

Yuriy Sirenko
Lyudmyla Velychko *Editors*

Electromagnetic Waves in Complex Systems

Selected Theoretical and Applied
Problems

Springer Series on Atomic, Optical, and Plasma Physics

Volume 91

Editor-in-chief

Gordon W.F. Drake, Windsor, Canada

Series editors

James Babb, Cambridge, USA

Andre D. Bandrauk, Sherbrooke, Canada

Klaus Bartschat, Des Moines, USA

Philip George Burke, Belfast, UK

Robert N. Compton, Knoxville, USA

Tom Gallagher, Charlottesville, USA

Charles J. Joachain, Bruxelles, Belgium

Peter Lambropoulos, Iraklion, Greece

Gerd Leuchs, Erlangen, Germany

Pierre Meystre, Tucson, USA

The Springer Series on Atomic, Optical, and Plasma Physics covers in a comprehensive manner theory and experiment in the entire field of atoms and molecules and their interaction with electromagnetic radiation. Books in the series provide a rich source of new ideas and techniques with wide applications in fields such as chemistry, materials science, astrophysics, surface science, plasma technology, advanced optics, aeronomy, and engineering. Laser physics is a particular connecting theme that has provided much of the continuing impetus for new developments in the field, such as quantum computation and Bose-Einstein condensation. The purpose of the series is to cover the gap between standard undergraduate textbooks and the research literature with emphasis on the fundamental ideas, methods, techniques, and results in the field.

More information about this series at <http://www.springer.com/series/411>

Yuriy Sirenko · Lyudmyla Velychko
Editors

Electromagnetic Waves in Complex Systems

Selected Theoretical and Applied Problems

 Springer

Editors

Yuriy Sirenko
Usikov Institute for Radiophysics
and Electronics
Kharkiv
Ukraine

Lyudmyla Velychko
Usikov Institute for Radiophysics
and Electronics
Kharkiv
Ukraine

ISSN 1615-5653

ISSN 2197-6791 (electronic)

Springer Series on Atomic, Optical, and Plasma Physics

ISBN 978-3-319-31630-7

ISBN 978-3-319-31631-4 (eBook)

DOI 10.1007/978-3-319-31631-4

Library of Congress Control Number: 2016935966

© Springer International Publishing Switzerland 2016

This work is subject to copyright. All rights are reserved by the Publisher, whether the whole or part of the material is concerned, specifically the rights of translation, reprinting, reuse of illustrations, recitation, broadcasting, reproduction on microfilms or in any other physical way, and transmission or information storage and retrieval, electronic adaptation, computer software, or by similar or dissimilar methodology now known or hereafter developed.

The use of general descriptive names, registered names, trademarks, service marks, etc. in this publication does not imply, even in the absence of a specific statement, that such names are exempt from the relevant protective laws and regulations and therefore free for general use.

The publisher, the authors and the editors are safe to assume that the advice and information in this book are believed to be true and accurate at the date of publication. Neither the publisher nor the authors or the editors give a warranty, express or implied, with respect to the material contained herein or for any errors or omissions that may have been made.

Printed on acid-free paper

This Springer imprint is published by Springer Nature

The registered company is Springer International Publishing AG Switzerland

Preface

Our aim in writing this manuscript was to provide young researchers and graduate students with a book that combines examples of solving serious research problems in electromagnetics and original results that encourage further investigations. The book contains seven papers on various aspects of resonant wave propagation and scattering written by different authors. Each paper solves one original problem. However, all of the papers are unified by authors' desire to show the advantages of rigorously justified approaches to all stages of the study: from problem formulation and selection of the method of attack to interpretation of the results.

A glance at the Contents will reveal a range of physical problems raised in the book. Mostly, those are the problems associated with wave propagation and scattering in natural and artificial environments or with designing the elements and units for antenna feeders. The authors invoke both theoretical (analytical and numerical) and experimental techniques for handling the problems. Considerable attention is given to the mathematical simulation issues, problems of computational efficiency, and physical interpretation of the results of numerical or full-scale experiments. Most of the presented results are original and have not been published earlier.

The need for rigorous theoretical justification of mathematical modeling and computational experiments—the widely used methodologies of obtaining new knowledge—is evident. Underformulated problems, neglect of the estimation of stability and convergence of numerical schemes cannot guarantee reliability of the results. Furthermore, the rigorous theoretical basis of the laboratory and full-scale experiments allows to conduct research saving time and material resources, to safely test simulated devices in a variety of operating conditions. To demonstrate the advantages of rigorous approaches and their realizability is the heart of the ideology of this book. And we address it to those young researchers who are going to work actively and fruitfully in the field of theoretical and applied physics, electronics, and optics.

The authors of this book are mostly current or former employees of the Department of Mathematical Physics at the O.Ya. Usikov Institute for Radiophysics

and Electronics of the National Academy of Sciences (Kharkiv, Ukraine). Professor Yuriy Sirenko, who has been at the head of the department over the last 25 years, initiated the writing of this rather unusual in its conception book. He has had a major influence on it, both scientific and organizational, and managed to inspire other colleagues with his idea.

The assumed background of the reader is mostly limited to standard undergraduate topics in physics and mathematics.

Kharkiv, Ukraine

Lyudmyla Velychko

Contents

1	New Analytical Solutions of Selected Electromagnetic Problems in Wave Diffraction Theory	1
	Leonid Pazyinin	
1.1	Introduction	1
1.2	Wave Propagation Near an Irregular Impedance Structure	3
1.2.1	Wave Propagation Over a Plane Surface of Variable Conductivity	3
1.2.2	A Field of Linear Magnetic Current in a Plane Waveguide with Smoothly Varying Impedance of Its Walls	7
1.3	The Cycle Slipping Phenomenon and the Degeneracy of Waveguide Modes	21
1.3.1	Introduction	21
1.3.2	Problem Formulation and Solution	24
1.3.3	The Watson Transformation	31
1.3.4	A Numerical Experiment	35
1.4	Pulsed Radiation from a Line Electric Current Near a Planar Interface	40
1.4.1	Problem Formulation	41
1.4.2	Reduction to Single Integrals	44
1.4.3	The Field in the First Medium	48
1.4.4	The Field in the Second Medium	51
1.4.5	Discussion and Conclusion	52
1.5	Transition Radiation of a Longitudinal Magnetic Dipole in the Case of Diffuse Interface	54
1.5.1	Problem Formulation and Solution	54
1.5.2	The Criterion of the Interface ‘Sharpness’	61
1.6	The Biisotropic Epstein Transition Layer	63
1.6.1	Equations for the Electromagnetic Field in a Biisotropic Medium	63

1.6.2	Problem Formulation and Solution	65
1.6.3	Analysis of the Reflected and Transmitted Fields	68
1.7	Negative Refraction in Isotropic Double-Negative Media	71
1.7.1	Negative Refraction Phenomenon in Homogeneous Double-Negative Media	71
1.7.2	A Model of Smoothly Inhomogeneous Flat-Layered Double Negative Medium. Solution of the Problem of Transmission of a Plane Wave.	73
1.7.3	Analysis of the Expressions for Fields	76
1.8	Distorting Coatings as an Alternative to Masking Coatings	78
1.8.1	Transformation Optics, Masking Coatings, Distorting Coatings	78
1.8.2	Radical Distortion of Radar Image by Applying a Special Coating on the Metamaterial Surface	79
1.9	Conclusion	83
	References	85
2	Dyadic Green's Function for Biaxial Anisotropic Media	91
	Leonid Pazyinin, Seil Sautbekov and Yuriy Sirenko	
2.1	Introduction.	91
2.2	Formulation of the Problem.	92
2.3	Initial Representation for Dyadic Green's Function.	93
2.4	Transformation of the Original Representation. Singular Part of Dyadic Green's Function	94
2.5	Regular Part of Dyadic Green's Function	96
2.6	The Physical Solution.	98
2.7	Conclusion	101
	References	102
3	Operator Fresnel Formulas in the Scattering Theory of Waveguide Modes	103
	Igor Petrusenko and Yuriy Sirenko	
3.1	Introduction.	103
3.2	The Mode-Matching Technique in the Problem of a Waveguide Step-like Discontinuity	106
3.2.1	The Classical Mode-Matching Technique: An Example of Application.	106
3.2.2	The Mode-Matching Technique in the Problem of a Step Discontinuity in a Waveguide: Standard Approach	108
3.2.3	New Formulation of the Problem of Scattering of Waveguide Modes	114
3.3	Matrix Operator Formalism in the Scalar Mode Analysis	114

- 3.4 Generalized Mode-Matching Technique in the Step Discontinuity Problem 119
 - 3.4.1 Derivation of the Operator Fresnel Formulas 119
 - 3.4.2 Reciprocity Principle and Energy Conservation Law in the Operator Form. 123
 - 3.4.3 Correctness of the Matrix-Operator Model. 127
- 3.5 Justification of the Truncation Technique for Solving Operator Equations. 129
 - 3.5.1 Construction of Projection Approximations for the Fresnel Formulas 130
 - 3.5.2 Unconditional Convergence of the Truncation Technique 133
 - 3.5.3 Rate of Convergence of the Approximations of Scattering Operators 135
- 3.6 Mittra Rule for Scattering Operators. 139
- 3.7 Novel Matrix Models for the Problem of a Step Discontinuity in a Waveguide 143
- 3.8 The Conservation Laws in Operator Form for Two Classes of Mode Diffraction Problems 148
- 3.9 Universality of the Operator Fresnel Formulas 155
 - 3.9.1 Step-Like Discontinuity in a Waveguide 155
 - 3.9.2 Generalized Operator Fresnel Formulas for Resonant Discontinuities 157
- 3.10 Matrix Scattering Operators. 159
 - 3.10.1 Properties of Reflection and Transmission Operators. 159
 - 3.10.2 Basic Operator Properties of the Generalized Scattering Matrix 164
- 3.11 Conclusion 172
- Appendix A: Vectors and Their Spaces 175
- Appendix B: Infinite Systems of Linear Algebraic Equations 179
- Appendix C: Operator Forms of the Energy Conservation Law Under Time Reversal. 184
- References 185
- 4 Two-Dimensionally Periodic Gratings: Pulsed and Steady-State Waves in an Irregular Floquet Channel 187**

Lyudmyla Velychko

 - 4.1 Introduction. 187
 - 4.2 Fundamental Equations, Domain of Analysis, Initial and Boundary Conditions 189
 - 4.3 Time Domain: Initial Boundary Value Problems 192
 - 4.4 Exact Absorbing Conditions for the Rectangular Floquet Channel 194
 - 4.5 Some Important Characteristics of Transient Fields in the Rectangular Floquet Channel 197

4.6	Transformation Operator Method	202
4.6.1	Evolutionary Basis of a Signal and Transformation Operators	202
4.6.2	Equations of the Operator Method in the Problems for Multilayered Periodic Structures	206
4.7	Some Important Properties of Steady-State Fields in the Rectangular Floquet Channel	208
4.7.1	Excitation by a <i>TM</i> -Wave	208
4.7.2	Excitation by a <i>TE</i> -Wave	212
4.7.3	General Properties of the Grating's Secondary Field	213
4.7.4	Corollaries of the Reciprocity Relations and the Energy Conservation Law	215
4.8	Elements of Spectral Theory for Two-Dimensionally Periodic Gratings	217
4.8.1	Canonical Green Function	217
4.8.2	Qualitative Characteristics of the Spectrum	219
4.9	Conclusion	223
	References	223
5	The Exact Absorbing Conditions Method in the Analysis of Open Electrodynamical Structures	225
	Kostyantyn Sirenko and Yuriy Sirenko	
5.1	Introduction	225
5.2	Circular and Coaxial Waveguides	228
5.2.1	Formulation of the Model Problem	228
5.2.2	Radiation Conditions for Outgoing Waves	230
5.2.3	Nonlocal Exact Absorbing Conditions	235
5.2.4	Local Exact Absorbing Conditions	237
5.2.5	Equivalence Theorem	241
5.3	Compact Axially Symmetric Structures	245
5.3.1	Formulation of the Model Problem	245
5.3.2	Radiation Conditions for Outgoing Waves	246
5.3.3	Far-Field Zone Problem, Extended and Remote Sources	254
5.3.4	Virtual Feed Lines in Compact Open Structures	259
5.4	Characteristics of Steady-State and Transient Fields in Axially Symmetric Structures	263
5.4.1	Frequency-Domain Prototypes for Initial Boundary Value Problems	263
5.4.2	Electrodynamical Characteristics of Open Axially Symmetric Structures	265
5.4.3	Spectral Characteristics of Open Resonators	269
5.5	Plane Models for Open Electrodynamical Structures	275
5.5.1	The Key Problem	275

- 5.5.2 Exact Absorbing Conditions for Parallel-Plate Waveguides. 277
- 5.5.3 Exact Absorbing Conditions for Cylindrical Virtual Boundary in Free Space. 283
- 5.5.4 Exact Absorbing Conditions for Rectangular Virtual Boundary in Free Space. 286
- 5.5.5 Frequency-Domain Formalism and Main Characteristics of Open Plane Structures 291
- 5.6 3-D Vector Models 292
 - 5.6.1 Exact Absorbing Conditions for Regular Hollow Waveguides. 294
 - 5.6.2 Radiation Conditions and Exact Absorbing Conditions for Spherical Virtual Boundary in Free Space 300
 - 5.6.3 TM-Excitation: Frequency-Domain Characteristics 306
 - 5.6.4 TE-Excitation: Frequency-Domain Characteristics. 310
- 5.7 Accurate and Efficient Calculations 311
 - 5.7.1 General Questions 311
 - 5.7.2 Nonlocal or Local Conditions?. 312
 - 5.7.3 The Blocked FFT-Based Acceleration Scheme. 314
 - 5.7.4 Efficiency and Accuracy of the Blocked FFT-Based Acceleration Scheme. Numerical Results. 317
 - 5.7.5 Test Problems 320
- 5.8 Conclusion 322
- References 324
- 6 High-Power Short Pulses Compression: Analysis and Modeling 327**

Vadym Pazynin, Kostyantyn Sirenko and Yuriy Sirenko

 - 6.1 Introduction. 327
 - 6.2 Exact Absorbing Conditions Method: 2-D Case 329
 - 6.2.1 Planar Structures 329
 - 6.2.2 Axially Symmetric Structures 337
 - 6.3 Energy Accumulation in Direct-Flow Waveguide Compressors 343
 - 6.3.1 Slot Switches. 343
 - 6.3.2 Active Compressors Based on Circular and Coaxial Waveguides. 348
 - 6.3.3 Distributed Switches and Active Compressors Based on Rectangular Waveguides. 352
 - 6.4 Radiation of High-Power Short Pulses 358
 - 6.4.1 Radiation of Compressed Pulses by Simple Antennas. 360
 - 6.4.2 Novel Antenna Array Design with Combined Compressor/Radiator Elements. 367
 - 6.5 Compression of Frequency-Modulated Electromagnetic Pulses in Hollow Waveguides 371

- 6.5.1 Transport Operators for Regular Waveguides. 373
- 6.5.2 Pulse Compression in Regular Waveguides 375
- 6.6 Conclusion 382
- References 383
- 7 Diffraction Radiation Phenomena: Physical Analysis and Applications. 387**
 Seil Sautbekov, Kostyantyn Sirenko, Yuriy Sirenko, Alexey Vertiy and Anatoliy Yevdokymov
- 7.1 Introduction. 387
- 7.2 Periodic Structures and Dielectric Waveguides: Analysis Techniques 389
 - 7.2.1 Plane Models for Infinite Gratings: Time-Domain Representations 389
 - 7.2.2 Plane Models for Infinite Gratings: Frequency-Domain Representations 394
 - 7.2.3 Infinite Gratings as Open Resonators or Open Waveguides. 397
 - 7.2.4 Some Further Comments. 397
- 7.3 Diffraction Radiation Phenomena. 400
 - 7.3.1 Reflecting Gratings in the Field of a Density-Modulated Electron Flow 400
 - 7.3.2 Finite Gratings: Plane and Axially Symmetric Models 408
 - 7.3.3 Near-Field to Far-Field Conversion by Finite Periodic Structures. Plane Models 411
 - 7.3.4 Near-Field to Far-Field Conversion by Finite Periodic Structures. Axially Symmetric Models 416
- 7.4 Synthesis of Diffraction Antenna Components and Units. 423
 - 7.4.1 Synthesis of Radiators with Predetermined Amplitude-Phase Field Distribution on the Aperture 423
 - 7.4.2 Maintenance of Antenna Operability on Coupling Level 429
- 7.5 The Low-Side-Lobe Planar Antenna. 432
 - 7.5.1 Radiator’s Characteristics 432
 - 7.5.2 Antenna Design 435
 - 7.5.3 Experimental Data 438
- 7.6 Conclusion 440
- References 440
- Index 443**

Contributors

Leonid Pazynin O.Ya. Usikov Institute for Radiophysics and Electronics, National Academy of Sciences, Kharkiv, Ukraine

Vadym Pazynin O.Ya. Usikov Institute for Radiophysics and Electronics, National Academy of Sciences, Kharkiv, Ukraine

Igor Petrusenko University of Customs and Finance, Dnipropetrovsk, Ukraine

Seil Sautbekov L.N. Gumilyov Eurasian National University, Astana, Republic of Kazakhstan

Kostyantyn Sirenko King Abdullah University of Science and Technology, Thuwal, Saudi Arabia

Yuriy Sirenko O.Ya. Usikov Institute for Radiophysics and Electronics, National Academy of Sciences, Kharkiv, Ukraine; L.N. Gumilyov Eurasian National University, Astana, Republic of Kazakhstan

Lyudmyla Velychko O.Ya. Usikov Institute for Radiophysics and Electronics, National Academy of Sciences, Kharkiv, Ukraine

Alexey Vertiy L.N. Gumilyov Eurasian National University, Astana, Republic of Kazakhstan

Anatoliy Yevdokymov O.Ya. Usikov Institute for Radiophysics and Electronics, National Academy of Sciences, Kharkiv, Ukraine

Chapter 1

New Analytical Solutions of Selected Electromagnetic Problems in Wave Diffraction Theory

Leonid Pazyinin

Abstract The chapter presents explicit analytical solutions for some sophisticated electromagnetic problems. The analysis of these solutions made it possible, in particular, to explain the physics of a cycle slipping phenomenon when very long electromagnetic waves propagate in the Earth-ionosphere waveguide, to establish the rigorous criterion of the boundary ‘sharpness’ for transient radiation and to show that the well-known negative refraction phenomenon in isotropic double-negative media is a direct consequence of the energy conservation law and Maxwell’s equations.

1.1 Introduction

Exact analytical solutions of the basic problems of physics—boundary value and initial boundary value—are important not only as a reference for verifying numerical results but also as an effective tool for a deeper understanding of the nature of the model under study. To obtain such solutions for new physical problems, one should invoke, as a rule, new mathematical methods or significantly modify the available ones. Thus, for example, in quantum mechanics, novel approaches have resulted in a sharp increase in the number of exactly solvable problems and raised interest in the subject in the recent years [1]. In theoretical radio physics, this was the case in mid-twentieth century, after publishing of the book by Wiener and Hopf [2]. This work has been of vital importance, which is why the method presented therein takes its name from the authors—the *Wiener-Hopf method*. As applied to diffraction problems, it was first used in [3–5]. In the review [6] the authors attempted to describe the areas of application and discussed the future development of this method.

Mention should be made of the detailed study of the *integral convolution equations* in the book by Gakhov and Cherskiy [7], which although not mentioned

L. Pazyinin (✉)

O.Ya. Usikov Institute for Radiophysics and Electronics, National Academy of Sciences, Kharkiv, Ukraine

e-mail: pazyinin@ire.kharkov.ua

in [6] can be considered as part of the development of this method. In the first two sections of this chapter, we apply their methodology of solving integral convolution equations to the new problems on wave propagation near a plane surface of varying conductivity, thereby reducing those problems to exactly solvable boundary value ones. Thus, in Sect. 1.2 of this chapter, using the technique suggested in [7] for solving the so-called smooth transition equation, we obtain analytical solutions for two two-dimensional problems, namely, we find analytical expressions for the field generated by a linear current above a plane surface whose impedance varies continuously from Z_1 to Z_2 in a given direction, and for the field generated by the same source in a planar waveguide with a wall of the same impedance distribution. These solutions generalize the known ones in which the surface impedance changes stepwise. In Sect. 1.3 we investigate a model of a ring waveguide of constant cross-section with variable in azimuth impedance of one of the walls. We have found a class of distributions of these impedances, for which the analytical solution of the excitation problem for this waveguide had been obtained. This result is used for simulation of the known *cycle slipping phenomenon* occurring when very long electromagnetic waves propagate in the *Earth-ionosphere waveguide*. A possible cause of this phenomenon is discussed.

The remaining sections of the chapter are not associated with the Wiener-Hopf method. In Sect. 1.4 a novel technique is suggested for the analysis of a transient electromagnetic field generated by a pulsed line current that is located near a planar interface between two dielectric nonabsorbing and nondispersive media. As distinct from the *Cagniard-de Hoop method*, which is widely used for the study of transient fields both in electrodynamics and in the theory of acoustic and seismic waves, our approach is based on the transformation of the domain of integration in the integral expression for the field in the space of two complex variables. As a result, it will suffice to use the standard procedure of finding the roots of the algebraic equation rather than construct auxiliary Cagniard's contours. A new representation for the field has been derived in the form of an integral along a finite contour.

In Sect. 1.5 we discuss the transient radiation of a *moving longitudinal magnetic dipole* whose trajectory crosses a soft boundary between two media. The obtained analytical representation for the dipole field ensures a rigorous *criterion of the boundary 'sharpness'* thus significantly improving the now known approximate version.

In Sect. 1.6 the isotropic *Epstein transition layer* was generalized to the case of a *biisotropic plane stratified medium*. An explicit analytical solution to the problem of normal incidence of a linearly polarized electromagnetic plane wave onto the Epstein layer was obtained for this extension. The derived transmission and reflection coefficients are indicative of the presence of the total transmission mode in such media.

In Sect. 1.7 we suggest a model for a smoothly inhomogeneous isotropic flat-layered medium that includes domains with *double-positive* and *double-negative media*. The analytical solution derived for a plane wave propagating through this medium shows that the well-known *negative refraction phenomenon* in the isotropic double-negative medium is a direct consequence of Maxwell's equations and of the *energy conservation law*.

In Sect. 1.8, using as an example a perfectly conducting sphere, we rigorously prove the possibility of drastic *distortion* of its *radar image* by applying a *meta-material coating* on the sphere surface. We have found such radial distributions of the coating dielectric and magnetic permeabilities that the scattered field everywhere outside the object coincides with the field scattered by a perfectly conducting sphere of any given smaller radius. Requirements on the material parameters of such distorting coating are smaller than they are in the case of a masking coating.

1.2 Wave Propagation Near an Irregular Impedance Structure

One of the problems solved at the early stage of the development of the Wiener-Hopf method was related to the electromagnetic wave propagation above a plane whose impedance changed step-wise from Z_1 to Z_2 in a given direction [8]. A waveguide analog of this problem was studied in [9] for acoustic waves and in [10] for electromagnetic waves. The electromagnetic model presented in [8] was given the name '*the coastal refraction problem*' since it was used for calculation of a radar error arising when the radar crosses a shoreline.

It is well known that in the case of the stratified medium, whose permittivity is given by the hyperbolic tangent or by hyperbolic secant, the solution of the wave propagation problem can be written in explicit form. These two media have been named asymmetric and symmetric Epstein layers, respectively. In this section we will show that the problem of wave propagation near a plane surface, whose impedance is given by the hyperbolic tangent, is also explicitly resolvable. At the same time, attempts to obtain similar results for an impedance analog of the symmetric Epstein layer (the permittivity is given by the hyperbolic secant) were unsuccessful, because in this case we are led to *three-element Carleman's problem* whose solution is unknown.

1.2.1 Wave Propagation Over a Plane Surface of Variable Conductivity

Electrical properties of real underlying surfaces vary smoothly and the assumption as to their step-wise change (for example, when crossing the boundary land/sea) can only be justified for sufficiently large values of the wavelength λ . However, the discontinuity of the function $Z(x)$, which characterizes the surface impedance distribution on the plane $z = 0$ in classical two-dimensional ($\partial/\partial y \equiv 0$) problems, is incompatible with a mere concept of the surface impedance.

The question arises as to the existence of such continuous and reasonable (from the physical point of view) surface impedance distributions that they allow an exact analytical solution of the problems like those discussed in [8–10].

It has been shown [11] that such a distribution does exist. It is the impedance version of the Epstein transition layer [12]

$$Z(x) = \frac{Z_2 + Z_1 \exp(-\tau x)}{1 + \exp(-\tau x)}; \quad -\infty < x < \infty, \quad (1.1)$$

where $Z_1 = Z(-\infty)$ and $Z_2 = Z(+\infty)$ are the limiting values of impedance. The parameter $0 < \tau < \infty$ determines the width of the transition region in the impedance distribution. The Grinberg-Fock model of the step-wise change in impedance [8] represents the limiting case $\tau \rightarrow \infty$.

Let us consider the following two-dimensional problem: a field generated by a filament of linear magnetic current $\vec{J}^{(m)} = I^{(m)} \delta(g - g_0) \exp(-i\omega t) \vec{y}$, which is parallel to the impedance plane $z = 0$, is to be found. Here, $\delta(\dots)$ is the δ -Dirac function; $g = \{x, z\}$ and $g_0 = \{x_0, z_0\}$ are the points of the space \mathbb{R}^2 ; \vec{x} , \vec{y} , and \vec{z} are the Cartesian basis vectors. The current self-field can be represented as $\vec{E}^0 = i\omega\mu\mu_0 \text{rot } \vec{\Pi}^{(m)}$, where $\Pi_y^{(m)} = -I^{(m)}(4\omega\mu\mu_0)^{-1} H_0^{(1)}(k|g - g_0|)$ and $\Pi_x^{(m)} = \Pi_z^{(m)} = 0$ are the components of the magnetic Hertz potential; $H_0^{(1)}(\dots)$ is the Hankel function; $k = \omega\sqrt{\varepsilon\varepsilon_0\mu\mu_0}$; ε and μ are the relative dielectric permittivity and magnetic permeability of the medium. The surface impedance is given by relation (1.1).

Basing, as in [8], on the *integral Green formula* and using the impedance boundary condition $\partial E_z(g)/\partial z = -ikZ(x)E_z(g)|_{z=0}$ [13, 14], we arrive at the following 1-D integral equation:

$$f(x) = q(x) - \frac{k}{2} Z(x) \int_{-\infty}^{\infty} f(\tilde{x}) H_0^{(1)}(k|x - \tilde{x}|) d\tilde{x}, \quad (1.2)$$

where $f(x) = Z(x)E_z(x, 0)$, $q(x) = 2Z(x)E_z^0(x, 0)$; $E_z^0(x, z)$ and $E_z(x, z)$ are the vertical components of the primary and total electrical fields, respectively.

Equation (1.2) belongs to the class of the so-called *smooth transition equations* introduced by Cherskiy [7]:

$$f(x) + \frac{1}{\sqrt{2\pi}} \int_{-\infty}^{\infty} K_1(x - \tilde{x}) f(\tilde{x}) d\tilde{x} - q(x) + e^{-x} \left\{ f(x) + \frac{1}{\sqrt{2\pi}} \int_{-\infty}^{\infty} K_2(x - \tilde{x}) f(\tilde{x}) d\tilde{x} - q(x) \right\} = 0; \quad -\infty < x < \infty. \quad (1.3)$$

For this equation to be normally solvable in the space $L_2(-\infty, \infty)$ and have a finite index it is necessary and sufficient to have $1 + \tilde{K}_j(\xi) \neq 0, j = 1, 2$, where $\tilde{K}_j(\xi)$ is the Fourier transform of $K_j(x)$. In our case, we have

$$\tilde{K}_j(\xi) = \kappa Z_j \int_0^\infty H_0^{(1)}(\kappa s) \cos \xi s ds = \kappa Z_j (\kappa^2 - \xi^2)^{-1/2},$$

where $\kappa = k/\tau$, and $\sqrt{\kappa^2 - \xi^2} \rightarrow i\xi$ with $\xi \rightarrow +\infty$.

In [7], the authors prove the solvability in quadratures of (1.3) in the space $L_2(-\infty, \infty)$ with the complementary condition that $q(x) \in L_2(-\infty, \infty)$.

Let us apply the Fourier transform to (1.2), following [7]. Then we are led to Carleman’s two-element boundary value problem for a strip $0 < \text{Im} \xi < 1$. Later on, with the use of some conformal mapping $v = \exp(2\pi\xi)$, we will rearrange this problem to yield the Riemann problem, which is as follows: on the real axis of the complex plane of variable $v = v' + iv''$ two functions, $D(v')$ and $H(v')$, are given; it is required to find two functions $F^\pm(v)$, which are analytic in the upper complex half-plane ($v'' > 0$) and in the lower complex half-plane ($v'' < 0$), respectively, and which also satisfy the boundary condition $F^+(v') = D(v')F^-(v') + H(v')$. The value $\chi = (2\pi i)^{-1} [\ln D(v')] |_{-\infty}^\infty$ is known as the index of the Riemann problem. For the two problems considered in this section, we have $\chi = 0$. Using the well-known solution of this problem [7], we can write the solution of (1.2) in the following form:

$$f(x) = -\frac{i}{4} I^{(m)} \frac{1}{\sqrt{2\pi}} \int_{-\infty}^\infty [\tau Q(\xi) + e^{\pi\xi} \omega + (e^{2\pi\xi})] \frac{\sqrt{\kappa^2 - \xi^2} \cdot e^{-i\bar{x}\xi}}{\sqrt{\kappa^2 - \xi^2} + \kappa Z_1} d\xi, \quad (1.4)$$

where $\bar{x} = x\tau, \bar{z} = z\tau$, and

$$Q(\xi) = \sqrt{\frac{2}{\pi}} \frac{\partial}{\partial \bar{x}_0} \int_{-\infty}^\infty \frac{Z_2 + Z_1 e^{-\eta}}{1 + e^{-\eta}} H_0^{(1)}\left(\kappa \sqrt{(\eta - \bar{x}_0)^2 + \bar{z}_0^2}\right) e^{i\xi\eta} d\eta,$$

$$\omega + (e^{2\pi\xi}) = -i\tau X + (e^{2\pi\xi})\kappa(Z_1 - Z_2) \int_{-\infty}^\infty \frac{Q(\zeta) e^{\pi\zeta} d\zeta}{\left(\sqrt{\kappa^2 - \zeta^2} + \kappa Z_2\right) X + (e^{2\pi\zeta})(e^{2\pi\zeta} - e^{2\pi\xi})},$$

$$X^\pm(e^{2\pi\zeta}) = \exp\left\{ \left(1 - ie^{2\pi\zeta}\right) \int_{-\infty}^\infty \ln \frac{\sqrt{\kappa^2 - \sigma^2} + \kappa Z_1}{\sqrt{\kappa^2 - \sigma^2} + \kappa Z_2} \frac{e^{2\pi\sigma} d\sigma}{(e^{2\pi\sigma} + i)(e^{2\pi\sigma} - e^{2\pi\zeta})} \right\}.$$

The contour of integration passes below the pole for the functions marked by ‘+’ and above the pole for the functions marked by ‘-’.

These relations represent an explicit expression for the vertical component of the electric field on an impedance plane considered without any restriction on the parameters of the model.

In the case of grazing propagation of a plane wave ($x_0 \rightarrow -\infty$) and for $Z_1 = 0$, the integral in the representation of the function $\omega^+[\exp(2\pi\xi)]$ can be calculated. To do this, let us transform the formula for $Q(\xi)$ using the *Parseval equality* for Fourier integrals and then apply the *saddle-point technique*. As a result we get the following asymptotic estimate for $k|x_0| \gg 1$:

$$Q(\xi) = 2 \exp(-i\pi/4) \frac{\exp(ik|x_0|)}{\sqrt{k|x_0|}} \frac{1}{\text{sh}[\pi(\kappa + \xi)]} \left(1 + O\left(\frac{1}{k|x_0|}\right) \right).$$

Hence, for the vertical component of the total electric field we have

$$E_z(x, 0) = 2e^{ikx} - \frac{i\kappa Z_2}{X^-[\exp(2\pi(-\kappa + i))]} \int_{-\infty}^{\infty} \frac{X^+[\exp(2\pi\xi)] \exp(-i\bar{x}\xi) d\xi}{\sqrt{\kappa^2 - \xi^2} \text{sh}[\pi(\kappa + \xi)]}, \quad (1.5)$$

where the integration contour passes above the pole $\xi = -\kappa$. The representation in the form of (1.5) is convenient for $x < 0$. The first term represents the plane wave on a perfectly conducting planar surface, while the integral term describes the field scattered by the impedance inhomogeneity.

Taking into account characteristics of the *factorization function* $X^\pm[\exp(2\pi\xi)]$, we obtain the representation, which is convenient for the area $x > 0$:

$$E_z(x, 0) = -\frac{i\kappa Z_2}{X^-[\exp(2\pi(-\kappa + i))]} \int_{-\infty}^{\infty} \frac{X^-[\exp(2\pi(\xi + i))] \exp(-i\bar{x}\xi) d\xi}{(\sqrt{\kappa^2 - \xi^2 + \kappa Z_2}) \text{sh}[\pi(\kappa + \xi)]}, \quad (1.6)$$

where the integration contour passes below the pole $\xi = -\kappa$. Using the following decomposition

$$\frac{1}{\text{sh}[\pi(\kappa + \xi)]} = \frac{1}{\pi} \sum_{n=-\infty}^{\infty} \frac{(-1)^n}{\xi + \kappa + in},$$

it is easy to show that (1.6) transforms for $\tau \rightarrow \infty$ into the well-known formula [8] for $E_z(x, 0)$ on the plane whose impedance equals Z_2 for $x > 0$ and is zero for $x < 0$.

Notice that the solution obtained in [8] represents the dominant term of the long-wave asymptotic of the solution to the problem considered by us. This is the case, where the wavelength of the source is much greater than the width of the transition region on the impedance surface ($2k \ll \tau$).

1.2.2 A Field of Linear Magnetic Current in a Plane Waveguide with Smoothly Varying Impedance of Its Walls

In this section, we construct the exact *Green function* of the *Helmholtz equation* for a band with the non-homogeneous boundary condition of the third kind on one of its boundaries. The coefficient $Z(x)$ in this boundary condition is an impedance analogue for the permittivity of the known Epstein transition layer [12]. We use this Green function below for analyzing the electromagnetic field induced by a linear magnetic current in a gradient junction between two regular impedance waveguides. This solution comprises the stepped impedance distribution as a limiting case [10]. In [15], we considered a related problem of the electromagnetic *TM-wave* propagation in a planar waveguide with the perfectly conducting upper wall and the lower wall with conductivity changing as $\text{th}\tau x$.

In Sect. 1.2.2.1, the boundary value problem is reduced to the integral equation of the second kind. In the next section, we derive the analytical solution by reducing this equation to the Riemann problem of the linear conjugation of two analytical functions on the real axis. For this purpose we invoke the Fourier transform and the conforming mapping. In Sect. 1.2.2.3, the Green function is expressed as the double Fourier integral, which is transformed further, by employing the *Cauchy-Poincaré theorem*, into series in residues. Section 1.2.2.4 is devoted to the analysis of these series as applied to the transformation of the eigenwaves of the regular section of the waveguide junction. We also rigorously estimate the *adiabatic approximation* for the considered waveguides.

1.2.2.1 Reduction of the Problem to an Integral Equation

A Solution to the Following Two-Dimensional Boundary Value Problem

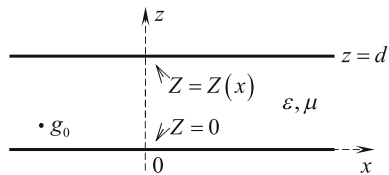
$$\left(\frac{\partial^2}{\partial x^2} + \frac{\partial^2}{\partial z^2} + \omega^2 \varepsilon \varepsilon_0 \mu \mu_0 \right) G^t = -\delta(g - g_0), \quad (1.7a)$$

$$\frac{\partial}{\partial z} G^t = 0 \quad \text{for } z = 0, \quad (1.7b)$$

$$\frac{\partial}{\partial z} G^t + i\omega \varepsilon \varepsilon_0 Z(x) G^t = 0 \quad \text{for } z = d \quad (1.7c)$$

is to be found in the band $\{0 < z < d, -\infty < x < \infty\}$ (see Fig. 1.1). Here $g = \{x, z\}$, $g_0 = \{x_0, z_0\}$, and the function

Fig. 1.1 The geometry of the problem



$$Z(x) = \frac{Z_2 + Z_1 \exp(-\tau x)}{Z + \exp(-\tau x)}; \quad \tau > 0, \quad Z = \exp(i\varphi), \quad -\pi < \varphi < \pi \quad (1.8)$$

is the complex-valued function describing the gradient transition from $Z(-\infty) = Z_1 = Z_l$ to $Z(+\infty) = Z_2/Z = Z_r$. Its hodograph represents a circular arc having the angular size of $|2\varphi|$ and joining the points Z_l and Z_r . In the course of solution, the imaginary part of the wave number $k = \omega\sqrt{\varepsilon\varepsilon_0\mu\mu_0}$ is assumed to be positive, whereas in the final formulas we put it equal to zero.

We seek the solution to the problem (1.7a, 1.7b, 1.7c) in the form of a sum

$$G^t(g, g_0) = G^0(g, g_0) + G(g, g_0), \quad (1.9)$$

where

$$G^0(g, g_0) = -\frac{1}{2\pi} \int_{-\infty}^{\infty} \frac{d(\eta, z, z_0)}{R_l(\eta)} \exp[-i(\bar{x} - \bar{x}_0)\eta] d\eta$$

is the solution to (1.7a, 1.7b, 1.7c) with the fixed $Z(x) = Z_l$, and

$$G(g, g_0) = \int_{-\infty}^{\infty} F_0(\eta, \bar{g}_0) \cos(v\bar{z}) \exp[-i(\bar{x} - \bar{x}_0)\eta] d\eta \quad (1.10)$$

is the solution of the homogeneous equation (1.7a) with condition (1.7b). Here, $d(\eta, z, z_0) = \cos(v\bar{z}_<)[\cos(v(\delta - \bar{z}_>)) - i\bar{Z}_l \sin(v(\delta - \bar{z}_>))]/v$,

$R_z(\eta) = v \sin v\delta + i\bar{Z}_z \cos v\delta$, $v = v(\eta) = \sqrt{\kappa^2 - \eta^2}$, $\bar{Z}_\alpha = Z_\alpha \omega \varepsilon / \tau$, $\alpha = l$ or r , $\kappa = k/\tau$, $\delta = d\tau$, $\bar{z}_< = \min(\bar{z}, \bar{z}_0)$, $\bar{z}_> = \max(\bar{z}, \bar{z}_0)$, $\bar{x} = x\tau$, $\bar{z} = z\tau$, and d is the waveguide height. With this representation of the function G^t , the requirements (1.7a), (1.7b) are satisfied automatically. The condition (1.7c) leads to the following integral equation

$$\int_{-\infty}^{\infty} F(\eta) [e^{2iv\delta} - 1 - \bar{Z}(\bar{x})(e^{2iv\delta} + 1)/v] \exp(-i\bar{x}\eta) d\eta = -\sqrt{2\pi} Q(\bar{x}); \quad (1.11)$$

$$Q(\bar{x}) = i(2\pi)^{-3/2} (\bar{Z}_l - \bar{Z}(\bar{x})) \int_{-\infty}^{\infty} \frac{\cos(v\bar{z}_0)}{R_l(\eta)} \exp[-i(\bar{x} - \bar{x}_0)\eta] d\eta, \quad -\infty < \bar{x} < \infty$$

with respect to the unknown function

$$F(\eta) = \frac{1}{2i} v \exp[-i(v\delta - \eta\bar{x}_0)] F_0(\eta, \bar{g}_0). \tag{1.12}$$

By using the known formula [16]

$$2\exp(iv\delta) = v \int_{-\infty}^{\infty} H_0^{(1)}\left(\kappa\sqrt{\xi^2 + \delta^2}\right) \exp(i\eta\xi) d\xi,$$

we can easily go from (1.11) to the equation of the second kind

$$f(\bar{x}) + \int_{-\infty}^{\infty} \tilde{K}(\bar{x}, \bar{x} - \xi) f(\xi) d\xi = Q(\bar{x}); \quad -\infty < \bar{x} < \infty \tag{1.13}$$

with respect to the Fourier transform of $F(\eta)$

$$f(\bar{x}) = \frac{1}{\sqrt{2\pi}} \int_{-\infty}^{\infty} F(\eta) \exp(-i\eta\bar{x}) d\eta. \tag{1.14}$$

The kernel looks like

$$\begin{aligned} \tilde{K}(\bar{x}, \bar{x} - \xi) = & \frac{1}{2} \bar{Z}(\bar{x}) H_0^{(1)} \left[\kappa \sqrt{(\bar{x} - \xi)^2 + (2\delta)^2} \right] + \frac{1}{2} \bar{Z}(\bar{x}) H_0^{(1)} (\kappa|\bar{x} - \xi|) \\ & - \frac{1}{4i} \frac{\partial}{\partial \delta} H_0^{(1)} \left[\kappa \sqrt{(\bar{x} - \xi)^2 + (2\delta)^2} \right]. \end{aligned}$$

Rewrite finally (1.13) in the form

$$\begin{aligned} Zf(\bar{x}) + \frac{1}{\sqrt{2\pi}} \int_{-\infty}^{\infty} K_2(\bar{x} - \xi) f(\xi) d\xi - ZQ(\bar{x}) \\ + \exp(-\bar{x}) \left\{ f(\bar{x}) + \frac{1}{\sqrt{2\pi}} \int_{-\infty}^{\infty} K_1(\bar{x} - \xi) f(\xi) d\xi - Q(\bar{x}) \right\} = 0; \quad -\infty < \bar{x} < \infty, \end{aligned} \tag{1.15}$$

where

$$\frac{1}{\sqrt{2\pi}}K_j(\bar{x} - \xi) = \frac{1}{2}\bar{Z}_j \left[H_0^{(1)} \left[\kappa \sqrt{(\bar{x} - \xi)^2 + (2\delta)^2} \right] + H_0^{(1)}(\kappa|\bar{x} - \xi|) \right] - \frac{1}{4i}Z_j^{-1} \frac{\partial}{\partial \delta} H_0^{(1)} \left[\kappa \sqrt{(\bar{x} - \xi)^2 + (2\delta)^2} \right]; \quad j = 1, 2.$$

1.2.2.2 Solution of the Integral Equation

For $Z = 1$, a similar equation was discussed in [17], where a method of obtaining its analytical solution was proposed. Following the basic ideas introduced in this work, let us find the analytical solution of the more general equation (1.15) by reducing it to the Riemann conjugation problem. To this end, we introduce a new unknown function

$$\Phi(\bar{x}) = f(\bar{x}) + \frac{1}{\sqrt{2\pi}} \int_{-\infty}^{\infty} K_1(\bar{x} - \xi) f(\xi) dt - Q(\bar{x}); \quad -\infty < \bar{x} < \infty. \quad (1.16)$$

By subjecting (1.15) and (1.16) to the Fourier transform, we obtain a system of functional equations

$$\begin{cases} ZF(\bar{\xi}) + \tilde{K}_2(\bar{\xi})F(\bar{\xi}) - Z\tilde{Q}(\bar{\xi}) + \tilde{\Phi}(\bar{\xi} + i) = 0 \\ \tilde{\Phi}(\bar{\xi}) = F(\bar{\xi}) + \tilde{K}_1(\bar{\xi})F(\bar{\xi}) - \tilde{Q}(\bar{\xi}), \end{cases} \quad (1.17)$$

where $\tilde{K}_1(\bar{\xi})$, $\tilde{K}_2(\bar{\xi})$, $\tilde{\Phi}(\bar{\xi})$, and $\tilde{Q}(\bar{\xi})$ are the Fourier transforms of the functions $K_1(\bar{x})$, $K_2(\bar{x})$, $\Phi(\bar{x})$, and $Q(\bar{x})$, respectively. Eliminating $F(\bar{\xi})$, we arrive at the equation

$$\tilde{\Phi}(\bar{\xi}) = -D(\bar{\xi})\tilde{\Phi}(\bar{\xi} + i) + H(\bar{\xi}); \quad -\infty < \bar{\xi} < \infty, \quad (1.18)$$

where

$$D(\bar{\xi}) = R_l(\bar{\xi})/[ZR_r(\bar{\xi})] \quad \text{and} \quad H(\bar{\xi}) = i(\bar{Z}_l - \bar{Z}_r)\cos(\nu\delta)\tilde{Q}(\bar{\xi})/R_r(\bar{\xi}).$$

This is the Carleman problem: to find the analytical function $\tilde{\Phi}(\bar{\xi})$ in the band $0 < \text{Im}\bar{\xi} < 1$ of the complex plane $\bar{\xi} = \bar{\xi} + i\bar{\zeta}$ from the condition (1.18) on the band boundary. Applying the conformal mapping $\zeta = \exp(2\pi\bar{\xi})$ to (1.18), we pass to the new unknown function $\omega(\zeta) = \zeta^{-1/2}\Phi(\ln \zeta/2\pi)$. Then this problem is transformed into the Riemann problem of finding two analytical functions $\omega^\pm(\zeta)$ (in the upper and lower half-planes of the complex plane $\zeta = \xi + i\zeta$) from the boundary condition on the real axis ξ

$$\omega^+(\zeta) = \bar{D}(\zeta)\omega^-(\zeta) + \bar{H}(\zeta); \quad -\infty < \zeta < \infty \quad (1.19)$$

with the discontinuous coefficient

$$\begin{aligned} \bar{D}(\zeta) &= \{D(\bar{\zeta}) \text{ for } \zeta > 0; 1 \text{ for } \zeta < 0\} \quad \text{and} \\ \bar{H}(\zeta) &= \left\{ e^{-\pi\bar{\zeta}} H(\bar{\zeta}) \text{ for } \zeta > 0; 0 \text{ for } \zeta < 0 \right\}; \quad \bar{\zeta} = \ln \zeta / 2\pi. \end{aligned} \quad (1.20)$$

The branches of the functions $\ln \zeta$ and $\sqrt{\zeta}$ are determined by the value $\arg \zeta = 0$ on the upper edge of the cut made along the ray $\zeta \geq 0$.

The analytical solution to the homogeneous Riemann problem

$$\omega^+(\zeta) = \bar{D}(\zeta)\omega^-(\zeta); \quad -\infty < \zeta < \infty \quad (1.21)$$

in the case where the function $\bar{D}(\zeta)$ is continuous along the whole of the real axis, including the infinitely distant point, is well known [7]. The function in (1.20) is discontinuous at the points $\zeta = 0$ and $\zeta = \infty$. Represent it as a product

$$\bar{D}(\zeta) = \bar{D}_1(\zeta)\bar{D}_2(\zeta)$$

of the continuous function

$$\bar{D}_1(\zeta) = \{R_l(\bar{\zeta})/R_r(\bar{\zeta}) \text{ for } \zeta > 0; 1 \text{ for } \zeta < 0\} \quad (1.22)$$

and the discontinuous function

$$\bar{D}_2(\zeta) = \{Z^{-1} \text{ for } \zeta > 0; 1 \text{ for } \zeta < 0\}.$$

Obviously, if the solutions $\omega_j(\zeta)$ of the problems

$$\omega_j^+(\zeta) = \bar{D}_j(\zeta)\omega_j^-(\zeta); \quad j = 1, 2, \quad -\infty < \zeta < \infty \quad (1.23)$$

are known, then $\omega(\zeta) = \omega_1(\zeta)\omega_2(\zeta)$ is a solution to the problem in (1.21). Let us find $\omega_2(\zeta)$. Since

$$\ln \omega_2^+(\zeta) = \ln \omega_2^-(\zeta) - i\varphi \{1 \text{ for } \zeta > 0; 0 \text{ for } \zeta < 0\}; \quad -\infty < \zeta < \infty,$$

then the desired function is analytical in the plane ζ containing a cut along the real positive semiaxis; the discontinuity value on it is $-i\varphi = -\ln Z$. We take for such a function the function

$$\omega_2(\zeta) = \exp\left\{\frac{\varphi}{2\pi} \cdot \ln \zeta\right\}.$$

The solution of the problem in (1.23) for $\omega_1(\zeta)$ can be derived by using the known mathematical technique of factorizing the Riemann problem coefficient [7, 17]

$$\omega_1^+(\zeta) = \exp\{\Gamma^+(\zeta)\},$$

where

$$\Gamma^+(\zeta) = \frac{1}{2\pi i} \int_{-\infty}^{\infty} \ln \bar{D}_1(\xi) \frac{(\zeta + i)d\xi}{(\xi - \zeta)(\xi + i)}; \quad \text{Im}\zeta > 0.$$

Let us introduce a function

$$X^+(\bar{\zeta}) = \omega_1^+[\exp(2\pi\bar{\zeta})] = \exp\{\Gamma^+[\exp(2\pi\bar{\zeta})]\},$$

$$\Gamma^+[\exp(2\pi\bar{\zeta})] = \frac{1}{2i} \int_{-\infty}^{\infty} \ln \frac{R_l(\eta)}{R_r(\eta)} \cdot \frac{\text{ch}[\pi(\bar{\zeta} - i/4)]d\eta}{\text{ch}[\pi(\eta - i/4)]\text{sh}[\pi(\eta - \bar{\zeta})]}; \quad \text{Im}\bar{\zeta} > 0.$$

With the representation

$$\frac{R_l(\eta)}{R_r(\eta)} = \prod_{n=0}^{\infty} \frac{\eta^2 - (\eta_n^l)^2}{\eta^2 - (\eta_n^r)^2},$$

it can be shown that

$$X^+(\bar{\zeta}) = \prod_{n=0}^{\infty} \frac{\gamma(\bar{\zeta}, \eta_n^l, \eta_n^r)}{\gamma(\bar{\zeta}, \eta_n^r, \eta_n^l)}, \quad (1.24)$$

where $\gamma(\eta, \eta_n^l, \eta_n^r) = \Gamma[1 - i(\eta_n^l - \eta)] \cdot \Gamma[-i(\eta_n^r + \eta)]$, $\Gamma(\dots)$ is the gamma-function [16], and $\eta_n^\alpha = \sqrt{\kappa^2 - (v_n^\alpha)^2}$, $\text{Im}\eta_n^\alpha \geq 0$, where v_n^α are the roots of the following dispersion equation for a regular waveguide with the impedance \bar{Z}_α of one of the waveguide walls:

$$v_n^\alpha \text{tg}(v_n^\alpha \delta) + i\bar{Z}_\alpha = 0; \quad \alpha = l \text{ or } r. \quad (1.25)$$

The expression for $X^-(\bar{\zeta})$ is evident from (1.23), (1.24).

The coefficient of problem (1.19) can be written now as

$$\bar{D}(\zeta) = \frac{\omega_1^+(\zeta)\omega_2^+(\zeta)}{\omega_1^-(\zeta)\omega_2^-(\zeta)},$$

whereas (1.19) takes the form

$$\frac{\omega^+(\zeta)}{\omega_1^+(\zeta)\omega_2^+(\zeta)} = \frac{\omega^-(\zeta)}{\omega_1^-(\zeta)\omega_2^-(\zeta)} + \frac{\bar{H}(\zeta)}{\omega_1^+(\zeta)\omega_2^+(\zeta)}; \quad -\infty < \zeta < \infty.$$

The solution of this problem on the discontinuity [7] is the Cauchy integral

$$\Psi^+(\zeta) \equiv \frac{\omega^+(\zeta)}{\omega_1^+(\zeta)\omega_2^+(\zeta)} = \frac{1}{2\pi i} \int_0^\infty \frac{H(\bar{\zeta}') \exp(-\pi\bar{\zeta}')}{\omega_1^+(\zeta')\omega_2^+(\zeta')(\zeta' - \zeta)} d\zeta';$$

$$\bar{\zeta} = \ln \zeta' / 2\pi, \quad \text{Im} \zeta > 0.$$

Hence,

$$\exp(\pi\bar{\zeta})\Psi^+[\exp(2\pi\bar{\zeta})] = \frac{1}{2i} \int_{-\infty}^\infty \frac{H(\bar{\zeta}') \exp(-\varphi\bar{\zeta}')}{X(\bar{\zeta}') \text{sh}[\pi(\bar{\zeta}' - \bar{\zeta})]} d\bar{\zeta}'; \quad \text{Im} \bar{\zeta} > 0, \quad (1.26)$$

where $X(\bar{\zeta}) = \omega_1(\exp(2\pi\bar{\zeta}))$ and

$$H(\bar{\zeta}) = \frac{-i(\bar{Z}_l - \bar{Z}_r)^2 \exp(\varphi\bar{\zeta}) \cos[v(\bar{\zeta})\delta]}{4\pi R_r(\bar{\zeta})} \int_{-\infty}^\infty \frac{\cos[v(\eta)\bar{z}_0] \exp(i\bar{x}_0\eta) d\eta}{R_l(\eta) \exp(\varphi\eta) \text{sh}[\pi(\bar{\zeta} - \eta)]}.$$

The pole at the point $\eta = \bar{\zeta}$ lies above the integration contour. Since according to (1.22) we have $\omega_1^+(\zeta) = \omega_1^-(\zeta)$ for $\zeta < 0$, therefore the functions $\omega_1^\pm(\zeta)$ represent a unified analytical function $\omega_1(\zeta)$. Hence in what follows, we will not use the superscripts ‘±’.

When calculating the function in (1.26), the following integral arises

$$U(\eta, \bar{\zeta}) = \int_{-\infty}^\infty \frac{\cos[v(\bar{\zeta}')\delta] d\bar{\zeta}'}{R_r(\bar{\zeta}') X(\bar{\zeta}') \text{sh}[\pi(\bar{\zeta}' - \eta)] \text{sh}[\pi(\bar{\zeta}' - \bar{\zeta})]},$$

in which the integration contour passes above the pole $\bar{\zeta}' = \eta$ and below the pole $\bar{\zeta}' = \bar{\zeta}$. Let us consider the auxiliary integral $\tilde{U}(\eta, \bar{\zeta})$ along the boundary of the band $0 < \text{Im} \bar{\zeta} < 1$. From the above we have

$$\tilde{U}(\eta, \bar{\zeta}) = \int \frac{d\bar{\zeta}'}{X(\bar{\zeta}') \text{sh}[\pi(\bar{\zeta}' - \eta)] \text{sh}[\pi(\bar{\zeta}' - \bar{\zeta})]}$$

$$= \int_{-\infty}^\infty \left[1 - \frac{X(\bar{\zeta}')}{X(\bar{\zeta}' + i)} \right] \frac{d\bar{\zeta}'}{X(\bar{\zeta}') \text{sh}[\pi(\bar{\zeta}' - \eta)] \text{sh}[\pi(\bar{\zeta}' - \bar{\zeta})]} = i(\bar{Z}_r - \bar{Z}_l) U(\eta, \bar{\zeta}).$$

Here we have used the equality $X(\bar{\zeta})R_r(\bar{\zeta}) = X(\bar{\zeta} + i)R_l(\bar{\zeta})$ following from (1.24). At the same time, the integral $\tilde{U}(\eta, \bar{\zeta})$ equals to a sum of residues at the points $\bar{\zeta}' = \eta + i$ and $\bar{\zeta}'' = \bar{\zeta}$, and hence

$$U(\eta, \bar{\zeta}) = \frac{2(\bar{Z}_r - \bar{Z}_l)^{-1}}{\text{sh}[\pi(\bar{\zeta} - \eta)]} \left[\frac{1}{X(\bar{\zeta})} - \frac{1}{X(\bar{\zeta} + i)} \right].$$

If we substitute this formula into (1.26) and take into consideration that the solution of the Carleman's boundary value problem (1.18) is

$$\tilde{\Phi}(\bar{\zeta}) = \exp(\pi\bar{\zeta})\Psi[\exp(2\pi\bar{\zeta})]X(\bar{\zeta})\exp(\varphi\bar{\zeta}); \quad 0 \leq \text{Im } \bar{\zeta} \leq 1,$$

we derive from (1.14), (1.17) the desired solution of the integral (1.15):

$$\begin{aligned} f(\bar{x}) &= \frac{i(\bar{Z}_l - \bar{Z}_r)}{4(2\pi)^{3/2}} \int_{-\infty}^{\infty} \frac{\exp(-i\bar{x}\eta')X(\eta')v(\eta')d\eta'}{\exp(-\varphi\eta')\exp[iv(\eta')\delta]R_l(\eta')} \\ &\times \int_{-\infty}^{\infty} \frac{\cos[v(\eta)\bar{z}_0]\exp(i\bar{x}_0\eta)d\eta}{R_l(\eta)\exp(\varphi\eta)X(\eta)\text{sh}[\pi(\eta - \eta')]} \end{aligned}$$

1.2.2.3 Residue Series Representation

Having regard to the equality $X(\eta)X(-\eta) = R_l(\eta)/R_r(\eta)$ following from (1.24), we obtain from (1.10), (1.12), and (1.14) that

$$\begin{aligned} G(g, g_0) &= \frac{(\bar{Z}_l - \bar{Z}_r)}{4\pi} \int_{-\infty - \alpha_1}^{\infty - \alpha_1} \frac{\cos[v(x_1)\bar{z}] \exp(i\bar{x}x_1) dx_1}{X(x_1)R_r(x_1)} \\ &\times \int_{-\infty}^{\infty} \frac{X(x_2) \cos[v(x_2)\bar{z}_0] \exp(-i\bar{x}_0x_2) \exp[\varphi(x_2 - x_1)] dx_2}{R_l(x_2) \text{sh}\pi[(x_2 - x_1)]}, \end{aligned} \quad (1.27)$$

where α_1 is a small positive value. In view of equalities (1.9), (1.10), we get the expression for the Green function $G^f(g, g_0)$.

Let us transform the integral representation of $G(g, g_0)$ in (1.27) into residue series. To do this, let us deform the integration surface $S = \{z_1, z_2 : z_j = x_j + iy_j, j = 1, 2, x_j \in \mathbb{R}^1, y_1 = -\alpha_1, y_2 = 0\}$ in the space $\mathbb{C} \times \mathbb{C}$ of two complex variables z_1

and z_2 into the Leray coboundary [18] enclosing the analytical set A of the singularities of the integrand. We rewrite (1.27) in the form

$$G(g, g_0) = \frac{1}{4\pi} (\bar{Z}_l - \bar{Z}_r) \int_S \omega, \tag{1.28}$$

where the differential form is given by

$$\begin{aligned} \omega &= f(z_1)q(z_2)h(z_2 - z_1) \exp(i\bar{x}z_1 - i\bar{x}_0z_2) dz_1 \wedge dz_2, \\ f(z_1) &= \frac{\cos[v(z_1)\bar{z}]}{R_r(z_1)X(z_1)}, \quad q(z_2) = \frac{X(z_2) \cos[v(z_2)\bar{z}_0]}{R_l(z_2)}, \\ h(z) &= \exp(\varphi z) / \text{sh}(\pi z). \end{aligned}$$

The set A comprises the following families of planes $z_1 = -\eta_{nk}^l, z_1 = \eta_{nk}^r, z_2 = \eta_{nk}^l, z_2 = -\eta_{nk}^r, z_2 - z_1 = \pm im, n, k, m = 0, 1, 2, \dots$, where $\eta_{nk}^\alpha = \eta_n^\alpha + ik$ and $\alpha = \{l \text{ or } r\}$. The behavior of the integrand in (1.28) at infinity is governed by the sign of $\text{Re}(i\bar{x}z_1 - i\bar{x}_0z_2) = -\bar{x}y_1 + \bar{x}_0y_2$. Consequently, let us introduce the following three-dimensional chains:

$$\begin{aligned} C_1^\pm &= \left\{ z_1, z_2 : x_{1,2} \in \mathbb{R}^1, \begin{pmatrix} y_1 > -\alpha_1 \\ y_1 < -\alpha_1 \end{pmatrix}, y_2 = 0 \right\}, \\ C_2^\pm &= \left\{ z_1, z_2 : x_{1,2} \in \mathbb{R}^1, y_1 = -\alpha_1, \begin{pmatrix} y_2 > 0 \\ y_2 < 0 \end{pmatrix} \right\}, \end{aligned}$$

for which the integration surface S is a common boundary. If one of four inequalities $\bar{x} > 0, \bar{x} < 0, \bar{x}_0 > 0$ or $\bar{x}_0 < 0$ is satisfied, then we can use the *Cauchy-Poincare theorem* [18] in C_1^+, C_1^-, C_2^- or C_2^+ , respectively, and deform S into the Leray coboundary enclosing the polar straight lines, along which the analytical planes A and the chains C_j^\pm intersect.

It suffices to restrict ourselves to the case of $\bar{x}_0 < 0$. In C_2^+ , the equations for polar straight lines are

$$\begin{aligned} P_{nk} &= \{z_1 = s, z_2 = \eta_{nk}^l\}, \quad Q_m = \{z_1 = s, z_2 = s + im\}; \\ &-\infty < s < \infty, \quad n, k = 0, 1, 2, \dots, \quad m = 1, 2, 3, \dots, \end{aligned}$$

whereas the equations for their coboundaries are as follows:

$$\begin{aligned} \delta P_{nk} &= \{z_1 = s, z_2 = \Delta \exp(i\theta) + \eta_{nk}^l\} \quad \text{and} \\ \delta Q_m &= \left\{ z_1 = \left(s - \sqrt{2}\Delta \cos \theta \right) / 2, z_2 = \left(s + \sqrt{2}\Delta \cos \theta \right) + i\Delta \sin \theta + im \right\}; \\ 0 < \Delta &\ll 1, \quad 0 \leq \theta \leq 2\pi. \end{aligned}$$

Therefore, the double integral in (1.28) can be represented as a sum of two single integrals

$$G(g, g_0) = \frac{1}{4\pi} (\bar{Z}_l - \bar{Z}_r) \left[\sum_{n,k=0}^{\infty} I_{nk} + \sum_{m=1}^{\infty} I_m \right],$$

where

$$I_{nk} = \lim_{\delta \rightarrow 0} \int_{\delta P_{nk}} \omega = 2\pi i (-1)^k \exp(ik\varphi - i\bar{x}_0 \eta_{nk}^l) \cos[v(\eta_{nk}^l) \bar{z}_0] \psi_{nk}^{-1} J_n^1(\bar{x}),$$

$$I_m = \lim_{\delta \rightarrow 0} \int_{\delta Q_m} \omega = 2i (-1)^m \exp(im\varphi + m\bar{x}_0) J_m^2(\bar{x} - \bar{x}_0)$$

with

$$\psi_{nk} = \frac{d[R_l(\eta)/X(\eta)]}{d\eta} \Big|_{\eta=\eta_{nk}^l}, \quad J_n^1(\bar{x}) = \int_{-\infty}^{\infty} f(\zeta) h(\eta_n^1 - \zeta) \exp(i\bar{x}\zeta) d\zeta,$$

$$J_m^2(\bar{x}) = \int_{-\infty}^{\infty} f(\zeta) q(\zeta + im) \exp[i(\bar{x} - \bar{x}_0)\zeta] d\zeta.$$

With allowance made for the asymptotics of $X(\zeta)$ for $|\zeta| \gg 1$ and the fact that $f(\zeta)$ and $q(\zeta)$ are meromorphic functions, the above integrals can be reduced to residue series. As a result, we obtain the following representation for the Green function of problem (1.7a, 1.7b, 1.7c) in the form of the expansion in a two-parameter family of inhomogeneous plane waves:

$$G^l(g, g_0) = \begin{cases} \sum_{n,k=0}^{\infty} g_{nk}^+(\bar{g}_0) \cos(v_{nk}^r \bar{z}) \exp(i\eta_{nk}^r \bar{x}); & \bar{x} > 0 \\ \sum_{n,k=0}^{\infty} g_{nk}^-(\bar{g}_0) \cos(v_{nk}^l \bar{z}) \exp(-i\eta_{nk}^l \bar{x}) \\ \quad + \sum_{n,k=0}^{\infty} q_{nk}^+(\bar{g}_0) \cos(v_{n,-k}^l \bar{z}) \exp(i\eta_{n,-k}^l \bar{x}); & \bar{x}_0 < \bar{x} < 0 \\ \sum_{n,k=0}^{\infty} g_{nk}^-(\bar{g}_0) \cos(v_{nk}^l \bar{z}) \exp(-i\eta_{nk}^l \bar{x}) \\ \quad + \sum_{n,k=0}^{\infty} q_{nk}^-(\bar{g}_0) \cos(v_{nk}^l \bar{z}) \exp(-i\eta_{nk}^l \bar{x}); & \bar{x} < \bar{x}_0. \end{cases}$$

Here,

$$g_{nk}^+(\bar{g}_0) = \pi(\bar{Z}_r - \bar{Z}_l)\varphi_{nk}^{-1} \sum_{p,q=0}^{\infty} \left\{ (-1)^{q-k} \psi_{pq}^{-1} \exp[i\varphi(q-k)] \frac{\exp\left[\varphi\left(\eta_p^l - \eta_n^r\right)\right]}{\text{sh}\left[\pi\left(\eta_p^l - \eta_n^r\right)\right]} \right. \\ \left. \times \cos\left(v_{pq}^l \bar{z}_0\right) \exp\left(-i\eta_{pq}^l \bar{x}_0\right) \right\}, \quad (1.29a)$$

$$g_{nk}^-(\bar{g}_0) = \pi(\bar{Z}_r - \bar{Z}_l)\psi_{nk}^{-1} \sum_{p,q=0}^{\infty} \left\{ (-1)^{q-k} \psi_{pq}^{-1} \exp[i\varphi(q+k)] \frac{\exp\left[\varphi\left(\eta_p^l + \eta_n^l\right)\right]}{\text{sh}\left[\pi\left(\eta_p^l + \eta_n^l\right)\right]} \right. \\ \left. \times \cos\left(v_{pq}^l \bar{z}_0\right) \exp\left(-i\eta_{pq}^l \bar{x}_0\right) \right\}, \quad (1.29b)$$

$$q_{nk}^+(\bar{g}_0) = (\bar{Z}_r - \bar{Z}_l) \left[R_r\left(\eta_{n,-k}^l\right) X\left(\eta_{n,-k}^l\right) \right]^{-1} \sum_{q=0}^{\infty} \left\{ (-1)^{q-k} \psi_{nq}^{-1} \exp[i\varphi(q+k)] \right. \\ \left. \times \cos\left(v_{nq}^l \bar{z}_0\right) \exp\left(-i\eta_{nq}^l \bar{x}_0\right) \right\}, \quad (1.29c)$$

$$q_{nk}^-(\bar{g}_0) = (\bar{Z}_r - \bar{Z}_l)\psi_{nk}^{-1} \sum_{q=0}^{\infty} \left\{ (-1)^{q-k} \left[R_r\left(\eta_{n,-q}^l\right) X\left(\eta_{n,-q}^l\right) \right]^{-1} \exp[i\varphi(q+k)] \right. \\ \left. \times \cos\left(v_{n,-q}^l \bar{z}_0\right) \exp\left(i\eta_{n,-q}^l \bar{x}_0\right) \right\} \quad (1.29d)$$

with $\varphi_{nk} = d[R_r(\eta)X(\eta)]/d\eta|_{\eta=\eta_{nk}^r}$.

Direct substitution of (1.29a, 1.29b, 1.29c, 1.29d) and (1.27) into (1.7a, 1.7b, 1.7c) assures that we have found the desired solutions.

1.2.2.4 Transformation of Eigenmodes on the Waveguide Junction

The Obtained Green Function Determines the Electromagnetic Field

$$H_y = i\omega\varepsilon\varepsilon_0 I^{(m)} G^t, \quad E_x = I^{(m)} \frac{\partial}{\partial z} H_y, \quad E_z = -I^{(m)} \frac{\partial}{\partial x} H_y,$$

generated by a linear magnetic current of density $\vec{J}^{(m)} = I^{(m)} \delta(g - g_0) \exp(-i\omega t) \vec{y}$ in a plane waveguide whose bottom wall is perfectly conducting, while the surface impedance distribution of the top wall is defined by (1.8).

If the source and the observation point are well off the irregular section of the impedance distribution $Z(x)$, $|x_0| > |x| \gg 1/\tau$, then the functions in (1.29a, 1.29b, 1.29c, 1.29d) become expansions in terms of eigenmodes of the regular waveguides:

$$H_n^\alpha(g) = a_n^\alpha \cos(v_n^\alpha \tau z) \exp(\pm i \eta_n^\alpha \tau x); \quad \alpha = l \text{ or } r, \quad n = 0, 1, 2, \dots \quad (1.30)$$

Here, the normalization $a_n^\alpha = i[R'_\alpha(\eta_n^\alpha) \cos(v_n^\alpha \tau d)]^{1/2}$ has been chosen such that the energy transported by each mode (1.30) does not depend on the indices n and α . Taking into account that the modes are orthogonal in these systems, we deduce that in the irregular segment the m -th mode of the left waveguide transforms into the n -th modes of the right and left regular waveguides with the transmission coefficient

$$T_{mn} = \left[-\pi \frac{R_r(\eta_m^l) R_l(\eta_n^r)}{R'_r(\eta_n^r) R'_l(\eta_m^l)} \right]^{1/2} \frac{X(\eta_m^l) \exp[(\eta_m^l - \eta_n^r) \varphi]}{X(\eta_n^r) \text{sh}[\pi(\eta_m^l - \eta_n^r)]}; \quad n, m = 0, 1, 2, \dots \quad (1.31)$$

and the reflection coefficient

$$R_{mn} = \left[\pi \frac{R_r(\eta_m^l) R_r(\eta_n^l)}{R'_l(\eta_n^l) R'_l(\eta_m^l)} \right]^{1/2} X(\eta_n^l) X(\eta_m^l) \frac{\exp[(\eta_m^l + \eta_n^r) \varphi]}{\text{sh}[\pi(\eta_m^l + \eta_n^r)]}; \quad n, m = 0, 1, 2, \dots, \quad (1.32)$$

where

$$\begin{aligned} R_\alpha(\eta_m^\beta) &= i(\bar{Z}_\alpha - \bar{Z}_\beta) \cos(v_m^\beta \tau d) \text{ for } \alpha \neq \beta, \\ R'_\alpha(\eta_n^\alpha) &= -\eta_n^\alpha \gamma_n^\alpha (v_n^\alpha)^{-2} \cos(v_n^\alpha \tau d), \quad \text{and} \quad \gamma_n^\alpha = \tau d \left[(v_n^\alpha)^2 - \bar{Z}_\alpha^2 \right] - i\bar{Z}_\alpha; \\ \alpha, \beta &= l \text{ or } r. \end{aligned}$$

It is not hard to prove the invariance of R_{mn} with respect to a permutation of subscripts and the invariance of T_{mn} with respect to a simultaneous permutation of subscripts and impedances $Z_l \leftrightarrow Z_r$, or, in other words, to prove the reciprocity theorem for the waveguide under study.

Let us estimate the error of *adiabatic approximation* with the use of (1.31). This approximate description of wave processes in slightly irregular waveguides with no regard for the mode interconversion [19] is named by analogy with the Born-Oppenheimer method in solid-state physics. Up to now, the error for this approach has not been estimated. For ease of estimation, let us restrict ourselves to the case of purely imaginary limiting values $Z_l = iQ_l$, and $Z_r = iQ_r$, which is the

same to the absence of absorption in the walls of the regular sections of the waveguide. Hodographs for the complex-valued surface impedance functions $Z(x, \varphi)$ ($-\pi < \varphi < 0$ for $Q_l < Q_r$ and $0 \leq \varphi < \pi$ for $Q_l > Q_r$) represent a family of circular arcs of radius $Q^- / \sin \varphi$ centered at $iQ^+ - Q^- \text{ctg} \varphi$, $2Q^\pm = Q_l \pm Q_r$ (for $\varphi = 0$ it is a straight line) and connecting the points iQ_l and iQ_r in the right half-plane of physically realizable impedances. In this case, the following equalities for the propagation constants are valid:

$$\text{Im } \eta_s^\alpha = 0 \text{ for } 0 \leq s \leq s^\alpha \quad \text{and} \quad \text{Re } \eta_s^\alpha = 0 \text{ for } s^\alpha < s, \tag{1.33}$$

where s^α is the maximum number of the mode (1.30) propagating in the α -regular waveguide without attenuation.

Since, by hypothesis, the waveguide properties vary slowly over the distance of a wavelength, then $|\eta_s^\alpha| = |h_s^\alpha \tau^{-1}| \gg 1$, where h_s^α is the longitudinal wavenumber of the s -mode and τ^{-1} is the characteristic dimension of the irregular section of $Z(x)$. Then, with the asymptotic Stirling formula for gamma functions, we obtain from (1.31)

$$T_{mn} \approx \frac{e_m^r(-\eta_m^l) e_n^l(-\eta_n^r) e_m^l(-\eta_m^l)}{e_m^r(\eta_m^l) e_n^l(\eta_n^r) e_n^r(-\eta_n^r)} \cdot \frac{\exp[\varphi(\eta_m^l - \eta_n^r)]}{2\text{sh}[\pi(\eta_m^l - \eta_n^r)]} \cdot \frac{\Pi_m(\eta_m^l)}{\Pi_n(\eta_n^r)}, \tag{1.34}$$

where $e_m^\alpha(\eta) = \exp\{-i(\eta_m^\alpha - \eta) \ln[-i(\eta_m^\alpha - \eta)]\}$, the principal branch of $\ln z$ with a cut joining the points $z = 0$ and $z = -\infty$ has been chosen, and

$$\Pi_m(\eta) = \prod_{\substack{s=0 \\ s \neq m}}^{\infty} \frac{e_s^l(\eta) e_s^r(-\eta)}{e_s^l(-\eta) e_s^r(\eta)}$$

In view of (1.33), we derive from (1.34) the following expression (with a finite number of multipliers) for absolute values of the transmission coefficients for the undumped mode $H_m^l(g)$, $0 \leq m \leq s^l$ incoming from the left waveguide and transformed into undumped modes $H_n^r(g)$, $0 \leq n \leq s^r$ of the right waveguide:

$$|T_{mn}| \approx \left\{ \prod_{s=m}^{n-1} \exp[\pi(\eta_{s+1}^l - \eta_s^r)] \text{ for } m < n, 1 \text{ for } m = n, \text{ and} \right. \\ \left. \exp[2\pi(\eta_m^l - \eta_n^r)] \prod_{s=n}^{m-1} \exp[\pi(\eta_s^r - \eta_{s+1}^l)] \text{ for } m > n \right\} \exp[\varphi(\eta_m^l - \eta_n^r)]; \tag{1.35}$$

$$Q_l < Q_r$$

and

$$|T_{mn}| \approx \left\{ \exp[2\pi(\eta_n^r - \eta_m^l)] \prod_{s=m}^{n-1} \exp[\pi(\eta_s^l - \eta_{s+1}^r)] \text{ for } m < n, 1 \text{ for } m = n, \text{ and} \right. \\ \left. \prod_{s=n}^{m-1} \exp[\pi(\eta_{s+1}^r - \eta_s^l)] \text{ for } m > n \right\} \exp[\varphi(\eta_m^l - \eta_n^r)]; \quad Q_l > Q_r. \quad (1.36)$$

In particular, in the case of two-mode operation ($s^l = s^r = 1$), as zero mode $H_0^l(g)$ runs against the inhomogeneity, we can write

$$|T_{01}| \approx \exp\{-[\pi(\eta_0^r - \eta_1^l) + |\varphi|(\eta_0^l - \eta_1^r)]\} < 1; \quad -\pi < \varphi \leq 0, \quad Q_l < Q_r \quad (1.37)$$

and

$$|T_{01}| \approx \exp[(\varphi - \pi)(\eta_0^l - \eta_1^r)] < 1; \quad 0 \leq \varphi < \pi, \quad Q_l > Q_r. \quad (1.38)$$

An interesting feature is exhibited when comparing the amplitudes of zero (principal) mode $H_0^r(g)$ and the first mode $H_1^l(g)$ travelling into the right waveguide:

$$\left| \frac{T_{01}}{T_{00}} \right| \approx \exp\{-[\pi(\eta_0^r - \eta_1^l) + |\varphi|(\eta_0^r - \eta_1^r)]\} < 1; \quad -\pi < \varphi \leq 0, \quad Q_l < Q_r \quad (1.39)$$

and

$$\left| \frac{T_{01}}{T_{00}} \right| \approx \exp\{-[\pi(\eta_0^l - \eta_1^r) - \varphi(\eta_0^r - \eta_1^r)]\}; \quad 0 \leq \varphi < \pi, \quad Q_l > Q_r. \quad (1.40)$$

In the latter case we have $|T_{01}/T_{00}| < 1$ with small φ , whereas for $\varphi \rightarrow \pi$ this value tends to $\exp[\pi(\eta_0^r - \eta_0^l)]$ and is greater than unity. That is, for $Q_l > Q_r$, starting with the hodograph $Z(x)$ of sufficiently large radius, the efficiency of transformation (when passing the irregular segment) of the zeroth mode into the first mode ($H_0^l \rightarrow H_1^l$) is greater than into the zeroth one ($H_0^l \rightarrow H_0^r$).

This effect is caused by the familiar phenomenon of the interconversion of two adjacent modes in the vicinity of the degeneracy regime. Among the wave structures with mode degeneracy is a regular impedance waveguide. It is known [20] that in such a waveguide, for each two adjacent modes H_j^z and H_{j+1}^z , the impedance value $Z_{j,j+1}^{\text{deg}}$ exists such that the solutions v_j^z and v_{j+1}^z of the dispersion equation in (1.25) coincide. The analysis of the behavior of these roots on the trajectories

passing around the point $Z_{j,j+1}^{\text{deg}}$ reveals [21] that the complete mode interconversion $H_j^z \leftrightarrow H_{j+1}^z$ occurs as a result of this bypass.

In the above case of the two-mode operation (1.40), as φ increases, the arc of the hodograph $Z(x)$ occupies increasingly more space in the right half-plane of physically realizable impedances, into which the point Z_{01}^{deg} falls starting with some value φ_0 . It is then that the transformation $H_0^l \rightarrow H_1^r$ becomes dominant, by virtue of the mode interconversion $H_0^z \leftrightarrow H_1^z$. These phenomena are of great interest for clarifying the effects of abnormal propagation of radio waves in the Earth-ionosphere waveguide along the paths intersecting the terminator [22]. It is interesting to note that in the case of $Q_l < Q_r$, the asymptotics in (1.39) do not show the effect at all, as well as in the case of a linear hodograph ($\varphi = 0$).

As obvious from the asymptotics in (1.35), (1.36), the adiabatic approximation error is defined by products of the exponentials $\exp\left(-\pi\left|\eta_i^\alpha - \eta_j^\beta\right|\right)$, where $\alpha, \beta = \{l \text{ or } r\}$, $i = 0, 1, \dots, s^\alpha$, $j = 0, 1, \dots, s^\beta$. If the arguments of these exponentials are of the order of unity, the adiabatic approximation is impossible. For example, for large positive Q_l and large negative Q_r , the value of $\eta_0^l - \eta_1^r$ is small and $|T_{01}|$ in (1.38) is of the order of unity as $\varphi \approx \pi$.

Finally note that rigorous error estimates are also lacking for the main theoretical approach used in the study of irregular waveguides with slowly varying parameters, namely, for the *cross-section method* [23] suggested by Stevenson [24]. The exact Green function derived in the present section provides such estimates as applied to the irregular impedance waveguides of fixed cross-section. In particular, it is seen from (1.29a, 1.29b, 1.29c, 1.29d) that for these structures the fields should be expanded in terms of two-parameter set of functions, whereas the cross-section method is based on the expansion in one-parameter set, namely, in the eigenfunctions of an auxiliary regular waveguide.

1.3 The Cycle Slipping Phenomenon and the Degeneracy of Waveguide Modes

1.3.1 Introduction

Electromagnetic wave propagation in the Earth-ionosphere waveguide has been studied intensively in the last five decades [25–28]. General formulation of the problems arising in the analysis of such waveguide processes is very complicated since it requires the inclusion of both the inhomogeneity of the Earth and the inhomogeneity and anisotropy of the ionosphere. In this section we restrict our analysis by the case of very low-frequency (VLF) waves, i.e. the electromagnetic oscillations whose frequency varies from 1.0 to 60 kHz. The main advantage of the waves of this range is their high stability against random variation of the

ionospheric parameters. In particular, the analysis of peculiarities of the wave processes inherent in this range is of importance in developing global navigation systems.

We will examine the diurnal variations of the VLF field occurring when the ‘transmitter-receiver’ path crosses the dividing ‘day-night’ line. The propagation conditions vary significantly along this path during 24 h period. The decrease of the electron density in the lower ionosphere at night increases the effective height of the Earth-ionosphere waveguide and changes the properties of the upper wall of the waveguide, which in the modeling are usually characterized by the surface impedance. As a consequence, there is a marked increase in the field amplitude at night; the phase of the received signal changes as well. The standard view of these relationships, which has become known as *the amplitude and phase of trapezoids*, is shown in [29], Fig. 1.1. It is well explained by the simple single-mode propagation model.

However, a significant distinction from the specified standard form of the amplitude and phase dependencies of VLF signals can be observed on long paths [29, 30]. This difference consists in that the initial and final phases of the signal differ by $\pm 2\pi m$ (as a rule, $m = 1$) in diurnal phase records. This kind of abnormal diurnal field dependency at the point of reception is called a *cycle slipping* (CS) phenomenon.

From Fig. 1.2, which shows typical abnormal diurnal field variations, we notice that the CS phenomenon corresponds to an extremely deep fading of the received signal. This phenomenon can be explained qualitatively by assuming [22] that not

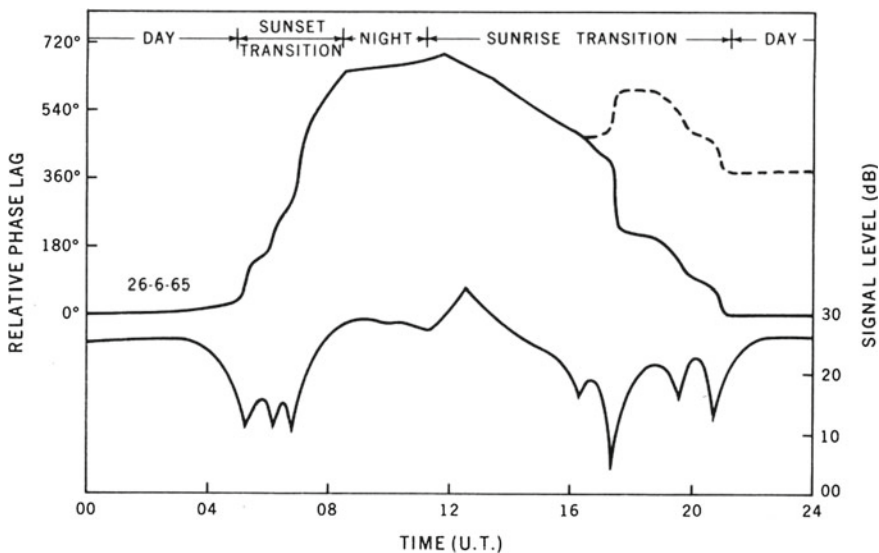


Fig. 1.2 (from paper [29]). Typical diurnal phase and signal level variations in NLK signals received at Smithfield (South Australia). Path length is equal to 13,420 km, $f = 18.6$ kHz. The broken line shows the phase record when cycle slipping occurs

only the principal (first) mode arrives at the observation point but also do the second mode and the higher-order modes resulting from the transformation of the principal mode on a waveguide discontinuity at the intersection of the path and the terminator (i.e. the sunrise or sunset line).

It is not difficult to see [27] that to observe the cycle slipping phenomenon, first of all, the field of the second mode should be greater at some moment of time than the field of the fundamental mode. Indeed, let at the point of reception two oscillations with the complex amplitudes $r_1 \exp(i\varphi_1)$ and $r_2 \exp(i\varphi_2)$ be added up. In order for the diurnal variation in the argument of the amplitude of the total signal $r_1 \exp(i\varphi_1)[1 + (r_2/r_1) \exp(i(\varphi_2 - \varphi_1))]$ be equal to 2π , the variation in the argument of the second factor must be 2π as well. (The phase variation of the first factor is zero, because during 24 h period it makes a symmetric trapezoidal oscillation.) Consequently, it is necessary that the ratio r_2/r_1 is greater than unity, at least, when $\varphi_2 - \varphi_1 = \pi$. It is just the fact that the ratio should be greater than unity, when the first and the second modes are in antiphase, which leads to that the cycle slipping phenomenon is usually accompanied by an abnormally deep minimum of the amplitude (Fig. 1.2). The most important here is the requirement of the large coefficient of conversion of the fundamental mode into the second mode.

A number of different modifications of irregular waveguides have been investigated by employing numerical simulation of the CS phenomenon. For example, the coefficient of conversion from the first into the second mode has been calculated by the method of partial domains for a number of two-dimensional impedance waveguides without considering the reflection from the discontinuity [30, 31]. Even for a stepwise change in the waveguide height, it did not exceed 0.5. In [32], to estimate this coefficient, the authors invoked the method of cross sections [23] developed for waveguide structures with slowly varying parameters over a wavelength distance. A two-dimensional model was used to represent a coaxial waveguide whose cross section and the surface impedance Z of one wall vary in azimuth. The coefficient of conversion reached 1.2, which, as the authors noted, was also too small to explain the CS phenomenon occurring mostly away from the terminator. The approach developed in [31] was extended in a number of papers to the waveguides whose top wall is a flat-layered anisotropic medium [33].

Only in one study [34], in contrast to all the above mentioned papers, the authors provide different *qualitative explanation* for this phenomenon in terms of the crude adiabatic approximation, by linking it with the degeneracy of the fundamental modes.

These investigations have cast doubt on the statement that the CS phenomenon can be explained solely by the conversion of the fundamental mode into the higher-order modes in the waveguide of variable cross section. In regular waveguides with walls of finite conductivity, which is constant along the structure, a more efficient mode-interconversion mechanism takes place. It is well known [35] that there exist values of the normalized surface impedance of the walls $\eta_{i,i+1}^{\text{deg}}$ such that the propagation constants v_i and v_{i+1} of two adjacent (i and $i+1$) waveguide modes coincide. Here $\eta = Z/\eta_0$, where $\eta_0 = \sqrt{\mu_0/\epsilon_0}$ is the wave resistance of

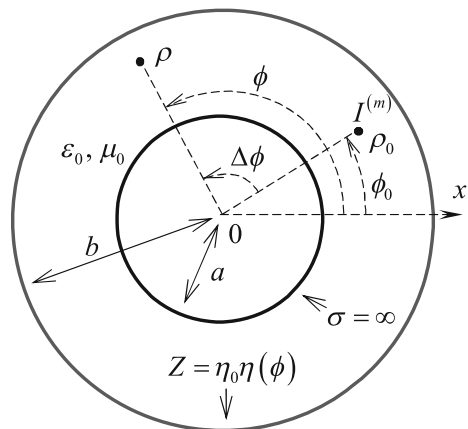
vacuum. These modes and the associated impedance values are said to be degenerate. *Mode interconversion* occurs in the neighborhood of the degeneracy regime [21]. For example, by varying the complex-valued impedance $\eta(z)$ of the wall of a regular waveguide such that it draws a closed curve around the degeneracy point $\eta_{i,i+1}^{\text{deg}}$, we get a complete interconversion of the i and $i + 1$ modes. In particular, the degeneracy of two VLF modes in a natural waveguide has been discussed in [36].

Our purpose is to clear up the role of the mode interconversion taking place in the neighborhood of the degeneracy regime in the occurrence of CS [37]. In Sect. 1.3.2, we present a model of the irregular waveguide with a constant cross section and the impedance varying in azimuth, which is a simplified version of the model given in [32]. This model allows us to exclude from consideration the diffraction effect of wave transformation on spatial inhomogeneities of the waveguide walls and to obtain the analytical solution of the associated boundary value problem for some class of surface impedance distributions. In the next section, with the help of the well-known *Watson method*, the solution will be transformed into a rapidly converging series for large wave sizes of the model. In Sect. 1.3.4 we present results of a numerical experiment.

1.3.2 Problem Formulation and Solution

Consider in the cylindrical coordinates ρ, ϕ, z a coaxial waveguide whose inner wall, $\rho = a$, is perfectly conducting and the outer wall, $\rho = b$, has variable surface impedance (Fig. 1.3). A filament of linear magnetic current with the time dependence $\exp(-i\omega t)$ disposed at $g_0 = \{\rho_0, \phi_0\}$ such that it is parallel to the z -axis, generates a field $\vec{E} = i\omega\mu_0\{\partial U/\rho\partial\phi, -\partial U/\partial\rho, 0\}$, $\vec{H} = k^2\{0, 0, U\}$. The Hertz potential U is a solution of the equation

Fig. 1.3 The waveguide cross-section geometry



$$\left[\frac{1}{\rho} \frac{\partial}{\partial \rho} \rho \frac{\partial}{\partial \rho} + \frac{1}{\rho^2} \frac{\partial^2}{\partial \phi^2} + k^2 \right] U(g, g_0) = -\frac{iI^{(m)}}{\omega \mu_0 \rho} \delta(g - g_0); \tag{1.41}$$

$$a < \rho, \rho_0 < b, \quad -\pi \leq \phi, \phi_0 \leq \pi$$

with the boundary conditions

$$\left. \frac{\partial U}{\partial \rho} \right|_{\rho=a} = 0, \quad \left. \left[\frac{\partial U}{\partial \rho} - ik\eta(\phi)U \right] \right|_{\rho=b} = 0, \tag{1.42}$$

where $k = \omega \sqrt{\epsilon_0 \mu_0}$ is the wavenumber and $I^{(m)}$ is the linear magnetic current density.

Let the normalized surface impedance of the wall $\rho = b$ be given in the form

$$\eta(\phi) = \eta_3 \frac{e^{i\phi} + \eta_1}{e^{i\phi} + \eta_2} \tag{1.43}$$

with the arbitrary complex parameters $\eta_j, j = 1, 2, 3$. Then the values of the function $\eta(\phi)$ form in the plane of the complex variable η a circle (the hodograph curve) of radius $r_{\text{imp}} = |\eta_3(\eta_1 - \eta_2)| / |1 - |\eta_2|^2|$ centered at the point $\eta_{\text{imp}} = \eta_3(1 - \eta_1\eta_2^*) / (1 - |\eta_2|^2)$.

In order to find the function U , we will use the Green formula

$$U(g, g_0) = U_0(g, g_0) + \int_S \left[U(g_1, g_0) \frac{\partial}{\partial \vec{n}} G(g_1, g) - \frac{\partial}{\partial \vec{n}} U(g_1, g_0) G(g_1, g) \right] ds_1, \tag{1.44}$$

where \vec{n} is the outer normal to the boundary S of the ring domain $\{a < \rho_1 < b, -\pi < \phi_1 < \pi\}$. By choosing as the function $G(g_1, g)$ the Green function of the space containing a perfectly conducting cylinder of radius a

$$G(g_1, g) = -\frac{i}{8} \sum_{n=-\infty}^{\infty} \exp[in(\phi_1 - \phi)] H_n^{(1,0)}(ka, k\rho_{<}) \frac{H_n^{(1)}(k\rho_{>})}{H_n^{(1)'}(ka)} = G(\rho_1, \rho, \phi_1 - \phi) \tag{1.45}$$

and as the function $U_0(g, g_0)$ the Hertz potential of the field generated by a linear magnetic current in the presence of the conducting cylinder $\rho = a$

$$U_0(g, g_0) = -\frac{iI^{(m)}}{k} G(\rho_0, \rho, \phi_0 - \phi) = U_0(\rho_0, \rho, \phi_0 - \phi), \tag{1.46}$$

we satisfy (1.41) and the first of the boundary conditions (1.42). In (1.45), the following notation is used:

$$H_n^{(j_1, j_2)}(x_1, x_2) = \frac{\partial^{j_1}}{\partial x_1^{j_1}} \frac{\partial^{j_2}}{\partial x_2^{j_2}} \left[H_n^{(1)}(x_1) H_n^{(2)}(x_2) - H_n^{(2)}(x_1) H_n^{(1)}(x_2) \right]; \quad j_1, j_2 = 0, 1,$$

$H_n^{(j)}(\dots)$ stands for the Hankel functions, $\rho_< = \min(\rho, \rho_1)$, $\rho_> = \max(\rho, \rho_1)$.

In order to satisfy the remained boundary condition from (1.42), one can make in (1.44) the passage $\rho \rightarrow b$ and then substitute the value of $\partial U / \partial \rho$ on the boundary $\rho = b$. Then the equality (1.44) turns into an integral equation of the second kind with a strong kernel singularity [38]. To avoid this, let us consider formula (1.44) on the circle $\rho = b - \Delta$, where Δ is a small positive value. Then we have:

$$\begin{aligned} U(b - \Delta, \rho_0, \phi, \phi_0) &= U_0(\rho_0, b - \Delta, \phi_0 - \phi) \\ &+ b \int_{-\pi}^{\pi} \left[\frac{\partial}{\partial \rho} G(\rho, b - \Delta, \bar{\phi} - \phi) \right]_{\rho=b}^{-ik\eta(\bar{\phi})} G(b, b - \Delta, \bar{\phi} - \phi) U(b, \rho_0, \bar{\phi}, \phi_0) d\bar{\phi}. \end{aligned} \quad (1.47)$$

Let us denote the direct and inverse Fourier transform operators as

$$\begin{aligned} W_\phi[a_n] &= A(\phi) = \sum_{n=-\infty}^{\infty} a_n \exp(in\phi), \\ W_n^{-1}[A(\phi)] &= a_n = \frac{1}{2\pi} \int_{-\pi}^{\pi} A(\phi) \exp(-in\phi) d\phi. \end{aligned}$$

For the inverse Fourier transform the following relationships are valid:

$$W_n^{-1} \left[\frac{1}{2\pi} \int_{-\pi}^{\pi} A(\bar{\phi} - \phi) B(\phi) d\phi \right] = a_{-n} b_n, \quad W_n^{-1}[\exp(ip\phi) A(\phi)] = a_{n-p}. \quad (1.48)$$

Applying the operator W_n^{-1} to (1.47), we obtain in view of (1.48):

$$\begin{aligned} W_{n-1}^{-1} \left[\frac{U(b - \Delta, \rho_0, \phi, \phi_0)}{\exp(i\phi) + \eta_2} \right] + \eta_2 W_{n-1}^{-1} \left[\frac{U(b - \Delta, \rho_0, \phi, \phi_0)}{\exp(i\phi) + \eta_2} \right] &= W_{n-1}^{-1}[U_0(\rho_0, b - \Delta, \phi_0 - \phi)] \\ + 2\pi b W_{n-1}^{-1} \left[\frac{\partial G(\rho, b - \Delta, \phi)}{\partial \rho} \right]_{\rho=b} &\left\{ W_{n-1}^{-1} \left[\frac{U(b, \rho_0, \phi, \phi_0)}{\exp(i\phi) + \eta_2} \right] + \eta_2 W_{n-1}^{-1} \left[\frac{U(b, \rho_0, \phi, \phi_0)}{\exp(i\phi) + \eta_2} \right] \right\} \\ - 2\pi b i k \eta_3 W_{n-1}^{-1}[G(b, b - \Delta, \phi)] &\left\{ W_{n-1}^{-1} \left[\frac{U(b, \rho_0, \phi, \phi_0)}{\exp(i\phi) + \eta_2} \right] + \eta_1 W_{n-1}^{-1} \left[\frac{U(b, \rho_0, \phi, \phi_0)}{\exp(i\phi) + \eta_2} \right] \right\}, \end{aligned} \quad (1.49)$$

where

$$\begin{aligned}
 W_n^{-1}[U_0(\rho_0, b - \Delta, \phi_0 - \phi)] &= -\frac{I^{(m)}}{8k} \exp(-in\phi_0) \frac{H_n^{(1,0)}(x, k\rho_0)}{H_n^{(1)'}(x)} H_n^{(1)}[k(b - \Delta)], \\
 W_n^{-1}[G(b, b - \Delta, \phi)] &= -\frac{i}{8} \frac{H_n^{(1,0)}(x, k(b - \Delta))}{H_n^{(1)'}(x)} H_n^{(1)}(y), \\
 W_n^{-1}\left[\frac{\partial G(\rho, b - \Delta, \phi)}{\partial \rho}\right]_{\rho=b} &= -\frac{ik}{8} \frac{H_n^{(1,0)}(x, k(b - \Delta))}{H_n^{(1)'}(x)} H_n^{(1)'}(y); \quad -\infty < n < \infty,
 \end{aligned}$$

and $H_n^{(j)'}(x) = dH_n^{(j)}(x)/dx$. One can pass to the limit $\Delta \rightarrow 0$ in these relationships. Considering that $H_{-n}^{(j)}(x) = (-1)^n H_n^{(j)}(x)$, we obtain the following finite-difference equation [7]

$$u_n = -\eta_2^{-1}(1 + s_n)u_{n-1} + g_n; \quad -\infty < n < \infty. \tag{1.50}$$

Here

$$(1 + s_n) = \frac{H_{n,1}^{(1,1)(1,0)}(x, y)}{H_{n,\delta}^{(1,1)(1,0)}(x, y)}, \quad g_n = -\frac{I^{(m)} \exp(-in\phi_0)}{2\pi i k y \eta_2} \frac{H_n^{(1,0)}(x, k\rho_0)}{H_{n,\delta}^{(1,1)(1,0)}(x, y)} \tag{1.51}$$

and $H_{n,\delta}^{(1,1)(1,0)}(x, y) = H_n^{(1,1)}(x, y) - in_3 \delta H_n^{(1,0)}(x, y)$, $H_{n,1}^{(1,1)(1,0)}(x, y) = H_{n,\delta}^{(1,1)(1,0)}(x, y)|_{\delta=1}$, $u_n = W_n^{-1}[U(b, \rho_0, \phi, \phi_0)/[\exp(i\phi) + \eta_2]]$, $s_{-n} = s_n$, $x = ka$, $y = kb$, $\delta = \eta_1/\eta_2$.

Let us apply the *factorization method* [7] to solve (1.50). Represent the multiplier in (1.50) in the following form:

$$(1 + s_n) = \frac{x_n}{x_{n-1}^\gamma}, \tag{1.52}$$

where the exponent $\gamma > 1$ is an auxiliary parameter. Taking the logarithm of (1.52) and then applying the operators W and W^{-1} , we can easily show that

$$\ln x_n = W_n^{-1}[W_\theta[\ln(1 + s_n)]]/[1 - \gamma \exp(i\theta)] = -\gamma^n \sum_{m=n+1}^\infty \ln(1 + s_m) \gamma^{-m}. \tag{1.53}$$

Estimate the convergence of this series. Using the known asymptotics

$$J_\nu(z) \approx (2\pi\nu)^{-1/2} \left(\frac{eZ}{2\nu}\right)^\nu, \quad H_\nu^{(1)}(z) \approx -2i(2\pi\nu)^{-1/2} \left(\frac{eZ}{2\nu}\right)^{-\nu}, \tag{1.54}$$

for fixed z and $|v| \gg 1$, $|\arg v| < \pi/2$, one can show that $\ln(1+s_n) = i\eta_3(\delta-1)yn^{-1} + O(n^{-2})$. In other words, the convergence of the series in (1.53) is too weak to pass to the limit $\gamma \rightarrow 1$ under the sum sign. The elements of the factorization sequence x_n are defined up to an arbitrary factor without violating the equality (1.52). This allows us to solve the problem of convergence of the series in (1.53). Let us take the logarithm of the right-hand side of (1.52) and rearrange it in the following way:

$$\begin{aligned} \ln x_n - \gamma \ln x_{n-1} &= -\gamma^n \sum_{m=n+1}^{\infty} \gamma^{-m} \ln(1+s_m) + \gamma^n \sum_{m=n}^{\infty} \gamma^{-m} \ln(1+s_m) \\ &\quad + \gamma^n \sum_{m=0}^{\infty} \gamma^{-m} \ln(1+s_m) - \gamma^n \sum_{m=0}^{\infty} \gamma^{-m} \ln(1+s_m) \\ &= \gamma^n \sum_{m=0}^n \gamma^{-m} \ln(1+s_m) - \gamma^n \sum_{m=0}^{n-1} \gamma^{-m} \ln(1+s_m); \quad n \geq 1, \\ \ln x_0 - \gamma \ln x_{-1} &= -\sum_{m=1}^{\infty} \gamma^{-m} \ln(1+s_m) + \sum_{m=0}^{\infty} \gamma^{-m} \ln(1+s_m) \\ &\quad + \sum_{m=0}^{\infty} \gamma^{-m} \ln(1+s_m) - \sum_{m=0}^{\infty} \gamma^{-m} \ln(1+s_m) = \ln(1+s_0) - 0; \quad n = 0, \\ \ln x_{-1} - \gamma \ln x_{-2} &= -\gamma^{-1} \sum_{m=0}^{\infty} \gamma^{-m} \ln(1+s_m) + \gamma^{-1} \sum_{m=-1}^{\infty} \gamma^{-m} \ln(1+s_m) \\ &\quad + \gamma^{-1} \sum_{m=0}^{\infty} \gamma^{-m} \ln(1+s_m) - \gamma^{-1} \sum_{m=0}^{\infty} \gamma^{-m} \ln(1+s_m) = 0 - \ln(1+s_{-1})^{-1}; \quad n = -1, \end{aligned}$$

and

$$\ln x_n - \gamma \ln x_{n-1} = -\gamma^n \sum_{m=-1}^{n+1} \gamma^{-m} \ln(1+s_m) + \gamma^n \sum_{m=-1}^n \gamma^{-m} \ln(1+s_m); \quad n \leq -2.$$

So we can pass to the limit $\gamma \rightarrow 1$ and get

$$x_n = \left\{ \prod_{m=0}^n (1+s_m) \text{ for } n \geq 0; 1 \text{ for } n = -1; \prod_{m=-1}^{n+1} (1+s_m)^{-1} \text{ for } n \leq -2 \right\}. \quad (1.55)$$

It is easy to verify that this sequence satisfies (1.52) with $\gamma = 1$. By substituting (1.52) with $\gamma = 1$ into (1.50), we arrive at the equation

$$\frac{u_n}{x_n} = -\eta_2^{-1} \frac{u_{n-1}}{x_{n-1}} + \frac{g_n}{x_n}; \quad -\infty < n < \infty.$$

The solution of this equation is similar to that of the equation for $\ln x_n$, which can be derived by taking the logarithm of (1.52), and is as follows

$$\frac{u_n}{x_n} = W_n^{-1} \left[\frac{W_\theta(g_n/x_n)}{1 + \eta_2^{-1} \exp(i\theta)} \right] = \frac{1}{2\pi} \int_{-\pi}^{\pi} \sum_{m=-\infty}^{\infty} \frac{g_m \exp[i(m-n)\theta]}{x_m 1 + \eta_2^{-1} \exp(i\theta)} d\theta. \quad (1.56)$$

The integrand here has no singularities on the path of integration as far as its denominator coincides with the denominator of the function $\eta(\phi)$, while the surface impedance distribution of the waveguide is naturally assumed to be a limited function. Equations (1.44)–(1.46), (1.51), (1.55), and (1.56) allows us to obtain a closed expression for the Hertz potential U . One should distinguish two cases: $|\eta_2| < 1$ and $|\eta_2| > 1$. Let us do the relevant calculations for the first case.

The calculation of the integral in (1.56), by substituting $\exp(i\theta) = z$, is reduced to the calculation of residues at the points $z = 0$ and $z = -\eta_2$. As a result we have

$$\frac{u_n}{x_n} = - \sum_{m=n+1}^{\infty} \frac{g_m}{x_m} (-\eta_2)^{m-n}.$$

Then we find the Hertz potential distribution on the impedance wall $\rho = b$:

$$\begin{aligned} U(b, \rho_0, \phi, \phi_0) &= [\exp(i\phi) + \eta_2] W_\phi[u_n] \\ &= -[\exp(i\phi) + \eta_2] \sum_{n=-\infty}^{\infty} x_n \sum_{m=n+1}^{\infty} \frac{g_m}{x_m} (-\eta_2)^{m-n} \exp(in\phi). \end{aligned}$$

The potential inside the waveguide, as follows from (1.44), is

$$U(\rho, \rho_0, \phi, \phi_0) = U_0(\rho_0, \rho, \phi_0 - \phi) + b \int_{-\pi}^{\pi} H(\phi_1, \phi) U(b, \rho_0, \phi_1, \phi_0) d\phi_1, \quad (1.57)$$

where

$$H(\phi_1, \phi) = -\frac{ik}{8} \sum_{l=-\infty}^{\infty} \exp[iil(\phi_1 - \phi)] H_l^{(1,0)}(x, k\rho) \left[H_l^{(1)'}(y) - i\eta(\phi) H_l^{(1)}(y) \right] / H_l^{(1)'}(x).$$

The integration in (1.57) results in the following expression for the potential

$$U(g, g_0) = -\frac{I^{(m)}}{8k} [U_0(g, g_0) + U_1(g, g_0)], \quad (1.58)$$

where (see formulas (1.45), (1.46))

$$U_0(g, g_0) = \sum_{n=-\infty}^{\infty} \exp[in(\phi_0 - \phi)] H_n^{(1,0)}(x, k\rho_{<}) H_n^{(1)}(k\rho_{>}) / H_n^{(1)'}(x)$$

and

$$U_1(g, g_0) = - \sum_{n=-\infty}^{\infty} \exp(in\phi) \sum_{m=n+1}^{\infty} \frac{x_n H_m^{(1,0)}(x, k\rho_0)}{x_m H_{m,\delta}^{(1,1)(1,0)}(x, y)} \exp(-im\phi_0) (-\eta_2)^{m-n-1}, \\ \times \left[\eta_2 \frac{H_n^{(1,0)}(x, k\rho)}{H_n^{(1)'}(x)} H_n^\delta(y) + \exp(i\phi) \frac{H_{n+1}^{(1,0)}(x, k\rho)}{H_{n+1}^{(1)'}(x)} H_{n+1}^1(y) \right],$$

$H_n^\delta(y) = H_n^{(1)'}(y) - i\eta_3 \delta H_n^{(1)}(y)$, $H_n^1(y) = H_n^\delta(y)|_{\delta=1}$, $\rho_{<} = \min(\rho_0, \rho)$, $\rho_{>} = \max(\rho_0, \rho)$, and x_n is given by (1.55).

In a similar way, transformations are made for $|\eta_2| > 1$. It would be convenient to separate the regular and irregular parts of the potential in (1.58). After lengthy transformations, we arrive at the following expression for the Hertz potential

$$U(g, g_0) = \frac{I^{(m)}}{8k} [U_{reg}(g, g_0) + U_{ireg}(g, g_0)], \quad (1.59)$$

where its regular part with the simple angular dependence in the form of $\phi - \phi_0$ is

$$U_{reg}(g, g_0) = \sum_{n=-\infty}^{\infty} \exp[in(\phi - \phi_0)] \frac{H_n^{(1,0)}(x, k\rho_{<})}{H_{n,\alpha}^{(1,1)(1,0)}(x, y)} H_{n,\alpha}^{(1,0)(0,0)}(y, k\rho_{>}), \quad (1.60)$$

$$\alpha = \{1 \text{ if } |\eta_2| < 1, \delta \text{ if } |\eta_2| > 1\}, \quad \rho_{<} = \min(\rho_0, \rho_1), \quad \rho_{>} = \max(\rho_0, \rho_1),$$

while its irregular part is

$$U_{ireg}(g, g_0) = -4 \frac{\eta_3(1 - \delta)}{\pi y} \sum_{n=-\infty}^{\infty} \exp[in(\phi - \phi_0)] \frac{H_n^{(1,0)}(x, k\rho)}{H_{n,1}^{(1,1)(1,0)}(x, y)} U_n(g_0), \quad (1.61)$$

$$U_n(g_0) = \sum_{m=1}^{\infty} \exp(-im\phi_0) (-\eta_2)^m \prod_{j=1}^m \frac{H_{n+j,\delta}^{(1,1)(1,0)}(x, y)}{H_{n+j,1}^{(1,1)(1,0)}(x, y)} \frac{H_{n+m}^{(1,0)}(x, k\rho_0)}{H_{n+m,\delta}^{(1,1)(1,0)}(x, y)}; \quad |\eta_2| < 1, \quad (1.62)$$

$$U_n(g_0) = - \sum_{m=1}^{\infty} \exp(im\phi_0) (-\eta_2)^{-m} \prod_{j=0}^{m-1} \frac{H_{n-j,1}^{(1,1)(1,0)}(x, y)}{H_{n-j,\delta}^{(1,1)(1,0)}(x, y)} \frac{H_{n-m}^{(1,0)}(x, k\rho_0)}{H_{n-m,\delta}^{(1,1)(1,0)}(x, y)}; \quad |\eta_2| > 1. \quad (1.63)$$

The first term in (1.59) coincides with the solution to the problem where the source excites the regular coaxial waveguide whose reduced surface impedance of the wall $\rho = b$ equals $\eta_3\alpha$.

It is easy to show the uniform convergence of the series, which determines the second term in (1.59), within the interval $a \leq \rho, \rho_0 \leq b$. Hence in this region the function $U_{\text{ireg}}(g, g_0)$ is analytic and satisfies the homogeneous Helmholtz equation.

Following the methodology in [39], one can make certain that the function $U(g, g_0)$ in (1.59) is really the desired Green function of the Helmholtz (1.41) in the ring region with irregular boundary conditions (1.42).

1.3.3 The Watson Transformation

The series in n in (1.60), (1.61) represent expansions in terms of radially propagating waves. Since the number of the terms contributing significantly to the field are of the order of $O(ka)$ [20, 40], (1.59) is convenient for analysis only for $ka \ll 1$.

For the applications considered in the present section, the range of interest is $ka \gg 1$, where the expansions in terms of azimuthally propagating ‘creeping’ waves (alternative to the series in (1.60), (1.61)), obtainable from (1.59) by using the so called *Watson transformation* [20, 39, 41], are rapidly convergent.

The method leading to the Watson transformation was proposed in the early twentieth century in the works of H. Poincare and J.W. Nicholson and was first used in the electromagnetic theory by G.N. Watson [42]. This mathematical apparatus is also used in quantum mechanics, in the theory of potential scattering [42].

As applied to series like in (1.60), (1.61), the initial statement of this method is as follows: if the function of complex variable $B(v)$ is analytic in the neighborhood of the real axis, then the equality is valid

$$\sum_{n=-\infty}^{\infty} \exp(in\phi)B(n) = \frac{i}{2} \int_C \frac{\exp[iv(\phi - \pi)]}{\sin \pi v} B(v)dv, \tag{1.64}$$

, where C is the contour formed by two straight lines $\text{Im}v = \pm\alpha, \alpha \ll 1$ and bypassing the real axis in a clockwise direction. Let us first consider the regular part of the field:

$$U_{\text{reg}}(g, g_0) = \sum_{n=-\infty}^{\infty} \exp(in\Delta\phi)B_{\text{reg}}(n), \tag{1.65}$$

$$B_{\text{reg}}(n) = \frac{H_n^{(1,0)}(x, k\rho_{<})}{H_{n,\alpha}^{(1,1)(1,0)}(x, y)} H_{n,\alpha}^{(1,0)(0,0)}(y, k\rho_{>}), \quad \Delta\phi = \phi - \phi_0 > 0. \tag{1.66}$$

If the analytical properties of the function $B_{\text{reg}}(v)$ allow the contour of integration C to be deformed to infinity, then the integral in (1.64) can be represented as a series of residues at the poles $B_{\text{reg}}(v)$. This series is just the Watson transform of the initial series.

Consider the function $B_{\text{reg}}(v)$. Since for the Hankel functions with complex index the following relationships are valid: $H_{-v}^{(1)}(z) = \exp(i\pi v)H_v^{(1)}(z)$, $H_{-v}^{(2)}(z) = \exp(-i\pi v)H_v^{(2)}(z)$, then we have $B_{\text{reg}}(-v) = B_{\text{reg}}(v)$; hence it is sufficient to clear up the properties of this function in the half-plane $\text{Re} v > 0$. Using the asymptotics (1.54) we find:

$$B_{\text{reg}}(v) \approx \frac{2i}{\pi v} \left(\frac{\rho_{<}}{\rho_{>}} \right)^v \quad \text{for } |v| \gg 1, \quad |\arg v| < \pi/2.$$

Hence, the integral in (1.64) is reduced to a sum of the residues at the poles v_s obtainable from the formula

$$\begin{aligned} H_{v,\alpha}^{(1,1)(1,0)}(x,y) &\equiv \left[H_v^{(1)'}(x)H_v^{(2)'}(y) - H_v^{(2)'}(x)H_v^{(1)'}(y) \right] \\ &\quad - i\eta_3\alpha \left[H_v^{(1)'}(x)H_v^{(2)}(y) - H_v^{(2)'}(x)H_v^{(1)}(y) \right] = 0; \quad 0 < x < y. \end{aligned} \quad (1.67)$$

Let us determine the location of zeros of this equation in the v -plane. Following the paper [43], on the assumption that x and y are fixed and $|v| \gg 1 + y^2$, we obtain the following approximation:

$$v_{\pm 1} \approx \pm \sqrt{i\eta_3\alpha y / \ln(y/x)}, \quad v_s \approx \frac{\eta_3\alpha y}{\pi(s-1)} + \frac{i\pi(s-1)}{\ln(y/x)} \quad \text{for } s = 2, 3, \dots$$

and

$$v_s \approx \frac{\eta_3\alpha y}{\pi(s+1)} + \frac{i\pi(s+1)}{\ln(y/x)} \quad \text{for } s = -2, -3, \dots$$

Thus the roots of (1.67) are located symmetrically in the first ($s = 1, 2, 3, \dots$) and the third ($s = -1, -2, -3, \dots$) quadrants of the v -plane.

By finding the residues at these points, we arrive at the representation

$$U_{\text{reg}}(g, g_0) = -2\pi \sum_{s=1}^{\infty} \frac{\cos[v_s(\pi - \Delta\phi)]H_{v_s}^{(1,0)}(x, k\rho_{<})}{\sin(\pi v_s)\tilde{H}_{v_s,\alpha}^{(1,1)(1,0)}(x,y)} H_{v_s,\alpha}^{(1,0)(0,0)}(y, k\rho_{>}), \quad (1.68)$$

where the following notation is used: $\tilde{H}_{v_s,\alpha}^{(1,1)(1,0)}(x,y) = \partial H_{v_s,\alpha}^{(1,1)(1,0)}(x,y) / \partial v \Big|_{v=v_s}$.

For the irregular part of the field, the manipulations are similar though more cumbersome:

$$U_{\text{ireg}}(g, g_0) = \frac{4\eta_3(1 - \delta)}{\pi kb} \sum_{n=-\infty}^{\infty} \exp(in\Delta\phi) B_{\text{ireg}}(n),$$

where

$$B_{\text{ireg}}(v) = - \sum_{l=1}^{\infty} \exp(-il\phi_0) (-\eta_2)^l \frac{H_v^{(1,0)}(x, k\rho)}{H_{v,\delta}^{(1,1)(1,0)}(x, y)} \Pi_l(v) \frac{H_{v+l}^{(1,0)}(x, k\rho_0)}{H_{v+l,\delta}^{(1,1)(1,0)}(x, y)},$$

$$\Pi_l(v) = \prod_{j=0}^l \frac{H_{v+j,\delta}^{(1,1)(1,0)}(x, y)}{H_{v+j,1}^{(1,1)(1,0)}(x, y)} \quad \text{for } |\eta_2| < 1$$

and

$$B_{\text{ireg}}(v) = \sum_{l=1}^{\infty} \exp(il\phi_0) (-\eta_2)^l \frac{H_v^{(1,0)}(x, k\rho)}{H_{v,1}^{(1,1)(1,0)}(x, y)} \tilde{\Pi}_l(v) \frac{H_{v-l}^{(1,0)}(x, k\rho_0)}{H_{v-l,1}^{(1,1)(1,0)}(x, y)},$$

$$\tilde{\Pi}_l(v) = \prod_{j=0}^l \frac{H_{v-j,1}^{(1,1)(1,0)}(x, y)}{H_{v-j,\delta}^{(1,1)(1,0)}(x, y)} \quad \text{for } |\eta_2| > 1.$$

The poles of the function $B_{\text{ireg}}(v)$ for $|\eta_2| < 1$ are located at the points $v_s - j$, where v_s are the roots of the equation (1.67) with $\alpha = 1$. For $|\eta_2| > 1$, they are located at the points $v_s + j$, where v_s are the roots of the equation (1.67) with $\alpha = \delta$. By finding the residues at these points, we arrive at the following expressions:

$$U_{\text{ireg}}(g, g_0) = \frac{4i}{y} \eta_3^2 (1 - \delta)^2 \sum_{s=1}^{\infty} \frac{H_{v_s}^{(1,0)}(x, y)}{\sin(\pi v_s) \tilde{H}_{v_s, \alpha}^{(1,1)(1,0)}(x, y)} \times [\exp[iv_s(\Delta\phi - \pi)]U(g, g_0, v_s) + \exp[-iv_s(\Delta\phi - \pi)]U(g, g_0, -v_s)],$$

(1.69)

where

$$U(g, g_0, v_s) = \sum_{m=1}^{\infty} \exp(-im\phi_0) (-\eta_2)^m \sum_{l=0}^m \exp(-il\Delta\phi) \Pi_m^{(l)}(v_s - l) \times \frac{H_{v_s-l}^{(1,0)}(x, k\rho) H_{v_s-l+m}^{(1,0)}(x, k\rho_0)}{H_{v_s-l,\delta}^{(1,1)(1,0)}(x, y) H_{v_s-l+m,\delta}^{(1,1)(1,0)}(x, y)} \quad \text{for } |\eta_2| < 1,$$

(1.70)

$$U(g, g_0, v_s) = \sum_{m=1}^{\infty} \exp(im\phi_0)(-\eta_2)^{-m} \sum_{l=0}^m \exp(il\Delta\phi) \tilde{\Pi}_m^{(l)}(v_s + l) \quad (1.71)$$

$$\times \frac{H_{v_s+l}^{(1,0)}(x, k\rho) H_{v_s+l-m}^{(1,0)}(x, k\rho_0)}{H_{v_s+l,1}^{(1,1)(1,0)}(x, y) H_{v_s+l-m,1}^{(1,1)(1,0)}(x, y)} \quad \text{for } |\eta_2| > 1,$$

$$\Pi_m^{(l)}(v) = \prod_{\substack{j=0 \\ j \neq l}}^m \frac{H_{v+j,\delta}^{(1,1)(1,0)}(x, y)}{H_{v+j,1}^{(1,1)(1,0)}(x, y)}, \quad \tilde{\Pi}_m^{(l)}(v) = \prod_{\substack{j=0 \\ j \neq l}}^m \frac{H_{v-j,1}^{(1,1)(1,0)}(x, y)}{H_{v-j,\delta}^{(1,1)(1,0)}(x, y)}, \quad (1.72)$$

$$\tilde{H}_{v_s,\alpha}^{(1,1)(1,0)}(x, y) = \left. \frac{d}{dv} H_{v,\alpha}^{(1,1)(1,0)}(x, y) \right|_{v=v_s}, \quad \Delta\phi = \phi - \phi_0 > 0,$$

and v_s are the roots of the equation (1.67).

In the analysis which follows, we restrict ourselves to the case of $|\eta_2| < 1$. The CS phenomenon has been detected for the waves coming to the receiver by the shortest route. Therefore, separating them out in (1.68)–(1.72) and placing the receiver and the source onto the boundary $\rho = a$ at the points with angular coordinates ϕ and ϕ_0 , respectively, we arrive at the following expression for the Hertz vector

$$\frac{4k}{I^{(m)}} U(g, g_0) \Big|_{\rho=\rho_0=a} = -\frac{4}{x} \sum_{s=1}^{\infty} \frac{\exp(iv_s \Delta\phi)}{\tilde{H}_{v_s,1}^{(1,1)(1,0)}(x, y)} V_s(\phi, \phi_0), \quad (1.73)$$

$$V_s(\phi, \phi_0) = V_{\text{reg}}(v_s) + V_{\text{ireg}}(\phi, \phi_0, v_s), \quad (1.74)$$

$$V_{\text{reg}}(v_s) = H_{v_s,1}^{(1,0)(0,0)}(y, x), \quad (1.75)$$

$$V_{\text{ireg}}(\phi, \phi_0, v_s) = \frac{-16i\eta_3}{\pi^2 xy} (1 - \delta) \left\{ u_s^+(\phi_0) + \left[1 + i\eta_3(1 - \delta) H_{v_s}^{(1,0)}(x, y) u_s^+(\phi_0) \right] u_s^-(\phi) \right\}, \quad (1.76)$$

$$u_s^{\pm}(\phi) = \sum_{m=1}^{\infty} \exp(-im\phi)(-\eta_2)^m \prod_{j=1}^m \frac{H_{v_s \pm j, \delta}^{(1,1)(1,0)}(x, y)}{H_{v_s \pm j, 1}^{(1,1)(1,0)}(x, y)} \cdot \frac{1}{H_{v_s \pm m, \delta}^{(1,1)(1,0)}(x, y)}. \quad (1.77)$$

To simulate the CS phenomenon let us fix the angular distance $\Delta\phi$ between the receiver and the source. In this case, the function

$$\tilde{U}(\phi) = \left[4k / I^{(m)} \right] U(g, g_0) \Big|_{\substack{\rho = \rho_0 = a \\ \phi_0 = \phi - \Delta\phi}}; \quad 0 \leq \phi \leq 2\pi$$

may be considered as the ‘diurnal dependence’ of the received signal. To ensure a nonzero diurnal phase change, the curve $V_s(\phi, \phi_0)$ in the complex plane must enclose the origin of coordinates. Since the regular term V_{reg} in (1.75) does not depend on ϕ , while the irregular term V_{ireg} is proportional to $\exp(-i\phi)$ for $\phi_0 = \phi - \Delta\phi$, the inequality

$$|V_{\text{reg}}(v_s)| < |V_{\text{ireg}}(\phi, \phi_0, v_s)| \tag{1.78}$$

is the necessary condition for the CS to occur in the model considered.

1.3.4 A Numerical Experiment

Let us calculate the Hertz potential $\tilde{U}(\phi)$ from (1.73)–(1.77) for the frequency $f = 10\text{kHz}$ and waveguide dimensions $a = 6370\text{ km}$ and $b - a = 60\text{ km}$. Since $x = ka = 1335.06 \gg 1$, we will use *Olver’s uniform asymptotic representation* [44] to calculate the Hankel functions $H_v^{(j)}(x)$ along with their derivatives with respect to the argument and the index. The roots of the transcendental equation in (1.67) for $\alpha = 1$ can be found by the *Newton-Raphson method* [45]. For better understanding of the peculiarities that characterize the waveguide mode interconversion, one should analyze the location of several first roots of the equation (1.67) as a function of the complex parameter η_3 .

Figure 1.4 illustrates typical trajectories of the first two roots $v_s, s = 1, 2$ in the complex v -plane for several fixed values of $\arg \eta_3$ as $|\eta_3|$ increases. The real values v_1^0 and v_2^0 correspond to zero impedance. The sign ‘+’ indicates the degenerate value v_{12}^{deg} of these two roots corresponding to the impedance $\eta_{12}^{\text{deg}} \approx 0.1826 - i0.1127$

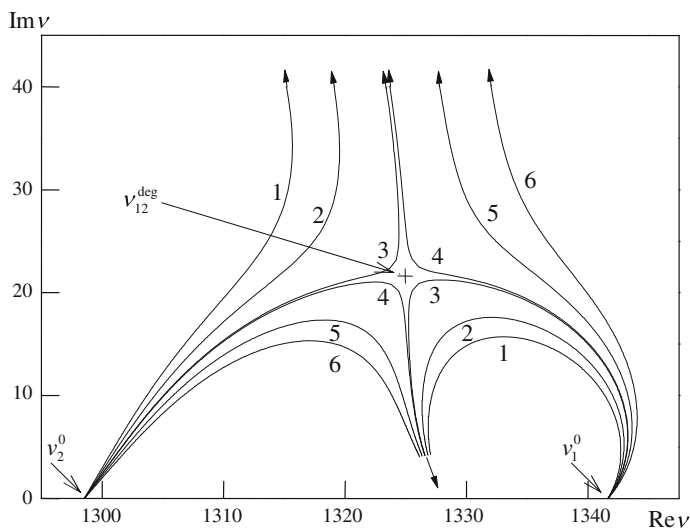


Fig. 1.4 The trajectories of the first two roots, v_1 and v_2 , of (1.67) in the complex v -plane for several fixed values of $\arg \eta_3$ with increasing $|\eta_3|, 0 \leq |\eta_3| \leq 0.5$: $\arg(i\eta_3)$ equals (1) 63.43° , (2) 60.94° , (3) 58.39° , (4) 58.21° , (5) 55.83° , (6) 53.37°

(see [21, 46]). It is easily seen that an abrupt change in the behavior of the eigenvalues of waveguide modes occurs when crossing the ray $\arg \eta_3 = \arg \eta_{12}^{\text{deg}}$.

Let us first consider the case of weakly irregular waveguides ($\delta \approx 1$). Then for $|\eta_2| \ll 1$ we have from (1.76)

$$V_{\text{ireg}}(\phi, \phi_0, v_s) = (\eta_1 - \eta_2)V_0(\phi, \phi_0, v_s), \quad (1.79)$$

$$V_0(\phi, \phi_0, v_s) = -\frac{16 i \eta_3}{\pi^2 xy} \exp(-i\phi_0) \left[\frac{1}{H_{v_s+1,1}^{(1,1)(1,0)}(x,y)} + \frac{\exp(-i\Delta\phi)}{H_{v_s-1,1}^{(1,1)(1,0)}(x,y)} \right] + O(1-\delta). \quad (1.80)$$

In Fig. 1.5, the level curves of the function $|V_0(\phi, \phi_0, v)|$ (for $\phi_0 = \phi - \Delta\phi$) are shown in the complex v -plane for the most interesting domain of variation of the eigenvalues of the first and the second modes for the impedance $i\eta_3 = H_v^{(1,1)}(x,y)/H_v^{(1,0)}(x,y)$ satisfying (1.67).

The angular distance between the receiver and the transmitter is $\Delta\phi = 114.6^\circ$, therefore, as it follows from numerical estimations, the contribution of the third and higher modes can be neglected. Minimal values of $|V_0(\phi, \phi_0, v)|$ are located in the vicinity of the points v_1^0 and v_2^0 , while the maximum is close to v_{12}^{deg} . By comparing these results with the level curves of $|V_{\text{reg}}(v)|$ from Fig. 1.6, we can conclude that

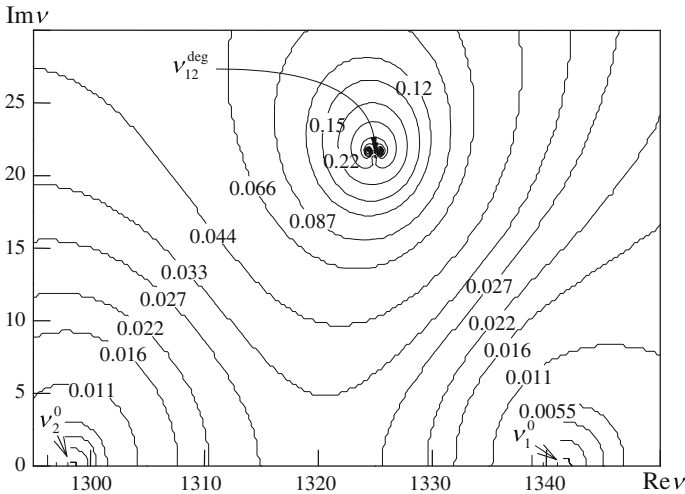
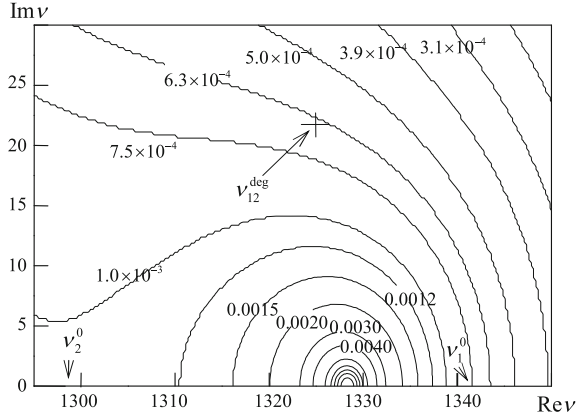


Fig. 1.5 The level curves of the function $|V_0(\phi_0 + \Delta\phi, \phi_0, v)|$ for $\Delta\phi = 114.6^\circ$: $\max_v |V_0(\phi_0 + \Delta\phi, \phi_0, v)| = 3.0517$, $v_{\text{max}} = 1325.5 + i21.75$, $|V_0(\phi_0 + \Delta\phi, \phi_0, v_1^0)| = 1.2593 \cdot 10^{-4}$, $|V_0(\phi_0 + \Delta\phi, \phi_0, v_2^0)| = 4.5397 \cdot 10^{-5}$

Fig. 1.6 The level curves of the function $|V_{\text{reg}}(v)|$, $\max_v |V_{\text{reg}}(v)| = 0.1561$, $v_{\text{max}} = 1328.25$



for small η_3 , for which $r_{\text{imp}} \ll 1$ and $v_{1,2} \rightarrow v_{1,2}^0$, the inequality $|V_{\text{reg}}(v)| > |V_0(\phi, \phi_0, v)|$ holds, and hence, CS is impossible in view of (1.78), (1.79). Let η_3 be increasing and approaching η_{12}^{deg} . At the same time, the center r_{imp} of the impedance circle $\eta_{\text{imp}} \rightarrow \eta_{12}^{\text{deg}}$ increases too, while the eigenvalues of the first and second modes approach the point v_{12}^{deg} , in the vicinity of which the amplitude of the irregular part of $|V_0(\phi, \phi_0, v)|$ is maximal.

Then for not too small values of $|\eta_1 - \eta_2|$, the inequality (1.78) holds. In other words, it follows from the foregoing numerical estimates for the functions $|V_{\text{reg}}(v)|$ and $|V_0(\phi, \phi_0, v)|$ for weakly irregular waveguides that there exists a *threshold value* of the hodograph radius $r_{\text{imp}}^{\text{cs}}$ of the impedance $\eta(\phi)$ (1.43) such that the CS phenomenon is impossible for $r_{\text{imp}} < r_{\text{imp}}^{\text{cs}}$, while for $r_{\text{imp}} > r_{\text{imp}}^{\text{cs}}$ it occurs at least for the hodographs located in the vicinity of η_{12}^{deg} . As the angular distance $\Delta\phi$ increases, the probability that the phenomenon in question will occur is growing too, all factors being equal. A similar situation holds when a degree of the waveguide irregularity grows, i.e. with increasing r_{imp} .

Let us now turn back to the general case of arbitrary index of a waveguide irregularity δ . Figure 1.7 present the simulated diurnal record of the received signal or, in other words, the ϕ -dependencies, $\Delta\phi \leq \phi \leq 2\pi + \Delta\phi$, of the normalized value

$$W(\phi) = \left[\lg \left(\max_{0 \leq \phi \leq 2\pi} |\tilde{U}(\phi)| \right) \tilde{U}(\phi) \right] / \left[\lg(|\tilde{U}(\phi)|) |\tilde{U}(\phi)| \right],$$

for the fixed angular distance $\Delta\phi = 114.6^\circ$ between the source and the receiver. On the curves three following values of the received signal are marked: ‘0’ corresponds to the initial moment of the record ($\phi = 0$), ‘r’ (‘r’) corresponds to the moment of time when the receiver (the transmitter) is passing through the waveguide cross section $\phi = \phi_{\text{cr}}$, where the surface impedance is closest to η_{12}^{deg} (see Fig. 1.8).

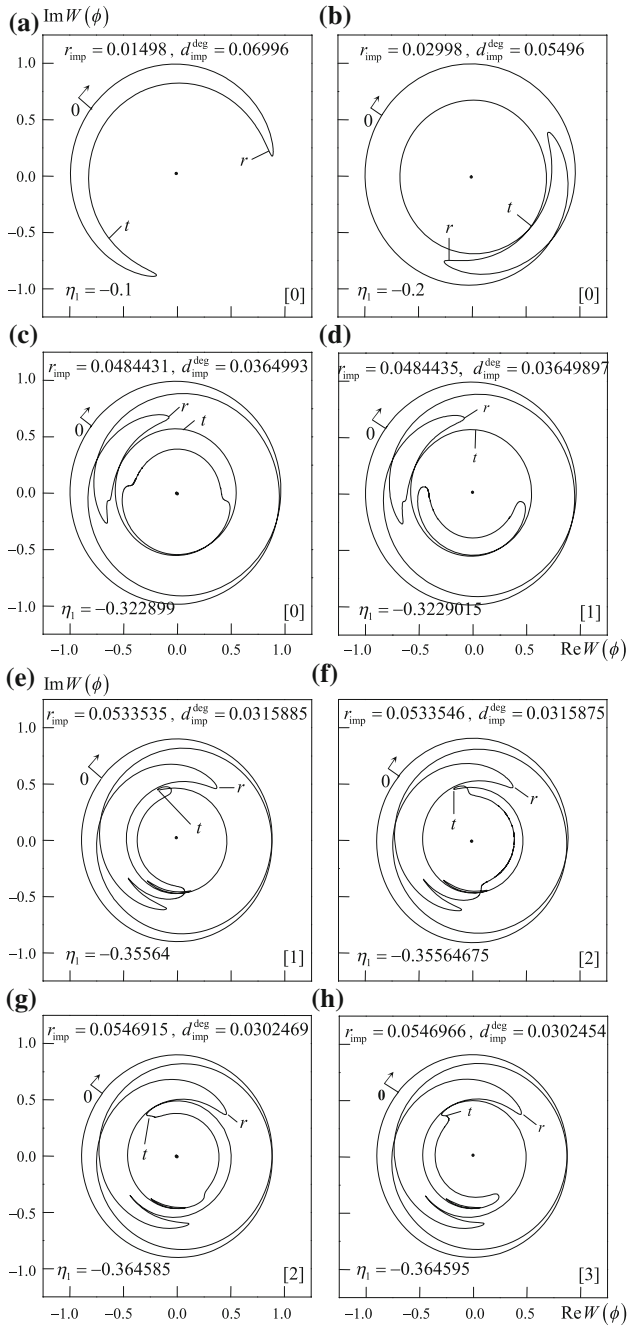
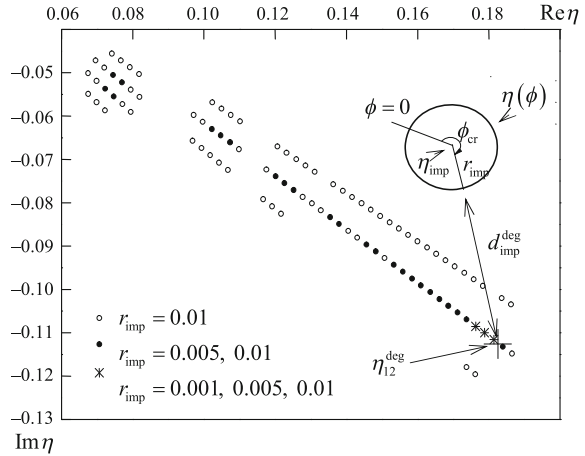


Fig. 1.7 The normalized diurnal records of the received signal $W(\phi)$: $\eta_3 = 0.1455 - i0.03638$, $\eta_2 = 0.0001$, $\Delta\phi = 114.6^\circ$

Fig. 1.8 The domains in the complex plane of the impedance η , where the CS occurs with the given radius r_{imp} and the angle $\Delta\phi = 114.6^\circ$



The number of lost phase cycles are shown in the figures in square brackets $[m]$; $d_{\text{imp}}^{\text{deg}}$ is the distance from the impedance circle to the point η_{12}^{deg} . The numerical experiment has shown that the CS phenomenon does not occur for the hodographs of the impedance $\eta(\phi)$ remote from the segment $l_{\text{cs}} = \left\{ 0 < |\eta| \leq \eta_{12}^{\text{deg}}, \arg \eta = \arg \eta_{12}^{\text{deg}} \right\}$ (Fig. 1.7a, b, c). As r_{imp} increases, $W(\phi)$ behavior becomes more complex; when the circle $\eta(\phi)$ intersects l_{cs} , CS occurs (Fig. 1.7d) for $\eta_3 = 0.1455 - i0.03638$ and $r_{\text{imp}} \approx 0.0484435$. At the same time, the signal amplitude decreases within a small variation interval of ϕ (of the order of 0.01°).

As r_{imp} grows, at $r_{\text{imp}} \approx 0.0533546$ (Fig. 1.7f), the CS phenomenon for two cycles, at $r_{\text{imp}} \approx 0.0546966$ (Fig. 1.7h) for three cycles, and so forth is observable. A similar situation holds for the circle $\eta(\phi)$, whose center is located in the vicinity of l_{cs} (Fig. 1.8); however, the CS occurs at lesser values of r_{imp} . Each CS phenomenon is accompanied by a sharp decrease in signal amplitude, which is typical for a CS in a natural waveguide [22, 32]. In the context of the given model, the role played by the segment l_{cs} in the initiation of the CS phenomenon can be explained as follows: only for the impedances in the vicinity of this segment, the eigenvalues v_1 and v_2 have closely spaced imaginary parts, and consequently, the amplitudes of the first and the second modes are nearly equal. In addition, when η_3 is moving along l_{cs} towards the point η_{12}^{deg} , the real parts of v_1 and v_2 come close together (curves 3 or 4 in Fig. 1.4), and consequently, the phase velocities of these modes approach each other.

Of some interest is a localization of the domains in the complex η -plane, for which the CS phenomenon takes place at the given radius r_{imp} and angle $\Delta\phi$. In Fig. 1.8 dots indicate center positions of the hodographs of radiuses 0.001, 0.005 and 0.01, for which CS occurs at $\Delta\phi = 114.6^\circ$. It is seen that with increasing r_{imp} the CS phenomenon develops initially in the immediate vicinity of the point η_{12}^{deg} , and then, as r_{imp} grows, this area is extending occupying a constantly increasing

part of the segment l_{cs} . For the hodographs with fixed centers, the CS phenomenon having developed at some r_{imp} , persists for larger values of the radius.

In conclusion note the following. We have proposed a model of the ring waveguide of a fixed cross section whose irregularity is caused only by the behavior of the surface impedance of its wall. Hence we have excluded from consideration the diffraction effect of wave transformation on a spatial inhomogeneity of the wall; only the mode degeneracy effect being inherent in the waveguides with finite absorption is analyzed. We have obtained the analytical solution of the corresponding boundary value problem for a class of circular hodographs of surface impedance. It is the first problem of the excitation of a finite irregular waveguide with continuously varying properties, for which the analytical solution is found.

The results of the numerical experiment for widely separated ($1 \leq \Delta\phi \leq \pi$) transmitter and receiver have shown that the CS phenomenon here is directly related to the degeneracy of the first and the second modes. This phenomenon is threshold-like and it occurs in waveguides with sufficiently high irregularity of the walls whose impedance is distributed in the neighborhood of the degenerate value η_{12}^{deg} . Once the phenomenon is developed, it persists as the radius of the impedance hodograph increases. At the same time, the domain of the complex plane of the impedance, where the CS takes place, is extending occupying a constantly increasing part of the segment joining the origin of coordinates and the point η_{12}^{deg} .

It has been demonstrated with a waveguide of fixed cross section that the CS in irregular lossy waveguides may be caused by the interconversion of two dominant waveguide modes in the neighborhood of their degeneracy rather than by the diffraction effect of rescattering of the principal mode into the higher modes on a spatial inhomogeneity of the waveguide wall, as it is customary to assume.

1.4 Pulsed Radiation from a Line Electric Current Near a Planar Interface

The classical problem of transient electromagnetic fields generated by pulsed currents located near a planar boundary between layered media are the subject of constant theoretical research starting with the B. van der Pol paper [47]. The approaches based on the *Cagniard method* [48, 49] is the most efficient tool in this study. A.T. de Hoop [50] has suggested a modification of Cagniard's method with the help of which exact solutions have been obtained for a number of problems of a dipole or a line source near an interface [51–54]. Various modifications of Cagniard's technique have found wide application in the study of transient acoustic and seismic wave propagation. Following paper [50], the modifications of de Hoop's technique [55, 56] as well as the alternative approaches free from some drawbacks to this method [57, 58] have been suggested.

In this section, following the paper [59], we use the approach alternative to Cagniard's technique to study the transient field generated by line sources located in a flat-layered media. The suggested approach is applied to the already solved problem, namely, the problem of finding the electromagnetic field generated by a pulsed line source located near a planar interface between two nonabsorbing and nondispersive media. The most complete solution to this problem have been obtained and discussed in considerable detail by A.T. de Hoop in [54]. In this paper, we applied the one-sided Laplace transform with respect to time and two-sided Laplace transform with respect to a horizontal spatial variable. The electromagnetic field is represented in the form of a double integral. This integral can be efficiently calculated by the *Cagniard-de Hoop method* (CHM). The essence of the method is as follows. The original path of integration for one of two integrals forming the double integral is deformed into a so-called *modified Cagniard contour*. It is chosen such that upon the corresponding change of the integration variable in the integral along the modified contour, the original double integral turns into a composition of the direct and inverse Laplace transform for the known function. The central problem with this method is to find, generally speaking, numerically, the modified Cagniard contour. It should be noted that the shape of this contour changes as the observation point changes.

The key point of the approach proposed here consists in the following. To calculate the double integral efficiently, we suggest deforming its domain of integration (the real plane) in the $C \times C$ -space of two complex variables rather than to deform one contour in the complex C -plane, as has been done in CHM. It is shown that in this case the integral reduces to a sum of residues. The use of powerful apparatus of the residue theory instead of somewhat artificial way used in CHM is a reason to hope that this new approach can be efficient in the situations where the CHM is failed, for example, for anisotropic media. Our method can be extended to multilayered media and arbitrary dipole sources.

1.4.1 Problem Formulation

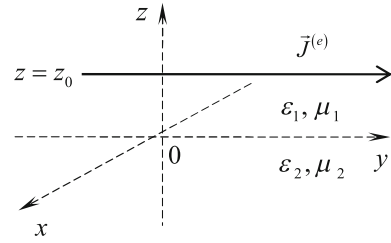
The field generated by a pulsed line electric current

$$\vec{J}^{(e)} = I^{(e)} \delta(x) \delta(z - z_0) \delta(t) \vec{y}; \quad z_0 > 0, \quad (1.81)$$

which is located near a planar interface (Fig. 1.9), is to be found. The source excites the E -polarized field

$$E_y \neq 0, \quad E_x = E_z = H_y = 0, \quad \frac{\partial H_x}{\partial t} = \frac{1}{\mu\mu_0} \frac{\partial E_y}{\partial z}, \quad \frac{\partial H_z}{\partial t} = -\frac{1}{\mu\mu_0} \frac{\partial E_y}{\partial x}. \quad (1.82)$$

Fig. 1.9 A pulsed line source near the interface between two semi-infinite media



The function E_y is the solution of the wave equation

$$\left(\frac{\partial^2}{\partial x^2} + \frac{\partial^2}{\partial z^2} - \epsilon \epsilon_0 \mu \mu_0 \frac{\partial^2}{\partial t^2} \right) E_y = \mu_1 \mu_0 \frac{\partial J_y^{(e)}}{\partial t} \quad (1.83)$$

that satisfies the conditions of continuity of E_y - and H_x -components on the interface $z = 0$ and the causality principle. Here, $\epsilon = \epsilon_1$, $\mu = \mu_1$ for $z > 0$ and $\epsilon = \epsilon_2$, $\mu = \mu_2$ for $z < 0$.

The Fourier transform in time

$$F(x, z, \omega) = \frac{1}{2\pi} \int_{-\infty}^{\infty} E_y(x, z, t) e^{i\omega t} dt, \quad E_y(x, z, t) = \int_{-\infty}^{\infty} F(x, z, \omega) e^{-i\omega t} d\omega \quad (1.84)$$

applied to the boundary value problem in (1.83) results in the following problem

$$\begin{cases} \left(\frac{\partial^2}{\partial x^2} + \frac{\partial^2}{\partial z^2} + \omega^2 \epsilon_1 \epsilon_0 \mu_1 \mu_0 \right) F^1 = -I_0 \delta(x) \delta(z - z_0); & z > 0 \\ \left(\frac{\partial^2}{\partial x^2} + \frac{\partial^2}{\partial z^2} + \omega^2 \epsilon_2 \epsilon_0 \mu_2 \mu_0 \right) F^2 = 0; & z < 0 \end{cases} \quad (1.85)$$

with the boundary conditions on $z = 0$

$$F^1 = F^2, \quad \mu_2 \frac{\partial F^1}{\partial z} = \mu_1 \frac{\partial F^2}{\partial z}, \quad (1.86)$$

where $I_0 = i\omega \mu_1 \mu_0 I^{(e)}/2\pi$. The solution of the equations in (1.85) is conveniently represented in the form [41]

$$F^1 = I_0 (F^0 + F_s^1) \text{ for } z > 0 \quad \text{and} \quad F^2 = I_0 F_s^2 \text{ for } z < 0, \quad (1.87)$$

where

$$F^0 = \frac{i}{4\pi} \int_{-\infty}^{\infty} \frac{\exp\left[i\zeta x + i\sqrt{k_1^2 - \zeta^2}|z - z_0|\right]}{\sqrt{k_1^2 - \zeta^2}} d\zeta = \frac{1}{4} H_0^{(1)}(k_1 R_-), \tag{1.88}$$

$$F_s^1 = \frac{i}{4\pi} \int_{-\infty}^{\infty} \frac{\exp\left[i\zeta x + i\sqrt{k_1^2 - \zeta^2}(z + z_0)\right]}{\sqrt{k_1^2 - \zeta^2}} \Gamma_1(\zeta, \omega) d\zeta, \tag{1.89}$$

$$F_s^2 = \frac{i}{4\pi} \int_{-\infty}^{\infty} \frac{\exp\left[i\zeta x - i\sqrt{k_2^2 - \zeta^2}z + i\sqrt{k_1^2 - \zeta^2}z_0\right]}{\sqrt{k_1^2 - \zeta^2}} \Gamma_2(\zeta, \omega) d\zeta, \tag{1.90}$$

$\Gamma_j(\zeta, \omega)$ are the unknown functions, $\text{Im}\sqrt{k_j^2 - \zeta^2} \geq 0$, $k_j^2 = \omega^2 n_j^2$, $n_j^2 = \epsilon_j \epsilon_0 \times \mu_j \mu_0$, $j = 1, 2$, $R_-^2 = x^2 + (z - z_0)^2$. From the boundary conditions in (1.86), we have:

$$1 + \Gamma_1 = \Gamma_2, \quad -\mu_2 \sqrt{k_1^2 - \zeta^2} + \mu_1 \sqrt{k_1^2 - \zeta^2} \Gamma_1 = -\mu_1 \sqrt{k_2^2 - \zeta^2} \Gamma_2,$$

or

$$\Gamma_1(\zeta, \omega) = \frac{\mu_2 \sqrt{k_1^2 - \zeta^2} - \mu_1 \sqrt{k_2^2 - \zeta^2}}{\mu_2 \sqrt{k_1^2 - \zeta^2} + \mu_1 \sqrt{k_2^2 - \zeta^2}}, \tag{1.91}$$

$$\Gamma_2(\zeta, \omega) = \frac{2\mu_2 \sqrt{k_1^2 - \zeta^2}}{\mu_2 \sqrt{k_1^2 - \zeta^2} + \mu_1 \sqrt{k_2^2 - \zeta^2}}. \tag{1.92}$$

Thus we obtain the required field in the form of the following double integrals taken over the plane P of real variables ω and ζ :

$$E_y^j(x, z, t) = E_0 \frac{\partial}{\partial t} G^j(x, z, t); \quad j = 0, 1, 2, \tag{1.93}$$

$$G^0(x, z, t) = \frac{1}{4\pi i} \iint_P \exp\left[i\zeta x + i\sqrt{\omega^2 n_1^2 - \zeta^2}|z - z_0| - i\omega t\right] \frac{d\omega d\zeta}{\sqrt{\omega^2 n_1^2 - \zeta^2}}; \quad z > 0, \tag{1.94}$$

$$G^1(x, z, t) = \frac{1}{4\pi i} \iint_{\mathbf{P}} \exp \left[i\xi x + i\sqrt{\omega^2 n_1^2 - \xi^2} (z + z_0) - i\omega t \right] \frac{\Gamma_1(\xi, \omega) d\omega d\xi}{\sqrt{\omega^2 n_1^2 - \xi^2}}; \quad (1.95)$$

$$z > 0,$$

$$G^2(x, z, t) = \frac{1}{4\pi i} \iint_{\mathbf{P}} \exp \left[i\xi x - i\sqrt{\omega^2 n_2^2 - \xi^2} z + i\sqrt{\omega^2 n_1^2 - \xi^2} z_0 - i\omega t \right] \times \frac{\Gamma_2(\xi, \omega) d\omega d\xi}{\sqrt{\omega^2 n_1^2 - \xi^2}}; \quad (1.96)$$

$$z < 0,$$

where $E_0 = I^{(e)} \mu_1 \mu_0 / 2\pi$ and $\text{Im} \sqrt{\omega^2 n_j^2 - \xi^2} \geq 0, j = 1, 2$.

1.4.2 Reduction to Single Integrals

In formulas (1.94)–(1.96), the integrands allow analytic continuation from the real plane $\mathbf{P} = \{\omega, \xi : \omega'' = \xi'' = 0\}$ into the $\mathbf{C} \times \mathbf{C}$ -space of two complex variables $\omega = \omega' + i\omega''$ and $\xi = \xi' + i\xi''$. As the previous analysis has shown, there is no need to operate with the whole of real four-dimensional space $\mathbf{C} \times \mathbf{C}$. To calculate the integrals in (1.94)–(1.96), it is sufficient to restrict our consideration to a three-dimensional space $\mathbf{R}^3 = \{\omega, \xi : \xi'' = 0\} \subset \mathbf{C} \times \mathbf{C}$ containing \mathbf{P} . In \mathbf{R}^3 , one should choose the single-valued branches of two square roots in the integrands.

Consider a function $\kappa(\omega, \xi) = \sqrt{\omega^2 n^2 - \xi^2}$ in \mathbf{R}^3 assuming that the refractive index $n = n' + in''$ ($n', n'' > 0$) is complex-valued.

The surface

$$\text{Re} \kappa^2 = (n^2 - n''^2) \omega'^2 - (n^2 - n''^2) \omega''^2 - 4n'n'' \omega' \omega'' - \xi'^2 = 0 \quad (1.97)$$

has the following invariants [60]: $I = -1, J = -|n|^4, D = -J, A = 0, A' = D$. Therefore it represents a two-pole elliptic cone, which is symmetrical with respect to the plane $\xi' = 0$, with its vertex at the origin of coordinates. Let us locate the axis of the cone. The lines of intersection of the cone with the symmetry plane $\xi' = 0$ are two mutually orthogonal straight lines $(n' \mp n'') \omega'' \pm (n' \pm n'') \omega' = 0$ with the bisecting lines $n' \omega'' + n'' \omega' = 0$ and $n' \omega' - n'' \omega'' = 0$. Consequently, the cone axis is determined by the equations $n' \omega'' + n'' \omega' = 0$ and $\xi' = 0$.

The surface

$$\text{Im} \kappa^2 = n'n'' (\omega'^2 - \omega''^2) + \omega' \omega'' (n^2 - n'^2) = 0 \quad (1.98)$$

has the following invariants: $I = 0$, $D = -|n|^4/4$, $A = 0$. Therefore it represents two mutually orthogonal planes intersecting along the ζ' -axis and determined by the equations $n'\omega'' + n''\omega' = 0$ and $n''\omega'' - n'\omega' = 0$. The first plane contains the axis of the cone (1.97) being its another symmetry plane. From (1.97) and (1.98), we derive the following equations for the branch lines of $\kappa(\omega, \xi)$:

$$n'\omega' - n''\omega'' \pm \zeta' = 0, \quad n'\omega'' + n''\omega' = 0.$$

In Fig. 1.10, the distribution of signs for $\text{Re}\kappa^2$ and $\text{Im}\kappa^2$ in \mathbb{R}^3 is shown. In (1.94)–(1.96), a single-valued branch of the function $\kappa(\omega, \xi)$, for which $\text{Im}\kappa(\omega, \xi) \geq 0$, is determined on the real plane $P = \{\zeta', \omega'\}$. The above mentioned inequality is hold everywhere in \mathbb{R}^3 , if the following condition is satisfied: $0 \leq \arg \kappa^2 < 2\pi$. In other words, the cut S in \mathbb{R}^3 that separates this branch should be determined by the conditions $\text{Re}\kappa^2 \geq 0$, $\text{Im}\kappa^2 = 0$. As is seen from Fig. 1.10, this takes place for a double sector formed by the intersection of the inner part of the cone (1.97) with its symmetry plane $n'\omega'' + n''\omega' = 0$. In \mathbb{R}^3 , with the cut of this kind (Fig. 1.11), we have $\text{Im}\kappa(\omega, \xi) \geq 0$.

A similar approach to choose a branch of the square root is given in [61] for the case of a single variable. When passing to the lossless medium $\alpha = 0$, the cut surface S is shifted into the plane $\omega'' = 0$ representing the double sector, which contains the ω' -axis and is bounded by the straight branch lines $n'\omega' \pm \zeta' = 0$.

Thus we have shown that for a lossless media the cut surface ensuring a choice of the branch, for which we have $\text{Im}\sqrt{\omega^2 n_j^2 - \zeta^2} \geq 0$ in \mathbb{R}^3 , is a double sector S_j (Fig. 1.11), which lies in the plane $\omega'' = 0$, contains the ω' -axis, and is bounded by the branch lines $n_j\omega' \pm \zeta' = 0, j = 1, 2$. The root is positive on the upper side of the right-hand sector $\{\omega' > 0, \omega'' = 0 + 0\}$ and on the bottom side of the left-hand

Fig. 1.10 The sign distribution for $\text{Re} \kappa^2$ and $\text{Im} \kappa^2$ in the plane $\zeta' = 0$. Straight lines indicate the lines of intersection with the plane $\zeta' = 0$: the bold lines—for the cone $\text{Re} \kappa^2 = 0$, the dashed lines—for the planes $\text{Im} \kappa^2 = 0$. Symbols (\pm) specify the sign of $\text{Re} \kappa^2$, while $[\pm]$ specify the sign of $\text{Im} \kappa^2$; $\sin \alpha = -n''/|n|$, l_0 is the axis of the cone (1.97)

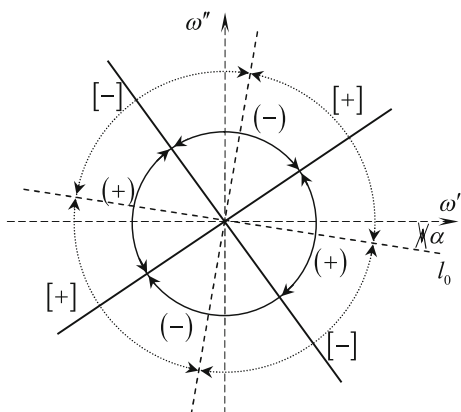
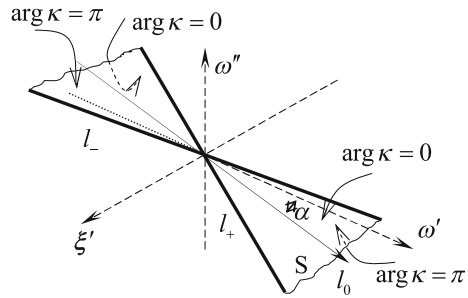


Fig. 1.11 The location of the branch lines l_{\pm} and the cut surface S ensuring the choice of the branch for which $\text{Im} k(\omega, \xi) \geq 0$ in \mathbb{R}^3 -space; l_0 is the axis of the cone (1.97)



sector $\{\omega' < 0, \omega'' = 0 - 0\}$, while it is negative on the other sides. Since the integrands in (1.94)–(1.96) are uniquely defined in the \mathbb{R}^3 -space with the specified cuts, one can apply the Cauchy-Poincare theorem [18] to deform the surface of integration P in $\mathbb{R}^3 \setminus (S_1 \cup S_2)$.

In accordance with the causality principle, the cut surfaces S_1 and S_2 have to adjoin the real plane P from the bottom ($\omega'' = 0 - 0$). Then, the integrands have no singularities in the half-space $\omega'' > 0$, and we have $E_y(x, z, t) \equiv 0$ for all $t < 0$, according to the mentioned theorem.

For the positive values of t , the P -plane can be deformed to a half-space $\omega'' < 0$. Then we have for E_y^0 an integral over the surface P_{c1} , while for E_y^1, E_y^2 we have integrals over the surface $P_c = P_{c1} \cup P_{c2}$. Here P_{cj} stands for the closed surface enveloping the cut S_j .

Using the function $G^1(x, z, t)$ as an example, let us demonstrate how the integrals describing the secondary field in (1.95), (1.96) can be simplified. Denoting the integrand in (1.95) by $f(\omega, \xi')$, consider the following integral over the surface P_c :

$$\iint_{P_c} f(\omega, \xi') ds = I_1 + I_2, \tag{1.99}$$

where $I_j = \iint_{P_{cj}} f(\omega, \xi') ds$. Let P_{cj}^+ and P_{cj}^- be the right-hand ($\omega' > 0$) and the left-hand ($\omega' < 0$) cavities of the surface P_{cj} ; $L_{\omega'j}$ is the closed contour generated by the intersection of the surface P_{cj} with the coordinate plane $\omega' = \text{const}$. Then we have

$$\begin{aligned} I_1 &= \sum_{\pm} \iint_{P_{c1}^{\pm}} f(\omega, \xi') ds = \int_0^{\infty} d\omega' \int_{L_{\omega'1}} df(\omega, \xi') + \int_{-\infty}^0 d\omega' \int_{L_{\omega'1}} df(\omega, \xi') \\ &= \int_0^{\infty} d\omega' \left[\int_{L_{\omega'1}} df(\omega, \xi') - \int_{L_{\omega'1}} df(-\omega, -\xi') \right]. \end{aligned} \tag{1.100}$$

In the second integral, we made the following change of variables $\omega \rightarrow -\omega$, $\xi' \rightarrow -\xi'$. Taking into account the evenness of the chosen branches of the square roots entering the function $f(\omega, \xi')$ with respect to this change of variables and performing another change of variables $\xi' = \omega\eta$, we arrive at the following expression for the integral in (1.95):

$$I_1 = \int_0^\infty d\omega \int_{L_1} d\eta \left(\exp \left\{ i\omega \left[\eta x + \sqrt{n_1^2 - \eta^2} (z + z_0) - t \right] \right\} - \exp \left\{ i\omega \left[-\eta x + \sqrt{n_1^2 - \eta^2} (z + z_0) + t \right] \right\} \right) \tilde{\Gamma}_1(\eta) / \sqrt{n_1^2 - \eta^2}, \tag{1.101}$$

where

$$\tilde{\Gamma}_1(\eta) = \frac{\mu_2 \sqrt{n_1^2 - \eta^2} - \mu_1 \sqrt{n_2^2 - \eta^2}}{\mu_2 \sqrt{n_1^2 - \eta^2} + \mu_1 \sqrt{n_2^2 - \eta^2}}. \tag{1.102}$$

The contour L_1 envelops the segment $(-n_1, n_1)$ in the complex η -plane. Let us introduce the accessory parameter $\delta > 0$ for the sake of convergence acceleration, then rewrite (1.101) in the form

$$\begin{aligned} I_1 &= \lim_{\delta \rightarrow 0} \int_0^\infty d\omega \int_{L_1} d\eta \left(\exp \left\{ i\omega \left[i\delta + \eta x + \sqrt{n_1^2 - \eta^2} (z + z_0) - t \right] \right\} - \exp \left\{ i\omega \left[i\delta - \eta x + \sqrt{n_1^2 - \eta^2} (z + z_0) + t \right] \right\} \right) \tilde{\Gamma}_1(\eta) / \sqrt{n_1^2 - \eta^2} \\ &= i \lim_{\delta \rightarrow 0} \int_{L_1} \left[\frac{1}{\eta x + \sqrt{n_1^2 - \eta^2} (z + z_0) - t + i\delta} - \frac{1}{-\eta x + \sqrt{n_1^2 - \eta^2} (z + z_0) + t + i\delta} \right] \frac{\tilde{\Gamma}_1(\eta) d\eta}{\sqrt{n_1^2 - \eta^2}}. \end{aligned} \tag{1.103}$$

For the second integral in (1.99), I_2 , we obtain a representation similar to (1.103) with L_1 replaced by L_2 , where L_2 is the contour enveloping the segment $(-n_2, n_2)$. Thus, for the function given by (1.95), which determines the secondary field in the first medium (see (1.93)), we arrive at the following expression

$$G^1(x, z, t) = \frac{1}{4\pi} \lim_{\delta \rightarrow 0} \int_L \left[\frac{1}{\eta x + \sqrt{n_1^2 - \eta^2} (z + z_0) - t_-} - \frac{1}{-\eta x + \sqrt{n_1^2 - \eta^2} (z + z_0) + t_+} \right] \frac{\tilde{\Gamma}_1(\eta) d\eta}{\sqrt{n_1^2 - \eta^2}}, \tag{1.104}$$

where $t_{\pm} = t \pm i\delta$, L is the contour enveloping the segment $(-n_{\max}, n_{\max})$, $n_{\max} = \max(n_1, n_2)$. The root branches are determined by the inequalities $-\pi < \arg \sqrt{n_j^2 - \eta^2} < \pi$ with zero argument on the bottom side of the cut along the segment $(-n_j, n_j)$.

Similarly, for the function G^2 , describing the field in the second medium, we obtain from (1.96):

$$G^2(x, z, t) = \frac{1}{4\pi} \lim_{\delta \rightarrow 0} \int_L \left[\frac{1}{\eta x + \sqrt{n_1^2 - \eta^2} z_0 - \sqrt{n_2^2 - \eta^2} z - t_-} - \frac{1}{-\eta x + \sqrt{n_1^2 - \eta^2} z_0 - \sqrt{n_2^2 - \eta^2} z + t_+} \right] \frac{\tilde{T}_2(\eta) d\eta}{\sqrt{n_1^2 - \eta^2}}, \quad (1.105)$$

where $\tilde{T}_2(\eta) = 1 + \tilde{T}_1(\eta)$. The integrands in (1.104) and (1.105) are analytic in the plane of complex variable η with the specified cut and decreasing at infinity as η^{-2} . Therefore, these integrals can be reduced to the residues determined by zeros of the denominators in the square brackets:

$$\eta x + \sqrt{n_1^2 - \eta^2} (z + z_0) - t_- = 0, \quad -\eta x + \sqrt{n_1^2 - \eta^2} (z + z_0) + t_+ = 0 \quad \text{for} \quad (1.104), \quad (1.106)$$

$$\begin{aligned} \eta x + \sqrt{n_1^2 - \eta^2} z_0 - \sqrt{n_2^2 - \eta^2} z - t_- &= 0, \\ -\eta x + \sqrt{n_1^2 - \eta^2} z_0 - \sqrt{n_2^2 - \eta^2} z + t_+ &= 0 \quad \text{for} \quad (1.105). \end{aligned} \quad (1.107)$$

1.4.3 The Field in the First Medium

The roots of (1.106) are readily determined and can be written as

$$\begin{aligned} \eta_1^- &= \left(x t_- - (z + z_0) \sqrt{n_1^2 R_+^2 - t_-^2} \right) R_+^{-2} \quad \text{and} \\ \eta_1^+ &= \left(x t_+ + (z + z_0) \sqrt{n_1^2 R_+^2 - t_+^2} \right) R_+^{-2}, \end{aligned} \quad (1.108)$$

where $R_+^2 = x^2 + (z + z_0)^2$. For the square root $\sqrt{n_1^2 R_+^2 - t^2}$, we determined the same branch in the complex plane of variable t as for $\sqrt{n_j^2 - \eta^2}$ in the η -plane. By calculating the corresponding residues, we get from (1.104):

$$\begin{aligned}
 G^1(x, z, t) &= \frac{i}{2} \lim_{\delta \rightarrow 0} \left\{ \frac{\tilde{T}_1(\eta)}{x\sqrt{n_1^2 - \eta^2} - (z + z_0)\eta} \Big|_{\eta=\eta_1^-} + \frac{\tilde{T}_1(\eta)}{x\sqrt{n_1^2 - \eta^2} + (z + z_0)\eta} \Big|_{\eta=\eta_1^+} \right\} \\
 &= \frac{i}{2} \lim_{\delta \rightarrow 0} \left\{ \frac{\tilde{T}_1(\eta_1^-)}{\sqrt{n_1^2 R_+^2 - t_-^2}} + \frac{\tilde{T}_1(\eta_1^+)}{\sqrt{n_1^2 R_+^2 - t_+^2}} \right\}.
 \end{aligned} \tag{1.109}$$

Here we used the equality

$$\sqrt{n_1^2 - (\eta_1^\mp)^2} = \left[x\sqrt{n_1^2 R_+^2 - (t_\mp)^2} \pm (z + z_0)t_\mp \right] R_+^{-2}. \tag{1.110}$$

It is easy to verify that the following relationships are hold for the chosen branches of the square roots:

$$\begin{aligned}
 \sqrt{n_1^2 R_+^2 - (t^*)^2} &= \exp(i\pi) \left(\sqrt{n_1^2 R_+^2 - t^2} \right)^*, \\
 \sqrt{n_j^2 - (\eta^*)^2} &= \exp(i\pi) \left(\sqrt{n_j^2 - \eta^2} \right)^*
 \end{aligned} \tag{1.111}$$

(the asterisk stands for a complex conjugation). Therefore,

$$\begin{aligned}
 \eta_1^- &= \left[xt_+^* - (z + z_0) \exp(i\pi) \left(\sqrt{n_1^2 R_+^2 - t_+^2} \right)^* \right] R_+^{-2} \\
 &= \left[xt_+ + (z + z_0) \sqrt{n_1^2 R_+^2 - t_+^2} \right]^* R_+^{-2} = (\eta_1^+)^*, \\
 \sqrt{n_j^2 - (\eta_1^-)^2} &= \exp(i\pi) \left(\sqrt{n_j^2 - [(\eta_1^-)^*]^2} \right)^* = - \left[\sqrt{n_j^2 - (\eta_1^+)^2} \right]^*, \\
 \tilde{T}_1(\eta_1^-) &= [\tilde{T}_1(\eta_1^+)]^*.
 \end{aligned} \tag{1.112}$$

The wave reflected from the interface comes at some point in the first medium at time $t_{\text{ref}} = n_1 R_+$. For the time interval $0 < t < t_{\text{ref}}$, in view of (1.112), we obtain

$$\begin{aligned}
 G^1(x, z, t) &= \frac{i}{2} \lim_{\delta \rightarrow 0} \left[\frac{\tilde{T}_1^*(\eta_1^+)}{\sqrt{n_1^2 R_+^2 - t_-^2}} + \frac{\tilde{T}_1(\eta_1^+)}{\sqrt{n_1^2 R_+^2 - t_+^2}} \right] = \frac{i}{2} \lim_{\delta \rightarrow 0} \frac{[\tilde{T}_1^*(\eta_1^+) - \tilde{T}_1(\eta_1^+)]}{\sqrt{n_1^2 R_+^2 - t^2}} \\
 &= \text{Im} \tilde{T}_1(\eta_1^<) / \sqrt{n_1^2 R_+^2 - t^2},
 \end{aligned} \tag{1.113}$$

where $\eta_1^< = \eta_1^+ |_{\delta=0} = [xt - (z + z_0) \sqrt{n_1^2 R_+^2 - t^2}] R_+^{-2}$.

For the time interval $t_{\text{ref}} < t$, we have

$$G^1(x, z, t) = \frac{i}{2} \lim_{\delta \rightarrow 0} \left[\frac{\tilde{\Gamma}_1^*(\eta_1^+)}{i\sqrt{t^2 - n_1^2 R_+^2}} + \frac{\tilde{\Gamma}_1(\eta_1^+)}{i\sqrt{t^2 - n_1^2 R_+^2}} \right] = \frac{\text{Re}\tilde{\Gamma}_1(\eta_1^>)}{\sqrt{t^2 - n_1^2 R_+^2}}, \quad (1.114)$$

where $\eta_1^> = \eta_1^+ \big|_{\delta=0} = \left[xt + i(z + z_0)\sqrt{t^2 - n_1^2 R_+^2} \right] R_+^{-2}$.

The behavior of the secondary field in the first medium for the times $0 < t < t_{\text{ref}}$ essentially depends on the relation between the refractive indices for the first (n_1) and second (n_2) media.

For an arbitrary point in the first medium, both of the roots entering $\tilde{\Gamma}_1(\eta_1^<)$ are real (see (1.110)) if $n_1 < n_2$. Consequently, we have $\text{Im}\tilde{\Gamma}_1(\eta_1^<) = 0$, and the secondary field given by (1.113) is zero ($G^1(x, z, t) \equiv 0$) up to the moment of arrival of the reflected wave.

In the case that $n_1 > n_2$, a more detailed analysis of the function $n_2^2 - (\eta_1^<)^2$ is required. Let us use the following notation: $x/R_+ = \sin\theta$, $(z + z_0)/R_+ = \cos\theta$, $n_2/n_1 = \sin\theta_{\text{tot}}$, where θ_{tot} stands for the angle of total internal reflection [41, 62]. Let us also introduce the parameter $\tau = \arccos(t/t_{\text{ref}})$ such that $\cos\tau = t/t_{\text{ref}}$ and the principal branch $0 < \tau < \pi$ of this function is chosen. Then we arrive at

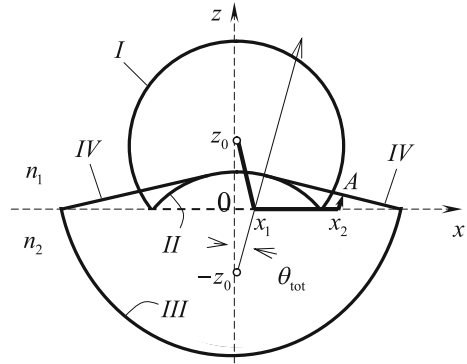
$$\begin{aligned} n_2^2 - (\eta_1^<) ^2 &= n_1^2 \left\{ \left[\frac{x}{R_+} \sqrt{1 - \left(\frac{t}{n_1 R_+} \right)^2} + \frac{(z + z_0)}{R_+} \frac{t}{n_1 R_+} \right]^2 - \left(1 - \frac{n_2^2}{n_1^2} \right) \right\} \\ &= n_1^2 [\cos^2(\tau - \theta) - \cos^2\theta_{\text{tot}}] = n_1^2 \sin(\theta_{\text{tot}} - \theta + \tau) \sin(\theta_{\text{tot}} + \theta - \tau). \end{aligned} \quad (1.115)$$

Since we have $0 < \theta, \theta_{\text{tot}}, \tau < \pi/2$ for the space-time domain considered, then the arguments of the sine functions in (1.115) find themselves within the interval $(-\pi/2, \pi)$. Therefore, the function given by (1.115) has two roots, $\tau_1 = \theta - \theta_{\text{tot}}$ and $\tau_2 = \theta + \theta_{\text{tot}}$, corresponding to the time points $t_1 = t_{\text{ref}} \cos(\theta - \theta_{\text{tot}})$ and $t_2 = t_{\text{ref}} \cos(\theta + \theta_{\text{tot}})$. There is no difficulty to show (the trajectory $z_0 x_1 x_2 A$ in Fig. 1.12) that

$$t_1 = n_1 z_0 / \cos\theta_{\text{tot}} + n_2 [x - (z + z_0) \text{tg}\theta_{\text{tot}}] + n_1 z / \cos\theta_{\text{tot}} = t_{\text{dif}},$$

where t_{dif} is the time of arrival of the so-called side wave [41] (or diffraction wave [62]) at the observation point located in the first medium in the region $\theta > \theta_{\text{tot}}$. For $\theta < \theta_{\text{tot}}$, the variable τ_1 goes to the unphysical sheet of the function $\arccos(t/t_{\text{ref}})$, and the side wave does not occur in this region. By virtue of the causality principle, for the times $t < t_{\text{dif}}$, there is no secondary field and so the other zero (τ_2) is of no importance ($t_2 < t_1$).

Fig. 1.12 The wave fronts of the field generated by a pulsed line current located near a planar interface for $n_1 > n_2$: the primary (I), reflected (II), transmitted (III), and side (IV) waves; z_0 x_1 x_2 A is the trajectory determining the time of arrival of the side wave at the point A , θ_{tot} is the angle of total internal reflection



Let us find the value of $\text{sign} [n_2^2 - (\eta_1^<)^2]$ for $t_{\text{dif}} < t < t_{\text{ref}}$ in the region $\theta > \theta_{\text{tot}}$. Here the following relationships for the arguments of the sine functions in (1.113) are valid:

$$\begin{aligned}
 & -\pi/2 < \theta_{\text{tot}} - \theta < \theta_{\text{tot}} - \theta + \tau < \theta_{\text{tot}} - \theta + \tau_1 = 0, \\
 & 0 < 2\theta_{\text{tot}} = \theta_{\text{tot}} + \theta - \tau_1 < \theta_{\text{tot}} + \theta - \tau < \theta_{\text{tot}} + \theta < \pi,
 \end{aligned}$$

which means that $n_2^2 - (\eta_1^<)^2 < 0$. Considering that $\text{Im} \sqrt{n_1^2 - (\eta_1^<)^2} = 0$, we have $\text{Im} \tilde{F}_1(\eta_1^<) \neq 0$.

Thus for $n_1 > n_2$ and $t_{\text{dif}} < t < t_{\text{ref}}$, in the region $\theta > \theta_{\text{tot}}$, the side wave is generated, which is given by the function in (1.113).

From (1.113), (1.114), through the substitutions $\tilde{F}_1 \rightarrow 1$, $z + z_0 \rightarrow z - z_0$, we arrive at the following expression for the function G^0 characterizing the primary field:

$$G^0(x, z, t) = \left[0 \text{ for } 0 < t < t_0; 1 / \sqrt{t^2 - t_0^2} \text{ for } t_0 < t \right], \tag{1.116}$$

where $t_0 = n_1 R_-$ is the time of arrival of the primary wave at the observation point in the first medium.

1.4.4 The Field in the Second Medium

Denote the roots of the equation (1.107) by η_2^- and η_2^+ . Then the integral in (1.105) takes the form

$$G^2(x, z, t) = \frac{i}{2} \lim_{\delta \rightarrow 0} \left[\operatorname{Res}_{\eta = \eta_2^-} \frac{\tilde{\Gamma}_2(\eta)}{x\eta + z_0\sqrt{n_1^2 - \eta^2} - z\sqrt{n_2^2 - \eta^2} - t_-} - \operatorname{Res}_{\eta = \eta_2^+} \frac{\tilde{\Gamma}_2(\eta)}{-x\eta + z_0\sqrt{n_1^2 - \eta^2} - z\sqrt{n_2^2 - \eta^2} + t_+} \right] = \frac{i}{2} \lim_{\delta \rightarrow 0} \left[\frac{\tilde{\Gamma}_2(\eta_2^-)}{x - Z(\eta_2^-)} + \frac{\tilde{\Gamma}_2(\eta_2^+)}{x + Z(\eta_2^+)} \right], \quad (1.117)$$

where

$$Z(\eta) = \left[\frac{z_0}{\sqrt{n_1^2 - \eta^2}} - \frac{z}{\sqrt{n_2^2 - \eta^2}} \right] \eta \quad \text{and} \quad \tilde{\Gamma}_2(\eta) = \frac{\tilde{\Gamma}_2(\eta)}{\sqrt{n_1^2 - \eta^2}}. \quad (1.118)$$

The roots η_2^\pm can be written explicitly, in the form of the solutions of the associated algebraic quartic equations. However, they are too lengthy because of six parameters entering (1.107) and will not be used. In view of the causality principle, we have $G^2(x, z, t) \equiv 0$ for $t < t_{\text{tr}}$, where t_{tr} is the time of arrival of the transmitted wave at the observation point in the second medium. For $t > t_{\text{tr}}$, the roots η_2^\pm are complex and, as evident from (1.107), in terms of (1.111), we have $\eta_2^- = (\eta_2^+)^*$. Therefore, taking into account formulas in (1.112), we obtain for $t > t_{\text{tr}}$

$$G^2(x, z, t) = \frac{i}{2} \lim_{\delta \rightarrow 0} \left[\frac{\tilde{\Gamma}_2(\eta_2^+)}{x + Z(\eta_2^+)} - \frac{\tilde{\Gamma}_2(\eta_2^{+*})}{x - Z(\eta_2^{+*})} \right] = \frac{i}{2} \lim_{\delta \rightarrow 0} \left\{ \left[\frac{\tilde{\Gamma}_2(\eta_2^+)}{x + Z(\eta_2^+)} \right] - \left[\frac{\tilde{\Gamma}_2(\eta_2^+)}{x + Z(\eta_2^+)} \right]^* \right\} \\ = - \lim_{\delta \rightarrow 0} \operatorname{Im} \frac{\tilde{\Gamma}_2(\eta_2^+)}{x + Z(\eta_2^+)} = - \operatorname{Im} \frac{\tilde{\Gamma}_2(\eta_2^>)}{x + Z(\eta_2^>)}, \quad (1.119)$$

where $\eta_2^> = \eta_2^+ \big|_{\delta=0}$.

1.4.5 Discussion and Conclusion

Formulas (1.93) and (1.116) for the primary field, formulas (1.113) and (1.114) for the secondary field in the first medium, as well as formula (1.119) for the secondary field in the second medium coincide with the corresponding expressions derived with the help of CHM in [54].

The main result of our study is a new representation for the field generated by a pulsed line current in a two-media configuration in the form of the integrals along finite contours (1.104), (1.105). This method, like the CHM, is applicable to the problems of pulsed electromagnetic radiation from linear sources in the medium

formed by an arbitrary finite number N of homogeneous parallel layers with permittivity ε_j and permeability μ_j , $j = 1, 2, \dots, N$. In this case, for the field in the layers, the integrals along the contour enveloping the interval $(-n_{\max}, n_{\max})$, where $n_{\max} = \max\{n_1, n_2, \dots, n_N\}$, are similar to representations (1.104), (1.105). Two methods for calculating these integrals are possible.

The first way is to reduce them, by the Cauchy theorem, to a sum of residues at the poles of the integrand. These poles are determined by the roots of algebraic equations that coincide with the equations for the modified Cagniard contours [54]. Therefore this technique, being alternative to the CHM in an analytical sense, is equivalent to it in a calculating sense.

Another way is to estimate numerically the integrals in (1.104), (1.105). It is easy to show that they can be reduced to the integrals over the interval $(0, n_{\max})$. For example, the field in the first medium (1.104) can be represented for $n_2 > n_1$, $t > t_{\text{ref}}$ in the following form:

$$G^1(x, z, t) = -\frac{2}{\pi}t \left[\int_0^{n_1} f(\eta) \tilde{\Gamma}_{\sim 1}(\eta) d\eta + \frac{2}{n_2^2 - n_1^2} \int_{n_1}^{n_2} f(\eta) \sqrt{n_2^2 - \eta^2} d\eta \right],$$

where

$$f(\eta) = \frac{x^2\eta^2 + (n_1^2 - \eta^2)(z + z_0)^2 - t^2}{\left[x^2\eta^2 - (n_1^2 - \eta^2)(z + z_0)^2 + t^2 \right]^2 - 4x^2t^2\eta^2}, \quad \tilde{\Gamma}_{\sim 1}(\eta) = \frac{\tilde{\Gamma}_1(\eta)}{\sqrt{n_1^2 - \eta^2}}.$$

We can use a standard integration procedure of any mathematical package to calculate G^1 by this formula. Comparison of the data obtained by this way with the explicit expression given by (1.114) has demonstrated high efficiency and accuracy of the approach.

The key point of the CHM is the solution of the algebraic equation determining the modified Cagniard contour. To do this, the iterative numerical methods are used. The greatest difficulty inherent in these methods is to choose the initial value that is close enough to the required zero of the equation [63]. In the paper [54], such an initial approximation has been proposed for the medium consisting of N isotropic layers. The efficiency of the iterative method has been demonstrated for $N = 2$. For more complex structures containing anisotropic layers, the initial approximation of this kind is unknown. (The CHM allows us to study as yet the simplest situation where the source and the observation point are located on the boundary of an anisotropic medium [64].)

Our approach, being free from such complications, reduces the calculation of the field generated by a line dipole in a multilayered medium to the standard procedure of numerical integration along a finite interval.

1.5 Transition Radiation of a Longitudinal Magnetic Dipole in the Case of Diffuse Interface

In the overwhelming number of studies on *transition radiation* (see reviews [65, 66]) the medium models are used in which spatial properties change abruptly. The transition radiation that occurs when an electric charge moves across the diffuse interface of two media was first discussed in the paper [67]. The authors used the *asymmetric Epstein layer* of relative permittivity $\varepsilon(z) = 1 + \alpha/[1 + \exp(-dz)]$. This model problem is of particular value since its exact solution, if it were obtained, would allow one to determine the conditions under which the transition radiation on the diffuse boundary can be considered approximately the same as in the case of the sharp boundary. This problem in [67] is reduced to the solution of the one-dimensional scalar Helmholtz equation with the coefficient involving $\sqrt{\varepsilon}(1/\sqrt{\varepsilon})''$ instead of $\varepsilon(z)$. Since the analytic solution of this equation is not known, the authors were forced to make an additional assumption about smallness of $\text{grad } \varepsilon(z)$. Furthermore, the variation of the function $\varepsilon(z)$ is supposed to be also small since the authors of [67] limited themselves by the case of the radiation from an ultrarelativistic charge at frequencies larger than optical frequencies. These assumptions, weakening the initial rigorous formulation, do not allow one to establish a reliable *criterion of the interface 'sharpness'*, which is free from those restrictions.

In this section, for the medium like an asymmetric Epstein layer, we will show the possibility to solve rigorously the problem of the transition radiation of a longitudinal magnetic dipole [68].

1.5.1 Problem Formulation and Solution

We assume that a longitudinal magnetic dipole with moment $\vec{m} = m_z \vec{z}$ is moving with constant velocity $\vec{V} = V_z \vec{z}$, $V_z > 0$ in an isotropic layered medium with constant relative permeability μ and relative permittivity

$$\varepsilon(z) = \varepsilon_1 + \frac{\varepsilon_2 - \varepsilon_1}{1 + \exp(-\tau z)}; \quad \tau > 0. \quad (1.120)$$

For simplicity, we assume that the condition of *Vavilov-Cherenkov radiation* is not satisfied. The initial equations are [67]:

$$\begin{aligned} \text{rot } \vec{H} &= \frac{\partial \vec{D}}{\partial t} + \vec{J}^{(m)}, \quad \text{rot } \vec{E} = -\frac{\partial \vec{B}}{\partial t}, \quad \vec{D} = \varepsilon \varepsilon_0 \vec{E}, \quad \vec{B} = \mu \mu_0 \vec{H}, \\ \vec{J}^{(m)} &= \sqrt{1 - V_z^2/c^2} m_z [\nabla_t \times \vec{z}] \delta(\vec{r}_\perp) \delta(z - V_z t), \quad c = (\sqrt{\varepsilon_0 \mu_0})^{-1}, \quad \nabla_t = \frac{\partial}{\partial x} \vec{x} + \frac{\partial}{\partial y} \vec{y}, \\ \vec{r}_\perp &= x \vec{x} + y \vec{y}. \end{aligned}$$

For a plane-layered isotropic medium, these equations with a harmonic time dependence can be reduced [41] to two scalar equations

$$\begin{aligned} \left(\varepsilon \frac{\partial}{\partial z} \frac{1}{\varepsilon} \frac{\partial}{\partial z} + k^2 + \nabla_t^2 \right) ([\nabla_t \times \vec{z}] \cdot \vec{H}_\omega^t) &= \varepsilon \frac{\partial}{\partial z} \frac{1}{\varepsilon} \left(\nabla_t \cdot \vec{J}_\omega^{(m)} \right), \\ \left(\frac{\partial^2}{\partial z^2} + k^2 + \nabla_t^2 \right) ([\nabla_t \times \vec{z}] \cdot \vec{E}_\omega^t) &= -i\omega\mu\mu_0 \left([\nabla_t \times \vec{z}] \cdot \vec{J}_\omega^{(m)} \right), \end{aligned}$$

where $k^2 = k_0^2 \varepsilon \mu$, $k_0 = \omega \sqrt{\varepsilon_0 \mu_0}$, and \vec{E}_ω^t , \vec{H}_ω^t are the projections of the corresponding vectors on the plane xOy . In this case,

$$\begin{aligned} (\nabla_t \cdot \vec{E}_\omega^t) &= \frac{1}{i\omega\varepsilon\varepsilon_0} \left((\nabla_t \cdot \vec{J}_\omega^{(m)}) - \frac{\partial}{\partial z} ([\nabla_t \times \vec{z}] \cdot \vec{H}_\omega^t) \right), \\ (\nabla_t \cdot \vec{H}_\omega^t) &= \frac{1}{i\omega\mu\mu_0} \frac{\partial}{\partial z} ([\nabla_t \times \vec{z}] \cdot \vec{E}_\omega^t), \quad E_{z\omega} = \frac{1}{i\omega\varepsilon} ([\nabla_t \times \vec{z}] \cdot \vec{H}_\omega^t), \\ H_{z\omega} &= -\frac{1}{i\omega\mu\mu_0} ([\nabla_t \times \vec{z}] \cdot \vec{E}_\omega^t). \end{aligned}$$

Since the problem is homogeneous in time and in the direction perpendicular to the velocity of the dipole, we represent all the functions in Maxwell's equations in the form of the Fourier integrals

$$\vec{F}(\vec{r}, t) = \int \vec{F}_{\omega, \vec{k}}(z) \exp[i(\vec{k} \cdot \vec{r}_\perp) - i\omega t] d\omega d\vec{k}; \quad \vec{k} = \kappa_x \vec{x} + \kappa_y \vec{y}, \quad \vec{r} = \vec{r}_\perp + z\vec{z}$$

with

$$\vec{J}_{\omega, \vec{k}}^{(m)}(z) = \frac{i\sqrt{1 - V_z^2/c^2}}{(2\pi)^3 V_z} m_z \exp(i\omega z/V_z) [\vec{k} \times \vec{z}].$$

Then, by introducing the scalar function $u(z) = ([\vec{k} \times \vec{z}] \cdot \vec{E}_{\omega, \vec{k}}^t)$, we arrive at the equation

$$\begin{aligned} \left[\frac{d^2}{dz^2} + k_0^2 \varepsilon(z) \mu - \kappa^2 \right] u(z) &= A \exp(i\omega z/V_z); \\ A &= \frac{\sqrt{4\pi\varepsilon_0\omega\mu\mu_0}}{(2\pi)^3 V_z} \sqrt{1 - V_z^2/c^2} m_z \kappa^2. \end{aligned} \tag{1.121}$$

The spectral components of the field can be recovered from the solution of this equation by the formulas

$$\begin{aligned}\vec{E}_{\omega, \vec{\kappa}}^t &= -\frac{i}{\kappa^2}[\vec{\kappa} \times \vec{z}]u(z), & E_{z, \omega, \vec{\kappa}} &= 0, & \vec{H}_{\omega, \vec{\kappa}}^t &= -\frac{i}{\sqrt{4\pi\epsilon_0\omega\mu\mu_0}\kappa^2}\vec{\kappa}\frac{d}{dz}u(z), \\ H_{z, \omega, \vec{\kappa}} &= -\frac{1}{\sqrt{4\pi\epsilon_0\omega\mu\mu_0}}u(z).\end{aligned}$$

The magnetic field vector lies in the radiation plane, which passes through the vectors $\vec{\kappa}$ and \vec{V} , that is, the field is an H -polarized wave [69].

We now seek the solution of homogeneous (1.121). By introducing a new independent variable $x = -\exp(-\tau z)$ and a new function $y(x) = (-x)^{-v}u(z)$ [12, 67], we pass from (1.121) to the following hypergeometric equation

$$x(1-x)y''(x) + [s - (a+b+1)x]y'(x) - aby(x) = 0 \quad (1.122)$$

with the parameters $a = v + \lambda$, $b = v - \lambda$, $s = 1 + 2v$,
 $v = (\tau)^{-1}\sqrt{\kappa^2 - \omega^2\epsilon_2\epsilon_0\mu\mu_0}$, $\lambda = (\tau)^{-1}\sqrt{\kappa^2 - \omega^2\epsilon_1\epsilon_0\mu\mu_0}$,
 $\text{Re}\sqrt{\kappa^2 - \omega^2\epsilon_{1,2}\epsilon_0\mu\mu_0} \geq 0$.

Let us choose two linearly independent solutions of (1.122) that are regular at zero [70]:

$$y_1(x) = F(a, b, s, x), \quad y_5(x) = x^{1-s}F(a+1-s, b+1-s, 2-s, x),$$

where $F(\dots)$ is the hypergeometric function. The corresponding solutions of homogeneous (1.121) are

$$\begin{aligned}u_1(z) &= \exp(-v\tau z)F(v + \lambda, v - \lambda, 1 + 2v, -\exp(-\tau z)), \\ u_5(z) &= \exp(v\tau z)F(\lambda - v, -\lambda - v, 1 - 2v, -\exp(-\tau z)).\end{aligned}$$

The general solution of inhomogeneous (1.121) is given by

$$\begin{aligned}\frac{W}{A}u(z) &= -u_1(z) \int u_5(z) \exp(i\omega z/V_z) dz + u_5(z) \int u_1(z) \exp(i\omega z/V_z) dz \\ &+ C_1 u_1(z) + C_2 u_5(z)\end{aligned} \quad (1.123)$$

with the Wronskian $W = \lim_{z \rightarrow \infty} (u_1 u_5' - u_1' u_5) = 2\tau v$. To calculate these integrals we use the *Barnes representation* [70]

$$F(a, b, s, \xi) = \frac{1}{2\pi i} \frac{\Gamma(s)}{\Gamma(a)\Gamma(b)} \int_{\gamma-i\infty}^{\gamma+i\infty} \frac{\Gamma(a+t)\Gamma(b+t)\Gamma(-t)}{\Gamma(s+t)} (-\xi)^t dt,$$

where $|\arg(-\xi)| < \pi$, $\gamma > 0$ and all the poles of $\Gamma(-t)$ are located to the right of the contour of integration. Let us introduce the notation $\sigma = i\omega/V_z\tau$, $\zeta = \tau z$ and consider the case where $z < 0$. Then,

$$\begin{aligned}
 I_1 &= \int u_5(z) \exp(i\omega z/V_z) dz \\
 &= \frac{1}{\tau} \int F(\lambda - v, -\lambda - v, 1 - 2v, -\exp(-\zeta)) \exp[(\sigma + v)\zeta] d\zeta \\
 &= \frac{1}{2\pi i \tau} \frac{\Gamma(1 - 2v) \exp[(\sigma + v)\zeta]}{\Gamma(\lambda - v) \Gamma(-\lambda - v)} \int_{\gamma - i\infty}^{\gamma + i\infty} \frac{\Gamma(\lambda - v + t) \Gamma(-\lambda - v + t) \Gamma(-t)}{\Gamma(1 - 2v + t) (\sigma + v - t)} \exp(-\zeta t) dt.
 \end{aligned}$$

The integrand allows us to close the integration contour in the left half-plane $\text{Re } t < \gamma$. Upon calculating the residues at the poles $t_n = -n - \lambda + v$, $t'_m = -m + \lambda + v$, $n, m = 0, 1, 2, \dots$ and $t^+ = \sigma + v$, we obtain

$$\begin{aligned}
 I_1 &= \frac{1}{\tau} \frac{\exp(\sigma\zeta) \Gamma(1 - 2v)}{\Gamma(\lambda - v) \Gamma(-\lambda - v)} \left\{ \exp(\lambda\zeta) \sum_{n=0}^{\infty} \frac{(-1)^n \Gamma(-2\lambda - n) \Gamma(-v + \lambda + n)}{n! \Gamma(1 - v - \lambda - n) (\sigma + \lambda + n)} \exp(n\zeta) \right. \\
 &\quad + \exp(-\lambda\zeta) \sum_{n=0}^{\infty} \frac{(-1)^n \Gamma(2\lambda - n) \Gamma(-v - \lambda + n)}{n! \Gamma(1 - v + \lambda - n) (\sigma - \lambda + n)} \exp(n\zeta) \\
 &\quad \left. - \frac{\Gamma(\lambda + \sigma) \Gamma(-\lambda + \sigma) \Gamma(-\sigma - v)}{\Gamma(1 + \sigma - v)} \exp(-\sigma\zeta) \right\}.
 \end{aligned}$$

Similarly,

$$\begin{aligned}
 I_2 &= \int u_1(z) \exp(i\omega z/V_z) dz = \frac{1}{\tau} \int F(v + \lambda, v - \lambda, 1 + 2v, -\exp(-\zeta)) \exp[(\sigma - v)\zeta] d\zeta \\
 &= \frac{1}{2\pi i \tau} \frac{\Gamma(1 + 2v) \exp[(\sigma - v)\zeta]}{\Gamma(v + \lambda) \Gamma(v - \lambda)} \int_{\gamma - i\infty}^{\gamma + i\infty} \frac{\Gamma(v + \lambda + t) \Gamma(v - \lambda + t) \Gamma(-t)}{\Gamma(1 + 2v + t) (\sigma - v - t)} \exp(-\zeta t) dt.
 \end{aligned}$$

Upon calculating the residues at the poles $t_n = -n - \lambda - v$, $t'_m = -m + \lambda - v$, $n, m = 0, 1, 2, \dots$, and $t^- = \sigma - v$ in the half-plane $\text{Re } t < \gamma$, we obtain

$$\begin{aligned}
 I_2 &= \frac{1}{\tau} \frac{\exp(\sigma\zeta) \Gamma(1 + 2v)}{\Gamma(v + \lambda) \Gamma(v - \lambda)} \left\{ \exp(\lambda\zeta) \sum_{n=0}^{\infty} \frac{(-1)^n \Gamma(-2\lambda - n) \Gamma(v + \lambda + n)}{n! \Gamma(1 + v - \lambda - n) (\sigma + \lambda + n)} \exp(n\zeta) \right. \\
 &\quad + \exp(-\lambda\zeta) \sum_{n=0}^{\infty} \frac{(-1)^n \Gamma(2\lambda - n) \Gamma(v - \lambda + n)}{n! \Gamma(1 + v + \lambda - n) (\sigma - \lambda + n)} \exp(n\zeta) \\
 &\quad \left. - \frac{\Gamma(\lambda + \sigma) \Gamma(\sigma - \lambda) \Gamma(-\sigma + v)}{\Gamma(1 + \sigma + v)} \exp(-\sigma\zeta) \right\}.
 \end{aligned}$$

Applying the formula $\pi(-1)^{n+1} = \sin(\pi\alpha) \Gamma(\alpha + 1 - n) \Gamma(-\alpha + n)$ [70], we find that

$$\begin{aligned}
\frac{W}{A}u(z) = & -u_1(z)\exp(\sigma\zeta)\frac{\Gamma(1-2\nu)}{\tau\Gamma(\lambda-\nu)\Gamma(-\lambda-\nu)}\left\{-\exp(\lambda\zeta)S_1(\zeta)\frac{\sin[\pi(\nu+\lambda)]}{\sin(2\pi\lambda)}\right. \\
& + \left.\exp(-\lambda\zeta)S_2(\zeta)\frac{\sin[\pi(\nu-\lambda)]}{\sin(2\pi\lambda)} - \frac{\Gamma(\lambda+\sigma)\Gamma(-\lambda+\sigma)\Gamma(-\sigma-\nu)}{\Gamma(1+\sigma-\nu)}\exp(-\sigma\zeta)\right\} \\
& + u_5(z)\exp(\sigma\zeta)\frac{\Gamma(1+2\nu)}{\tau\Gamma(\nu+\lambda)\Gamma(\nu-\lambda)}\left\{-\exp(\lambda\zeta)S_1(\zeta)\frac{\sin[\pi(\lambda-\nu)]}{\sin(2\pi\lambda)}\right. \\
& - \left.\exp(-\lambda\zeta)S_2(\zeta)\frac{\sin[\pi(\lambda+\nu)]}{\sin(2\pi\lambda)} - \frac{\Gamma(\lambda+\sigma)\Gamma(-\lambda+\sigma)\Gamma(-\sigma+\nu)}{\Gamma(1+\sigma+\nu)}\exp(-\sigma\zeta)\right\} \\
& + C_1u_1(z) + C_2u_5(z),
\end{aligned} \tag{1.124}$$

where

$$\begin{aligned}
S_1(\zeta) &= \sum_{n=0}^{\infty} \frac{(-1)^n \Gamma(-\nu+\lambda+n)\Gamma(\nu+\lambda+n)}{n!\Gamma(1+2\lambda+n)(\sigma+\lambda+n)} \exp(n\zeta) \quad \text{and} \\
S_2(\zeta) &= \sum_{n=0}^{\infty} \frac{(-1)^n \Gamma(\nu-\lambda+n)\Gamma(-\nu-\lambda+n)}{n!\Gamma(1-2\lambda+n)(\sigma-\lambda+n)} \exp(n\zeta).
\end{aligned}$$

The linearly independent solutions u_1 and u_5 are regular for positive z . We are interested in $z < 0$, therefore, let us continue these solutions analytically into this domain [70]: $u_1 = \Gamma_{13}u_3 + \Gamma_{14}u_4$, $u_5 = \Gamma_{53}u_3 + \Gamma_{54}u_4$. Here

$$\begin{aligned}
\Gamma_{13} &= \frac{\Gamma(1+2\nu)\Gamma(-2\lambda)}{\Gamma(\nu-\lambda+1)\Gamma(\nu-\lambda)}, & \Gamma_{14} &= \frac{\Gamma(1+2\nu)\Gamma(2\lambda)}{\Gamma(\nu+\lambda+1)\Gamma(\nu+\lambda)}, \\
\Gamma_{53} &= \frac{\Gamma(1-2\nu)\Gamma(-2\lambda)}{\Gamma(-\nu-\lambda+1)\Gamma(-\nu-\lambda)}, & \Gamma_{54} &= \frac{\Gamma(1-2\nu)\Gamma(2\lambda)}{\Gamma(-\nu+\lambda+1)\Gamma(-\nu+\lambda)}.
\end{aligned}$$

By substituting the above expressions into (1.124), we obtain for $z < 0$

$$u(z) = u^m(z) + u^r(z), \tag{1.125}$$

where

$$\begin{aligned}
\frac{W}{A}u^m(z) &= \frac{\nu}{\tau\lambda}\exp(\sigma\zeta)\left\{-u_4(z)\exp(\lambda\zeta)S_1(\zeta)\frac{\Gamma(1+2\lambda)}{\Gamma(\lambda-\nu)\Gamma(\nu+\lambda)}\right. \\
& \quad \left.+ u_3(z)\exp(-\lambda\zeta)S_2(\zeta)\frac{\Gamma(1-2\lambda)}{\Gamma(-\lambda-\nu)\Gamma(\nu-\lambda)}\right\}, \\
\frac{W}{A}u^r(z) &= \frac{1}{\tau}u_3(z)\{\Gamma_{13}[\Gamma(\sigma,\lambda,-\nu) + \tau C_1] - \Gamma_{53}[\Gamma(\sigma,\lambda,\nu) - \tau C_2]\} \\
& \quad + \frac{1}{\tau}u_4(z)\{\Gamma_{14}[\Gamma(\sigma,\lambda,-\nu) + \tau C_1] - \Gamma_{54}[\Gamma(\sigma,\lambda,\nu) - \tau C_2]\}, \\
\Gamma(\sigma,\lambda,\nu) &= \frac{\Gamma(1+2\nu)\Gamma(\sigma+\lambda)\Gamma(\sigma-\lambda)\Gamma(-\sigma+\nu)}{\Gamma(\nu+\lambda)\Gamma(\nu-\lambda)\Gamma(1+\sigma+\nu)}.
\end{aligned}$$

With $z \rightarrow -\infty$ we have $u_3(z) \approx \exp(\lambda\zeta)$, $u_4(z) \approx \exp(-\lambda\zeta)$, consequently

$$u^m(z) \approx -\frac{\sqrt{4\pi\epsilon_0\omega\mu\mu_0m_z}}{(2\pi)^3V_z}\kappa^2\sqrt{1-V_z^2/c^2}\frac{\exp(i\omega z/V_z)}{\kappa^2-\omega^2\epsilon_1\epsilon_0\mu\mu_0+\omega^2/V_z^2},$$

i.e. for $z \rightarrow -\infty$ the term $u^m(z)$ changes into the self field of the longitudinal magnetic dipole [69]. The term $u^r(z)$ represents the radiation field. For propagating waves, the inequality $k_0^2\epsilon_{1,2}\mu > \kappa^2$ holds; choosing the root branch $\arg\sqrt{\kappa^2-k_0^2\epsilon_{1,2}\mu} = -\pi/2$, we have

$$v = -\frac{i}{\tau}\sqrt{\omega^2\epsilon_2\epsilon_0\mu\mu_0-\kappa^2}, \quad \lambda = -\frac{i}{\tau}\sqrt{\omega^2\epsilon_1\epsilon_0\mu\mu_0-\kappa^2}.$$

Consequently, for $z \rightarrow -\infty$, $u_3(z)$ is the wave outgoing to $-\infty$, while $u_4(z)$ is the wave incoming from $-\infty$. Since the latter should not exist, the coefficient at $u_4(z)$ must be zero:

$$\Gamma_{14}[\Gamma(\sigma, \lambda, -v) + \tau C_1] = \Gamma_{54}[\Gamma(\sigma, \lambda, v) - \tau C_2]. \tag{1.126}$$

Another condition for the constants C_1 and C_2 we obtain from the representation (1.123) for the total field for $z > 0$. In this case, $\exp(-\zeta) < 1$ in the integral I_1 , which allows us to close the contour of integration in the half-plane $\text{Re}t > \gamma$, where the poles $t_n = n$, $n = 0, 1, 2, \dots$ are located. As a result we have for $z > 0$

$$\begin{aligned} \frac{W}{A}u(z) &= -u_1(z)\frac{\exp[(\sigma+v)\zeta]\Gamma(1-2v)}{\Gamma(\lambda-v)\Gamma(-\lambda-v)\tau}\sum_{n=0}^{\infty}\frac{(-1)^n\Gamma(\lambda-v+n)\Gamma(-\lambda-v+n)}{n!\Gamma(1-2v+n)(\sigma+v-n)}e^{-n\zeta} \\ &+ u_5(z)\frac{\exp[(\sigma-v)\zeta]\Gamma(1+2v)}{\Gamma(v+\lambda)\Gamma(v-\lambda)\tau}\sum_{n=0}^{\infty}\frac{(-1)^n\Gamma(v+\lambda+n)\Gamma(v-\lambda+n)}{n!\Gamma(1+2v+n)(\sigma-v-n)} \\ &+ C_1u_1(z) + C_2u_5(z). \end{aligned}$$

With $z \rightarrow \infty$, $u_1 \approx \exp(-v\zeta)$ is the wave outgoing to $+\infty$, while $u_5 \approx \exp(v\zeta)$ is the wave incoming from $+\infty$. That is why the coefficient at $u_5(z)$ must be zero, $C_2 = 0$, and (1.126) turns into

$$\begin{aligned} C_1 &= [\Gamma_{54}\Gamma(\sigma, \lambda, v) - \Gamma_{14}\Gamma(\sigma, \lambda, -v)]\frac{1}{\Gamma_{14}\tau} \\ &= -\frac{\Gamma(1+v+\lambda)\Gamma(\sigma+\lambda)\Gamma(-\sigma+v)\Gamma(-\sigma-v)}{\tau\Gamma(2v)\Gamma(\lambda-v)\Gamma(1-\sigma+\lambda)}. \end{aligned}$$

If we introduce, by analogy with [67], the function

$$v(v, \lambda, \sigma, \exp(-\zeta)) = F(-v + \lambda, -v - \lambda, 1 - 2v, -\exp(-\zeta)) \\ \times \frac{\Gamma(1 + 2v)}{\Gamma(v - \lambda)\Gamma(v + \lambda)} \sum_{n=0}^{\infty} \frac{(-1)^n \Gamma(v - \lambda + n)\Gamma(v + \lambda + n)}{n!\Gamma(1 + 2v + n)(-\sigma + v + n)} \exp(-n\zeta),$$

then, for $z > 0$ the field can be written as

$$u(z) = \frac{A}{2\tau^2 v} \exp(\sigma\zeta) \{-v[v, -\lambda, \sigma, \exp(-\zeta)] + v[-v, -\lambda, \sigma, \exp(-\zeta)]\} \\ - \frac{A}{\tau^2} \frac{\Gamma(v + \lambda)\Gamma(1 + v + \lambda)}{\Gamma(1 + 2v)\Gamma(1 + 2\lambda)} \Gamma(-\sigma, -v, \lambda) u_1(z), \quad (1.127)$$

while for $z < 0$ it is

$$u(z) = \frac{A}{2\tau^2 \lambda} \exp(\sigma\zeta) \{-v[\lambda, v, -\sigma, \exp(\zeta)] + v[-\lambda, v, -\sigma, \exp(\zeta)]\} \\ - \frac{A}{\tau^2} \frac{\Gamma(v + \lambda)\Gamma(1 + v + \lambda)}{\Gamma(1 + 2v)\Gamma(1 + 2\lambda)} \Gamma(\sigma, -\lambda, v) u_3(z). \quad (1.128)$$

In what follows, we will be interested only in the radiation field away from the boundary ($|z| \gg 1/\tau$). From (1.128) we obtain for this field

$$u^{\text{rad}}(z) = -\frac{A}{\tau^2} \times \begin{cases} \Gamma(\sigma, \lambda, v) \exp(\lambda\zeta); & z < 0 \\ \Gamma(-\sigma, v, \lambda) \exp(-v\zeta); & z > 0, \end{cases} \quad (1.129)$$

where

$$\Gamma(\sigma, \lambda, v) = \frac{\Gamma(1 + v + \lambda)\Gamma(\sigma + \lambda)\Gamma(\sigma - \lambda)\Gamma(-\sigma + v)}{\Gamma(1 + 2\lambda)\Gamma(v - \lambda)\Gamma(1 + v + \sigma)}.$$

The energy of the forward radiation into the half-space $z > 0$ is [69]

$$W_2^r = \frac{m_z^2 (1 - V_z^2/c^2) \mu \mu_0}{4\pi^2 V_z^2 \tau^4} \int_0^{\infty} d\omega \int_0^{\infty} \omega \kappa^2 |\Gamma(-\sigma, v, \lambda)|^2 \sqrt{\omega^2 \varepsilon_2 \varepsilon_0 \mu \mu_0 - \kappa^2} d\kappa^2, \quad (1.130)$$

where the integration is performed over the domain $\kappa^2 < \omega^2 \varepsilon_2 \varepsilon_0 \mu \mu_0$, which corresponds to the waves propagating in the right half-space away from the boundary. For such κ , complex conjugation of the parameters v and μ gives $v^* = -v$, $\lambda^* = -\lambda$. Taking into account the properties of the gamma function $\Gamma^*(z) = \Gamma(z^*)$, $\Gamma(z)\Gamma(1 - z) = \pi/\sin(\pi z)$, we obtain

$$|\Gamma(-\sigma, v, \lambda)|^2 = \frac{\pi (\lambda^2 - v^2) \sin(2\pi v) \sin[\pi(\lambda - v)] \sin[\pi(\sigma - \lambda)]}{2v (\sigma^2 - v^2)(\sigma^2 - \lambda^2) \sin[\pi(v + \lambda)] \sin[\pi(\sigma + \lambda)]} \times \frac{1}{\sin[\pi(\sigma - v)] \sin[\pi(\sigma + v)]}. \tag{1.131}$$

Formulas (1.127)–(1.131) are valid for arbitrary values of the parameter τ , which characterizes the degree of boundary diffusiveness.

1.5.2 The Criterion of the Interface ‘Sharpness’

Let us consider the transition to the sharp interface: $\tau \rightarrow \infty$. The expansion of (1.131) in the power series in the small parameter $1/\tau$ requires the smallness of the absolute values of $2v$, $\lambda - v$, $\sigma - \lambda$, $\sigma + \lambda$, $\sigma - v$, $\sigma + v$, $\lambda + v$, which can be expressed via four independent values: $\sigma \pm v$, $\sigma \pm \lambda$. Denote

$$L_1^\pm = \frac{2\pi}{\tau|\sigma \pm \lambda|} = \frac{2\pi}{\left| \frac{\omega}{v_c} \mp \sqrt{k_0^2 \epsilon_{1\mu} - \kappa^2} \right|}, \quad L_2^\pm = \frac{2\pi}{\tau|\sigma \pm v|} = \frac{2\pi}{\left| \frac{\omega}{v_c} \mp \sqrt{k_0^2 \epsilon_{2\mu} - \kappa^2} \right|}$$

and suppose the following inequalities hold:

$$2\pi/\tau \ll L_1^\pm, \quad 2\pi/\tau \ll L_2^\pm. \tag{1.132}$$

Then we have

$$\frac{\sin(2\pi v) \sin[\pi(\lambda - v)] \sin[\pi(\sigma - \lambda)]}{\sin[\pi(v + \lambda)] \sin[\pi(\sigma + \lambda)] \sin[\pi(\sigma - v)] \sin[\pi(\sigma + v)]} = \frac{2v(\sigma - \lambda)(\lambda - v)}{\pi(v + \lambda)(\sigma + \lambda)(\sigma^2 - v^2)} \left[1 + \frac{1}{3}\pi^2(\sigma + v)(\sigma - v + 2\lambda) + \dots \right]$$

and for $\tau \rightarrow \infty$

$$|\Gamma(-\sigma, v, \lambda)|^2 = \frac{(\lambda - v)^2}{(\sigma + \lambda)^2(\sigma^2 - v^2)^2}. \tag{1.133}$$

Substituting this formula into (1.130), we obtain the expression for the radiation energy, which coincides exactly with the results given in [69] for the case of a sharp boundary.

In evaluating the sharpness of the interface between two media an important role is played by the notion of *the radiation-forming region*. In the case of a diffuse interface, the radiation can be considered approximately the same as in the case of a

sharp interface if the characteristic width of the transition boundary layer Δz is much smaller than the length of the radiation-forming region. During the qualitative evaluation [69] based on the determination of the distance at which the field of a moving source and the radiation field, moving away from the boundary, are separated, the following conditions were obtained

$$\Delta z \ll L_1^-, \quad \Delta z \ll L_2^+. \quad (1.134)$$

They are equivalent to the conditions in (1.132) ($\tau = 2\pi/\Delta z$). Here, L_1^- and L_2^+ are the lengths of the radiation-forming regions for the radiation moving away from the interface in the first and second media, respectively.

These two conditions are not enough to transfer from the general solution (1.131) to the solution (1.133) for a sharp boundary. Two additional conditions in (1.132) estimate the distance from the boundary, at which the field of the source and the radiation field incoming on the boundary are separated. Since $L_{1,2}^+ > L_{1,2}^-$, the conditions under which the interface between two media can be considered sharp, are:

$$\Delta z \ll L_1^-, \quad \Delta z \ll L_2^-. \quad (1.135)$$

The error of the condition (1.134), as compared with the exact condition (1.135), shows itself in the situation where the source moves from a less dense into a more dense medium.

In the paper [67], the following two inequalities were chosen as a criterion of the interface sharpness:

$$\Delta z \ll L_1^+, \quad \Delta z \ll L_2^+, \quad (1.136)$$

which were less restrictive than those in (1.135). Within the frequency range $\omega^2 \gg \omega_{pe}^2 = 4\pi N_e e^2/m_e$, considered in [67], where N_e is the electron density of the material and m_e is the electron mass, the conditions in (1.136) are sufficient for passing to the case of a sharp interface in the general relationships for the spectral density of the radiation, produced at small angles by an ultrarelativistic charge in the medium with a *diffuse boundary*.

Thus, we have formulated the problem of transition radiation for a medium with a diffuse boundary. For the first time, we obtained the rigorous analytical solution of this problem, without imposing any restrictions on the parameters of the model. By analyzing the passage to the limiting case of a sharp boundary in this solution, we have found an exact criterion of the interface ‘sharpness’ in the form of two inequalities (1.135). It substantially improves the well-known criterion (1.134) and, in contrast to another version of this criterion (1.136), does not require any restrictions on the frequency range, the charge velocity and the change in the permittivity $\varepsilon_2 - \varepsilon_1$.

1.6 The Biisotropic Epstein Transition Layer

The isotropic linear media having the properties of chirality and nonreciprocity are referred to as *biisotropic*. Chirality leads to circular dichroism and optical activity—the rotation of the polarization vector as in the *Faraday effect*, but regardless of the direction of propagation. If a medium has the property of nonreciprocity, the electric and magnetic field vectors are not orthogonal, and the phase velocity depends on the nonreciprocity index [71]. These effects may be important for new microwave applications [72, 73], if such a medium is realized.

Analysis of electromagnetic waves in inhomogeneous biisotropic media began from the works [74, 75]. The authors of these papers considered diffraction of a plane electromagnetic wave on a boundary of the half-space filled with a chiral medium. In [76] a similar problem was solved for the general case of an arbitrary *biisotropic medium*. In a number of works, a similar problem for homogeneous biisotropic layers has been studied in detail [77]. The papers [78, 79], which use numerical and analytical methods, are devoted to the investigation of the electromagnetic scattering in biisotropic stratified media with *continuously* varying parameters. Within the class of inhomogeneous biisotropic media, we proposed in [80] a model of the medium, for which one can write the *analytical* solution to the problem of the plane electromagnetic wave that propagates in this medium along the normal to the layers. Such a medium is a generalization to the biisotropic case of the known [12] isotropic Epstein transition layer, which describes a smooth transition in a plane-layered isotropic medium between the regions with different refractive indices n_1 and n_2 . In this section, we discuss in detail the methodology for obtaining this solution. The solution can be expressed in terms of the known hypergeometric series, as well as for the isotropic Epstein layer. The analytical expressions for the reflection and transmission coefficients have been derived, from which it follows that in such a medium the total transmission may occur.

1.6.1 Equations for the Electromagnetic Field in a Biisotropic Medium

It is well known that biisotropic media are marked by the magnetoelectric coupling, in which both electric and magnetic excitation leads simultaneously both to the electric and magnetic polarization. To describe the most general form of such a medium, in addition to the relative permittivity ε and the permeability μ , the nonreciprocity parameter χ and the chirality parameter κ are used. The constitutive equations for this medium, on the assumption of harmonic excitation (time dependence is defined by $\exp(-i\omega t)$), are as follows [71]:

$$\vec{D} = \varepsilon\varepsilon_0\vec{E} + \sqrt{\varepsilon_0\mu_0}(\chi + i\kappa)\vec{H}, \quad \vec{B} = \sqrt{\varepsilon_0\mu_0}(\chi - i\kappa)\vec{E} + \mu\mu_0\vec{H}, \quad (1.137)$$

where ε_0 , μ_0 are the permittivities of free space. For lossless media, the dimensionless parameters ε , μ , χ , and κ are the real functions of coordinates.

The Maxwell's equations, in view of (1.137), can be written as

$$\text{rot}\vec{E} = ik_0\eta_0\mu\vec{H} + k_0(\kappa + i\chi)\vec{E}, \quad \text{rot}\vec{H} = -ik_0\eta_0^{-1}\varepsilon\vec{E} + k_0(\kappa - i\chi)\vec{H}, \quad (1.138)$$

where $k_0 = \omega\sqrt{\varepsilon_0\mu_0}$, $\eta_0 = \sqrt{\mu_0/\varepsilon_0}$. By eliminating \vec{H} from (1.138), we arrive at the vector Helmholtz equation

$$\frac{1}{k_0}\text{rot}\frac{1}{\mu}\text{rot}\vec{E} - \text{rot}\frac{\kappa + i\chi}{\mu}\vec{E} - \frac{\kappa - i\chi}{\mu}\text{rot}\vec{E} + k_0\left(\frac{\kappa^2 + \chi^2}{\mu} - \varepsilon\right)\vec{E} = 0. \quad (1.139)$$

The parameters ε , χ , κ of the plane-parallel medium depend only on the coordinate z ; the magnetic permeability μ is considered constant in the whole space. The electromagnetic wave that propagates in such a medium perpendicularly to the layers, does not depend on the transversal coordinates x , y . Therefore, (1.139) is transformed into the system:

$$\begin{cases} \frac{d^2 E_x}{dz^2} - 2k_0\kappa\frac{dE_y}{dz} - k_0^2(\kappa^2 + \chi^2 - \varepsilon\mu)E_x - k_0\frac{d(\kappa + i\chi)}{dz}E_y = 0 \\ \frac{d^2 E_y}{dz^2} + 2k_0\kappa\frac{dE_x}{dz} + k_0\frac{d(\kappa + i\chi)}{dz}E_x - k_0^2(\kappa^2 + \chi^2 - \varepsilon\mu)E_y = 0 \\ E_z = 0. \end{cases} \quad (1.140)$$

Hence, introducing the auxiliary functions $E_{\pm} = E_x \pm iE_y$, we obtain two independent equations

$$\frac{d^2 E_{\pm}}{d\tilde{z}^2} \pm 2i\kappa\frac{dE_{\pm}}{d\tilde{z}} + [(n^2 - \kappa^2 - \chi^2) \pm i(\kappa' + i\chi')]E_{\pm} = 0, \quad (1.141)$$

where $\tilde{z} = k_0z$, $n = \sqrt{\varepsilon\mu}$, $\kappa' + i\chi' = d(\kappa + i\chi)/d\tilde{z}$. Removing the term with the first derivative by the substitution

$$E_{\pm} = \tilde{E}_{\pm}(z)e^{\mp}(\tilde{z}), \quad e^{\mp}(\tilde{z}) = \exp\left[\mp i \int \kappa(\tilde{z})d\tilde{z}\right], \quad (1.142)$$

we arrive at the following equation for the function $\tilde{E}_{\pm}(\tilde{z})$:

$$\frac{d^2 \tilde{E}_{\pm}}{d\tilde{z}^2} + (n^2 - \chi^2 \mp \chi')\tilde{E}_{\pm} = 0. \quad (1.143)$$

1.6.2 Problem Formulation and Solution

Consider the following version of the plane-layered medium

$$\begin{aligned} n^2(\tilde{z}) = \varepsilon(\tilde{z}) &= 0.5(1 + \tilde{n}^2) + 0.5(1 - \tilde{n}^2)\text{th}(\tilde{\tau}\tilde{z}), & \chi(\tilde{z}) &= 0.5\tilde{\chi}[1 - \text{th}(\tilde{\tau}\tilde{z})], \\ \kappa(\tilde{z}) &= 0.5\tilde{\kappa}[1 - \text{th}(\tilde{\tau}\tilde{z})], & \mu &= 1, & |\tilde{\chi}| &\leq \tilde{n}, & \tilde{\tau} &= \tau/k_0, \end{aligned} \quad (1.144)$$

which is the generalization of the known isotropic Epstein transition layer on the biisotropic case [12]. For $\tilde{z} = -\infty$, the inhomogeneous biisotropic medium (1.144) smoothly transits into a homogeneous biisotropic medium with the parameters \tilde{n}^2 , $\tilde{\chi}$, $\tilde{\kappa}$, while for $\tilde{z} = +\infty$ it transits into the isotropic medium with $\varepsilon = \mu = 1$, $\chi = \kappa = 0$. The value $\Delta = 2k_0/\tau$ can be considered an effective width of the transition layer (1.144), which describes the degree of diffusiveness of the boundary between the isotropic and biisotropic media.

In view of (1.144), (1.143) takes the form

$$\frac{d^2\tilde{E}_\pm}{d\tilde{z}^2} + n_\pm^2(\tilde{z})\tilde{E}_\pm = 0, \quad (1.145)$$

where

$$\begin{aligned} n_\pm^2(\tilde{z}) &= 1 - N \frac{\exp(-2\tilde{\tau}\tilde{z})}{1 + \exp(-2\tilde{\tau}\tilde{z})} - 4M_\pm \frac{\exp(-2\tilde{\tau}\tilde{z})}{[1 + \exp(-2\tilde{\tau}\tilde{z})]^2}; \\ N &= 1 - \tilde{n}^2 + \tilde{\chi}^2, & 4M_\pm &= -\tilde{\chi}(\tilde{\chi} \pm 2\tilde{\tau}). \end{aligned}$$

Let a plane linearly polarized electromagnetic wave of unit amplitude be incident from $\tilde{z} = +\infty$ on the biisotropic medium (1.144). The resulting electromagnetic field is to be found.

It is known [12] that solutions of the equations like the one in (1.145) can be represented as

$$\tilde{E}_\pm(\tilde{z}) = (\zeta')^{-1/2} \zeta^{\gamma/2} (1 - \zeta)^{(\alpha + \beta - \gamma + 1)/2} u(\zeta), \quad (1.146)$$

where $\zeta = -\exp(-2\tilde{\tau}\tilde{z})$, while the function $u(\zeta)$ is the general solution to the *hypergeometric Gauss equation*

$$\zeta(1 - \zeta) \frac{d^2u}{d\zeta^2} - [(\alpha + \beta + 1)\zeta - \gamma] \frac{du}{d\zeta} - \alpha\beta u = 0. \quad (1.147)$$

The parameters α , β , γ are representable through the parameters $\tilde{\tau}$, N , M_\pm of the model:

$$\alpha_{\pm} = \frac{1}{2} + \frac{1}{2}\sqrt{1 - 4M_{\pm}\tilde{\tau}^{-2}} + \frac{i}{2\tilde{\tau}}\left(1 - \sqrt{1 - N}\right),$$

$$\beta_{\pm} = \frac{1}{2} + \frac{1}{2}\sqrt{1 - 4M_{\pm}\tilde{\tau}^{-2}} + \frac{i}{2\tilde{\tau}}\left(1 + \sqrt{1 - N}\right).$$

Substituting N and M_{\pm} , we obtain

$$\alpha_{\pm} = 1 + \frac{1}{2\tilde{\tau}}\left[\pm\tilde{\chi} + i\left(1 - \sqrt{\tilde{n}^2 - \tilde{\chi}^2}\right)\right], \quad \beta_{\pm} = 1 + \frac{1}{2\tilde{\tau}}\left[\pm\tilde{\chi} + i\left(1 + \sqrt{\tilde{n}^2 - \tilde{\chi}^2}\right)\right],$$

$$\gamma = 1 + \frac{i}{\tilde{\tau}},$$
(1.148)

where the imaginary parts of the roots is nonnegative.

Equation (1.147) has three proper critical points $\zeta = 0, 1, \infty$, in the vicinity of which the two linearly independent solutions of this equation can be represented in the form of the converging hypergeometric series u_i , $i = 1, 2, 3, 4, 5, 6$ [70].

The transmitted wave should be outgoing as $\tilde{z} \rightarrow -\infty$, i.e. for $\zeta \rightarrow -\infty$. In the vicinity of an infinitely distant point of the complex plane ζ , the linearly independent solutions of (1.147) are

$$u_3 = (-\zeta)^{-\alpha}F(\alpha, \alpha - \gamma + 1, \alpha - \beta + 1, \zeta^{-1}),$$

$$u_4 = (-\zeta)^{-\beta}F(\beta, \beta - \gamma + 1, \beta - \alpha + 1, \zeta^{-1}),$$
(1.149)

where $-\zeta = \zeta \exp(i\pi)$ and $F(\alpha, \beta, \gamma, \zeta) \equiv {}_2F_1(\alpha, \beta, \gamma, \zeta)$ is a hypergeometric series [70].

The asymptotics as $\tilde{z} \rightarrow -\infty$ of the functions in (1.146)

$$\tilde{E}_{\pm}(z) = \exp[(1 - \gamma)\tilde{\tau}\tilde{z}][1 + \exp(-2\tilde{\tau}\tilde{z})]^{(\alpha_{\pm} + \beta_{\pm} - \gamma + 1)/2}u(\zeta)$$

that correspond to the solutions (1.149) are

$$\tilde{E}_{\pm}^{(3)}(\tilde{z}) \approx \exp[(\alpha_{\pm} - \beta_{\pm})\tilde{\tau}\tilde{z}], \quad \tilde{E}_{\pm}^{(4)}(\tilde{z}) \approx \exp[(\beta_{\pm} - \alpha_{\pm})\tilde{\tau}\tilde{z}].$$

Since $\alpha_{\pm} - \beta_{\pm} = -i\sqrt{\tilde{n}^2 - \tilde{\chi}^2}/\tilde{\tau}$ and $\sqrt{\tilde{n}^2 - \tilde{\chi}^2} > 0$, then $\tilde{E}_{\pm}^{(3)}$ corresponds to the waves outgoing to $\tilde{z} = -\infty$, while $\tilde{E}_{\pm}^{(4)}$ corresponds to the ones incoming from $\tilde{z} = -\infty$. Consequently, one should take as solutions the functions

$$\tilde{E}_{\pm}^{(3)}(z) = \exp[(1 - \gamma)\tilde{\tau}\tilde{z}][1 + \exp(-2\tilde{\tau}\tilde{z})]^{(\alpha_{\pm} + \beta_{\pm} - \gamma + 1)/2}u_3(\zeta),$$

whose behavior at $\tilde{z} \rightarrow +\infty$ ($\zeta \rightarrow 0$) is determined by the following *Kummer's formula* [70]:

$$u_3 = \frac{\Gamma(1-\gamma)\Gamma(\alpha_{\pm}+1-\beta_{\pm})}{\Gamma(1-\beta_{\pm})\Gamma(\alpha_{\pm}+1-\gamma)}u_1 - \frac{\Gamma(\gamma)\Gamma(1-\gamma)\Gamma(\alpha_{\pm}+1-\beta_{\pm})}{\Gamma(2-\gamma)\Gamma(\gamma-\beta_{\pm})\Gamma(\alpha_{\pm})}u_5, \quad (1.150)$$

where

$$u_1 = F(\alpha, \beta, \gamma, \zeta), u_5 = \zeta^{1-\gamma}F(\alpha - \gamma + 1, \beta - \gamma + 1, 2 - \gamma, \zeta),$$

and $\Gamma(\dots)$ is the gamma function. The asymptotics of the solutions of (1.145) that correspond to the functions u_1, u_5 are

$$\begin{aligned} \tilde{E}_{\pm}^{(1)}(\tilde{z}) &\approx \exp[(1-\gamma)\tilde{z}] = \exp(-i\tilde{z}), & \tilde{E}_{\pm}^{(5)}(\tilde{z}) &\approx \exp[(1-\gamma)\tilde{z}] \\ &\times [-\exp(-2\tilde{z})]^{1-\gamma} = (-1)^{1-\gamma}\exp[-(1-\gamma)\tilde{z}] = (-1)^{1-\gamma}\exp(i\tilde{z}). \end{aligned} \quad (1.151)$$

i.e. $\tilde{E}_{\pm}^{(1)}$ corresponds to the wave incoming from $\tilde{z} = +\infty$, while $\tilde{E}_{\pm}^{(5)}$ corresponds to the wave outgoing to $\tilde{z} = +\infty$. It follows from (1.150) that

$$\begin{aligned} &\frac{\Gamma(1-\beta_{\pm})\Gamma(\alpha_{\pm}+1-\gamma)}{\Gamma(1-\gamma)\Gamma(\alpha_{\pm}+1-\beta_{\pm})}\tilde{E}_{\pm}^{(3)}(\tilde{z}) \\ &= \tilde{E}_{\pm}^{(1)}(\tilde{z}) - \frac{\Gamma(\gamma)\Gamma(1-\beta_{\pm})\Gamma(\alpha_{\pm}+1-\gamma)}{\Gamma(2-\gamma)\Gamma(\gamma-\beta_{\pm})\Gamma(\alpha_{\pm})}(-1)^{\gamma-1}\tilde{E}_{\pm}^{(5)}(\tilde{z}). \end{aligned} \quad (1.152)$$

Since for $\tilde{z} \rightarrow +\infty$ the behavior of the functions $\tilde{E}_{\pm}^{(1)}(\tilde{z})$ and $(-1)^{\gamma-1}\tilde{E}_{\pm}^{(5)}(\tilde{z})$ are determined by the asymptotics (1.151) and for $\tilde{z} \rightarrow -\infty$ we have $\tilde{E}_{\pm}^{(3)}(\tilde{z}) \approx \exp(-i\sqrt{\tilde{n}^2 - \tilde{\chi}^2}\tilde{z})$, then these functions define the primary, reflected, and transmitted waves, respectively, while the factors in (1.152) are the transmission coefficients

$$T_{\pm} = \frac{\Gamma(1-\beta_{\pm})\Gamma(\alpha_{\pm}+1-\gamma)}{\Gamma(1-\gamma)\Gamma(\alpha_{\pm}+1-\beta_{\pm})} \quad (1.153)$$

and the reflection coefficients

$$R_{\pm} = \frac{\Gamma(\gamma-1)\Gamma(1-\beta_{\pm})\Gamma(\alpha_{\pm}+1-\gamma)}{\Gamma(1-\gamma)\Gamma(\gamma-\beta_{\pm})\Gamma(\alpha_{\pm})}. \quad (1.154)$$

The left and right parts of the equation (1.152) are two representations of the solutions of (1.145) $\tilde{E}_{\pm}(\tilde{z})$ for $\tilde{z} < 0$ and for $\tilde{z} > 0$, respectively.

1.6.3 Analysis of the Reflected and Transmitted Fields

As evident from (1.142) and (1.144), the electromagnetic field components can be written in the form

$$E_x = \frac{1}{2}(\tilde{E}_+ e^- + \tilde{E}_- e^+), \quad E_y = \frac{1}{2i}(\tilde{E}_+ e^- - \tilde{E}_- e^+),$$

where

$$e^\mp(\tilde{z}) = \exp\left\{\mp \frac{i}{2}\tilde{\kappa}[\tilde{z} - \tilde{\tau}^{-1} \ln(\exp(\tilde{\tau}\tilde{z}) + \exp(-\tilde{\tau}\tilde{z}))]\right\}.$$

Let us consider the field structure away from the region, whose dimensions are determined by the effective width of the layer, $|\tilde{z}| \gg \Delta$.

In the region $\tilde{z} \gg \Delta$, where the medium differs little from the isotropic one, we have

$$\begin{aligned} e^\mp(\tilde{z}) &= 1 + O[\exp(-2\tilde{\tau}\tilde{z})], \quad \tilde{E}_\pm \approx \exp(-i\tilde{z}) + R_\pm \exp(i\tilde{z}), \\ E_x &\approx \exp(-i\tilde{z}) + \frac{1}{2}(R_+ + R_-) \exp(i\tilde{z}), \quad E_y \approx \frac{1}{2i}(R_+ - R_-) \exp(i\tilde{z}). \end{aligned}$$

In other words, the primary wave is linearly polarized along the x -axis, while the reflected wave is

$$\vec{E}_{\text{ref}} = \left[\frac{1}{2}(R_+ + R_-)\vec{x} - \frac{i}{2}(R_+ - R_-)\vec{y} \right] \exp(i\tilde{z}) = \vec{E}_{\text{ref}}^r + \vec{E}_{\text{ref}}^l,$$

where $\vec{E}_{\text{ref}}^{r,l} = 0.5R^{r,l}(\vec{x} \pm i\vec{y}) \exp(i\tilde{z})$ (the upper sign is associated with the superscript r , the bottom sign is associated with l), \vec{E}_{ref}^r is the right-hand circularly polarized wave, \vec{E}_{ref}^l is the left-hand circularly polarized wave. The reflection coefficients of these two waves can be represented in the form

$$R^{r,l} = R_\mp = \frac{\tilde{\chi} \pm i(1 + \sqrt{\tilde{n}^2 - \tilde{\chi}^2})}{\tilde{\chi} \mp i(1 - \sqrt{\tilde{n}^2 - \tilde{\chi}^2})} \frac{\Gamma(\gamma - 1)}{\Gamma(1 - \gamma)} R, \quad (1.155)$$

where

$$R = \frac{\Gamma(\Delta[\tilde{\chi} - i(1 + \sqrt{\tilde{n}^2 - \tilde{\chi}^2})])\Gamma(\Delta[-\tilde{\chi} - i(1 + \sqrt{\tilde{n}^2 - \tilde{\chi}^2})])}{\Gamma(\Delta[\tilde{\chi} + i(1 - \sqrt{\tilde{n}^2 - \tilde{\chi}^2})])\Gamma(\Delta[-\tilde{\chi} + i(1 - \sqrt{\tilde{n}^2 - \tilde{\chi}^2})])}. \quad (1.156)$$

The reflected wave takes the form

$$\vec{E}_{\text{ref}} = \frac{R}{1 - 2\sqrt{\tilde{n}^2 - \tilde{\chi}^2} + \tilde{n}^2} \frac{\Gamma(2i\Delta)}{\Gamma(-2i\Delta)} [(\tilde{n}^2 - 1)\vec{x} - 2\tilde{\chi}\vec{y}] \exp(i\tilde{z}). \quad (1.157)$$

When passing to the sharp boundary ($\Delta = 0$), we get

$$\vec{E}_{\text{ref}} = [(1 - \tilde{n}^2)\vec{x} + 2\tilde{\chi}\vec{y}] \left(1 + 2\sqrt{\tilde{n}^2 - \tilde{\chi}^2} + \tilde{n}^2\right)^{-1} \exp(i\tilde{z}). \quad (1.158)$$

As seen from (1.157) and regardless of the width of the layer, when a plane linearly polarized wave is reflected from a biisotropic half-space with $n^2 = \varepsilon = \tilde{n}^2 > 1$, $\chi = \tilde{\chi} > 0$ ($\chi = \tilde{\chi} < 0$), the plane of polarization rotates anticlockwise (clockwise) by the angle of

$$\varphi_{\text{ref}} = \text{arctg} \frac{2\tilde{\chi}}{1 - \tilde{n}^2}, \quad (1.159)$$

if viewed in the direction of the reflected wave.

Expressions (1.158) and (1.159) differ from those obtained in [76] by the sign of $\tilde{\chi}$. It is interesting to note that the reflection from the biisotropic transition layer (1.144), in contrast to the isotropic layer, may disappear completely. Indeed, if the following conditions on the non-reciprocity parameter $\tilde{\chi} = \tilde{\chi}_0$, the refraction index $\tilde{n} = \tilde{n}_0$, and the layer width $\Delta = \Delta_0$ are satisfied:

$$\tilde{\chi}_0 = \sqrt{\tilde{n}_0^2 - 1}, \quad \tilde{\chi}_0 \Delta_0 = m; \quad m = 1, 2, \dots, \quad (1.160)$$

then the coefficients $R^{r,l}$ (1.155) vanish due to the second gamma function in the denominator (1.156).

With the increase in the width of the transition layer, the coefficients $R^{r,l}$ decay exponentially to zero. Using the known formulas for gamma functions, we obtain from (1.155)

$$|R^{r,l}| \approx \begin{cases} \exp(-2\pi\Delta) \text{ for } |\tilde{\chi}| < \tilde{\chi}_0, \\ \exp\left(-2\pi\Delta\sqrt{\tilde{n}^2 - \tilde{\chi}^2}\right) \text{ for } |\tilde{\chi}| > \tilde{\chi}_0 \end{cases}; \quad \Delta \gg 1, \quad (1.161)$$

where $\tilde{\chi}_0$ is defined by (1.160).

Consider the field transmitted into the biisotropic media, away from the transition layer. For $\tilde{z} \ll -\Delta$ we have

$$\begin{aligned}
e^{\mp}(\tilde{z}) &= \exp(\mp i\tilde{k}\tilde{z})[1 + O(\exp(2\tilde{\tau}\tilde{z}))], \quad \tilde{E}_{\pm} = T_{\pm}\tilde{E}_{\pm}^{(3)} \approx T_{\pm} \exp\left(-i\tilde{z}\sqrt{\tilde{n}^2 - \tilde{\chi}^2}\right), \\
E_x &\approx \frac{1}{2}\left[T_+ \exp\left(-i\tilde{z}\sqrt{\tilde{n}^2 - \tilde{\chi}^2} - i\tilde{k}\tilde{z}\right) + T_- \exp\left(-i\tilde{z}\sqrt{\tilde{n}^2 - \tilde{\chi}^2} + i\tilde{k}\tilde{z}\right)\right], \\
E_y &\approx \frac{1}{2i}\left[T_+ \exp\left(-i\tilde{z}\sqrt{\tilde{n}^2 - \tilde{\chi}^2} - i\tilde{k}\tilde{z}\right) - T_- \exp\left(-i\tilde{z}\sqrt{\tilde{n}^2 - \tilde{\chi}^2} + i\tilde{k}\tilde{z}\right)\right].
\end{aligned}$$

Hence, the wave transmitted through the transition layer is

$$\vec{E}_{\text{tr}} = \vec{E}_{\text{tr}}^r + \vec{E}_{\text{tr}}^l, \quad (1.162)$$

where $\vec{E}_{\text{tr}}^r = 0.5T^r(\vec{x} - i\vec{y}) \exp(-ik^+ \tilde{z})$ is the right-hand circularly polarized wave, while $\vec{E}_{\text{tr}}^l = 0.5T^l(\vec{x} + i\vec{y}) \exp(-ik^- \tilde{z})$ is the left-hand circularly polarized wave with the propagation constants $k^{\pm} = \sqrt{\tilde{n}^2 - \tilde{\chi}^2} \pm \tilde{k}$, $T^r = T_+$, $T^l = T_-$. It is easy to verify that

$$\frac{T^r}{T^l} = \frac{1 + \tilde{n} \left(\sqrt{1 - \tilde{\chi}^2} + i\tilde{\chi} \right)}{1 + \tilde{n} \left(\sqrt{1 - \tilde{\chi}^2} - i\tilde{\chi} \right)} = \frac{1 + \tilde{n} \exp(i\theta)}{1 + \tilde{n} \exp(-i\theta)} = \exp(i\psi_{\text{tr}}), \quad (1.163)$$

where $\tilde{\chi} = \tilde{\chi}/\tilde{n} = \sin \theta$, $|\theta| \leq \pi/2$, and

$$\psi_{\text{tr}} = \text{arctg} \frac{2\tilde{n} \sin \theta + \tilde{n}^2 \sin 2\theta}{1 + 2\tilde{n} \cos \theta + \tilde{n}^2 \cos 2\theta}, \quad |\psi_{\text{tr}}| \leq \pi - \text{arctg} \frac{2\tilde{n}}{\tilde{n}^2 - 1}. \quad (1.164)$$

Thus, regardless of the width of the transition layer Δ , the two waves, \vec{E}_{tr}^r and \vec{E}_{tr}^l , into which the primary wave is split (when transmitting into the biisotropic medium), have the amplitudes equal in absolute values and shifted in phase by ψ_{tr} . By representing T^l in the form

$$T^l = \frac{\Gamma\left(\Delta\left[\tilde{\chi} - i\left(1 + \sqrt{\tilde{n}^2 - \tilde{\chi}^2}\right)\right]\right) \Gamma\left(2i\Delta\sqrt{\tilde{n}^2 - \tilde{\chi}^2}\right) \sin\left(2\pi i\Delta\sqrt{\tilde{n}^2 - \tilde{\chi}^2}\right)}{\Gamma\left(\Delta\left[\tilde{\chi} + i\left(1 + \sqrt{\tilde{n}^2 - \tilde{\chi}^2}\right)\right]\right) \Gamma(-2i\Delta) \sin\left\{\pi\Delta\left[\tilde{\chi} + i\left(1 + \sqrt{\tilde{n}^2 - \tilde{\chi}^2}\right)\right]\right\}}, \quad (1.165)$$

we find that

$$|T^r| = |T^l| = \left| \frac{\Gamma\left(2i\Delta\sqrt{\tilde{n}^2 - \tilde{\chi}^2}\right)}{\Gamma(-2i\Delta)} \right| \cdot \left| \frac{\sin\left(2\pi i\Delta\sqrt{\tilde{n}^2 - \tilde{\chi}^2}\right)}{\sin\left\{\pi\Delta\left[\tilde{\chi} + i\left(1 + \sqrt{\tilde{n}^2 - \tilde{\chi}^2}\right)\right]\right\}} \right|, \quad (1.166)$$

and with no reflection (see (1.160)) we get $|T^r| = |T^l| = 1$. From notions of \vec{E}_{tr}^r and \vec{E}_{tr}^l , we can see that in this case all the energy of the primary wave is distributed between these two waves.

Thus, the isotropic Epstein transition layer has been generalized to the case of biisotropic medium. We have also found the explicit analytical solution to the problem of a linearly polarized wave normally incident onto the Epstein layer. The main results are as follows.

- The reflected wave does not depend on the chirality of the medium and has, regardless of the width Δ , the polarization shifted by an angle of φ_{ref} as compared to the case of the isotropic half-space with the same refraction index $n = \tilde{n}$.
- In a biisotropic half-space, the transmitted wave is split into the right-hand and the left-hand circularly polarized waves that are equal in amplitude and shifted in phase by an angle of ψ_{tr} .
- Regimes with zero reflection coefficients, which occur only in the case of the nonreciprocal medium ($\chi \neq 0$) with a diffuse boundary ($\Delta \neq 0$), have been revealed. They are determined by the following relationships between the nonreciprocity index $\tilde{\chi} = \tilde{\chi}_0$, the refraction index $\tilde{n} = \tilde{n}_0$, and the effective width of the transition layer $\Delta = \Delta_0 : \tilde{\chi}_0 = \sqrt{\tilde{n}_0^2 - 1}$, $\tilde{\chi}_0 \Delta_0 = m$, $m = 1, 2, \dots$

1.7 Negative Refraction in Isotropic Double-Negative Media

1.7.1 Negative Refraction Phenomenon in Homogeneous Double-Negative Media

In recent years, a growing number of publications have analyzed the unusual effects in the propagation of electromagnetic waves in the isotropic media with negative relative permittivity ε and permeability μ —the so-called double negative (DNG) or *left-handed media*. One such effect is the so-called *negative refraction* (NR), in which the beam refracted in a DNG medium lies in the plane of incidence on the same side of the normal to the interface, as the incident beam. At the same time, the wave vector of the transmitted wave is directed towards the interface. Since there is no isotropic media with $\varepsilon < 0$, $\mu < 0$ in the natural environment, then, in the experiments, the artificial composite materials in the form of three-dimensional periodic structures [81] are used as DNG media. As is well known [82], when an electromagnetic wave, whose wavelength is comparable to the period, is propagating through a periodic medium, the NR effect may also occur. In this case, it is impossible to introduce the effective permeabilities of the medium. Since in the experiments [83, 84] revealed the NR, the values of ε and μ , as well as the wavelength inside the material, were not determined directly and were assessed implicitly, the authors of some works expressed doubt [85] about that this effect is

inherent in a continuous isotropic medium with negative permittivity rather than it is caused by the periodicity of the material.

In this section, following the approach outlined in [86], we explore the possibility that the NR effect occurs in isotropic media. A model is suggested of an inhomogeneous isotropic flat-layered lossless medium comprising spatial regions with conventional and DNG media and smooth, monotonic transition between them. The analytical description of the plane electromagnetic wave propagating through such a medium is found, which demonstrates the NR effect in the region occupied by a DNG isotropic medium. For the first time, this is shown without any additional assumptions, as a direct consequence of Maxwell's equations and the energy conservation law. In addition, letting the size of the transition region to zero, we verify the conditions on a sharp interface between the conventional and the DNG homogeneous media. The proposed model has allowed us to obtain for the first time the accurate description for the electromagnetic field distribution in the vicinity of the point at which the medium permeabilities ε and μ are zero.

When an electromagnetic wave is passing from a conventional medium to a DNG medium, the NR effect can be seen from the standard *Fresnel formulas*, if we assume that they remain valid in the case where one of the media is DNG. If the E -polarized wave $\vec{E}^t = \exp(i\vec{k}_2\vec{r} - i\omega t)\vec{y}$, $\vec{k}_2 = \{k_2 \sin \theta_0, 0, -k_2 \cos \theta_0\}$, $\vec{r} = x\vec{x} + y\vec{y} + z\vec{z}$ is incident from the half-space $z > 0$ with the relative permeabilities $\varepsilon_2 > 0$ and $\mu_2 > 0$ at an angle θ_0 , the wave transmitted into the half-space $z < 0$ with the relative permeabilities $\varepsilon_1 > \varepsilon_2$, $\mu_1 > \mu_2$ has the form [87]

$$\vec{E}^t = \frac{2\mu_1 k_2 \cos \theta_0}{\mu_1 k_2 \cos \theta_0 + \mu_2 \sqrt{k_1^2 - k_2^2 \sin^2 \theta_0}} \exp(i\vec{k}_1\vec{r} - i\omega t)\vec{y}. \quad (1.167)$$

Its wave vector is

$$\vec{k}_1 = \left\{ k_2 \sin \theta_0, 0, -\sqrt{k_1^2 - k_2^2 \sin^2 \theta_0} \right\}; \quad k_j^2 = \omega^2 \varepsilon_0 \mu_0 \varepsilon_j \mu_j, \quad j = 1, 2, \quad (1.168)$$

while the average energy flux is

$$\vec{\Pi}_1 = |\vec{E}^t|^2 \vec{k}_1 / 2\mu_1 \mu_0 \omega. \quad (1.169)$$

In the denominator of (1.167) we have the sum of two positive values.

Let us pass to the case where $\varepsilon_1 < 0$ and $\mu_1 < 0$. Then the first term in the denominator in (1.167) will be negative; and for the denominator not to be zero, we should choose the second branch of the square root, that is replace $\sqrt{k_1^2 - k_2^2 \sin^2 \theta_0}$ by $-\sqrt{k_1^2 - k_2^2 \sin^2 \theta_0}$. At the same time, as it seen from (1.168), (1.169), the signs of the longitudinal component of \vec{k}_1 and the transversal component of $\vec{\Pi}_1$ change.

Thus, assuming that the Fresnel formulas for DNG media are valid, we arrive at the NR effect. However, this assumption is not obvious, since the boundary conditions for a pair of conventional media and the radiation condition suggesting that the wave vector of the transmitted wave is directed away from the interface are used in the derivation of these formulas from Maxwell's equations.

To avoid any suggestion, one should consider a medium without sharp boundaries, with the permeabilities being smooth (analytic) functions of the spatial variable and changing from positive to negative values.

1.7.2 A Model of Smoothly Inhomogeneous Flat-Layered Double Negative Medium. Solution of the Problem of Transmission of a Plane Wave

The propagation of electromagnetic waves in an inhomogeneous isotropic stratified lossless medium with the permeabilities $\varepsilon(z)$ and $\mu(z)$ is described for E -polarization by the equations:

$$\begin{aligned} \frac{\partial^2 E_y}{\partial x^2} + \frac{\partial^2 E_y}{\partial z^2} + \left(\mu \frac{d}{dz} \frac{1}{\mu} \right) \frac{\partial E_y}{\partial z} + \omega^2 \varepsilon \varepsilon_0 \mu \mu_0 E_y &= 0, \\ \frac{\partial E_y}{\partial z} = -i\omega \mu \mu_0 H_x, \quad \frac{\partial E_y}{\partial x} = i\omega \mu \mu_0 H_z, \quad E_x = E_z = H_y &= 0. \end{aligned} \quad (1.170)$$

The substitutions $\vec{E} \rightarrow \vec{H}$, $\vec{H} \rightarrow -\vec{E}$, $\varepsilon \varepsilon_0 \rightarrow \mu \mu_0$, $\mu \mu_0 \rightarrow \varepsilon \varepsilon_0$ in (1.170) yield the corresponding equations for H -polarization.

A plane E -polarized wave in such a medium can be represented as

$$E_y = Z(z) \exp(i\kappa_\infty x - i\omega t). \quad (1.171)$$

It follows from (1.170) that the unknown amplitude function $Z(z)$ is the solution of the following equation

$$\frac{d^2 Z}{dz^2} - \frac{1}{\mu} \frac{d\mu}{dz} \frac{dZ}{dz} + (\omega^2 \varepsilon \varepsilon_0 \mu \mu_0 - \kappa_\infty^2) Z = 0; \quad -\infty < z < \infty, \quad (1.172)$$

with the evident condition $z \rightarrow +\infty$. Here $\kappa_\infty = k_\infty \sin \theta$, $k_\infty = \omega \sqrt{\varepsilon_\infty \varepsilon_0 \mu_\infty \mu_0}$, θ is the angle of incidence of the primary wave, $\varepsilon_\infty = \varepsilon(\infty) > 0$, $\mu_\infty = \mu(\infty) > 0$.

In order to describe a smooth transition from the conventional medium ($\varepsilon > 0$, $\mu > 0$ for $z > 0$) to the DNG medium ($\varepsilon < 0$, $\mu < 0$ for $z < 0$), consider the following distribution of the permeabilities:

$$\varepsilon = \varepsilon_\infty \alpha(z), \quad \mu = \mu_\infty \alpha(z), \quad \alpha(z) = \text{th}(z/\Delta), \quad (1.173)$$

where the parameter $\Delta > 0$ defines the width of the transition region in the vicinity of the point $z = 0$. With the help of the substitution

$$Z(z) = \xi^q u(\xi), \quad \xi = \text{ch}^{-2}(z/\Delta), \quad q = \frac{1}{2} ik_\infty \Delta \cos \theta, \quad (1.174)$$

(1.172) is rearranged to the hypergeometric equation

$$\xi(1 - \xi) \frac{d^2 u}{d\xi^2} + [c - (a + b + 1)\xi] \frac{du}{d\xi} - abu = 0 \quad (1.175)$$

with the parameters

$$a = \frac{1}{2} ik_\infty \Delta (1 + \cos \theta), \quad b = -\frac{1}{2} ik_\infty \Delta (1 - \cos \theta), \quad c = 1 + ik_\infty \Delta \cos \theta. \quad (1.176)$$

The function $\xi(z)$ maps the strip $|\text{Im}z| < \pi\Delta/2$ of the complex plane z onto a double-sheeted Riemann surface of the complex variable ξ with the branch points $\xi = 0$ and $\xi = 1$. At the same time, the real semiaxis $(-\infty < z < 0)$ is mapped onto a segment $(0 < \xi < 1, \arg(1 - \xi) = 2\pi)$ of the first sheet, while the semiaxis $0 < z < \infty$ is mapped onto a segment $(1 > \xi > 0, \arg(1 - \xi) = 0)$ of the second sheet.

Following the general theory of hypergeometric equations [70], we find the desired solution of (1.175). It is known that the points $\xi = 0, 1, \infty$ are the singular points of this equation, in the vicinity of which the standard pairs of its linearly independent solutions are determined: u_1 and u_5 , u_2 and u_6 , u_3 and u_4 , respectively.

Let us choose as a solution of (1.175) in the vicinity of the point $\xi = 0$ of the first sheet of the Riemann surface (this point corresponds to the value $z = -\Delta \ln[(1 + \sqrt{1 - \xi})/\sqrt{\xi}]|_{\xi=0} = -\infty$) the function [70]

$$u_1 = F(a, b, c, \xi) = \sum_{n=0}^{\infty} \frac{(a)_n (b)_n}{(c)_n n!} \xi^n; \quad |\xi| \leq 1. \quad (1.177)$$

The alternative, with a choice of the function u_5 as a solution of (1.175) in the vicinity of the point $\xi = 0$ will be discussed below.

To obtain the solution of (1.175), and, therefore, in view of (1.174), of (1.172) as well, on the entire axis $-\infty < z < \infty$, one should perform the following steps: (i) to continue analytically, on the first sheet of the Riemann surface, the function $u_1(\xi)$ from the neighborhood of the point $\xi = 0$ to the neighborhood of the point $\xi = 1$; (ii) to go onto the second sheet in this neighborhood; (iii) to perform the analytic continuation on this sheet into a vicinity of the point $\xi = 0$.

Since for $z \rightarrow -\infty$ we have $\xi \approx 4 \exp(2z/\Delta) \approx 0$, $u_1 \approx 1$, then the function

$$Z \approx \xi^q \approx 4^q \exp(ik_\infty z \cos \theta) \quad (1.178)$$

in view of (1.171), will describe the field that is a plane wave, whose phase velocity is directed towards positive z as $z \rightarrow -\infty$. For the analysis of the field at small $|z|$, as seen from (1.174), the function $u_1(\xi)$ must be analytically continued into a neighborhood of the point $\xi = 1$. Given that the parameters (1.176) are related by the equation $c - a - b = 1$, to do this, one should use the equality [70]

$$F(a, b, a + b + 1, \xi) = \frac{\Gamma(c)}{\Gamma(a + 1)\Gamma(b + 1)} - \frac{\Gamma(c)}{\Gamma(a)\Gamma(b)} (1 - \xi) \sum_{n=0}^{\infty} \frac{(a + 1)_n (b + 1)_n}{(n + 1)_n n!} \times [h_n'' - \ln(1 - \xi)] (1 - \xi)^n; \quad |1 - \xi| < 1, \tag{1.179}$$

where $h_n'' = \psi(n + 1) + \psi(n + 2) - \psi(a + n + 1) - \psi(b + n + 1)$, $\Gamma(\dots)$ is the gamma function and $\psi(x)$ is the logarithmic derivative of the gamma function. Hence, it follows that when the point $\xi = 1$ is passed around once in the negative direction $(1 - \xi) \rightarrow (1 - \xi) \exp(-2\pi i)$, the following transformation occurs:

$$u_1(\xi) \rightarrow \tilde{u}_1(\xi) = u_1(\xi) - 2\pi i a b u_0 u_6(\xi); \quad |1 - \xi| < 1, \tag{1.180}$$

where $\tilde{u}_1(\xi)$ stands for the values of the solution $u_1(\xi)$ on the second sheet,

$$u_0 = \frac{\Gamma(c)}{\Gamma(a + 1)\Gamma(b + 1)}, \quad \text{and} \quad u_6(\xi) = (1 - \xi)F(a + 1, b + 1, 2, 1 - \xi).$$

Now continue the function $\tilde{u}_1(\xi)$ from the vicinity of the point $\xi = 1$ on the second sheet into the vicinity of the point $\xi = 0$, using the following Kummer's relationship [70]

$$u_6 = \Gamma_{61} u_1 + \Gamma_{65} u_5, \tag{1.181}$$

where

$$\Gamma_{61} = \frac{\Gamma(c + 1 - a - b)\Gamma(1 - c)}{\Gamma(1 - a)\Gamma(1 - b)}, \quad \Gamma_{65} = \frac{\Gamma(c + 1 - a - b)\Gamma(c - 1)}{\Gamma(c - a)\Gamma(c - b)}.$$

Upon the substitution of (1.181) into (1.180) we obtain for $|\xi| < 1$ on the second sheet of the *Riemann surface*:

$$\tilde{u}_1 = B_{11} u_1 + B_{15} u_5, \tag{1.182}$$

where

$$u_5 = \xi^{1-c} F(-a, -b, 2-c, \xi), \quad B_{11} = \frac{\text{ch}(\pi k_\infty \Delta) - \exp(-\pi k_\infty \Delta \cos \theta)}{\text{sh}(\pi k_\infty \Delta \cos \theta)},$$

$$B_{15} = 2\pi i \frac{(ik_\infty \Delta \cos \theta) \Gamma^2(ik_\infty \Delta \cos \theta)}{(0.5ik_\infty \Delta \sin \theta)^2 \Gamma^2[0.5ik_\infty \Delta (\cos \theta + 1)] \Gamma^2[0.5ik_\infty \Delta (\cos \theta - 1)]}.$$

Taking into account that $\xi \sim 4 \exp(-2z/\Delta) \sim 0$ as $z \rightarrow +\infty$, from equalities (1.174) and (1.182) we get

$$Z = \xi^q (B_{11} u_1 + B_{15} u_5) \approx 4^q B_{11} \exp(-ik_\infty z \cos \theta) + 4^{1-c+q} B_{15} \exp(ik_\infty z \cos \theta). \quad (1.183)$$

Since for $z \rightarrow +\infty$ the medium (1.173) goes into a conventional medium with constant permeabilities ε_∞ and μ_∞ , then the first term in (1.183) describes the wave incoming on the transition region while the second term describes the reflected wave. Expressions (1.178) and (1.183) are the principal terms in the expansions for large $|z|$ of the function $Z(z)$ for $z < 0$ and $z > 0$, respectively. Normalizing this function by the factor at the first exponent in (1.183), we obtain the coefficients of reflection and transmission for the plane wave (1.171) propagating through the transition layer (1.173):

$$R = 4^{1-c} B_{15} B_{11}^{-1}, \quad T = B_{11}^{-1}. \quad (1.184)$$

In view of the known formula $|\Gamma(iy)|^2 = \pi/y \sin(\pi y)$, we find their absolute values:

$$|R| = \frac{\text{ch}(\pi k_\infty \Delta) - \text{ch}(\pi k_\infty \Delta \cos \theta)}{\text{ch}(\pi k_\infty \Delta) - \exp(-\pi k_\infty \Delta \cos \theta)}, \quad |T| = \frac{\text{sh}(\pi k_\infty \Delta \cos \theta)}{\text{ch}(\pi k_\infty \Delta) - \exp(-\pi k_\infty \Delta \cos \theta)}. \quad (1.185)$$

1.7.3 Analysis of the Expressions for Fields

In going to a sharp boundary ($\Delta \rightarrow 0$), the coefficients behave, as they must [81], like $|R| \rightarrow 0$, $|T| \rightarrow 1$. As seen from (1.178), (1.183) and (1.184), the field components and the *Poynting vector* away from the transition region ($|z| \gg \Delta$) are as follows:

$$E_y = \exp[ik_\infty(-z \cos \theta + x \sin \theta) - i\omega t], \quad H_x = \eta_\infty \cos \theta E_y, \quad H_z = \eta_\infty \sin \theta E_y,$$

$$\vec{\Pi} = \frac{1}{2} \eta_\infty \{\sin \theta, 0, -\cos \theta\}, \quad \eta_\infty = \sqrt{\varepsilon_\infty / \mu_\infty} \quad (1.186)$$

for the incident wave,

$$\begin{aligned}
E_y &= R \exp[ik_\infty(z \cos \theta + x \sin \theta) - i\omega t], \quad H_x = -\eta_\infty \cos \theta E_y, \quad H_z = \eta_\infty \sin \theta E_y, \\
\vec{\Pi} &= \frac{1}{2} \eta_\infty |R|^2 \{\sin \theta, 0, \cos \theta\}
\end{aligned}
\tag{1.187}$$

for the reflected wave, and

$$\begin{aligned}
E_y &= T \exp[ik_\infty(z \cos \theta + x \sin \theta) - i\omega t], \quad H_x = \eta_\infty \cos \theta E_y, \quad H_z = -\eta_\infty \sin \theta E_y, \\
\vec{\Pi} &= \frac{1}{2} \eta_\infty |T|^2 \{-\sin \theta, 0, -\cos \theta\}
\end{aligned}
\tag{1.188}$$

for the transmitted wave.

It is easy to verify that the NR occurs for the wave transmitted into the region with negative ε and μ . The above relations are also valid for all z in the limiting case $\Delta \rightarrow 0$ of a sharp interface between the conventional and DNG homogeneous media. It follows from (1.186), (1.187) and (1.188) that the well-known continuity conditions are fulfilled on this boundary for the tangential components of \vec{E} and \vec{H} and for the normal components of \vec{D} and \vec{B} .

Now find, using (1.179), the field in the transition region between two media for small $|z|$. Since for $|z| \ll \Delta$ we have:

$$\begin{aligned}
\xi &= 1 - (z/\Delta)^2 + O[(z/\Delta)^4], \\
u_1(\xi) &= u_0 \left\{ 1 - ab[h_0'' - \ln(1 - \xi)](1 - \xi) + O[(1 - \xi)^2 \ln(1 - \xi)] \right\}, \\
\ln(1 - \xi) &= \ln(z/\Delta)^2 + 2\pi i \{0 \text{ for } z > 0; 1 \text{ for } z < 0\} + O[(z/\Delta)^2].
\end{aligned}$$

Then we arrive at the following representations for the field components:

$$\begin{aligned}
E_y &= u_0 \left\{ 1 - [abh^\pm + q - ab \ln z^2] \left(\frac{z}{\Delta}\right)^2 + O\left[\left(\frac{z}{\Delta}\right)^4 \ln\left(\frac{z}{\Delta}\right)\right] \right\} \\
&\quad \times \exp(i\kappa_\infty x - i\omega t), \\
H_x &= \frac{2u_0}{i\omega\mu_\infty\Delta} \left\{ [abh^\pm + q - ab \ln z^2] + O\left[\left(\frac{z}{\Delta}\right)^2 \ln\left(\frac{z}{\Delta}\right)\right] \right\} \\
&\quad \times \exp(i\kappa_\infty x - i\omega t), \\
H_z &= \eta_\infty \Delta \frac{u_0 \sin \theta}{z} \left\{ 1 - \left[abh^\pm + q - \frac{1}{3} - ab \ln z^2\right] \left(\frac{z}{\Delta}\right)^2 + O\left[\left(\frac{z}{\Delta}\right)^4 \ln\left(\frac{z}{\Delta}\right)\right] \right\} \\
&\quad \times \exp(i\kappa_\infty x - i\omega t),
\end{aligned}
\tag{1.189}$$

where

$$h^{\pm} = h_0'' + 2 \ln \Delta - 2\pi i \begin{cases} 0 & \text{for } z > 0 \\ 1 & \text{for } z < 0 \end{cases}.$$

As seen from these expansions, the components of the magnetic field intensity have singularities at $z = 0$: $H_x \approx \ln z$, $H_z \approx 1/z$. It is interesting that in the case of oblique incidence of the H -polarized wave onto the conventional flat-layered medium ($\varepsilon(z), \mu = \text{const} > 0$) in a neighborhood of zero of its dielectric permittivity, the respective components of the electric field have the same singularities, as has been shown in [88–90]. These singularities disappear at normal incidence, as well as for all angles θ when passing to a sharp interface. For arbitrary values of the model parameters, this is the case when taking into account the absorption in the medium.

Returning to formula (1.177), we would like to note that if the function u_5 , instead of u_1 , is chosen as a solution in the vicinity of the point $\xi = 0$, then we get the usual refraction law for a plane wave transmitted into a medium with negative ε and μ . As this takes place, we have the following expressions for absolute values of the reflection and transmission coefficients:

$$|R| = \frac{|\text{ch}(\pi k_{\infty} \Delta) - \exp(\pi k_{\infty} \Delta \cos \theta)|}{\text{ch}(\pi k_{\infty} \Delta) - \text{ch}(\pi k_{\infty} \Delta \cos \theta)}, \quad |T| = \frac{\text{sh}(\pi k_{\infty} \Delta \cos \theta)}{\text{ch}(\pi k_{\infty} \Delta) - \text{ch}(\pi k_{\infty} \Delta \cos \theta)}.$$

The nonphysical nature of these formulas is evident: at normal incidence, the coefficients become infinite. That is, the selection of the function u_5 results in the usual refraction law, but violates the energy conservation law.

Thus, we have shown the following. There exist two formal solutions of Maxwell's equations that describe the transmission of a plane wave from a conventional to a DNG media. One of them, which corresponds to the conventional refraction of a plane wave, is inconsistent with the energy conservation law and should be disregarded. The other, correct, solution obeying this law corresponds to the NR in the considered medium.

1.8 Distorting Coatings as an Alternative to Masking Coatings

1.8.1 Transformation Optics, Masking Coatings, Distorting Coatings

One of urgent problems in the applied radio physics is the radar camouflage with the help of special electromagnetic materials. In recent years, there was a conceptual and methodological breakthrough in this field [91]. A novel approach to this problem based on the idea of ‘wave flow’ was presented in 2006, in the works [92,

93]. Its physical meaning is that a masking coating has to bend the propagation direction of the electromagnetic radiation incident on it and cause the wave to pass round the masked region, after which the initial direction of propagation is restored maintaining the desired phase. Thus, the electromagnetic waves cannot penetrate into the area bounded by this coating; and any object being placed inside it becomes invisible. To find the parameters of such a coating, the method of coordinate transformations is used, which is based on the fact that Maxwell's equations are invariant with respect to arbitrary coordinate transformations, if the permittivity and the permeability are properly redefined. This approach received the name *transformation optics* (TO) [94]. With the help of the TO, a wide range of masking coatings has been studied [91]. The overwhelming majority of the works listed in the review [91] are based on numerical experiments; for three-dimensional models only the case of spherical surfaces has been studied analytically [95–98]. It has been shown that all these coatings are anisotropic gradient materials, whose permittivity and permeability tensor elements are less than unity. The problem of practical realization of such materials is extremely complex and far from being solved [99]. In addition to the inhomogeneity and anisotropy, for a number of important types of coatings, including spherical, the vanishing of the permittivity and permeability components on its inner surface is also required. That is, the surface consists entirely of critical points, which greatly complicates both the analysis of the corresponding electrodynamic problem and the practical implementation of such coatings.

In this section, we investigate the alternative way of the object masking—the distortion of its image, instead of using masking coatings [100].

1.8.2 Radical Distortion of Radar Image by Applying a Special Coating on the Metamaterial Surface

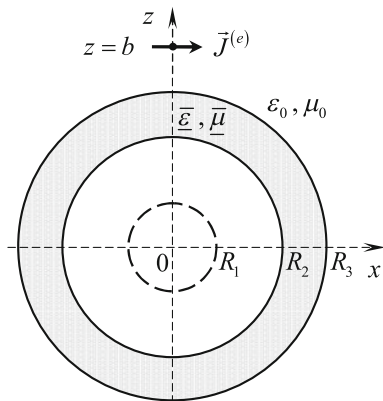
The geometry of the problem is shown in Fig. 1.13. In the spherical coordinate system r, ϑ, ϕ , a horizontal electric dipole is located at the point $\{r, \vartheta, \phi\} = \{b, 0, 0\}$, $b > R_3$; the time dependence is given by $\exp(-i\omega t)$.

Suppose one should construct the coating in the form of a spherical layer $R_2 < r < R_3$ on a perfectly conducting sphere of radius $r = R_2$. Following the TO methodology, let us consider the coordinate transformation

$$\tilde{r} = \frac{R_3 - R_1}{R_3 - R_2}(r - R_2) + R_1 = f(r), \quad \tilde{\vartheta} = \vartheta, \quad \tilde{\phi} = \phi, \quad (1.190)$$

which maps the spherical layer $0 < R_1 < R_2 \leq r \leq R_3$ onto the spherical layer $R_1 \leq \tilde{r} \leq R_3$. Under this transformation, Maxwell's equations for a homogeneous isotropic medium with permittivity ε_0 and permeability μ_0 pass into Maxwell's equations for the inhomogeneous anisotropic medium, whose relative permittivity and permeability are defined by the following diagonal tensors [101]:

Fig. 1.13 Geometry of the problem



$$\bar{\underline{\epsilon}} = \bar{\underline{\mu}} = \text{diag} \left\{ \frac{Q_{\tilde{\vartheta}} Q_{\tilde{\phi}}}{Q_{\tilde{r}}}, \frac{Q_{\tilde{r}} Q_{\tilde{\phi}}}{Q_{\tilde{\vartheta}}}, \frac{Q_{\tilde{r}} Q_{\tilde{\vartheta}}}{Q_{\tilde{\phi}}} \right\}, \quad (1.191)$$

where

$$Q_{\tilde{r}} = \frac{h_{\tilde{r}} \partial \tilde{r}}{h_r \partial r}, \quad Q_{\tilde{\vartheta}} = \frac{h_{\tilde{\vartheta}} \partial \tilde{\vartheta}}{h_{\vartheta} \partial \vartheta}, \quad Q_{\tilde{\phi}} = \frac{h_{\tilde{\phi}} \partial \tilde{\phi}}{h_{\phi} \partial \phi},$$

and $h_r = 1$, $h_{\vartheta} = r$, $h_{\phi} = r \sin \vartheta$, $h_{\tilde{r}} = 1$, $h_{\tilde{\vartheta}} = \tilde{r}$, $h_{\tilde{\phi}} = \tilde{r} \sin \tilde{\vartheta}$.

Thus we get for the permittivity and the permeability:

$$\bar{\underline{\epsilon}} = \bar{\underline{\mu}} = \text{diag} \{ \alpha_{rr}, \alpha_{\vartheta\vartheta}, \alpha_{\phi\phi} \},$$

$$\alpha_{rr} = \frac{R_3 - R_1}{R_3 - R_2} \left(1 - \frac{R_2 - R_1}{R_3 - R_1} \frac{R_3}{r} \right)^2, \quad \alpha_{\vartheta\vartheta} = \alpha_{\phi\phi} = \frac{R_3 - R_1}{R_3 - R_2}. \quad (1.192)$$

It is easily seen that $\bar{\underline{\epsilon}}$ and $\bar{\underline{\mu}}$ do not vanish in the layer $R_2 \leq r \leq R_3$.

Now we use the expansion in vector spherical harmonics $\vec{Y}_{lm}^{(j)}(\vartheta, \phi)$, where $j = -1, 0, 1$, to find the fields [102]. In the region $R_3 < r$, the total electromagnetic field is equal to the sum of the field of a horizontal electric dipole

$$\vec{E}^i = \frac{J^{(e)}}{4\sqrt{\pi} br} \sqrt{\frac{\mu_0}{\epsilon_0}} \sum_{l=1}^{\infty} \sum_{m=\pm 1} \sqrt{2l+1} \left\{ m \zeta_l^{(1)'}(k_0 b) \left[\psi_l'(k_0 r) \vec{Y}_{lm}^{(1)}(\vartheta, \phi) + \frac{\sqrt{l(l+1)}}{k_0 r} \psi_l(k_0 r) \vec{Y}_{lm}^{(-1)}(\vartheta, \phi) \right] - \zeta_l^{(1)}(k_0 b) \psi_l(k_0 r) \vec{Y}_{lm}^{(0)}(\vartheta, \phi) \right\}, \quad (1.193)$$

$$\begin{aligned} \vec{H}^i = & -\frac{J^{(e)}}{4\sqrt{\pi}br} \sum_{l=1}^{\infty} \sum_{m=\pm 1} \sqrt{2l+1} \left\{ m\zeta_l^{(1)'}(k_0b)\psi_l(k_0r)\bar{Y}_{lm}^{(0)}(\vartheta, \phi) \right. \\ & \left. + \zeta_l^{(1)}(k_0b) \left[\psi_l'(k_0r)\bar{Y}_{lm}^{(1)}(\vartheta, \phi) + \frac{\sqrt{l(l+1)}}{k_0r}\psi_l(k_0r)\bar{Y}_{lm}^{(-1)}(\vartheta, \phi) \right] \right\} \end{aligned} \quad (1.194)$$

and the scattered field

$$\begin{aligned} \vec{E}^s = & \frac{1}{r} \sum_{l=1}^{\infty} \sum_{m=\pm 1} \left\{ \tilde{E}_{lm}\zeta_l^{(1)}(k_0r)\bar{Y}_{lm}^{(0)}(\vartheta, \phi) \right. \\ & \left. - \tilde{H}_{lm} \left[\sqrt{\frac{\mu_0}{\varepsilon_0}}\zeta_l^{(1)'}(k_0r)\bar{Y}_{lm}^{(1)}(\vartheta, \phi) + \frac{\sqrt{l(l+1)}}{\omega\varepsilon_0r}\zeta_l^{(1)}(k_0r)\bar{Y}_{lm}^{(-1)}(\vartheta, \phi) \right] \right\}, \end{aligned} \quad (1.195)$$

$$\begin{aligned} \vec{H}^s = & \frac{1}{r} \sum_{l=1}^{\infty} \sum_{m=\pm 1} \left\{ \tilde{H}_{lm}\zeta_l^{(1)}(k_0r)\bar{Y}_{lm}^{(0)}(\vartheta, \phi) \right. \\ & \left. + \tilde{E}_{lm} \left[\sqrt{\frac{\varepsilon_0}{\mu_0}}\zeta_l^{(1)'}(k_0r)\bar{Y}_{lm}^{(1)}(\vartheta, \phi) + \frac{\sqrt{l(l+1)}}{\omega\mu_0r}\zeta_l^{(1)}(k_0r)\bar{Y}_{lm}^{(-1)}(\vartheta, \phi) \right] \right\}. \end{aligned} \quad (1.196)$$

Here, $k_0 = \omega\sqrt{\varepsilon_0\mu_0}$, $J^{(e)}$ is the amplitude of the elementary electric current, $\zeta_l^{(1)'}(k_0b) = d\zeta_l^{(1)}(x)/dx|_{x=k_0b}$, $\psi_l'(k_0r) = d\psi_l(x)/dx|_{x=k_0r}$. The *Riccati-Bessel functions* [103] can be expressed in terms of the cylindrical functions as

$$\psi_l(x) = \sqrt{\pi x/2} J_{l+1/2}(x), \quad \zeta_l^{(1)}(x) = \sqrt{\pi x/2} H_{l+1/2}^{(1)}(x).$$

Formulas (1.193) and (1.194) are given for $r < b$. For $b < r$, one should substitute $\zeta_l^{(1)} \leftrightarrow \psi_l$.

In the anisotropic layer $R_2 < r < R_3$, the total field can be represented as the expansion [104]:

$$\begin{aligned} \vec{E} = & \frac{1}{r} \sum_{l=1}^{\infty} \sum_{m=\pm 1} \left\{ \left[\hat{E}_{lm}^{(1)}f_l^{(1)}(r) + \hat{E}_{lm}^{(2)}f_l^{(2)}(r) \right] \bar{Y}_{lm}^{(0)}(\vartheta, \phi) \right. \\ & - \frac{1}{\omega\varepsilon_r} \left[\hat{H}_{lm}^{(1)}g_l^{(1)'}(r) + \hat{H}_{lm}^{(2)}g_l^{(2)'}(r) \right] \bar{Y}_{lm}^{(1)}(\vartheta, \phi) \\ & \left. - \frac{\sqrt{l(l+1)}}{\omega\varepsilon_r r} \left[\hat{H}_{lm}^{(1)}g_l^{(1)}(r) + \hat{H}_{lm}^{(2)}g_l^{(2)}(r) \right] \bar{Y}_{lm}^{(-1)}(\vartheta, \phi) \right\}, \end{aligned} \quad (1.197)$$

$$\begin{aligned}
\vec{H} = & \frac{1}{r} \sum_{l=1}^{\infty} \sum_{m=\pm 1} \left\{ \left[\widehat{H}_{lm}^{(1)} g_l^{(1)}(r) + \widehat{H}_{lm}^{(2)} g_l^{(2)}(r) \right] \widehat{Y}_{lm}^{(0)}(\vartheta, \phi) \right. \\
& + \frac{1}{\omega \mu_t} \left[\widehat{E}_{lm}^{(1)} f_l^{(1)'}(r) + \widehat{E}_{lm}^{(2)} f_l^{(2)'}(r) \right] \widehat{Y}_{lm}^{(1)}(\vartheta, \phi) \\
& \left. + \frac{\sqrt{l(l+1)}}{\omega \mu_r r} \left[\widehat{E}_{lm}^{(1)} f_l^{(1)}(r) + \widehat{E}_{lm}^{(2)} f_l^{(2)}(r) \right] \widehat{Y}_{lm}^{(-1)}(\vartheta, \phi) \right\},
\end{aligned} \tag{1.198}$$

where $f_l^{(j)}(r)$ are the independent solutions of the equation

$$\mu_r \frac{d}{dr} \frac{1}{\mu_t} \frac{df_l}{dr} + \left[\omega^2 \varepsilon_t \mu_r - \frac{l(l+1)}{r^2} \right] f_l = 0, \tag{1.199}$$

while $g_l^{(j)}(r)$ are the independent solutions of the equation

$$\varepsilon_r \frac{d}{dr} \frac{1}{\varepsilon_t} \frac{dg_l}{dr} + \left[\omega^2 \varepsilon_r \mu_t - \frac{l(l+1)}{r^2} \right] g_l = 0; \tag{1.200}$$

$$\varepsilon_r = \varepsilon_0 \alpha_{rr}, \quad \varepsilon_t = \varepsilon_0 \alpha_{\vartheta\vartheta} = \varepsilon_0 \alpha_{\phi\phi}, \quad \mu_r = \mu_0 \alpha_{rr}, \quad \mu_t = \mu_0 \alpha_{\vartheta\vartheta} = \mu_0 \alpha_{\phi\phi},$$

and $g_l^{(j)'}(r) = dg_l^{(j)}(r)/dr$, $f_l^{(j)'}(r) = df_l^{(j)}(r)/dr$. Taking into account (1.192), one can easily obtain the independent solutions of (1.199) and (1.200):

$$\begin{aligned}
f_l^{(1)} = g_l^{(1)} = \zeta_l^{(2)}(k_0 \widehat{r}), \quad f_l^{(2)} = g_l^{(2)} = \zeta_l^{(1)}(k_0 \widehat{r}); \\
\widehat{r} = \frac{R_3 - R_1}{R_3 - R_2} r - R_3 \frac{R_2 - R_1}{R_3 - R_2}.
\end{aligned} \tag{1.201}$$

The continuity conditions for the tangential components of the total field on the boundary $r = R_3$ yield:

$$\begin{aligned}
\widehat{H}_{lm}^{(1)} g_l^{(1)'}(R_3) + \widehat{H}_{lm}^{(2)} g_l^{(2)'}(R_3) &= \left[\widetilde{H}_{lm} \zeta_l^{(1)'}(k_0 R_3) \right. \\
&\quad \left. - \frac{J^{(e)} m}{4\sqrt{\pi} b} \sqrt{2l+1} \zeta_l^{(1)'}(k_0 b) \psi_l'(k_0 R_3) \right] k_0 \frac{\varepsilon_t}{\varepsilon_0}, \\
\widehat{E}_{lm}^{(1)} f_l^{(1)}(R_3) + \widehat{E}_{lm}^{(2)} f_l^{(2)}(R_3) &= \widetilde{E}_{lm} \zeta_l^{(1)}(k_0 R_3) - \frac{J^{(e)}}{4\sqrt{\pi} b} \sqrt{\frac{\mu_0}{\varepsilon_0}} \sqrt{2l+1} \zeta_l^{(1)}(k_0 b) \psi_l(k_0 R_3), \\
\widehat{H}_{lm}^{(1)} g_l^{(1)}(R_3) + \widehat{H}_{lm}^{(2)} g_l^{(2)}(R_3) &= \widetilde{H}_{lm} \zeta_l^{(1)}(k_0 R_3) - \frac{J^{(e)} m}{4\sqrt{\pi} b} \sqrt{2l+1} \zeta_l^{(1)'}(k_0 b) \psi_l(k_0 R_3), \\
\widehat{E}_{lm}^{(1)} f_l^{(1)'}(R_3) + \widehat{E}_{lm}^{(2)} f_l^{(2)'}(R_3) &= \left[\widetilde{E}_{lm} \zeta_l^{(1)'}(k_0 R_3) \right. \\
&\quad \left. - \frac{J^{(e)}}{4\sqrt{\pi} b} \sqrt{\frac{\mu_0}{\varepsilon_0}} \sqrt{2l+1} \zeta_l^{(1)'}(k_0 b) \psi_l'(k_0 R_3) \right] k_0 \frac{\mu_t}{\mu_0}.
\end{aligned}$$

While the conditions on the perfectly conducting sphere $r = R_2$ yield:

$$\widehat{E}_{lm}^{(1)} f_l^{(1)}(R_2) + \widehat{E}_{lm}^{(2)} f_l^{(2)}(R_2) = 0, \quad \widehat{H}_{lm}^{(1)} g_l^{(1)'}(R_2) + \widehat{H}_{lm}^{(2)} g_l^{(2)'}(R_2) = 0.$$

Solving the system of all these equations with respect to the unknown values $\widehat{E}_{lm}^{(1)}$, $\widehat{E}_{lm}^{(2)}$, $\widehat{H}_{lm}^{(1)}$, $\widehat{H}_{lm}^{(2)}$, and \tilde{E}_{lm} , \tilde{H}_{lm} we obtain, in particular,

$$\tilde{E}_{lm} = \frac{J^{(e)}}{4\sqrt{\pi}b} \sqrt{\frac{\mu_0}{\varepsilon_0}} \sqrt{2l+1} \zeta_l^{(1)}(k_0b) \frac{\psi_l(k_0R_1)}{\zeta_l^{(1)}(k_0R_1)}, \quad (1.202)$$

$$\tilde{H}_{lm} = \frac{J^{(e)}m}{4\sqrt{\pi}b} \sqrt{2l+1} \zeta_l^{(1)'}(k_0b) \frac{\psi_l'(k_0R_1)}{\zeta_l^{(1)'}(k_0R_1)}. \quad (1.203)$$

Substituting these values into (1.195), (1.196) gives the expression for the scattered field that results from the interaction of a horizontal electric dipole with a perfectly conducting sphere of radius R_2 , coated with a layer of a magneto-dielectric material of thickness $R_3 - R_2$ and with the permittivity and permeability given by (1.192). It is easy to see that outside the layer (that is for $r > R_3$), this field is exactly the same as the field generated by the same source and scattered by the perfectly conducting sphere of radius $R_1 < R_2$ [105].

Thus, by using a perfectly conducting sphere as an example, we have rigorously proved that the application of some special coating onto its surface allows one to obtain the scattered electromagnetic field that will be exactly the same as the field scattered by the perfectly conducting sphere of any smaller radius. At the same time, it is much easier to make such a *distorting coating*, since it does not require the vanishing of certain components of its permittivity and permeability, as in the case of a *masking coating*.

In [106], the authors demonstrate the possibility of a complete *replacement of the image* of the real object with the image of any other object without using the wave flow method (the so-called *illusion optics*). However, this complex procedure, based on the double application of the TO method, can be simulated only numerically.

1.9 Conclusion

In this chapter, analytical solutions have been obtained for the following electromagnetic problems associated with wave propagation.

- *Wave Propagation in a Homogeneous Medium Bounded by a Surface with Variable Impedance.* We proposed a more realistic compared to the known [8] model of electromagnetic wave propagation over a plane surface with impedance that varies smoothly in the given direction; we found the analytic representation for the field generated by a line current located above this plane; the case of rapidly varying impedance function $Z(x)$ (see (1.1)) has been considered

($\tau \gg 2k$); it is shown that the principal term in the asymptotic approximation for the obtained electromagnetic field coincides with the known expression derived in [8] for the case, where the surface impedance changes step-wise.

We constructed the exact Green's function of the Helmholtz equation for a plane waveguide with smoothly varying impedance of its wall. As in the previous problem, the coefficient $Z(x)$ in the boundary condition is an impedance analogue of the permittivity of the Epstein 'transition' layer. The obtained solution was used for the analysis of the field induced by a linear magnetic current in the gradient junction between two regular impedance waveguides. In the limiting case, this solution goes to a well-known expression for the field in the waveguide with the stepped impedance distribution. The error of adiabatic approximation for smoothly irregular waveguides has been estimated. It has been also revealed that there exists a regime with the abnormally efficient transformation of zero fundamental mode into the first mode. The asymptotics, for large dimensions of the transition region, makes it possible to estimate the error of the well-known heuristic approach to the study of the waveguides with slowly varying parameters (the cross-section method).

A model of the irregular circular waveguide of constant cross-section, with variable in azimuth impedance of its wall, has been proposed; it has been found the class of the impedance functions, for which the analytical solution of the excitation problem for such a waveguide is obtained; this solution allowed us to find the cause of the well-known *cycle slipping phenomenon*, which occurs when VLF electromagnetic waves propagate in the Earth-ionosphere waveguide; it is the first exact analytical solution of the excitation problem for the finite irregular waveguide, whose properties vary continuously.

- *Wave Propagation in Inhomogeneous Media.* The problem of the transition radiation in a medium with a diffuse boundary has been formulated; for this problem, a rigorous analytical solution has been obtained for the first time without imposing any restrictions on the model parameters. The limiting transition to the sharp boundary in this solution allowed us to find the precise criterion of boundary sharpness in the form of two inequalities, which essentially clarify the known criterion.

The known isotropic Epstein transition layer, describing a smooth transition between the regions with different refractive indices n_1 and n_2 in a flat-layered isotropic medium, is extended to the case of biisotropic media. An analytical solution to the problem of a plane electromagnetic wave propagating in such a medium in the normal-to-layer direction has been obtained. The analytical expressions for the reflection and transmission coefficients, which suggest the existence of the total transition mode, are derived.

A model of a smoothly inhomogeneous isotropic flat-layered medium that involves domains of conventional and double-negative media is proposed. The analytical solution derived for a plane wave travelling through this medium shows that the well-known negative refraction phenomenon in isotropic

double-negative medium is a direct consequence of Maxwell's equations and the energy conservation law.

- *Pulsed Radiation from a Line Electric Current near a Planar Interface: a Novel Technique.* A novel technique has been proposed for the analysis of a transient electromagnetic field generated by a pulsed line current that is located near a planar interface between two dielectric nonabsorbing and nondispersive media. As distinct from the Cagniard-de Hoop method, which is widely used for the study of transient fields both in electrodynamics and in the theory of acoustic and seismic waves, our approach is based on the transformation of the domain of integration in the integral expression for the field in the space of two complex variables. As a result, it will suffice to use the standard procedure of finding the roots of the algebraic equation rather than construct auxiliary Cagniard's contours. We have represented the field in the form of an integral along a finite contour. The algorithm based on such representation may work as the most effective tool for calculating fields in multilayered media. The suggested method allows extension to the case of arbitrary dipole sources.
- *Radical Distortion of Radar Image Caused by a Special Coating Applied on the Surface of Metamaterial.* We have rigorously proved, by the example of a perfectly conducting sphere, that by applying a special coating on it one can ensure that the scattered electromagnetic field will be exactly the same as the field scattered by a perfectly conducting sphere of any given smaller radius. At the same time, it is much easier to make such a *distorting coating*, since it does not require vanishing of certain components of its permittivity and permeability, as in the case of a *masking coating*.

Another two papers need to be mentioned. In [107], for a quasi-homogeneous random medium with the dispersion varying in some direction as hyperbolic tangent, the average Green's function is obtained as an exact solution of Dyson's equation in the bilocal approximation. The coherent part of the plane wave, which is incident on a bounded, randomly fluctuating medium with a diffuse boundary, is studied in detail. It is shown that in the case of small-scale fluctuations such a medium is a random analogue of the transient Epstein layer. Paper [108] is devoted to the study of the radiation from a uniformly moving charge in the nonstationary medium, whose time dependence of the permittivity is given by the formula similar to that for the symmetric Epstein layer:

$$\varepsilon(t) = \varepsilon_0 [1 + \alpha / [\operatorname{ch}^2(t/\Delta t) - \alpha]].$$

References

1. Krylov, G.G.: Exactly and Quasi-Exactly Solvable Problems in Quantum Mechanics and Statistical Dynamics. Belarusian State Univ. Press, Minsk (2011). (in Russian)
2. Wiener, N., Hopf, E.: Über eine klassensingularer integralgleichungen. S.B.Preuss. Akad. Wiss., 696–706 (1931)

3. Copson, E.T.: On an integral equation arising in the theory of diffraction. *Q. J. Math.* **17**, 19–34 (1946)
4. Carlson, J.F., Heins, A.E.: The reflection of an electromagnetic plane wave by an infinite set of plates. *Q. Appl. Math.* **4**, 313–329 (1947)
5. Weinshtein, L.A.: On the reflection of a sound wave from the open end of a tube. *Doklady Akademii Nauk SSSR*, **58**(9), 1957–1960 (1947). (in Russian)
6. Lawrie, J.B., Abrahams, I.D.: A brief historical perspective of the Wiener-Hopf technique. *J. Eng. Math.* **59**(4), 351–358 (2007)
7. Gakhov, F.D., Cherskiy, Y.I.: *Equations of Convolution Type*. Nauka, Moscow (1978). (in Russian)
8. Grinberg, G.A., Fok, V.A.: On the theory of coastal refraction of electromagnetic waves. In: Vvedenskii, B.A. (ed.) *Book chapter, Investigations on Propagation of Radio Waves*, 69–111. AN SSSR Press, Moscow (1948)
9. Heins, A.E., Feshbach, H.: The coupling of two acoustical ducts. *J. Math. Phys.* **26**, 143–155 (1947)
10. Talanov, V.I.: About electromagnetic wave diffraction on the jump of surface impedance in a waveguide. *Izvestiya Vuzov. Radiofizika*, **1**(3), 64–72 (1958). (in Russian)
11. Pazynin, L.A.: New exactly solvable problems in the theory of wave propagation near an irregular impedance plane. *Telecommun. Radio Eng.* **55**(10-11), 22–29 (2001)
12. Brekhovskikh, L.M.: *Waves in Layered Media*. Academic Press, New York (1960)
13. Weinshtein, L.A.: *The Theory of Diffraction and the Factorization Method*. The Golem Press, Boulder (1969)
14. Senior, T.B.A., Volakis, J.L.: Generalized impedance boundary conditions in scattering. *Proc. IEEE* **79**(10), 1413–1420 (1991)
15. Pazynin, V.L., Pazynin, L.A.: Electromagnetic waves in planar impedance irregular waveguide. *Radio Phys. Radio Astron.* **4**(1), 49–53 (1999). (in Russian)
16. Gradshteyn, I.S., Ryzhik, I.M.: *Table of Integrals, Series, and Products*. Academic Press, San Diego, London (2000)
17. Cherskiy, Y.I.: Normally solvable smooth-transition equation. *Doklady Akademii Nauk SSSR*, **190**(1), 57–60 (1970). (in Russian)
18. Shabat, B.V.: *Introduction to Complex Analysis. Part II. Functions of Several Variables*. American Mathematical Society, Providence, RI (1992)
19. Pierce, A.D.: Extension of the method of normal modes to sound propagation in an almost-stratified medium. *J. Acoust. Soc. Am.* **37**, 19–27 (1965)
20. Makarov, G.I., Novikov, V.V., Rybachek, S.T.: *Radiowave Propagation in the Earth-Ionosphere Waveguide and in the Ionosphere*. Nauka, Moscow (1994). (in Russian)
21. Krasnushkin, P.Y., Fedorov, Y.N.: About multiplicity of wave numbers of normal modes in stratified media. *Radiotekhnika i Elektronika*, **17**(6), 1129–1140 (1972). (in Russian)
22. Walker, D.: Phase steps and amplitude fading of VLF signals at dawn and dusk. *Radio Sci.* **69D**(11), 1435–1443 (1965)
23. Katsenelenbaum, B.Z., Mercader, R.L., Pereyaslavets, M.M., Sorolla, A.M., Tumm, M.: *Theory of Nonuniform Waveguides: the Cross-Section Method*. Published by the Institution of Electrical Engineers, London (1998)
24. Stevenson, A.F.: Exact and approximate equations for wave propagation in acoustic horns. *J. Appl. Phys.* **22**(12), 1461–1463 (1951)
25. Johler, J.R., Berry, L.A.: *Propagation Radio Waves at Frequencies Below 300kc/s*. Pergamon Press, Oxford-Paris (1964)
26. Alpert, Y.L., Guseva, E.G., Fligel, D.S.: *Propagation of Low-Frequency Electromagnetic Waves in the Earth-Ionosphere Waveguide*. Nauka, Moscow (1967). (in Russian)
27. Makarov, G.I., Novikov, V.V., Orlov, A.B.: The current status of research on the VLF propagation in the earth-ionosphere waveguide. *Izvestiya Vuzov. Radiofizika*, **13**(3), 321–355 (1970). (in Russian)

28. Simpson, J.J., Taflove, A.: A review of progress in FDTD Maxwell's Equations modeling of impulsive subionospheric propagation below 300 kHz. *IEEE Trans. Antennas Propag.* **55**(6), 1582–1590 (2007)
29. Lynn, K.J.W.: Anomalous sunrise effects observed on a long transequatorial VLF propagation path. *Radio Sci.* **2**(6), 521–530 (1967)
30. Bahar, E., Wait, J.R.: Propagation in a model terrestrial waveguide of nonuniform height: theory and experiment. *Radio Sci.* **69D**(11), 1445–1463 (1965)
31. Wait, J.R.: Mode conversion and refraction effects in the Earth–ionosphere waveguide for VLF radio waves. *J. Geophys. Res.* **73**(11), 3537–3548 (1968)
32. Bolotovskiy, Y.E., Makarov, G.I.: Intersection of VLF-signal path and the 'day–night' boundary. *Problems of Diffraction and Wave Propagation*, vol.11, pp. 142–158. Leningrad State University. Press (1972). (in Russian)
33. Pappert, R.A., Ferguson, J.A.: VLF/LF mode conversion model calculations for air to air transmissions in the earth-ionosphere waveguide. *Radio Sci.* **21**(4), 551–558 (1986)
34. Perel, M.V., Stesik, O.L.: Numerical simulation of cycle slipping in diurnal variation of phase of VLF field. *Radio Sci.* **32**(1), 199–217 (1997)
35. Budden, K.G.: The critical coupling of modes in a tapered earth–ionosphere waveguide. *Math. Proc. Cambridge Philos. Soc.* **77**, 567–580 (1975)
36. Foley, G., Wang, I.C., Jones, T.B.: Studies of the modal parameters of VLF radiowaves propagated below the night–time ionosphere. *J. Atmos. Terr. Phys.* **35**(12), 2111–2122 (1973)
37. Pazynin, L.A.: The cycle slipping phenomenon and the degeneration effect of guided-wave modes. *Prog. Electromagn. Res. M* **6**, 75–90 (2009)
38. Vaganov, R.B., Katsenelenbaum, B.Z.: *Foundations of Diffraction Theory*. Nauka, Moscow (1982). (in Russian)
39. Tyras, G.: *Radiation and Propagation of Electromagnetic Waves*. Academic Press, New York and London (1969)
40. Valagiannopoulos, C.A.: An overview of the Watson transformation presented through a simple example. *Progr. Electromagn. Res.* **75**, 137–152 (2007)
41. Felsen, L.B., Marcuvitz, N.: *Radiation and Scattering of Waves*. Prentice-Hall, Englewood Cliffs, NJ (1973)
42. Newton, R.G.: *Theory of Waves and Particles*. McGraw-Hill, New York (1969)
43. Keller, J.B., Rubinow, S.I., Goldstein, M.: Zeros of Hankel functions and poles of scattering amplitudes. *J. Math. Phys.* **4**(6), 829–832 (1963)
44. Paknys, R.: Evaluation of Hancel functions with complex argument and complex order. *IEEE Trans. Antennas Propag.* **40**(5), 569–578 (1992)
45. Tian, Y.B., Qian, J.: Ultraconveniently finding multiple solutions of complex transcendental equations based on genetic algorithm. *J. Electromagn. Waves Appl.* **20**(4), 475–488 (2006)
46. Hanson, G.W., Yakovlev, A.B.: Investigation of mode interaction on planar dielectric waveguides with loss and gain. *Radio Sci.* **34**(6), 1349–1359 (1999)
47. van der Pol, B.: On discontinuous electromagnetic waves and the occurrence of a surface wave. *IRE Tran. Antennas Propag.* **AP-4**, 288–293 (1956)
48. Cagniard, L.: *Reflexion et Refraction des Ondes Seismiques Progressives*. Gauthier-Villars, Paris (1939)
49. Cagniard, L.: *Reflection and Refraction of Progressive Seismic Waves*. McGraw-Hill, New York (1962)
50. de Hoop, A.T.: A modification of Cagniard's method for solving seismic pulse problems. *Appl. Sci. Res.* **B8**, 349–356 (1960)
51. de Hoop, A.T., Frankena, H.J.: Radiation of pulses generated by a vertical electric dipole above a plane, non-conducting Earth. *Appl. Sci. Res.*, **B8**, 369–377 (1960)
52. Frankena, H.J.: Transient phenomena associated with Sommerfeld's horizontal dipole problem. *Appl. Sci. Res.*, **B8**, 357–368 (1960)
53. Langenberg, K.J.: The transient response of a dielectric layer. *Appl. Phys.* **3**(3), 179–188 (1974)

54. de Hoop, A.T.: Pulsed electromagnetic radiation from a line source in a two-media configuration. *Radio Sci.* **14**(2), 253–268 (1979)
55. Kooij, B.J.: The transient electromagnetic field of an electric line source above a plane conducting Earth. *IEEE Trans. Electromagn. Capab.* **33**, 19–24 (1991)
56. Murrell, H.C., Ungar, A.: From Cagniard's method for solving seismic pulse problems to the method of the differential transform. *Comput. Math Appl.* **8**(2), 103–118 (1982)
57. Bleistein, N., Cohen, J.K.: An alternative approach to the Cagniard de Hoop method. *Geophys. Prospect.* **40**(6), 619–649 (1991)
58. Beh-Hador, R., Buchen, P.: A new approach to Cagniard's problem. *Applied Mathematics Letters* **12**(8), 65–72 (1999)
59. Pazynin, L.A.: Pulsed radiation from a line electric current near a planar interface: a novel technique. *IEEE Trans. Antennas Propag.* **59**(12), 4733–4739 (2011)
60. Korn, G.A., Korn, T.M.: *Mathematical Handbook for Scientists and Engineers.* McGraw-Hill, New York (1961)
61. Mittra, R., Lee, S.W.: *Analytical Techniques in the Theory of Guided Waves.* Macmillan, New York (1971)
62. Friedlander, F.G.: *Sound Pulses.* Cambridge University Press, Cambridge (1958)
63. Forsythe, G.E., Malcolm, M.A., Moler, C.B.: *Computer Methods for Mathematical Computations.* Prentice-Hall, Upper Saddle River, NJ (1977)
64. Lihh, W., Nam, S.: Time-domain electromagnetic fields radiating along the horizontal interface between vertically uniaxial half-space media. *IEEE Trans. Antennas Propag.* **55**(5), 1305–1317 (2007)
65. Bass, F.G., Yakovenko, V.M.: Theory of radiation from a charge passing through an electrically inhomogeneous medium. *Soviet Physics-Uspexhi* **8**(3), 420–444 (1965)
66. Ginzburg, V.L., Tsytoich, V.N.: Several problems of the theory of transition radiation and transition scattering. *Phys. Rep.* **49**(1), 1–89 (1979)
67. Amatuni, A., Korhmazyan, N.: Transition radiation in the case of a diffuse boundary between two media. *Zhurnal Experimental'noy I Teoreticheskoy Fiziki*, **39**(4,10), 1011–1019 (1960). (in Russian)
68. Pazynin, L.A.: Radiation of the longitudinal magnetic dipole for non-sharp boundary between two media. *Radiofizika I Elektronika*, **4**(2), 14–18 (1999). (in Russian)
69. Ginzburg, V.L., Tsytoich, V.N.: *Transition Radiation and Transition Scattering.* A Hilger, Bristol, New York (1990)
70. Bateman, H.: *Higher Transcendental Functions*, vol. I. McGraw-Hill, New York (1953)
71. Lindel, I.V., Sihvola, A.H., Tretyakov, S.A., Viitanen, A.J.: *Electromagnetic Waves on Chiral and Bi-Isotropic Media.* Artech House, Norwood, MA (1994)
72. Lindel, I.V., Tretykov, S.A., Oksanen, M.I.: Conductor-backed Tellegen slab as twist polarizer. *Electron. Lett.* **28**, 281–282 (1992)
73. Viitanen, A.J., Lindel, I.V.: Chiral slab polarization transformer for aperture antennas. *IEEE Trans. Antennas Propag.* **46**(9), 1395–1397 (1998)
74. Silverman, M.P.: Reflection and refraction at the surface of a chiral medium, comparison of gyrotropic constitutive relations invariant or noninvariant under a duality transformation. *J. Opt. Soc. Am. A*, **3-A**(6), 830–837 (1986)
75. Bassiri, S., Papas, C.H., Engheta, N.: Electromagnetic wave propagation through a dielectric-chiral interface and through a chiral slab. *J. Opt. Soc. Am. A*, **5-A**(9), 1450–1456 (1988)
76. Lindel, I.V., Viitanen, A.J.: Duality transformations for general bi-isotropic (nonreciprocal chiral) media. *IEEE Trans. Antennas Propag.* **40**(1), 91–95 (1992)
77. Tretyakov, S.A., Oksanen, M.I.: *Vector Circuit Theory for Multilayered Isotropic and Chiral Structures: Reflection and Transmission.* Electromagnetics Laboratory Helsinki University of Technology Reports, no. 50 (1989)
78. He, S.: A time-harmonic Green function technique and wave propagation in a stratified nonreciprocal chiral slab with multiple discontinuities. *J. Math. Phys.* **33**(12), 4103–4110 (1992)

79. He, S., Hu, Y.: Electromagnetic scattering from a stratified bi-isotropic (nonreciprocal chiral) slab: Numerical computations. *IEEE Trans. Antennas Propag.* **41**(8), 1057–1062 (1993)
80. Pazyinin, L.A.: Electromagnetic wave propagation through a biisotropic transition layer. *Radio Physics and Radio Astronomy*, **10**(3), 284–290 (2005). (in Russian)
81. Bliokh, K.Y., Bliokh, Y.P.: What are the left-handed media and what is interesting about them? *Physics-Uspekhi* **47**(4), 393–400 (2004)
82. Parkhomenko, M.P., Silin, R.A., Chepurnykh, I.P.: Experimental investigation of quasi-optical characteristics of artificial dielectrics with negative dispersion. *Radiotekhnika I Elektronika*, **49**(5), 624–628 (2004). (in Russian)
83. Smith, D.R., Padilla, W.J., Vier, D.C., Nemat-Nasser, S.C., Schultz, S.: Composite medium with simultaneously negative permeability and permittivity. *Phys. Rev. Lett.* **84**, 4184–4187 (2000)
84. Shelby, R.A., Smith, D.R., Schultz, S.: Experimental verification of a negative index of refraction. *Science* **292**, 77–79 (2001)
85. Vashkovskii, A.V., Lokk, E.G.: Properties of backward electromagnetic waves and the appearance of negative reflection in ferrite films. *Physics-Uspekhi* **49**(4), 389–399 (2006)
86. Pazyinin, L.A.: Negative reflection in isotropic double-negative media. *Elektromagnitnye Volny I Elektronnye Sistemy*, **14**(9), 45–50 (2009). (in Russian)
87. Stratton, J.A.: *Electromagnetic Theory*. McGraw-Hill, New York, London (1953)
88. Forsterling, K., Wuster, H.O.: Eutscheidung von oberwellen in der ionosphäre. *J. Atmos. Terr. Phys.* **2**, 22–31 (1951)
89. Denisov, N.G.: On a peculiarity of the electromagnetic wave propagating in an inhomogeneous plasma. *Zhurnal Experimental'noy I Teoreticheskoy Fiziki* **31**(4, 10), 609–619 (1956). (in Russian)
90. Ginzburg, V.: *The Propagation of Electromagnetic Waves in Plasmas*. Pergamon, Oxford (1970)
91. Dubinov, A.E., Mytareva, L.A.: Invisible cloaking of material bodies using the wave flow method. *Physics-Uspekhi* **53**(5), 455–479 (2010)
92. Pendry, J.B., Schurig, D., Smith, D.R.: Controlling electromagnetic fields. *Science* **312**, 1780–1782 (2006)
93. Leonhardt, U.: Notes on conformal invisibility devices. *New J. Phys.*, **8**(118) (2006)
94. Kildishev, A.V., Shalaev, V.M.: Enabling transformation optics through metamaterials. *Trans. Opt. Metamaterials. Physics-Uspekhi* **54**(1), 53–63 (2011)
95. Chen, H., Wu, B.-I., Zhang, B., et al.: Electromagnetic wave interactions with a metamaterial cloak. *Phys. Rev. Lett.*, **99**, ID 063903 (2007)
96. Gao, L., Fung, T.H., Yu, K.W. et al.: Electromagnetic transparency by coated spheres with radial anisotropy. *Phys. Rev.*, **E78**, ID 046609 (2008)
97. Qiu, C.W., Hu, L., Zhang, B., et al.: Spherical cloaking using nonlinear transformations for improved segmentation into concentric isotropic coatings. *Opt. Express* **17**(16), 13467–13478 (2009)
98. Meng, F.Y., Liang, Y., Wu, Q., et al.: Invisibility of a metamaterial cloak illuminated by spherical. *Appl. Phys. A* **95**, 881–888 (2009)
99. Cheng, X.X., Chen, H.S., Zhang, X.M.: Cloaking a perfectly conducting sphere with rotationally uniaxial nihility media in monostatic radar system. *Prog. Electromagn. Res.* **100**, 285–298 (2010)
100. Pazyinin, L.A.: Distorting coating as an alternative to the masking coating. *Fizicheskie Osnovy Priborostroeniya*, **2**(1), 72–77 (2013). (in Russian)
101. Chen, H.: Transformation optics in orthogonal coordinates. *J. Opt. A Pure Appl. Opt.* **11**, ID 075102 (2009)
102. Varshalovich, D.A., Moskalev, A.N., Chersonsky, V.K.: *Quantum Theory of Angular Momentum: Irreducible Tensors, Spherical Harmonics, Vector Coupling Coefficients, 3nj Symbols*. World Scientific, Singapore (1988)
103. Abramowitz, M., Stegun, I.A. (eds.): *Handbook of Mathematical Functions*. Dover, New York (1972)

104. Zhu, G.: Scalar theory of electromagnetic wave in a spherically symmetric radially anisotropic and inhomogeneous medium: Photonic atoms. *J. Appl. Phys.*, **108**, ID 073118 (2010)
105. Bowman, J.J., Senior, T.B.A., Uslenghi, P.L.F.: *Electromagnetic and Acoustic Scattering by Simple Shapes*. North-Holland Publishing Company, Amsterdam (1969)
106. Lai, Y., Ng, J., Chen, H. et al.: Illusion optics: The optical transformation of an object into another object. *Phys. Rev. Lett.* **102**, ID 253902 (2009)
107. Pazynin, L.A.: The random analogue of Epstein's transition layer. *Waves in Random Media* **7**, 545–556 (1997)
108. Pazynin, L.A.: Radiation of a uniformly moving charge in a nonstationary medium with the dependence of $\epsilon^{-1}(t)$ as $\text{sech}^2(t)$. *Elektromagnitnye Volny I Elektronnye Sistemy*, **5**(3), 70–75 (2000). (in Russian)

Chapter 2

Dyadic Green's Function for Biaxial Anisotropic Media

Leonid Pazyinin, Seil Sautbekov and Yuriy Sirenko

Abstract In this chapter, authors construct the dyadic Green's function for a biaxial anisotropic media. Among the obtained analytical results, worthy of mention are the representation of the singular part of the Green's function in an explicit form and the representation of its regular part in the form of a relatively simple double integral over a limited region. These results are aimed at developing efficient numerical algorithms and asymptotic representations in the problems of wave scattering in anisotropic media.

2.1 Introduction

The *Dyadic Green's function* (DGF) is the most efficient analytical tool in the analysis of radiation and propagation of electromagnetic waves in an unbounded medium [1]. The explicit closed-form expression for DGF is known for a uniaxial *anisotropic medium* [2–4]. In the case of biaxial and some more complex anisotropic media, DGF is represented usually as a three-dimensional Fourier integral in Cartesian [5], cylindrical [6, 7] or spherical [8–10] coordinates in the space K^3 of wave vectors \vec{k} . To obtain a unique solution from this physical representation, the following radiation condition at infinity is used: under the assumption of small loss in the anisotropic medium, DGF must tend to zero with the unbounded removal of the observation point $\vec{r} \in R^3$ [5]. It is not possible to reduce the mentioned three-dimensional integral to an explicit closed-form one, so the most part of the works in this field is devoted to the

L. Pazyinin (✉) · Y. Sirenko
O.Ya. Usikov Institute for Radiophysics and Electronics, National Academy
of Sciences, Kharkiv, Ukraine
e-mail: pazyinin@ire.kharkov.ua

Y. Sirenko
e-mail: yks@ire.kharkov.ua

S. Sautbekov · Y. Sirenko
L.N. Gumilyov Eurasian National University, Astana, Republic of Kazakhstan
e-mail: sautbek@mail.ru

transformation of this integral into a form that allow numerical analysis and asymptotic estimation in the near-field and far-field zones.

In the Cartesian and cylindrical coordinates, a single integration in standard three-dimensional integral is performed without any difficulties. However, the result—a double singular integral in the case of the Cartesian coordinate system or a double integral in the infinite limits of functions with double infinite sums in the case of the cylindrical coordinate system—is even less suitable for computations than the original one.

The most convenient for the development of computational algorithms for DGF, apparently, is an approach that is based on the use of spherical coordinates [8–10]. In [8] it is implemented in a standard way and the calculation of the integral over the radial variable results in representation of DGF in the form of a double integral over a finite region but with the appearance of a double sum in the integrand function. In [9], dealing with the construction of DGF for *bianisotropic medium*, and in [10] a spherical coordinate system is bound to the observation point $\vec{r} = x\vec{x} + y\vec{y} + z\vec{z}$. It allowed the authors of [9] to transform the integral over the radial variable k_r , $0 \leq k_r < \infty$ into the integral over the entire axis $-\infty < k_r < \infty$ and reduce it to the sum of residues, describing outgoing waves, that is, to fulfill the radiation condition at infinity. That is a good result, but in its derivation the modifications associated with the replacement of the original coordinate system by the systems oriented to an observation point, only the vector of independent variables \vec{k} , has been subjected to transformation, but transformation of the dyadic (tensor) Green's function has not been carried out.

DGF, which is a Fourier integral of a function nondecreasing at infinity, is a generalized function. It is convenient to consider it by breaking up into two parts: the singular one (generalized function) and regular one (normal function). In all above mentioned works, the singular part is calculated in the corresponding coordinate system, but without explicit extraction of the regular part, which may be more important for the future work.

In the present chapter, the proposed in the paper [9] idea of transition to a special spherical coordinate system is implemented, and inaccuracies made in [9], which we have pointed out above, are fixed. DGF is presented as a sum of singular and regular parts. An explicit, not depending on the coordinate system, representation for the singular part is found out; it generalizes the known expression for the singular part of the Green's function of the uniaxial anisotropic medium [11]. The regular part is represented as a double integral over a finite domain. This integral is convenient both for computations and for the construction of asymptotic representations.

2.2 Formulation of the Problem

For the anisotropic medium under consideration, Maxwell's equations describing a harmonically oscillating field (time dependence is determined by the factor $\exp(-i\omega t)$) can be written as

$$\text{rot}\vec{E}(\vec{r}) - i\omega\mu_0\mu\vec{H}(\vec{r}) = 0, \quad \text{rot}\vec{H}(\vec{r}) + i\omega\varepsilon_0\vec{\varepsilon}\vec{E}(\vec{r}) = \vec{j}(\vec{r}), \quad (2.1)$$

where ε_0 and μ_0 are permittivity and permeability of vacuum; $\vec{\varepsilon}$ is the relative permittivity tensor and μ is the relative magnetic permeability—they are defined by arbitrary complex numbers.

The solution of (2.1) for any external electric current density $\vec{j}(\vec{r})$ can be expressed by the integrals [3]

$$\vec{E}(\vec{r}) = \iiint \underline{\underline{G}}_{ee}(\vec{r}, \vec{r}_0)\vec{j}(\vec{r}_0)d\vec{r}_0, \quad \vec{H}(\vec{r}) = \iiint \underline{\underline{G}}_{me}(\vec{r}, \vec{r}_0)\vec{j}(\vec{r}_0)d\vec{r}_0, \quad (2.2)$$

where the dyadic Green's functions $\underline{\underline{G}}_{ee}$ and $\underline{\underline{G}}_{me}$ are solutions of the equations

$$\begin{cases} \text{rot}\underline{\underline{G}}_{ee}(\vec{r}, \vec{r}_0) - i\omega\mu_0\mu\underline{\underline{G}}_{me}(\vec{r}, \vec{r}_0) = 0 \\ \text{rot}\underline{\underline{G}}_{me}(\vec{r}, \vec{r}_0) + i\omega\varepsilon_0\vec{\varepsilon}\underline{\underline{G}}_{ee}(\vec{r}, \vec{r}_0) = \underline{\underline{I}}\delta(\vec{r} - \vec{r}_0). \end{cases} \quad (2.3)$$

Here $\delta(\dots)$ is the Dirac delta-function and $\underline{\underline{I}}$ is the identity tensor (dyadic). System (2.3) is equivalent to two equations of the second order

$$[\text{rot} \mu^{-1} \text{rot} \underline{\underline{I}} - k_0^2 \vec{\varepsilon}] \underline{\underline{G}}_{ee}(\vec{r}, \vec{r}_0) = i\omega\mu_0 \underline{\underline{I}} \delta(\vec{r} - \vec{r}_0), \quad (2.4)$$

$$[\text{rot} \vec{\varepsilon}^{-1} \text{rot} \underline{\underline{I}} - k_0^2 \mu] \underline{\underline{G}}_{me}(\vec{r}, \vec{r}_0) = i\omega\varepsilon_0 \underline{\underline{I}} \delta(\vec{r} - \vec{r}_0), \quad (2.5)$$

where $k_0 = \omega\sqrt{\varepsilon_0\mu_0}$.

We confine ourselves to finding DGF of electric type $\underline{\underline{G}}(\vec{r}, \vec{r}_0) = \underline{\underline{G}}_{ee}(\vec{r}, \vec{r}_0)/i\omega\mu_0\mu$ from the equation

$$\text{rot} \text{rot} \underline{\underline{G}}(\vec{r}) - k_0^2 \mu \vec{\varepsilon} \underline{\underline{G}}(\vec{r}) = \underline{\underline{I}} \delta(\vec{r}). \quad (2.6)$$

There is no need to solve (2.5), since due to the availability of $\underline{\underline{G}}$ the field $\vec{H}(\vec{r})$ is determined by the first equations from (2.1) and (2.2).

2.3 Initial Representation for Dyadic Green's Function

The solution of (2.6) can be represented as a triple Fourier integral [5, 8]

$$\underline{\underline{G}}(\vec{r}) = \iiint_{\mathbb{K}^3} \underline{\underline{g}}(\vec{k}) \exp(i\vec{k} \cdot \vec{r}) d\vec{k}, \quad (2.7)$$

where $\bar{\underline{g}}(\vec{k}) = (2\pi)^{-3} [\bar{\underline{A}}(\vec{k})]^{-1} = (2\pi)^{-3} \text{adj} [\bar{\underline{A}}(\vec{k})] / \det [\bar{\underline{A}}(\vec{k})]$, $\kappa_0^2 = k_0^2 \mu$, $\bar{\underline{A}}(\vec{k}) = k^2 \bar{\underline{I}} - \vec{k} \otimes \vec{k} - \kappa_0^2 \bar{\underline{\varepsilon}}$, and $\vec{a} \otimes \vec{b}$ is the *tensor product* of the vectors \vec{a} and \vec{b} , or, in other words, the tensor with components $a_\alpha b_\beta = [\vec{a} \otimes \vec{b}]_{\alpha\beta}$.

In a Cartesian coordinate system $\{x, y, z\}$ with axes directed along the axes of the medium anisotropy, we have

$$\bar{\underline{\varepsilon}} = \begin{bmatrix} \varepsilon_1 & 0 & 0 \\ 0 & \varepsilon_2 & 0 \\ 0 & 0 & \varepsilon_3 \end{bmatrix}, \quad \vec{k} \otimes \vec{k} = \begin{bmatrix} k_x^2 & k_x k_y & k_x k_z \\ k_x k_y & k_y^2 & k_y k_z \\ k_x k_z & k_y k_z & k_z^2 \end{bmatrix}, \quad \text{adj} [\bar{\underline{A}}(\vec{k})] = \begin{bmatrix} \tilde{a}_{11} & \tilde{a}_{12} & \tilde{a}_{13} \\ \tilde{a}_{21} & \tilde{a}_{22} & \tilde{a}_{23} \\ \tilde{a}_{31} & \tilde{a}_{32} & \tilde{a}_{33} \end{bmatrix}, \quad (2.8)$$

where $\varepsilon_1, \varepsilon_2, \varepsilon_3$ are arbitrary complex numbers,

$$\begin{aligned} \tilde{a}_{11} &= q_2 q_3 - k_y^2 q_3 - k_z^2 q_2, & \tilde{a}_{12} &= \tilde{a}_{21} = k_x k_y q_3, & \tilde{a}_{13} &= \tilde{a}_{31} = k_x k_z q_2, \\ \tilde{a}_{22} &= q_1 q_3 - k_x^2 q_3 - k_z^2 q_1, & \tilde{a}_{23} &= \tilde{a}_{32} = k_y k_z q_1, & \tilde{a}_{33} &= q_1 q_2 - k_x^2 q_2 - k_y^2 q_1, \\ \vec{k} &= k_x \vec{x} + k_y \vec{y} + k_z \vec{z}, & q_j &= k^2 - \kappa_0^2 \varepsilon_j; & j &= 1, 2, 3, \end{aligned}$$

and

$$\begin{aligned} \det [\bar{\underline{A}}(\vec{k})] &= -\kappa_0^2 \left\{ k^2 (k_x^2 \varepsilon_1 + k_y^2 \varepsilon_2 + k_z^2 \varepsilon_3) \right. \\ &\quad \left. - \kappa_0^2 [k_x^2 (\varepsilon_1 \varepsilon_2 + \varepsilon_1 \varepsilon_3) + k_y^2 (\varepsilon_1 \varepsilon_2 + \varepsilon_2 \varepsilon_3) + k_z^2 (\varepsilon_1 \varepsilon_3 + \varepsilon_2 \varepsilon_3)] + \kappa_0^4 \varepsilon_1 \varepsilon_2 \varepsilon_3 \right\}. \end{aligned} \quad (2.9)$$

2.4 Transformation of the Original Representation. Singular Part of Dyadic Green's Function

Let us write the *adjoint matrix* $\text{adj}[\dots]$ in the form of an expansion in powers of \vec{k} :

$$\text{adj} [\bar{\underline{A}}(\vec{k})] = k^2 \vec{k} \otimes \vec{k} - \kappa_0^2 \bar{\underline{A}}^{(2)}(\vec{k}) + \kappa_0^4 \bar{\underline{A}}^{(0)}. \quad (2.10)$$

Here,

$$\bar{\underline{A}}^{(2)}(\vec{k}) = \begin{bmatrix} k_x^2 (\varepsilon_2 + \varepsilon_3) + k_y^2 \varepsilon_2 + k_z^2 \varepsilon_3 & k_x k_y \varepsilon_3 & k_x k_z \varepsilon_2 \\ k_x k_y \varepsilon_3 & k_x^2 \varepsilon_1 + k_y^2 (\varepsilon_1 + \varepsilon_3) + k_z^2 \varepsilon_3 & k_y k_z \varepsilon_1 \\ k_x k_z \varepsilon_2 & k_y k_z \varepsilon_1 & k_x^2 \varepsilon_1 + k_y^2 \varepsilon_2 + k_z^2 (\varepsilon_1 + \varepsilon_2) \end{bmatrix} \quad (2.11)$$

and

$$\underline{\underline{A}}^{(0)} = \begin{bmatrix} \varepsilon_2 \varepsilon_3 & 0 & 0 \\ 0 & \varepsilon_1 \varepsilon_3 & 0 \\ 0 & 0 & \varepsilon_1 \varepsilon_2 \end{bmatrix}. \quad (2.12)$$

Let

$$D(\vec{k}) = -\frac{\kappa_0^2}{\det[\underline{\underline{A}}(\vec{k})]} = D_{(4)}(\vec{k}) + D_{(6)}(\vec{k}), \quad (2.13)$$

where $D_{(4)}(\vec{k}) = \left[k^2 \left(k_x^2 \varepsilon_1 + k_y^2 \varepsilon_2 + k_z^2 \varepsilon_3 \right) \right]^{-1}$, and the lower index (n) is equal to the order of decrease of $D_{(n)}(\vec{k})$ as $k \rightarrow \infty$.

Transform the integrand in (2.7) according to the representation

$$-(2\pi)^3 \kappa_0^2 \underline{\underline{g}}(\vec{k}) = \underline{\underline{g}}^{\text{sing}}(\vec{k}) + \underline{\underline{g}}_{(2)}^{\text{reg}}(\vec{k}) + \underline{\underline{g}}_{(4)}^{\text{reg}}(\vec{k}), \quad (2.14)$$

where $\underline{\underline{g}}^{\text{sing}}(\vec{k}) = k^2 \vec{k} \otimes \vec{k} D_{(4)}(\vec{k})$, $\underline{\underline{g}}_{(2)}^{\text{reg}}(\vec{k}) = k^2 \vec{k} \otimes \vec{k} D_{(6)}(\vec{k}) - \kappa_0^2 \underline{\underline{A}}^{(2)}(\vec{k}) D_{(4)}(\vec{k})$, and $\underline{\underline{g}}_{(4)}^{\text{reg}}(\vec{k}) = -\kappa_0^2 \underline{\underline{A}}^{(2)}(\vec{k}) D_{(6)}(\vec{k}) + \kappa_0^4 \underline{\underline{A}}^{(0)}(\vec{k}) D(\vec{k})$. Consequently, DGF breaks up into three terms:

$$\underline{\underline{G}}(\vec{r}) = \underline{\underline{G}}^{\text{sing}}(\vec{r}) + \underline{\underline{G}}_{(2)}^{\text{reg}}(\vec{r}) + \underline{\underline{G}}_{(4)}^{\text{reg}}(\vec{r}). \quad (2.15)$$

Transform the first one to the form

$$\begin{aligned} \underline{\underline{G}}^{\text{sing}}(\vec{r}) &= -\frac{1}{(2\pi)^3 \kappa_0^2} \iiint_{\mathbb{K}^3} k^2 \vec{k} \otimes \vec{k} D_{(4)}(\vec{k}) \exp(i\vec{k} \cdot \vec{r}) d\vec{k} \\ &= \frac{1}{(2\pi)^3 \kappa_0^2} (\nabla \otimes \nabla) \iiint_{\mathbb{K}^3} \frac{\exp(i\vec{k} \cdot \vec{r}) d\vec{k}}{k_x^2 \varepsilon_1 + k_y^2 \varepsilon_2 + k_z^2 \varepsilon_3} \\ &= \frac{1}{4\pi \kappa_0^2} (\nabla \otimes \nabla) \frac{1}{r_\varepsilon \sqrt{\varepsilon_1 \varepsilon_2 \varepsilon_3}}; \quad r_\varepsilon^2 = x^2/\varepsilon_1 + y^2/\varepsilon_2 + z^2/\varepsilon_3, \\ \nabla &= \frac{\partial}{\partial x} \vec{x} + \frac{\partial}{\partial y} \vec{y} + \frac{\partial}{\partial z} \vec{z}, \end{aligned} \quad (2.16)$$

using the result from [12] for calculating the last integral in (2.16).

It is known that $-(4\pi)^{-1} \nabla^2 r^{-1} = \delta(r)$ for $r^2 = x^2 + y^2 + z^2$ [12]. Therefore, one can assume that the function $\underline{\underline{G}}^{\text{sing}}(\vec{r})$ generalizes the function $\delta(r)$ in the case of

biaxial anisotropic medium. In the particular case of the uniaxial medium, it arrives to the known expression for the singular part of the corresponding DGF [11].

2.5 Regular Part of Dyadic Green's Function

The function $\overline{\underline{G}}_{(2)}^{\text{reg}}(\vec{r})$ from (2.15) can be represented as a sum of two terms:

$$\begin{aligned} & -\frac{1}{(2\pi)^3 \kappa_0^2} \iiint_{\mathbb{K}^3} (\vec{k} \otimes \vec{k}) k^2 D_{(6)}(\vec{k}) \exp(i\vec{k} \cdot \vec{r}) d\vec{k} \\ & = \frac{1}{(2\pi)^3 \kappa_0^2} (\nabla \otimes \nabla) \iiint_{\mathbb{K}^3} k^2 D_{(6)}(\vec{k}) \exp(i\vec{k} \cdot \vec{r}) d\vec{k} \end{aligned} \quad (2.17)$$

and

$$\begin{aligned} & \frac{1}{(2\pi)^3} \iiint_{\mathbb{K}^3} \overline{\underline{A}}^{(2)}(\vec{k}) D_{(4)}(\vec{k}) \exp(i\vec{k} \cdot \vec{r}) d\vec{k} \\ & = -\frac{1}{(2\pi)^3} \overline{\underline{A}}^{(2)}(\nabla) \iiint_{\mathbb{K}^3} D_{(4)}(\vec{k}) \exp(i\vec{k} \cdot \vec{r}) d\vec{k}, \end{aligned} \quad (2.18)$$

where

$$\overline{\underline{A}}^{(2)}(\nabla) = \begin{bmatrix} (\varepsilon_2 + \varepsilon_3) \partial_{xx}^2 + \varepsilon_2 \partial_{yy}^2 + \varepsilon_3 \partial_{zz}^2 & \varepsilon_3 \partial_{xy}^2 & \varepsilon_2 \partial_{xz}^2 \\ \varepsilon_3 \partial_{xy}^2 & \varepsilon_1 \partial_{xx}^2 + (\varepsilon_1 + \varepsilon_3) \partial_{yy}^2 + \varepsilon_3 \partial_{zz}^2 & \varepsilon_1 \partial_{yz}^2 \\ \varepsilon_2 \partial_{xz}^2 & \varepsilon_1 \partial_{yz}^2 & \varepsilon_1 \partial_{xx}^2 + \varepsilon_2 \partial_{yy}^2 + (\varepsilon_1 + \varepsilon_2) \partial_{zz}^2 \end{bmatrix}. \quad (2.19)$$

Thus

$$\begin{aligned} \overline{\underline{G}}_{(2)}^{\text{reg}}(\vec{r}) & = \frac{1}{(2\pi)^3} \left[\frac{1}{\kappa_0^2} (\nabla \otimes \nabla) \iiint_{\mathbb{K}^3} k^2 D_{(6)}(\vec{k}) \exp(i\vec{k} \cdot \vec{r}) d\vec{k} \right. \\ & \quad \left. - \overline{\underline{A}}^{(2)}(\nabla) \iiint_{\mathbb{K}^3} D_{(4)}(\vec{k}) \exp(i\vec{k} \cdot \vec{r}) d\vec{k} \right] \end{aligned} \quad (2.20)$$

and

$$\begin{aligned} \overline{\underline{G}}_{(4)}^{\text{reg}}(\vec{r}) & = -\frac{1}{(2\pi)^3} \left[\overline{\underline{A}}^{(2)}(\nabla) \iiint_{\mathbb{K}^3} D_{(6)}(\vec{k}) \exp(i\vec{k} \cdot \vec{r}) d\vec{k} \right. \\ & \quad \left. + \kappa_0^2 \overline{\underline{A}}^{(0)} \iiint_{\mathbb{K}^3} D(\vec{k}) \exp(i\vec{k} \cdot \vec{r}) d\vec{k} \right]. \end{aligned} \quad (2.21)$$

The sums (2.20) and (2.21) give us the regular part of DGF:

$$\begin{aligned} \underline{\underline{G}}^{reg}(\vec{r}) = & \frac{1}{(2\pi)^3} \left[\frac{1}{\kappa_0^2} (\nabla \otimes \nabla) \iiint_{\mathbb{K}^3} k^2 D_{(6)}(\vec{k}) \exp(i\vec{k} \cdot \vec{r}) d\vec{k} \right. \\ & \left. - \left[\overline{\underline{\underline{A}}}^{(2)}(\nabla) + \kappa_0^2 \overline{\underline{\underline{A}}}^{(0)} \right] \iiint_{\mathbb{K}^3} D(\vec{k}) \exp(i\vec{k} \cdot \vec{r}) d\vec{k} \right]. \end{aligned} \quad (2.22)$$

The matrix operator

$$\overline{\underline{\underline{T}}}(\vartheta, \phi) = \begin{bmatrix} \sin \vartheta \cos \phi & \sin \vartheta \sin \phi & \cos \vartheta \\ \cos \vartheta \cos \phi & \cos \vartheta \sin \phi & -\sin \vartheta \\ -\sin \phi & \cos \phi & 0 \end{bmatrix} \quad (2.23)$$

for the transition in \mathbb{R}^3 -space from the Cartesian ($\{x, y, z\}$) to the spherical coordinates

$$\{r, \vartheta, \phi\} : \begin{cases} x = r \sin \vartheta \cos \phi \\ y = r \sin \vartheta \sin \phi \\ z = r \cos \vartheta \end{cases} \quad (2.24)$$

transforms (2.22) into

$$\underline{\underline{G}}^{reg}(\vec{r}) = \frac{1}{(2\pi)^3} \left[\frac{1}{\kappa_0^2} (\nabla \otimes \nabla)_{\text{sph}} U_{(6)}(\vec{r}) - \left(\overline{\underline{\underline{A}}}^{(2)}(\nabla) + \kappa_0^2 \overline{\underline{\underline{A}}}^{(0)} \right)_{\text{sph}} U(\vec{r}) \right]. \quad (2.25)$$

Here,

$$U_{(6)}(\vec{r}) = \iiint_{\mathbb{K}^3} k^2 D_{(6)}(\vec{k}) \exp(i\vec{k} \cdot \vec{r}) d\vec{k}, \quad U(\vec{r}) = \iiint_{\mathbb{K}^3} D(\vec{k}) \exp(i\vec{k} \cdot \vec{r}) d\vec{k}, \quad (2.26)$$

and

$$(\dots)_{\text{sph}} = \overline{\underline{\underline{T}}}(\vartheta, \phi) (\dots) \overline{\underline{\underline{T}}}^T(\vartheta, \phi) \quad (2.27)$$

(the upper index T in $\overline{\underline{\underline{T}}}^T(\vartheta, \phi)$ denotes the transpose operation of the matrix $\overline{\underline{\underline{T}}}(\vartheta, \phi)$), \vec{r} is defined by formula (2.24). Cartesian components of the operator ∇ are expressed in terms of spherical coordinates by the formulas [13]

$$\begin{aligned} \frac{\partial}{\partial x} &= \sin \vartheta \cos \phi \frac{\partial}{\partial r} + \frac{\cos \vartheta \cos \phi}{r} \frac{\partial}{\partial \vartheta} - \frac{\sin \phi}{r \sin \vartheta} \frac{\partial}{\partial \phi}, \\ \frac{\partial}{\partial y} &= \sin \vartheta \sin \phi \frac{\partial}{\partial r} + \frac{\cos \vartheta \sin \phi}{r} \frac{\partial}{\partial \vartheta} + \frac{\cos \phi}{r \sin \vartheta} \frac{\partial}{\partial \phi}, \\ \frac{\partial}{\partial z} &= \cos \vartheta \frac{\partial}{\partial r} - \frac{\sin \vartheta}{r} \frac{\partial}{\partial \vartheta}. \end{aligned}$$

2.6 The Physical Solution

To meet the radiation condition, we transform the coordinate system in the integration space K^3 . First, make the transition from the original Cartesian system $\{k_x, k_y, k_z\}$ to the new Cartesian coordinate system $\{k_{\tilde{x}}, k_{\tilde{y}}, k_{\tilde{z}}\}$, with the axis $k_{\tilde{z}}$ directed to the observation point $\vec{r} = \vec{r}(r, \vartheta, \phi)$ of the space R^3 (see, for example, Fig. 2.1 and [9]; the $k_{\tilde{x}}$ -axis lies in the $k_x 0 k_y$ -plane, the angles $\tilde{\vartheta}$ and $\tilde{\phi}$ are spherical angles in the rotated system). This transition, $\vec{k} = \underline{T}_1(\vartheta, \phi)\vec{k}$, is described by the rotation matrix

$$\underline{T}_1(\vartheta, \phi) = \begin{bmatrix} \sin \phi & -\cos \phi & 0 \\ \cos \vartheta \cos \phi & \cos \vartheta \sin \phi & -\sin \vartheta \\ \sin \vartheta \cos \phi & \sin \vartheta \sin \phi & \cos \vartheta \end{bmatrix}. \quad (2.28)$$


Then we make the second transform in K^3 , namely, change from the Cartesian coordinate system to spherical coordinates in the representation of the vector \vec{k} :

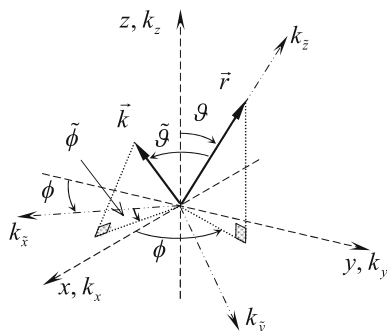
$$\begin{cases} k_{\tilde{x}} = k \sin \tilde{\vartheta} \cos \tilde{\phi} \\ k_{\tilde{y}} = k \sin \tilde{\vartheta} \sin \tilde{\phi} \\ k_{\tilde{z}} = k \cos \tilde{\vartheta} \end{cases}. \quad (2.29)$$

Then we have

$$\vec{k} = \vec{k}(\tilde{\vartheta}, \tilde{\phi}, \vartheta, \phi) = k\vec{k}(\tilde{\vartheta}, \tilde{\phi}, \vartheta, \phi) = \underline{T}_1^T(\vartheta, \phi)\vec{k}(\tilde{\vartheta}, \tilde{\phi}), \quad (2.30)$$

where $\vec{k}(\tilde{\vartheta}, \tilde{\phi}) = \{k_{\tilde{x}}, k_{\tilde{y}}, k_{\tilde{z}}\}$ and

Fig. 2.1 Original and new Cartesian coordinate systems:
—right angle



$$\begin{aligned} \underline{k}_x &= \sin \phi \sin \tilde{\vartheta} \cos \tilde{\phi} + \cos \vartheta \cos \phi \sin \tilde{\vartheta} \sin \tilde{\phi} + \sin \vartheta \cos \phi \cos \tilde{\vartheta}, \\ \underline{k}_y &= -\cos \phi \sin \tilde{\vartheta} \cos \tilde{\phi} + \cos \vartheta \sin \phi \sin \tilde{\vartheta} \sin \tilde{\phi} + \sin \vartheta \sin \phi \cos \tilde{\vartheta}, \\ \underline{k}_z &= -\sin \vartheta \sin \tilde{\vartheta} \sin \tilde{\phi} + \cos \vartheta \cos \tilde{\vartheta}, \quad (\vec{k} \cdot \vec{r}) = kr \cos \tilde{\vartheta}. \end{aligned}$$

In the new coordinates $\{k, \tilde{\vartheta}, \tilde{\phi}\}$ the integrals (2.26) in (2.25) for the regular part of DGF take the form

$$U_{(6)}(\vec{r}) = \int_0^\infty k^4 dk \int_0^\pi \sin \tilde{\vartheta} d\tilde{\vartheta} \int_0^{2\pi} D_{(6)}(\vec{k}) \exp(ikr \cos \tilde{\vartheta}) d\tilde{\phi}, \quad (2.31)$$

$$U(\vec{r}) = \int_0^\infty k^2 dk \int_0^\pi \sin \tilde{\vartheta} d\tilde{\vartheta} \int_0^{2\pi} D(\vec{k}) \exp(ikr \cos \tilde{\vartheta}) d\tilde{\phi}. \quad (2.32)$$

In these representations it is possible to carry out the analytical integration over k . To do this, first we express the determinant of (2.9) through the roots of the dispersion equation:

$$\det[\bar{A}(\vec{k})] = -\kappa_0^2 (ak^4 + bk^2 + c) = -\kappa_0^2 a (k^2 - k_1^2) (k^2 - k_2^2). \quad (2.33)$$

Here,

$$k_{1,2}^2 = k_{1,2}^2(\tilde{\vartheta}, \tilde{\phi}, \vartheta, \phi) = \frac{-b \pm \sqrt{b^2 - 4ac}}{2a}, \quad (2.34)$$

$$a = a(\tilde{\vartheta}, \tilde{\phi}, \vartheta, \phi) = \underline{k}_x^2 \varepsilon_1 + \underline{k}_y^2 \varepsilon_2 + \underline{k}_z^2 \varepsilon_3, \quad (2.35)$$

$$b = b(\tilde{\vartheta}, \tilde{\phi}, \vartheta, \phi) = -\kappa_0^2 \left[\underline{k}_x^2 \varepsilon_1 (\varepsilon_2 + \varepsilon_3) + \underline{k}_y^2 \varepsilon_2 (\varepsilon_1 + \varepsilon_3) + \underline{k}_z^2 \varepsilon_3 (\varepsilon_1 + \varepsilon_2) \right], \quad (2.36)$$

$$c = c(\tilde{\vartheta}, \tilde{\phi}, \vartheta, \phi) = \kappa_0^4 \varepsilon_1 \varepsilon_2 \varepsilon_3. \quad (2.37)$$

Then we derive from (2.13) that

$$\begin{aligned} D(\vec{k}) &= \frac{1}{a(k^2 - k_1^2)(k^2 - k_2^2)} = D(k^2, \tilde{\vartheta}, \tilde{\phi}, \vartheta, \phi), \\ D_{(6)}(\vec{k}) &= \frac{-(bk^2 + c)}{a^2 k^4 (k^2 - k_1^2)(k^2 - k_2^2)} = D_{(6)}(k^2, \tilde{\vartheta}, \tilde{\phi}, \vartheta, \phi). \end{aligned} \quad (2.38)$$

Both of these functions are invariant with respect to the change of variables $\tilde{\vartheta} = \pi - \underline{\tilde{\vartheta}}$, $\tilde{\phi} = \pi + \underline{\tilde{\phi}}$. This allows one to transform the integration in (2.31), (2.32) over the unit sphere to the integration over the closest to the observation point hemisphere. Consider, for example, the integral (2.32). Given the fact that

$$\begin{aligned} & \int_{\pi/2}^{\pi} \sin \tilde{\vartheta} d\tilde{\vartheta} \int_0^{2\pi} D(k^2, \tilde{\vartheta}, \tilde{\phi}, \vartheta, \phi) \exp(ikr \cos \tilde{\vartheta}) d\tilde{\phi} \\ &= - \int_{\pi/2}^0 \sin \tilde{\vartheta} d\tilde{\vartheta} \int_{-\pi}^{\pi} D(k^2, \tilde{\vartheta}, \tilde{\phi}, \vartheta, \phi) \exp(-ikr \cos \tilde{\vartheta}) d\tilde{\phi} \\ &= \int_0^{\pi/2} d\underline{\tilde{\vartheta}} \sin \underline{\tilde{\vartheta}} \int_0^{2\pi} D(k^2, \underline{\tilde{\vartheta}}, \underline{\tilde{\phi}}, \vartheta, \phi) \exp(-ikr \cos \underline{\tilde{\vartheta}}) d\underline{\tilde{\phi}}, \end{aligned}$$

we have

$$\begin{aligned} U(\vec{r}) &= \int_0^{\infty} k^2 dk \int_0^{\pi/2} \sin \tilde{\vartheta} d\tilde{\vartheta} \int_0^{2\pi} D(k^2, \tilde{\vartheta}, \tilde{\phi}, \vartheta, \phi) \exp(ikr \cos \tilde{\vartheta}) d\tilde{\phi} \\ &+ \int_0^{\infty} k^2 dk \int_0^{\pi/2} \sin \tilde{\vartheta} d\tilde{\vartheta} \int_0^{2\pi} D(k^2, \tilde{\vartheta}, \tilde{\phi}, \vartheta, \phi) \exp(-ikr \cos \tilde{\vartheta}) d\tilde{\phi} \quad (2.39) \\ &= \int_{-\infty}^{\infty} k^2 dk \int_0^{\pi/2} \sin \tilde{\vartheta} d\tilde{\vartheta} \int_0^{2\pi} D(k^2, \tilde{\vartheta}, \tilde{\phi}, \vartheta, \phi) \exp(ikr \cos \tilde{\vartheta}) d\tilde{\phi}. \end{aligned}$$

Similarly, we also obtain that

$$U_{(6)}(\vec{r}) = \int_{-\infty}^{\infty} k^4 dk \int_0^{\pi/2} \sin \tilde{\vartheta} d\tilde{\vartheta} \int_0^{2\pi} D_{(6)}(k^2, \tilde{\vartheta}, \tilde{\phi}, \vartheta, \phi) \exp(ikr \cos \tilde{\vartheta}) d\tilde{\phi}. \quad (2.40)$$

Apply now the radiation condition in order to extract the unique (physical) solution of the problem. Suppose that the medium has small absorption: $\text{Im}\kappa_0$ is a small positive number. Then, as seen from (2.34), two out of four poles

$$k_{1,2,3,4} = \pm \sqrt{\left(-b \pm \sqrt{b^2 - 4ac}\right) / 2a}$$

of the integrand in (2.39), (2.40) have positive imaginary parts. Properties of the integrand functions of the integrals over k in (2.39), (2.40) enable the closing of the corresponding integration contour in the upper half plane of the complex variable k . By finding the corresponding to these functions residues at the poles $k = k_1, k_2$ ($\text{Im}k_j > 0$ for $j = 1, 2,$) we obtain

$$U_{(6)}(\vec{r}) = -\pi i \int_0^{\pi/2} \sin \tilde{\vartheta} d\tilde{\vartheta} \times \int_0^{2\pi} \frac{k_1^{-1}(bk_1^2 + c)\exp(ik_1 r \cos \tilde{\vartheta}) - k_2^{-1}(bk_2^2 + c)\exp(ik_2 r \cos \tilde{\vartheta})}{a\sqrt{b^2 - 4ac}} d\tilde{\varphi}, \quad (2.41)$$

$$U(\vec{r}) = \pi i \int_0^{\pi/2} \sin \tilde{\vartheta} d\tilde{\vartheta} \int_0^{2\pi} \frac{k_1 \exp(ik_1 r \cos \tilde{\vartheta}) - k_2 \exp(ik_2 r \cos \tilde{\vartheta})}{\sqrt{b^2 - 4ac}} d\tilde{\varphi}. \quad (2.42)$$

Thus the representation for $\overline{\mathcal{G}}^{reg}(\vec{r})$ (see formulas (2.25)–(2.27)) is constructed. The finiteness of the domain of integration in (2.41), (2.42) and regularity of the integrand functions allowed using this representation both for numerical and asymptotic estimations of DGF.

Going to the limiting case of an isotropic medium in these formulas, we obtain the well-known relations [3, 11]. We failed to derive the relationships for the uniaxial anisotropic medium, but in the course of the computational experiments we fully confirmed the identity of the results following from (2.41), (2.42) and the results presented in [11]. In this context, it should be noted that the authors of [11] for some reason discarded the static part of the regular component of the Green's function for the uniaxial anisotropic medium without any comments. In our numerical experiments, we have taken into account the corresponding difference in the analytical results.

2.7 Conclusion

The dyadic Green's function for an unbounded biaxial anisotropic medium is treated analytically. The original triple integral is represented as a sum of singular and regular terms. For the first time, the first term has been evaluated analytically and presented in the general dyadic form, not related to the coordinate system. It is a

generalization of the well-known result for uniaxial anisotropy [11] to the case of a biaxial medium. In view of the radiation conditions at infinity, the regular part of DGF has been reduced to double integrals (2.41), (2.42) over a finite domain that are convenient for numerical calculations and for obtaining asymptotic estimates. These integrals also allow seeing the fundamental difference in analytics in the cases of biaxial and uniaxial anisotropic media. The integral over the variable $\tilde{\phi}$ can be represented as a contour integral over the unit circle. The square root in the denominator of the integrand generally has two branch points inside the contour and two out of it. The contour of integration is located between the two cut lines. In the transition to a uniaxial medium, the radical expression becomes a complete square, the branch points are transformed to the poles and the integral is easily calculated.

References

1. Tai, C.T.: *Dyadic Green's Functions in Electromagnetic Theory*. IEEE Press, New York (1994)
2. Chen, H.C.: *Theory of Electromagnetic Waves: A Coordinate-Free Approach*. McGraw-Hill, New York (1983)
3. Weiglhofer, W.S.: Dyadic Green's functions for general uniaxial media. In: *IEEE Proceedings–H: Microwaves, Antennas and Propagation*, vol. 137, no. 1, pp. 5–10 (1990)
4. Sautbekov, S., Kanymgazieva, I., Frangos, P.: The generalized solutions of Maxwell equation for the uniaxial crystal. *J. Appl. Electromagn.* **10**(2), 43–55 (2008)
5. Cottis, P.G., Kondylis, G.D.: Properties of the dyadic Green's function for an unbounded anisotropic medium. *IEEE Trans. Antennas Propag.* **43**(2), 154–161 (1995)
6. Cottis, P.G., Vazouras, C.N., Spyrou, C.: Green's function for an unbounded biaxial medium in cylindrical coordinates. *IEEE Trans. Antennas Propag.* **47**(1), 195–199 (1999)
7. Li, K., Park, S.O.: Dyadic Green's function for an unbounded anisotropic medium in cylindrical coordinates. *Prog. Electromagn. Res.* **35**, 115–125 (2002)
8. Kaklamani, D.I., Uzunoglu, N.K.: Radiation of a dipole in an infinite triaxial anisotropic medium. *Electromagnetics* **12**(2), 231–245 (1992)
9. Jakoby, B., Olyslager, F.: Asymptotic expansions for Green's dyadics in bianisotropic media. *Prog. Electromagn. Res.* **12**, 277–302 (1996)
10. Zhuck, N.P., Omar, A.S.: Radiation and low-frequency scattering of EM waves in a general anisotropic homogeneous medium. *IEEE Trans. Antennas Propag.* **47**(8), 1364–1373 (1999)
11. Potemkin, A.S., Poddubny, A.N., Belov, P.A., Kivshar, Y.S.: Green function for hyperbolic media. *Phys. Rev. A* **85**, 023848 (2012)
12. Vladimirov, V.S.: *Equations of Mathematical Physics*. Dekker, New York (1971)
13. Varshalovich, D.A., Moskalev, A.N., Chersonsky, V.K.: *Quantum Theory of Angular Momentum: Irreducible Tensors, Spherical Harmonics, Vector Coupling Coefficients, 3nj Symbols*. World Scientific, Singapore (1988)

Chapter 3

Operator Fresnel Formulas in the Scattering Theory of Waveguide Modes

Igor Petrusenko and Yuriy Sirenko

Abstract A novel formulation of the problem of wave diffraction by abrupt and volume discontinuities in a waveguide is presented in this chapter. In the context of this formulation, the authors succeeded in solving a number of the long-discussed problems concerning mathematical properties of matrix models of the mode-matching technique. In particular, they rigorously justified the possibility to use the truncation technique, unconditionally converging in the norm of a space of infinite sequences, for numerical implementation of the developed matrix models. The operator-matrix analysis of the mode-matching technique has shown that the proposed approach leads to the operator Fresnel formulas, which generalize properly the well-known Fresnel formulas to the scattering operators.

3.1 Introduction

Scattering of a plane time-harmonic wave being incident normally on the plane Ω , where the wave properties of a continuous medium occupying all space are changing abruptly, is described by the well-known *Fresnel formulas*

$$r = \frac{d^2 - 1}{d^2 + 1}, \quad t = \frac{2d}{d^2 + 1} \quad (3.1)$$

I. Petrusenko (✉)

University of Customs and Finance, Dnipropetrovsk, Ukraine
e-mail: petrusigor@gmail.com

Y. Sirenko

National Academy of Sciences, O.Ya. Usikov Institute for Radiophysics
and Electronics, Kharkiv, Ukraine
e-mail: yks@ire.kharkov.ua

Y. Sirenko

L.N. Gumilyov Eurasian National University, Astana, Republic of Kazakhstan

for the amplitude reflection (r) and transmission (t) coefficients. In these equalities, the dimensionless parameter d characterizes the jump discontinuity of the *medium impedance* on the boundary Ω .

The original Fresnel formulas were related to the description of regularities attributed to the scattering of transverse waves in a hypothetical ether. A.-J. Fresnel himself stated [1] that the reflection formula had been originally given by T. Young, and then C.-D. Poisson had obtained it for longitudinal vibrations of highly elastic ether. For these two problems, the derivation of formulas of type (3.1) was based on the equality of the frequencies of the incident, reflected and transmitted waves.

In classical electrodynamics, the Fresnel formulas follow directly from the boundary conditions

$$\vec{E}_{tg}^{(1)}(\omega) = \vec{E}_{tg}^{(2)}(\omega) \quad \text{and} \quad \vec{H}_{tg}^{(1)}(\omega) = \vec{H}_{tg}^{(2)}(\omega) \quad \text{on the surface} \quad \Omega. \quad (3.2)$$

They are also known as the matching conditions for the tangential components of the vector complex amplitudes (i.e. vector phasors) of the electromagnetic field of angular frequency ω existing on both sides (1 and 2) of the interface Ω (due to a large number of published studies, we refer the reader to the basic reference [2]).

For normal incidence of a *TEM*-wave on a plane interface Ω between two linear homogeneous isotropic media, we have

$$r^{11} = \pm r, \quad t^{21} = t, \quad d = \sqrt{\theta_{21}}; \quad \left\{ \begin{array}{l} H_{\perp} - \text{case} \\ E_{\perp} - \text{case} \end{array} \right\} \quad (3.3)$$

for the two possible polarizations (H_{\perp} and E_{\perp}) with respect to the observation plane. Here, r^{11} is the reflection coefficient in the first medium, t^{21} is the transmission coefficient from medium 1 to medium 2, while θ_{21} stands for the relative impedance/admittance of these two media. The substitution $(\pm) \rightarrow (\mp)$ in the first equality in (3.3) gives the expression for the reflection coefficient r^{22} in the second medium, with the coefficient $t^{12} = t$ being characteristic of the wave transmission from medium 2 into medium 1.

In this chapter we will show that the wave scattering law in the form of (3.1), (3.3), but for the *reflection and transmission matrix operators*

$$R^{11} = \pm \frac{D_0 D_0^T - I}{D_0 D_0^T + I}, \quad T^{21} = (D_0 D_0^T + I)^{-1} 2D_0; \quad \left\{ \begin{array}{l} H - \text{case} \\ E - \text{case} \end{array} \right\} \quad (3.4)$$

holds for the *H*-or *E*-plane two-port waveguide junction, where the *Poynting vector* of the incident wave is perpendicular to the aperture plane Ω of the step discontinuity in a waveguide (i.e., having its own volume $V_{\text{int}} = 0$) and where the matching conditions (3.2) are satisfied. In formulas (3.4) the matrix operator $D_0 = D_0(\omega)$ acting in the *Hilbert space* l_2 , is defined by the given geometry of the problem, I is the unit operator, and the superscript ' T ' indicates transposition. Similarly to the above-mentioned properties of formulas (3.3), simultaneous substitutions

$(\pm) \rightarrow (\mp)$ and $D_0 \rightleftharpoons D_0^T$ in (3.4) give expressions for the reflection and transmission operators, R^{22} and T^{12} , respectively. There are other parallels between formulas (3.1), (3.3) and operator expressions (3.4), which will be discussed in the relevant sections of this chapter.

Considering the generally recognized name of (3.1), we will call formulas like (3.4) *operator Fresnel formulas*. It is clear that they generalize their scalar analogues (3.1), (3.3) to the case of an infinite (but countable) number of the waveguide modes.

In this chapter we will also show that the relationships similar to (3.1) but for the generalized scattering matrix S of the N -port wave transformer (i.e. for the $N \times N$ operator matrix acting in the Hilbert space $h_N = l_2^N$, $N = 2, 3, \dots$; $l_2^2 = l_2 \times l_2$, and so on), take place in the case of the ‘volume’ ($V_{\text{int}} \neq 0$) waveguide discontinuities:

$$S = \frac{W - I_h}{W + I_h}, \quad K = (W + I_h)^{-1} 2W_0. \quad (3.5)$$

Here, the given operator of the problem has the formal representation $W = W_0 W_0^T$, the unit operator is $I_h : h_N \rightarrow h_N$, while the introduced operator matrix K characterizes the oscillating field in the cavity V_{int} . Since formulas (3.5) represent the next step of generalization—the transition from matrix operators to operator matrices—we will call them *generalized operator Fresnel formulas*.

In computational electrodynamics, boundary conditions (3.2) are regarded as the initial equalities of rigorous methods for solving diffraction problems that involve real or virtual boundaries separating different regions of wave propagation. In particular, among those methods is the mode-matching technique (also known as the method of partial (contiguous) regions or re-expansion method), which remains popular in engineering practice over a very long period of time and seems to be the most widespread tool for calculating waveguide paths.

All the known matrix models of the mode-matching technique have the form of infinite systems of linear algebraic equations. They appear in connection with a commonly used formulation of the mode diffraction problem.

The conventional statement of the problem of mode diffraction by a waveguide discontinuity is as follows: a specified single waveguide mode is scattered by a discontinuity and it is necessary to find the amplitudes of the excited modes (both propagating and evanescent ones). Such problem formulation leads to infinite systems of linear algebraic equations, in which identifying the operator Fresnel formulas is quite a challenge.

In accordance with the developed approach, we propose to change the problem formulation in the following way. The electromagnetic wave of a finite power is scattered by a given discontinuity in the waveguide; the field of this wave is an infinite set of modes with any known distribution of amplitudes; it is necessary to find the scattering operators.

If the diffraction problem is posed as suggested above, then the application of the mode-matching technique yields an equation with respect to the scattering operator rather than an infinite system of linear algebraic equations.

This new approach to solving diffraction problems appears to be more efficient. In particular, it allows one to

- rigorously prove the existence, uniqueness and stability of the solutions of the matrix-operator equations of the mode-matching technique for two classes of the problems considered;
- clarify that the correctness of the operator Fresnel formulas is a direct consequence of the energy conservation law;
- prove the unconditional convergence of the projection approximations of the truncation technique to the actual scattering operators;
- investigate the rate of convergence of approximate solutions;
- estimate analytically the condition number for both the infinite and the truncated matrix of the final model.

From the formal mathematical point of view, the proposed approach means that the unknown vector of the Fourier coefficients in the modal expansion of the field is replaced by the desired matrix scattering operator. This idea is not new in mathematical physics—it will suffice to mention Heisenberg’s matrix quantum mechanics. In computational electromagnetics this idea probably was first consistently implemented in the method of matrix operators [4]. The approach applied in this chapter can also be seen as a further development of the method of spectral scattering operators [5–7].

Thus, we assert that the considered mode-matching technique is of a matrix-operator nature and, therefore, the theory of operators in the Hilbert space and, as will be shown, in the *Pontryagin space* [8] provides an adequate mathematical tool for solving mode diffraction problems.

3.2 The Mode-Matching Technique in the Problem of a Waveguide Step-like Discontinuity

Let us analyze the application of the mode-matching technique to the problem of diffraction of waveguide modes.

3.2.1 *The Classical Mode-Matching Technique: An Example of Application*

The best known guidance on the application of the classical mode-matching technique is the book by Mittra and Lee [3]. The method therein is applied to the

analytically solvable canonical problem of a waveguide bifurcation in the H -plane [9]. In the proposed approach one can identify the following key points [3]:

- *Formulation of the problem.* The fundamental mode with unit amplitude is incident on a discontinuity in a parallel plane waveguide with perfectly conducting walls. The scattered field is to be found.

The desired field is a complete set of waveguide modes with the same polarization as the incident wave, since the problem under consideration is invariant with respect to displacement along the Cartesian axis perpendicular to the H -plane. Just as for the incident wave, all the components of the scattered field are completely determined by the complex amplitude of the single component of the electric field $U(g, \omega)$, $g = \{y, z\}$ (throughout the chapter we will use the uniform notation other than that used in the book [3]). This scalar function satisfies the wave equation, the homogeneous *Dirichlet conditions* on perfectly conducting surfaces, the condition at infinity for waveguides and the condition on a sharp edge [10].

- *Construction of the matrix model.* The geometry of the problem allows partition of the entire domain of the field determination into simple partial contiguous subregions, which is why the mode-matching technique is sometimes called the method of partial regions. The partial region is called simple if it allows one to find the general solution of the given boundary value problem by using the method of separation of variables in a suitable coordinate system.

The function $U(g, \omega)$ is sought in each of the regions as a series of a complete set of waveguide modes with their amplitudes to be determined. For the propagating modes, these amplitudes are the reflection and transmission coefficients.

The matching of the tangential electric and magnetic field components on the common (virtual) boundary of partial regions, results in a system of functional equations. Application of the *Galerkin procedure*, i.e. projection of the obtained equations on the complete set of the transversal eigenfunctions of the waveguides, yields a dual infinite system of linear algebraic equations (SLAE) for the desired complex coefficients of the modal expansion of the field.

- *The analytical solution of the infinite SLAE.* The constructed SLAE can be solved analytically both by the truncation technique and by the method of residues [3]. In the first case, the infinite SLAE is first truncated, what is the same to taking into account the finite number of modes M and N in the corresponding partial regions. Then the solution of the SLAE reduced to the order of $(M + N) \times (M + N)$ is obtained by the classical *Cramer rule*. Finally, the passage to the limit at $M, N \rightarrow \infty$ is performed.
- *The analysis of the obtained analytical solution.* As it was found, the approximate solution of the infinite SLAE obtained by the truncation procedure is not the only one, and it depends on the ratio M/N . This phenomenon has been called *relative convergence*, while the rule of determination of such M/N that leads to the true solution is often referred to as *Mittra rule*. The relative convergence

effect is confirmed by numerous computations for various problems of mode diffraction by waveguide step-like discontinuities.

- *Software implementation of the exact solution of the infinite SLAE.* Numerical experiments show that the exact analytical solution of the matrix equation is, generally speaking, poorly adapted for practical computations. It was found that the problems arising in the calculation of slowly converging infinite products and series as a rule require significant additional efforts. Therefore, the approximate solutions of the diffraction problems may reduce computational burden as compared with the rigorous analytical results.

Based on a literal understanding of the problem statement [3], one could expect that the declared purpose of the study is to find the scattered field. However, in the book [3], as in many other works, neither the function $U(g, \omega)$ nor, especially, the components of the electromagnetic field are calculated. Instead, the found coefficients of the modal expansion for the function $U(g, \omega)$ are declared as the solution of the problem.

3.2.2 *The Mode-Matching Technique in the Problem of a Step Discontinuity in a Waveguide: Standard Approach*

In this subsection we present an example of the commonly accepted practice of using the mode-matching technique in the typical case where the problem has no exact analytical solution, but is important for engineering.

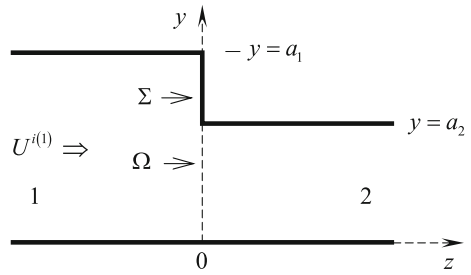
The problem of the mode scattering by a step discontinuity in the H - or E -plane rectangular (or parallel-plate) waveguide is a canonical problem of the applied electrodynamics. All the features of the application of the mode-matching technique for the analysis of this elementary discontinuity can be transferred, as will be seen in Sect. 3.9, on the whole class of problems usually called the problems of *abrupt waveguide discontinuities*. (The rigorous criterion of dividing all the mode diffraction problems into two different classes will be formulated in Sect. 3.8.) Of course, the list of papers devoted to this problem is very long. We will rely basically on the work [11], where an extensive bibliography is also available.

Let us apply the mode-matching technique to the problem of step discontinuity in a waveguide following the above scheme.

The contour of the discontinuity under study and the used Cartesian coordinate system are shown in Fig. 3.1. We consider an infinite hollow rectangular waveguide with an abrupt change in its cross-section in the plane $z = 0$ from $a_1 \times a_3$ to $a_2 \times a_3$. The plane, where the cross-section changes stepwise and in which the aperture of the discontinuity is lying, we take as a reference plane.

Referring to Fig. 3.1, the waveguide is divided into two simple partial regions, namely, two semi-infinite arms 1 and 2. The ratio a_2/a_1 is arbitrary ($0 < a_2/a_1 < 1$).

Fig. 3.1 Geometry of the problem



All the metal walls of the waveguide are assumed to be perfectly conducting surfaces.

Suppose that the r th waveguide mode of unit amplitude ($r \geq 0$ is an arbitrary integer) be incident onto the step (Fig. 3.1) from the region 1. To simplify the analysis we assume that the field of this mode does not change along the x -axis in case of H -plane discontinuity, while in the case of the E -plane step one variation of the field occurs. In what follows we will consider both of these problems simultaneously, indicating formulas by H -case or E -case, respectively.

Depending on the polarization of the incident wave, we write the x -component of the field as

$$\begin{aligned} E_x &= U(g, \omega) \exp(-i\omega t) && \text{for } H\text{-case and} \\ H_x &= U(g, \omega) \sin(\pi x/a_3) \exp(-i\omega t) && \text{for } E\text{-case.} \end{aligned} \quad (3.6)$$

The remaining field components can be expressed via the continuous function $U(g, \omega)$, which is the solution of the two-dimensional homogeneous Helmholtz equation

$$\left(\frac{\partial^2}{\partial y^2} + \frac{\partial^2}{\partial z^2} + \chi^2 \right) U = 0; \quad \chi^2 = \begin{cases} k^2; & H\text{-case} \\ k^2 - (\pi/a_3)^2; & E\text{-case} \end{cases} \quad (3.7)$$

in any finite domain of the field determination. Here, $k = \sqrt{\epsilon_0 \mu_0} \omega$ is the wavenumber and $\text{Re } k > 0, \text{Im } k = 0$.

Let us denote the values of the function U in the regions 1 and 2 by $U^{(1)}$ and $U^{(2)}$, respectively. Then the conditions ensuring the existence and uniqueness of the solution of this electrodynamic problem takes the following form:

- homogeneous boundary conditions

$$\begin{aligned} U(g, \omega)|_{g \in \Sigma} &= 0 && \text{for } H\text{-case and} \\ \partial U(g, \omega) / \partial \vec{n}|_{g \in \Sigma} &= 0 && \text{for } E\text{-case} \end{aligned} \quad (3.8)$$

on the all perfectly conducting walls $\Sigma = \Sigma_x \times [0 < x < a_3]$ of the waveguide junction; Σ_x is the trace of these walls in yOz -plane and \vec{n} is the surface normal;

- condition of continuity of the tangential components of the electric and magnetic fields on the interface Ω between the two partial regions (i.e. the matching condition)

$$U^{(1)}(g, \omega) = U^{(2)}(g, \omega) \quad \text{and} \quad \partial U^{(1)} / \partial z = \partial U^{(2)} / \partial z; \quad g \in \Omega; \quad (3.9)$$

- condition at infinity for waveguides in the form

$$\lim_{z \rightarrow -\infty} \exp(-i\beta_{m1}z) = 0 \quad \text{and} \quad \lim_{z \rightarrow +\infty} \exp(i\beta_{m2}z) = 0 \quad \text{for} \quad (3.10)$$

$$m : \chi^2 < \lambda_{mj}^2 = (m\pi/a_j)^2; \quad j = 1, 2,$$

where

$$\beta_{mj} = \sqrt{\chi^2 - \lambda_{mj}^2} \quad (3.11)$$

are the propagation constants of modes in the j th partial region;

- condition of finiteness of the field energy in any bounded field domain S , which is written in the form [11]

$$W(S) = \int_S \left[|U|^2 + \left| \frac{\partial U}{\partial y} \right|^2 + \left| \frac{\partial U}{\partial z} \right|^2 \right] ds \equiv \|U\|_{L_2(S)}^2 + \|\nabla_{yz}U\|_{L_2(S)}^2 < \infty \quad (3.12)$$

with $\lim_{S \rightarrow 0} W(S) = 0$.

The last-mentioned condition excludes the sources/sinks of the field inside the finite domain S , including those at the points of geometrical singularities (for this problem—on the sharp edge of the step $\{y, z\} = \{a_2, 0\}$) [10]. This ‘*edge condition*’ defines the functional space, in which the complex amplitude $U(g, \omega)$ should be sought. Namely, according to (3.12), this function should belong to the *Sobolev space* W_2^1 (see, for example, book [12]).

It follows from (3.10) and from the principle of limiting absorption for undamped modes (with the numbers m such that $\chi^2 > \lambda_{mj}^2$) that the propagation constant β_{mj} is given by the branch of the square root (3.11) such that $\text{Re } \beta_{mj} \geq 0$ and $\text{Im } \beta_{mj} \geq 0$. We exclude the critical frequencies k_{mj}^+ of the waveguides that correspond to $\beta_{mj} = 0$ for some values of m as non-physical.

The waveguide modes of the partial regions are given by the complete orthonormal sets of real-valued eigenfunctions

$$\mu_{mj}(y) = \begin{cases} \sqrt{\frac{2}{a_j}} \sin(\lambda_{mj}y); & m = 1, 2, 3, \dots, \quad H - \text{case} \\ \sqrt{\frac{2 - \delta_0^m}{a_j}} \cos(\lambda_{mj}y); & m = 0, 1, 2, \dots, \quad E - \text{case} \end{cases}; \quad y \in (0, a_j), \quad j = 1, 2 \quad (3.13)$$

whose scalar product is determined in the usual manner:

$$(\mu_{mj}, \mu_{nj})_{(0, a_j)} \equiv \int_0^{a_j} \mu_{mj}(y) \mu_{nj}(y) dy = \delta_m^n = \begin{cases} 1 & \text{if } m = n \\ 0 & \text{if } m \neq n. \end{cases} \quad (3.14)$$

In accordance with the physics of the of scattering phenomenon, we represent the field in the first partial region as a sum of the incident and reflected waves

$$\begin{aligned} U^{(1)}(g, \omega) &= U^{i(1)}(g, \omega) + U^{s(1)}(g, \omega) \\ &= \mu_{r1}(y) \exp(i\beta_{p1}z) + \sum_{m=(0)1}^{\infty} x_{m1} \mu_{m1}(y) \exp(-i\beta_{m1}z); \quad z \leq 0, \end{aligned} \quad (3.15)$$

while in the second region—as the transmitted wave

$$U^{(2)}(g, \omega) = U^{s(2)}(g, \omega) = \sum_{n=(0)1}^{\infty} x_{n2} \mu_{n2}(y) \exp(i\beta_{nj}z); \quad z \geq 0. \quad (3.16)$$

If we substitute these modal expansions into the integral in (3.12) and then integrate over any finite domain S , we find that $\{x_{m1}\}_{m=(0)1}^{\infty}$, $\{x_{n2}\}_{n=(0)1}^{\infty} \in \tilde{l}_2$, where

$$\tilde{l}_2 = \left\{ a \equiv \{a_m\}_m; \sum_m m |a_m|^2 = \|a\|_+^2 < \infty \right\} \quad (3.17)$$

is the Hilbert space of sequences of complex numbers. (Appendix A gives basic information about all vector spaces used in this chapter.)

Problem 3.1 Verify: $\{x_{m1}\}_{m=(0)1}^{\infty}$, $\{x_{n2}\}_{n=(0)1}^{\infty} \in \tilde{l}_2$.

The matching condition (3.9) applied to the fields in the partial regions at the aperture Ω of the discontinuity together with the boundary condition (3.8) at the face of the step lead to the following functional equations

$$\mu_{r1}(y) + \sum_{m=(0)1}^{\infty} x_{m1} \mu_{m1}(y) = \begin{cases} 0; & y \in (a_2, a_1), \quad H - \text{case only} \\ \sum_{n=(0)1}^{\infty} x_{n2} \mu_{n2}(y); & y \in (0, a_2), \end{cases} \quad (3.18a)$$

$$\beta_{r1} \mu_{r1}(y) - \sum_{m=(0)1}^{\infty} x_{m1} \beta_{m1} \mu_{m1}(y) = \begin{cases} 0; & y \in (a_2, a_1), \quad E - \text{case only} \\ \sum_{n=(0)1}^{\infty} x_{n2} \beta_{n2} \mu_{n2}(y); & y \in (0, a_2). \end{cases} \quad (3.18b)$$

Performing projection onto the *complete and orthonormal set of eigenfunctions* $\{\mu_{mj}(y)\}_{m=(0)1}^{\infty}$, $y \in (0, a_j)$, $j = 1, 2$, we obtain the dual infinite SLAE

$$\begin{cases} \delta_m^r + x_{m1} = \sum_{n=(0)1}^{\infty} x_{n2} (\mu_{n2}, \mu_{m1}); & m = 1, 2, 3, \dots \\ \frac{\beta_{r1}}{\beta_{n2}} (\mu_{r1}, \mu_{n2}) - \sum_{m=(0)1}^{\infty} x_{m1} \frac{\beta_{m1}}{\beta_{n2}} (\mu_{m1}, \mu_{n2}) = x_{n2}; & n = 1, 2, 3, \dots \end{cases} \quad \text{for } H - \text{case}, \quad (3.19)$$

or

$$\begin{cases} (\mu_{r1}, \mu_{n2}) + \sum_{m=0}^{\infty} x_{m1} (\mu_{m1}, \mu_{n2}) = x_{n2}; & n = 0, 1, 2, \dots \\ \delta_m^r - x_{m1} = \sum_{n=0}^{\infty} x_{n2} \frac{\beta_{n2}}{\beta_{m1}} (\mu_{n2}, \mu_{m1}); & m = 0, 1, 2, \dots \end{cases} \quad \text{for } E - \text{case}. \quad (3.20)$$

The scalar product of the eigenfunctions can be found explicitly:

$$(\mu_{m1}, \mu_{n2}) \equiv (\mu_{n2}, \mu_{m1}) = \frac{\sin[(\lambda_{m1} - \lambda_{n2})a_2]}{\lambda_{m1}^2 - \lambda_{n2}^2} \begin{cases} \frac{2}{\sqrt{a_1 a_2}} \lambda_{n2}; & H - \text{case} \\ \sqrt{\frac{(2 - \delta_0^m)(2 - \delta_0^n)}{a_1 a_2}} \lambda_{m1}; & E - \text{case} \end{cases}. \quad (3.21)$$

Excluding x_{n2} from the systems (3.19) and (3.20), we arrive at the final infinite SLAE:

$$x_{m1} + \sum_{q=(0)1}^{\infty} D_{mq} x_{q1} = \mp [\delta_m^r - D_{mr}]; \quad m = (0)1, 2, \dots, \quad \begin{cases} H - \text{case} \\ E - \text{case} \end{cases}. \quad (3.22)$$

Here we introduced the notation

$$D_{mq} = \begin{cases} 4 \frac{\beta_{q1}}{a_1 a_2} \sum_{n=1}^{\infty} \frac{\lambda_{n2}^2}{\beta_{n2}} \frac{\sin[(\lambda_{m1} - \lambda_{n2})a_2]}{\lambda_{m1}^2 - \lambda_{n2}^2} \frac{\sin[(\lambda_{n2} - \lambda_{q1})a_2]}{\lambda_{n2}^2 - \lambda_{q1}^2}, & H - \text{case} \\ \sqrt{(2 - \delta_0^m)(2 - \delta_0^q)} \frac{\lambda_{m1} \lambda_{q1}}{\beta_{m1} a_1 a_2} \sum_{n=0}^{\infty} (2 - \delta_0^n) \beta_{n2} \frac{\sin[(\lambda_{m1} - \lambda_{n2})a_2]}{\lambda_{m1}^2 - \lambda_{n2}^2} \\ \times \frac{\sin[(\lambda_{n2} - \lambda_{q1})a_2]}{\lambda_{n2}^2 - \lambda_{q1}^2}; & E - \text{case} \end{cases} .$$

The analytical solution of infinite SLAE (3.22) is not known, and this situation is typical for most of the problems that are important for applications. The way out is to prove the correctness of the constructed matrix model and to justify the truncation procedure for finding finite-dimensional approximations.

A considerable effort was made to implement this approach (see, for example, [11]). Many researchers believed that the knowledge of the explicit form of all elements of the infinite matrix $D = \{D_{mq}\}_{m,q=(0)1}^{\infty}$ had to provide the knowledge of all its operator properties. However, the results of these studies, in general, have not met these expectations.

Problem 3.2 (research) On the basis of the exact expression for the matrix elements of the operator D, show its boundedness on the pair of spaces $\tilde{l}_2 \rightarrow \tilde{l}_2$. A simple proof of this fact, but by the other way, will be given in Sect. 3.4.1.

As noted by P.R. Halmos in his famous book [13]: ‘While the algebra of infinite matrices is more or less reasonable, the analysis is not. Questions about norms and spectra are likely to be recalcitrant. Each of the few answers that are known is considered a respectable mathematical accomplishment.’ Appendix B to this chapter provides an overview of applied results of the theory of matrix operators in frequently used *Banach spaces*. As one can see, these results are of little use for the problem under consideration.

Moreover, it turned out to be almost impossible to justify rigorously the applicability of the truncation procedure for finding approximate solutions of matrix equations of the type (3.22).

It is extremely rare to find in today’s publications a discussion of the existence and uniqueness of the solution obtained by the mode-matching technique or by any related method (for example, by the method of moments). A discussion of the stability of the solution and the validity of the truncation procedure is replaced, in the best case, by the analysis of the ‘practical convergence’ of the results of computer calculations and by the numerical evaluation of the condition number for a truncated SLAE. The study of the above-mentioned phenomenon of the relative convergence of approximations resulting in a numerical catastrophe has also for many years been in a theoretical impasse.

The current unfavorable situation in the theory of the mode-matching technique can be resolved, as will be shown, by changing the formulation of the problem of mode diffraction.

3.2.3 New Formulation of the Problem of Scattering of Waveguide Modes

Earlier we have used the conventional formulation of the problem of mode diffraction. We assumed that a specified waveguide mode is scattered by a given discontinuity. (Note that in practice the analysis is most often restricted by the fundamental mode $r = 1$ for H -case or $r = 0$ for E -case.) As a result, the mode-matching technique always leads to infinite SLAE with respect to the desired amplitudes $\{x_{m1}\}_{m=(0)1}^{\infty}$, $\{x_{n2}\}_{n=(0)1}^{\infty}$.

We propose a new and, in our view, a more natural statement of the problem. Let us assume that an electromagnetic wave of finite energy, whose field is a complete set of modes with any given distribution of complex amplitudes, be incident on a discontinuity. It is required to find scattering operators.

A way to introduce these operators is to replace the infinite-dimensional vectors of the Fourier coefficients $\{x_{m1}\}_{m=(0)1}^{\infty}$, $\{x_{n2}\}_{n=(0)1}^{\infty} \in \tilde{l}_2$, by the infinite reflection and transmission matrices $X_1, X_2 : \tilde{l}_2 \rightarrow \tilde{l}_2$ (i.e., by the scattering matrix operators).

With this formulation of the problem, the mode-matching technique leads to the equation with respect to the desired scattering matrix operator. For the diffraction by a step-like discontinuity in a waveguide, these operator relationships have the form of the Fresnel formulas

$$R = \frac{D_0 D_0^T - I}{D_0 D_0^T + I}, \quad T = (D_0 D_0^T + I)^{-1} 2D_0 \quad (3.23)$$

for the reflection (R) and transmission (T) operators acting in the Hilbert space l_2 . In these formulas, the elementary matrix operator of the problem, D_0 , is determined by the geometry of the waveguide discontinuity and depends on the frequency.

In order to obtain the solution of the problem in the form of (3.23) as simply as to derive the infinite systems of (3.22), it is convenient to use the matrix operator method. The basics of the relevant mathematical formalism are outlined below as applied to the problem of a step discontinuity in a waveguide.

3.3 Matrix Operator Formalism in the Scalar Mode Analysis

Let us combine the unknown Fourier coefficients of waveguide mode expansions (3.15), (3.16) into the infinite-dimensional row vectors $x_1 = \{x_{m1}\}_{m=(0)1}^{\infty}$ and $x_2 = \{x_{n2}\}_{n=(0)1}^{\infty}$, while the transverse eigenfunctions of the partial regions (3.13)—

into the column vector $\mu_j(y) = \{\mu_{mj}(y)\}_{m=(0)1}^\infty$, $j = 1, 2$. The properties of this vector-function are determined by the equalities

$$\mu_j^T(y)\mu_j(\bar{y}) = \delta(y - \bar{y}), \quad \left(\mu_j, \mu_j^T\right)_{(0,a_j)} = I. \quad (3.24)$$

Here we use the usual notation for the Dirac delta function and the *bilinear tensor-scalar product of vector-functions*.

Let us introduce the diagonal matrix operator describing mode propagation $E_j(z) = \{\delta_m^n \exp(-i\beta_{mj}z)\}_{m,n=(0)1}^\infty$, $j = 1, 2$, such that $E_j(0) = I$ is the unit operator. Then the decompositions of the complex amplitudes (or phasors) of the reflected and transmitted waves into waveguide modes (3.15), (3.16) take the form

$$\begin{aligned} U^{s(1)}(g, \omega) &= x_1 E_1(z) \mu_1(y); \quad z \leq 0 \quad \text{and} \\ U^{s(2)}(g, \omega) &= x_2 E_2(-z) \mu_2(y); \quad z \geq 0. \end{aligned} \quad (3.25)$$

Using these formulas, the derivative of the complex amplitudes along the waveguide axis z can be written as

$$\begin{aligned} \partial U^{s(1)}(g, \omega) / \partial z &= x_1 E_1^\beta(z) \mu_1(y); \quad z \leq 0 \quad \text{and} \\ \partial U^{s(2)}(g, \omega) / \partial z &= -x_2 E_2^\beta(-z) \mu_2(y); \quad z \geq 0, \end{aligned} \quad (3.26)$$

where $E_1^\beta(z) = \{-i\delta_m^n \beta_{mj} \exp(-i\beta_{mj}z)\}_{m,n=(0)1}^\infty$ is another diagonal matrix operator, which generates the ‘*similarity operator*’ $I_j^\beta \equiv E_j^\beta(0) = \{-i\delta_m^n \beta_{mj}\}_{m,n=(0)1}^\infty$, $j = 1, 2$.

The flux of the reflected oscillating power through the aperture Ω of the discontinuity is determined by the value

$$F_{\text{osc}}^{s(1)} = \left[\left(U^{s(1)}(g, \omega), \frac{\partial U^{s(1)}(g, \omega)}{\partial z} \right)_{(0,a_1)} \right]_{z=-0} = x_1 I_1^\beta x_1^T = \tilde{x}_1 \tilde{x}_1^T, \quad (3.27)$$

while the flux of the reflected complex power—by the value

$$F_{\text{comp}}^{s(1)} = \left[\left(U^{s(1)}(g, \omega), \frac{\partial [U^{s(1)}(g, \omega)]^*}{\partial z} \right)_{(0,a_1)} \right]_{z=-0} = x_1 \left(I_1^\beta \right)^* x_1^\dagger = \tilde{x}_1 U_1 \tilde{x}_1^\dagger, \quad (3.28)$$

where $\tilde{x}_1 = x_1 \left(I_1^\beta \right)^{1/2}$, and the superscripts ‘*’ and ‘†’ stand for the complex conjugation and *Hermitian conjugation*, respectively. In (3.28) we introduced the diagonal operator of the waveguide port (or *portal operator*)

$$U_1 \equiv \left(I_1^\beta \right)^{-1/2} \left(I_1^\beta \right)^* \left(I_1^{\beta*} \right)^{-1/2} = \left\{ \delta_m^n \exp[-i \arg(-i\beta_{m1})] \right\}_{m,n=(0)1}^\infty, \quad (3.29)$$

which is uniquely defined, provided $\beta_{m1} \neq 0$ for $\forall m$.

Suppose that in the first waveguide p_1 (*H*-case) or $p_1 + 1$ (*E*-case) types of modes propagate at the given frequency. Let us introduce the *orthoprojectors*

$$P_1 = \left\{ \sum_{q=(0)1}^{p_1} \delta_m^q \delta_q^n \right\}_{m,n=(0)1}^\infty, \quad Q_1 = \left\{ \sum_{q=p_1+1}^\infty \delta_m^q \delta_q^n \right\}_{m,n=(0)1}^\infty \quad (3.30)$$

such that $\tilde{x}_{1-} = \tilde{x}_1 P_1$ and $\tilde{x}_{1+} = \tilde{x}_1 Q_1$ are the row vectors of the amplitudes of the propagating modes and all evanescent modes, respectively. Then from the definition (3.29), in view of the condition at infinity (3.10), it follows that

$$U_1 = Q_1 + iP_1. \quad (3.31)$$

From (3.29) and (3.31) it is obvious that the portal operator is unitary, $U_1^{-1} = U_1^\dagger$, and that its numerical range lies entirely in the first quadrant of the complex plane. Such operators are usually called *cramped unitary operators*.

Problem 3.3 Find the portal operator U_1 for the field with time dependence $\exp(i\omega t)$. Answer: $U_1 = \left\{ \delta_m^n \exp[-i \arg(-i\beta_{m1})] \right\}_{m,n=(0)1}^\infty = Q_1 - iP_1$.

Instead of the condition of finiteness of the stored energy (3.12) for the field $U = U^{s(1)}(g, \omega)$, let us postulate the equivalent requirement of finiteness of the flux of reflected complex power through the waveguide: $\left| F_{\text{comp}}^{s(1)} \right| < \infty$.

Problem 3.4 Prove the equivalence of the conditions (3.12) and $\left| F_{\text{comp}} \right| < \infty$ for the solution $U(g, \omega)$ of the Helmholtz equation.

Problem 3.5 Show that estimate $\left| F_{\text{osc}} \right| < \infty$ follows immediately from the finiteness of the flux of complex power.

By substituting (3.31) into (3.28), we find:

$$F_{\text{comp}}^{s(1)} = \|\tilde{x}_{1+}\|^2 + i\|\tilde{x}_{1-}\|^2. \quad (3.32)$$

Here, the notation $\|\tilde{x}_{1\pm}\|^2 = \tilde{x}_{1\pm} \tilde{x}_{1\pm}^\dagger$ has been used (see Appendix A). Consequently, $\|x_{1+}\|^2 = \text{Re } F_{\text{comp}}^{s(1)} \leq \left| F_{\text{comp}}^{s(1)} \right| < \infty$. So, we have $\tilde{x}_1 \in l_2 \leftrightarrow x_1 \in \tilde{l}_2$, where

$$l_2 = \left\{ a \equiv \{a_m\}_m: \sum_m |a_m|^2 = \|a\|^2 < \infty \right\} \quad (3.33)$$

is the standard Hilbert space of the sequences of complex numbers (see also Appendix A).

Problem 3.6 Verify that $\tilde{x}_1 \in l_2$.

In a similar way, if in the second waveguide p_2 (H -case) or $p_2 + 1$ (E -case) modes propagate at the same frequency, we can define the orthoprojectors:

$$P_2 = \left\{ \sum_{q=(0)1}^{p_2} \delta_m^q \delta_q^n \right\}_{m,n=(0)1}^{\infty}, \quad Q_2 = \left\{ \sum_{q=p_2+1}^{\infty} \delta_m^q \delta_q^n \right\}_{m,n=(0)1}^{\infty}, \quad (3.34)$$

while for the unitary operator for the second port we obtain

$$U_2 = \left(I_2^\beta \right)^{-1/2} \left(I_2^\beta \right)^* \left(I_2^{\beta^*} \right)^{-1/2} = \left\{ \delta_m^n \exp[-i \arg(-i\beta_{m2})] \right\}_{m,n=(0)1}^{\infty} = Q_2 + iP_2. \quad (3.35)$$

From the requirement of finiteness of the flux of transmitted complex power, $|F_{\text{comp}}^{s(2)}| < \infty$, it follows that $x_2 \in \tilde{l}_2$ and $\tilde{x}_2 = x_2 \left(I_2^\beta \right)^{1/2} \in l_2$. This will automatically give $|F_{\text{osc}}^{s(1)}| < \infty$.

According to the new formulation of the diffraction problem, let us represent the unknown complex amplitude as the scalar product of the infinite-dimensional vectors:

$$U(g, \omega) = \tilde{b} \cdot u(g, \omega) = \sum_{m=(0)1}^{\infty} \tilde{b}_m u_m(g, \omega), \quad (3.36)$$

where the given row vector $\tilde{b} = \{\tilde{b}_m\}_{m=(0)1}^{\infty} \in \tilde{l}_2$ describes the incident wave, while $u(g, \omega) = \{u_m(g, \omega)\}_{m=(0)1}^{\infty}$ is the column vector of the functions to be found.

It is easy to see that the validity of the postulated representation (3.36) follows from the linearity of the Helmholtz equation. Indeed, assume that in the entire infinite domain of the field determination, the unknown functions $u_m(g, \omega)$ satisfy the inhomogeneous equation

$$\left(\frac{\partial^2}{\partial y^2} + \frac{\partial^2}{\partial z^2} + \chi^2 \right) u_m(g, \omega) = \phi_m(g), \quad (3.37)$$

while the functions $\phi_m(g)$, $m = (0)1, 2, \dots$ form a basis in the volume occupied by the field source. Multiplying both sides of (3.37) by the known constants \tilde{b}_m and summing the resulting expression in accordance with the superposition principle, we obtain the equation

$$\left(\frac{\partial^2}{\partial y^2} + \frac{\partial^2}{\partial z^2} + \chi^2 \right) U(g, \omega) = \phi(g, \omega) \quad (3.38)$$

in which $\phi(g, \omega) = \sum_m \tilde{b}_m \phi_m(g, \omega)$ is the field source function. Note that there is actually no need to know or to construct the functions ϕ and ϕ_m , since we are dealing with the problem of the diffraction of the incident wave (more precisely, of the given set of waveguide modes) rather than with the problem of the excitation of the field in a waveguide by the known source.

Since the vector $\tilde{b} \in \tilde{l}_2$ in (3.36) is specified arbitrary, the standard formulation of the electrodynamic problem is transferred onto the vector function $u(g, \omega)$. Then each unknown function $u_m(g, \omega)$, $m = (0)1, 2, \dots$, must satisfy the Helmholtz equation and obey the conditions (3.8)–(3.12). Therefore, in two regular waveguides, we obtain the standard expansion in waveguide modes for each of these functions:

$$\begin{aligned} u^{s(1)}(g, \omega) &= X_1 E_1(z) \mu_1(y); \quad z \leq 0 \quad \text{and} \\ u^{s(2)}(g, \omega) &= X_2 E_2(-z) \mu_2(y); \quad z \geq 0. \end{aligned} \quad (3.39)$$

But now, in contrast to formula (3.25), the matrix operators X_1 and X_2 are to be found. Comparing (3.25) with formulas (3.36) and (3.39), we obtain

$$\tilde{b} X_1 = x_1, \quad \tilde{b} X_2 = x_2. \quad (3.40)$$

Thus, according to (3.39), the representation of the considered complex amplitude in the form of the series (3.36) is equivalent to the replacement of the Fourier coefficients $\{x_{n1}\}_{n=(0)1}^\infty$ and $\{x_{n2}\}_{n=(0)1}^\infty$ in the modal expansion of the field (3.15), (3.16) by the elements of the infinite matrices $X_1 : \tilde{l}_2 \rightarrow \tilde{l}_2$ and $X_2 : \tilde{l}_2 \rightarrow \tilde{l}_2$, having the meaning of the reflection and transmission operators, respectively.

In what follows we will use the standardized reflection and transmission operators $R : l_2 \rightarrow l_2$ and $T : l_2 \rightarrow l_2$, which are introduced as follows. The reflected power flux is determined by the vector $\tilde{x}_1 \in l_2$ from formulas (3.27) and (3.28), while the transmitted power flux—by the vector $\tilde{x}_2 \in l_2$. In accordance with (3.40), we find

$$\begin{aligned} \tilde{x}_1 &= x_1 \left(I_1^\beta \right)^{1/2} = \left(\tilde{b} \left(I_1^\beta \right)^{1/2} \right) \left(I_1^\beta \right)^{-1/2} X_1 \left(I_1^\beta \right)^{1/2} = \tilde{c} R^{11}, \\ \tilde{x}_2 &= x_2 \left(I_2^\beta \right)^{1/2} = \left(\tilde{b} \left(I_1^\beta \right)^{1/2} \right) \left(I_1^\beta \right)^{-1/2} X_2 \left(I_2^\beta \right)^{1/2} = \tilde{c} T^{21}, \end{aligned} \quad (3.41)$$

where we have introduced the vector $\tilde{c} = \tilde{b} \left(I_1^\beta \right)^{1/2} \in l_2$. Hence two pairs of the required scattering operators are related by the formulas:

$$\begin{cases} X_1 = \left(I_1^\beta \right)^{1/2} R^{11} \left(I_1^\beta \right)^{-1/2} \\ X_2 = \left(I_1^\beta \right)^{1/2} T^{21} \left(I_2^\beta \right)^{-1/2} \end{cases} \leftrightarrow \begin{cases} R^{11} = \left(I_1^\beta \right)^{-1/2} X_1 \left(I_1^\beta \right)^{1/2} \\ T^{21} = \left(I_1^\beta \right)^{-1/2} X_2 \left(I_2^\beta \right)^{1/2} \end{cases}. \quad (3.42)$$

Thus, with the new formulation of the problem of mode diffraction, the expressions for the fields in the first and second partial regions are as follows

$$\begin{aligned} U^{i(1)}(g, \omega) + U^{s(1)}(g, \omega) &= \tilde{c} \left[\left(I_1^\beta \right)^{-1/2} E_1(-z) + R^{11} \left(I_1^\beta \right)^{-1/2} E_1(z) \right] \mu_1(y); \quad z \leq 0, \\ U^{s(2)}(g, \omega) &= \tilde{c} T^{21} \left(I_2^\beta \right)^{-1/2} E_2(-z) \mu_2(y); \quad z \geq 0 \end{aligned} \quad (3.43)$$

instead of the usual expansions (3.15) and (3.16).

Note that the boundedness of the matrix reflection and transmission operators, R and T , in the space l_2 follows directly from the finiteness of the power flux through the cross section of the waveguide. In what follows we will use the fact that all matrix operators studied in this chapter belong to the *Banach algebra* $B(l)$ of bounded operators defined throughout the Hilbert space l .

As will be shown in the further analysis, the operator properties of the infinite matrices U_j , Q_j and P_j , $j = 1, 2$, defined by formulas (3.30), (3.31), (3.34) and (3.35) play a decisive role in the rigorous justification of the mode-matching technique.

3.4 Generalized Mode-Matching Technique in the Step Discontinuity Problem

3.4.1 Derivation of the Operator Fresnel Formulas

For the problem under consideration (Fig. 3.1), we assume that the independent sources, labeled with numbers 1 and 2, which generate monochromatic fields of the same frequency and, in general, of different power, are located in the corresponding waveguide arms. The mutual independence of the field sources means that the two wave generators can be switched on/off separately.

Suppose that the function $U^{(q,p)}(g, \omega)$ is the complex amplitude, which determines in the q th waveguide all the field components whose source is located in the p th waveguide, $p, q = 1, 2$. The field of this source contains a full set of the

corresponding modes with known amplitudes given by the row vector $b^{(p)} = \left\{ b_m^{(p)} \right\}_{m=(0)1}^{\infty} \in l_2$.

According to the generalized mode-matching technique, we can now present the complex amplitude in the form of the scalar product of the infinite-dimensional vectors:

$$U^{(q,p)}(g, \omega) = b^{(p)} u^{(q,p)}(g, \omega). \quad (3.44)$$

The condition (3.9) of continuity of the tangential components of the electric and magnetic fields at the aperture of the discontinuity leads to the implication that

$$\begin{cases} b^{(p)} [u^{(1,p)}(g, \omega) - u^{(2,p)}(g, \omega)] = 0 \\ b^{(p)} \frac{\partial}{\partial z} [u^{(1,p)}(g, \omega) - u^{(2,p)}(g, \omega)] = 0 \end{cases}; \quad \forall b^{(p)} \in l_2 \quad \rightarrow \quad (3.45)$$

$$\begin{cases} u^{(1,p)}(g, \omega) = u^{(2,p)}(g, \omega) \\ \frac{\partial}{\partial z} u^{(1,p)}(g, \omega) = \frac{\partial}{\partial z} u^{(2,p)}(g, \omega) \end{cases}; \quad y \in (0, a_2), \quad z = 0, \quad p = 1, 2.$$

The key point here is that the vector $b^{(p)}$ is common to both partial regions. Similar considerations lead to the homogeneous boundary conditions

$$\begin{cases} u^{(1,p)}(g, \omega) = 0; & H - \text{case} \\ \frac{\partial}{\partial z} u^{(1,p)}(g, \omega) = 0; & E - \text{case} \end{cases}, \quad y \in (a_2, a_1), \quad z = 0 \quad (3.46)$$

on the step face.

Starting from (3.43), we can write the modal expansion for the functions under study on the reference plane $z = 0$ ($p, q = 1, 2$):

$$u^{(q,p)}(y, 0, \omega) = \begin{cases} (I + R^{pp}) \left(I_p^\beta \right)^{-1/2} \mu_p(y); & q = p \\ T^{qp} \left(I_q^\beta \right)^{-1/2} \mu_q(y); & q \neq p \end{cases}, \quad y \in (0, a_2), \quad (3.47)$$

$$\frac{\partial}{\partial z} u^{(q,p)}(y, 0, \omega) = \begin{cases} \mp (I - R^{pp}) \left(I_p^\beta \right)^{1/2} \mu_p(y); & q = p \\ \mp T^{qp} \left(I_q^\beta \right)^{1/2} \mu_q(y); & q \neq p \end{cases}, \quad p = \begin{cases} 1 \\ 2 \end{cases}, \quad (3.48)$$

$$y \in (0, a_2).$$

Substituting (3.47) and (3.48) into (3.45), we obtain the following system of matrix-functional equations for $y \in (0, a_2)$:

$$\begin{cases} (I + R^{pp}) \left(I_p^\beta \right)^{-1/2} \mu_p(y) = T^{qp} \left(I_q^\beta \right)^{-1/2} \mu_q(y) \\ (I - R^{pp}) \left(I_p^\beta \right)^{1/2} \mu_p(y) = T^{qp} \left(I_q^\beta \right)^{1/2} \mu_q(y) \end{cases}; \quad q \neq p. \quad (3.49)$$

From the boundary conditions (3.46) we find

$$\left\{ \begin{array}{l} (I \pm R^{11}) \left(I_1^\beta \right)^{\mp 1/2} \mu_1(y) = 0 \\ T^{12} \left(I_1^\beta \right)^{\mp 1/2} \mu_1(y) = 0 \end{array} \right. ; \quad y \in (a_2, a_1), \quad \left\{ \begin{array}{l} H - \text{case} \\ E - \text{case} \end{array} \right\}. \quad (3.50)$$

Applying the *Galerkin procedure* to relations (3.49) and (3.50), we formally obtain the desired solution

$$\left\{ \begin{array}{l} R^{11} = \pm (D_1 - I)(D_1 + I)^{-1} \\ T^{21} = (D_1 + I)^{-1} 2D_0 \end{array} \right. \quad \text{and} \quad \left\{ \begin{array}{l} R^{22} = \mp (D_2 - I)(D_2 + I)^{-1} \\ T^{12} = (D_2 + I)^{-1} 2D_0^T \end{array} \right. ; \quad \left\{ \begin{array}{l} H - \text{case} \\ E - \text{case} \end{array} \right\}, \quad (3.51)$$

where we have introduced the following notation:

$$D_1 = D_0 D_0^T, \quad D_2 = D_0^T D_0, \quad D_0 = \left(I_1^\beta \right)^{\pm 1/2} (\mu_1, \mu_2^T) \left(I_2^\beta \right)^{\mp 1/2} ; \quad \left\{ \begin{array}{l} H - \text{case} \\ E - \text{case} \end{array} \right\}. \quad (3.52)$$

The resulting solution (3.51) represents the Fresnel formulas for the reflection and transmission operators.

Problem 3.7 Derive the operator Fresnel formulas (3.51) from (3.49) and (3.50).

The existence of a bounded inverse operators in (3.51) follows from the law of conservation of complex power and will be rigorously proved in Sect. 3.4.3. Here we mention the symmetry properties of the obtained solution. Indeed, we find from the first operator Fresnel formula

$$R_p = I - 2(D_p + I)^{-1} = R_p^T, \quad R_p \equiv \left\{ \begin{array}{ll} \pm R^{11} & \text{for } p = 1 \\ \mp R^{22} & \text{for } p = 2 \end{array} \right., \quad \left\{ \begin{array}{l} H - \text{case} \\ E - \text{case} \end{array} \right\}, \quad (3.53)$$

since by definition (3.52) we have $D_p^T = D_p$, $p = 1, 2$. The symmetry property of the transmission operators $(T^{qp})^T = T^{pq}$ is verified by the direct substitution.

Note that the first Fresnel formula in (3.51) is also known as the *Cayley transformation*. From here on we will use both the names interchangeably. (Strictly speaking, the name ‘Cayley transformation’ was used in the book by H. Weyl [14] as applied to finite matrices, however, this term has long been used in the functional analysis to describe this linear fractional transformation of a linear operator). If the condition of the existence of such a transform is satisfied (i.e., if the spectrum of the operator D_p , $p = 1, 2$ does not contain the number -1), the transformation is invertible:

$$R_p = \frac{D_p - I}{D_p + I} \leftrightarrow D_p = \frac{I + R_p}{I - R_p}. \quad (3.54)$$

In these formulas the Cayley transforms are written in Weyl's form [14].

Let us prove that the elementary operator D_0 (3.52) is bounded on a pair of spaces $l_2 \rightarrow l_2$. To this end, we introduce another Hilbert space (see Appendix A):

$$\tilde{l}_2 = \left\{ a \equiv \{a_m\}_m: \sum_m m^{-1} |a_m|^2 = \|a\|_-^2 < \infty \right\}. \quad (3.55)$$

It is easily seen that for three spaces (3.17), (3.33) and (3.55) the inclusions $\tilde{l}_2 \subset l_2 \subset \tilde{l}_2$ are valid. Let us show that the matrix operator $\Psi_{pq} = (\mu_p, \mu_q^\dagger)$, $p, q = 1, 2$ is bounded in each of these spaces. (We recall that according to the accepted definition (3.21) the scalar product of functions (\dots, \dots) means integration over the transverse coordinate $0 < y < a_2$). Indeed, the matrix operators

$$\Xi_p \equiv \Psi_{pq} \Psi_{pq}^\dagger = (\mu_p, \mu_p^\dagger), \quad (3.56)$$

$$\Xi_q \equiv \Psi_{pq}^\dagger \Psi_{pq} = (\mu_q, \mu_q^\dagger) \quad (3.57)$$

are defined in all these spaces; they are bounded and self-adjoint. Furthermore, by virtue of the completeness of the system of eigenfunctions (3.24), the operators (3.56) and (3.57) are *idempotent operators*, $\Xi_{p(q)}^2 = \Xi_{p(q)}$. Consequently, the operator $\Xi_{p(q)}$ is the *orthoprojector* and $\|\Xi_{p(q)}\|_\diamond = 1$, where the norm $\|\dots\|_\diamond$ is any of the norms (3.17), (3.33) or (3.55). (More precisely, depending on the value of the subscripts $p, q = 1, 2$, $p \neq q$ one of the operators (3.56) or (3.57) is the identity I , while the other one is an orthoprojector.) Then from (3.56) and (3.57) it follows that $\|\Psi_{pq}\|_\diamond = 1$.

Next, taking into account the asymptotic behavior of the propagation constant $\beta_{mp} \approx im \cdot \text{const}(p)$ with $m \gg 1$, it is easy to verify that the similarity operator $(I_j^\beta)^{\pm 1/2} = \left\{ \delta_m^n (-i\beta_{mj})^{\pm 1/2} \right\}_{m,n=(0)1}^\infty$ is bounded on a pair of spaces $\tilde{l}_2 \rightleftarrows l_2, l_2 \rightleftarrows \tilde{l}_2$ for all finite values of the wavenumber k . Therefore, the product of three matrix operators

$$F_{pq}^\pm = (I_p^\beta)^{\pm 1/2} (\mu_p, \mu_q^T) (I_q^\beta)^{\mp 1/2}, \quad p, q = 1, 2 \quad (3.58)$$

is a bounded operator in the space l_2 .

Thus, the elementary operator under study and its products

$$D_0 = F_{12}^{\pm}; \quad \left\{ \begin{array}{l} H - \text{case} \\ E - \text{case} \end{array} \right\} \quad \text{and} \quad D_p = \left\{ \begin{array}{ll} D_0 D_0^T & \text{for } p = 1 \\ D_0^T D_0 & \text{for } p = 2 \end{array} \right. \quad (3.59)$$

are bounded matrix operators in the Hilbert space l_2 . Then, according to (3.51), the scattering operators are also bounded, what was implicitly assumed in the previous sections where they were introduced.

Problem 3.8 Prove the boundedness of the operator $\Xi_{p(q)}$ in the space \tilde{l}_2 .

Problem 3.9 Demonstrate the boundedness of the operator (3.58) in the space l_2 .

The next step is to validate the correctness of the obtained matrix-operator model (3.51) of the mode-matching technique. We will prove it starting from the conservation law in a generalized form.

3.4.2 Reciprocity Principle and Energy Conservation Law in the Operator Form

In the electromagnetic field theory, two energy laws are of first importance; namely, they are the Poynting theorem and the Lorentz reciprocity theorem. When passing to monochromatic fields in the domain of complex amplitudes (i.e. the phasor domain), the number of the fundamental laws doubles. This fact is evident from the representation of the product of the field components ${}^{\alpha}\vec{E}(t)$ and ${}^{\beta}\vec{H}(t)$ via the complex amplitudes ${}^{\alpha}\vec{E}(\omega)$ and ${}^{\beta}\vec{H}(\omega)$, like, for example, the following expression for the cross product:

$${}^{\alpha}\vec{E}(t) \times {}^{\beta}\vec{H}(t) = \frac{1}{2} \text{Re} \left\{ {}^{\alpha}\vec{E}(\omega) \times {}^{\beta}\vec{H}^*(\omega) + [{}^{\alpha}\vec{E}(\omega) \times {}^{\beta}\vec{H}(\omega)] \exp(\pm i 2\omega t) \right\}. \quad (3.60)$$

Here and everywhere below the indices α and β stand for the independent field sources. As previously mentioned, this independence implies the possibility of their independent switching on/off and, in general, different amplitude distributions in the modal expansion of the field.

When describing a time-harmonic field through complex amplitudes, the Poynting theorem generates the well-known complex power theorem, as well as the theorem on oscillating power [15]. For the problem under consideration, the Lorentz theorem yields two universal reciprocity relations as well. The first one, containing the initial complex amplitudes and thus corresponding to the second term in (3.60), is the well-known Lorenz lemma. The second relation, which contains the complex conjugate values, will be referred to as the *second Lorenz lemma* [16].

All four power laws can be derived from Maxwell's equations for complex amplitudes in the same manner (see, for example, [17]). The difference between the two pairs of these laws arises from the different number of the field sources taken into account. Indeed, both oscillating power and complex power theorems are formulated for a single source, $\alpha \equiv \beta$, while the two Lorentz lemmas operate with two separate sources α and β . Generally speaking, it can be any number of different sources, but they all obey two Lorentz lemmas in pairs.

For the problem considered, two independent field sources may be present both in different partial regions, as suggested above in Sect. 3.4.1, and in the same waveguide arm. Therefore, in some contrast to formula (3.44), we represent the field complex amplitude and its derivative with respect to the normal $\vec{n} = \pm \vec{z}$ to the reference plane in the form

$$\begin{aligned} \alpha^{(\beta)} U^{(q)}(y, 0, \omega) &= \alpha^{(\beta)} b^{(p)} u^{(q,p)}(y, 0, \omega), \\ \left. \frac{\partial}{\partial \vec{n}} \alpha^{(\beta)} U^{(q)}(g, \omega) \right|_{z=0} &= \alpha^{(\beta)} b^{(p)} \left. \frac{\partial}{\partial \vec{n}} u^{(q,p)}(g, \omega) \right|_{z=0}, \end{aligned} \quad (3.61)$$

where the given vector $\alpha^{(\beta)} b^{(p)} = \{ \alpha^{(\beta)} b_m^{(p)} \}_{m=(0)1}^\infty$ is associated with the corresponding source in the p th waveguide port, while the vector functions (3.47) and (3.48) determine the scattering characteristics of these waves in the q th waveguide.

The continuity condition for a flux of oscillating power through the aperture of the discontinuity yields two equalities:

$$\left(\alpha^{(\beta)} U^{(1)}, \frac{\partial}{\partial \vec{n}} \alpha^{(\beta)} U^{(1)} \right)_{(0,a_1)} \Big|_{z=-0} = \left(\alpha^{(\beta)} U^{(2)}, \frac{\partial}{\partial \vec{n}} \alpha^{(\beta)} U^{(2)} \right)_{(0,a_2)} \Big|_{z=+0}. \quad (3.62)$$

Two more equalities can be derived from the first Lorentz lemma:

$$\left(\alpha^{(\beta)} U^{(1)}, \frac{\partial}{\partial \vec{n}} \beta^{(\alpha)} U^{(1)} \right)_{(0,a_1)} \Big|_{z=-0} = \left(\alpha^{(\beta)} U^{(2)}, \frac{\partial}{\partial \vec{n}} \beta^{(\alpha)} U^{(2)} \right)_{(0,a_2)} \Big|_{z=+0}. \quad (3.63)$$

Substituting the representation for the field (3.61) into (3.62) and (3.63), taking into account the modal expansions (3.47), (3.48) and applying the orthogonal property of the transverse eigenfunctions (3.24), we find the required relationships between the scattering operators.

Suppose first that both of the field sources are located in the p th waveguide, $p = 1, 2$, then from (3.63) we obtain four equations, which can be written in the common form:

$$\alpha^{(\beta)} b^{(p)} \{ (I + R^{pp}) [I - (R^{pp})^T] - T^{qp} (T^{qp})^T \} \left(\beta^{(\alpha)} b^{(p)} \right)^T = 0; \quad p, q = 1, 2, \quad p \neq q. \quad (3.64)$$

If these sources are placed in two different waveguide arms, we can similarly write

$$b^{(p)} \{ T^{qp} [I - (R^{qq})^T] - (I + R^{pp})(T^{pq})^T \} (b^{(p)})^T = 0; \quad p, q = 1, 2, \quad p \neq q. \quad (3.65)$$

We have omitted the indices α and β because the source is uniquely defined by the number of a waveguide port. From (3.64), four fundamental relations follow immediately

$$(R^{pp})^T = R^{pp}, \quad (R^{pp})^2 + T^{qp}(T^{qp})^T = I; \quad p, q = 1, 2, \quad p \neq q. \quad (3.66)$$

Four additional basic properties of the scattering operators

$$(T^{qp})^T = T^{pq}, \quad R^{pp}T^{qp} + (R^{qq}T^{pq})^T = 0; \quad p, q = 1, 2, \quad p \neq q \quad (3.67)$$

follow from (3.65).

Problem 3.10 Prove that if $bAd^T = 0$ for $\forall b, d \in l_2$, then $A = 0$.

Problem 3.11 Derive the properties (3.66), (3.67) of the scattering operators.

The oscillating power theorem (3.62) in its turn leads to the equation

$$b^{(p)} \{ (I + R^{pp}) [I - (R^{pp})^T] - T^{qp}(T^{qp})^T \} (b^{(p)})^T = 0; \quad p, q = 1, 2, \quad p \neq q \quad (3.68)$$

giving the second formula in (3.66).

Problem 3.12 Prove that if $bAb^T = 0$ for $\forall b \in l_2$, then $A = -A^T$.

Problem 3.13 Derive the operator relationship $(R^{pp})^2 + T^{qp}(T^{qp})^T = I$ from (3.68).

Next, we write the continuity condition for the complex power flux through the aperture of the discontinuity as

$$\left(\alpha^{(\beta)} U^{(1)}, \frac{\partial}{\partial \vec{n}} \left(\alpha^{(\beta)} U^{(1)} \right)^* \right)_{(0, a_1)} \Big|_{z=-0} = \left(\alpha^{(\beta)} U^{(2)}, \frac{\partial}{\partial \vec{n}} \left(\alpha^{(\beta)} U^{(2)} \right)^* \right)_{(0, a_2)} \Big|_{z=+0}. \quad (3.69)$$

The second Lorentz lemma yields the following two equalities:

$$\left(\alpha^{(\beta)} U^{(1)}, \frac{\partial}{\partial \vec{n}} \left(\beta^{(\alpha)} U^{(1)} \right)^* \right)_{(0, a_1)} \Big|_{z=-0} = \left(\alpha^{(\beta)} U^{(2)}, \frac{\partial}{\partial \vec{n}} \left(\beta^{(\alpha)} U^{(2)} \right)^* \right)_{(0, a_2)} \Big|_{z=+0}. \quad (3.70)$$

Substituting the field into formula (3.70) as indicated above and using the properties of the transverse eigenfunctions of regular waveguides (3.24), we arrive at the equations ($p, q = 1, 2, p \neq q$)

$${}^{\alpha(\beta)}b^{(p)} \left\{ (I + R^{pp})U_p \left[I - (R^{pp})^\dagger \right] - T^{qp} U_q (T^{qp})^\dagger \right\} \left({}^{\beta(x)}b^{(p)} \right)^\dagger = 0, \quad (3.71)$$

$$b^{(p)} \left\{ T^{qp} U_q \left[I - (R^{qq})^\dagger \right] - (I + R^{pp})U_p (T^{pq})^\dagger \right\} \left(b^{(q)} \right)^\dagger = 0. \quad (3.72)$$

We have omitted the indices α and β in formula (3.72) for the same reason as for (3.65).

Problem 3.14 Derive formulas (3.71) and (3.72) from (3.69), (3.70).

From (3.71) and (3.72), the required relations for scattering operators ($p, q = 1, 2, p \neq q$) follow:

$$(I + R^{pp})U_p \left[I - (R^{pp})^\dagger \right] - T^{qp} U_q (T^{qp})^\dagger = 0, \quad (3.73)$$

$$T^{qp} U_q \left[I - (R^{qq})^\dagger \right] - (I + R^{pp})U_p (T^{pq})^\dagger = 0. \quad (3.74)$$

The complex power theorem (3.69) leads to the equation

$$b^{(p)} \left\{ (I + R^{pp})U_p \left[I - (R^{pp})^\dagger \right] - T^{qp} U_q (T^{qp})^\dagger \right\} \left(b^{(p)} \right)^\dagger = 0; \quad p, q = 1, 2, \\ p \neq q, \quad (3.75)$$

which repeatedly gives operator relationship (3.73).

Problem 3.15 Derive equality (3.73) from (3.75). Show first that if $bAb^\dagger = 0$ for $\forall b \in l_2$, then $A = 0$.

For the problem under discussion, the energy laws for fields are expressed completely by formulas (3.62), (3.63) and (3.69), (3.70). Therefore, there are no other basic relationships between scattering operators, except the above derived formulas (3.66), (3.67), (3.73) and (3.74).

The obtained relationships will be generalized and written in a compact form in Sect. 3.8, after the introduction of the basic operator matrix—the generalized scattering matrix S .

3.4.3 Correctness of the Matrix-Operator Model

In the derivation of the operator Fresnel formulas (3.51), we formally assumed that the operator $A_p \equiv (D_p + I)^{-1}$, $p = 1, 2$ is bounded in the space l_2 . The next important step of the generalized mode-matching technique is a rigorous proof of this fact.

We turn first to the question of the correctness of the scalar Fresnel formulas (3.1) and (3.3) (see Sect. 3.1). For the finite value of $\theta_{21} \neq 0$, a pair of linear fractional transformations follows from the first Fresnel formula:

$$r = \frac{\theta_{21} - 1}{\theta_{21} + 1} \leftrightarrow \theta_{21} = \frac{1+r}{1-r}, \quad (3.76)$$

from which follows the two-sided implication

$$\operatorname{Re} \theta_{21} > 0 \leftrightarrow |r| < 1. \quad (3.77)$$

From a physical point of view, these inequalities correspond to the energy condition for ordinary passive media whose permittivities and permeabilities lie in the first quadrant of the complex plane (recall that the time dependence is taken as $\exp(-i\omega t)$). The scalar Fresnel formulas (3.1) and (3.3) for such media are correct since the condition (3.77) ensures that $\theta_{21} \neq -1$ and $r \neq 1$.

Correctness of the operator Fresnel formulas (3.51) follows in just the same way from the basic energy conservation law. The concept of the correctness of this solution involves three properties of formulas (3.51): existence, uniqueness and stability.

Our proof is based on the known properties of the two operators forming the first Fresnel formula (3.54). Namely, if for the given matrix operator D_p the localization of its spectrum $\sigma(D_p)$ is unknown, then the main characteristics of the entire spectrum $\sigma(R_p)$ of the sought-for reflection operator R^{pp} are completely determined by the energy conservation law (3.73). The relationship of these two operators in the form of the Cayley transform (3.54) allows us to find all of their required properties.

Lemma 3.1 *The spectrum $\sigma(R_p)$ of the reflection operator lies inside the unit disc with each nonreal point of the spectrum being an eigenvalue of finite multiplicity and the rest of the spectrum lies on the real axis.*

This statement is a consequence of two facts, the proof of which will be given in Sect. 3.10.1. Firstly, it follows from the energy conservation law (3.73) that the reflection operator R_p , $p = 1, 2$ is *quasi-Hermitian*. This means that its imaginary part $\operatorname{Im} R_p \equiv (R_p - R_p^\dagger) / (2i)$ is a *compact operator*. Such non-self-adjoint operators are rather well studied (see, for example, [18, 19]). Secondly, the reflection operator is a strict contraction, $\|R_p\| < 1$ [20]. In Sect. 3.10.1, in order to

find these basic properties of the operator R_p , we will use the concepts and ideas of the operator theory in the space with indefinite metric (here, in a *Pontryagin space* [8]), as well as the geometric properties of the Hilbert space.

Theorem 3.1 *The solution of the problem of mode diffraction on a step discontinuity in a waveguide in the form of the Fresnel formulas for the scattering operators (3.51) is correct.*

Proof According to the above lemma $1 \notin \sigma(R_p)$, and hence the Cayley transform of the reflection operator

$$W(R_p) = \frac{I + R_p}{I - R_p} \quad (3.78)$$

exists. Then the Cayley transform $D_p = W(R_p)$ is a symmetric quasi-Hermitian operator, $D_p^T = D_p$, because R_p is a symmetric quasi-Hermitian operator, $R_p^T = R_p$. As corollary of the familiar spectral mapping theorem (see, for example, [21]),

$$\sigma(D_p) = \sigma(W(R_p)) = W(\sigma(R_p)), \quad (3.79)$$

we obtain that the spectrum of the operator D_p lies entirely within the right half-plane, $\operatorname{Re} \nu > 0$ for $\forall \nu \in \sigma(D_p)$; each nonreal point of this spectrum is an eigenvalue of finite multiplicity, and the rest of the spectrum lies on the real axis. Thus we have $-1 \notin \sigma(D_p)$, and therefore there exists the inverse Cayley transform

$$R_p = W^{-1}(D_p) = \frac{D_p - I}{D_p + I}. \quad (3.80)$$

The uniqueness of the considered solution follows from its existence, i.e. if there were a second solution of the problem obtained in the same way, it would have the form of (3.51) and coincide with the first solution.

Let us represent the operator A_p introduced above in the form of $A_p = (I - R_p)/2$; then we have $\|A_p\| < 1$, and for the *condition number* $\operatorname{cond} A_p \equiv \|A_p\| \|A_p^{-1}\|$ the following estimate is true:

$$1 \leq \operatorname{cond}(A_p) \leq 1 + \|D_p\| < \infty. \quad (3.81)$$

Hence it follows that the obtained solution (3.51) is stable on a set of bounded operators that act in the space l_2 . \square

Problem 3.16 Derive estimate (3.81).

Note that in fact the operators D_p and A_p possess additional (and stronger) properties, which have not been used in the above proof. Namely, the operator D_p is accretive, $\operatorname{Re} D_p \equiv (D_p + D_p^\dagger)/2 > 0$, while the operator A_p is accretive

contraction, $\operatorname{Re} A_p > A_p A_p^\dagger > 0$. The mentioned properties of these operators are inextricably entwined with the basic properties of the reflection operator, and we will prove them rigorously in Sect. 3.10.1.

3.5 Justification of the Truncation Technique for Solving Operator Equations

The method most frequently used for solving infinite SLAE is a three-step-algorithm truncation technique. At the first stage, the truncation procedure is used, i.e. the first M rows and M columns are cut from the matrix operator $D = \{D_{mq}\}_{m,q=(0)1}^\infty$ of SLAE (3.22) and each matrix entry is replaced by the N th partial sum of the series for D_{mq} . In the second step, the solution of the finite $M \times M$ system of equations is obtained, and finally, at the third step, the passing to the limit $M, N \rightarrow \infty$ is performed.

In fact, this passing to the limit is impossible in numerical implementation of the method. Instead, one finds numerical approximations to the required Fourier coefficients x_{m1} , $m = (0)1, 2, \dots, M$ for some ascending sequences of the finite values M and N . The results of such calculations, presented as tables or schematic graphs, make possible to demonstrate the so-called ‘practical convergence’ of approximations obtained by the truncation procedure.

Let us write the infinite SLAE (3.22) in the operator form

$$(I + D)x_1 = f, \quad (3.82)$$

where the vector in the right-hand side is $f \equiv \mp \{\delta_m^p - D_{mp}\}_{m=(0)1}^\infty \in \tilde{l}_2$. Then, the above-described truncation technique can be classified as a *fully discrete method*, involving two sequential approximations of the equation (3.82). Indeed, initially the approximate operator $D_N : \tilde{l}_2 \rightarrow \tilde{l}_2$ is introduced which should give a certain approximate representation of the initial matrix operator $D_N \rightarrow D$ with $N \rightarrow \infty$, and only then the standard projection scheme is applied to the obtained approximate equation (see, for example, [21]):

$$P_M(I + D_N)x_1^{(M,N)} = P_M f^{(N)}; \quad M, N = 1, 2, \dots \quad (3.83)$$

Here, P_M is the operator of the projection onto M -dimensional subspace of the space \tilde{l}_2 , $x_1^{(M,N)} \in P_M \tilde{l}_2$ is the required projection approximation, while $f^{(N)}$ is the corresponding approximation to the right-hand side of (3.82) such that $f^{(N)} \rightarrow f$ as $N \rightarrow \infty$. Equation (3.83) reveals the problem of the relative (or conditional) convergence common to the mode-matching technique: whether the double passing to the limit, $M, N \rightarrow \infty$, will lead to a result different from the true solution?

In the generalized mode-matching technique, we are dealing with the equations for the unknown scattering operators and not with infinite SLAE. For the problem of mode diffraction on a step-like discontinuity in a waveguide, the operator equations are the Fresnel formulas for matrix reflection and transmission operators. Therefore, the generalized mode-matching technique is beyond the scope of the theory of projection methods [21] for solving linear equations like (3.82).

In this section, we will perform the generalization of the standard *projection method* in order to construct the approximations for the operator Fresnel formulas (3.51) and will study analytically the basic characteristics of the convergence of these approximations.

3.5.1 Construction of Projection Approximations for the Fresnel Formulas

To find the desired finite-dimensional approximations, let us construct the orthoprojectors by the formulas

$$P_K \equiv \left\{ p_{mn}^{(K)} = \sum_{q=(0)1}^K \delta_m^q \delta_q^n \right\}_{m,n=(0)1}^{\infty} = \begin{pmatrix} I_K & 0 \\ 0 & 0 \end{pmatrix}, \quad Q_K = I - P_K. \quad (3.84)$$

From now on, when describing the special 2×2 block structure of a matrix operator, we will follow the agreement that in the top left cell there is a finite-dimensional matrix, on the secondary diagonal there are the corresponding ‘semi-infinite’ matrices, and at the bottom of the main diagonal an infinite matrix is placed. Thus any additional notation to distinguish semi-infinite and endless matrices is not used.

In the definitions (3.84), $K = M$ or $K = N$ means the highest number of the waveguide mode taken into account in the partial region, while I_K is the K -dimensional identity matrix. In order to unify the formulas given in this section we will assume that the field in the p th region, $p = 1, 2$, is reduced to the sum of M (H -case) or $M + 1$ (E -case) modes, whereas N or $N + 1$ modes, respectively, is taken into account in the adjacent partial region.

Problem 3.17 Show that premultiplication (postmultiplication) by the orthoprojector P_K cuts from the infinite matrix either K (H -case) or $K + 1$ (E -case) rows (columns), making it ‘semi-infinite’.

The truncation of the accountable modes results in the $M \times M$ matrices

$$\tilde{D}_p = \begin{cases} \tilde{D}_0 \tilde{D}_0^T; & p = 1 \\ \tilde{D}_0^T \tilde{D}_0; & p = 2, \end{cases} \quad (3.85)$$

$$\tilde{A}_p = (\tilde{D}_p + I_M)^{-1}, \quad \tilde{A}_p \tilde{A}_p^{-1} = \tilde{A}_p^{-1} \tilde{A}_p = I_M, \quad (3.86)$$

and the required finite-dimensional approximations to the scattering operators take the form:

$$\tilde{R}_p = \frac{\tilde{D}_p - I_M}{\tilde{D}_p + I_M} = I_M - 2\tilde{A}_p, \quad (3.87)$$

$$\tilde{T}^{qp} = 2\tilde{A}_p \left\{ \begin{array}{c} \tilde{D}_0^T \\ \tilde{D}_0 \end{array} \right\}; \quad p \neq q = \left\{ \begin{array}{c} 1 \\ 2 \end{array} \right\}. \quad (3.88)$$

Formula (3.87) is the Cayley transform of the finite ‘matrix of the problem’ \tilde{D}_p .

As in the case of the exact solution (3.51), the correctness of the projection approximations (3.87), (3.88) is a consequence of the continuity condition for the energy flux through the aperture Ω . Indeed, matching on the reference plane the approximate representations for the tangential components of the fields in two partial regions in the form of the truncated modal expansions, we subject these approximations to the four energy laws mentioned in Sect. 3.4.2. Performing the same calculations as in the case of the exact solution, we obtain from the first Lorentz lemma and the oscillating power theorem the following relationships:

$$\begin{aligned} (\tilde{R}^{pp})^T &= \tilde{R}^{pp}, & (\tilde{T}^{qp})^T &= \tilde{T}^{pq}, & (\tilde{R}^{pp})^2 + \tilde{T}^{qp}(\tilde{T}^{qp})^T &= I_M, \\ \tilde{R}^{pp} \tilde{T}^{qp} + (\tilde{R}^{qq} \tilde{T}^{pq})^T &= 0. \end{aligned} \quad (3.89)$$

The second Lorentz lemma together with the complex power theorem yields the energy conservation law in a matrix form:

$$(I_M + \tilde{R}^{pp}) \tilde{U}_p \left[I_M - (\tilde{R}^{pp})^\dagger \right] - \tilde{T}^{qp} \tilde{U}_q (\tilde{T}^{qp})^\dagger = 0, \quad (3.90)$$

$$\tilde{T}^{qp} \tilde{U}_q \left[I_N - (\tilde{R}^{qq})^\dagger \right] - (I_M + \tilde{R}^{pp}) \tilde{U}_p (\tilde{T}^{pq})^\dagger = 0. \quad (3.91)$$

Here $\tilde{U}_j, j = 1, 2$, is the finite-dimensional $K \times K$ approximation to the operator of the waveguide ports (3.29) and (3.35). Obviously that \tilde{U}_j is also a cramped unitary matrix, i.e. its numerical range lies entirely in the first quadrant of the complex plane (for the time dependence $\exp(-i \omega t)$).

Problem 3.18 Derive relationships (3.89)–(3.91).

Let the (finite-dimensional) row vector $\tilde{b} \in P_M l_2, \|\tilde{b}\| = 1$, be the *eigenvector of reflection matrix*, $\tilde{b} \tilde{R}^{pp} = \lambda \tilde{b}$. Multiplying (3.90) from the left and from the right by this eigenvector, we obtain the equality

$$(1 + \lambda)(1 - \lambda^*)\tilde{b} \tilde{U}_p \tilde{b}^\dagger = \tilde{b} \tilde{T}^{qp} \tilde{U}_q (\tilde{T}^{qp})^\dagger \tilde{b}^\dagger. \quad (3.92)$$

The multiplication of the latter by $(\tilde{b} \tilde{U}_p \tilde{b}^\dagger)^\dagger = \tilde{b} \tilde{U}_p^\dagger \tilde{b}^\dagger$ gives, in its turn, the relation

$$(1 + \lambda)(1 - \lambda^*) \left| \tilde{b} \tilde{U}_p \tilde{b}^\dagger \right|^2 = \left(\tilde{b} \tilde{T}^{qp} \tilde{U}_q (\tilde{T}^{qp})^\dagger \tilde{b}^\dagger \right) \left(\tilde{b} \tilde{U}_p^\dagger \tilde{b}^\dagger \right), \quad (3.93)$$

from which we find:

$$\text{sign Re} \{(1 + \lambda)(1 - \lambda^*)\} = \text{sign Re} \left\{ \left(\tilde{b} \tilde{T}^{qp} \tilde{U}_q (\tilde{T}^{qp})^\dagger \tilde{b}^\dagger \right) \left(\tilde{b} \tilde{U}_p^\dagger \tilde{b}^\dagger \right) \right\}. \quad (3.94)$$

In view of the properties of the cramped unitary operators \tilde{U}_q and \tilde{U}_p^\dagger , the result of the multiplying of the two values in the right-hand side of formula (3.93) will always belong to the right half of the complex plane. Therefore, from (3.94) it follows that $1 - |\lambda|^2 > 0$, i.e. the *spectrum of reflection matrix* \tilde{R}^{pp} lies completely within the unit disc. According to the above mentioned spectral mapping theorem, this means that $-1 \notin \sigma(\tilde{D}_p)$, and consequently, the Cayley transform (3.87) exists.

Basic properties of the finite matrices \tilde{D}_p , \tilde{R}^{pp} and \tilde{A}_p are completely similar to the properties of the corresponding matrix operators in (3.52), (3.53) and (3.81). The proof of these properties requires fairly sophisticated methods of the operator theory and hence is considered in Sect. 3.10.1. However, in what follows we consider as proved the fact that the operator A_p and the matrix \tilde{A}_p are strict contractions, i.e. their norm is less than one.

Taking these properties and definitions (3.85), (3.86) into account, we obtain the uniform estimate for the condition number $\text{cond}(\tilde{A}_p) \equiv \|\tilde{A}_p\| \|\tilde{A}_p^{-1}\|$ of the matrix (3.86)

$$1 \leq \text{cond}(\tilde{A}_p) \leq 1 + \|\tilde{D}_0\| \|\tilde{D}_0^T\| < \infty \quad \text{for } \forall M, N, \quad (3.95)$$

ensuring the computational stability.

Since in the conventional statement of the diffraction problem the convergence of the finite-dimensional approximations, which have been obtained by the standard mode-matching technique, has no substantiation, the efforts were made to find empirical criteria to evaluate the accuracy of these approximations. In due time, one believed that such a natural and easily applicable criterion is to verify the complex power conservation law. However, it was soon discovered that all obtained numerical solutions satisfy this law, regardless of the remaining number of waveguide modes, of the problem geometry and the operating frequency.

According to the rule generally accepted today, the balance ratio between the incident, reflected and transmitted electromagnetic energy (which is a special case of general formula (3.90)) is adequate only to check algebra, programming and roundoff errors, but is not a proper measure of the accuracy of approximations.

The above result allows us to understand the true role of the complete fulfillment of the energy conservation law in the mode-matching technique, which is difficult to identify with the traditional approach. Namely, the subjection of each approximate solution (3.87), (3.88) to the generalized energy conservation law (3.90), (3.91) ensures the nonsingularity of the matrix of the truncated SLAE (3.85) and the stable computations for any number of waveguide modes taken into account.

3.5.2 Unconditional Convergence of the Truncation Technique

In order to analyze the convergence of projection approximations in the space l_2 , one should extend the finite matrices given above to infinite matrix operators by using zeros. The formulas providing such an extension can be different, but the result will be the same. From general considerations, we prefer to introduce the extended elementary operator of the problem in the form of

$$\bar{D}_0 = \left\{ \begin{matrix} P_M \\ P_N \end{matrix} \right\} D_0 \left\{ \begin{matrix} P_N \\ P_M \end{matrix} \right\} = \begin{pmatrix} \tilde{D}_0 & 0 \\ 0 & 0 \end{pmatrix}, \quad p = \left\{ \begin{matrix} 1 \\ 2 \end{matrix} \right\}. \quad (3.96)$$

Then, using the given matrix of the problem

$$\bar{D}_p \equiv \begin{pmatrix} \tilde{D}_p & 0 \\ 0 & 0 \end{pmatrix} = \begin{cases} \tilde{D}_0 \tilde{D}_0^T; & p = 1 \\ \tilde{D}_0^T \tilde{D}_0; & p = 2 \end{cases} \rightarrow \bar{D}_p + I = \begin{pmatrix} \tilde{A}_p^{-1} & 0 \\ 0 & I \end{pmatrix}, \quad (3.97)$$

we arrive at the relations

$$\begin{aligned} \bar{A}_p \equiv (\bar{D}_p + I)^{-1} &= \begin{pmatrix} \tilde{A}_p & 0 \\ 0 & I \end{pmatrix}, & I - 2\bar{A}_p &= \begin{pmatrix} \tilde{R}_p & 0 \\ 0 & -I \end{pmatrix}, \\ \bar{A}_p \bar{A}_p^{-1} &= \bar{A}_p^{-1} \bar{A}_p = I. \end{aligned} \quad (3.98)$$

Consequently, the required infinite dimensional extension of the reflection matrix $M \times M$ has the form

$$\bar{R}_p \equiv (I - 2\bar{A}_p)P_M = P_M(I - 2\bar{A}_p) = \begin{pmatrix} \tilde{R}_p & 0 \\ 0 & 0 \end{pmatrix}. \quad (3.99)$$

Representing the exact and approximate reflection operators in the form of

$$R_p = I - 2A_p, \quad \bar{R}_p = P_M - 2\bar{A}_p P_M, \quad (3.100)$$

and using the definitions of the operators A_p and \bar{A}_p , we find the difference

$$P_M R_p P_M - \bar{R}_p = 2\bar{A}_p (P_M D_p - \bar{D}_p) A_p P_M. \quad (3.101)$$

In view of the inequality $\|A_p P_M\| < 1$, we obtain the following estimate for projection approximations of the reflection operator:

$$\|b(P_M R_p P_M - \bar{R}_p)\| < \|d(P_M D_p - \bar{D}_p)\|; \quad d = 2b\bar{A}_p, \quad \forall b \in l_2. \quad (3.102)$$

Further, by constructing in a similar manner the infinite extension of the matrix $M \times N$ (3.88)

$$\bar{T}^{qp} \equiv \begin{pmatrix} \bar{T}^{qp} & 0 \\ 0 & 0 \end{pmatrix} = 2\bar{A}_p \left\{ \begin{matrix} \bar{D}_0 \\ \bar{D}_0^T \end{matrix} \right\}; \quad q \neq p = \left\{ \begin{matrix} 1 \\ 2 \end{matrix} \right\}, \quad (3.103)$$

we find the estimate for projection approximations of the transmission operator:

$$\|b(P_M T^{qp} P_N - \bar{T}^{qp})\| \leq \frac{\sqrt{2}}{2} \|d(P_M D_p - \bar{D}_p)\|; \quad (3.104)$$

$$d = 2b\bar{A}_p, \quad \forall b \in l_2, \quad q \neq p = \left\{ \begin{matrix} 1 \\ 2 \end{matrix} \right\}.$$

Inequalities (3.102) and (3.104) allow us to consider the convergence in the form

$$\lim_{M, N \rightarrow \infty} \left\{ \begin{matrix} \|b(P_M R_p P_M - \bar{R}_p)\| \\ \|b(P_M T^{qp} P_N - \bar{T}^{qp})\| \end{matrix} \right\} = 0, \quad \forall b \in l_2, \quad (3.105)$$

which is known as *strong projection convergence* (or *P-convergence*) [21].

Problem 3.19 Based on the inequality $\|T^{qp}\| \leq \sqrt{2}$ obtain the estimate (3.104).

Problem 3.20 Prove that in the space l_2 strong convergence of the operators follows from their strong *P-convergence* and vice versa.

According to the estimates (3.102) and (3.104), strong *P-convergence* of the constructed projection approximations is fully determined by strong *P-convergence* of the known matrix \bar{D}_p to the given operator D_p . Thus the problem is to examine the conditions of convergence of the difference of two known operators, $P_M D_p - \bar{D}_p \equiv \Lambda_{M, N}^{(p)}$, to the null operator.

Lemma 3.2 *The operator $\Lambda_{M,N}^{(p)}$ strongly converges to the null operator: $\|d \Lambda_{M,N}^{(p)}\| \rightarrow 0$ for $\forall d \in l_2$ if $M, N \rightarrow \infty$.*

Proof Using the definitions (3.52) and (3.97) let us write this operator as

$$\Lambda_{M,N}^{(p)} = P_M D_p - \bar{D}_p = \begin{cases} P_M D_0 Q_N D_0^T + P_M D_0 P_N D_0^T Q_M; & p = 1 \\ P_M D_0^T Q_N D_0 + P_M D_0^T P_N D_0 Q_M; & p = 2. \end{cases} \quad (3.106)$$

Our assertion follows immediately from this representation as a result of strong (but nonuniform) convergence of the orthoprojector P_K , $K = M, N$, to the unit operator in the space l_2 :

$$\lim_{K \rightarrow \infty} \|d(I - P_K)\| = \lim_{K \rightarrow \infty} \|d Q_K\| = 0 \quad \text{for } \forall d \in l_2. \quad (3.107)$$

The presence of two terms in (3.106) implies that both passages to the limit, $M \rightarrow \infty$ and $N \rightarrow \infty$, should be performed simultaneously and independently. \square

Problem 3.21 Derive formula (3.106).

Problem 3.22 Derive the formula $\Lambda_{M,N}^{(1)} = P_M D_0 Q_N D_0^T P_M + P_M D_0 D_0^T Q_M$, which is alternative to (3.106).

Lemma 3.2 and the derived estimates (3.102) and (3.104) lead to the following result:

Theorem 3.2 *The finite-dimensional approximations \tilde{R}^{pp} and \tilde{T}^{qp} always exhibit strong P -convergence to the corresponding scattering operators.*

As a consequence, there is no conditional (or relative) strong P -convergence of the projection approximations for the mathematical model of the generalized mode-matching technique in the form of operator Fresnel formulas (3.51).

In Sect. 3.6, we will obtain an alternative representation for the operator $\Lambda_{M,N}^{(p)}$ suitable for the study of more subtle convergence properties of the approximations constructed.

3.5.3 Rate of Convergence of the Approximations of Scattering Operators

Our next goal will be to estimate analytically the rate of decrease

$$\left\| b \bar{A}_p \Lambda_{M,N}^p \right\| \rightarrow 0 \quad \text{as } M, N \rightarrow \infty \quad (3.108)$$

for the norm of the approximation error vector, given by formulas (3.102) and (3.104). We will consider a practical problem where the r th waveguide mode is

scattered by the discontinuity ($r \leq M, N$, for H -case or $r \leq (M+1), (N+1)$, for E -case), i.e., $b = \{\delta_r^m\}_{m=(0)1}^\infty$. The key to the success lies in the equivalent transformation of the product $\bar{A}_p \Lambda_{M,N}^{(p)}$ of the matrix operators.

First, using an alternative to formula (3.106) (see Problem 3.22)

$$\Lambda_{M,N}^{(p)} = P_M D_p Q_M + P_M \begin{Bmatrix} D_0 \\ D_0^T \end{Bmatrix} Q_N \begin{Bmatrix} D_0^T \\ D_0 \end{Bmatrix} P_M; \quad p = \begin{Bmatrix} 1 \\ 2 \end{Bmatrix}, \quad (3.109)$$

we obtain the equality

$$2 \bar{A}_p \Lambda_{M,N}^{(p)} = [2 \bar{A}_p P_M D_p] Q_M + \left[2 \bar{A}_p P_M \begin{Bmatrix} D_0 \\ D_0^T \end{Bmatrix} \right] Q_N \begin{Bmatrix} D_0^T \\ D_0 \end{Bmatrix} P_M; \quad p = \begin{Bmatrix} 1 \\ 2 \end{Bmatrix}. \quad (3.110)$$

Here, the square brackets mark two combinations of matrix operators

$$2 \bar{A}_p P_M D_p = P_M + \bar{R}_p; \quad 2 \bar{A}_p P_M \begin{Bmatrix} D_0 \\ D_0^T \end{Bmatrix} = \bar{T}^{qp}; \quad p = \begin{Bmatrix} 1 \\ 2 \end{Bmatrix}, \quad (3.111)$$

that generate new projection approximations \bar{R}_p and \bar{T}^{qp} , which, as it is easy to see, converge to the corresponding scattering operators. Indeed, from the formulas for the exact solution

$$I + R_p = 2 A_p D_p, \quad T^{qp} = 2 A_p \begin{Bmatrix} D_0 \\ D_0^T \end{Bmatrix}; \quad p = \begin{Bmatrix} 1 \\ 2 \end{Bmatrix}, \quad (3.112)$$

we find, firstly, an expression akin to (3.101):

$$P_M R_p - \bar{R}_p = -2 \bar{A}_p (P_M D_p - \bar{D}_p) A_p D_p, \quad (3.113)$$

and, secondly, a similar formula for the transmission operator

$$P_M T^{qp} - \bar{T}^{qp} = -2 \bar{A}_p (P_M D_p - \bar{D}_p) A_p \begin{Bmatrix} D_0 \\ D_0^T \end{Bmatrix}; \quad p = \begin{Bmatrix} 1 \\ 2 \end{Bmatrix}. \quad (3.114)$$

Strong P -convergence of the approximations \bar{R}_p and \bar{T}^{qp} as $M, N \rightarrow \infty$ follows from Lemma 3.2.

Further, when using formulas (3.113) and (3.114) to eliminate the auxiliary operators \bar{R}_p and \bar{T}^{qp} from formulas (3.111), the latter take the form

$$\begin{aligned}
2\bar{A}_p P_M D_p &= \left(P_M + \bar{A}_p \Lambda_{M,N}^{(p)} \right) (I + R_p), \\
2\bar{A}_p P_M \begin{Bmatrix} D_0 \\ D_0^T \end{Bmatrix} &= \left(P_M + \bar{A}_p \Lambda_{M,N}^{(p)} \right) T^{qp}; \quad p = \begin{Bmatrix} 1 \\ 2 \end{Bmatrix}.
\end{aligned} \tag{3.115}$$

Then, taking these relationships into account, formula (3.110) is transformed into the equation below

$$\bar{A}_p \Lambda_{M,N}^{(p)} = \left(P_M + \bar{A}_p \Lambda_{M,N}^{(p)} \right) \frac{1}{2} \Phi_{M,N}^{(p)}, \tag{3.116}$$

in which the following notation is used:

$$\begin{aligned}
\Phi_{M,N}^{(p)} &\equiv (I + R_p) Q_M + T^{qp} Q_N \begin{Bmatrix} D_0^T \\ D_0 \end{Bmatrix} P_M = T^{qp} \left[\begin{Bmatrix} D_0^T \\ D_0 \end{Bmatrix} - P_N \begin{Bmatrix} D_0^T \\ D_0 \end{Bmatrix} P_M \right]; \\
p &= \begin{Bmatrix} 1 \\ 2 \end{Bmatrix}.
\end{aligned} \tag{3.117}$$

Note that we have used formulas (3.112) when deriving (3.115) and (3.117).

Problem 3.23 Derive (3.116).

To solve (3.116) with respect to $\bar{A}_p \Lambda_{M,N}^{(p)}$, we will use the following lemma.

Lemma 3.3 *The operator $\frac{1}{2} \Phi_{M,N}^{(p)}$ is a strict contraction: $\frac{1}{2} \|\Phi_{M,N}^{(p)}\| < 1$ for $\forall M, N$.*

Proof This follows from the second form of the matrix operator (3.117) and from the fact that the operator

$$\frac{1}{2} T^{qp} \begin{Bmatrix} D_0^T \\ D_0 \end{Bmatrix} = A_p D_p; \quad p = \begin{Bmatrix} 1 \\ 2 \end{Bmatrix},$$

is an *accretive contraction* (see also Sect. 3.10.1):

$$\|A_p D_p\| = \frac{1}{2} \|I + R_p\| \leq \frac{1}{2} (1 + \|R_p\|) < 1. \quad \square$$

Therefore, the inverse operator $\left(I - \frac{1}{2} \Phi_{M,N}^{(p)} \right)^{-1}$ exists and is bounded, while operator (3.116) has a bounded solution

$$\bar{A}_p \Lambda_{M,N}^{(p)} = \frac{1}{2} P_M \Phi_{M,N}^{(p)} \left(I - \frac{1}{2} \Phi_{M,N}^{(p)} \right)^{-1}. \tag{3.118}$$

Accordingly, the estimates given by (3.102) and (3.104) can be written as

$$\left. \begin{aligned} & \|b(P_M R_p P_M - \bar{R}_p)\| \\ & \|b(P_M T^{qp} P_N - \bar{T}^{qp})\| \end{aligned} \right\} < \frac{\|b P_M \Phi_{M,N}^{(p)}\|}{1 - \frac{1}{2} \|\Phi_{M,N}^{(p)}\|}; \quad \forall b \in l_2, \quad (3.119)$$

where $\|b P_M \Phi_{M,N}^{(p)}\| \rightarrow 0$ as $M, N \rightarrow \infty, \forall M, N$.

Next, we use the first form of the operator (3.117) to represent the infinite vector under consideration as

$$b P_M \Phi_{M,N}^{(p)} = b P_M (I + R_p) Q_M + b P_M T^{qp} Q_N \left\{ \begin{matrix} D_0^T \\ D_0 \end{matrix} \right\} P_M; \quad p = \left\{ \begin{matrix} 1 \\ 2 \end{matrix} \right\}. \quad (3.120)$$

Since P_M and Q_M are a pair of *complementary orthoprojectors*, $P_M Q_M = Q_M P_M = 0$, we find from the Pythagorean theorem that

$$\|b P_M \Phi_{M,N}^{(p)}\|^2 = \|b P_M (I + R_p) Q_M\|^2 + \|b P_M T^{qp} Q_N \left\{ \begin{matrix} D_0^T \\ D_0 \end{matrix} \right\} P_M\|^2; \quad p = \left\{ \begin{matrix} 1 \\ 2 \end{matrix} \right\}. \quad (3.121)$$

The infinite vectors $b P_M (I + R_p)$ and $b P_M T^{qp}$ are the Fourier coefficients in the modal expansion of the field. The asymptotic law of decrease of these coefficients is determined, as is well known, by the *condition on the sharp edge* [3, 11]. Setting the space of the solutions and the geometry of the sharp edge, we a priori know the behavior of these Fourier coefficients. If the solution of our problem is represented by the vectors $x_1 = \{x_{m1}\}_{m=(0)1}^\infty \in \tilde{l}_2$ and $x_2 = \{x_{m2}\}_{m=(0)1}^\infty \in \tilde{l}_2$, the law of decrease of these coefficients is the power law, $x_{m1}, x_{m2} = O(m^{-5/3}), m \gg 1$ [3]. When passing to the Hilbert space l_2 , we have the dependence $O(m^{-7/6})$, and therefore

$$\|b P_M (I + R_p) Q_M\|^2 = O(M^{-4/3}), \quad \|b P_M T^{qp} Q_N\|^2 = O(N^{-4/3}); \quad M, N \gg 1. \quad (3.122)$$

Above, we have used the asymptotic estimate

$$\sum_{m=M+1}^\infty \left(\frac{const}{m^{7/6}} \right)^2 = \frac{const^2}{M^{4/3}} [1 + O(M^{-1})]; \quad M \gg 1.$$

Thus, a rough lower estimate for the rate of convergence of the constructed projection approximations has the form

$$\left. \begin{aligned} & \|b(P_M R_p P_M - \bar{R}_p)\| \\ & \|b(P_M T^{qp} P_N - \bar{T}^{qp})\| \end{aligned} \right\} < \frac{1}{1 - \frac{1}{2} \|\Phi_{M,N}^{(p)}\|} \sqrt{\frac{\text{const}_1^2}{M^{4/3}} + \frac{\text{const}_2^2}{N^{4/3}}}, \quad (3.123)$$

$$M, N \gg 1, \quad b = \{\delta_r^m\}_{m=(0)1}^\infty.$$

Note that the denominator in the right-hand side of this inequality depends on the ratio M/N . This conclusion follows, in particular, from formula (3.117) for the operator $\Phi_{M,N}^{(p)}$. We will study the impact of this dependence upon the rate of convergence in the following section.

3.6 Mittra Rule for Scattering Operators

We will study the subtle effects of P -convergence for the projection approximations, which have been constructed in the previous section, using the theory of distributions (see, for example, [22]).

In our analysis, the key role is played by the distributions

$$({}^\mp)G^{(p)}(y, \bar{y}) = \mu_p^T(y) \left(I_p^\beta\right)^{\mp 1} \mu_p(\bar{y}); \quad y, \bar{y} \in (0, a_2), \quad p = 1, 2, \quad (3.124)$$

which have the meaning of traces of Green’s function for the p th partial region (the upper minus sign) and of its second derivative (the lower plus sign) at the aperture Ω of the discontinuity. These functions of two variables are the kernels of the integral expressions

$$\left({}^\mp\right)G^{(p)}\mu_{mq}(y) = \int_0^{a_2} \left({}^\mp\right)G^{(p)}(y, \bar{y})\mu_{mq}(\bar{y})d\bar{y}; \quad p, q = 1, 2, \quad (3.125)$$

or, in other words, they induce the integral operators $({}^\mp)G^{(p)}$. More specifically, the distributions (3.124) induce the *integral operator of Hilbert-Schmidt type* $(-)G^{(p)}$, the *hypersingular integral operator* $(+)G^{(p)}$ and the difference operators $({}^\mp)B^{(qp)} = ({}^\mp)G^{(q)} - ({}^\mp)G^{(p)}$, $p, q = 1, 2, p \neq q$. In their turn, these integral operators generate the matrix operators

$$\begin{aligned} D_p &= \left(I_p^\beta\right)^{\pm 1/2} \left(\mu_p, ({}^\mp)G^{(q)}\mu_p^T\right) \left(I_p^\beta\right)^{\pm 1/2}, \quad ({}^\pm)F_p ({}^\mp)F_p = \left(I_p^\beta\right)^{\pm 1/2} \left(\mu_p, ({}^\mp)G^{(p)}\mu_p^T\right) \left(I_p^\beta\right)^{\pm 1/2}, \\ B &= \left(I_p^\beta\right)^{\pm 1/2} \left(\mu_p, ({}^\mp)B^{(qp)}\mu_p^T\right) \left(I_p^\beta\right)^{\pm 1/2}; \quad \left\{ \begin{matrix} p \\ q \end{matrix} \right\} = \left\{ \begin{matrix} 1, 2 \\ 2, 1 \end{matrix} \right\}. \end{aligned} \quad (3.126)$$

Hereinafter in this section, for the first partial region, the upper sign corresponds to the case of H -plane, while the lower sign corresponds to the E -plane, and vice versa for the second region.

If a finite number of modes is taken into account in regular waveguides, the functions (3.124) take the form

$$({}^{\mp})G_K^{(p)}(y, \bar{y}) = \left[\mu_p^T(y) P_K \right] \left(I_p^\beta \right)^{\mp 1} \left[P_K \mu_p(\bar{y}) \right]; \quad K = M, N,$$

while the corresponding finite-dimensional matrix operators are

$$\begin{aligned} \bar{D}_p &= \left(I_p^\beta \right)^{\pm 1/2} \left(\mu_p, ({}^{\mp})G_N^{(q)} \mu_p^T \right) \left(I_p^\beta \right)^{\pm 1/2}, \\ ({}^{\pm})F_p P_K ({}^{\mp})F_p &= \left(I_p^\beta \right)^{\pm 1/2} \left(\mu_p, ({}^{\mp})G_K^{(p)} \mu_p^T \right) \left(I_p^\beta \right)^{\pm 1/2}, \\ B_{NM} &= \left(I_p^\beta \right)^{\pm 1/2} \left(\mu_p, ({}^{\mp})B_{NM}^{(qp)} \mu_p^T \right) \left(I_p^\beta \right)^{\pm 1/2}; \quad \begin{cases} p \\ q \end{cases} = \begin{cases} 1, 2 \\ 2, 1 \end{cases}, \end{aligned} \quad (3.127)$$

where, by definition, we have $({}^{\mp})B_{NM}^{(qp)} = ({}^{\mp})G_N^{(q)} - ({}^{\mp})G_M^{(p)}$.

From (3.126) and (3.127), the desired equivalent representation for the matrix operator (3.106) is

$$\Lambda_{M,N}^{(p)} = P_M (B - B_{NM}) P_M + P_M B Q_M + \bar{\Xi}_M, \quad (3.128)$$

where the third summand is

$$\bar{\Xi}_M = P_M ({}^{\pm})F_p \left(Q_M ({}^{\mp})F_p + P_M ({}^{\mp})F_p Q_M \right). \quad (3.129)$$

In the obtained representation (3.128), we are interested in convergence of difference between two known operators, $B - B_{NM} \equiv \Delta B_{NM}$, to the null operator.

Lemma 3.4 *The operator ΔB_{NM} converges strongly to the null operator: $\forall b \|\Delta B_{NM}\| \rightarrow 0$ as $N, M \rightarrow \infty$.*

Proof This follows immediately from definitions (3.126) and (3.127), in view of strong convergence of the orthoprojector (3.107). \square

Next, let us examine in detail the properties of the convergence $\Delta B_{NM} \rightarrow 0$, $N, M \rightarrow \infty$. Separating the main (or static) parts $({}^{\mp})g^{(p)}(y, \bar{y})$ in the distributions (3.124), we obtain for the induced integral operators: $({}^{\mp})G^{(p)} = ({}^{\mp})g^{(p)} + ({}^{\mp})\theta^{(p)}$, $p = 1, 2$, where the remainders $(-)\theta^{(p)}$ and $(+)\theta^{(p)}$ are a nuclear operator and a Hilbert-Schmidt operator, respectively. With a finite number of waveguide modes taken into account in the partial regions, we have the corresponding integral operators with the degenerate kernel $({}^{\mp})G_K^{(p)} = ({}^{\mp})g_K^{(p)} + ({}^{\mp})\theta_K^{(p)}$, $K = M, N$.

Consider the difference of the matrix operators in formula (3.128):

$$B - B_{NM} \equiv \Delta B_{NM} = \left(I_p^\beta\right)^{\pm 1/2} \left(\mu_p, {}^{(\mp)}\Delta B_{NM}^{(qp)} \mu_p^T\right) \left(I_p^\beta\right)^{\pm 1/2}. \quad (3.130)$$

Here, we used the notation

$${}^{(\mp)}\Delta B_{NM}^{(qp)} = {}^{(\mp)}\Delta g_{NM}^{(qp)} + {}^{(\mp)}\Delta \theta_{NM}^{(qp)}, \quad (3.131)$$

where

$$\begin{aligned} {}^{(\mp)}\Delta g_{NM}^{(qp)} &= {}^{(\mp)}\Delta g_N^{(q)} - {}^{(\mp)}\Delta g_M^{(p)}, & {}^{(\mp)}\Delta \theta_{NM}^{(qp)} &= {}^{(\mp)}\Delta \theta_N^{(q)} - {}^{(\mp)}\Delta \theta_M^{(p)}; & \begin{Bmatrix} p \\ q \end{Bmatrix} &= \begin{Bmatrix} 1, 2 \\ 2, 1 \end{Bmatrix} \\ \text{and } {}^{(\mp)}\Delta g_K^{(p)} &= {}^{(\mp)}g^{(p)} - {}^{(\mp)}g_K^{(p)}, & {}^{(\mp)}\Delta \theta_K^{(p)} &= {}^{(\mp)}\theta^{(p)} - {}^{(\mp)}\theta_K^{(p)}; & K &= M, N. \end{aligned}$$

Let us introduce six bounded matrix operators by the formula

$$\begin{Bmatrix} (\pm)C^{(p)} \\ (\pm)\Delta C_{NM}^{(qp)} \\ (\pm)\Delta \Theta_{NM}^{(qp)} \end{Bmatrix} = \left(I_p^\beta\right)^{\pm 1/2} \left(\mu_p, \begin{Bmatrix} {}^{(\mp)}g^{(p)} \\ {}^{(\mp)}\Delta g_{NM}^{(qp)} \\ {}^{(\mp)}\Delta \theta_{NM}^{(qp)} \end{Bmatrix} \mu_p^T\right) \left(I_p^\beta\right)^{\pm 1/2}. \quad (3.132)$$

Then from (3.130) and (3.131) follows:

$$\Delta B_{NM} = {}^{(\mp)}\Delta C_{NM}^{(qp)} + {}^{(\mp)}\Delta \Theta_{NM}^{(qp)}.$$

Here, the first term is the main part of the operator under study, and the remainder is a nuclear operator such that

$$\lim_{M, N \rightarrow \infty} \left\| {}^{(\mp)}\Delta \Theta_{NM}^{(qp)} \right\| = 0; \quad \forall M/N.$$

Consequently, the ascertained strong convergence $\Delta B_{NK} \rightarrow 0$ will be determined by the estimate

$$\|b \Delta B_{NM}\| \leq \left\| b {}^{(\mp)}\Delta C_{NM}^{(qp)} \right\| + \left\| {}^{(\mp)}\Delta \Theta_{NM}^{(qp)} \right\| \|b\|; \quad \forall b \in l_2. \quad (3.133)$$

Further, if we consider the first region, then we assume $N = tM$ (and correspondingly, $M = tN$ for the second region), where $t > 0$. Then we sum the kernel of the integral operator ${}^{(\mp)}\Delta g_{NM}^{(qp)}$ (i.e., the kernel of the principal part of the operator ${}^{(\mp)}\Delta B_{NM}^{(qp)}$) over the index M (or N) = 1, 2, 3, ... Upon introducing the dimensionless variables $\alpha = \pi y/a_2$, $\bar{\alpha} = \pi \bar{y}/a_2$, and the geometric parameter $\tau = a_2/a_1 \leq 1$, the result of the summation is given by the formula

$$\begin{aligned} \sum_{M=1}^{\infty} (\mp) \Delta g_{tM,M}^{(21)}(\alpha, \bar{\alpha}) &= - \sum_{N=1}^{\infty} (\mp) \Delta g_{N,tN}^{(12)}(\alpha, \bar{\alpha}) = \mp (\tau^{-1} - t^{-1}) \left\{ \frac{\delta(\alpha - \bar{\alpha})}{\frac{d^2 \delta(x)}{dx^2} \Big|_{x=\alpha-\bar{\alpha}}} \right\} \\ &+ (\mp) g^{(1)}(\alpha, \bar{\alpha}) - \frac{1}{2} \left[(\mp) g^{(2)}(\alpha, \bar{\alpha}) + (\mp) g(t\alpha, t\bar{\alpha}) \right], \end{aligned} \quad (3.134)$$

where

$$\begin{aligned} (\mp) g(t\alpha, t\bar{\alpha}) &= \left\{ \begin{array}{l} -\frac{2}{\pi} \int \Phi(t\alpha, t\bar{\alpha}) d\alpha \\ \frac{2\pi}{\alpha^2} \frac{\partial}{\partial \alpha} \Phi(t\alpha, t\bar{\alpha}) \end{array} \right\} \rightarrow (\mp) g(t\alpha, t\bar{\alpha}) \Big|_{t=\tau} = \frac{1}{\tau} (\mp) g^{(1)}(\alpha, \bar{\alpha}) \\ \text{and } \Phi(t\alpha, t\bar{\alpha}) &= \frac{1}{2} \left[\text{ctg} \left(t \frac{\alpha - \bar{\alpha}}{2} \right) \mp \text{ctg} \left(t \frac{\alpha + \bar{\alpha}}{2} \right) \right]; \quad \left\{ \begin{array}{l} H - \text{case} \\ E - \text{case} \end{array} \right\}. \end{aligned}$$

The obtained sum (3.134) together with the definition (3.132) allow us to construct the operator series, which will be convergent or divergent depending on the ratio $t = M/N$ of the number of accounted modes in the waveguide arms. Namely, if $t = \tau$, then the first term in the right-hand side of (3.134) vanishes and, according to (3.132), we obtain the convergent operator series of the form

$$2 \sum_{M=1}^{\infty} (\mp) \Delta C_{\tau M, M}^{(21)} = -2 \sum_{N=1}^{\infty} (\mp) \Delta C_{N, \tau N}^{(12)} = \frac{2\tau - 1}{\tau} (\mp) C^{(1)} - (\mp) C^{(2)}. \quad (3.135)$$

Otherwise if $t \neq \tau$, it is easy to see that δ -singularities in the sum (3.134) generate the unbounded in l_2 matrix operators

$$\text{const} \cdot (\tau^{-1} - t^{-1}) \left(I_p^\beta \right)^{\pm 1/2} \left(\mu_p, \left\{ \begin{array}{l} \mu_p^T \\ d^2 \mu_p^T / dy^2 \end{array} \right\} \right) \left(I_p^\beta \right)^{\pm 1/2}; \quad p = 1, 2. \quad (3.136)$$

Hence, in this case, a convergent operator series cannot be constructed in the space $B(l_2)$ of bounded operators on the basis of formula (3.134).

Problem 3.24 Using relations (3.132) and (3.134), obtain the series (3.135) and operators (3.136).

Thus, the rate of decrease of the first term in (3.133), which is given as $\left\| b \left((\mp) \Delta C_{NM}^{(qp)} \right)^T \right\| \rightarrow 0$, $M, N \rightarrow \infty$, depends on the ratio $t = M/N$. It can be sufficient for the series in (3.135) to converge ($t = \tau$) or not ($\forall t \neq \tau$).

So, the Mittra rule for the scattering operators of the problem under consideration can be formulated as follows:

Theorem 3.3 *If the relation $N/M = \tau$, where $\tau = a_2/a_1$ is a predetermined geometrical parameter of the problem, holds, then the rate of convergence of the approximations is higher than with any other ratio of the numbers of accounted modes.*

Taking into account formulas (3.102) and (3.128), we conclude that for $N/M = \tau$ the previously established strong P -convergence of the projection approximations is characterized by the estimate

$$\|b(P_M R_p - \tilde{R}_p)\| < 2\|b \Delta B_{\tau M, M}\| + \|d (P_M B Q_M + \bar{\Xi}_M)\|, \quad (3.137)$$

where $d = 2b\tilde{A}_p, \forall b \in l_2$.

3.7 Novel Matrix Models for the Problem of a Step Discontinuity in a Waveguide

Let us represent the found solution (3.51) via the operator $A_p \equiv (D_p + I)^{-1}$, $p = 1, 2$, in the form of the following table:

$$\left. \begin{matrix} R^{11} = \pm(I - 2A_1) & T^{21} = 2A_1 D_0 \\ T^{12} = 2A_2 D_0^T & R^{22} = \mp(I - 2A_2) \end{matrix} \right\}; \quad \left\{ \begin{matrix} H - \text{case} \\ E - \text{case} \end{matrix} \right\}. \quad (3.138)$$

To the left of the equality sign in the table is a 2×2 operator matrix—the generalized scattering matrix

$$S \equiv \begin{bmatrix} R^{11} & T^{21} \\ T^{12} & R^{22} \end{bmatrix}, \quad (3.139)$$

operating in the space $h_2 = l_2 \times l_2 \equiv l_2^2$. Owing to the established order of the scattering operators in the entries of matrix (3.139), the symmetry properties of the operators (3.66) and (3.67) can now be expressed as $S^T = S$.

Next, if we specially construct three diagonal operator matrices

$$J = \begin{bmatrix} I & 0 \\ 0 & -I \end{bmatrix}, \quad A = \begin{bmatrix} A_1 & 0 \\ 0 & A_2 \end{bmatrix}, \quad V = \begin{bmatrix} 0 & D_0 \\ D_0^T & 0 \end{bmatrix}, \quad (3.140)$$

then the Table (3.138) can be brought in obvious way to the compact form:

$$S = \pm J + 2A(V \mp J), \quad \left\{ \begin{matrix} H - \text{case} \\ E - \text{case} \end{matrix} \right\}. \quad (3.141)$$

Here, according to the definition (3.140), J is the *canonical symmetry* of the space h_2 , $J = J^\dagger = J^{-1}$ (see Appendix A), A is the accretive contraction,

$\operatorname{Re} A > AA^\dagger > 0$, while V is the given operator matrix of the problem. From the structure of three operator matrices in (3.140) it follows that they are symmetrical with respect to a transposition operation.

Since $A : h_2 \rightarrow h_2$ is the accretive contraction, then there exists a unique bounded and accretive operator C (which is also contraction) such that $C^2 = A$. Since the original operator is symmetric, $A^T = A$, then the operator C will inherit this property: $C^T = C$. As is customary in operator theory, we will use the notation $C \equiv A^{1/2}$. To find this operator matrix, notice that from the relation

$$(V \mp J)^2 = V^2 + I_h = \begin{bmatrix} D_1 + I & 0 \\ 0 & D_2 + I \end{bmatrix} = A^{-1} \quad (3.142)$$

it follows that $A^{1/2} = (V \mp J)^{-1} = A (V \mp J)$. Here, I_h is the unit operator acting in the space h_2 .

Thus, the solution (3.141) takes the remarkably simple form

$$S = \pm J + 2 (V \mp J)^{-1} = 2A^{1/2} \pm J, \quad \left\{ \begin{array}{l} H - \text{case} \\ E - \text{case} \end{array} \right\}. \quad (3.143)$$

This equality can be interpreted as the inner structure of the generalized scattering matrix (3.139).

Problem 3.25 Using (3.143), prove that the generalized scattering matrix of the studied waveguide junction is an involutory operator: $S^2 = I_h$.

Below we will be interested in formula (3.143) in terms of convergence of the projection approximations to the desired generalized scattering matrix.

Let us combine the earlier introduced orthoprojectors (3.84) into the operator matrices

$$P = \begin{bmatrix} P_M & 0 \\ 0 & P_N \end{bmatrix}, \quad Q = I_h - P = \begin{bmatrix} Q_M & 0 \\ 0 & Q_N \end{bmatrix}, \quad (3.144)$$

where M (N) is now the number of the modes taken into account in the first (second) region. The computed finite-dimensional approximations have the form of the $(M+N) \times (M+N)$ block (or partitioned) matrices

$$\tilde{S} = \begin{bmatrix} \tilde{R}^{11} & \tilde{T}^{21} \\ \tilde{T}^{12} & \tilde{R}^{22} \end{bmatrix} = 2\tilde{A}^{1/2} \pm \tilde{J}, \quad \tilde{A} \equiv \begin{bmatrix} \tilde{A}_1 & 0 \\ 0 & \tilde{A}_2 \end{bmatrix}, \quad \tilde{J} \equiv \begin{bmatrix} \tilde{I}_M & 0 \\ 0 & -\tilde{I}_N \end{bmatrix}; \quad \left\{ \begin{array}{l} H - \text{case} \\ E - \text{case} \end{array} \right\}, \quad (3.145)$$

where the operators in the submatrices are given by formulas (3.86)–(3.88).

Basing on the operator (3.96), we construct the infinite-dimensional extension by zeros of the given finite matrix in the form

$$\bar{V} \equiv PVP = \begin{bmatrix} 0 & \bar{D}_0 \\ \bar{D}_0^T & 0 \end{bmatrix} \rightarrow \bar{V}^2 = \begin{bmatrix} \bar{D}_1 & 0 \\ 0 & \bar{D}_2 \end{bmatrix}, \quad (3.146)$$

where the operator \bar{D}_p , $p = 1, 2$ is given by formula (3.97). We also use the operator (3.98) to extend by zeros the operator matrix of accretive contraction

$$\bar{A} \equiv \begin{bmatrix} \bar{A}_1 & 0 \\ 0 & \bar{A}_2 \end{bmatrix}, \quad \bar{A}_p \bar{A}_p^{-1} = \bar{A}_p^{-1} \bar{A}_p = I_h, \quad (3.147)$$

for which the analog of (3.142) is

$$(PVP \mp J)^2 = \bar{V}^2 + I_h = \begin{bmatrix} \bar{D}_1 + I & 0 \\ 0 & \bar{D}_2 + I \end{bmatrix} = \bar{A}^{-1}. \quad (3.148)$$

Problem 3.26 Derive formula (3.148).

With the help of the operator (3.147) we form the required projection approximation

$$\bar{S} = 2P\bar{A}^{1/2} \pm PJ = 2\bar{A}^{1/2}P \pm JP = \begin{bmatrix} \bar{R}^{11} & \bar{T}^{21} \\ \bar{T}^{12} & \bar{R}^{22} \end{bmatrix}; \quad \left\{ \begin{array}{l} H - \text{case} \\ E - \text{case} \end{array} \right\} \quad (3.149)$$

as well as the difference between the operator matrices

$$PSP - \bar{S} = -2PA^{1/2}QVPA^{1/2}. \quad (3.150)$$

In view of the estimate $\|P\bar{A}^{1/2}\|_{h_2} < 1$ and the equality $P2A^{1/2}Q = PSQ$, which is a consequence of (3.143) and the orthogonality of the projectors, expression (3.150) leads to the following estimate for the projection approximation error:

$$\|b(PSP - \bar{S})\|_{h_2} < \|dQ\|_{h_2} \|QVP\|_{h_2}; \quad d = bPS, \quad \forall b \in h_2. \quad (3.151)$$

Strong convergence of the approximations follows from this estimate as a consequence of strong convergence of the orthoprojector P to the unit operator in the space h_2 :

$$\lim_{M, N \rightarrow \infty} \|dQ\|_{h_2} = \lim_{M, N \rightarrow \infty} \|d(I_h - P)\|_{h_2} = 0; \quad \forall d \in h_2. \quad (3.152)$$

Thus the projection approximation (3.145) always strongly P -converges to the true solution (3.143), while the relative convergence of these approximations is lacking.

The rate of strong convergence can be obtained from the behavior of the given vector d . First note that the following equality is valid:

$$\|dQ\|_{h_2}^2 = \|d_1Q_M\|^2 + \|d_2Q_N\|^2, \quad (3.153)$$

where

$$d = \{d_1, d_2\}, \quad d_1 = b_1P_MR^{11} + b_2P_NT^{12}, \quad d_2 = b_1P_MT^{21} + b_2P_NR^{22}; \quad (3.154) \\ \forall b_1, b_2 \in l_2.$$

As in Sect. 3.5.3, we will consider the scattering of the r th mode of the first waveguide port ($r \leq M$ for H -case or $r \leq M + 1$ for E -case), $b_1 = \{\delta_m^r\}_{m=(0)1}^\infty$, and the s th mode of the second port ($s \leq N$ for H -case or $s \leq N + 1$ for E -case), $b_2 = \{\delta_m^s\}_{m=(0)1}^\infty$.

At this step we will use the results of the study presented in [3] regarding the rate of decrease of the Fourier coefficients of the modal expansion in the aperture of the discontinuity in order to find the asymptotics $d_1, d_2 = \{O(m^{-7/6}); m \gg 1\}$ (see Sect. 3.5.3 for details). Then the required estimate takes the form

$$\|b(PSP - \bar{S})\|_{h_2} < \|QVP\|_{h_2} \sqrt{\frac{const_1^2}{M^{4/3}} + \frac{const_2^2}{N^{4/3}}}; \quad M, N \gg 1, \quad b = \{b_1, b_2\}, \quad (3.155)$$

where the multiplier $\|QVP\|_{h_2}$ depends on the ratio M/N , confirming the findings of [3, 11].

Let us use the canonical problem of diffraction of the principal mode of a rectangular waveguide on the H -plane step discontinuity to illustrate numerically the obtained analytical results. Chose the modulus $|r_{11}^{11}| = 0.478458$ and the argument $\arg r_{11}^{11} = 2.9771$ of the reflection coefficient ($R^{11} = \{r_{mr}^{11}\}_{m,r=1}^\infty$, r is the number of the incident wave) calculated accurately in [11] for the parameters $a_1/\lambda = 1.300001$ and $a_2/a_1 = 0.5001$, as test values.

Figure 3.2 shows a stable ‘practical convergence’ of the approximations to the reference values (shown by the dashed line). In full agreement with the above results, the relative convergence of the approximations is not observed. At the same time, the rate of convergence depends substantially on the ratio of the numbers of modes taken into account M/N . As expected, compliance with the Mittra rule, $M/N = 2.0$, gives the best results.

In the numerical computations, the largest size of the reduced matrix reached 7200×7200 . At the same time, the maximum matrix condition number did not exceed 1.75.

The high stability of calculations is explained by the structure of the considered block matrix. The ‘mountain profile’ of this matrix is visualized for $M = 15$ and $N = 10$ in Fig. 3.3. This figure shows that the main diagonal of this matrix contains

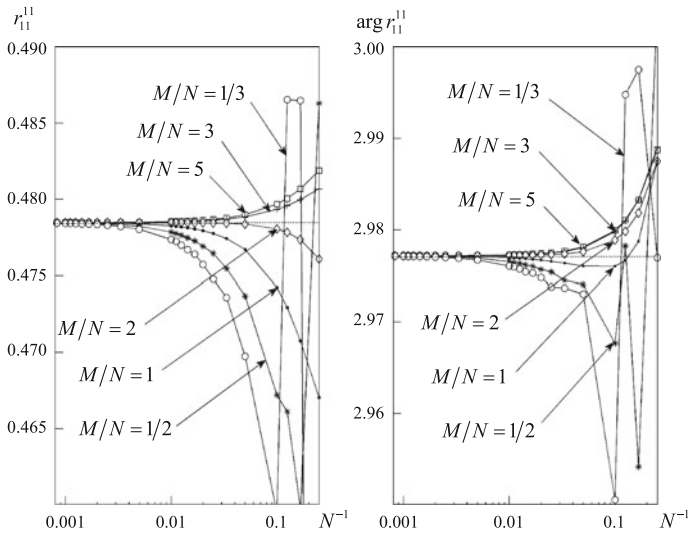


Fig. 3.2 Numerical convergence of projection approximations

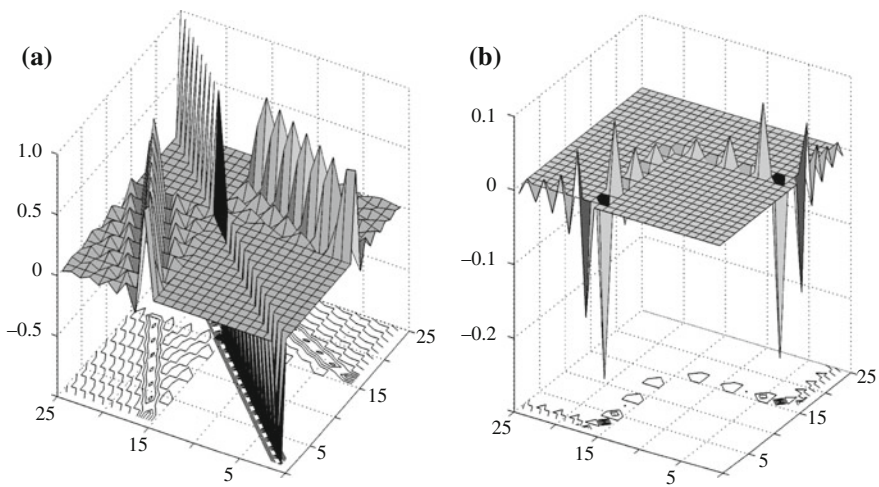


Fig. 3.3 The profile of the 25×25 -size invertible matrix $\tilde{A}^{-1/2}$: **a** the real part of the matrix; **b** the imaginary part of the matrix

extreme elements ± 1 independent of the numbers M and N . At the same time, the elements of the submatrices \tilde{D}_0 and \tilde{D}_0^T , whose magnitude depends on the ratio M/N , are located at the periphery of the matrix.

Figure 3.4 shows the level lines for the norm of the relative error of projection approximations (3.151) for the observed range of variation of the truncation numbers M and N and for different values of the geometric parameter a_2/a_1 .

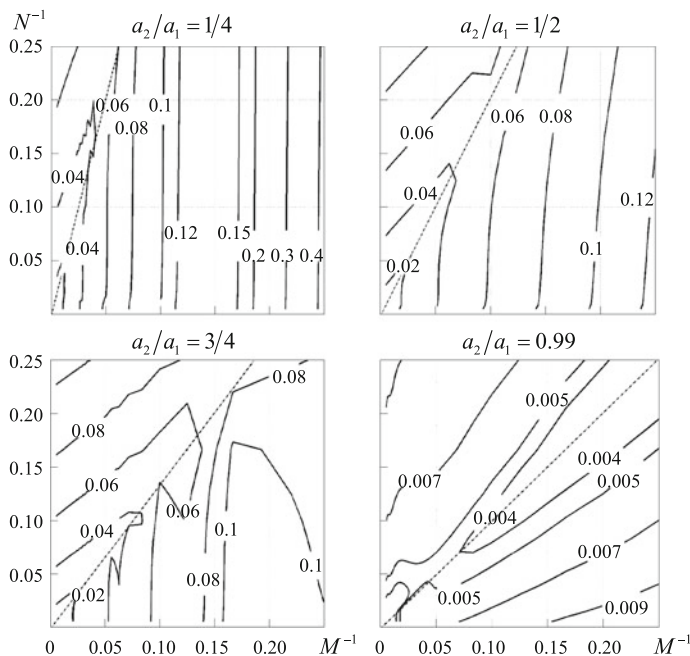


Fig. 3.4 The norm of the approximation error for different values of a_2/a_1

The approximation calculated for $M = N = 250$ has been taken for a true generalized scattering matrix. This profile has a unique ravine-type minimum (marked by the dashed line) corresponding to the Mittra rule $M/N = a_2/a_1$.

Thus, the presented numerical results fully confirm the findings of our previous analytical study.

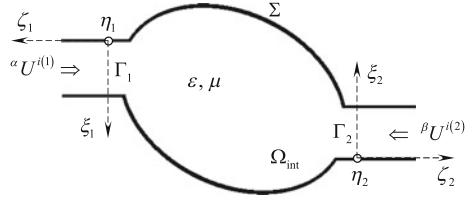
3.8 The Conservation Laws in Operator Form for Two Classes of Mode Diffraction Problems

Our next goal will be to apply the developed approach to the analysis of H - and E -plane waveguide transformers of a general shape.

In this section, we will study a two-port waveguide transformer with relatively arbitrary geometry of coupling cavity. The configuration and the coordinate systems used are shown in Fig. 3.5. Here, the orthogonal coordinates $\{\eta_j, \xi_j, \zeta_j\}$, $j = 1, 2$ stand for either Cartesian $\{x, y, z\}$ or cylindrical $\{\eta = z, \xi = \rho, \zeta = \phi\}$ coordinate systems.

In this way we introduce the uniformly curved waveguides of rectangular cross-section, in which the modes LM_{0n} , $n = 1, 2, \dots$ (H -case) or LE_{1n} , $n = 0, 1, \dots$ (E -case) form a complete orthogonal set. (Note that in our notation, n equals to the

Fig. 3.5 Configuration of the wave transformer and the coordinate systems



number of field variations along the straight $O\xi$ -axis.) For such regular waveguides, the mode propagation along the uniformly curved coordinate axis is described by the exponential function $\exp(\pm i\beta_n \phi)$, where $\{\beta_n\}_{n=(0)}^\infty$ are the angular propagation constants. (There exists a large number of works on uniform bends of rectangular waveguides; the generalized mode-matching technique has been applied to the analysis of such waveguide bend in [23].)

In Fig. 3.5, the coupling region is a cylindrical cavity that is geometrically uniform along the straight η_1 -axis or η_2 -axis; the height of the cavity is a_3 . Denote the volume confined by the metal walls together with the reference planes $\Sigma_j = \Gamma_j \times (0, a_3)$, $j = 1, 2$, disposed in the regular waveguides, as $V_{\text{int}} \equiv \Omega_{\text{int}} \times (0, a_3)$, and the reference surface as $S = \Sigma_1 \cup \Sigma_2$. This volume is supposed to be source free, which ensures the fulfillment of the edge condition (3.12). We can let $\Omega_{\text{int}} \rightarrow 0$ to form the aperture of an abrupt waveguide discontinuity, which is now considered as a special case of the wave transformer (obviously, in this case $V_{\text{int}} \rightarrow 0$). All metal surfaces are assumed to be perfect electric conductors. The waveguide transformer is filled with a homogeneous lossless medium and the waveguide arms are terminated in matching loads.

Let us mark two independent sources of the field as α and β . These sources generate the fields $\{\alpha\vec{E}, \alpha\vec{H}\}$, and respectively $\{\beta\vec{E}, \beta\vec{H}\}$, in the volume V_{int} . In view of the geometry (Fig. 3.5) and the homogeneous boundary conditions on the metal walls, the first and second Lorentz lemmas take the form

$$\int_S (\alpha\vec{E} \times \beta\vec{H} - \beta\vec{E} \times \alpha\vec{H}) \cdot \vec{n} ds = 0 \tag{3.156}$$

and

$$\int_S (\alpha\vec{E} \times \beta\vec{H}^* + \beta\vec{E}^* \times \alpha\vec{H}) \cdot \vec{n} ds = 0, \tag{3.157}$$

respectively. The oscillating power theorem and the complex power theorem yields two relations

$$\int_S (\vec{E} \times \vec{H}) \cdot \vec{n} ds = i\omega \int_{V_{\text{int}}} (\varepsilon\varepsilon_0 \vec{E}^2 + \mu\mu_0 \vec{H}^2) dV \quad (3.158)$$

$$\int_S (\vec{E} \times \vec{H}^*) \cdot \vec{n} ds = -i\omega \int_{V_{\text{int}}} (\varepsilon\varepsilon_0 |\vec{E}|^2 - \mu\mu_0 |\vec{H}|^2) dV \quad (3.159)$$

where ε and μ are the relative permittivity and permeability, and the common index α or β is omitted. In all formulas (3.156)–(3.159), the unit vector \vec{n} is the outward normal to the reference surface S .

In the domain of complex amplitudes, the oscillation power theorem (3.158) and the complex power theorem (3.159) together with two Lorentz lemmas (3.156) and (3.157) form a complete set of basic electromagnetic laws in the sense that there are no other independent energy relations for two fields generated by independent sources. The presence or absence of the volume integrals in the right-hand sides of formulas (3.158) and (3.159) naturally divides mode diffraction problems into two classes. We assign the wave scattering by resonant discontinuities of volume $V_{\text{int}} / = 0$ to the first class and abrupt discontinuities in waveguides ($V_{\text{int}} = 0$)—to the second class. For these two classes of problems the energy conservation laws are evidently different.

For the planar wave transformers considered herein, the electromagnetic field can be expressed in terms of η -components of the electric (H -plane case) or magnetic (E -plane case) fields. The corresponding complex amplitude (i.e. the phasor) we will denote, as earlier in (3.6), by $U(g, \omega)$, $g = \{y, z\}$ in Cartesian coordinates and $g = \{\rho, \phi\}$ in cylindrical coordinates.

We now substitute the continuous scalar function $U(g, \omega)$ expanded in the complete set of orthonormal transverse eigenfunctions of regular waveguides into the left-hand sides of (3.156) and (3.158). Taking into account the orthogonality of these eigenfunctions, we get two relations for the generalized scattering matrix

$$S^T = S, \quad b(I_h - S^2)b^T = \int_{\Omega_{\text{int}}} \left\{ [\nabla_{\parallel}({}^{\alpha}U + {}^{\beta}U)]^2 - \chi^2({}^{\alpha}U + {}^{\beta}U)^2 \right\} ds, \quad (3.160)$$

where $\nabla_{\parallel} \equiv \nabla_{\xi\xi}$ stands for the longitudinal part of the gradient. The first equality in (3.160) (which have been cited earlier for the canonical problem of a step in a waveguide) is associated with the reciprocity property of a waveguide transformer, while the second one describes the oscillating power in the coupling cavity.

Problem 3.27 Derive (3.160) from the laws (3.156) and (3.158).

Similarly, from the second pair of equations in (3.157) and (3.159) one can obtain a combined relation, which can be written as

$$bGb^\dagger = \int_{\Omega_{\text{int}}} \left\{ |\nabla_{\parallel}(\alpha U + \beta U)|^2 - \chi^2 |\alpha U + \beta U|^2 \right\} ds. \quad (3.161)$$

Here, we have introduced the characteristic operator

$$G \equiv (I_h + S)U(I_h - S^\dagger), \quad (3.162)$$

which involves the ‘portal operator matrix’

$$U \equiv \begin{bmatrix} U_1 & 0 \\ 0 & U_2 \end{bmatrix} = \begin{bmatrix} Q_1 + iP_1 & 0 \\ 0 & Q_2 + iP_2 \end{bmatrix} = Q + iP. \quad (3.163)$$

The matrix operators U_m , Q_m , and P_m , $m = 1, 2$, have been previously defined in (3.30), (3.31), (3.34) and (3.35). With the last two operators, we have formed the operator matrix P and $Q = I_h - P$ (see (3.144)) of projection onto all propagating modes and, accordingly, onto all evanescent modes in the two waveguide ports. The existence of two mutually orthogonal subspaces of the vectors Ph_2 and Qh_2 composed of the amplitudes of propagating and evanescent modes, respectively, necessitates introduction of a special vector space. The ratio between the energy transferred by the propagating modes (i.e., the norm of the vectors from the subspace Ph_2) and the energy stored by the oscillating field (i.e., the norm of the vectors from the subspace Qh_2) may be arbitrary. Therefore, this space is of indefinite metric. Since for any finite wavenumber χ (see formula (3.7)), the number of propagating modes is always limited and equal to p_j (H -case) or $p_j + 1$ (E -case), $j = 1, 2$ (see (3.30) and (3.34)), then P is the operator of finite rank $\nu = \text{Tr}(P) = p_1 + p_2$ (H -case) or $\nu = (p_1 + 1) + (p_2 + 1)$ (E -case). Consequently, the space $\Pi_\nu = Ph_2 \cup Qh_2$ with an indefinite metric is a Pontryagin space [8]. The canonical symmetry of this space is given by the following formula (see Appendix A):

$$J \equiv Q - P = I_h - 2P \quad \rightarrow \quad J = J^\dagger = J^{-1}. \quad (3.164)$$

In what follows, the operators S , U , and G will be treated as ones acting both in the space $h_2 = l_2^2$, and in the space Π_ν .

In addition, to write the results in a compact form, it is convenient to use the conventional notation for two components of any linear operator L :

$$\text{Re} L = \frac{1}{2}(L + L^\dagger), \quad \text{Im} L = \frac{1}{2i}(L - L^\dagger). \quad (3.165)$$

Refer now to the base relation (3.161), which can be rewritten as

$$b G b^\dagger = \|\nabla_{\parallel}(\alpha U + \beta U)\|_{L_2(\Omega_{\text{int}})}^2 - \chi^2 \|\alpha U + \beta U\|_{L_2(\Omega_{\text{int}})}^2. \quad (3.166)$$

Problem 3.28 Derive (3.166) from the laws (3.157) and (3.159).

In the absence of loss (i.e., when χ is a real number), equality (3.166) implies the Hermiticity of the characteristic operator, $G^\dagger = G$, which is equivalent to the relationships

$$\text{Im } G = P - S P S^\dagger + 2\text{Im}(S Q) = 0, \quad (3.167)$$

$$G = \text{Re } G = Q - S Q S^\dagger - 2\text{Im}(S P). \quad (3.168)$$

We emphasize that these expressions are valid for any real value of the wavenumber χ , i.e. for any (finite) number of propagating modes existing in the waveguide ports (Fig. 3.5).

The found property of the generalized scattering matrix S in the form of the corollary (3.167) of formula (3.166) has a clear electrodynamic meaning. Namely, this matrix-operator expression reflects the fact that the active power flux through the surface enclosing any source-free and lossless volume V_{int} equals zero:

$$\text{Re} \int_S (\vec{E} \times \vec{H}^*) \cdot \vec{n} \, ds = 0.$$

Thus the property (3.167) of the generalized scattering matrix S is the energy conservation law in a generalized (or operator) form.

Evidently this law in the form of (3.167) is not the only possible representation, and below we will give its useful modifications. By adding and subtracting (3.167) and (3.168), we obtain a new representation of the characteristic operator:

$$G = I_h - S S^\dagger + 2\text{Im}(S J) = J - S J S^\dagger - 2\text{Im } S. \quad (3.169)$$

The operator matrices

$$V_{\pm} = \left(\frac{1}{2}\right)^{1/2} (I_h \mp i S J) \quad (3.170)$$

play an important role in further mathematical manipulations. With the use of them equalities (3.169) can be written in a compact form:

$$\frac{1}{2}G = I_h - V_- V_-^\dagger = J - V_+ J V_+^\dagger, \quad (3.171)$$

$$\frac{1}{2}JG^T J = I_h - V_-^\dagger V_- = J - V_+^\dagger J V_+. \quad (3.172)$$

Problem 3.29 Derive formulas (3.169), (3.171) and (3.172).

To derive other forms of the energy conservation law, we use the identities

$$I_h + SS^\dagger = V_+ V_+^\dagger + V_- V_-^\dagger, \quad (3.173)$$

$$2\text{Im}(SJ) = V_+ V_+^\dagger - V_- V_-^\dagger, \quad (3.174)$$

which represent, respectively, the Pythagorean theorem and an indefinite form in the space $h_2 \times h_2$ (these formulas were derived in [24] for a more general problem).

Problem 3.30 Verify the validity of identities (3.173) and (3.174) by direct substitution of the operator (3.170).

Combining relations (3.171)–(3.174), we find the following equivalent forms of the energy conservation law (3.167):

$$\frac{1}{2}(I_h - SS^\dagger) = Q - V_+ Q V_+^\dagger, \quad (3.175)$$

$$\text{Im} S = -P + V_- P V_-^\dagger, \quad (3.176)$$

$$\text{Im}(SJ) = -P + V_+ P V_+^\dagger, \quad (3.177)$$

whose meaning will be clarified in Sect. 3.10.2.

Problem 3.31 (*research*) Derive formulas (3.175)–(3.177).

For the second class of the problems of wave scattering by an abrupt waveguide discontinuity one has to pass to the limit $\Omega_{\text{int}} \rightarrow 0$ in formulas (3.160) and (3.161). Since there are no sources and sinks of field both in the interior of Ω_{int} , and at the points of geometrical singularities of the boundary, the integrals in the right-hand sides of (3.160) and (3.161) vanish.

Now, in order to represent the required energy conservation laws, let us introduce the reflection and transmission operator matrices

$$S_R \equiv \begin{bmatrix} R^{11} & 0 \\ 0 & R^{22} \end{bmatrix}, \quad S_T \equiv \begin{bmatrix} 0 & T^{21} \\ T^{12} & 0 \end{bmatrix}, \quad (3.178)$$

respectively. From the first equality in (3.160) it follows that both of these matrices are symmetric with respect to the transposition operation: $S_R^T = S_R$, $S_T^T = S_T$. (Note that, generally speaking, the generalized scattering matrix could be defined by the

operators (3.178) using the formula $S_{\pm} = S_R \pm S_T$, since all the relationships derived in this chapter are valid for both signs).

From the oscillating power theorem and the first Lorentz lemma, we obtain

$$S_R^2 + S_T^2 = I_h, \quad (3.179)$$

$$S_R S_T + S_T S_R = 0. \quad (3.180)$$

In view of these equations, the relation

$$S_T U \left(I_h - S_R^{\dagger} \right) = (I_h + S_R) U S_T^{\dagger}, \quad (3.181)$$

which arise from the second Lorentz lemma, turns into a corollary of the complex power theorem

$$(I_h + S_R) U \left(I_h - S_R^{\dagger} \right) = S_T U S_T^{\dagger}, \quad (3.182)$$

and vice versa. Therefore, formula (3.182) can be taken as a generalized form of the energy conservation law for the step-like discontinuities in a waveguide considered herein.

It should be mentioned that simple formulas (3.179)–(3.182) cannot be extended to the case of a waveguide junction with more than two ports.

Problem 3.32 (*research*) Derive the properties (3.179)–(3.182) and show their interdependence.

Separating the real and imaginary parts of the operator (3.182), and then summing and subtracting the obtained expressions, we get the power conservation law in the equivalent forms

$$I_h - V_{R-} V_{R-}^{\dagger} = \frac{1}{2} S_T S_T^{\dagger}, \quad (3.183)$$

$$J - V_{R+} J V_{R+}^{\dagger} = \frac{1}{2} S_T J S_T^{\dagger}, \quad (3.184)$$

where

$$V_{R\pm} = \left(\frac{1}{2} \right)^{1/2} (I_h \mp i S_R J). \quad (3.185)$$

Note that from (3.183) immediately follows the estimate

$$\|S_T\| \leq \sqrt{2}, \quad \|V_{R-}\| \leq 1. \quad (3.186)$$

Problem 3.33 (*research*) Derive the energy conservation law in the forms of (3.183) and (3.184).

Other equivalent forms of the energy conservation law are

$$\frac{1}{2} \left(I_h - S_R S_R^\dagger \right) = Q - V_{R+} Q V_{R+}^\dagger + \frac{1}{2} S_T P S_T^\dagger = P - V_{R+} P V_{R+}^\dagger + \frac{1}{2} S_T Q S_T^\dagger, \quad (3.187)$$

$$\text{Im } S_R = -P + V_{R-} P V_{R-}^\dagger + \frac{1}{2} S_T P S_T^\dagger = Q - V_{R-} Q V_{R-}^\dagger - \frac{1}{2} S_T Q S_T^\dagger. \quad (3.188)$$

They can be obtained by combining (3.183), (3.184) and the identities

$$I_h + S_R S_R^\dagger = V_{R+} V_{R+}^\dagger + V_{R-} V_{R-}^\dagger, \quad (3.189)$$

$$2\text{Im}(S_R J) = V_{R+} V_{R+}^\dagger - V_{R-} V_{R-}^\dagger, \quad (3.190)$$

which are completely analogous to formulas (3.173) and (3.174). From the first equation in (3.188) it follows that the operator matrix S_R is a quasi-Hermitian operator.

Problem 3.34 (*research*) Derive the energy conservation law in the forms of (3.187) and (3.188).

Note that since the operator matrices (3.178) are ‘diagonal’, the relations similar to (3.179)–(3.188) are also obtained for the initial matrix operators R^{pp} and T^{qp} . In particular, from (3.179), (3.180) formulas (3.66) and (3.67) follow, while (3.181), (3.182) yields formulas (3.73) and (3.74).

3.9 Universality of the Operator Fresnel Formulas

The operator Fresnel formulas (3.51) identically satisfy the energy conservation laws derived above, which is easily verified by direct substitution. We will now show that these energy relations, which are valid for the entire class of problems considered, in their turn lead to the operator Fresnel formulas.

3.9.1 Step-Like Discontinuity in a Waveguide

Let us rewrite, for completeness and clarity, the energy laws (3.66), (3.67) (or, what is the same, formulas (3.179), (3.180)) as

$$(R^{pp})^T = R^{pp}, \quad (T^{qp})^T = T^{pq}, \quad (3.191)$$

$$(I \pm R^{pp})(I \mp R^{pp})^T = T^{qp}(T^{qp})^T, \quad (3.192)$$

$$R^{pp}T^{qp} + (R^{qq}T^{pq})^T = 0, \quad (3.193)$$

$p, q = 1, 2$ and $p \neq q$. We treat equality (3.192) as an equation with respect to the required reflection and transmission operators. It follows from this equation that the spectrum points $\lambda \in \sigma(R^{pp})$ and $\tau \in \sigma(T^{qp}(T^{qp})^T)$ lie on the algebraic curve

$$\lambda^2 + \tau = 1; \quad \lambda, \tau \in \mathbb{C} \quad (3.194)$$

(where \mathbb{C} is the complex plane), for which we know the solution of the uniformization problem in the form of rational functions (see, for example, [25]). Let us write this solution in the following form:

$$\lambda = \frac{t-1}{t+1}, \quad \tau = \frac{4t}{(t+1)^2}; \quad t \neq -1. \quad (3.195)$$

Based on the previously mentioned spectral mapping theorem and the first formula in (3.195), we conclude that there exists a quasi-Hermitian operator D_p such that its spectral points are $t = (1 + \lambda)/(1 - \lambda) \in \sigma(D_p)$; therefore, the following representation is true

$$R_p = \frac{D_p - I}{D_p + I} \rightarrow \begin{cases} I - R_p = 2(D_p + I)^{-1} \\ I + R_p = 2(D_p + I)^{-1}D_p \end{cases} \quad (3.196)$$

(here we have used the notation (3.53)). Substituting the last two expressions into (3.192), we find

$$T^{qp}(T^{qp})^T = \left[2(D_p + I)^{-1}D_p\right] \left[2(D_p + I)^{-1}\right]. \quad (3.197)$$

Taking into account the symmetry of the reflection operator (3.191), we put $D_p = MM^T$ (or $D_p = M^T M$), where $M : l_2 \rightarrow l_2$ is some bounded matrix operator. Then from (3.197) the second Fresnel formula follows:

$$T^{qp} = (D_p + I)^{-1}2D_0 \quad \text{or} \quad T^{qp} = (D_p + I)^{-1}2\bar{D}_0. \quad (3.198)$$

Here, we have introduced the notation $D_0 = MC$ and $\bar{D}_0 = M^T C$. The second multiplier in these formulas possesses the property $CC^T = I$. So we can immediately put $D_p = D_0 D_0^T$ (or $D_p = D_0^T D_0$). Now, the bounded matrix operator D_0 should be redefined with the use of the complex energy conservation law.

Note that it seems impossible to otherwise distribute the rational functions in (3.195) since this would result in violation of (3.191) and (3.193).

Problem 3.35 Verify the last mentioned statement.

Thus the possibility to parameterize the algebraic curve (3.194) by using single-valued functions (3.195), in this case, ensures the existence of a single operator of the problem, D_p , which defines the laws of mode reflection and transmission in the form of (3.196), (3.198).

The obtained result can be formulated as the following statement.

Theorem 3.4 *For each problem of mode diffraction by a step-like waveguide discontinuity, there exists a matrix-operator model in the form of the operator Fresnel formulas (3.196) and (3.198), if the reciprocity theorem (Lorentz lemma) and the oscillating power theorem for this problem hold in the form of (3.191)–(3.193).*

Notice that the properties (3.191) and (3.193) of the scattering operators play an important role in the above reasoning. Namely, these relationships provide a uniqueness of the solution (3.195) for the problem of uniformization of the curve (3.194). Again, formula (3.180) relating the reflection and transmission operator matrices, S_R and S_T , is of decisive importance as well. Despite the fact that equality (3.179) also results in the algebraic curve in the form of (3.194), the property (3.180) does not allow to obtain the Fresnel formulas for these operator matrices.

Problem 3.36 (*research*) Prove that the operator S_R has no Cayley transform. Hint: show that $\pm 1 \in \sigma(S_R)$.

3.9.2 Generalized Operator Fresnel Formulas for Resonant Discontinuities

Here we will construct the operator model for the problem of a resonant discontinuity in a waveguide ($V_{\text{int}} \neq 0$) by using the developed technique.

The first Lorentz lemma and the oscillating power theorem yield for this problem two relationships (3.160), which can be rewritten in the form

$$S^T = S, \quad b(I_h \pm S)(I_h \mp S)b^T = \int_{\Omega_{\text{int}}} \left\{ [\nabla_{\parallel}({}^{\alpha}U + {}^{\beta}U)]^2 - \chi^2({}^{\alpha}U + {}^{\beta}U)^2 \right\} ds. \quad (3.199)$$

As will be shown in Sect. 3.10.2, the generalized scattering matrix S is a quasi-Hermitian operator. Therefore, every nonreal point of its spectrum $\sigma(S)$ is an eigenvalue of finite multiplicity, while all singular spectral elements located on the real axis [18, 19]. These latter points correspond to the eigenvalues of the closed boundary value problem for the Helmholtz equation (3.7) in the region Ω_{int} (see Fig. 3.5), and we exclude them from consideration as non-physical ones.

Substituting into (3.199) the eigenvector b_{λ} , which corresponds to the eigenvalue $\lambda \in \sigma(S)$ of the operator matrix S , we obtain the equality

$$1 - \lambda^2 = \tau; \quad \lambda, \tau \in \mathbb{C}, \quad (3.200)$$

where

$$\tau = \frac{1}{b_\lambda b_\lambda^T} \int_{\Omega_{\text{int}}} \left\{ [\nabla_{\parallel}(\alpha U + \beta U)]^2 - \chi^2(\alpha U + \beta U)^2 \right\} ds. \quad (3.201)$$

Solution of the uniformization problem for the algebraic curve (3.200) is given above in the form of rational functions (3.195). Only this solution agrees with the symmetry property $S = S^T$ and, therefore, it is unique.

Consequently, there exists the operator $W : h_2 \rightarrow h_2$, which possesses by the eigenvectors $\{b_\lambda\}$ and the spectrum $\sigma(W) = \{(1 + \lambda)/(1 - \lambda)\}$. This single operator of the problem is related with the desired generalized scattering matrix by the Cayley transform

$$W = \frac{I_h + S}{I_h - S} \quad \leftrightarrow \quad S = \frac{W - I_h}{W + I_h}. \quad (3.202)$$

From the symmetry of the generalized scattering matrix (3.199) it follows that $W^T = W$, which is equivalent to the representation $W = W_0 W_0^T$ (or $W = W_0^T W_0$), where $W_0 : h_2 \rightarrow h_2$ is a bounded operator that requires redefinition by using the energy conservation law in the generalized form (3.167).

Problem 3.37 (*research*) Construct the operator model in the form of (3.202) for some problem of mode scattering by a resonant discontinuity in a waveguide.

Next, we introduce a new operator matrix by the formula

$$K = (W + I_h)^{-1} 2W_0, \quad (3.203)$$

then the second equality in (3.199) takes the form

$$b K K^T b^T = \int_{\Omega_{\text{int}}} \left\{ [\nabla_{\parallel}(\alpha U + \beta U)]^2 - \chi^2(\alpha U + \beta U)^2 \right\} ds. \quad (3.204)$$

It follows that the matrix operator K determines the oscillating field in the bulk of the discontinuity V_{int} .

Problem 3.38 (*yet to be solved*) Find the explicit form of the operator K for some mode diffraction problem.

The resulting matrix-operator model

$$\begin{cases} S = \frac{W - I_h}{W + I_h}, & W = W_0 W_0^T, \\ K = (W + I_h)^{-1} 2W_0 \end{cases} \quad (3.205)$$

resembles the operator Fresnel formulas (3.196) and (3.198); moreover, the characteristic equation is valid (compare with formula (3.192)):

$$S^2 + KK^T = I_h. \quad (3.206)$$

The difference is that the formulas for the operator matrices (3.205) have no scalar analogues. As noted above, we call these equalities the generalized operator Fresnel formulas.

The obtained result can be formulated as the following statement.

Theorem 3.5 *For each problem of mode diffraction in a waveguide transformer with the coupling cavity $V_{\text{int}} \neq 0$, there exists a matrix-operator model in the form of the generalized operator Fresnel formulas (3.205), if the reciprocity theorem (the Lorentz lemma) and the oscillating power theorem (3.199) hold true for this problem.*

3.10 Matrix Scattering Operators

In this section we will determine the main properties of the matrix reflection operator R_p and the generalized scattering matrix S . For this purpose, we will use a number of notions and theorems of the theory of bounded operators in the Hilbert space.

3.10.1 Properties of Reflection and Transmission Operators

The energy conservation law in the form of (3.73), (3.74) (see Sect. 3.4.2) takes a simple form in terms of the Cayley transform $D_p = W(R_p)$ (3.54), which allows one to explore the basic properties of this operator, and thereby to clarify the basic properties of the reflection operator $R_p = W^{-1}(D_p)$.

The substitution of the operator Fresnel formulas (3.51) into (3.73) and (3.74), which were obtained from the complex power theorem and the second Lorentz lemma, yields the expressions

$$\left. \begin{array}{l} D_1 U_1 \\ U_1 D_1^\dagger \end{array} \right\} = D_0 U_2 D_0^\dagger, \quad \left. \begin{array}{l} U_2 D_2^\dagger \\ D_2 U_2 \end{array} \right\} = D_0^T U_1 D_0^*, \quad \left. \begin{array}{l} D_0 U_2 D_2^\dagger = D_1 U_1 D_0^* \\ D_0^T U_1 D_1^\dagger = D_2 U_2 D_0^\dagger \end{array} \right\}; \quad \left\{ \begin{array}{l} H - \text{case} \\ E - \text{case} \end{array} \right\}, \quad (3.207)$$

$$D_0^T U_1 = U_2 D_0^\dagger \quad \text{for } H - \text{case} \quad \text{and} \quad D_0 U_2 = U_1 D_0^* \quad \text{for } E - \text{case}. \quad (3.208)$$

Taking into consideration that, by definition, $D_1 = D_0 D_0^T$ and $D_2 = D_0^T D_0$, we come to the conclusion that equalities (3.208) form the basis of (3.207).

Problem 3.39 Verify the above statement.

Thus, all the operator relations of the complex power conservation law follow from the sole condition (3.208), which can be rewritten as

$$D_0 = \left\{ \begin{array}{c} U_1^\dagger \\ U_1 \end{array} \right\} D_0^* \left\{ \begin{array}{c} U_2 \\ U_2^\dagger \end{array} \right\}; \quad \left\{ \begin{array}{l} H - \text{case} \\ E - \text{case} \end{array} \right\}. \quad (3.209)$$

It is precisely this condition that sets apart the elementary operator D_0 from the entire set of bounded matrix operators acting in the space l_2 .

For the canonical problem of a step discontinuity in a rectangular waveguide, considered in Sect. 3.4.1, (3.209) can be given in more detail. Using the following properties of the portal operator

$$\left(I_p^\beta\right)^{1/2} U_p = \left(\left(I_p^\beta\right)^{1/2}\right)^*, \quad \left(\left(I_p^\beta\right)^{-1/2}\right)^* U_p = \left(I_p^\beta\right)^{-1/2}, \quad (3.210)$$

we can write (3.209) in the form

$$\left(I_1^\beta\right)^{\mp 1/2} D_0 \left(I_2^\beta\right)^{\pm 1/2} = \left(\left(I_1^\beta\right)^{\mp 1/2} D_0 \left(I_2^\beta\right)^{\pm 1/2}\right)^*; \quad \left\{ \begin{array}{l} H - \text{case} \\ E - \text{case} \end{array} \right\}. \quad (3.211)$$

Substituting into (3.211) the definition (3.52) of the operator D_0 , we get

$$\left(\mu_1, \mu_2^T\right) = \left(\mu_1, \mu_2^T\right)^*. \quad (3.212)$$

Thus the fact that the bilinear scalar product (3.212) of the transverse eigenfunctions of regular waveguides is real lies in the basis of the complex power conservation law (3.73), (3.74) and (3.167).

Let us now clarify the properties of the operator $D_p U_p$, $p = 1, 2$. From the energy conservation law in the form of (3.207) we obtain

$$\operatorname{Re}(D_p U_p) > 0, \quad \operatorname{Im}(D_p U_p) > 0. \quad (3.213)$$

Indeed, taking into account the properties of the unitary portal operator $U_p = Q_p + iP_p$, $p = 1, 2$ (see definitions (3.31) and (3.35) in Sect. 3.3), we find from the first two relationships in (3.207) that

$$\begin{aligned}
b \operatorname{Re} (D_p U_p) b^\dagger &= d \operatorname{Re} U_q d^\dagger = d Q_q d^\dagger = \|d_+\|^2 > 0; \\
b \operatorname{Im} (D_p U_p) b^\dagger &= d \operatorname{Im} U_q d^\dagger = d P_q d^\dagger = \|d_-\|^2 > 0; \\
\forall b \in l_2, \quad q \neq p, \quad d &\equiv \begin{cases} b D_0 \\ b D_0^T \end{cases}; \quad \begin{cases} H\text{-case} \\ E\text{-case} \end{cases}.
\end{aligned} \tag{3.214}$$

Thus, the numerical range of the operator $D_p U_p$, which is metrically equal to the operator D_p , lies entirely in the first quadrant of the complex plane. The inequality $\operatorname{Re} (D_p U_p) > 0$ determines the accretive operator, while the inequality $\operatorname{Im} (D_p U_p) > 0$ means that at the same time this operator is dissipative (regarding the terminology, see, for example, the book [27] and the Mathematical Encyclopedia [26]). For such operators, we introduce the term ‘accretive-dissipative operators’.

Similarly, it follows from (3.207) that the operator $D_p U_p^\dagger$, $p = 1, 2$ is *accretive-accumulative operator*, which means that $\operatorname{Re} (D_p U_p^\dagger) > 0$ (accretivity of the operator $D_p U_p^\dagger$) and, at the same time, $\operatorname{Im} (D_p U_p^\dagger) < 0$ (accumulativity of $D_p U_p^\dagger$ [27]). In other words, the numerical range of the operator $D_p U_p^\dagger$ lies completely in the fourth quadrant of the complex plane.

Below, we will use the properties of the operator $D_p U_p$ to prove the fundamental fact that the operators D_1 (*H-case*) and D_2 (*E-case*) are accretive operators. These properties for the other two operators D_2 (*H-case*) and D_1 (*E-case*) can be proved in a similar way with the use of the properties of the operator $D_p U_p^\dagger$; proof is suggested as an exercise.

In what follows, we omit the subscript $p = 1, 2$ for simplicity.

Our analysis is based on the following statements, which we formulate for some bounded operator L .

Lemma 3.5 $\operatorname{Re} L \geq 0$ if and only if $(L - \alpha I)(L - \alpha I)^\dagger \geq \alpha^2$, $\forall \alpha < 0$.

Proof For any real value of the parameter α we have

$$(L - \alpha I)(L - \alpha I)^\dagger - \alpha^2 = LL^\dagger - \alpha(L + L^\dagger) = LL^\dagger - \alpha 2\operatorname{Re} L.$$

If the left-hand side is nonnegative for $\forall \alpha < 0$, then

$$2\alpha \operatorname{Re} L \leq LL^\dagger \quad \rightarrow \quad \operatorname{Re} L \geq \frac{1}{2\alpha} LL^\dagger.$$

Passing to the limit for $\alpha \rightarrow -\infty$, we have $\operatorname{Re} L \geq 0$. If, conversely, $\operatorname{Re} L \geq 0$, then for any $\alpha < 0$ we have

$$\operatorname{Re} L \geq 0 \geq \frac{1}{2\alpha} LL^\dagger \quad \rightarrow \quad LL^\dagger \geq \alpha 2 \operatorname{Re} L. \quad \square$$

Lemma 3.6 Suppose $Z_R \stackrel{\text{def}}{=} \{z : \operatorname{Re} z \geq 0\}$ and $M(L)$ is the numerical range of the operator L , then $M(L) \subset Z_R$ if and only if

$$(L - \lambda I)(L - \lambda I)^\dagger \geq (\operatorname{Re} \lambda)^2; \quad \forall \lambda \notin Z_R.$$

Proof $M(L) \subset Z_R$ if and only if $\operatorname{Re} L \geq 0$, since $b \operatorname{Re} L b^\dagger = \operatorname{Re} (b L b^\dagger)$. Let $\lambda = \alpha + i\beta$ (α and β as usual are real), then we have $L - \lambda I = \bar{L} - \alpha I$, where $\bar{L} = L - i\beta I$ and $\operatorname{Re} \bar{L} = \operatorname{Re} L$. According to the previous Lemma 3.5 we get

$$(\bar{L} - \alpha I)(\bar{L} - \alpha I)^\dagger \geq \alpha^2; \quad \forall \alpha < 0,$$

if and only if $\operatorname{Re} \bar{L} \geq 0$. □

Corollary Let $L = -iM$, then $\operatorname{Re} L = \operatorname{Im} M$; and we obtain

$$(iM - \lambda I)(iM - \lambda I)^\dagger = (M + i\lambda I)(M + i\lambda I)^\dagger \geq (\operatorname{Re} \lambda)^2; \quad \forall \lambda \notin Z_R,$$

if and only if $\operatorname{Im} M \geq 0$.

Based on the definition of the vector norm (see Appendix A), we can rewrite the obtained results in the form of the following two-sided implications:

- for $\lambda = -\alpha - i\beta$, $\alpha > 0$, $-\infty < \beta < \infty$ we have

$$\operatorname{Re} L \geq 0 \quad \leftrightarrow \quad \|(L - \lambda I)b^T\|^2 \geq \alpha^2 \|b\|^2; \quad \forall b \in l_2; \quad (3.215)$$

- for $\bar{\lambda} = i\lambda = \beta - i\alpha$, $\alpha > 0$, $-\infty < \beta < \infty$ we have

$$\operatorname{Im} M \geq 0 \quad \leftrightarrow \quad \|(M - \bar{\lambda} I)b^T\|^2 \geq \alpha^2 \|b\|^2; \quad \forall b \in l_2. \quad (3.216)$$

We now use these relations to prove the main result of this section.

Theorem 3.6 The Cayley transform $D = W(R)$ is an accretive operator, $\operatorname{Re} D > 0$.

Proof Inequalities (3.213) indicate that the operator DU is accretive-dissipative. Then, according to (3.215) and (3.216), the following estimates are true

$$\left. \begin{aligned} \|(DU - \lambda I)b_+^T\| &\geq \alpha \|b_+\| \\ \|(DU - i\lambda I)b_-^T\| &\geq \alpha \|b_-\| \end{aligned} \right\}; \quad \forall b_\pm \in l_2,$$

where $\lambda = -\alpha - i\beta$, $\alpha > 0$, $b_+ = bQ$ and $b_- = bP$. These two equalities together give

$$\|(DU - \lambda I)b_+^T\|^2 + \|(DU - i\lambda I)b_-^T\|^2 \geq \alpha^2 \|b\|^2; \quad \forall b \in l_2, \quad (3.217)$$

since $\|b\|^2 = \|b_+\|^2 + \|b_-\|^2$. Transform the left-hand side of (3.217) by using the *parallelogram rule* to the form

$$\|(DU - \lambda I)b_+^T\|^2 + \|(DU - i\lambda I)b_-^T\|^2 = \frac{1}{2} \left(\|(D - \lambda I)d^T\|^2 + \|(D - \lambda I)Jd^T\|^2 \right), \quad (3.218)$$

where $J = Q - P$ is the canonical symmetry of the Pontryagin space $\Pi = Ql_2 \cup Pl_2$ and the notation $d = bU$ is used, where $U = Q - iP$ is the unitary portal operator.

Use the following estimate for the right-hand part of equality (3.218):

$$\|(D - \lambda I)d^T\|^2 + \|(D - \lambda I)Jd^T\|^2 \leq 2\|(D - \lambda I)c^T\|^2, \quad (3.219)$$

where $\|(D - \lambda I)c^T\| = \max\{\|(D - \lambda I)d^T\|, \|(D - \lambda I)Jd^T\|\}$. Then, on the basis of two formulas, (3.217) and (3.218), we obtain the following inequality:

$$\|(D - \lambda I)c^T\|^2 \geq \alpha^2 \|c\|^2.$$

We have taken into account that $\|c\| = \|d\| = \|dJ\| = \|b\|$. Thus we found that

$$\|(D - \lambda I)c^T\| \geq \alpha \|c\|; \quad \forall c \in l_2.$$

Referring again to the corollary (3.215) of Lemma 3.6, we obtain $\operatorname{Re} D \geq 0$. \square

Corollary *The reflection operator is a contraction, $\|R\| \leq 1$.*

Indeed, for the Cayley transform $D = W(R)$ the following relations are true

$$\frac{1}{4} \left\{ \begin{array}{c} I - RR^\dagger \\ I - R^\dagger R \end{array} \right\} = \left\{ \begin{array}{c} (D+I)^{-1} \\ (D^\dagger+I)^{-1} \end{array} \right\} \operatorname{Re} D \left\{ \begin{array}{c} (D^\dagger+I)^{-1} \\ (D+I)^{-1} \end{array} \right\},$$

i.e., the inequality $\operatorname{Re} D \geq 0$ is equivalent to $RR^\dagger \leq I$, $R^\dagger R \leq I$ or $\|R\|^2 = \|RR^\dagger\| \leq 1$.

Problem 3.40 (*research*) Using the similar reasoning, prove that $\operatorname{Im}(JR) \leq 0$ and $\operatorname{Im}(RJ) \leq 0$.

3.10.2 Basic Operator Properties of the Generalized Scattering Matrix

Completing generalization of the previous results, consider mode diffraction in an H - or E -plane N -port waveguide transformer (N is arbitrary integer). General configuration of the structure is shown in Fig. 3.6.

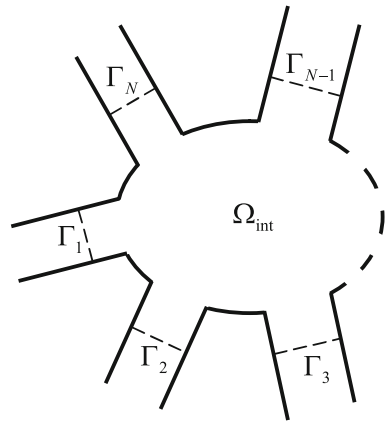
We suppose that the resonant volume $V_{\text{int}} = \Omega_{\text{int}} \times a_3 \neq 0$ and the feeding regular waveguides are uniform along the Cartesian axis that is perpendicular to the H - or E -plane. The volume V_{int} is bounded by the metal walls of the coupling region and the reference planes $\Sigma_n = \Gamma_n \times (0, a_3)$, $n = 1, 2, \dots, N$, which are located in the waveguide arms, and is free from sources/sinks of the field. As before, we suppose that the device is filled with a homogeneous lossless medium and all metal walls are perfectly conducting, while the waveguide arms are terminated in matching loads.

Assume that in each of N inputs, the mode composition of the incident field is described by the infinite row vector of complex amplitudes $b^{(n)} \in l_2$, $n = 1, 2, \dots, N$. Then the vector $b \equiv \{b^{(1)}, b^{(2)}, \dots, b^{(N)}\}$ of the amplitudes of the given sources belongs to the Hilbert space $h_N = l_2^N$ (see Appendix A).

Let p_n be the number of modes above cutoff in the n th port. The corresponding orthoprojector we denote as P_n and then use it to create the operator matrix of projections onto all modes propagating in N ports:

$$P = \begin{bmatrix} P_1 & 0 & \cdots & 0 \\ 0 & P_2 & \cdots & 0 \\ \vdots & \vdots & \ddots & \vdots \\ 0 & 0 & \cdots & P_N \end{bmatrix}. \quad (3.220)$$

Fig. 3.6 Geometry of the planar N -port waveguide transformer



According to this definition, P is an operator of finite rank $v = \text{Tr}(P) = \sum_{n=1}^N p_n$ (we will assume that $v \neq 0$ unless otherwise stated). The orthoprojector onto all evanescent modes $Q = I_h - P$ involves, obviously, the orthoprojectors $Q_n = I - P_n$, $n = 1, 2, \dots, N$, on the main diagonal.

We will characterize the n th port by the matrix reflection operator $R^{nn} : l_2 \rightarrow l_2$ and by the unitary operator $U_n = Q_n + iP_n$. We will also denote the matrix operator of the mode transmission from p th waveguide into q th waveguide as $T^{qp} : l_2 \rightarrow l_2$.

The wave transformer under consideration is fully described by the portal operator matrix

$$U = \begin{bmatrix} U_1 & 0 & \cdots & 0 \\ 0 & U_2 & \cdots & 0 \\ \vdots & \vdots & \ddots & \vdots \\ 0 & 0 & \cdots & U_N \end{bmatrix} \tag{3.221}$$

and the generalized scattering matrix

$$S = \begin{bmatrix} R^{11} & T^{21} & \cdots & T^{N1} \\ T^{12} & R^{22} & \cdots & T^{N2} \\ \vdots & \vdots & \ddots & \vdots \\ T^{1N} & T^{2N} & \cdots & R^{NN} \end{bmatrix}. \tag{3.222}$$

These two operator matrices comprise the characteristic operator

$$G = (I_h + S)U(I_h - S^\dagger) : h_N \rightarrow h_N. \tag{3.223}$$

All the operators in (3.220)–(3.223) act also in the Pontrjagin space $\Pi_v = Ph_N \cup Qh_N$, which is introduced in the same way as in Sect. 3.8. The canonical symmetry of this space is the operator $J = Q - P$, for which we have $J^\dagger = J^{-1} = J$.

With the idealizations stated previously, the following fundamental electromagnetic laws are valid:

- the first Lorentz lemma, from which the symmetry

$$S^T = S \tag{3.224}$$

- of the generalized scattering matrix follows;
- the oscillating power theorem yielding the relationship

$$b(I_h \pm S)(I_h \mp S^T)b^T = \int_{\Omega_{\text{int}}} \left\{ (\nabla_{\parallel} U_V)^2 - \chi^2 U_V^2 \right\} ds, \quad (3.225)$$

in which U_V stands for the total complex amplitude in the region Ω_{int} ; as before, $\nabla_{\parallel} U_V$ is the gradient of this complex amplitude in the H - or E -plane;

- the complex power theorem and the second Lorentz lemma, which give together the equality

$$b\hat{G}b^\dagger = \|\nabla_{\parallel} U_V\|_{L_2(\Omega_{\text{int}})}^2 - \chi^2 \|U_V\|_{L_2(\Omega_{\text{int}})}^2. \quad (3.226)$$

With $\text{Im } \chi = 0$, we have from (3.226) that $G^\dagger = G$ (i.e. the operator G is self-adjoint), or alternatively, in view of definition (3.223),

$$\text{Im } G = 0 \quad \rightarrow \quad \begin{cases} P - SPS^\dagger = i(SQ - QS^\dagger) \\ P - S^\dagger PS = i(QS - S^\dagger Q). \end{cases} \quad (3.227)$$

This relationship is the energy conservation law in the most general form, for the entire class of the mode diffraction problems under consideration.

In applied research, various truncated forms of this law are widely used. One of its widespread particular forms can be derived from (3.227) as follows. Let us introduce the operator $S_0 \equiv P S P$, which is obtained from the classical (finite) scattering matrix of circuit theory by extending it by zeroes to the infinite matrix. Multiplying (3.227) from the left and right by the orthoprojector P and taking into account its properties $P^\dagger = P$, $P^2 = P$ and $PQ = QP = 0$, we obtain the desired result

$$S_0 S_0^\dagger = S_0^\dagger S_0 = P, \quad (3.228)$$

or, in expanded form, we have

$$\sum_{s=(0)1}^{P_p} R_{sm}^{pp} (R_{sn}^{pp})^* + \sum_{q=1}^N \sum_{s=(0)1}^{P_q} T_{sm}^{qp} (T_{sn}^{qp})^* = \delta_m^n; \quad m, n \leq P_p, \quad p = 1, 2, \dots, N. \\ q \neq p \quad (3.229)$$

Equalities (3.228) imply that the operator S_0 is partially isometric in the space h_N (or, what is the same thing, it is an isometry of the subspace Ph_N). Formula (3.229), commonly known as the energy conservation law for propagating modes, has been used in practice since the methods of the microwave network theory are transferred to waveguide systems.

Note that separation of diagonal operator blocks of the operator matrix (3.227) results in a more general expression as compared with (3.229):

$$\sum_{s=(0)1}^{P_p} R_{sm}^{pp} (R_{sn}^{pp})^* + \sum_{q=1}^N \sum_{s=(0)1}^{P_q} T_{sm}^{qp} (T_{sn}^{qp})^* = \begin{cases} \delta_m^n; & m, n \leq p_p \\ 0; & m > p_p, \quad n \leq p_p \\ 2\text{Im} R_{nm}^{pp}; & n > p_p, \quad \forall m, \end{cases} \quad (3.230)$$

where $p = 1, 2, \dots, N$. This formula is also the well-known generalization of the energy conservation law onto evanescent modes. (The frequently used special cases of formula (3.230) can be found, for example, in the book [6].)

It follows from (3.227) that, in particular, the generalized scattering matrix S is not a unitary operator. The measure of its deviation from unitarity is given by the formula

$$\frac{1}{2} (I_h - SS^\dagger) = Q - V_+ Q V_+^\dagger; \quad V_+ \equiv \left(\frac{1}{2}\right)^{1/2} (I_h - iSJ), \quad (3.231)$$

which is one more generalized form of the energy conservation law equivalent to (3.227). Namely, the greater the number of propagating modes in the waveguide ports, the closer (in the sense of (3.231)) S to a unitary operator, never reaching this limit.

If the wavenumber χ is less than its lower critical value, then there are no propagating modes in the waveguide ports: $P = 0$, $Q = I_h$ and equality (3.227) give $S^\dagger = S$. In this case, the Hermiticity property of the generalized scattering matrix corresponds to the closed system. Generally a measure of the deviation of S from self-adjointness is given by the formula

$$\text{Im} S = -P + V_- P V_-^\dagger; \quad V_- \equiv \left(\frac{1}{2}\right)^{1/2} (I_h + iSJ), \quad (3.232)$$

which is one more generalized form of the energy conservation law.

Problem 3.41 (*research*) Derive the energy conservation law in the form of (3.231) and (3.232). Hint: the required formulas are combinations of the relations similar to (3.171)–(3.174), but for the N-port waveguide transformer.

As already noted, the orthoprojector P is the operator of finite rank, since for any wavenumber χ only a finite number of modes can propagate in the waveguide ports. Then, from (3.232) it follows that the imaginary part of the generalized scattering matrix $\text{Im} S$ belongs to the class of compact operators. This means that the operator S is quasi-Hermitian [19]. This subclass of non-self-adjoint operators had previously been investigated in studies [18, 19], the results of which we widely use in this chapter.

The quasi-Hermitian character of the generalized scattering matrix means, in particular, that all the singular elements of its spectrum $\sigma(S)$ lie on the real axis, while all the nonreal points of this spectrum are the eigenvalues of finite multiplicity (i.e., the regular elements of the point spectrum) [18, 19]. For the considered problem, the real points of the spectrum $\sigma(S)$ correspond to the eigenfrequencies of the homogeneous boundary value problem for the Helmholtz equation in the region $\Omega_{\text{int}} \neq 0$, which is enclosed along the corresponding reference planes in the waveguide arms by electric (in the H -case) or magnetic (in the E -case) walls. At these eigenfrequencies, the right-hand sides of (3.225) and (3.226) vanish:

$$b(I_h \pm S)(I_h \mp S^T)b^T = 0 \quad \rightarrow \quad S^2 = I_h, \quad (3.233)$$

$$bGb^\dagger = 0 \quad \rightarrow \quad G \equiv (I_h + S)U(I_h - S^\dagger) = 0 \quad (3.234)$$

(for the proof of these implications see Problems 3.12 and 3.15 above). Relation (3.233) together with the symmetry property $S^T = S$ make appropriate to introduce special operators

$$\begin{aligned} Q_S = \frac{1}{2}(I_h + S) \\ P_S = \frac{1}{2}(I_h - S) \end{aligned} \quad \rightarrow \quad \begin{cases} Q_S + P_S = I_h \\ Q_S - P_S = S, \end{cases} \quad (3.235)$$

which, evidently, possess the properties

$$Q_S^T = Q_S, \quad P_S^T = P_S, \quad Q_S^2 = Q_S, \quad P_S^2 = P_S, \quad Q_S P_S = P_S Q_S = 0. \quad (3.236)$$

In other words, the operators P_S and Q_S are the complementary projectors (in the case of $S^\dagger = S$ they become the orthoprojectors and hence $\|P_S\| = \|Q_S\| = 1$). Since the projector spectrum consists only of two points $\{0; 1\}$ of infinite multiplicity, then from the relationships

$$S = I_h - 2P_S = 2Q_S - I_h \quad (3.237)$$

we find that the eigenfrequency of the region Ω_{int} corresponds to the points of the real axis $\lambda = -1$ or $\lambda = +1$, also of infinite multiplicity.

Problem 3.42 (research) Show that each eigenfrequency of the region Ω_{int} corresponds to the point $\lambda = -1 \in \sigma(S)$ in the case of the H -plane transformer or the point $\lambda = +1 \in \sigma(S)$ in the E -plane case.

Note that for any operating frequency relations (3.233) and (3.234) characterize the arbitrary abrupt waveguide discontinuity, for which $\Omega_{\text{int}} = 0$ by definition. The above arguments show that in this case the spectrum of the generalized scattering matrix consists of only two points of infinite multiplicity, $\sigma(S) = \{-1; +1\}$, lying on the real axis. The energy conservation law (3.234) written as

$$Q_S U P_S^\dagger = 0 \quad \rightarrow \quad Q_S Q P_S^\dagger = -i Q_S P P_S^\dagger, \quad (3.238)$$

shows that in this case P_S and/or Q_S are compact operators, since the orthoprojector P in the right-hand side of the second equality in (3.238) is an operator of finite rank. According to (3.237), this means that the generalized scattering matrix S of the step-like discontinuity in a waveguide can be represented as a sum of unit and compact operators.

The characteristic property (3.234), $G = 0$, can also be written in the expanded form:

$$Q - S Q S^\dagger = \frac{1}{i} (S P - P S^\dagger), \quad (3.239)$$

or, more compactly, as

$$V_- V_-^\dagger = V_-^\dagger V_- = I_h, \quad V_+ J V_+^\dagger = V_+^\dagger J V_+ = J. \quad (3.240)$$

Hence, for any abrupt discontinuity in a waveguide, the operator matrix V_- is a unitary operator, while the operator matrix V_+ is a J -unitary operator. Finally, the addition and subtraction of (3.227) and (3.239) give the representations

$$\frac{1}{2} (I_h - S S^\dagger) = -\text{Im}(S J), \quad \frac{1}{2} (J - S^\dagger J S) = \text{Im}(S), \quad (3.241)$$

i.e., in the case of an abrupt discontinuity in a waveguide the left-hand sides of these equations are compact operators.

We now turn to the characteristic operator G . It can be seen from (3.223) that it makes sense to introduce a linear fractional transformation of the generalized scattering matrix S . To this end, we eliminate from the frequency axis the eigenfrequencies of the region Ω_{int} , which correspond to the point $-1 \in \sigma(S)$ with the boundary condition $U_V|_{\Sigma_m} = 0$, $m = 1, 2, \dots, N$, and to the point $+1 \in \sigma(S)$ provided that $(\partial U_V / \partial \vec{n}_m)|_{\Sigma_m} = 0$ where \vec{n}_m is the outward normal to the corresponding reference plane Σ_m , see Fig. 3.6.

Now we can introduce the Cayley transform of the operator S

$$W_\mp = \frac{I_h \mp S}{I_h \pm S}; \quad \left\{ \begin{array}{l} H \text{ - case} \\ E \text{ - case} \end{array} \right\}, \quad (3.242)$$

which exists under the restrictions $-1 \notin \sigma(S)$ (H -case) and $+1 \notin \sigma(S)$ (E -case).

In microwave engineering, the following terminology borrowed from the network theory is adopted: $Z = W_+$ is the generalized impedance matrix, $Y = W_-$ is the generalized admittance matrix, and W_\pm is the generalized immittance matrix. Note that it is important to remember that the above operator matrices are not necessarily exist because of the constituent parts of the spectrum $\sigma(S)$ [28].

For the mode diffraction problem under study, the Cayley transform W_{\pm} is the given operator matrix. Having obtained this operator (by using the proposed generalization of the mode-matching technique or by any other method based on the modal expansion of the field), we have immediately (i.e., before calculating the generalized scattering matrix S) the generalized admittance matrix Y (in the case of H -plane) or the generalized impedance matrix Z (in the case of E -plane) in an explicit analytic form.

In terms of the Cayley transform (3.242), the characteristic operator (3.223) takes the form

$$\frac{1}{4}G = (W_{\mp} + I_h)^{-1} \left\{ \begin{array}{l} U W_{\mp}^{\dagger} \\ W_{\mp} U \end{array} \right\} (W_{\mp}^{\dagger} + I_h)^{-1}; \quad \left\{ \begin{array}{l} H - \text{case} \\ E - \text{case} \end{array} \right\} \quad (3.243)$$

and the energy conservation law (3.227) is

$$\text{Im} \left\{ \begin{array}{l} W_{-} U^{\dagger} \\ W_{+} U \end{array} \right\} = 0; \quad \left\{ \begin{array}{l} H - \text{case} \\ E - \text{case} \end{array} \right\}. \quad (3.244)$$

The last equality can also be equivalently represented as the Cayley transform property:

$$W_{\mp} = \left\{ \begin{array}{l} U \\ U^{\dagger} \end{array} \right\} W_{\mp}^{\dagger} \left\{ \begin{array}{l} U \\ U^{\dagger} \end{array} \right\}; \quad \left\{ \begin{array}{l} H - \text{case} \\ E - \text{case} \end{array} \right\}. \quad (3.245)$$

Note that this relation is similar to the above (3.209); it represents the basic property of the column vector of the transverse eigenfunctions μ and of an infinite set of mode propagation constants, which forms the basis of the energy conservation law (3.244).

Thus, for the canonical problem of the right-angle bend of a rectangular waveguide, formula (3.245) can be written in the following form:

$$\begin{aligned} \left(\left(\frac{\partial^2 G^D}{\partial \bar{n}_p \partial \bar{n}_q}, \mu_q \right)_{\Sigma_q}, \mu_p^T \right)_{\Sigma_p} &= \left(\left(\frac{\partial^2 G^D}{\partial \bar{n}_p \partial \bar{n}_q}, \mu_q \right)_{\Sigma_q}, \mu_p^T \right)_{\Sigma_p}^*; & H - \text{case} \\ \left((G^N, \mu_q)_{\Sigma_q}, \mu_p^T \right)_{\Sigma_p} &= \left((G^N, \mu_q)_{\Sigma_q}, \mu_p^T \right)_{\Sigma_p}^*; & E - \text{case} \end{aligned} \quad \text{for } \forall p, q = 1, 2 \quad (3.246)$$

(compare with (3.212)). Here $G^{D(N)}$ is the well-known Green function of a rectangular coupling region Ω_{int} , which satisfies homogeneous Dirichlet (Neumann) boundary conditions. For this diffraction problem, the basic property (3.246) follows from the characteristics of traces of the Green function and its second derivative on the reference planes Σ_p , $p = 1, 2$, as well as from the fact that the functions μ_p are real-valued. For a discrete set of the wavenumbers that correspond

to the eigenfrequencies of the region Ω_{int} , the Green function is not defined and the power conservation law (3.244), (3.245) becomes meaningless.

Problem 3.43 (*research*) Using the generalized mode-matching technique, construct a matrix-operator model for a right-angle bend of a rectangular waveguide in the form of the generalized operator Fresnel formulas. Derive the corollary of the energy conservation law in the form of (3.246). Hint: the derivation of the properties (3.246) is similar to that of (3.212).

Let us multiply (3.244) from the left and right by the row eigenvector b_λ of the quasi-Hermitian operator S . Then for the spectrum points $\tau \in \sigma(W_\pm)$ we find

$$\text{Im}\tau = \pm \text{tg}(\varphi_b) \text{Re}\tau; \quad \begin{cases} H - \text{case} \\ E - \text{case} \end{cases}, \quad (3.247)$$

where φ_b is the argument of the complex number $b_\lambda U b_\lambda^\dagger$, which, by the properties of the portal operator, belongs to the first quadrant of the complex plane. Geometrically, we have the equation of the bundle of lines passing through the spectrum point $\tau = 0$ with the slopes $\pm \text{tg}(\varphi_b)$, $0 < \varphi_b < \pi/2$.

Equation (3.247) implies that if the energy conservation law in the form of (3.244), (3.245) is valid, then the condition $-1 \notin \sigma(W_\pm)$ necessarily fulfills, and therefore, the following inverse Cayley transform hold true:

$$S = \pm \frac{I_h - W_\mp}{I_h + W_\mp}; \quad \begin{cases} H - \text{case} \\ E - \text{case} \end{cases}. \quad (3.248)$$

In other words, the solution in the form of (3.248) of each problem of mode diffraction by the H - or E -plane waveguide discontinuity with the resonant volume $V_{\text{int}} \neq 0$ exists and is unique for all the wavenumbers, except for the eigenfrequencies of the region Ω_{int} . The boundedness of the operator $A = (I_h + W_\mp)^{-1}$ ensures the stability of the solution throughout the frequency axis, except the vicinities of the eigenfrequencies, where $\text{cond}(A) \equiv \|A\| \cdot \|A^{-1}\| \rightarrow \infty$.

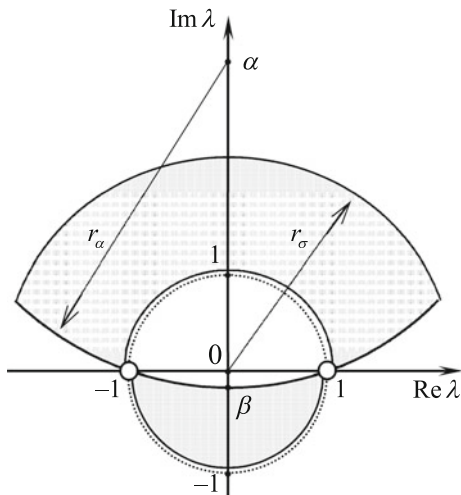
We now investigate the localization of the spectrum $\sigma(S)$ of the generalized scattering matrix. By analogy with the derivation of (3.247), we multiply (3.223) from the left and right by the row eigenvector b_λ of the operator matrix S . Thus obtained from (3.226) equation

$$(1 + \lambda)(1 - \lambda^*) b_\lambda U b_\lambda^\dagger = C_b; \quad C_b \equiv \left\| \nabla_{\parallel} U_V^{\text{eig}} \right\|_{L_2(\Omega_{\text{int}})}^2 - \chi^2 \left\| U_V^{\text{eig}} \right\|_{L_2(\Omega_{\text{int}})}^2 \quad (3.249)$$

yields the system of equalities

$$\begin{cases} 1 - |\lambda|^2 = C_\lambda \\ 2\text{Im}(\lambda) = -C_\lambda \text{tg}(\varphi_b) \end{cases} \quad (3.250)$$

Fig. 3.7 Localization of the spectrum $\sigma(S)$ of the generalized scattering matrix



the right-hand parts of which depend on the parameter $C_\lambda \equiv C_b \left| b_\lambda U b_\lambda^\dagger \right|^{-1} \cos(\varphi_b)$, and $C_\lambda < 1$.

Equations (3.250) give the required localization of the entire spectrum $\{\lambda\} \in \sigma(S)$ in the complex plane (Fig. 3.7). In Fig. 3.7, r_σ stands for the spectral radius of the operator S , $r_\sigma \leq \|S\|_{h_N}$, $r_\alpha = \csc(\varphi_b^{\min})$ is the radius of the circle centered at the point $\alpha = \text{ctg}(\varphi_b^{\min})$ on the imaginary axis, $\varphi_b^{\min} \equiv \min_{\forall b_\lambda}(\varphi_b)$, $0 < \varphi_b^{\min} < \pi/2$; the positive value $\beta = \text{tg}(\varphi_b^{\min}/2) < 1$ is also marked on this axis.

3.11 Conclusion

In this chapter, we have presented the rigorous solution of the mode-diffraction problem in operator form using the canonical problem of H - (E -) plane step discontinuity in a rectangular waveguide as an example. It has been shown how the modal expansion of the complex amplitude $U(g, \omega)$ in two regular partial regions together with the matching condition for tangential components of the electric and magnetic fields in the aperture of the discontinuity (the mode-matching technique in the theory of mode diffraction) leads to the matrix models possessing different properties. Let us outline these models in the sequence in which they appear in the text above.

The first matrix model is the known infinite SLAE (3.22), the solution of which—the required vector of the Fourier coefficients—has the form

$$x_p = A_p f_p; \quad A_p \equiv (I + D_p)^{-1}, \quad x_p, f_p \in l_2, \quad p = 1, 2.$$

Here, the given operator of the problem, D_p , is bounded in the space l_2 , but is not a contraction or a compact operator; besides, it does not meet the known regularity criteria (see Appendix B). Consequently, the proof of the correctness of the above-mentioned matrix model remained important for decades. Another unsolved problem was to justify the applicability of the truncation procedure to the solution of the infinite SLAE and to determine the convergence conditions for the approximate solutions.

As was shown above, the key to overcoming these mathematical difficulties is the integration of an infinite number of the vectors x_p into a matrix operator. To realize this idea we give a new formulation of the mode-diffraction problem, which leads to a generalization of the widespread version of the mode-matching technique.

The proposed approach, in essence, consists in replacing the unknown Fourier coefficients in the modal expansion of the field by the elements of the desired matrix scattering operator. This matrix-operator technique allows one to introduce scattering operators as the unknown values of the mode-matching technique.

Implementing this approach, we observe that the matrix model in the form of an infinite SLAE is a truncation of the general matrix-operator equation, which results in the loss of basic information about the properties of both the required solution and the given operator of the problem. For example, only in the context of this approach, it was possible to establish the quasi-Hermitian character of the scattering operators and the given operator of the problem. This means that these operators belong to the class of non-self-adjoint operators with compact imaginary parts, which have relatively simple structure of the spectrum. We emphasize that the quasi-Hermitian character, as well as other revealed important properties of the operators under study, are a corollary of the energy conservation law.

When describing time-harmonic fields in the domain of complex amplitudes, we must take into account four basic energy laws: the complex power theorem, the oscillating power theorem, as well as the first and second Lorentz lemmas. Thus, using jointly the complex Poynting's theorem and the second Lorentz lemma [16] we have derived the energy conservation law in a generalized form—the operator equality (3.227). The contribution of each of these theorems into the law is quite clear. The operator relations on the main diagonal of the resultant operator matrix are the corollary of the complex power theorem, whereas all the off-diagonal operator blocks follow from the second Lorentz lemma.

Since the complex Poynting theorem and the second Lorentz lemma form the full list of basic electromagnetic laws concerning a complex power flux, we argue that the derived forms of the energy conservation law (3.227), (3.231) and (3.232) are maximum complete in this sense for the considered range of problems. They can also be interpreted as the generalized optical theorem in operator form, which is proved for mode scattering in lossless reciprocal waveguides.

The second matrix model (3.51) is the Fresnel formulas for the reflection and transmission operators

$$R_p = I - 2A_p, \quad T^{qp} = 2A_p \begin{cases} D_0 & \text{for } q = 2; \\ D_0^T & \text{for } q = 1; \end{cases} \quad p \neq q, \quad p = 1, 2.$$

For this model, we have rigorously proved that the given operator of the problem $D_p = A_p^{-1} - I$ is accretive ($\text{Re } D_p > 0$), the entire spectrum of the reflection operator $\sigma(R_p)$ lies strictly inside the unit disc, and that all nonreal points of the spectrum are the eigenvalues of finite multiplicity. Based on the known properties of the Cayley transform, it has been shown that the reflection operator is a contraction, $\|R_p\| < 1$, while the amplitude operator A_p is an accretive contraction, $\text{Re } A_p > A_p A_p^\dagger > 0$.

The operator Fresnel formulas appear as a solution to the problem of mode diffraction by an abrupt discontinuity in a waveguide (i.e., the waveguide discontinuity with zero volume, $V_{\text{int}} = 0$). If we assume that there exists the unique operator D_p , which is determined by the problem geometry and is frequency-dependent (the given operator of the problem), then the existence of the Fresnel formulas for the required scattering operators follows from the above mentioned fundamental energy laws.

Combination of the reflection and transmission matrix operators of the problem into one operator matrix has enabled us to obtain the compact *third model*, which represents the generalized scattering matrix as

$$S = 2A^{1/2} \pm J; \quad \begin{cases} H - \text{case} \\ E - \text{case} \end{cases}, \quad A \equiv \begin{bmatrix} A_1 & 0 \\ 0 & A_2 \end{bmatrix}, \quad J \equiv \begin{bmatrix} I & 0 \\ 0 & -I \end{bmatrix},$$

and has some good points (in particular, this matrix model is remarkably stable).

Application of the generalized mode-matching technique to the analysis of waveguide transformers with coupling cavity leads to the solution in the form of the operator Fresnel formula for the generalized scattering matrix:

$$S = \frac{W - I_h}{W + I_h}.$$

To construct the solution in such general form, it is sufficient that the operator of the problem, W , exists and the energy conservation laws (3.160), (3.167) hold. The correctness of the generalized operator Fresnel formulas, $-1 \notin \sigma(W)$, is also a corollary of the energy conservation law.

The energy conservation law also allows one to reveal the important properties of the generalized scattering matrix S of a waveguide transformer, including the main characteristics of its entire spectrum. We have found that the generalized scattering matrix is a quasi-Hermitian and non-unitary operator, and the rank of its non-Hermiticity is equal to the total number of propagating waves in the ports of the waveguide transformer. The essential spectrum of the operator matrix S lies on the

real axis at the points ± 1 , and each nonreal point of its spectrum is an eigenvalue of finite multiplicity.

In the context of the generalized mode-matching technique, the convergence of projection approximations to the true solution of the problem has been established analytically. It has been proved that the complex energy conservation law and the second Lorentz lemma in the operator form provide, for any number of the modes taken into account in waveguide ports, the mandatory fulfillment of the requirements that ensure the unconditional convergence of projection approximations.

Using as an example the operator Fresnel formulas for a canonical problem of wave diffraction by an H - or E -plane step discontinuity in a rectangular waveguide, we studied the characteristics of convergence of finite-dimensional approximations, including the estimation of the rate of convergence. For the considered matrix model, the problem of estimation of the approximation error was reduced to the study of the projection convergence (or P -convergence) of the finite known matrices to a given matrix operator. As a result, we have rigorously shown the absence of relative or conditional convergence of the approximations. We have also established analytically that the condition number of the truncated matrix equation is a uniformly bounded value, which ensures stability of numerical computations.

It has been found that for the canonical problem of a step discontinuity in a waveguide, the compliance with the Mittra rule when truncating the field expansions in the partial regions implies the fastest strong convergence to zero of a certain matrix operator. The mentioned matrix operator is generated by the difference of the traces of the Green functions of these regions on the aperture of the discontinuity and it determines a part of the approximation error.

In this chapter, we used a new formulation of the mode diffraction problem to overcome significant mathematical difficulties in the rigorous justification of the mode-matching technique. On the other hand, when implementing this approach, we used the concepts and methods of the modern operator theory in the Hilbert space and Pontryagin space with indefinite metric. To derive the operator Fresnel formulas and their approximations we applied the techniques that generalize the classical Galerkin procedure and the theory of projection approximations.

The developed and rigorously justified generalized mode-matching technique should be considered as alternative to the standard version of this method widely used in computational electrodynamics.

Appendix A: Vectors and Their Spaces

Vectors in the Hilbert Spaces l_2 , \tilde{l}_2 and $\tilde{\tilde{l}}_2$

The linear space l_2 consists of infinite-dimensional row vectors $a = (a_1, a_2, \dots)$, $b = (b_1, b_2, \dots)$, etc., with complex elements $a_m \in \mathbb{C}$, $b_m \in \mathbb{C}$, $m = 1, 2, 3, \dots$. The norm $\|a\|_{l_2} \in \mathbb{R}^1$ of a vector in l_2 is defined by $\|a\|_{l_2}^2 = \sum_m |a_m|^2$ and its value

measures the length of the vector. By definition, the space l_2 consists only of the vectors of finite length: $\|a\|_{l_2} < \infty$. Here, \mathbb{C} is the plane of complex variable and \mathbb{R}^1 is the one-dimensional Euclidean space.

Addition is defined element by element: $a + b = (a_1 + b_1, a_2 + b_2, \dots)$. The sum belongs to the space l_2 because $\|a + b\|_{l_2} \leq \|a\|_{l_2} + \|b\|_{l_2} < \infty$ for $\forall a, b \in l_2$. Multiplication by a scalar λ is defined element by element: $\lambda a = (\lambda a_1, \lambda a_2, \dots)$. Consequently, $\|\lambda a\|_{l_2} = |\lambda| \|a\|_{l_2} < \infty$.

The conjugate space consists of infinite-dimensional column vectors $a^\dagger = (a_1^*, a_2^*, \dots)^T$, $b^\dagger = (b_1^*, b_2^*, \dots)^T$, etc., with the same linear operations and the norm $\|a^\dagger\|_{l_2} \equiv \|a\|_{l_2}$, $\|b^\dagger\|_{l_2} \equiv \|b\|_{l_2}$, and so on. Here the dagger ‘ \dagger ’ denotes Hermitian conjugation, the asterisk ‘ $*$ ’ is for complex conjugation, and the superscript T denotes transposition.

The scalar product is defined by $(a, b^\dagger) \equiv a \cdot b^\dagger = \sum_m a_m b_m^* \in \mathbb{C}$. This multiplication generates a finite complex number, because $|(a, b^\dagger)| \leq \|a\|_{l_2} \|b\|_{l_2} < \infty$ for $\forall a, b \in l_2$. Two vectors a and b are said to be orthogonal if $a \cdot b^\dagger = 0$ and $\|a\|_{l_2}, \|b\|_{l_2} \geq 0$, where $\|a\|_{l_2} = \sqrt{a \cdot a^\dagger}$, $\|b\|_{l_2} = \sqrt{b \cdot b^\dagger}$.

The *matrix product* $a^\dagger \cdot b = A_{ab}$ generates a matrix operator (i.e. an infinite matrix)

$$A_{ab} = \begin{pmatrix} a_1^* b_1 & a_1^* b_2 & \cdots \\ a_2^* b_1 & a_2^* b_2 & \cdots \\ \vdots & \vdots & \ddots \end{pmatrix},$$

which is bounded in l_2 . Specifically, the matrix operator A_{aa} is positive, $A_{aa} \geq 0$, and belongs to the class of nuclear operators in l_2 , because $\text{Tr}(A_{aa}) = \sum_m |a_m|^2 = \|a\|^2 < \infty$.

By definition, the spaces \tilde{l}_2 and $\tilde{\tilde{l}}_2$ are the complex Hilbert spaces for infinite-dimensional vectors a, b, \dots with the scalar products

$$\langle a, b^\dagger \rangle_{\pm} \equiv a I_{\mu}^{\pm 1} b^\dagger = \sum_{m=1}^{\infty} m^{\pm 1} a_m b_m^* \in \mathbb{C}; \quad \left\{ \begin{matrix} \tilde{l}_2 \\ \tilde{\tilde{l}}_2 \end{matrix} \right\},$$

respectively, and with the norm

$$\|a\|_{\pm} = \langle a, a^\dagger \rangle_{\pm}^{1/2} = \left[\sum_{m=1}^{\infty} m^{\pm 1} |a_m|^2 \right]^{1/2} < \infty; \quad \left\{ \begin{matrix} \tilde{l}_2 \\ \tilde{\tilde{l}}_2 \end{matrix} \right\},$$

and also

$$\left| \langle a, b^\dagger \rangle_\pm \right| \leq \|a\|_\pm \cdot \|b\|_\pm < \infty, \quad \|a + b\|_\pm \leq \|a\|_\pm + \|b\|_\pm < \infty; \quad \text{for } \forall a, b \in \left\{ \begin{matrix} \tilde{l}_2 \\ \tilde{l}_2 \end{matrix} \right\}.$$

Here, the diagonal matrix operator $I_\mu \equiv \{m \delta_m^n\}_{m,n=1}^\infty$ is given by its eigenvalues $m = 1, 2, 3, \dots$ and is positively defined, $I_\mu > 0$.

Sometimes the spaces \tilde{l}_2 and \tilde{l}_2 are referred to as ‘energetic spaces of the matrix operator $I_\mu^{\pm 1}$ ’.

Vectors in the Hilbert Space $h_N \equiv l_2^N, N \geq 2$

The linear space h_N consists of row vectors $a = (a^{(1)}, a^{(2)}, \dots, a^{(N)})$, $b = (b^{(1)}, b^{(2)}, \dots, b^{(N)})$, etc., with n vector elements $a^{(n)} \in l_2, b^{(n)} \in l_2, n = 1, 2, \dots, N$.

Addition and multiplication by a scalar λ are defined in a natural way: $a + b = (a^{(1)} + b^{(1)}, a^{(2)} + b^{(2)}, \dots, a^{(N)} + b^{(N)})$, $\lambda a = (\lambda a^{(1)}, \lambda a^{(2)}, \dots, \lambda a^{(N)})$.

Hermitian conjugation gives the column vectors $a^\dagger = \left((a^{(1)})^\dagger, (a^{(2)})^\dagger, \dots, (a^{(N)})^\dagger \right)^T$, $b^\dagger = \left((b^{(1)})^\dagger, (b^{(2)})^\dagger, \dots, (b^{(N)})^\dagger \right)^T$, etc., with the same linear operations.

The scalar product in the space h_N and the norm $\|a\|_{h_N} < \infty$ are defined by the equalities

$$\begin{aligned} (a, b^\dagger) &\equiv a \cdot b^\dagger = \sum_{n=1}^N \left(a^{(n)}, (b^{(n)})^\dagger \right) \in \mathbb{C} \quad \text{and} \\ \|a\|_{h_N}^2 &\equiv a \cdot a^\dagger = \sum_{n=1}^N \|a^{(n)}\|^2 \in \mathbb{R}^1, \end{aligned}$$

respectively; therefore, $\left| (a, b^\dagger) \right| \leq \|a\|_{h_N} \|b\|_{h_N} < \infty, \forall a, b \in h_N$.

The usual matrix product $a^\dagger \cdot b = A_{ab}$ generates an $N \times N$ operator matrix $A_{ab} = \{A_{ij}\}_{i,j=1}^N$ that is bounded in h_N , because each operator $A_{ij} \equiv A_{a^{(i)}b^{(j)}} = (a^{(i)})^\dagger \cdot b^{(j)} : l_2 \rightarrow l_2$ is the bounded one. Specifically, the operator matrix $A_{aa} = \{A_{a^{(i)}a^{(j)}}\}_{i,j=1}^N$ is positive, $A_{aa} > 0$; its trace $\text{Tr}(A_{aa}) = \sum_{n=1}^N A_{a^{(n)}a^{(n)}}$ is a nuclear operator in l_2 .

Operator Vectors in the Space $V_N \equiv (l_2 \rightarrow l_2)^N$, $N \geq 2$

Let us define the operator vectors $A = (A^{(1)}, A^{(2)}, \dots, A^{(N)})$, $B = (B^{(1)}, B^{(2)}, \dots, B^{(N)})$, etc., with N bounded in l_2 matrix operators $A^{(n)}, B^{(n)} : \|A^{(n)}\|_{l_2} < \infty$, $\|B^{(n)}\|_{l_2} < \infty$, $n = 1, 2, \dots, N$.

Addition and multiplication by a scalar λ are defined element by element:
 $A + B = \{A^{(1)} + B^{(1)}, A^{(2)} + B^{(2)}, \dots, A^{(N)} + B^{(N)}\}$,

$\lambda A = \{\lambda A^{(1)}, \lambda A^{(2)}, \dots, \lambda A^{(N)}\}$.

Hermitian conjugation gives the operator vectors $A^\dagger = \left((A^{(1)})^\dagger, (A^{(2)})^\dagger, \dots, (A^{(N)})^\dagger \right)^T$, $B^\dagger = \left((B^{(1)})^\dagger, (B^{(2)})^\dagger, \dots, (B^{(N)})^\dagger \right)^T$, etc., with the same linear operations.

The scalar product in V_N is defined by $(A, B^\dagger) \equiv AB^\dagger = \sum_{n=1}^N A^{(n)}(B^{(n)})^\dagger$, this product represents a bounded operator in l_2 . Specifically, $\|AA^\dagger\|_{l_2} \leq \sum_{n=1}^N \|A^{(n)}\|_{l_2}^2 < \infty$.

The matrix product of operator vectors $A^\dagger B = D$ generates the operator matrix $D = \{D_{ij}\}_{i,j=1}^N$ that is bounded in V_N , since each operator $D_{ij} = (A^{(i)})^\dagger B^{(j)} : l_2 \rightarrow l_2$ is bounded.

Pontryagin Space Π_ν with Indefinite Metric

A sesquilinear Hermitian Q -form $[a, b^\dagger] \equiv \sum_{m=1}^{\infty} \mu_m a_m b_m^* \in \mathbb{C}$, $\mu_m \in \mathbb{R}^1$, $\forall a, b \in G$

defines the indefinite metric (or Q -metric) of the linear vector space G , with the real number $[a, a^\dagger]$ being negative, or positive, or equal to zero as $a \neq 0$. Therefore, in the space with indefinite metric there is no isolated element, with respect to which the distance to any other element is measured.

The Hilbert space G with Q -metric (or the *Krein space*) allows a canonical decomposition $G = P_+G \oplus P_-G$ via two mutually complementary orthoprojectors P_+ and P_- . For all vectors $a \in G$ we have

$$a = a_+ + a_-, \quad (a, a^\dagger) \equiv \|a\|^2 = \|a_+\|^2 + \|a_-\|^2, \quad [a, a^\dagger] \equiv \|a_+\|^2 - \|a_-\|^2,$$

where $a_+ \in P_+G$, $a_- \in P_-G$ and the ratio $\|a_+\|/\|a_-\|$ is arbitrary. All the norms defined by different canonical decompositions are equivalent.

A linear operator $J = P_+ - P_-$ is the canonical symmetry of the Krein space G , which is self-adjoint, $J = J^\dagger$, involutive, $J^{-1} = J$, and unitary, $J^{-1} = J^\dagger$.

The basic relationships between the Q -metric and the Hilbert metric (a, b^\dagger) in the Krein space are $(a, b^\dagger) = [aJ, b^\dagger]$, $[a, b^\dagger] = (aJ, b^\dagger)$, $\forall a, b \in G$. By definition, the Pontryagin space Π_ν is the Krein space $G = P_+G \oplus P_-G$ with finite rank of indefiniteness $\nu = \min\{\dim(P_+G), \dim(P_-G)\} < \infty$.

Suppose that $a, b \in l_2$ and the Q -form is

$$[a, b^\dagger] = \sum_{m=1}^{\nu} a_m b_m^* - \sum_{m=\nu+1}^{\infty} a_m b_m^*,$$

then $l_2 = \Pi_\nu$ (L.S. Pontryagin, 1944).

Appendix B: Infinite Systems of Linear Algebraic Equations

Below we give a brief reference on the theory of infinite systems of linear algebraic equations (SLAE), composed of the information available to us and, therefore, not claiming to be exhausted.

For the infinite system of linear equations in a matrix form under consideration $(I + A)x = b$ the following notation is used: I is the identity operator (idem-factor); $A = \{a_{mn}\}_{m,n=1}^\infty$ is the given matrix operator; $x = \{x_n\}_{n=1}^\infty$ is the required vector; $b = \{b_m\}_{m=1}^\infty$ is the given vector of the right-hand side.

The main classes of matrix operators are related by inclusions:

of finite rank \subset nuclear \subset Hilbert – Schmidt \subset compact \subset bounded.

By the truncation technique we understand truncation of the matrix operator to the matrix A_{NN} of size $N \times N$, obtaining the solution of the corresponding finite-dimensional system and finding the limit for this solution as $N \rightarrow \infty$.

Early Results of the Theory

The truncation technique is applicable if the following conditions are met:

- $\sum_{m,n=1}^\infty |a_{mn}| < \infty$, $b \in l_\infty \equiv \{b = \{b_m\}_{m=1}^\infty : \sup_m |b_m| < \infty\}$ (then there exists a ‘normal determinant’ of the system, $\det(I + A)$; G.W. Hill, 1886);
- $\sum_{m=1}^\infty |a_{mm}| < \infty$, $\sum_{m,n=1}^\infty |a_{mn}|^2 < \infty$, $b \in l_2$ (i.e., $A : l_2 \rightarrow l_2$ is a nuclear operator; Helge von Koch, 1913);

- $\sum_{m,n=1}^{\infty} |a_{mn}|^2 < \infty$, $b \in l_2$ (the solution of this ‘Hilbert system’ reduces to the solution of the truncated $N \times N$ system and some number of infinite systems with small (in norm) operators; the number N is found from the condition $\sum_{m,n=N+1}^{\infty} |a_{mn}|^2 < 1$; L.V. Kantorovich, 1948).

Completely Regular Systems

By definition, the system is completely regular if the matrix operator $A : l_{\infty} \rightarrow l_{\infty}$ is a strict contraction: $\|A\|_{l_{\infty}} = \sup_m \sum_{n=1}^{\infty} |a_{mn}| = q < 1$, $b \in l_{\infty}$.

The system can be solved by the *method of successive approximations* (or the *method of simple iteration*). For a completely regular system, a principal solution $x \in l_{\infty}$ (i.e., the solution obtained when starting with a zero initial approximation) exists and is unique. The difference between the principal solution and k th successive approximation is estimated by the inequality $\|x - x^{(k)}\|_{l_{\infty}} \leq q^k (1 - q)^{-1} \|b\|_{l_{\infty}}$, i.e., strong convergence occurs in the space l_{∞} .

A completely regular SLAE is solvable by the truncation technique that provides a weak convergent in the space l_{∞} and convergent in the norm of the space l_{∞} , if x , b belong to the space $c_0 \subset l_{\infty}$ of the sequences converging to zero (sufficient condition; Yu.I. Griбанov, 1964).

Regular Systems

By definition, the system is regular if a given matrix operator has unit norm (the limiting case of completely regular systems): $\|A\|_{l_{\infty}} = \sup_m \sum_{n=1}^{\infty} |a_{mn}| = 1$, $b \in l_{\infty}$.

The principal solution of this system can be found by the truncation technique (L.V. Kantorovich 1948) or by the successive approximation method (P.O. Kuzmin, 1934) if the Kojalovich condition is met: $|b_m| \leq \text{const} \cdot (1 - \sum_{n=1}^{\infty} |a_{mn}|)$, $\forall m$.

We have the following criterion of uniqueness of a bounded solution: if a regular system satisfies the Kojalovich condition and transforms back to a regular system (or, possibly, completely regular) with the transformation $x_n = \omega_n y_n$, such that $\omega_n \neq 0$, $\forall n$ and $\lim_{n \rightarrow \infty} \omega_n = \infty$, then the initial infinite SLAE has a unique solution (P.S. Bondarenko, 1951).

B.M. Kojalovich (1932) considered the dual infinite SLAE

$$\begin{cases} x_m = \sum_{n=1}^{\infty} a_{mn}y_n + f_m \\ y_m = \sum_{n=1}^{\infty} \alpha_{mn}x_n + g_m \end{cases}$$

with the following restrictions: (i) $a_{mn}, \alpha_{mn} \geq 0, \forall m, n$; (ii) $\sum_{n=1}^{\infty} a_{mn} = 1 - \varphi(m), \sum_{n=1}^{\infty} \alpha_{mn} = 1 - \psi(m)$ (these are the generalized conditions of regularity with the possibility $\lim_{m \rightarrow \infty} \varphi(m) = \lim_{m \rightarrow \infty} \psi(m) = 0$); (iii) $|f_m| \leq K\varphi(m), |g_m| \leq K\psi(m), K = const$ (Kojalovich conditions).

Conditions (ii) and (iii) ensure existence of the principal solution $|x_n| \leq K, \forall n$. At the same time: (1) the principal solution can be found by the truncation technique or by the method of simple iteration; (2) if $f_m, g_m \geq 0$, then $x_n, y_n \geq 0$; (3) the values of the first unknowns in the principal solution determine the limits for all other unknown values, i.e., there exist the values p and q such that for $m > p$ and $n > q$ we have $h \leq x_m \leq H$ and $h \leq y_n \leq H$.

If the following additional conditions are met:

- (iv) there exist numbers $l, L \geq 0$ such that

$$l \leq \frac{a_{mn}}{\varphi(m)} \leq L, \quad l \leq \frac{\alpha_{mn}}{\psi(m)} \leq L \quad \text{for } \forall n < m \quad \text{and } \forall m;$$

- (v) there exists $\theta > 0$ such that

$$\begin{aligned} \varphi(m) + \sum_{n=1}^p a_{mn} &\geq \theta; \quad m = (p+1), (p+2), \dots, 2p \quad \text{and} \\ \psi(m) + \sum_{n=1}^p \alpha_{mn} &\geq \theta \quad \text{for } \forall p \end{aligned}$$

then $\{x_n\}_n$ and $\{y_n\}_n$ are the elements of the space $c \subset l_{\infty}$ of convergent sequences and the ‘law of asymptotic expressions’ $\lim_{n \rightarrow \infty} x_n = \lim_{n \rightarrow \infty} y_n = \sigma \neq 0$ holds true.

Quasi-regular Systems

By definition, the system is quasi-regular if a given matrix operator satisfies the following conditions:

- $A : l_{\infty} \rightarrow l_{\infty}$ is the bounded matrix operator, $\|A\|_{l_{\infty}} = \sup_m \sum_{n=1}^{\infty} |a_{mn}| < \infty$;

- $\sum_{n=1}^{\infty} |a_{mn}| < 1$ for $m = N, N + 1, \dots$;
- $|b_m| \leq \text{const} \cdot (1 - \sum_{n=N}^{\infty} |a_{mn}|)$, $m \geq N$.

The question of the existence of the solution reduces to the question of the existence of the solution of the truncated $N \times N$ SLAE. If the solutions of both the regular system

$$x_m = \sum_{n=N}^{\infty} a_{mn}x_n + \left(b_m + \sum_{n=1}^{N-1} a_{mn}x_n \right); \quad m = N, N + 1, \dots$$

and the truncated system are unique, then the solution of the initial system is unique as well (L.V. Kantorovich, 1936).

Matrix Contractions

By definition, a matrix operator is a strict contraction in space $l_p \equiv \left\{ a = \{a_m\}_{m=1}^{\infty} : \sum_{m=1}^{\infty} |a_m|^p < \infty \right\}$, $1 \leq p < \infty$, if its norm is less than unity: $\|A\|_p < 1$.

If $b \in l_p$, this infinite SLAE is uniquely solvable by the truncation technique, converging by the norm to the solution $x \in l_p$ (Yu.I. Gribanov, 1964). For the case of the space l_{∞} , see Sect. 3.B.2.

The Schur Test and the Young Inequality. Hilbert Matrices

To prove the boundedness of a given matrix operator $A : l_2 \rightarrow l_2$ and to estimate analytically its norm, one often uses the following sufficient condition known as the Schur test.

Suppose, $a_{mn} \geq 0$, $\forall m, n$ and $x_m, y_m > 0$, $\forall m$, while α and β are the positive numbers such that $\sum_{m=1}^{\infty} a_{mn}x_m \leq \alpha y_n$, $\forall n$ and $\sum_{n=1}^{\infty} a_{mn}y_n \leq \beta x_m$, $\forall m$. Then $A : l_2 \rightarrow l_2$ is the bounded operator of norm $\|A\| \leq \sqrt{\alpha\beta}$.

Another condition is known as the Young inequality: suppose $\mu = \max \left\{ \|A\|_{l_1}, \|A\|_{l_{\infty}} \right\} < \infty$, where $\|A\|_{l_1} = \sup_n \sum_{m=1}^{\infty} |a_{mn}|$ and $\|A\|_{l_{\infty}} = \sup_m \sum_{n=1}^{\infty} |a_{mn}|$, then the operator $A : l_p \rightarrow l_p$, $p \geq 1$ is bounded and $\|A\|_p \leq \mu$.

It has been proved by using the Schur test that the Hilbert-Hankel matrix operator $A = \left\{ (m+n+1)^{-1} \right\}_{m,n=0}^{\infty}$ has norm $\|A\|_{l_2} \leq \pi$.

If $\{a_k\}_{k=0}^\infty$ is the sequence of the Fourier coefficients of an essentially bounded function $f(x)$ in the basis $\{\exp(i2\pi kx)\}_{k=0}^\infty$, $x \in (0, 1)$, then the matrix operator defined by the elements $\{a_{m-n}\}_{m,n=0}^\infty$ is bounded on the pair of spaces $l_2 \rightarrow l_2$. The norm of this operator coincides with the norm of the function $f(x)$. From this follows the boundedness of the Hilbert-Toeplitz matrix operator $A = \left\{ (m-n)^{-1} \right\}_{m,n=0, m \neq n}^\infty$.

Compact (Completely Continuous) Operators

According to the Schur theorem, if the condition $\lim_{m \rightarrow \infty} \sum_{n=1}^\infty |a_{mn}| = 0$ is satisfied, the operator A is continuous on the pair of spaces $l_\infty \rightarrow c_0$ ($c_0 \subset l_\infty$ is the space of the numerical sequences converging to zero) and completely continuous on the pair of spaces $l_\infty \rightarrow l_\infty$.

A uniquely solvable SLAE with a compact matrix operator A is solvable by the truncation technique, which converges in the norm of the space l only if $b \in [l]$ (by definition, $[l_\infty] = c_0$, $[l_p] = l_p$ for $1 \leq p < \infty$) and otherwise converges weakly (Yu.I. Gribanov, 1964).

The Kojima and Toeplitz Matrix Operators

Suppose that for a given matrix operator the following conditions are satisfied:

- the operator $A : l_\infty \rightarrow l_\infty$ is bounded, $\|A\|_{l_\infty} = \sup_m \sum_{n=1}^\infty |a_{mn}| < \infty$;
- the ‘convergence by columns’ of the form $\lim_{m \rightarrow \infty} a_{mn} = \alpha_n, \forall n$ takes place.

Then,

- for $\alpha_n \equiv 0, \forall n$ the operator $A : c_0 \rightarrow c_0$ is bounded (the necessary and sufficient condition);
- if for some n we have $\alpha_n \neq 0$, then the operator $A : c_0 \rightarrow c$ is bounded (the necessary and sufficient condition).

In the general case, the Kojima-Schur theorem can be formulated as follows. Suppose, the limit $\lim_{m \rightarrow \infty} \sum_{n=1}^\infty a_{mn} = \alpha$ exists, then we have a ‘ K -matrix’—the bounded operator $A : c \rightarrow c$ (the necessary and sufficient condition).

At the same time, if $\lim_{n \rightarrow \infty} x_n = d$ and $\bar{x} = Ax$, then $\lim_{n \rightarrow \infty} \bar{x}_n = \alpha d + \sum_{n=1}^\infty \alpha_n (x_n - d)$, whence it follows that for $\alpha = 1$ and $\alpha_n = 0, \forall n$ the transformation $\bar{x} = Ax$ preserves the limit of the sequence $\{x_n\}_{n=1}^\infty$ (the Toeplitz-Silverman theorem). In this case, we have a ‘ T -matrix’ and the

transformation $\bar{x} = Ax$ is called regular. Notice that T -matrix is not a compact operator (the Steinhaus theorem).

A sum and a product of K -matrices exist and are K -matrices. K -matrices form an algebra, in which the addition is associative and commutative, while multiplication is distributive and associative, but, in general, is not commutative. The necessary (but not sufficient) condition for K -matrix to be a compact operator is the equality $\sum_{n=1}^{\infty} \alpha_n = \alpha$.

If K -matrix allows the representation $a_{mn} = (m)^{-1}f(n/m)$, $m, n = 1, 2, 3, \dots$ where the function $f(x) \in L_1(0, \infty)$ is monotonic for large x , then the following exact formulas are valid:

$$\lim_{m \rightarrow \infty} \sum_{n=1}^{\infty} a_{mn} = \lim_{m \rightarrow \infty} \frac{1}{m} \sum_{n=1}^{\infty} f\left(\frac{n}{m}\right) = \int_0^{\infty} f(x) dx,$$

$$\lim_{m \rightarrow \infty} \sum_{n=1}^{\infty} |a_{mn}| = \lim_{m \rightarrow \infty} \frac{1}{m} \sum_{n=1}^{\infty} \left| f\left(\frac{n}{m}\right) \right| = \int_0^{\infty} |f(x)| dx.$$

An illustrative example of T -matrix gives the operator with positive elements

$$a_{mn} = \frac{m^{1-\tau} n^{\tau}}{n^2 + m^2 \theta^2}; \quad 0 < \tau < 1, \quad \theta^2 > 0, \quad m, n = 1, 2, 3, \dots$$

Indeed, for $t = n/m$ we have $a_{mn} = (m)^{-1} t^{\tau} (t^2 + \theta^2)^{-1}$, and hence

$$\lim_{m \rightarrow \infty} \sum_{n=1}^{\infty} a_{mn} = \int_0^{\infty} \frac{t^{\tau} dt}{t^2 + \theta^2} = \frac{\pi \theta^{\tau-1}}{2 \cos(\pi \tau / 2)} \neq 0.$$

Considering that $\lim_{m \rightarrow \infty} a_{mn} = 0$, upon the correspondent normalization, we identify a T -matrix.

Appendix C: Operator Forms of the Energy Conservation Law Under Time Reversal

In this chapter, we have used the SI system of units and the time dependence is given by the factor $\exp(-i\omega t)$, where ω is the angular frequency.

Practicians often use a time dependence in the form of $\exp(+i\omega t)$. For such a choice, we give below some useful forms of the generalized energy conservation law in terms of the generalized scattering matrix. In the presence of a resonant volume $V_{\text{int}} \neq 0$, they are as follows:

- $P - SP S^\dagger - 2\text{Im}(SQ) = 0, \quad P - S^\dagger P S - 2\text{Im}(QS) = 0;$
- $I_h - V_+ V_+^\dagger = J - V_- J V_-^\dagger, \quad I_h - V_+^\dagger V_+ = J - V_-^\dagger J V_-;$
- $\frac{1}{2}(I_h - S S^\dagger) = Q - V_- Q V_-^\dagger;$
- $\text{Im} S = P - V_+ P V_+^\dagger;$
- $\text{Im}(S J) = P - V_- P V_-^\dagger.$

For an arbitrary abrupt discontinuity in a waveguide ($V_{\text{int}} = 0$) we have:

- $P - SP S^\dagger - 2\text{Im}(SQ) = 0, \quad Q - S Q S^\dagger + 2\text{Im}(SP) = 0;$
- $V_+ V_+^\dagger = V_+^\dagger V_+ = I_h, \quad V_- J V_-^\dagger = V_-^\dagger J V_- = J.$

All these forms are applicable for N -port waveguide transformer.

References

1. Fresnel, A.-J.: Mémoire sur la loi des modifications que la réflexion imprime à la lumière polarisée. Annales de chimie et de physique **XLVI**, 225–264 (1823) (in French)
2. Born, M., Wolf, E.: Principles of Optics: Electromagnetic Theory of Propagation, Interference and Diffraction of Light. Cambridge University Press, Cambridge (1999)
3. Mittra, R., Lee, S.: Analytical Techniques in the Theory of Guided Waves. Macmillan, New York (1971)
4. Shestopalov, V.P., Scherbak, V.V.: Matrix operators in diffraction problems. Radiophys. Quantum Electron. **11**(2), 161–166 (1968)
5. Shestopalov, V.P., Kirilenko, A.A., Masalov, S.A., Sirenko, Y.K.: Resonance Wave Scattering. Diffraction Gratings, vol. 1. Naukova Dumka, Kiev (1986). (in Russian)
6. Shestopalov, V.P., Kirilenko, A.A., Rud', L.A.: Resonance Wave Scattering. Waveguide Discontinuities, vol. 2. Naukova Dumka, Kiev (1986) (in Russian)
7. Lytvynenko, L.M., Prosvirnin, S.L.: Spectral Operators of Scattering in the Problems of Diffraction by Planar Screens. Naukova Dumka, Kiev (1984). (in Russian)
8. Azizov, T.Y., Iohvidov, I.S.: Linear Operators in Spaces with Indefinite Metric. Wiley, Chichester (1989)
9. Hurd, R.A., Gruenberg, H.: H-plane bifurcation of rectangular waveguides. Can. J. Phys. **32**, 694–701 (1954)
10. Hönl, H., Maue, A.W., Westpfahl, K.: Theorie der Beugung. Springer, Berlin (1961). (in German)
11. Shestopalov, V.P., Kirilenko, A.A., Masalov, S.A.: Matrix Convolution-Type Equations in the Diffraction Theory. Naukova Dumka, Kiev (1984). (in Russian)
12. Hutson, V.C.L., Pym, J.S.: Applications of Functional Analysis and Operator Theory. Academic Press, New York (1980)
13. Halmos, P.R.: A Hilbert Space Problem Book. Springer, Berlin (1982)
14. Weyl, H.: The Classical Groups: Their Invariants and Representations. Princeton University Press, Chichester (1997)
15. Collin, R.E.: Field Theory of Guided Waves. Wiley-IEEE Press, New York (1991)
16. Petrusenko, I.V., Sirenko, Y.K.: The lost 'second Lorentz theorem' in the phasor domain. Telecommun. Radio Eng. **68**(7), 555–560 (2009)
17. Rothwell, E.J., Cloud, M.J.: Electromagnetics. CRC Press, New York (2001)

18. Brodskii, M.S., Lifshits, M.S.: Spectral analysis of non-self-adjoint operators and intermediate systems. *Am. Math. Soc. Trans.* **13**(2), 265–346 (1960)
19. Lifshits, M.S.: *Operators, Oscillations, Waves*. Published by American Mathematical Society, Providence (1973)
20. Petrusenko, I.V., Sirenko, Y.K.: Abrupt discontinuities: The reflection operator is a contraction. *Telecommun. Radio Eng.* **67**(19), 1707–1709 (2008)
21. Trénoquigne, V.A.: *Analyse Fonctionnelle*. Editions MIR, Moscou (1985). (in French)
22. Vladimirov, V.S.: *Methods of the Theory of Generalized Functions*. Taylor & Francis, London (2002)
23. Petrusenko, I.V.: Analytic-numerical analysis of waveguide bends. *Electromagnetics* **24**(4), 237–254 (2004)
24. Petrusenko, I.V., Sirenko, Y.K.: Generalization of the power conservation law for scalar mode-diffraction problems. *Telecommun. Radio Eng.* **68**(16), 1399–1410 (2009)
25. von Hurwitz, A., von Courant, R.: *Allgemeine Funktionentheorie und Elliptische Funktionen. Geometrische Funktionentheorie*. Springer, Berlin (1964) (in German)
26. Vinogradov, I.M. (ed.): *Encyclopedia of Mathematics*. Kluwer, Boston (1995)
27. Gohberg, I.C., Krein, M.G.: *Introduction to the Theory of Linear Non-Self-Adjoint Operators*. Published by American Mathematical Society, New York (1969)
28. Petrusenko, I.V.: Basic properties of the generalized scattering matrix of waveguide transformers. *Electromagnetics* **26**(8), 601–614 (2006)

Chapter 4

Two-Dimensionally Periodic Gratings: Pulsed and Steady-State Waves in an Irregular Floquet Channel

Lyudmyla Velychko

Abstract This chapter presents a series of analytical results that serves as theoretical basis for numerical study of electromagnetic wave transformations in two-dimensionally periodic structures. Among them is the solution of the important problem of truncation of the computational space by artificial boundaries. The author establishes and analyzes fundamental characteristics of transient and steady-state fields in the regular part of the rectangular Floquet channel. For the first time, strict corollaries of Poynting's complex power theorem and Lorentz's lemma (the energy-balance equations and reciprocity relations) is presented for two-dimensionally periodic gratings of finite thickness illuminated by transverse-electric or transverse-magnetic plane waves. The method of transport operators (a space-time analogue of the generalized scattering matrices), developed in the chapter, can significantly reduce the computational resources required for calculation of wave scattering by multilayer periodic structures or by the structures on thick substrates. A number of questions concerning the spectral theory of two-dimensionally periodic gratings is answered—it is the result, which is essential for a reliable physical analysis of the resonant scattering of pulsed and monochromatic waves.

4.1 Introduction

Rigorous models of one-dimensionally periodic diffraction gratings made their appearance in the 1970s, when the corresponding theoretical problems had been considered in the context of classical mathematical disciplines such as mathematical physics, computational mathematics, and the theory of differential and integral equations. Periodic structures remain the subject of considerable attention. They are among the most called-for dispersive elements that provide efficient polarization, frequency, and spatial signal selection. Fresh insights into the physics of wave

L. Velychko (✉)

O.Ya. Usikov Institute for Radiophysics and Electronics, National Academy of Sciences,
Kharkiv, Ukraine
e-mail: lgv@ire.kharkov.ua

processes in diffraction gratings are being implemented into radically new devices operating in gigahertz, terahertz, and optical ranges, into new materials with inclusions ranging in size from micro- to nanometers, and into novel circuits for in situ measurements.

However, the potentialities of the classical two-dimensional models [1–7] are limited. The modern theory and practice invite further investigation of three-dimensional, vector models of periodic structures in increasing frequency. It is quite reasonable to base these models on the time-domain (TD) representations and implement them numerically by the mesh methods [8, 9]. It follows from the well-known facts: (i) TD-approaches are free from the idealizations inherent in the frequency domain; (ii) they are universal owing to minimal restrictions imposed on geometrical and material parameters of the objects under study; (iii) they allow *explicit computational schemes*, which do not require inversion of any operators and call for an adequate run time when implementing on present-day computers; (iv) they result in the data easy convertible into a standard set of frequency-domain characteristics. It should be also noted that in recent years both local and nonlocal *exact absorbing conditions* (EACs) have been derived and tested [6, 7]. They allow one to replace an *open initial boundary value problem* that occurs in electrodynamic theory of gratings with a *closed problem*. In addition, one can invoke the efficient fast Fourier transform accelerated finite-difference and finite-element schemes with EACs for characterizing different resonant structures [10, 11].

It is evident that the numerical algorithm solving a grating problem must be stable and convergent, computational error must be predictable, while the numerical results are bound to be unambiguously treated in physical terms. To comply with these requirements, it is important to theoretically justify each stage of the modeling process (formulation of boundary value or initial boundary value problems, determination of the correctness classes for them, analysis of singularities of the analytical continuation for the solutions of model boundary value problems into a domain of complex-valued frequencies, etc.).

Here we present a series of analytical results that provide the necessary theoretical background for the numerical solution of the initial boundary value problems associated with two-dimensionally periodic structures. First, we give general information required to formulate a model electrodynamic problem in a grating theory. Then, in Sects. 4.3 and 4.4, we dwell on the correct and efficient truncation of the computational space when solving the problems of spatial-temporal wave transformations in two-dimensionally periodic structures. Some important characteristics and properties of transient and steady-state fields in the regular parts of the rectangular Floquet channel are discussed in Sects. 4.5 and 4.7. In Sect. 4.6, the *method of transformation operators* (the TD-analog of the generalized scattering matrix method) is described; by applying this method, we can optimize the computational resources used in the calculation of multi-layered periodic structures or structures on thick substrates. In Sect. 4.8, we give the elements of the *spectral theory* for two-dimensionally periodic gratings in view of its importance in physical analysis of resonant scattering of pulsed or monochromatic waves by open periodic resonators.

4.2 Fundamental Equations, Domain of Analysis, Initial and Boundary Conditions

Space-time and space-frequency transformations of electromagnetic waves in diffraction gratings, waveguides, open resonators, radiators, etc. are described by the initial boundary value problems and boundary value problems for Maxwell's equations. In this chapter, we will consider the problems of the electromagnetic theory of gratings resulting from the following system of Maxwell's equations for the waves propagating in *stationary, locally inhomogeneous, isotropic, and frequency dispersive media* [9, 12]:

$$\begin{aligned} \operatorname{rot} \vec{H}(g, t) = \eta_0^{-1} \frac{\partial [\vec{E}(g, t) + \chi_\varepsilon(g, t) * \vec{E}(g, t)]}{\partial t} \\ + \chi_\sigma(g, t) * \vec{E}(g, t) + \vec{j}(g, t), \end{aligned} \quad (4.1)$$

$$\operatorname{rot} \vec{E}(g, t) = -\eta_0 \frac{\partial [\vec{H}(g, t) + \chi_\mu(g, t) * \vec{H}(g, t)]}{\partial t}. \quad (4.2)$$

Here, $g = \{x, y, z\}$ is a point in the three-dimensional space \mathbb{R}^3 ; $x, y,$ and z are the Cartesian coordinates; $\vec{E}(g, t) = \{E_x, E_y, E_z\}$ and $\vec{H}(g, t) = \{H_x, H_y, H_z\}$ are the electric and magnetic field vectors; $\eta_0 = (\mu_0/\varepsilon_0)^{1/2}$ is the intrinsic impedance of free space; ε_0 and μ_0 are the permittivity and permeability of free space; $\vec{j}(g, t)$ is the extraneous current density vector; $\chi_\varepsilon(g, t)$, $\chi_\mu(g, t)$, and $\chi_\sigma(g, t)$ are the electric, magnetic, and specific conductivity susceptibilities; $f_1(t) * f_2(t) = \int f_1(t - \tau)f_2(\tau) d\tau$ stands for the convolution operation. We use the SI system of units. From here on we will use the term 'time' for parameter t , which is measured in meters and has the meaning of the product of the natural time and the velocity of light in vacuum.

With no frequency dispersion in the domain $G \subset \mathbb{R}^3$, for the points $g \in G$ we have

$$\chi_\varepsilon(g, t) = \delta(t)[\varepsilon(g) - 1], \quad \chi_\mu(g, t) = \delta(t)[\mu(g) - 1], \quad \chi_\sigma(g, t) = \delta(t)\sigma(g),$$

where $\delta(t)$ is the Dirac delta-function; $\varepsilon(g)$, $\mu(g)$, and $\sigma(g)$ are the relative permittivity, relative permeability, and specific conductivity of a locally inhomogeneous medium, respectively. Then (4.1) and (4.2) take the form:

$$\operatorname{rot} \vec{H}(g, t) = \eta_0^{-1} \varepsilon(g) \frac{\partial \vec{E}(g, t)}{\partial t} + \sigma(g) \vec{E}(g, t) + \vec{j}(g, t), \quad (4.3)$$

$$\operatorname{rot} \vec{E}(g, t) = -\eta_0 \mu(g) \frac{\partial \vec{H}(g, t)}{\partial t}. \quad (4.4)$$

In vacuum, where we have $\varepsilon(g) = \mu(g) = 1$ and $\sigma(g) = 0$, they can be rewritten in the form of the following vector problems [6]:

$$\begin{cases} \left[\Delta - \text{grad div} - \frac{\partial^2}{\partial t^2} \right] \vec{E}(g, t) = \vec{F}_E(g, t), & \vec{F}_E(g, t) = \eta_0 \frac{\partial}{\partial t} \vec{j}(g, t) \\ \frac{\partial}{\partial t} \vec{H}(g, t) = -\eta_0^{-1} \text{rot} \vec{E}(g, t), \end{cases} \quad (4.5)$$

or

$$\begin{cases} \left[\Delta - \frac{\partial^2}{\partial t^2} \right] \vec{H}(g, t) = \vec{F}_H(g, t); & \vec{F}_H(g, t) = -\text{rot} \vec{j}(g, t) \\ \eta_0^{-1} \frac{\partial}{\partial t} \vec{E}(g, t) = \text{rot} \vec{H}(g, t) - \vec{j}(g, t). \end{cases} \quad (4.6)$$

By Δ we denote the Laplace operator. As shown in [6], the operator $\text{grad div} \vec{E}$ can be omitted in (4.5) due to the following reasons. By denoting the induced and external electric charge volume density through $\rho_1(g, t)$ and $\rho_2(g, t)$, we can write $\text{grad div} \vec{E} = \varepsilon_0^{-1} \text{grad}(\rho_1 + \rho_2)$. In a homogeneous medium, where ε and σ are positive and non-negative constants, respectively, we have $\rho_1(g, t) = \rho_1(g, 0) \exp(-t\eta_0\sigma/\varepsilon)$, and if $\rho_1(g, 0) = 0$, then $\rho_1(g, t) = 0$ for any $t > 0$. The remaining term $\varepsilon_0^{-1} \text{grad} \rho_2$ can be moved to the right-hand side of the wave equation in (4.5) as a part of the function defining current sources of the electric field.

To formulate the initial boundary value problem for hyperbolic equations (4.1)–(4.6), one should add initial conditions at $t = 0$ and boundary conditions on the external and internal boundaries of the domain of analysis Q [13]. In 3-D vector or scalar problems, the domain Q is a part of the R^3 -space bounded by the surfaces S that are the boundaries of the domains $\text{int}S$, filled with a perfect conductor: $Q = R^3 \setminus \overline{\text{int}S}$. In the so-called open problems, the domain of analysis may extend to infinity along one or more spatial coordinates.

The set of boundary conditions for the initial boundary value problems is formulated in the following way [12]:

- the tangential component of the electric field vector is zero on a perfectly conducting surface S at all times t

$$\vec{E}_{tg}(g, t)|_{g \in S} = 0 \quad \text{for } t \geq 0; \quad (4.7)$$

- the normal component of the magnetic field vector on S is equal to zero ($\vec{H}_{nr}(g, t)|_{g \in S} = 0$), and the function $\vec{H}_{tg}(g, t)|_{g \in S}$ defines the so-called surface currents generated on S by the external electromagnetic field;
- on the surfaces $S^{e, \mu, \sigma}$, where material properties of the medium have discontinuities, as well as all over the domain Q , the tangential components $\vec{E}_{tg}(g, t)$ and $\vec{H}_{tg}(g, t)$ of the electric and magnetic field vectors must be continuous;

- in the vicinity of singular points of the boundaries of Q , i.e. the points, where the tangents and normals are undetermined, the field energy density must be spatially integrable;
- if the domain Q is unbounded and the field $\{\vec{E}(g, t), \vec{H}(g, t)\}$ is generated by the sources that have bounded supports in Q , then for any finite time interval $(0, T)$ one can construct a closed virtual boundary $M \subset Q$ sufficiently removed from the sources such that

$$\{\vec{E}(g, t), \vec{H}(g, t)\} \Big|_{g \in M, t \in (0, T)} = 0. \quad (4.8)$$

The initial state of the system is determined by the initial conditions at $t = 0$. The reference states $\vec{E}(g, 0)$ and $\vec{H}(g, 0)$ in system (4.1), (4.2) or in system (4.3), (4.4) are the same as $\vec{E}(g, 0)$ and $[\partial \vec{E}(g, t) / \partial t]_{t=0}$ ($\vec{H}(g, 0)$ and $[\partial \vec{H}(g, t) / \partial t]_{t=0}$) in the differential forms of the second order (in terms of t), to which (4.1), (4.2) or (4.3), (4.4) are transformed if the vector \vec{H} (vector \vec{E}) is eliminated (see, for example, system (4.5), (4.6)). Thus, (4.5) should be complemented with the following initial conditions

$$\vec{E}(g, 0) = \vec{\varphi}(g), \quad \frac{\partial \vec{E}(g, t)}{\partial t} \Big|_{t=0} = \vec{\psi}(g); \quad g \in \bar{Q}. \quad (4.9)$$

The functions $\vec{\varphi}(g)$, $\vec{\psi}(g)$, and $\vec{F}(g, t)$ (we will call them the instantaneous and current source functions) usually have limited support in the closure of the domain Q . It is the practice to divide the current sources into hard and soft ones [9]: soft sources do not have material supports and thus they are not able to scatter electromagnetic waves. Instantaneous sources are obtained from the pulsed wave $\vec{U}^i(g, t)$ exciting an electrodynamic structure: $\vec{\varphi}(g) = \vec{U}^i(g, 0)$ and $\vec{\psi}(g) = [\partial \vec{U}^i(g, t) / \partial t]_{t=0}$. The pulsed signal $\vec{U}^i(g, t)$ itself should satisfy the corresponding wave equation and the causality principle. It is also important to demand that the pulsed signal has not yet reached the scattering boundaries by the moment $t = 0$.

The latter is obviously impossible if infinite structures (for example, gratings) are illuminated by the plane pulsed waves that propagate in the direction other than the normal to certain infinite boundary. Such waves are able to run through a part of the scatterer's surface by any moment of time. As a result, a mathematically correct modeling of the process becomes impossible: the input data required for the initial boundary value problem to be set are defined, as a matter of fact, by the solution of this problem.

4.3 Time Domain: Initial Boundary Value Problems

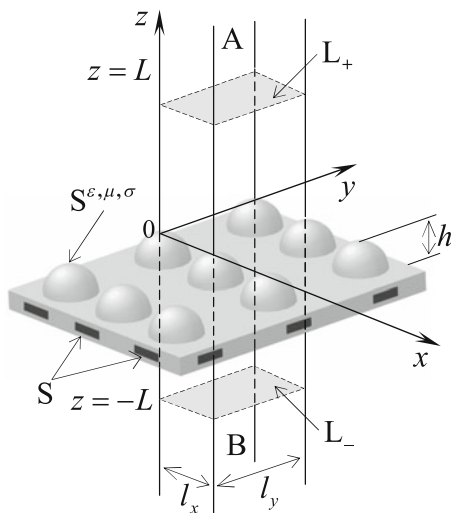
The vector problem describing transient states of the field nearby the gratings, whose geometry is presented in Fig. 4.1, can be written in the form

$$\left\{ \begin{array}{l} \operatorname{rot} \vec{H}(g, t) = \eta_0^{-1} \frac{\partial [\vec{E}(g, t) + \chi_\varepsilon(g, t) * \vec{E}(g, t)]}{\partial t} + \chi_\sigma(g, t) * \vec{E}(g, t) + \vec{j}(g, t), \\ \operatorname{rot} \vec{E}(g, t) = -\eta_0 \frac{\partial [\vec{H}(g, t) + \chi_\mu(g, t) * \vec{H}(g, t)]}{\partial t}; \quad g = \{x, y, z\} \in Q; \quad t > 0 \\ \vec{E}(g, 0) = \vec{\varphi}_E(g), \quad \vec{H}(g, 0) = \vec{\varphi}_H(g); \quad g \in \bar{Q} \\ \vec{E}_{tg}(g, t)|_{g \in S} = 0, \quad \vec{H}_{nr}(g, t)|_{g \in S} = 0; \quad t \geq 0. \end{array} \right. \quad (4.10)$$

Here, \bar{Q} is the closure of Q ; $\chi_\varepsilon(g, t)$, $\chi_\mu(g, t)$, and $\chi_\sigma(g, t)$ are piecewise continuous functions and the surfaces S are assumed to be sufficiently smooth. From this point on, it will be also assumed that the continuity conditions for tangential components of the field vectors are satisfied, if required. The domain of analysis $Q = \mathbb{R}^3 \setminus \overline{\operatorname{int} S}$ occupies a great deal of the \mathbb{R}^3 -space. The problem formulated for that domain can be resolved analytically or numerically only in two following cases:

- The problem (4.10) degenerates into a conventional Cauchy problem ($\overline{\operatorname{int} S} = \emptyset$, the medium is homogeneous and nondispersive, while the supports of the functions $\vec{F}(g, t)$, $\vec{\varphi}(g)$, and $\vec{\psi}(g)$ are bounded). With some inessential restrictions for the source functions, the classical and generalized solutions of the

Fig. 4.1 Geometry of a two-dimensionally periodic grating



Cauchy problem do exist; they are unique and described by the well-known Poisson formula [13].

- The functions $\vec{F}(g, t)$, $\vec{\varphi}(g)$, and $\vec{\psi}(g)$ have the same displacement symmetry as the periodic structure. In this case, the domain of analysis can be reduced to $Q^N = \{g \in Q : 0 < x < l_x; 0 < y < l_y\}$, by adding to problem (4.10) periodicity conditions [7] on the lateral surfaces of the rectangular Floquet channel $R = \{g \in R^3 : 0 < x < l_x; 0 < y < l_y\}$.

The domain of analysis can also be reduced to Q^N in a more general case. The objects of analysis are, in this case, not quite physical (*complex-valued sources and waves*). However, through simple mathematical transformations, all the results can be presented in the customary, physically correct form. There are several reasons (to one of them we have referred at the end of Sect. 4.2) why the modeling of physically realizable processes in the electromagnetic theory of gratings should start with the initial boundary value problems for the images $f^N(g, t, \Phi_x, \Phi_y)$ of the functions $f(g, t)$ describing the *actual real-valued sources*:

$$\begin{aligned}
 f(g, t) &= \int_{-\infty}^{\infty} \int_{-\infty}^{\infty} \tilde{f}(z, t, \Phi_x, \Phi_y) \exp(2\pi i \Phi_x \frac{x}{l_x}) \exp(2\pi i \Phi_y \frac{y}{l_y}) d\Phi_x d\Phi_y \\
 &= \int_{-\infty}^{\infty} \int_{-\infty}^{\infty} f^N(g, t, \Phi_x, \Phi_y) d\Phi_x d\Phi_y.
 \end{aligned}
 \tag{4.11}$$

From (4.11) it follows that

$$\begin{aligned}
 f^N \left\{ \frac{\partial f^N}{\partial x} \right\} (x + l_x, y, z, t, \Phi_x, \Phi_y) &= e^{2\pi i \Phi_x} f^N \left\{ \frac{\partial f^N}{\partial x} \right\} (x, y, z, t, \Phi_x, \Phi_y), \\
 f^N \left\{ \frac{\partial f^N}{\partial y} \right\} (x, y + l_y, z, t, \Phi_x, \Phi_y) &= e^{2\pi i \Phi_y} f^N \left\{ \frac{\partial f^N}{\partial y} \right\} (x, y, z, t, \Phi_x, \Phi_y),
 \end{aligned}$$

or, in other symbols,

$$\begin{aligned}
 D[f^N](x + l_x, y) &= e^{2\pi i \Phi_x} D[f^N](x, y), \\
 D[f^N](x, y + l_y) &= e^{2\pi i \Phi_y} D[f^N](x, y).
 \end{aligned}$$

The use of the sources $f^N(g, t, \Phi_x, \Phi_y)$ satisfying the foregoing conditions and *superposition principle* truncates the domain of analysis to the domain Q^N , which is a part of the Floquet channel R . Hence we can rewrite problem (4.10) in the form

$$\left\{ \begin{array}{l} \text{rot} \vec{H}^N(g, t) = \eta_0^{-1} \frac{\partial [\vec{E}^N(g, t) + \chi_\sigma(g, t) * \vec{E}^N(g, t)]}{\partial t} \\ \quad + \chi_\sigma(g, t) * \vec{E}^N(g, t) + \vec{J}^N(g, t), \\ \text{rot} \vec{E}^N(g, t) = -\eta_0 \frac{\partial [\vec{H}^N(g, t) + \chi_\mu(g, t) * \vec{H}^N(g, t)]}{\partial t}; \quad g \in Q^N, \quad t > 0 \\ \vec{E}^N(g, 0) = \vec{\varphi}_E^N(g), \quad \vec{H}^N(g, 0) = \vec{\varphi}_H^N(g); \quad g \in \bar{Q}^N \\ D[\vec{E}^N(\vec{H}^N)](l_x, y) = e^{2\pi i \Phi_x} D[\vec{E}^N(\vec{H}^N)](0, y) \quad \text{for } 0 \leq y \leq l_y, \\ D[\vec{E}^N(\vec{H}^N)](x, l_y) = e^{2\pi i \Phi_y} D[\vec{E}^N(\vec{H}^N)](x, 0) \quad \text{for } 0 \leq x \leq l_x, \\ \text{and } \vec{E}_{tg}^N(g, t)|_{g \in S} = 0, \quad \vec{H}_{nr}^N(g, t)|_{g \in S} = 0; \quad t \geq 0, \end{array} \right. \quad (4.12)$$

$$\begin{aligned} \vec{E}(g, t) &= \int_{-\infty}^{\infty} \int_{-\infty}^{\infty} \vec{E}^N(g, t, \Phi_x, \Phi_y) d\Phi_x d\Phi_y, \\ \vec{H}(g, t) &= \int_{-\infty}^{\infty} \int_{-\infty}^{\infty} \vec{H}^N(g, t, \Phi_x, \Phi_y) d\Phi_x d\Phi_y. \end{aligned} \quad (4.13)$$

It is known [6–8] that initial boundary value problems for the above discussed equations can be formulated such that they are uniquely solvable in the Sobolev space $W_2^1(Q^T)$, where $Q^T = Q \times (0, T)$ and $0 \leq t \leq T < \infty$ (the *observation interval*). On this basis, we will suppose in the subsequent discussion that the problem (4.12) for all $t \in [0, T]$ has also a generalized solution from the space $W_2^1(Q^{N,T})$ and that the uniqueness theorem is true in this space. Here symbol ‘ \times ’ stands for the direct product of two sets, $(0, T)$ and $[0, T]$ are open and closed intervals, $W_m^n(G)$ is a set of all elements $\vec{f}(g)$ from the space $L_m(G)$ whose generalized derivatives up to the order n inclusive also belong to $L_m(G)$, $L_m(G)$ is the space of the functions $\vec{f}(g) = \{f_x, f_y, f_z\}$ (for $g \in G$), such that the functions $|f_x(g)|^m$, $|f_y(g)|^m$, and $|f_z(g)|^m$ are integrable on the domain G .

4.4 Exact Absorbing Conditions for the Rectangular Floquet Channel

In this section, we present analytical results relative to the truncation of the computational space in open 3-D initial boundary value problems of the electromagnetic theory of gratings. In Sect. 4.3, by passing on to some special transforms of the functions describing physically realizable sources, the problem for infinite gratings have been reduced to that formulated in the rectangular Floquet channel R or, in other words, in the rectangular waveguide with quasi-periodic boundary conditions.

Now we perform further reduction of the domain Q^N to the region $Q_L^N = \{g \in Q^N : |z| < L\}$ (all the sources and inhomogeneities of the Floquet channel R are supposedly located in this domain). For this purpose the exact absorbing

conditions [6, 7, 10, 14, 15] for the artificial boundaries L_{\pm} ($z = \pm L$) of the domain Q_L^N will be constructed such that their inclusion into (4.12) does not change the correctness class of the problem and its solution $\vec{E}^N(g, t)$, $\vec{H}^N(g, t)$.

From here on we omit the superscripts N in (4.12). By applying the technique similar to that described in [14, 15], represent the solution $\vec{E}(g, t)$ of (4.12) in the closure of the domains $A = \{g \in \mathbb{R} : z > L\}$ and $B = \{g \in \mathbb{R} : z < -L\}$ in the following form:

$$\vec{E}(g, t) = \sum_{n,m=-\infty}^{\infty} \vec{u}_{nm}^{\pm}(z, t) \mu_{nm}(x, y); \quad \{x, y\} \in \bar{\mathbb{R}}_z, \quad t \geq 0, \quad (4.14)$$

where the superscript ‘+’ corresponds to $z \geq L$ and ‘-’ to $z \leq -L$, and the following notation is used: $\mathbb{R}_z = (0 < x < l_x) \times (0 < y < l_y)$; $\{\mu_{nm}(x, y)\}$ ($n, m = 0, \pm 1, \pm 2, \dots$) is the complete in $L_2(\mathbb{R}_z)$ orthonormal system of the functions $\mu_{nm}(x, y) = \exp(i\alpha_n x) \exp(i\beta_m y) / \sqrt{l_x l_y}$; $\alpha_n = 2\pi(\Phi_x + n) / l_x$, $\beta_m = 2\pi(\Phi_y + m) / l_y$, and $\lambda_{nm}^2 = \alpha_n^2 + \beta_m^2$. The *space-time amplitudes* $\vec{u}_{nm}^{\pm}(z, t)$ satisfy the equations

$$\begin{cases} \left[-\frac{\partial^2}{\partial t^2} + \frac{\partial^2}{\partial z^2} - \lambda_{nm}^2 \right] \vec{u}_{nm}^{\pm}(z, t) = 0; & t > 0 \\ \vec{u}_{nm}^{\pm}(z, 0) = 0, \quad \frac{\partial \vec{u}_{nm}^{\pm}(z, t)}{\partial t} \Big|_{t=0} = 0 \end{cases} \quad (4.15)$$

for $z \geq L$ and $z \leq -L$. Equations (4.14) and (4.15) are obtained by separating variables in the homogeneous boundary value problems for the equation $[\Delta - \partial^2 / \partial t^2] \vec{E}(g, t) = 0$ (see formula (4.5)) and taking into account that in the domains A and B we have $\text{grad div} \vec{E}(g, t) = 0$ and $\vec{F}_E(g, t) = 0$. It is also assumed that the field generated by the current and instantaneous sources located in Q_L has not yet reached the boundaries L_{\pm} by the moment of time $t = 0$.

For the solutions $\vec{u}_{nm}^{\pm}(z, t)$ of the vector problems (4.15), as well as in the case of the scalar problems [14, 15], we can write

$$\vec{u}_{nm}^{\pm}(\pm L, t) = \mp \int_0^t J_0[\lambda_{nm}(t - \tau)] \vec{u}_{nm}^{\pm}(\pm L, \tau) d\tau; \quad t \geq 0. \quad (4.16)$$

The above formula represents nonlocal EACs for the space-time amplitudes of the field $\vec{E}(g, t)$ in the cross-sections $z = \pm L$ of the Floquet channel R. The *exact nonlocal and local absorbing conditions* for the field $\vec{E}(g, t)$ on the *artificial boundaries* L_{\pm} follow immediately from (4.16) and (4.14):

$$\begin{aligned} \vec{E}(x, y, \pm L, t) = \mp \sum_{n, m=-\infty}^{\infty} \left\{ \int_0^t J_0[\lambda_{nm}(t-\tau)] \right. \\ \left. \times \left[\int_0^{l_x} \int_0^{l_y} \frac{\partial \vec{E}(\tilde{x}, \tilde{y}, z, \tau)}{\partial z} \Big|_{z=\pm L} \mu_{nm}^*(\tilde{x}, \tilde{y}) d\tilde{x} d\tilde{y} \right] d\tau \right\} \mu_{nm}(x, y); \quad (4.17) \\ \{x, y\} \in \bar{R}_z, \quad t \geq 0 \end{aligned}$$

and

$$\vec{E}(x, y, \pm L, t) = \frac{2}{\pi} \int_0^{\pi/2} \frac{\partial \vec{W}_E^{\pm}(x, y, t, \varphi)}{\partial t} d\varphi; \quad \{x, y\} \in \bar{R}_z, \quad t \geq 0, \quad (4.18a)$$

$$\begin{cases} \left[\frac{\partial^2}{\partial t^2} - \sin^2 \varphi \left(\frac{\partial^2}{\partial x^2} + \frac{\partial^2}{\partial y^2} \right) \right] \vec{W}_E^{\pm}(x, y, t, \varphi) = \mp \frac{\partial \vec{E}(g, t)}{\partial z} \Big|_{z=\pm L}; & \{x, y\} \in R_z, \quad t > 0 \\ \vec{W}_E^{\pm}(x, y, t, \varphi) \Big|_{t=0} = \frac{\partial \vec{W}_E^{\pm}(x, y, t, \varphi)}{\partial t} \Big|_{t=0} = 0; & \{x, y\} \in \bar{R}_z \\ D[\vec{W}_E^{\pm}](l_x, y) = e^{2\pi i \Phi_x} D[\vec{W}_E^{\pm}](0, y) & \text{for } 0 \leq y \leq l_y \quad \text{and} \\ D[\vec{W}_E^{\pm}](x, l_y) = e^{2\pi i \Phi_y} D[\vec{W}_E^{\pm}](x, 0) & \text{for } 0 \leq x \leq l_x; \quad t \geq 0. \end{cases} \quad (4.18b)$$

Here, $\vec{u}_{nm}^{\pm}(\pm L, \tau) = \partial \vec{u}_{nm}^{\pm}(z, \tau) / \partial z \Big|_{z=\pm L}$, $J_0(\dots)$ is the zero-order Bessel function, the superscript ‘*’ stands for the complex conjugation operation, $\vec{W}_E^{\pm}(x, y, t, \varphi)$ are some auxiliary functions, where the numerical parameter φ lies in the range $0 \leq \varphi \leq \pi/2$.

It is obvious that the magnetic field vector $\vec{H}(g, t)$ of the pulsed waves $\vec{U}(g, t) = \{\vec{E}(g, t), \vec{H}(g, t)\}$ outgoing towards the domains A and B satisfies similar boundary conditions on L_{\pm} . The boundary conditions for $\vec{E}(g, t)$ and $\vec{H}(g, t)$ (nonlocal or local) taken together reduce the computational space for the problem (4.12) to the domain Q_L (a part of the Floquet channel R) that contains all the sources and obstacles.

Now suppose that in addition to the sources $\vec{j}(g, t)$, $\vec{\varphi}_E(g)$, and $\vec{\varphi}_H(g)$, there exist sources $\vec{j}^A(g, t)$, $\vec{\varphi}_E^A(g)$, and $\vec{\varphi}_H^A(g)$ located in A and generating some pulsed wave $\vec{U}^i(g, t) = \{\vec{E}^i(g, t), \vec{H}^i(g, t)\}$ being incident on the boundary L_+ at times $t > 0$. The field $\vec{U}^i(g, t)$ is assumed to be nonzero only in the domain A. Since the boundary conditions (4.17), (4.18a, 4.18b) remain valid for any pulsed wave outgoing through L_{\pm} towards $z = \pm \infty$ [14, 15], then the total field $\{\vec{E}(g, t), \vec{H}(g, t)\}$ is the solution of the initial boundary value problem (4.12) in the domain Q_L with the

boundary conditions (4.17) or (4.18a, 4.18b) on L_- and the following conditions for the artificial boundary L_+

$$\begin{aligned} \vec{E}^s(x, y, L, t) = & - \sum_{n,m=-\infty}^{\infty} \left\{ \int_0^t J_0[\lambda_{nm}(t-\tau)] \right. \\ & \times \left. \left[\int_0^{l_x} \int_0^{l_y} \frac{\partial \vec{E}^s(\tilde{x}, \tilde{y}, z, \tau)}{\partial z} \Big|_{z=L} \mu_{nm}^*(\tilde{x}, \tilde{y}) d\tilde{x} d\tilde{y} \right] d\tau \right\} \mu_{nm}(x, y); \\ & \{x, y\} \in \bar{R}_z, \quad t \geq 0 \end{aligned} \quad (4.19)$$

or

$$\vec{E}^s(x, y, L, t) = \frac{2}{\pi} \int_0^{\pi/2} \frac{\partial \vec{W}_E^s(x, y, t, \varphi)}{\partial t} d\varphi; \quad \{x, y\} \in \bar{R}_z, \quad t \geq 0, \quad (4.20a)$$

$$\begin{cases} \left[\frac{\partial^2}{\partial t^2} - \sin^2 \varphi \left(\frac{\partial^2}{\partial x^2} + \frac{\partial^2}{\partial y^2} \right) \right] \vec{W}_E^s(x, y, t, \varphi) = -\frac{\partial \vec{E}^s(g, t)}{\partial z} \Big|_{z=L}; & \{x, y\} \in R_z, \quad t > 0 \\ \vec{W}_E^s(x, y, t, \varphi) \Big|_{t=0} = \frac{\partial \vec{W}_E^s(x, y, t, \varphi)}{\partial t} \Big|_{t=0} = 0; & \{x, y\} \in R_z \\ D[\vec{W}_E^s](l_x, y) = e^{2\pi i \Phi_x} D[\vec{W}_E^s](0, y) & \text{for } 0 \leq y \leq l_y \quad \text{and} \\ D[\vec{W}_E^s](x, l_y) = e^{2\pi i \Phi_y} D[\vec{W}_E^s](x, 0) & \text{for } 0 \leq x \leq l_x; \quad t \geq 0. \end{cases} \quad (4.20b)$$

Here, $\vec{U}^s(g, t) = \{\vec{E}^s(g, t), \vec{H}^s(g, t)\} = \vec{U}(g, t) - \vec{U}^i(g, t)$ ($g \in A$, $t > 0$) is the pulsed wave outgoing towards $z = +\infty$. It is generated by the incident wave $\vec{U}^i(g, t)$ ('reflection' from the virtual boundary L_+) and the sources $\vec{j}(g, t)$, $\vec{\varphi}_E(g)$, and $\vec{\varphi}_H(g)$.

4.5 Some Important Characteristics of Transient Fields in the Rectangular Floquet Channel

For numerical implementation of the computational schemes involving boundary conditions like (4.19) or (4.20a, 4.20b), the function $\vec{U}^i(g, t)$ for $t \in [0, T]$ and its normal derivative with respect to the boundary L_+ are to be known. To obtain the required data for the wave $\vec{U}^i(g, t)$ generated by a given set of sources $\vec{j}^A(g, t)$,

$\vec{\varphi}_E^A(g)$, and $\vec{\varphi}_H^A(g)$, the following initial boundary value problem for a regular hollow Floquet channel R is to be solved:

$$\left\{ \begin{array}{l} \left[-\frac{\partial^2}{\partial t^2} + \Delta \right] \left\{ \begin{array}{l} \vec{E}^i \\ \vec{H}^i \end{array} \right\} = \left\{ \begin{array}{l} \eta_0 \vec{\partial} \vec{J}^A / \partial t + \varepsilon_0^{-1} \text{grad} \rho_2^A \\ -\text{rot} \vec{J}^A \end{array} \right\} = \left\{ \begin{array}{l} \vec{F}_{z,E}^A \\ \vec{F}_{z,H}^A \end{array} \right\}; \\ g = \{x, y, z\} \in R, \quad t > 0 \\ \left\{ \begin{array}{l} \partial \vec{E}^i(g, t) / \partial t|_{t=0} = \eta_0 \text{rot} \vec{H}^i(g, 0) \\ \partial \vec{H}^i(g, t) / \partial t|_{t=0} = -\eta_0^{-1} \text{rot} \vec{E}^i(g, 0) \end{array} \right\} = \left\{ \begin{array}{l} \vec{\psi}_{z,E}^A \\ \vec{\psi}_{z,H}^A \end{array} \right\}, \\ \left\{ \begin{array}{l} \vec{E}^i(g, 0) \\ \vec{H}^i(g, 0) \end{array} \right\} = \left\{ \begin{array}{l} \vec{\varphi}_E^A \\ \vec{\varphi}_H^A \end{array} \right\}; \quad g \in \bar{R} \\ D[\vec{E}^i(\vec{H}^i)](l_x, y) = e^{2\pi i \Phi_x} D[\vec{E}^i(\vec{H}^i)](0, y) \quad \text{for } 0 \leq y \leq l_y \quad \text{and} \\ D[\vec{E}^i(\vec{H}^i)](x, l_y) = e^{2\pi i \Phi_y} D[\vec{E}^i(\vec{H}^i)](x, 0) \quad \text{for } 0 \leq x \leq l_x; \quad t \geq 0. \end{array} \right. \quad (4.21)$$

The function $\rho_2^A(g, t)$ here determines the volume density of foreign electric charge.

First we determine the longitudinal components E_z^i and H_z^i of the field $\{\vec{E}^i, \vec{H}^i\}$ at all points g of the domain R for all times $t > 0$. Let us consider the scalar initial boundary value problems following from (4.21):

$$\left\{ \begin{array}{l} \left[-\frac{\partial^2}{\partial t^2} + \Delta \right] \left\{ \begin{array}{l} E_z^i \\ H_z^i \end{array} \right\} = \left\{ \begin{array}{l} F_{z,E}^A \\ F_{z,H}^A \end{array} \right\}; \quad g \in R, \quad t > 0 \\ \left\{ \begin{array}{l} E_z^i(g, 0) \\ H_z^i(g, 0) \end{array} \right\} = \left\{ \begin{array}{l} \varphi_{z,E}^A \\ \varphi_{z,H}^A \end{array} \right\}, \quad \left\{ \begin{array}{l} \partial E_z^i(g, t) / \partial t|_{t=0} \\ \partial H_z^i(g, t) / \partial t|_{t=0} \end{array} \right\} = \left\{ \begin{array}{l} \psi_{z,E}^A \\ \psi_{z,H}^A \end{array} \right\}; \quad g \in \bar{R} \\ D[E_z^i(H_z^i)](l_x, y) = e^{2\pi i \Phi_x} D[E_z^i(H_z^i)](0, y) \quad \text{for } 0 \leq y \leq l_y \quad \text{and} \\ D[E_z^i(H_z^i)](x, l_y) = e^{2\pi i \Phi_y} D[E_z^i(H_z^i)](x, 0) \quad \text{for } 0 \leq x \leq l_x; \quad t \geq 0. \end{array} \right. \quad (4.22)$$

By separating the transverse variables x and y in (4.22), represent the solution of the problem as

$$\left\{ \begin{array}{l} E_z^i(g, t) \\ H_z^i(g, t) \end{array} \right\} = \sum_{n,m=-\infty}^{\infty} \left\{ \begin{array}{l} v_{nm(z,E)}(z, t) \\ v_{nm(z,H)}(z, t) \end{array} \right\} \mu_{nm}(x, y). \quad (4.23)$$

To determine the scalar functions $v_{nm(z,E)}(z, t)$ and $v_{nm(z,H)}(z, t)$, we have to invert the following Cauchy problems for the one-dimensional Klein-Gordon equations:

$$\left\{ \begin{array}{l} \left[-\frac{\partial^2}{\partial t^2} + \frac{\partial^2}{\partial z^2} - \lambda_{nm}^2 \right] \left\{ \begin{array}{l} v_{nm(z,E)}(z, t) \\ v_{nm(z,H)}(z, t) \end{array} \right\} = \left\{ \begin{array}{l} F_{nm(z,E)}^A \\ F_{nm(z,H)}^A \end{array} \right\}; \\ t > 0, \quad -\infty < z < \infty \\ \left\{ \begin{array}{l} v_{nm(z,E)}(z, 0) \\ v_{nm(z,H)}(z, 0) \end{array} \right\} = \left\{ \begin{array}{l} \varphi_{nm(z,E)}^A \\ \varphi_{nm(z,H)}^A \end{array} \right\}, \quad \left. \frac{\partial}{\partial t} \left\{ \begin{array}{l} v_{nm(z,E)}(z, t) \\ v_{nm(z,H)}(z, t) \end{array} \right\} \right|_{t=0} = \left\{ \begin{array}{l} \psi_{nm(z,E)}^A \\ \psi_{nm(z,E)}^A \end{array} \right\}; \\ -\infty < z < \infty, \quad n, m = 0, \pm 1, \pm 2, \dots \end{array} \right. \quad (4.24)$$

Here $F_{nm(z,E)}^A$, $\varphi_{nm(z,E)}^A$, $\psi_{nm(z,E)}^A$ and $F_{nm(z,H)}^A$, $\varphi_{nm(z,H)}^A$, $\psi_{nm(z,H)}^A$ are the amplitudes of the Fourier transforms of the functions $F_{z,E}^A$, $\varphi_{z,E}^A$, $\psi_{z,E}^A$ and $F_{z,H}^A$, $\varphi_{z,H}^A$, $\psi_{z,H}^A$ in the basic set $\{\mu_{nm}(x, y)\}_{n,m}$.

Let us continue the functions $v_{nm(z,E)}(z, t)$, $v_{nm(z,H)}(z, t)$ and $F_{nm(z,E)}^A$, $F_{nm(z,H)}^A$ by zero on the semi-axis $t < 0$ and pass on to the generalized formulation of the Cauchy problem (4.24) [13]:

$$\begin{aligned} B(\lambda_{nm}) \left[\begin{array}{l} v_{nm(z,E)}(z, t) \\ v_{nm(z,H)}(z, t) \end{array} \right] &\equiv \left[-\frac{\partial^2}{\partial t^2} + \frac{\partial^2}{\partial z^2} - \lambda_{nm}^2 \right] \left\{ \begin{array}{l} v_{nm(z,E)}(z, t) \\ v_{nm(z,H)}(z, t) \end{array} \right\} \\ &= \left\{ \begin{array}{l} F_{nm(z,E)}^A \\ F_{nm(z,H)}^A \end{array} \right\} - \delta^{(1)}(t) \left\{ \begin{array}{l} \varphi_{nm(z,E)}^A \\ \varphi_{nm(z,H)}^A \end{array} \right\} - \delta(t) \left\{ \begin{array}{l} \psi_{nm(z,E)}^A \\ \psi_{nm(z,H)}^A \end{array} \right\} = \left\{ \begin{array}{l} f_{nm(z,E)} \\ f_{nm(z,H)} \end{array} \right\}; \\ -\infty < z < \infty, \quad -\infty < t < \infty, \quad n, m = 1, \pm 2, \pm 3, \dots, \end{aligned} \quad (4.25)$$

where $\delta(t)$ and $\delta^{(m)}(t)$ are the Dirac delta-function and its derivative of the order m . Taking into account the properties of the *fundamental solution* $G(z, t, \lambda) = -(1/2) \chi(t - |z|) J_0(\lambda \sqrt{t^2 - z^2})$ of the operator $B(\lambda)$ [6, 14, 15] ($\chi(t)$ is the Heaviside step function), the solutions $v_{nm(z,E)}(z, t)$ and $v_{nm(z,H)}(z, t)$ of (4.25) can be written as

$$\begin{aligned} \left\{ \begin{array}{l} v_{nm(z,E)}(z, t) \\ v_{nm(z,H)}(z, t) \end{array} \right\} &= G(z, t, \lambda_{nm}) * \left\{ \begin{array}{l} f_{nm(z,E)} \\ f_{nm(z,H)} \end{array} \right\} \\ &= -\frac{1}{2} \left[\int_{-\infty}^{t-|z-\omega|} \int_{-\infty}^{\infty} J_0 \left(\lambda_{nm} \sqrt{(t-\tau)^2 - (z-\omega)^2} \right) \right. \end{aligned}$$

$$\times \left(\left\{ \begin{matrix} F_{nm(z,E)}^A \\ F_{nm(z,H)}^A \end{matrix} \right\} - \delta^{(1)}(t) \left\{ \begin{matrix} \varphi_{nm(z,E)}^A \\ \varphi_{nm(z,H)}^A \end{matrix} \right\} - \delta(t) \left\{ \begin{matrix} \psi_{nm(z,E)}^A \\ \psi_{nm(z,H)}^A \end{matrix} \right\} \right) d\omega d\tau \Big]; \quad (4.26)$$

$$-\infty < z < \infty, \quad t \geq 0, \quad n, m = 1, \pm 2, \pm 3, \dots$$

Relations (4.23) and (4.26) completely determine the longitudinal components of the field $\{\vec{E}^i, \vec{H}^i\}$.

Outside the bounded domain enclosing all the sources, in the domain $G \subset R$, where the waves generated by these sources propagate freely, the following relations [6, 15] are valid:

$$\begin{cases} \vec{E}^i = \left(\frac{\partial^2 U^E}{\partial x \partial z} - \frac{\partial^2 U^H}{\partial y \partial t} \right) \vec{x} + \left(\frac{\partial^2 U^E}{\partial y \partial z} + \frac{\partial^2 U^H}{\partial x \partial t} \right) \vec{y} + \left(\frac{\partial^2 U^E}{\partial z^2} - \frac{\partial^2 U^E}{\partial t^2} \right) \vec{z} \\ \eta_0 \vec{H}^i = \left(\frac{\partial^2 U^E}{\partial y \partial t} + \frac{\partial^2 U^H}{\partial x \partial z} \right) \vec{x} + \left(-\frac{\partial^2 U^E}{\partial x \partial t} + \frac{\partial^2 U^H}{\partial y \partial z} \right) \vec{y} + \left(\frac{\partial^2 U^H}{\partial z^2} - \frac{\partial^2 U^H}{\partial t^2} \right) \vec{z}. \end{cases} \quad (4.27)$$

Here,

$$U^{E,H}(g, t) = \sum_{n,m=-\infty}^{\infty} u_{nm}^{E,H}(z, t) \mu_{nm}(x, y) \quad (4.28)$$

are the scalar *Borgnis functions* such that $[\Delta - \partial^2/\partial t^2][\partial U^{E,H}(g, t)/\partial t] = 0$. Equations (4.23), (4.26)–(4.28) determine the field $\{\vec{E}^i, \vec{H}^i\}$ at all points g of the domain G for all times $t > 0$ provided that $\lambda_{nm} \neq 0$ for all n and m . The opposite case requires special consideration. Really, since at the time point $t = 0$ the domain G is undisturbed, then we have $[\Delta - \partial^2/\partial t^2]U^{E,H} = 0$ ($g \in G, t > 0$). Hence, in view of (4.27), (4.28), it follows:

$$E_z = \frac{\partial^2 U^E}{\partial z^2} - \frac{\partial^2 U^E}{\partial t^2} = - \left(\frac{\partial^2 U^E}{\partial x^2} + \frac{\partial^2 U^E}{\partial y^2} \right) = \sum_{n,m=-\infty}^{\infty} \lambda_{nm}^2 u_{nm}^E \mu_{nm},$$

$$\eta_0 H_z = \frac{\partial^2 U^H}{\partial z^2} - \frac{\partial^2 U^H}{\partial t^2} = - \left(\frac{\partial^2 U^H}{\partial x^2} + \frac{\partial^2 U^H}{\partial y^2} \right) = \sum_{n,m=-\infty}^{\infty} \lambda_{nm}^2 u_{nm}^H \mu_{nm}$$

and (see representation (4.23))

$$u_{nm}^E(z, t) = (\lambda_{nm})^{-2} v_{nm(z,E)}(z, t), \quad u_n^H(z, t) = \eta_0 (\lambda_{nm})^{-2} v_{nm(z,H)}(z, t). \quad (4.29)$$

Hence the functions $U^{E,H}(g, t)$ as well as the transverse components of the field $\{\vec{E}^i, \vec{H}^i\}$ are determined.

The foregoing suggests the following important conclusion: the fields generated in the reflection zone (the domain A) and transmission zone (the domain B) of the periodic structure are uniquely determined by their longitudinal (directed along z -

axis) components which can be represented in the following form (see also formulas (4.14) and (4.23)). For the incident wave we have

$$\left\{ \begin{array}{l} E_z^i(g, t) \\ H_z^i(g, t) \end{array} \right\} = \sum_{n,m=-\infty}^{\infty} \left\{ \begin{array}{l} v_{nm(z,E)}(z, t) \\ v_{nm(z,H)}(z, t) \end{array} \right\} \mu_{nm}(x, y); \quad g \in \bar{A}, \quad t \geq 0, \quad (4.30)$$

for the reflected wave $\vec{U}^s(g, t)$ (which coincides with the total field $\vec{U}(g, t)$ if $\vec{U}^i(g, t) \equiv 0$) we have

$$\left\{ \begin{array}{l} E_z^s(g, t) \quad \text{or} \quad E_z(g, t) \\ H_z^s(g, t) \quad \text{or} \quad H_z(g, t) \end{array} \right\} = \sum_{n,m=-\infty}^{\infty} \left\{ \begin{array}{l} u_{nm}^+(z,E)(z, t) \\ u_{nm}^+(z,H)(z, t) \end{array} \right\} \mu_{nm}(x, y); \quad g \in \bar{A}, \quad t \geq 0, \quad (4.31)$$

and for the transmitted wave (coinciding in the domain B with the total field $\vec{U}(g, t)$) we can write

$$\left\{ \begin{array}{l} E_z(g, t) \\ H_z(g, t) \end{array} \right\} = \sum_{n,m=-\infty}^{\infty} \left\{ \begin{array}{l} u_{nm}^-(z,E)(z, t) \\ u_{nm}^-(z,H)(z, t) \end{array} \right\} \mu_{nm}(x, y); \quad g \in \bar{B}, \quad t \geq 0. \quad (4.32)$$

In applied problems, the most widespread are situations where a periodic structure is excited by one of the partial components of *TE*-wave (with $E_z^i(g, t) = 0$) or *TM*-wave (with $H_z^i(g, t) = 0$) [7]. Consider, for example, a partial wave of order pq . Then we have

$$\vec{U}^i(g, t) = \vec{U}_{pq(H)}^i(g, t) : H_z^i(g, t) = v_{pq(z,H)}(z, t) \mu_{pq}(x, y)$$

or

$$\vec{U}^i(g, t) = \vec{U}_{pq(E)}^i(g, t) : E_z^i(g, t) = v_{pq(z,E)}(z, t) \mu_{pq}(x, y).$$

The excitation of this kind is implemented in our models in the following way. The time function $v_{pq(z,H)}(L, t)$ or $v_{pq(z,E)}(L, t)$ is defined on the boundary L_+ . This function determines the width of the pulse $\vec{U}^i(g, t)$, namely, the frequency range $[K_1, K_2]$ such that for all frequencies k from this range ($k = 2\pi/\lambda$, λ is the wavelength in free space) the value

$$\gamma = \frac{|\tilde{v}_{pq(z,H \text{ or } E)}(L, k)|}{\max_{k \in [K_1, K_2]} |\tilde{v}_{pq(z,H \text{ or } E)}(L, k)|},$$

where $\tilde{v}_{pq(z,H \text{ or } E)}(L, k)$ is the *spectral amplitude of the pulse* $v_{pq(z,H \text{ or } E)}(L, t)$, exceeds some given value $\gamma = \gamma_0$. All spectral characteristics $\tilde{f}(k)$ are obtainable from the temporal characteristics $f(t)$ by applying the Laplace transform

$$\tilde{f}(k) = \int_0^{\infty} f(t)e^{ikt} dt \quad \leftrightarrow \quad f(t) = \frac{1}{2\pi} \int_{i\alpha - \infty}^{i\alpha + \infty} \tilde{f}(k)e^{-ikt} dk; \quad 0 \leq \alpha \leq \text{Im } k. \quad (4.33)$$

For numerical implementation of the boundary conditions (4.19) and (4.20a, 4.20b) and for calculating space-time amplitudes of the transverse components of the wave $\vec{U}^i(g, t)$ in the cross-section $z = L$ of the Floquet channel (formulas (4.27) and (4.29)), the function $(v_{pq(z, H \text{ or } E)})'(L, t)$ is to be determined. To do this, we apply the following relation [7, 15]:

$$\vec{v}_{pq(H \text{ or } E)}(L, t) = \int_0^t J_0[\lambda_{pq}(t - \tau)] (\vec{v}_{pq(H \text{ or } E)})'(L, \tau) d\tau; \quad t \geq 0, \quad (4.34)$$

which is valid for all the amplitudes of the pulsed wave $\vec{U}^i(g, t)$ outgoing towards $z = -\infty$ and does not violate the causality principle.

4.6 Transformation Operator Method

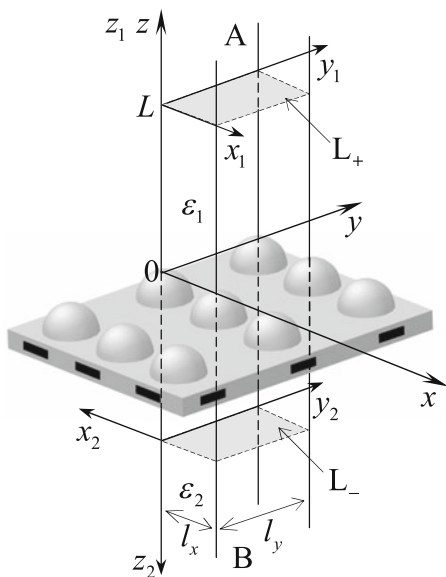
4.6.1 Evolutionary Basis of a Signal and Transformation Operators

Let us place an arbitrary periodic structure of finite thickness between two homogeneous dielectric half-spaces $z_1 = z - L > 0$ (with $\varepsilon = \varepsilon_1$) and $z_2 = -z - L > 0$ (with $\varepsilon = \varepsilon_2$). Let also a local coordinate system $g_j = \{x_j, y_j, z_j\}$ be associated with each of these half-spaces (Fig. 4.2).

Assume that the distant sources located in the domain A of the upper half-space generate a primary wave $\vec{U}_1^i(g, t) = \{\vec{E}_1^i(g, t), \vec{H}_1^i(g, t)\}$ being incident on the artificial boundary L_+ (on the plane $z_1 = 0$) as viewed from $z_1 = \infty$. Denote by $\vec{U}_j^s(g, t) = \{\vec{E}_j^s(g, t), \vec{H}_j^s(g, t)\}$ the fields resulting from scattering of the primary wave $\vec{U}_1^i(g, t)$ in the domains A (where the total field is $\vec{U}(g, t) = \{\vec{E}(g, t), \vec{H}(g, t)\} = \vec{U}_1^i(g, t) + \vec{U}_1^s(g, t)$) and B (where $\vec{U}(g, t) = \vec{U}_2^s(g, t)$). In Sect. 4.5, we have shown that the fields under consideration are uniquely determined by their longitudinal components, which can be given, for example, as:

$$\begin{Bmatrix} E_z^i(g, t) \\ H_z^i(g, t) \end{Bmatrix} = \sum_{n, m=-\infty}^{\infty} \begin{Bmatrix} v_{nm(1, E)}(z_1, t) \\ v_{nm(1, H)}(z_1, t) \end{Bmatrix} \mu_{nm}(x, y); \quad z_1 \geq 0, \quad t \geq 0, \quad (4.35)$$

Fig. 4.2 A
two-dimensionally periodic
grating between two dielectric
half-spaces as element of a
multi-layered structure



$$\left\{ \begin{array}{l} E_z^s(g, t) \\ H_z^s(g, t) \end{array} \right\} = \sum_{n,m=-\infty}^{\infty} \left\{ \begin{array}{l} u_{nm(j,E)}(z_j, t) \\ u_{nm(j,H)}(z_j, t) \end{array} \right\} \mu_{nm}(x, y); \quad z_j \geq 0, \quad t \geq 0, \quad j = 1, 2 \quad (4.36)$$

(see also formulas (4.30)–(4.32)). Here, as before, $\{\mu_{nm}(x, y)\}_{n,m=-\infty}^{\infty}$ is the complete (in $L_2(\mathbb{R}_z)$) orthonormal system of transverse eigenfunctions of the Floquet channel R (see Sect. 4.4), while the space-time amplitudes $u_{nm(j,E)}(z_j, t)$ and $u_{nm(j,H)}(z_j, t)$ are determined by the solutions of the following problems (see also problem (4.15)) for the one-dimensional Klein-Gordon equations:

$$\left\{ \begin{array}{l} \left[-\varepsilon_j \frac{\partial^2}{\partial t^2} + \frac{\partial^2}{\partial z_j^2} - \lambda_{nm}^2 \right] u_{nm(j,E \text{ or } H)}(z_j, t) = 0; \quad t > 0; \\ u_{nm(j,E \text{ or } H)}(z_j, 0) = 0, \quad \frac{\partial}{\partial t} u_{nm(j,E \text{ or } H)}(z_j, t) \Big|_{t=0} = 0 \\ z_j \geq 0, \quad j = 1, 2, \quad n, m = 0, \pm 1, \pm 2, \dots \end{array} \right. \quad (4.37)$$

Compose from the functions $v_{nm(1,E)}(z_1, t)$, $v_{nm(1,H)}(z_1, t)$, $u_{nm(j,E)}(z_j, t)$, $u_{nm(j,H)}(z_j, t)$ and the eigenvalues λ_{nm} ($n, m = 0, \pm 1, \pm 2, \dots$) the sets $v_{(1)}(z_1, t) = \{v_{p(1)}(z_1, t)\}_{p=-\infty}^{\infty}$, $u_{(j)}(z_j, t) = \{u_{p(j)}(z_j, t)\}_{p=-\infty}^{\infty}$, and $\{\lambda_p\}_{p=-\infty}^{\infty}$ such that their members are defined according to the rules depicted in Fig. 4.3. The sets $v_{(1)}(z_1, t)$ and $u_{(j)}(z_j, t)$ are said to be *evolutionary bases* of signals $\vec{U}_1^i(g, t)$ and $\vec{U}_j^s(g, t)$. They describe completely and unambiguously transformation of the

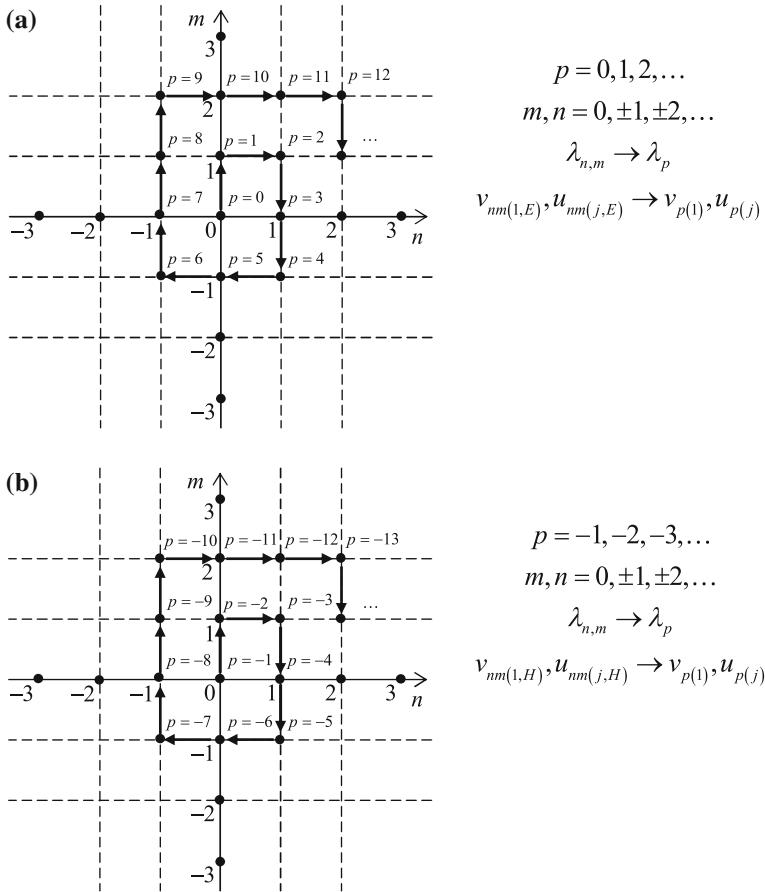


Fig. 4.3 Construction of sets of the values $v_{p(1)}, u_{p(j)}$, and λ_p ($p = 0, \pm 1, \pm 2, \dots$) from sets of the values $v_{nm(1,E)}, u_{nm(j,E)}, v_{nm(1,H)}, u_{nm(j,H)}$, and λ_{nm} ($m, n = 0, \pm 1, \pm 2, \dots$): **a** $p = 0, 1, 2, \dots$; **b** $p = -1, -2, -3, \dots$

corresponding nonsine waves in the regular Floquet channels A and B filled with dielectric.

Let us introduce by the relations

$$\begin{aligned}
 u_{p(j)}'(0, t) &\equiv \left. \frac{\partial}{\partial z_j} u_{p(j)}(z_j, t) \right|_{z_j=0} \\
 &= \int_0^t \sum_{q=-\infty}^{\infty} \left[S_{pq}^{AA}(t-\tau) \delta_j^1 + S_{pq}^{BA}(t-\tau) \delta_j^2 \right] v_{q(1)}(0, \tau) d\tau; \\
 t &\geq 0, \quad p = 0, \pm 1, \pm 2, \dots, \quad j = 1, 2,
 \end{aligned}
 \tag{4.38}$$

$$u_{(j)'}(0, t) = \{u_{p(j)'}(0, t)\}_p = \left[S^{AA} \delta_j^1 + S^{BA} \delta_j^2 \right] [v_{(1)}(0, \tau)]; \quad t \geq 0, \quad j = 1, 2 \tag{4.39}$$

the boundary (on the boundaries $z_j = 0$) *transformation operators* S^{AA} and S^{BA} of the evolutionary basis $v_{(1)}(z_1, t)$ of the wave $\vec{U}_1^i(g, t)$ incoming from the domain A. Here δ_m^n stands for the Kronecker delta, the operators' elements S_{nm}^{XY} specify the space-time energy transformation from the domain Y into the domain X and from the mode of order m into the mode of order n .

It is evident that the operators S^{AA} and S^{BA} working in the space of evolutionary bases are intrinsic characteristics of the periodic structure placed between two dielectric half-spaces. They totalize an impact of the structure on elementary excitations composing any incident signal $\vec{U}_1^i(g, t)$. Thus for $v_{q(1)}(0, t) = \delta_q^r \delta(t - \eta)$, where r is an integer and $\eta > 0$, we have $u_{p(1)'}(0, t) = S_{pr}^{AA}(t - \eta)$ and $u_{p(2)'}(0, t) = S_{pr}^{BA}(t - \eta)$. We use this example with an abstract nonphysical signal by methodological reasons, in order to associate the transformation operators' components $S_{pr}^{AA}(t - \tau)$ and $S_{pr}^{BA}(t - \tau)$ with an '*elementary excitation*'.

The operators S^{AA} and S^{BA} determine all the features of transient states on the upper and bottom boundaries of the layer enclosing the periodic structure. Secondary waves outgoing from these boundaries propagate freely in the regular Floquet channels A and B therewith undergoing deformations (see, for example, [6]). The space-time amplitudes $u_{p(j)}(z_j, t)$ of the partial components of these waves (the elements of the evolutionary bases of the signals $\vec{U}_j^s(g, t)$) vary differently for different values of p and j . These variations on any finite sections of the Floquet channels A and B are described by the diagonal *transporting operators* $Z_{0 \rightarrow z_1}^A$ and $Z_{0 \rightarrow z_2}^B$, which act according the rule:

$$u_{(j)}(z_j, t) = \{u_{p(j)}(z_j, t)\} = \left[Z_{0 \rightarrow z_1}^A \delta_j^1 + Z_{0 \rightarrow z_2}^B \delta_j^2 \right] [u_{(j)'}(0, \tau)]; \quad j = 1, 2. \tag{4.40}$$

The structure of the operators given by (4.40) can be detailed by the formula

$$u_{p(j)}(z_j, t) = -\frac{1}{\varepsilon_j} \int_0^{J_0} \left[\lambda_p \sqrt{\frac{(t - \tau)^2}{\varepsilon_j} - z_j^2} \right] \chi \left(\frac{t - \tau}{\sqrt{\varepsilon_j}} - z_j \right) u_{p(j)'}(0, \tau) d\tau; \tag{4.41}$$

$$t \geq 0, \quad z_j \geq 0, \quad p = 0, \pm 1, \pm 2, \dots, \quad j = 1, 2,$$

which reflects general properties of solutions of homogeneous problems (4.37), i.e. the solutions that satisfy zero initial conditions and are free from the components propagating in the direction of decreasing z_j . The derivation technique for (4.41) is discussed at length in [6, 14, 15].

4.6.2 Equations of the Operator Method in the Problems for Multilayered Periodic Structures

The operators S^{AA} and S^{BA} completely define properties of the periodic structure excited from the channel A. By analogy with (4.38) we can determine transformation operators S^{BB} and S^{AB} for evolutionary basis $v_{(2)}(z_2, t) = \{v_{p(2)}(z_2, t)\}_{p=-\infty}^{\infty}$ of the wave $\vec{U}_2^i(g, t) = \{\vec{E}_2^i(g, t), \vec{H}_2^i(g, t)\}$ incident onto the boundary $z_2 = 0$ from the channel B:

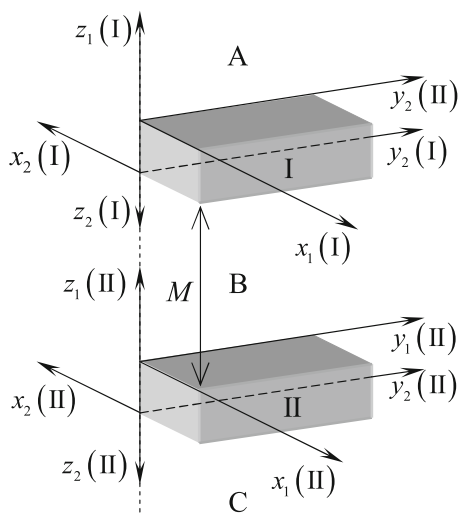
$$u_{p(j)}'(0, t) = \int_0^t \sum_{m=-\infty}^{\infty} \left[S_{pq}^{AB}(t - \tau) \delta_j^1 + S_{pq}^{BB}(t - \tau) \delta_j^2 \right] v_{q(2)}(0, \tau) d\tau; \tag{4.42}$$

$$t \geq 0, \quad p = 0, \pm 1, \pm 2, \dots, \quad j = 1, 2.$$

Let us construct an algorithm for calculating scattering characteristics of a multilayered structure consisting of two-dimensionally periodic gratings, for which the operators S^{AA} , S^{BA} , S_{pq}^{AB} , and S_{pq}^{BB} are known. Consider a double-layer structure, whose geometry is given in Fig. 4.4. Two semi-transparent periodic gratings I and II are separated by a dielectric layer of finite thickness M (here $\varepsilon = \varepsilon_2(\text{I}) = \varepsilon_1(\text{II})$) and placed between the upper and the bottom dielectric half-spaces with the permittivity $\varepsilon_1(\text{I})$ and $\varepsilon_2(\text{II})$, respectively. Let also a pulsed wave like (4.35) be incident onto the boundary $z_1(\text{I}) = 0$ from the Floquet channel A.

Retaining previously accepted notation (the evident changes are conditioned by the presence of two different gratings I and II), represent the solution of the corresponding initial boundary value problem in the regular domains A, B, and C

Fig. 4.4 Schematic drawing of a double-layered structure



in a symbolic form $U(\text{A}) = \sum_{p=-\infty}^{\infty} [v_{p(1)}(z_1(\text{I}), t) + u_{p(1)}(z_1(\text{I}), t)]\mu_p(x, y)$, $U(\text{B}) = \sum_{p=-\infty}^{\infty} [u_{p(2)}(z_2(\text{II}), t) + u_{p(1)}(z_1(\text{II}), t)]\mu_p(x, y)$, and $U(\text{C}) = \sum_{p=-\infty}^{\infty} u_{p(2)}(z_2(\text{II}), t)\mu_p(x, y)$.

The first terms here correspond to the waves propagating towards the domain C, while the second ones correspond to the waves propagating towards the domain A (Fig. 4.4). The set $\{\mu_p(x, y)\}_{p=-\infty}^{\infty}$ is formed by the functions $\mu_{nm}(x, y)$, $(n, m = 0, \pm 1, \pm 2, \dots)$ just as the set $\{\lambda_p\}_{p=-\infty}^{\infty}$ is composed from the values λ_{nm} , $(n, m = 0, \pm 1, \pm 2, \dots)$ (see Fig. 4.3).

By denoting

$$u_{(j)'}(\text{I}) \equiv \frac{\partial}{\partial z_j(\text{I})} u_{(j)}(z_j(\text{I}), t) \Big|_{z_j(\text{I})=0}, \quad u_{(j)}(\text{I}) = \{u_{p(j)}(z_j(\text{I}), t)\}_{z_j(\text{I})=0},$$

etc., and taking into account formulas (4.38)–(4.42), we construct the following system of operator equations:

$$\begin{cases} u_{(1)'}(\text{I}) = S^{\text{AA}}(\text{I})[v_{(1)}(\text{I})] + S^{\text{AB}}(\text{I})Z_{z_1(\text{II})=0 \rightarrow M}^{\text{B}}[u_{(1)'}(\text{II})] \\ u_{(2)'}(\text{I}) = S^{\text{BA}}(\text{I})[v_{(1)}(\text{I})] + S^{\text{BB}}(\text{I})Z_{z_1(\text{II})=0 \rightarrow M}^{\text{B}}[u_{(1)'}(\text{II})] \\ u_{(1)'}(\text{II}) = S^{\text{BB}}(\text{II})Z_{z_2(\text{I})=0 \rightarrow M}^{\text{B}}[u_{(2)'}(\text{I})] \\ u_{(2)'}(\text{II}) = S^{\text{CB}}(\text{II})Z_{z_2(\text{I})=0 \rightarrow M}^{\text{B}}[u_{(2)'}(\text{I})] \end{cases} \quad (4.43)$$

Equations (4.43) clearly represent step-by-step response of the complex structure on the excitation by the signal $\vec{U}_1^i(g, t)$ with the evolutionary basis $v_{(1)}(z_1(\text{I}), t) = \{v_{p(1)}(z_1(\text{I}), t)\}_{p=-\infty}^{\infty}$ (or simply $v_{(1)}(\text{I})$). Thus, for example, the first equation can be interpreted as follows. The signal $u_{(1)}(\text{I})$ (the secondary field in A) is a sum of two signals, where the first signal is a result of the reflection of the incident signal $v_{(1)}(\text{I})$ by the grating I, while another one is determined by the signal $u_{(1)}(\text{II})$ being deformed during propagation in the channel B and interaction with the grating I.

By method of elimination the system (4.43) is reduced to the operator equation of the second kind

$$u_{(2)'}(\text{I}) = S^{\text{BA}}(\text{I})[v_{(1)}(\text{I})] + S^{\text{BB}}(\text{I})Z_{z_1(\text{II})=0 \rightarrow M}^{\text{B}} S^{\text{BB}}(\text{II})Z_{z_2(\text{I})=0 \rightarrow M}^{\text{B}}[u_{(2)'}(\text{I})] \quad (4.44)$$

and some formulas for calculating the electromagnetic field components in all regions of the two-layered structure. The observation time t for the unknown function $u_{(2)'}(\text{I})$ from the left-hand side of (4.44) is strictly greater of any moment of time τ for the function $u_{(2)'}(\text{I})$ in the right-hand side of the equation (owing to finiteness of wave velocity). Therefore (4.44) can be inverted explicitly in the framework of standard algorithm of *step-by-step progression through time layers*. Upon realization of this scheme and calculation of the boundary operators by

(4.38), (4.42), the two-layered structure can be used as an ‘elementary’ unit of more complex structures.

Turning back to (4.38)–(4.42), we see that the operators entering these equations act differently than their analogues in the frequency domain, where the boundary operators relate a pair ‘field \rightarrow field’. Reasoning from the structure of the transport operators $Z_{0 \rightarrow z_1}^A$ and $Z_{0 \rightarrow z_2}^B$ (formulas (4.40) and (4.41)), we relate a pair ‘field \rightarrow directional derivative with respect to the propagation direction’ to increase numerical efficiency of the corresponding computational algorithms.

4.7 Some Important Properties of Steady-State Fields in the Rectangular Floquet Channel

4.7.1 Excitation by a *TM*-Wave

Let a grating (Fig. 4.1) be excited from the domain A by a pulsed *TM*-wave

$$\vec{U}^i(g, t) = \vec{U}_{pq(E)}^i(g, t) : E_z^i(g, t) = v_{pq(z,E)}(z, t) \mu_{pq}(x, y)$$

and the region Q_L is free from the sources $\vec{j}(g, t)$, $\vec{\varphi}_E(g)$, and $\vec{\varphi}_H(g)$. The field generated in the domains A and B is determined completely by its longitudinal components. They can be represented in the form of (4.31), (4.32). Define steady-state fields $\left\{ \vec{\tilde{E}}(g, k), \vec{\tilde{H}}(g, k) \right\}$ (see formula (4.33) with $\text{Im } k = 0$) corresponding to the pulsed fields $\left\{ \vec{E}^i, \vec{H}^i \right\}$, $\left\{ \vec{E}^s, \vec{H}^s \right\}$ in A and the pulsed field $\left\{ \vec{E}, \vec{H} \right\}$ in B, by their z -components [7]

$$\left\{ \begin{array}{l} \tilde{E}_z^i(g, k) \\ \tilde{H}_z^i(g, k) \end{array} \right\} = \left\{ \begin{array}{l} \tilde{v}_{pq(z,E)}(k) \\ 0 \end{array} \right\} e^{-i\Gamma_{pq}(z-L)} \mu_{pq}(x, y); \quad g \in \bar{A}, \quad (4.45)$$

$$\left\{ \begin{array}{l} \tilde{E}_z^s(g, k) \\ \tilde{H}_z^s(g, k) \end{array} \right\} = \sum_{n,m=-\infty}^{\infty} \left\{ \begin{array}{l} \tilde{u}_{nm(z,E)}^+(k) \\ \tilde{u}_{nm(z,H)}^+(k) \end{array} \right\} e^{i\Gamma_{nm}(z-L)} \mu_{nm}(x, y); \quad g \in \bar{A}, \quad (4.46)$$

$$\left\{ \begin{array}{l} \tilde{E}_z(g, k) \\ \tilde{H}_z(g, k) \end{array} \right\} = \sum_{n,m=-\infty}^{\infty} \left\{ \begin{array}{l} \tilde{u}_{nm(z,E)}^-(k) \\ \tilde{u}_{nm(z,H)}^-(k) \end{array} \right\} e^{-i\Gamma_{nm}(z+L)} \mu_{nm}(x, y); \quad g \in \bar{B}, \quad (4.47)$$

where the following notation is used: $\tilde{v}_{pq(z,E)}(k) \leftrightarrow v_{pq(z,E)}(L, t)$, $\tilde{u}_{nm(z,E \text{ or } H)}^\pm(k) \leftrightarrow u_{nm(z,E \text{ or } H)}^\pm(\pm L, t)$, and $\Gamma_{nm} = (k^2 - \lambda_{nm}^2)^{1/2}$; $\text{Re } \Gamma_{nm} \text{Re } k \geq 0$, $\text{Im } \Gamma_{nm} \geq 0$.

The amplitudes $\tilde{u}_{nm(z,E \text{ or } H)}^\pm(k)$ form the system of the so-called scattering coefficients of the grating, namely, the *reflection coefficients*

$$R_{pq(E)}^{nm(H)} = \frac{\tilde{u}_{nm(z,H)}^+(k)}{\tilde{v}_{pq(z,E)}(k)}, \quad R_{pq(E)}^{nm(E)} = \frac{\tilde{u}_{nm(z,E)}^+(k)}{\tilde{v}_{pq(z,E)}(k)}; \quad n, m = 0, \pm 1, \pm 2, \dots, \quad (4.48)$$

specifying efficiency of transformation of pq th harmonic of a monochromatic TM -wave into nm th harmonics of the scattered field $\{\tilde{E}^s, \tilde{H}^s\}$ in the reflection zone, and the *transmission coefficients*

$$T_{pq(E)}^{nm(H)} = \frac{\tilde{u}_{nm(z,H)}^-(k)}{\tilde{v}_{pq(z,E)}(k)}, \quad T_{pq(E)}^{nm(E)} = \frac{\tilde{u}_{nm(z,E)}^-(k)}{\tilde{v}_{pq(z,E)}(k)}; \quad n, m = 0, \pm 1, \pm 2, \dots, \quad (4.49)$$

determining the efficiency of excitation of the transmitted harmonics in the domain B.

These coefficients are related by the *energy balance equations*

$$\begin{aligned} & \sum_{n,m=-\infty}^{\infty} \frac{1}{\lambda_{nm}^2} \left[\left(|R_{pq(E)}^{nm(E)}|^2 + |T_{pq(E)}^{nm(E)}|^2 \right) \pm \eta_0^2 \left(|R_{pq(E)}^{nm(H)}|^2 + |T_{pq(E)}^{nm(H)}|^2 \right) \right] \begin{Bmatrix} \text{Re } \Gamma_{nm} \\ \text{Im } \Gamma_{nm} \end{Bmatrix} \\ &= \frac{1}{\lambda_{pq}^2} \begin{Bmatrix} \text{Re } \Gamma_{pq} + 2 \text{Im } \Gamma_{pq} \text{Im } R_{pq(E)}^{pq(E)} \\ \text{Im } \Gamma_{pq} - 2 \text{Re } \Gamma_{pq} \text{Im } R_{pq(E)}^{pq(E)} \end{Bmatrix} \mp \frac{1}{\varepsilon_0} \begin{Bmatrix} W_1 \\ W_2 \end{Bmatrix}; \quad p, q = 0, \pm 1, \pm 2, \dots, \end{aligned} \quad (4.50)$$

$$\begin{aligned} W_1 &= \frac{\varepsilon_0 \eta_0}{k} \int_{Q_L} \sigma(g, k) \left| \tilde{E}(g, k) \right|^2 dg, \\ W_2 &= \int_{Q_L} \left[\mu_0 \mu(g, k) \left| \tilde{H}(g, k) \right|^2 - \varepsilon_0 \varepsilon(g, k) \left| \tilde{E}(g, k) \right|^2 \right] dg. \end{aligned}$$

They follow from the *complex power theorem (Poynting theorem)* in the integral form [12]

$$\begin{aligned} \oint_{S_L} \left(\tilde{E} \times \tilde{H}^* \right) \cdot \vec{ds} &= \int_{Q_L} \text{div} \left(\tilde{E} \times \tilde{H}^* \right) dg \\ &= ik\eta_0 \int_{Q_L} \mu \left| \tilde{H} \right|^2 dg - \frac{ik}{\eta_0} \int_{Q_L} \varepsilon \left| \tilde{E} \right|^2 dg - \int_{Q_L} \sigma \left| \tilde{E} \right|^2 dg, \end{aligned} \quad (4.51)$$

where $\varepsilon(g, k) - 1 = \tilde{\chi}_\varepsilon(g, k) \leftrightarrow \chi_\varepsilon(g, t)$, $\mu(g, k) - 1 = \tilde{\chi}_\mu(g, k) \leftrightarrow \chi_\mu(g, t)$, $\sigma(g, k) = \tilde{\chi}_\sigma(g, k) \leftrightarrow \chi_\sigma(g, t)$, and \vec{ds} is the vector element of the surface S_L bounding the domain Q_L . Equations (4.50), (4.51) have been derived starting from

the following boundary value problem for a diffraction grating illuminated by a plane TM -wave $\tilde{U}_{pq(E)}^i(g, k) : \tilde{E}_z^i(g, k) = \exp[-i\Gamma_{pq}(z-L)]\mu_{pq}(x, y)$:

$$\left\{ \begin{array}{l} \eta_0 \text{rot} \tilde{H}(g, k) = -ik\bar{\varepsilon}(g, k)\tilde{E}(g, k), \\ \text{rot} \tilde{E}(g, k) = ik\eta_0\mu(g, k)\tilde{H}(g, k); \quad g \in Q_L \\ D\left[\tilde{E}\left(\tilde{H}\right)\right](l_x, y) = e^{2\pi i\Phi_x} D\left[\tilde{E}\left(\tilde{H}\right)\right](0, y) \quad \text{for } 0 \leq y \leq l_y \quad \text{and} \\ D\left[\tilde{E}\left(\tilde{H}\right)\right](x, l_y) = e^{2\pi i\Phi_y} D\left[\tilde{E}\left(\tilde{H}\right)\right](x, 0) \quad \text{for } 0 \leq x \leq l_x; \quad |z| < L \\ \left.\tilde{E}_{tg}^i(g, k)\right|_{g \in S} = 0, \quad \left.\tilde{H}_{nr}^i(g, k)\right|_{g \in S} = 0, \end{array} \right. \quad (4.52a)$$

$$\left\{ \begin{array}{l} \tilde{E}_z(g, k) \\ \tilde{H}_z(g, k) \end{array} \right\} = \left\{ \begin{array}{l} 1 \\ 0 \end{array} \right\} e^{-i\Gamma_{pq}(z-L)}\mu_{pq}(x, y) + \sum_{n,m=-\infty}^{\infty} \left\{ \begin{array}{l} R_{pq(E)}^{nm(E)}(k) \\ R_{pq(E)}^{nm(H)}(k) \end{array} \right\} \\ \times e^{i\Gamma_{nm}(z-L)}\mu_{nm}(x, y); \quad g \in \bar{A}, \quad (4.52b)$$

$$\left\{ \begin{array}{l} \tilde{E}_z(g, k) \\ \tilde{H}_z(g, k) \end{array} \right\} = \sum_{n,m=-\infty}^{\infty} \left\{ \begin{array}{l} T_{pq(E)}^{nm(E)}(k) \\ T_{pq(E)}^{nm(H)}(k) \end{array} \right\} e^{-i\Gamma_{nm}(z+L)}\mu_{nm}(x, y); \quad g \in \bar{B}. \quad (4.52c)$$

When deriving (4.50), we have also used the equations relating z -components of the eigenmode of the Floquet channel

$$\tilde{U}(g, k) : \tilde{E}_z(g, k) = Ae^{\pm i\Gamma z}\mu(x, y) \quad \text{and} \quad \tilde{H}_z(g, k) = Be^{\pm i\Gamma z}\mu(x, y)$$

(subscripts nm are omitted) with its longitudinal components:

$$\begin{aligned} \tilde{E}_x &= -\frac{\beta k \eta_0}{\lambda^2} \tilde{H}_z \mp \frac{\alpha \Gamma}{\lambda^2} \tilde{E}_z, & \tilde{E}_y &= \frac{\alpha k \eta_0}{\lambda^2} \tilde{H}_z \mp \frac{\beta \Gamma}{\lambda^2} \tilde{E}_z, \\ \tilde{H}_x &= \mp \frac{\alpha \Gamma}{\lambda^2} \tilde{H}_z + \frac{\beta k}{\eta_0 \lambda^2} \tilde{E}_z, & \tilde{H}_y &= \mp \frac{\beta \Gamma}{\lambda^2} \tilde{H}_z - \frac{\alpha k}{\eta_0 \lambda^2} \tilde{E}_z. \end{aligned} \quad (4.53)$$

Here, $\bar{\varepsilon}(g, k) = \varepsilon(g, k) + i\eta_0\sigma(g, k)/k$, $\mu(x, y) = (l_x l_y)^{-1/2} \exp(i\alpha x) \exp(i\beta y)$, $\Gamma = \sqrt{k^2 - \lambda^2}$, and $\lambda^2 = \alpha^2 + \beta^2$.

According to the *Lorentz lemma* [12], the fields $\{\tilde{E}^{(1)}, \tilde{H}^{(1)}\}$ and $\{\tilde{E}^{(2)}, \tilde{H}^{(2)}\}$, resulting from the interaction of a grating with two plane TM -waves

$$\tilde{U}_{pq(E)}^{i(1)}(g, k) : \tilde{E}_z^{i(1)}(g, k) = \exp[-i\Gamma_{pq}(\Phi_x, \Phi_y)(z-L)]\mu_{pq}(x, y, \Phi_x, \Phi_y)$$

and

$$\begin{aligned} \tilde{U}_{-r,-s(E)}^{i(2)}(g, k) : \tilde{E}_z^{i(2)}(g, k) &= \exp[-i\Gamma_{-r,-s}(-\Phi_x, -\Phi_y)(z-L)] \\ &\mu_{-r,-s}(x, y, -\Phi_x, -\Phi_y), \end{aligned}$$

satisfy the following equation

$$\oint_{S_L} \left(\tilde{E}^{(1)} \times \tilde{H}^{(2)} - \tilde{E}^{(2)} \times \tilde{H}^{(1)} \right) \cdot \vec{ds} = 0. \quad (4.54)$$

From (4.54), using (4.52b), (4.52c), and (4.53), we obtain

$$\begin{aligned} \frac{R_{pq(E)}^{rs(E)}(\Phi_x, \Phi_y) \lambda_{p,q}^2(\Phi_x, \Phi_y)}{\Gamma_{pq}(\Phi_x, \Phi_y)} &= \frac{R_{-r,-s(E)}^{-p,-q(E)}(-\Phi_x, -\Phi_y) \lambda_{-r,-s}^2(-\Phi_x, -\Phi_y)}{\Gamma_{-r,-s}(-\Phi_x, -\Phi_y)}; \\ p, q, r, s &= 0, \pm 1, \pm 2, \dots \end{aligned} \quad (4.55)$$

—the *reciprocity relations*, which are of considerable importance in the physical analysis of wave scattering by periodic structures as well as when testing numerical algorithms for boundary value problems (4.52a, 4.52b, 4.52c).

Assume now that the first wave

$$\begin{aligned} \tilde{U}_{pq(E)}^{i(1)}(g, k) : \tilde{E}_z^{i(1)}(g, k) &= \exp[-i\Gamma_{pq}(\Phi_x, \Phi_y)(z-L)] \mu_{pq}(x, y, \Phi_x, \Phi_y) \\ &= \tilde{U}_{pq(E)}^{i(1)}(g, k, A) \end{aligned}$$

be incident on the grating from the domain A, as in the case considered above, while another wave

$$\begin{aligned} \tilde{U}_{-r,-s(E)}^{i(2)}(g, k, B) : \tilde{E}_z^{i(2)}(g, k) &= \exp[i\Gamma_{-r,-s}(-\Phi_x, -\Phi_y)(z+L)] \\ &\mu_{-r,-s}(x, y, -\Phi_x, -\Phi_y) \end{aligned}$$

is incident from B. Both of these waves satisfy (4.54), whence we have

$$\begin{aligned} \frac{T_{pq(E)}^{rs(E)}(\Phi_x, \Phi_y, A) \lambda_{p,q}^2(\Phi_x, \Phi_y)}{\Gamma_{pq}(\Phi_x, \Phi_y)} &= \frac{T_{-r,-s(E)}^{-p,-q(E)}(-\Phi_x, -\Phi_y, B) \lambda_{-r,-s}^2(-\Phi_x, -\Phi_y)}{\Gamma_{-r,-s}(-\Phi_x, -\Phi_y)}; \\ p, q, r, s &= 0, \pm 1, \pm 2, \dots \end{aligned} \quad (4.56)$$

4.7.2 Excitation by a TE-Wave

Let a grating be excited from the domain A by a pulsed TE-wave

$$\vec{U}^i(g, t) = \vec{U}_{pq(H)}^i(g, t) : H_z^i(g, t) = v_{pq(z, H)}(z, t) \mu_{pq}(x, y)$$

and the region Q_L is free from the sources $\vec{j}(g, t)$, $\vec{\varphi}_E(g)$, and $\vec{\varphi}_H(g)$. The field generated in the domains A and B is determined completely by its longitudinal components. They can be represented in the form of (4.31), (4.32). Define steady-state fields $\{\vec{\tilde{E}}(g, k), \vec{\tilde{H}}(g, k)\}$ corresponding to the pulsed fields $\{\vec{E}^i, \vec{H}^i\}$, $\{\vec{E}^s, \vec{H}^s\}$ in A and the pulsed field $\{\vec{E}, \vec{H}\}$ in B by their z -components as was done for the TM-case (see (4.45)–(4.47)). Introduce the scattering coefficients $R_{pq(H)}^{nm(E)}$, $R_{pq(H)}^{nm(H)}$, $T_{pq(H)}^{nm(E)}$, and $T_{pq(H)}^{nm(H)}$ by the relations like (4.48), (4.49). These coefficients can be determined from the problem

$$\left\{ \begin{array}{l} \eta_0 \text{rot} \vec{\tilde{H}}(g, k) = -ik \vec{\tilde{E}}(g, k) \vec{\tilde{E}}(g, k), \\ \text{rot} \vec{\tilde{E}}(g, k) = ik \eta_0 \mu(g, k) \vec{\tilde{H}}(g, k); \quad g \in Q_L \\ D \left[\vec{\tilde{E}}(\vec{\tilde{H}}) \right] (l_x, y) = e^{2\pi i \Phi_x} D \left[\vec{\tilde{E}}(\vec{\tilde{H}}) \right] (0, y) \quad \text{for } 0 \leq y \leq l_y \quad \text{and} \\ D \left[\vec{\tilde{E}}(\vec{\tilde{H}}) \right] (x, l_y) = e^{2\pi i \Phi_y} D \left[\vec{\tilde{E}}(\vec{\tilde{H}}) \right] (x, 0) \quad \text{for } 0 \leq x \leq l_x; \quad |z| < L \\ \vec{\tilde{E}}_{tg}(g, k)|_{g \in S} = 0, \quad \vec{\tilde{H}}_{nr}(g, k)|_{g \in S} = 0, \end{array} \right. \quad (4.57a)$$

$$\left\{ \begin{array}{l} \vec{\tilde{E}}_z(g, k) \\ \vec{\tilde{H}}_z(g, k) \end{array} \right\} = \left\{ \begin{array}{l} 0 \\ 1 \end{array} \right\} e^{-i\Gamma_{pq}(z-L)} \mu_{pq}(x, y) + \sum_{n, m=-\infty}^{\infty} \left\{ \begin{array}{l} R_{pq(H)}^{nm(E)}(k) \\ R_{pq(H)}^{nm(H)}(k) \end{array} \right\} \\ \times e^{i\Gamma_{nm}(z-L)} \mu_{nm}(x, y); \quad g \in \bar{A}, \quad (4.57b)$$

$$\left\{ \begin{array}{l} \vec{\tilde{E}}_z(g, k) \\ \vec{\tilde{H}}_z(g, k) \end{array} \right\} = \sum_{n, m=-\infty}^{\infty} \left\{ \begin{array}{l} T_{pq(H)}^{nm(E)}(k) \\ T_{pq(H)}^{nm(H)}(k) \end{array} \right\} e^{-i\Gamma_{nm}(z+L)} \mu_{nm}(x, y); \quad g \in \bar{B} \quad (4.57c)$$

and satisfy the following relations, which are corollaries from the Poynting theorem and the Lorentz lemma:

$$\begin{aligned}
& \sum_{n,m=-\infty}^{\infty} \frac{1}{\lambda_{nm}^2} \left[\left(\left| R_{pq(H)}^{nm(H)} \right|^2 + \left| T_{pq(H)}^{nm(H)} \right|^2 \right) \pm \frac{1}{\eta_0^2} \left(\left| R_{pq(H)}^{nm(E)} \right|^2 + \left| T_{pq(H)}^{nm(E)} \right|^2 \right) \right] \begin{Bmatrix} \operatorname{Re} \Gamma_{nm} \\ \operatorname{Im} \Gamma_{nm} \end{Bmatrix} \\
&= \frac{1}{\lambda_{pq}^2} \begin{Bmatrix} \operatorname{Re} \Gamma_{pq} + 2 \operatorname{Im} \Gamma_{pq} \operatorname{Im} R_{pq(H)}^{pq(H)} \\ \operatorname{Im} \Gamma_{pq} - 2 \operatorname{Re} \Gamma_{pq} \operatorname{Im} R_{pq(H)}^{pq(H)} \end{Bmatrix} - \frac{1}{\mu_0} \begin{Bmatrix} W_1 \\ W_2 \end{Bmatrix}; \quad p, q = 0, \pm 1, \pm 2, \dots
\end{aligned} \tag{4.58}$$

and

$$\frac{R_{pq(H)}^{rs(H)}(\Phi_x, \Phi_y) \lambda_{p,q}^2(\Phi_x, \Phi_y)}{\Gamma_{pq}(\Phi_x, \Phi_y)} = \frac{R_{-r,-s(H)}^{-p,-q(H)}(-\Phi_x, -\Phi_y) \lambda_{-r,-s}^2(-\Phi_x, -\Phi_y)}{\Gamma_{-r,-s}(-\Phi_x, -\Phi_y)}; \tag{4.59}$$

$$p, q, r, s = 0, \pm 1, \pm 2, \dots$$

$$\frac{T_{pq(H)}^{rs(H)}(\Phi_x, \Phi_y, A) \lambda_{p,q}^2(\Phi_x, \Phi_y)}{\Gamma_{pq}(\Phi_x, \Phi_y)} = \frac{T_{-r,-s(H)}^{-p,-q(H)}(-\Phi_x, -\Phi_y, B) \lambda_{-r,-s}^2(-\Phi_x, -\Phi_y)}{\Gamma_{-r,-s}(-\Phi_x, -\Phi_y)};$$

$$p, q, r, s = 0, \pm 1, \pm 2, \dots$$

$$\tag{4.60}$$

4.7.3 General Properties of the Grating's Secondary Field

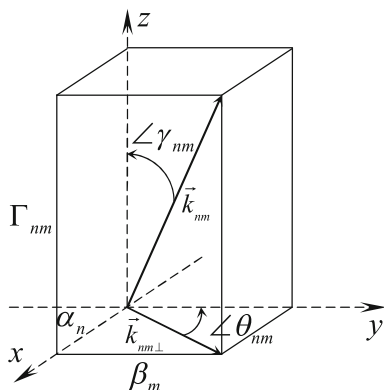
Let now k be a real positive frequency parameter, and let an arbitrary semi-transparent grating (Fig. 4.1) be excited from the domain A by a homogeneous *TM*- or *TE*-wave

$$\tilde{U}_{pq(E \text{ or } H)}^i(g, k) : \{ \tilde{E}_z^i(g, k) \text{ or } \tilde{H}_z^i(g, k) \} = e^{-i\Gamma_{pq}(z-L)} \mu_{pq}(x, y); \quad p, q : \operatorname{Im} \Gamma_{pq} = 0. \tag{4.61}$$

The terms of the infinite series in (4.52b), (4.52c) and (4.57b), (4.57c) are z -components of nm th harmonics of the scattered field for the domains A and B. The complex amplitudes $R_{pq(E \text{ or } H)}^{nm(E \text{ or } H)}$ and $T_{pq(E \text{ or } H)}^{nm(E \text{ or } H)}$ are the functions of k , Φ_x , Φ_y , as well as of the geometry and material parameters of the grating.

Every harmonic for which $\operatorname{Im} \Gamma_{nm} = 0$ and $\operatorname{Re} \Gamma_{nm} > 0$ is a homogeneous plane wave propagating away from the grating along the vector \vec{k}_{nm} : $k_x = \alpha_n$, $k_y = \beta_m$, $k_z = \Gamma_{nm}$ (in the domain A; see Fig. 4.5) or $k_z = -\Gamma_{nm}$ (in the domain B). The frequencies k such that $\Gamma_{nm}(k) = 0$ ($k = k_{nm}^\pm = \pm |\lambda_{nm}|$) are known as *threshold frequencies or sliding points* [1–6]. At those points, damped spatial harmonics of

Fig. 4.5 On determination of propagation directions for spatial harmonics of the field formed by a two-dimensionally periodic structure



order nm with $\text{Im } \Gamma_{nm} > 0$ are transformed into propagating homogeneous plane waves.

It is obvious that the propagation directions \vec{k}_{nm} of homogeneous harmonics of the secondary field depend on their order nm , on the values of k and on the directing vector of the incident wave \vec{k}_{pq}^i : $k_x^i = \alpha_p$, $k_y^i = \beta_q$, $k_z^i = -\Gamma_{pq}$.

According to (4.50) and (4.58), we can write the following formulas for the values, which determine the ‘energy content’ of harmonics, or in other words, the relative part of the energy directed by the structure into the relevant spatial radiation channel:

$$\begin{aligned} (WR)_{pq}^{nm} &= \left(|R_{pq(E)}^{nm(E)}|^2 + \eta_0^2 |R_{pq(E)}^{nm(H)}|^2 \right) \frac{\text{Re } \Gamma_{nm} \lambda_{pq}^2}{\lambda_{nm}^2 \Gamma_{pq}} = (WR)_{pq(E)}^{nm(E)} + (WR)_{pq(E)}^{nm(H)}, \\ (WT)_{pq}^{np} &= \left(|T_{pq(E)}^{nm(E)}|^2 + \eta_0^2 |T_{pq(E)}^{nm(H)}|^2 \right) \frac{\text{Re } \Gamma_{nm} \lambda_{pq}^2}{\lambda_{nm}^2 \Gamma_{pq}} = (WT)_{pq(E)}^{np(E)} + (WT)_{pq(E)}^{np(H)} \end{aligned} \quad (4.62)$$

(for *TM*-case) and

$$\begin{aligned} (WR)_{pq}^{nm} &= \left(|R_{pq(H)}^{nm(H)}|^2 + \frac{1}{\eta_0^2} |R_{pq(H)}^{nm(E)}|^2 \right) \frac{\text{Re } \Gamma_{nm} \lambda_{pq}^2}{\lambda_{nm}^2 \Gamma_{pq}} = (WR)_{pq(H)}^{nm(H)} + (WR)_{pq(H)}^{nm(E)}, \\ (WT)_{pq}^{np} &= \left(|T_{pq(H)}^{nm(H)}|^2 + \frac{1}{\eta_0^2} |T_{pq(H)}^{nm(E)}|^2 \right) \frac{\text{Re } \Gamma_{nm} \lambda_{pq}^2}{\lambda_{nm}^2 \Gamma_{pq}} = (WT)_{pq(H)}^{nm(H)} + (WT)_{pq(H)}^{nm(E)} \end{aligned} \quad (4.63)$$

(for *TE*-case). The channel corresponding to the nm th harmonic will be named ‘open’ if $\text{Im } \Gamma_{nm} = 0$. The regime with a single open channel ($nm = pq$) will be called the *single-mode regime*.

Since $|\vec{k}_{pq}^i| = |\vec{k}_{nm}| = k$, the nm th harmonic of the secondary field in the reflection zone propagates in opposition to the incident wave only if $\alpha_n = -\alpha_p$ and $\beta_m = -\beta_q$ or, in other notation, if

$$n = -2\Phi_x - p \quad \text{and} \quad m = -2\Phi_y - q. \tag{4.64}$$

Generation of the nonspecularly reflected mode of this kind is named *auto-collimation*.

Not all of the amplitudes $R_{pq(E \text{ or } H)}^{nm(E \text{ or } H)}$ or $T_{pq(E \text{ or } H)}^{nm(E \text{ or } H)}$ are of significance for the physical analysis. In the far-field zone, the secondary field is formed only by the *propagating harmonics* of the orders nm such that $\text{Re } \Gamma_{nm} \geq 0$. However, the radiation field in the immediate proximity of the grating requires consideration of the contribution of *damped harmonics* ($n, m : \text{Im } \Gamma_{nm} > 0$). Moreover, in some situations (resonance mode) this contribution is the dominating one [6].

4.7.4 Corollaries of the Reciprocity Relations and the Energy Conservation Law

Let us formulate several corollaries of the relations (4.50), (4.55), (4.56), and (4.58)–(4.60) basing on the results presented in [3, 7] for one-dimensionally periodic gratings and assuming that $\varepsilon(g, k) \geq 0$, $\mu(g, k) \geq 0$, and $\sigma(g, k) \geq 0$.

- The upper lines in (4.50) and (4.58) represent the energy conservation law for propagating waves. If $\text{Im } \Gamma_{pq} = 0$, the energy of the scattered field is clearly related to the energy of the incident wave. The energy of the wave $\tilde{U}_{pq(E \text{ or } H)}^i(g, k)$ is partially absorbed by the grating (only if $W_1 \neq 0$), and the remaining part is distributed between spatial *TM*- and *TE*-harmonics propagating in the domains A and B (it is reradiating into the directions $z = \pm\infty$). If a plane inhomogeneous wave be incident on the grating ($\text{Im } \Gamma_{pq} > 0$), the total energy is defined by the imaginary part of the reflection coefficient $R_{pq(E \text{ or } H)}^{pq(E \text{ or } H)}$, which in this case is nonnegative.
- The relations in the bottom lines in (4.50), (4.58) limit the values of $\sum_{n,m=-\infty}^{\infty} \left| R_{pq(E)}^{nm(E)} \right|^2 \lambda_{nm}^{-2} \text{Im } \Gamma_{nm}$, $\sum_{n,m=-\infty}^{\infty} \left| T_{pq(E)}^{nm(E)} \right|^2 \lambda_{nm}^{-2} \text{Im } \Gamma_{nm}$, etc. and determine thereby the class of infinite sequences

$$\bar{l}_2 = \left\{ a = \{a_{nm}\}_{n,m=-\infty}^{\infty} : \sum_{n,m=-\infty}^{\infty} \frac{|a_{nm}|^2}{\sqrt{n^2 + m^2}} < \infty \right\},$$

or *energetic space*, to which amplitudes of the scattered harmonics $R_{pq(E)}^{nm(E)}$, $T_{pq(E)}^{nm(E)}$, etc. belong.

- It follows from (4.55), (4.56), (4.59), and (4.60) that for all semi-transparent and reflecting gratings we can write

$$\begin{aligned} (WR)_{00(E \text{ or } H)}^{00(E \text{ or } H)}(\Phi_x, \Phi_y) &= (WR)_{00(E \text{ or } H)}^{00(E \text{ or } H)}(-\Phi_x, -\Phi_y), \\ (WT)_{00(E \text{ or } H)}^{00(E \text{ or } H)}(\Phi_x, \Phi_y, \mathbf{A}) &= (WT)_{00(E \text{ or } H)}^{00(E \text{ or } H)}(-\Phi_x, -\Phi_y, \mathbf{B}). \end{aligned} \quad (4.65)$$

The first equation in (4.65) proves that the efficiency of transformation of the *TM*- or *TE*-wave into the specular reflected wave of the same polarization remains unchanged if the grating is rotated in the plane about *z*-axis through 180°. The efficiency of transformation into the principal transmitted wave of the same polarizations does not also vary with the grating rotation about the axis lying in the plane and being normal to the vector \vec{k}_{00} (Fig. 4.5).

- When $r = s = p = q = 0$, we derive from (4.55), (4.56), (4.59), and (4.60) that

$$\begin{aligned} R_{00(E \text{ or } H)}^{00(E \text{ or } H)}(\Phi_x, \Phi_y) &= R_{00(E \text{ or } H)}^{00(E \text{ or } H)}(-\Phi_x, -\Phi_y), \\ T_{00(E \text{ or } H)}^{00(E \text{ or } H)}(\Phi_x, \Phi_y, \mathbf{A}) &= T_{00(E \text{ or } H)}^{00(E \text{ or } H)}(-\Phi_x, -\Phi_y, \mathbf{B}). \end{aligned} \quad (4.66)$$

That means that even if a semi-transparent or reflecting grating is non symmetric with respect to any plane, the reflection and transmission coefficients entering (4.66) do not depend on the proper changes in the angles of incidence of the primary wave.

- Relations (4.50), (4.55) allow the following regularities to be formulated for ideal ($\sigma(g, k) \equiv 0$) asymmetrical reflecting gratings. Let the parameters k , Φ_x , and Φ_y be such that $\text{Re } \Gamma_{00}(\Phi_x, \Phi_y) > 0$ and $\text{Re } \Gamma_{nm}(\Phi_x, \Phi_y) = 0$ for $n, m \neq 0$. If the incident wave is an inhomogeneous plane wave $\vec{U}_{\pm p, \pm q(E)}^i(g, k, \pm \Phi_x, \pm \Phi_y)$, then

$$\begin{aligned} &\left(\left| R_{\pm p, \pm q(E)}^{00(E)}(\pm \Phi_x, \pm \Phi_y) \right|^2 + n_0^2 \left| R_{\pm p, \pm q(E)}^{00(H)}(\pm \Phi_x, \pm \Phi_y) \right|^2 \right) \frac{\text{Re } \Gamma_{00}(\pm \Phi_x, \pm \Phi_y)}{\lambda_{00}^2(\pm \Phi_x, \pm \Phi_y)} \\ &= 2 \text{Im } R_{\pm p, \pm q(E)}^{\pm p, \pm q(E)}(\pm \Phi_x, \pm \Phi_y) \frac{\text{Im } \Gamma_{\pm p, \pm q}(\pm \Phi_x, \pm \Phi_y)}{\lambda_{\pm p, \pm q}^2(\pm \Phi_x, \pm \Phi_y)}. \end{aligned} \quad (4.67)$$

Since $R_{pq(E)}^{pq(E)}(\Phi_x, \Phi_y) = R_{-p, -q(E)}^{-p, -q(E)}(-\Phi_x, -\Phi_y)$, we derive from (4.67)

$$\begin{aligned} \left| R_{p,q(E)}^{00(E)}(\Phi_x, \Phi_y) \right|^2 + \eta_0^2 \left| R_{p,q(E)}^{00(H)}(\Phi_x, \Phi_y) \right|^2 = & \left| R_{-p,-q(E)}^{00(E)}(-\Phi_x, -\Phi_y) \right|^2 \\ & + \eta_0^2 \left| R_{-p,-q(E)}^{00(H)}(-\Phi_x, -\Phi_y) \right|^2. \end{aligned} \quad (4.68)$$

It is easy to realize a physical meaning of the equation (4.68) and of similar relation for TE -case, which may be of interest for diffraction electronics. If a grating is excited by a damped harmonic, the efficiency of transformation into the unique propagating harmonic of spatial spectrum is unaffected by the structure rotation in the plane xOy about z -axis through 180° .

The above stated corollaries are especially useful for testing numerical results and making their physical interpretation easier. The use of these corollaries may considerably reduce the amount of calculations.

4.8 Elements of Spectral Theory for Two-Dimensionally Periodic Gratings

The spectral theory of gratings studies singularities of analytical continuation of solutions of boundary value problems formulated in the frequency domain (see, for example, problems (4.53) and (4.57a, 4.57b, 4.57c)) into the domain of *complex-valued (non-physical) values of real parameters* (like frequency, propagation constants, etc.) and the role of these singularities in resonant and anomalous modes in monochromatic and pulsed wave scattering. The fundamental results of this theory for one-dimensionally periodic gratings are presented in [4, 6, 7]. We discuss the elements of the spectral theory for two-dimensionally periodic structures, which follow immediately from the results obtained in the previous sections. The frequency k acts as a spectral parameter; a two-dimensionally periodic grating is considered as an *open periodic resonator*.

4.8.1 Canonical Green Function

Let a solution $\tilde{G}_0(g, p, k)$ of the scalar problem

$$\left\{ \begin{aligned} & [\Delta_g + k^2] [\tilde{G}_0(g, p, k)] = \delta(g - p); g = \{x_g, y_g, z_g\} \in \mathbf{R}, \quad p = \{x_p, y_p, z_p\} \in \mathbf{Q}_L \\ & D[\tilde{G}_0](l_x, y_g) = e^{2\pi i \Phi_x} D[\tilde{G}_0](0, y_g) \quad \text{for } 0 \leq y_g \leq l_y \quad \text{and} \\ & D[\tilde{G}_0](x_g, l_y) = e^{2\pi i \Phi_y} D[\tilde{G}_0](x_g, 0) \quad \text{for } 0 \leq x_g \leq l_x; \quad |z_g| \leq L \\ & \tilde{G}_0(g, p, k) = \sum_{n,m=-\infty}^{\infty} \left\{ \begin{array}{l} A_{nm}(p, k) \\ B_{nm}(p, k) \end{array} \right\} e^{\pm i \Gamma_{nm}(z_g \mp L)} \mu_{nm}(x_g, y_g); \quad g \in \left\{ \begin{array}{l} \bar{\mathbf{A}} \\ \bar{\mathbf{B}} \end{array} \right\} \end{aligned} \right. \quad (4.69)$$

is named the canonical Green function for 2-D periodic gratings. In the case of the elementary periodic structure with the absence of any material scatterers, the problems of this kind but with arbitrary right-hand parts of the Helmholtz equation are formulated for the monochromatic waves generated by quasi-periodic current sources located in the region $|z| < L$.

Let us construct $\tilde{G}_0(g, p, k)$ as a superposition of free-space Green functions:

$$\tilde{G}_0(g, p, k) = -\frac{1}{4\pi} \sum_{n,m=-\infty}^{\infty} \frac{\exp[ik|g - p_{nm}|]}{|g - p_{nm}|} e^{2\pi i n \Phi_x} e^{2\pi i m \Phi_y}, \tag{4.70}$$

$$p_{nm} = \{x_p + nl_x, y_p + ml_y, z_p\}.$$

By using in (4.70) the Poisson summation formula [16] and the tabulated integrals [17]

$$\int_{-\infty}^{\infty} \frac{\exp(ip\sqrt{x^2 + a^2})}{\sqrt{x^2 + a^2}} e^{ibx} dx = \pi i H_0^{(1)}\left(a\sqrt{|p^2 - b^2|}\right),$$

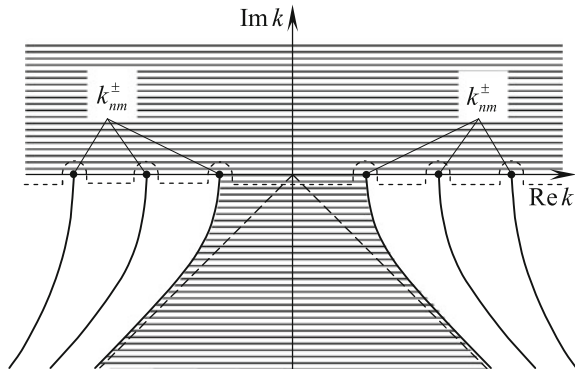
$$\int_{-\infty}^{\infty} H_0^{(1)}\left(p\sqrt{x^2 + a^2}\right) e^{ibx} dx = 2 \frac{\exp\left(ia\sqrt{p^2 - b^2}\right)}{\sqrt{p^2 - b^2}},$$

where $H_0^{(1)}(\dots)$ is the Hankel function of the first kind, we obtain

$$\tilde{G}_0(g, p, k) = -\frac{i}{2l_x l_y} \sum_{n,m=-\infty}^{\infty} e^{i[\alpha_n(x_g - x_p) + \beta_m(y_g - y_p)]} \frac{\exp[i|z_g - z_p|\Gamma_{nm}]}{\Gamma_{nm}}. \tag{4.71}$$

The surface K of analytic continuation of the canonical Green function (4.71) into the domain of complex-valued k is an infinite-sheeted Riemann surface consisting of the complex planes $k \in \mathbb{C}$ with cuts along the lines $(\text{Re } k)^2 - (\text{Im } k)^2 - \lambda_{nm}^2 = 0$ ($n, m = 0, \pm 1, \pm 2, \dots, \text{Im } k \leq 0$) (Fig. 4.6). The first

Fig. 4.6 Natural domain of variation of the spectral parameter k : the first sheet of the surface K



(physical) sheet C_k of the surface K is uniquely determined by the radiation conditions for $\tilde{G}_0(g, p, k)$ in the domains A and B, i.e. by the choice of $\operatorname{Re} \Gamma_{nm} \operatorname{Re} k \geq 0$ and $\operatorname{Im} \Gamma_{nm} \geq 0$ on the axis $\operatorname{Im} k = 0$. On this sheet, in the domain $0 \leq \arg k < \pi$, we have $\operatorname{Im} \Gamma_{nm} > 0$, while $\operatorname{Re} \Gamma_{nm} \geq 0$ for $0 < \arg k \leq \pi/2$ and $\operatorname{Re} \Gamma_{nm} \leq 0$ for $\pi/2 \leq \arg k < \pi$. In the domain $3\pi/2 \leq \arg k < 2\pi$ for finite number of functions $\Gamma_{nm}(k)$ (with n and m such that $(\operatorname{Re} k)^2 - (\operatorname{Im} k)^2 - \lambda_{nm}^2 > 0$), the inequalities $\operatorname{Im} \Gamma_{nm} < 0$ and $\operatorname{Re} \Gamma_{nm} > 0$ hold; for the rest of these functions we have $\operatorname{Im} \Gamma_{nm} > 0$ and $\operatorname{Re} \Gamma_{nm} \leq 0$. In the domain $\pi < \arg k \leq 3\pi/2$, the situation is similar, only the signs of $\operatorname{Re} \Gamma_{nm}$ are opposite. On the subsequent sheets (each of them with its own pair $\{k; \Gamma_{nm}(k)\}$), the signs (root branches) of $\Gamma_{nm}(k)$ are opposite to those they have on the first sheet for a finite number of n and m . The cuts (solid lines in Fig. 4.6) originate from the real algebraic branch points $k_{nm}^\pm = \pm|\lambda_{nm}|$.

In the vicinity of some fixed point $K \in K$ the function $\tilde{G}_0(g, p, k)$ can be expanded into a Loran series in terms of the local variable κ [18]:

$$\kappa = \begin{cases} k - K; & K \notin \{k_{nm}^\pm\} \\ \sqrt{k - K}; & K \in \{k_{nm}^\pm\} \end{cases}.$$

Therefore, this function is meromorphic on the surface K . Calculating the residues $\operatorname{Res}_{k=\bar{k}} \tilde{G}_0(g, p, k)$ at the simple poles $\bar{k} \in \{k_{nm}^\pm\}$, we obtain nontrivial solutions of homogeneous ($\tilde{U}^i(g, k) \equiv 0$) canonical ($\bar{e}(g, k) \equiv 1$, $\mu(g, k) \equiv 1$, $\overline{\operatorname{int} S} = \emptyset$) problems (4.52a, 4.52b, 4.52c) and (4.57a, 4.57b, 4.57c):

$$\begin{aligned} \tilde{E}(g, k_{nm}^\pm) &= \{\tilde{E}_x, \tilde{E}_y, \tilde{E}_z\}, \quad \tilde{E}_{x, y \text{ or } z} = a_{x, y \text{ or } z} \exp[i(\alpha_n x + \beta_m y)], \\ \text{and } \tilde{H}(g, k_{nm}^\pm) &= (ik_{nm}^\pm \eta_0)^{-1} \operatorname{rot} \tilde{E}(g, k_{nm}^\pm), \end{aligned} \tag{4.72}$$

where $a_{x, y \text{ or } z}$ are the arbitrary constants. These solutions determine free oscillations in the space stratified by the following conditions:

$$\begin{aligned} D[\tilde{E}(\tilde{H})](x + l_x, y) &= e^{2\pi i \Phi_x} D[\tilde{E}(\tilde{H})](x, y), \\ D[\tilde{E}(\tilde{H})](x, y + l_y) &= e^{2\pi i \Phi_y} D[\tilde{E}(\tilde{H})](x, y). \end{aligned}$$

4.8.2 Qualitative Characteristics of the Spectrum

Let a set Ω_k of the points $\{\bar{k}_j\}_j \in K$ such that for all $k \in \{\bar{k}_j\}_j$, the homogeneous (spectral) problem

$$\left\{ \begin{array}{l} \eta_0 \text{rot} \tilde{\tilde{H}}(g, k) = -ik\bar{\varepsilon}(g, k)\tilde{\tilde{E}}(g, k), \\ \text{rot} \tilde{\tilde{E}}(g, k) = ik\eta_0\mu(g, k)\tilde{\tilde{H}}(g, k); \quad g \in Q_L \\ D \left[\tilde{\tilde{E}} \left(\tilde{\tilde{H}} \right) \right] (l_x, y) = e^{2\pi i\Phi_x} D \left[\tilde{\tilde{E}} \left(\tilde{\tilde{H}} \right) \right] (0, y) \quad \text{for } 0 \leq y \leq l_y \quad \text{and} \\ D \left[\tilde{\tilde{E}} \left(\tilde{\tilde{H}} \right) \right] (x, l_y) = e^{2\pi i\Phi_y} D \left[\tilde{\tilde{E}} \left(\tilde{\tilde{H}} \right) \right] (x, 0) \quad \text{for } 0 \leq x \leq l_x; \quad |z| < L \\ \tilde{\tilde{E}}_{tg}(g, k) \Big|_{g \in S} = 0, \quad \tilde{\tilde{H}}_{nr}(g, k) \Big|_{g \in S} = 0, \end{array} \right. \quad (4.73a)$$

$$\left\{ \begin{array}{l} \tilde{\tilde{E}}_z(g, k) \\ \tilde{\tilde{H}}_z(g, k) \end{array} \right\} = \sum_{n,m=-\infty}^{\infty} \left\{ \begin{array}{l} A_{nm(E)}(k) \\ A_{nm(H)}(k) \end{array} \right\} e^{i\Gamma_{nm}(z-L)} \mu_{nm}(x, y); \quad g \in \bar{A}, \quad (4.73b)$$

$$\left\{ \begin{array}{l} \tilde{\tilde{E}}_z(g, k) \\ \tilde{\tilde{H}}_z(g, k) \end{array} \right\} = \sum_{n,m=-\infty}^{\infty} \left\{ \begin{array}{l} B_{nm(E)}(k) \\ B_{nm(H)}(k) \end{array} \right\} e^{-i\Gamma_{nm}(z+L)} \mu_{nm}(x, y); \quad g \in \bar{B} \quad (4.73c)$$

has a nontrivial (not necessarily unique) solution $\tilde{\tilde{U}}(g, \bar{k}_j) = \left\{ \tilde{\tilde{E}}(g, \bar{k}_j), \tilde{\tilde{H}}(g, \bar{k}_j) \right\}$ be called a *point spectrum* of the grating. It is obvious that these solutions characterize the so-called *free oscillations*, whose field pattern, structure of their spatial harmonics and behavior of these harmonics for large $|z|$ and t are determined by the value of $\bar{k}_j = \text{Re } \bar{k}_j + i \text{Im } \bar{k}_j$ and by a position of the point \bar{k}_j (the *eigenfrequency* associated with the free oscillation $\tilde{\tilde{U}}(g, \bar{k}_j)$) on the surface K [4, 6, 7]. By continuing analytically the problems (4.52a, 4.52b, 4.52c) and (4.57a, 4.57b, 4.57c) together with their solutions $\tilde{\tilde{U}}(g, k) = \left\{ \tilde{\tilde{E}}(g, k), \tilde{\tilde{H}}(g, k) \right\}$ into the domain K of the complex-valued k , we detect poles of the function $\tilde{\tilde{U}}(g, k)$ at the points $k = \bar{k}_j$. In the vicinity of these poles, the desired solutions can be represented by the *Loran series* in terms of the local on K variable κ [18]. The analytical findings of this kind may form the basis for detailed study of physical features of resonant wave scattering by one-dimensionally and two-dimensionally periodic structures [4, 6, 7, 19, 20].

Now, let us derive the conditions that constrain existence of nontrivial solutions of the problem (4.73a, 4.73b, 4.73c). These conditions can be considered as uniqueness theorems for the problems (4.52a, 4.52b, 4.57c) and (4.57a, 4.57b, 4.57c) formulated for different domains of the surface K . Notice that the study of the uniqueness allows one to estimate roughly a domain where elements of the set Ω_k are localized and simplify substantially the subsequent numerical solution of spectral problems owing to reduction of a search zone of the eigenfrequencies. The uniqueness theorems also serve as a basis for application of the ‘*meromorphic*’ *Fredholm theorem* [21] when constructing well grounded algorithms for solving diffraction problems as well as when studying qualitatively gratings’ spectra [4, 7].

Assume that grating scattering elements are nondispersive, that is $\varepsilon(g, k) = \varepsilon(g)$, $\mu(g, k) = \mu(g)$, and $\sigma(g, k) = \sigma(g)$. In this case, the analytical continuation of the spectral problem (4.73a, 4.73b, 4.73c) into the domain of complex-valued k are

simplified considerably. From the complex power theorem in the integral form formulated for the nontrivial solutions $\vec{U}(g, \bar{k}_j)$ like

$$\oint_{S_L} \left(\vec{E} \times \vec{H}^* \right) \cdot \vec{ds} = \int_{Q_L} \operatorname{div} \left(\vec{E} \times \vec{H}^* \right) dg = ik\eta_0 \int_{Q_L} \mu |\vec{H}|^2 dg - \frac{ik^*}{\eta_0} \int_{Q_L} \varepsilon |\vec{E}|^2 dg - \int_{Q_L} \sigma |\vec{E}|^2 dg \quad (4.74)$$

the following relations result:

$$\sum_{n,m=-\infty}^{\infty} \frac{1}{\lambda_{nm}^2} \left\{ \begin{array}{l} \left(\operatorname{Re} \Gamma_{nm} \operatorname{Re} k + \operatorname{Im} \Gamma_{nm} \operatorname{Im} k \right) \\ \left(\operatorname{Im} \Gamma_{nm} \operatorname{Re} k - \operatorname{Re} \Gamma_{nm} \operatorname{Im} k \right) \end{array} \right\} \left[\left(|A_{nm(E)}|^2 + |B_{nm(E)}|^2 \right) \pm \eta_0^2 \left(|A_{nm(H)}|^2 + |B_{nm(H)}|^2 \right) \right] = \frac{1}{\varepsilon_0} \left\{ \begin{array}{l} -\operatorname{Im} k (V_3 + V_2) - V_1 \\ \operatorname{Re} k (V_3 - V_2) \end{array} \right\}. \quad (4.75)$$

Notation: $k = \bar{k}_j$, $\vec{E} = \vec{E}(g, \bar{k}_j)$, $\Gamma_{nm} = \Gamma_{nm}(\bar{k}_j)$, $A_{nm(E)} = A_{nm(E)}(\bar{k}_j)$, etc., and

$$V_1 = \varepsilon_0 \eta_0 \int_{Q_L} \sigma |\vec{E}|^2 dg, \quad V_2 = \int_{Q_L} \varepsilon_0 \varepsilon |\vec{E}|^2 dg, \quad V_3 = \int_{Q_L} \mu_0 \mu |\vec{H}|^2 dg.$$

No free oscillations exist whose amplitudes do not satisfy (4.75). From this general statement, several important consequences follow. Below some of them are formulated for gratings with $\varepsilon(g) > 0$, $\mu(g) > 0$, and $\sigma(g) \geq 0$.

- There are no free oscillations whose eigenfrequencies \bar{k}_j are located on the upper half-plane ($\operatorname{Im} k > 0$) of the first sheet of the surface K . This can be verified by taking into account the upper relation in (4.75), the values of the function $\Gamma_{nm}(k)$ on C_k , and the inequalities $V_1 \geq 0$, $V_2 > 0$, $V_3 > 0$.
- If $\sigma(g) \equiv 0$ (the grating is non-absorptive), no free oscillations exist whose eigenfrequencies \bar{k}_j are located on the bottom half-plane ($\operatorname{Im} k < 0$) of the sheet C_k between the cuts corresponding to the smallest absolute values of k_{nm}^{\pm} . In Fig. 4.6, this region of the first sheet of K and the above-mentioned domain are shaded by horizontal lines.
- If $\sigma(g) > 0$ on some set of nonzero measure of points $g \in Q_L$, then there are no elements \bar{k}_j of grating's point spectrum Ω_k that are located on the real axis of the plane C_k .

Investigation of the entire spectrum of a grating, i.e. a set of the points $k \in K$, for which the diffraction problems given by (4.52a, 4.52b, 4.52c) and (4.57a, 4.57b, 4.57c) are not uniquely solvable, is a complicated challenge. Therefore, below we do no more than indicate basic stages for obtaining well-grounded results. The first stage is associated with regularization of the boundary value problem that describes

excitation of a metal-dielectric grating by the currents $\vec{j}(g, k) \leftrightarrow \vec{j}(g, t)$ located in the domain Q_L :

$$\begin{cases} \eta_0 \operatorname{rot} \vec{H}(g, k) = -ik\bar{\varepsilon}(g, k)\vec{E}(g, k) + \eta_0 \vec{j}(g, k), \\ \operatorname{rot} \vec{E}(g, k) = ik\eta_0 \mu(g, k)\vec{H}(g, k); \quad g \in Q_L \\ D\left[\vec{E}\left(\vec{H}\right)\right](l_x, y) = e^{2\pi i\Phi_x} D\left[\vec{E}\left(\vec{H}\right)\right](0, y) \quad \text{for } 0 \leq y \leq l_y \quad \text{and} \\ D\left[\vec{E}\left(\vec{H}\right)\right](x, l_y) = e^{2\pi i\Phi_y} D\left[\vec{E}\left(\vec{H}\right)\right](x, 0) \quad \text{for } 0 \leq x \leq l_x; \quad |z| < L \\ \vec{E}_{tg}(g, k)|_{g \in S} = 0, \quad \vec{H}_{nr}(g, k)|_{g \in S} = 0, \end{cases} \quad (4.76a)$$

$$\begin{cases} \vec{E}_z(g, k) \\ \vec{H}_z(g, k) \end{cases} = \sum_{n,m=-\infty}^{\infty} \begin{cases} A_{nm(E)}(k) \\ A_{nm(H)}(k) \end{cases} e^{i\Gamma_{nm}(z-L)} \mu_{nm}(x, y); \quad g \in \bar{A}, \quad (4.76b)$$

$$\begin{cases} \vec{E}_z(g, k) \\ \vec{H}_z(g, k) \end{cases} = \sum_{n,m=-\infty}^{\infty} \begin{cases} B_{nm(E)}(k) \\ B_{nm(H)}(k) \end{cases} e^{-i\Gamma_{nm}(z+L)} \mu_{nm}(x, y); \quad g \in \bar{B}. \quad (4.76c)$$

By *regularization* we mean (see, for example, [7]) a reduction of the boundary value problem to the equivalent operator *equation of the second kind*

$$[E + B(\tilde{G}_0, S, \bar{\varepsilon}, \mu, k)]X = Y, \quad EX = X \quad (4.77)$$

with a *compact* (in some space of vector fields) *finite-meromorphic* (in local on K variables κ) *operator-function* $B(\tilde{G}_0, S, \bar{\varepsilon}, \mu, k)$ [21, 22]. If the problem given by (4.76a, 4.76b, 4.76c) is considered separately for metal gratings ($\overline{\operatorname{int} S} \neq \emptyset$ and S are sufficiently smooth surfaces; $\bar{\varepsilon}(g, k) = \mu(g, k) \equiv 1$) and dielectric gratings ($\overline{\operatorname{int} S} = \emptyset$, $\bar{\varepsilon}(g, k) = \varepsilon(g)$ and $\mu(g, k) = \mu(g)$ are sufficiently smooth functions), then it can be regularized by applying the potential theory methods [4, 7, 23].

In the second stage, the following statements should be proved: (i) the *resolvent* $[E + B(k)]^{-1}$ ($k \in K$) of the problem (4.77) is a finite-meromorphic operator-function; (ii) its poles are located at the points $k = \bar{k}_j$ ($j = 1, 2, 3, \dots$); (iii) the entire spectrum coincides with its point spectrum Ω_k ; (iv) Ω_k is nothing more than a countable set without finite accumulation points. All these statements are corollaries of the previously proven '*meromorphic*' *Fredholm theorem* [4, 21, 22] and the uniqueness theorem.

By inverting the homogeneous operator (4.77), we can construct a numerical solution of the spectral problem given by (4.73a, 4.73b, 4.73c) [4, 6], in other words, calculate the complex-valued eigenfrequencies \bar{k}_j and associated eigenwaves $\vec{U}(g, \bar{k}_j) = \left\{ \vec{E}(g, \bar{k}_j), \vec{H}(g, \bar{k}_j) \right\}$ or free oscillations of an open two-dimensionally

periodic resonator. Commonly, this operation is reduced to an approximate solution of the *characteristic equation* like:

$$\det[C(k)] = 0. \quad (4.78)$$

Here $C(k)$ is some infinite matrix-function; the compactness of the operator $B(k)$ ensures (i) existence of the determinant $\det[C(k)]$ and (ii) the possibility to approximate the solutions \bar{k} of (4.78) by the solutions $\bar{k}(N)$ of the equation $\det[C(k, N)] = 0$ with the matrix $C(k, N)$ reduced to dimension $N \times N$.

Let \bar{k} be a root of characteristic equation (4.78) that does not coincide with any pole of the operator-function $B(k)$. The multiplicity of this root determines the multiplicity of the eigenvalue \bar{k} of the homogeneous operator (4.77), i.e. the value $M = M(1) + M(2) + \dots + M(Q)$ [22]. Here, Q is the number of linearly-independent eigenfunctions $\tilde{U}^{(q)}(g, \bar{k})$; $q = 1, 2, \dots, Q$ (the number of free oscillations) corresponding to the eigenvalue (eigenfrequency) \bar{k} , while $M(q) - 1$ is the number of the associated functions $\tilde{U}_{(m)}^{(q)}(g, \bar{k})$; $m = 1, 2, \dots, M(q) - 1$. The order of pole of the resolvent $[E + B(k)]^{-1}$ (and of the Green function $\tilde{G}(g, p, k)$ of the problem (4.76a, 4.76b, 4.76c)) for $k = \bar{k}$ is determined by the maximal value of $M(q)$.

4.9 Conclusion

The analytical results presented in the chapter are of much interest in the development of rigorous theory of two-dimensionally periodic gratings as well as in numerical solution of the associated initial boundary value problems. We derived exact absorbing boundary conditions that truncate the unbounded computational space of the initial boundary value problem for two-dimensionally periodic structures to a bounded part of the Floquet channel. Some important features of transient and steady-state fields in rectangular parts of the Floquet channel were discussed. The technique for calculating electrodynamic characteristics of a multi-layered structure consisting of two-dimensionally periodic gratings was developed by introducing the transformation operators similar to generalized scattering matrices in the frequency domain. In one of the last sections we discussed the elements of spectral theory for two-dimensionally periodic gratings. We also gave some practical guidelines related to fast enough and highly accurate numerical solution of gratings problems.

References

1. Shestopalov, V.P., Lytvynenko, L.M., Masalov, S.A., Sologub, V.G.: Wave Diffraction by Gratings. Kharkov State University Press, Kharkov (1973) (in Russian)
2. Petit, R. (ed.): Electromagnetic Theory of Gratings. Springer, New York (1980)

3. Shestopalov, V.P., Kirilenko, A.A., Masalov, S.A., Sirenko, Y.K.: Diffraction gratings. In: Resonance Wave Scattering, vol.1. Naukova Dumka, Kiev (1986) (in Russian)
4. Shestopalov, V.P., Sirenko, Y.K.: Dynamic Theory of Gratings. Naukova Dumka, Kiev (1989) (in Russian)
5. Neviere, M., Popov, E.: Light Propagation in Periodic Media: Differential Theory and Design. Dekker, New York (2003)
6. Sirenko, Y.K., Strom, S., Yashina, N.P.: Modeling and Analysis of Transient Processes in Open Resonant Structures: New Methods and Techniques. Springer, New York (2007)
7. Sirenko, Y.K., Strom, S. (eds.): Modern Theory of Gratings: Resonant Scattering: Analysis Techniques and Phenomena. Springer, New York (2010)
8. Ladyzhenskaya, O.A.: The Boundary Value Problems of Mathematical Physics. Springer, New York (1985)
9. Taflove, A., Hagness, S.C.: Computational Electrodynamics: The Finite-Difference Time-Domain Method. Artech House, Boston (2000)
10. Sirenko, K., Pazynin, V., Sirenko, Y., Bagci, H.: An FFT-accelerated FDTD scheme with exact absorbing conditions for characterizing axially symmetric resonant structures. *Prog. Electromagnet. Res.* **111**, 331–364 (2011)
11. Liu, M., Sirenko, K., Bagci, H.: An efficient discontinuous Galerkin finite element method for highly accurate solution of Maxwell equations. *IEEE Trans. Antennas Propag.* **60**(8), 3992–3998 (2012)
12. Rothwell, E.J., Cloud, M.J.: Electromagnetics. CRC Press, New York (2001)
13. Vladimirov, V.S.: Equations of Mathematical Physics. Dekker, New York (1971)
14. Sirenko, K.Y., Sirenko, Y.K.: Exact ‘absorbing’ conditions in the initial boundary value problems of the theory of open waveguide resonators. *Comput. Math. Math. Phys.* **45**(3), 490–506 (2005)
15. Kravchenko, V.F., Sirenko, Y.K., Sirenko, K.Y.: Electromagnetic Wave Transformation and Radiation by the Open Resonant Structures. Modelling and Analysis of Transient and Steady-State Processes. Fizmatlit, Moscow (2011) (in Russian)
16. Titchmarsh, E.: Introduction to the Theory of Fourier Integrals. Clarendon Press, Oxford (1948)
17. Gradshteyn, I.S., Ryzhik, I.M.: Table of Integrals, Series, and Products. Academic Press, San Diego, London (2000)
18. von Hurwitz, A.: Allgemeine Funktionentheorie und Elliptische Funktionen. von Courant, R.: Geometrische Funktionentheorie. Springer, Berlin (1964) (in German)
19. Sirenko, Y.K., Velychko, L.G., Erden, F.: Time-domain and frequency-domain methods combined in the study of open resonance structures of complex geometry. *Prog. Electromagnet. Res.* **44**, 57–79 (2004)
20. Velychko, L.G., Sirenko, Y.K., Velychko, O.S.: Time-domain analysis of open resonators. Analytical grounds. *Prog. Electromagnet. Res.* **61**, 1–26 (2006)
21. Reed, M., Simon, B.: Methods of Modern Mathematical Physics. IV: Analysis of Operators. Academic Press, New York (1978)
22. Høkhberg, I.Z., Seagul, Y.I.: Operator generalization of the theorem about logarithmic residue and the Rouché theorem. *Matematicheskiy Sbornik* **84**(4), 607–629 (1971) (in Russian)
23. Colton, D., Kress, R.: Integral Equation Methods in Scattering Theory. Wiley-Interscience, New York (1983)

Chapter 5

The Exact Absorbing Conditions Method in the Analysis of Open Electrodynamical Structures

Kostyantyn Sirenko and Yuriy Sirenko

Abstract The authors expound the method of exact absorbing boundary conditions, which solves one of the most important theoretical problems in computational electrodynamics, namely, the problem of equivalent replacement of an open (with infinite domain of analysis) initial boundary value problem by a closed (with bounded computation domain) one. This method, being mathematically strict, allows proper formulation and numerical study of transient and steady-state processes in various open resonant systems. The authors present local (in space and time) and non-local exact absorbing conditions for virtual boundaries located in cross-sections of regular waveguides or in free space. The elaborated concept of the so-called virtual feeding waveguides allows to solve many practically interesting radiation problems. The approach outlined in this chapter was implemented in software for solving both scalar (plane and axially symmetric) and vector problems.

5.1 Introduction

Exact absorbing conditions (EACs) are used in computational electrodynamics of non-sine waves to truncate computation domains via replacement of original initial boundary value problems formulated on open (unbounded) domains with modified problems on bounded domains [1–9].

K. Sirenko (✉)
King Abdullah University of Science and Technology,
Thuwal, Saudi Arabia
e-mail: k.sirenko@gmail.com

Y. Sirenko
O.Ya. Usikov Institute for Radiophysics and Electronics,
National Academy of Sciences, Kharkiv, Ukraine
e-mail: yks@ire.kharkov.ua

Y. Sirenko
L.N. Gumilyov Eurasian National University, Astana, Republic of Kazakhstan

The efficient truncation of computation domains of *open (unbounded) initial boundary value problems* (i.e. problems whose domains of analysis are infinite in one or more directions) is a vital issue in computational electrodynamics as well as in other physical disciplines using mathematical simulations and numerical experiments. Most of well-known and extensively used heuristic and approximate solutions to the truncation problem are based on absorbing boundary conditions (ABCs) [10–13] and perfectly matched layers (PMLs) [14–16]. Various modifications and improvements to ABCs and PMLs yield good results in various specific physical situations. However, it appears that for certain problems associated with the resonant wave scattering, the numerical implementation of ABCs or PMLs may cause unpredictable growth of the computational error for large observation times.

EACs-enabled methods [1–9, 17, 18] are outnumbered by approximate approaches utilizing ABCs or PMLs. However, careful numerical tests, and physical and applied results obtained with EACs-enabled methods (see, for example, [3, 5, 8, 18–27]), show their evident potential, especially, for simulations of open waveguides, periodic and compact resonators.

The essence of EACs-enabled methods for open (unbounded) scalar or vector problems, which are considered in the part Ω of two- or three-dimensional Euclidean space, is as follows. Assume that sources and scatterers are located in a bounded domain Ω_{int} of the unbounded analysis domain Ω . The propagation velocity of electromagnetic waves is finite. Therefore, within the finite time T , the waves will not leave some bounded domain $\Omega_{\text{int}, T} \subset \Omega$:

$$[U(g, t)]|_{g \in \Omega_{\text{ext}, T}, t \in [0, T]} = 0. \quad (5.1)$$

Here, $U(g, t)$ ($g \in \Omega$, $t \geq 0$) is the electromagnetic field function, $[0, T]$ is the observation interval $0 \leq t \leq T$, and $\Omega_{\text{ext}, T}$ is the complement of the domain $\Omega_{\text{int}, T}$ with respect to Ω .

The formula (5.1) is the well-known *radiation condition* for outgoing (from the domain Ω_{int}) pulsed waves $U(g, t)$. The only but essential limitation of this simple condition is associated with the fact that with growing observation time T the domain $\Omega_{\text{int}, T}$ is expanding, and its boundary is moving farther away from the domain Ω_{int} . That is why the condition (5.1) is not used for truncating computation domains of open problems. In EACs-enabled methods, the condition (5.1) is transferred from the field-free region $\Omega_{\text{ext}, T}$ onto some *virtual boundary* Γ located in a region, where the electromagnetic field can be arbitrary:

$$D[U(g, t)]|_{g \in \Gamma} = 0; \quad t \geq 0. \quad (5.2)$$

The electromagnetic waves $U(g, t)$ must be outgoing in this case as well, or in other words, they must intersect the boundary Γ in one direction only, moving away from sources and scatterers. Here, $D[U]$ is some integro-differential operator on the virtual boundary Γ .

The boundary Γ divides the unbounded domain Ω into two domains, namely, Ω_{int} and Ω_{ext} such that $\Omega = \Omega_{\text{int}} \cup \Omega_{\text{ext}} \cup \Gamma$. In the bounded computation domain

Ω_{int} , which contains all sources and scatterers, we can formulate the initial boundary value problem with respect to the function $U(g, t)$ using the boundary condition (5.2). This problem is called the *modified problem* as distinct from the *original initial boundary value problem* formulated in the unbounded domain Ω using the radiation condition (5.1). In the computation domain Ω_{int} , the function $U(g, t)$ can be computed using standard finite-difference [28] or finite-element [29] methods. To find the values of $U(g, t)$ in the domain Ω_{ext} using its values on the boundary Γ , EACs-enabled methods allow to derive the so-called *transport operators* $Z_{q \in \Gamma \rightarrow g \in \Omega_{\text{ext}}}(t)[U]$ [3, 8, 30, 31]

$$[U(g, t)] = Z_{q \in \Gamma \rightarrow g \in \Omega_{\text{ext}}}(t)[U(q, \tau)]; \quad 0 \leq \tau \leq t. \quad (5.3)$$

Analytical forms of the EAC operators $D[U]$ and the transport operators $Z[U]$ depend on the geometry of the domain Ω_{ext} , and, evidently, on problems' dimensions and coordinates systems. However, in all cases, the derivation of these operators is based on the common sequence of transformations widely used in the theory of hyperbolic equations [3, 32]: (i) isolation of the regular domain Ω_{ext} where the wave $U(g, t)$ propagates freely moving away from the domain Ω_{int} , which contains all sources and scatterers; (ii) separation of variables in the original initial boundary value problem for the domain Ω_{ext} , which results in a problem for the 1-D Klein-Gordon equation with respect to the space-time amplitudes of the field $U(g, t)$; (iii) integral transformations in the problem for 1-D Klein-Gordon equation; (iv) resolution of the auxiliary boundary value problem for ordinary differential equation with respect to the images of the field amplitudes; (v) inverse integral transformations.

As a result, nonlocal (in space and time) EACs on the virtual boundary Γ are derived. In some cases, the nonlocal conditions can be reduced to the local ones by replacing certain integral forms with differential ones [2, 3, 8]. EAC (5.2) can be included into standard finite-difference or finite-element algorithms with the computation domain truncated to Ω_{int} . However, one can confidently assert that relevant computational schemes are stable and convergent only when the modified problem is uniquely-solvable and equivalent to the original problem [33]. Although the corresponding assertions were formulated in some works (see, for example, [1, 3, 8]), they were proved analytically only in [9] for the initial boundary value problems describing TE_0 - and TM_0 -waves scattering on compact open axially symmetric structures. In Sect. 5.2.5 we replicate the proof for initial boundary value problems associated with compact discontinuities in circular and coaxial waveguides and demonstrate ipso facto that there is a strong reason to believe that it can be used for all other types of EACs as well.

In Sects. 5.2–5.4 of this chapter we construct EACs for axially symmetric electrodynamic structures illuminated by symmetric pulsed TE - and TM -waves (or TE_0 - and TM_0 -waves) and prove the equivalency of original (open) and modified (closed) initial boundary value problems. We present the following results: EACs for virtual boundaries in cross-sections of regular circular and coaxial waveguides (Sect. 5.2) and for spherical boundaries in free space (Sect. 5.3); transport operators relating near-zone and far-zone fields generated by compact structures in free space.

We also prove the unique solvability of modified closed problems and their equivalency to original open problems (Sect. 5.2) and solve the problem of extended and remote sources giving grounds for rigorous theoretical justification of EACs-enabled methods. Some important if not fundamental questions are discussed in Sect. 5.4, such as time domain to frequency domain transitions and algorithmization of the electrodynamic characteristics calculations. In the next sections, omitting details discussed in Sects. 5.2–5.4, we construct EACs for plane (2-D) electrodynamic structures illuminated by pulsed E - and H -polarized waves (Sect. 5.5) and EACs for 3-D vector initial boundary value problems describing electromagnetic field transformations in open waveguides and compact resonators (Sect. 5.6). Section 5.7 is devoted to the enhancement of computation efficiency of the results obtained in the previous sections.

5.2 Circular and Coaxial Waveguides

5.2.1 Formulation of the Model Problem

The 2-D initial boundary value problem describing the transformation of pulsed symmetric ($\partial/\partial\phi \equiv 0$) TE_0 - ($E_\rho = E_z = H_\phi \equiv 0$) and TM_0 -waves ($H_\rho = H_z = E_\phi \equiv 0$) in open axially symmetric waveguide structures is given (see [3, 8]) by

$$\left\{ \begin{array}{l} \left[-\varepsilon(g) \frac{\partial^2}{\partial t^2} - \sigma(g) \eta_0 \frac{\partial}{\partial t} + \frac{\partial^2}{\partial z^2} + \frac{\partial}{\partial \rho} \left(\frac{1}{\rho} \frac{\partial}{\partial \rho} \rho \right) \right] U(g, t) = F(g, t); \\ \quad t > 0, \quad g = \{\rho, z\} \in \Omega \\ U(g, t)|_{t=0} = \varphi(g), \quad \frac{\partial}{\partial t} U(g, t) \Big|_{t=0} = \psi(g); \quad g \in \bar{\Omega} \\ \vec{E}_{tg}(p, t) \Big|_{p=\{\rho, \phi, z\} \in \Sigma} = 0, \quad U(0, z, t) = 0 \quad \text{for } |z| < \infty; \quad t \geq 0. \end{array} \right. \quad (5.4)$$

Here, $\vec{E} = \{E_\rho, E_\phi, E_z\}$ and $\vec{H} = \{H_\rho, H_\phi, H_z\}$ are the electric and magnetic field vectors; $\{\rho, \phi, z\}$ are the cylindrical coordinates; $U(g, t) = E_\phi(g, t)$ for TE_0 -waves and $U(g, t) = H_\phi(g, t)$ for TM_0 -waves. By $\Sigma = \Sigma_\phi \times [0, 2\pi]$ we denote perfectly conducting surfaces obtained by rotating the piecewise smooth curves Σ_ϕ around the z -axis. The relative permittivity $\varepsilon(g)$ and specific conductivity $\sigma(g)$ are smooth non-negative functions inside Ω_{int} and take free space values outside (in the case of TE_0 -waves) or $\varepsilon(g) \equiv 1$ and $\sigma(g) \equiv 0$ (in TM_0 -case), $\eta_0 = (\mu_0/\varepsilon_0)^{1/2}$ is the impedance of free space, ε_0 and μ_0 are the electric and magnetic constants of vacuum. We use SI, the International System of Units, for all physical parameters except the ‘time’ t that is the product of the natural time and the velocity of light in vacuum, thus t is measured in meters.

The domain of analysis Ω is the part of the half-plane $\Omega_{\text{total}} = \{p = \{\rho, \phi, z\} : \rho > 0, |z| \geq 0, \phi = \pi/2\}$ bounded by Σ_ϕ . The domains Ω_{int} and $\Omega_{\text{add}} = \bigcup_{j=1}^J \Omega_j$

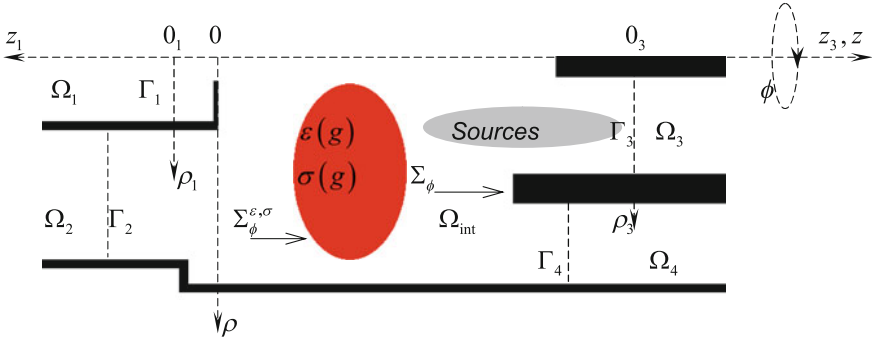


Fig. 5.1 Open axially symmetric waveguide transformer

(regular semi-infinite circular and coaxial waveguides) are separated by the virtual boundaries $\Gamma_j = \{g_j = \{\rho_j, z_j\} \in \Omega : z_j = 0\}$ and $\Omega = \Omega_{\text{int}} \cup \Omega_{\text{add}} \cup \Gamma_{\text{add}}$, $\Gamma_{\text{add}} = \cup_{j=1}^J \Gamma_j$. Here, $\{\rho_j, \phi_j, z_j\}$ is the local coordinate system associated with the waveguide Ω_j (see Fig. 5.1).

The functions $F(g, t)$, $\varphi(g)$, $\psi(g)$, $\sigma(g)$, and $\varepsilon(g) - 1$, which have compact supports in the closure of Ω , are supposed to satisfy the theorem on the unique solvability of the problem (5.4) in the Sobolev space $W_2^1(\Omega^T)$, $\Omega^T = \Omega \times (0, T)$, $(0, T) = \{t : 0 < t < T < \infty\}$ (see Statement 5.1 below and [3, 33]). The *current* and *instantaneous sources* given by the functions $F(g, t)$ and $\varphi(g)$, $\psi(g)$ as well as all scatterers described by the functions $\varepsilon(g)$, $\sigma(g)$ and by the contours Σ_ϕ are located in Ω_{int} . In axially symmetric problems, at the points $g = \{\rho, z\}$ such that $\rho = 0$, only H_z - or E_z -fields components are non-zero [2, 3, 8]. Hence, it follows that $U(0, z, t) = 0$ for $|z| < \infty$, $t \geq 0$ in (5.4).

Let us assume that $0 < v \leq 1/\varepsilon(g) \leq \mu < \infty$ ($g \in \Omega$) and the functions σ/ε , $\varepsilon'/\varepsilon^2$ are bounded in Ω . Then the following statement (see also [3, 33]) is true.

Statement 5.1. *Let $F(g, t)/\varepsilon(g) \in L_{2,1}(\Omega^T)$, $\varphi(g) \in W_2^1(\Omega)$ (for TE_0 -waves) or $\varphi(g) \in W_2^1(\Omega)$ (for TM_0 -waves), and $\psi(g) \in L_2(\Omega)$. Then the problem (5.4) has a generalized solution from $W_2^1(\Omega^T)$, and the uniqueness theorem is true in this space.*

Here, the following notations are used: ε' is the partial derivative of $\varepsilon(g)$ with respect to ρ or z ; $L_n(G)$ is the space of functions $f(g)$ ($g \in G$) for which the function $|f(g)|^n$ is integrable in G ; $W_m^l(G)$ is the set of all the elements $f(g)$ from $L_m(G)$ whose generalized derivatives up to the order l inclusive belong to $L_m(G)$; $L_{2,1}(G^T)$ is the space containing all elements $f(g, t) \in L_1(G^T)$ with finite norm $\|f\| = \int_0^T \left(\int_G |f|^2 dg \right)^{1/2} dt$; $\overset{\circ}{W}_2^1(G)$ is the subspace of space $W_2^1(G)$, where the set of functions, which have compact supports and infinitely differentiable in G , is a dense set.

5.2.2 Radiation Conditions for Outgoing Waves

In the domain Ω_j (see Fig. 5.2), where the wave $U(g, t)$ propagates freely to $z_j = \infty$ as $t \rightarrow \infty$, the 2-D initial boundary value problem (5.4) can be rewritten in the local coordinates $g_j = \{\rho_j, z_j\}$ in the following way:

$$\begin{cases} \left[-\frac{\partial^2}{\partial t^2} + \frac{\partial^2}{\partial z_j^2} + \frac{\partial}{\partial \rho_j} \left(\frac{1}{\rho_j} \frac{\partial}{\partial \rho_j} \rho_j \right) \right] U(g_j, t) = 0; & t > 0, \quad g_j \in \Omega_j \\ U(g_j, t)|_{t=0} = 0, \quad \frac{\partial}{\partial t} U(g_j, t)|_{t=0} = 0; & g_j = \{\rho_j, z_j\} \in \bar{\Omega}_j \\ \vec{E}_{tg}(p_j, t)|_{p_j=\{\rho_j, \phi_j, z_j\}} \in \Sigma = 0, \quad U(0, z_j, t) = 0 & \text{for } 0 \leq z_j \leq \infty; \quad t \geq 0. \end{cases} \quad (5.5)$$

Separation of variables in (5.5) results in

$$\begin{aligned} U(g_j, t) &= \sum_n u_{nj}(z_j, t) \mu_{nj}(\rho_j) \quad \text{and} \\ u_{nj}(z_j, t) &= \int_{0 \text{ or } b_j}^{a_j} U(g_j, t) \mu_{nj}(\rho_j) \rho_j d\rho_j; \quad g_j = \{\rho_j, z_j\} \in \Omega_j, \end{aligned} \quad (5.6)$$

where an orthonormal (with the weight factor ρ_j) system of the *transverse functions* $\mu_{nj}(\rho_j)$, and the *transverse eigenvalues* λ_{nj} are obtained from the homogeneous Sturm-Liouville problems

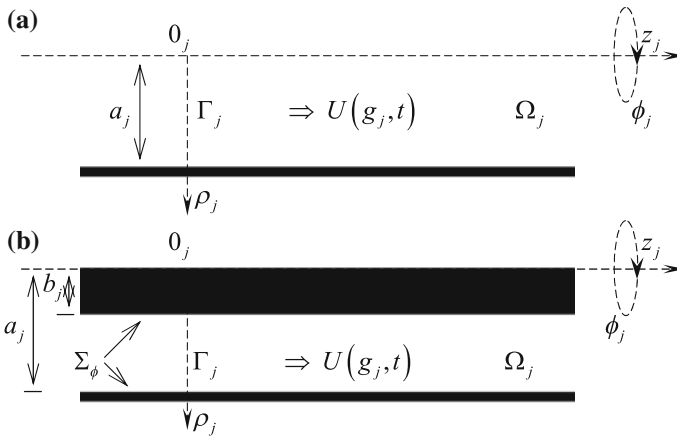


Fig. 5.2 Virtual boundary Γ_j in the regular **a** circular and **b** coaxial waveguide Ω_j

$$\left\{ \begin{array}{l} \left[\frac{d}{d\rho_j} \frac{1}{\rho_j} \frac{d}{d\rho_j} \rho_j + \lambda_{nj}^2 \right] \mu_{nj}(\rho_j) = 0; \quad \rho_j \in (0, a_j) \\ \mu_{nj}(0) = \mu_{nj}(a_j) = 0 \quad (TE_0\text{-waves}) \quad \text{or} \\ \mu_{nj}(0) = \left. \frac{d(\rho_j \mu_{nj}(\rho_j))}{d\rho_j} \right|_{\rho_j=a_j} = 0 \quad (TM_0\text{-waves}) \end{array} \right. \quad (5.7)$$

(if Ω_j is circular waveguide with $0 \leq \rho_j \leq a_j$) or

$$\left\{ \begin{array}{l} \left[\frac{d}{d\rho_j} \frac{1}{\rho_j} \frac{d}{d\rho_j} \rho_j + \lambda_{nj}^2 \right] \mu_{nj}(\rho_j) = 0; \quad \rho_j \in (b_j, a_j) \\ \mu_{nj}(b_j) = \mu_{nj}(a_j) = 0 \quad (TE_0\text{-waves}) \quad \text{or} \\ \left. \frac{d(\rho_j \mu_{nj}(\rho_j))}{d\rho_j} \right|_{\rho_j=b_j} = \left. \frac{d(\rho_j \mu_{nj}(\rho_j))}{d\rho_j} \right|_{\rho_j=a_j} = 0 \quad (TM_0\text{-waves}) \end{array} \right. \quad (5.8)$$

(if Ω_j is coaxial waveguide with $b_j \leq \rho_j \leq a_j$). Here and hereinafter, $n = 0, 1, 2, \dots$ only in the case of TM_0 -waves, and only for the coaxial waveguide Ω_j . In all other cases $n = 1, 2, 3, \dots$. The boundary conditions on waveguide walls for the case of TM_0 -waves in (5.7) and (5.8) are determined by the following relationships: $U(g, t) = H_\phi(g, t)$, $\vec{E}_{tg}(p_j, t)|_{p_j \in \Sigma}$ equals to $E_{z_j}(p_j, t)|_{p_j \in \Sigma}$, and [3]

$$\frac{\partial E_{z_j}}{\partial t} = \eta_0 \rho_j^{-1} \frac{\partial(\rho_j H_{\phi_j})}{\partial \rho_j}.$$

The *space-time amplitudes* $u_{n,j}(z_j, t)$ of the wave $U(g_j, t)$, $g_j \in \Omega_j$ are determined by a solution to the initial boundary value problem

$$\left\{ \begin{array}{l} \left[-\frac{\partial^2}{\partial t^2} + \frac{\partial^2}{\partial z_j^2} - \lambda_{nj}^2 \right] u_{n,j}(z_j, t) = 0; \quad t > 0, \quad z_j > 0 \\ u_{n,j}(z_j, 0) = 0, \quad \left. \frac{\partial}{\partial t} u_{n,j}(z_j, t) \right|_{t=0} = 0; \quad z_j \geq 0 \end{array} \right. \quad (5.9)$$

(it is assumed that the excitation $U(g, t)$, which is generated by the sources $\varphi(g)$, $\psi(g)$, and $F(g, t)$ located in Ω_{int} , has not yet reached the boundary $z_j = 0$ separating Ω_{int} and Ω_j by the moment of time $t = 0$).

Analytical representations for the solutions $\mu_{n,j}(\rho)$ and $\lambda_{n,j}$ to the problems (5.7), (5.8) are well-known [3, 8] and for TE_0 -waves are:

$$\left\{ \begin{array}{l} \mu_{nj}(\rho_j) = G_1(\lambda_{nj}, \rho_j) \sqrt{2} \left[a_j^2 G_0^2(\lambda_{nj}, a_j) - b_j^2 G_0^2(\lambda_{nj}, b_j) \right]^{-1/2}; \\ b_j < \rho_j < a_j \\ \lambda_{nj} > 0 \text{ are the roots of the equation } G_1(\lambda_j, a_j) = 0; \\ G_q(\lambda_j, \rho_j) = J_q(\lambda_j \rho_j) N_1(\lambda_j b_j) - N_q(\lambda_j \rho_j) J_1(\lambda_j b_j); \quad q = 0, 1 \end{array} \right. \quad (5.10)$$

for coaxial waveguide Ω_j and

$$\left\{ \begin{array}{l} \mu_{nj}(\rho_j) = J_1(\lambda_{nj} \rho_j) \sqrt{2} \left[a_j J_0(\lambda_{nj} a_j) \right]^{-1}; \quad 0 < \rho_j < a_j \\ \lambda_{nj} > 0 \text{ are the roots of the equation } J_1(\lambda_j a_j) = 0 \end{array} \right. \quad (5.11)$$

for circular waveguide Ω_j . For TM_0 -waves we have:

$$\left\{ \begin{array}{l} \mu_{nj}(\rho_j) = J_1(\lambda_{nj} \rho_j) \sqrt{2} \left[a_j J_1(\lambda_{nj} a_j) \right]^{-1}; \quad 0 < \rho_j < a_j \\ \lambda_{nj} > 0 \text{ are the roots of the equation } J_0(\lambda_j a_j) = 0 \end{array} \right. \quad (5.12)$$

for circular waveguide Ω_j and

$$\left\{ \begin{array}{l} \mu_{nj}(\rho_j) = \tilde{G}_1(\lambda_{nj}, \rho_j) \sqrt{2} \left[a_j^2 \tilde{G}_1^2(\lambda_{nj}, a_j) - b_j^2 \tilde{G}_1^2(\lambda_{nj}, b_j) \right]^{-1/2} \text{ for } n = 1, 2, \dots \\ \text{and } \mu_{0j}(\rho_j) = \left[\rho_j \sqrt{\ln(a_j/b_j)} \right]^{-1}; \quad b_j < \rho_j < a_j \\ \lambda_{nj} > 0 \text{ (} n = 1, 2, \dots \text{) are the roots of the equation } \tilde{G}_0(\lambda_j, b_j) = 0 \\ \text{and } \lambda_{0j} = 0; \\ \tilde{G}_q(\lambda_j, \rho_j) = J_q(\lambda_j \rho_j) N_0(\lambda_j a_j) - N_q(\lambda_j \rho_j) J_0(\lambda_j a_j); \quad q = 0, 1 \end{array} \right. \quad (5.13)$$

for coaxial waveguide Ω_j . Here, $J_q(\dots)$ and $N_q(\dots)$ are the Bessel and Neumann cylindrical functions.

Applying the cosine Fourier transform

$$\tilde{f}(\omega) = \sqrt{\frac{2}{\pi}} \int_0^\infty f(z_j) \cos(\omega z_j) dz_j \leftrightarrow f(z_j) = \sqrt{\frac{2}{\pi}} \int_0^\infty \tilde{f}(\omega) \cos(\omega z_j) d\omega \quad (5.14)$$

to the problem (5.9) and taking into account that

$$-\omega^2 \tilde{f}(\omega) - \sqrt{\frac{2}{\pi}} \left[\frac{d}{dz_j} f(z_j) \right] \Big|_{z_j=0} \leftrightarrow \frac{d^2}{dz_j^2} f(z_j)$$

[34], we obtain the following Cauchy problem for the images $\tilde{u}_{nj}(\omega, t)$ of $u_{nj}(z_j, t)$:

$$\begin{cases} D\left(\sqrt{\lambda_{nj}^2 + \omega^2}\right) [\tilde{u}_{nj}(\omega, t)] = -\sqrt{\frac{2}{\pi}}u_{nj}'(0, t); & \omega > 0, \quad t > 0 \\ \tilde{u}_{nj}(\omega, 0) = 0, \quad \frac{\partial}{\partial t}\tilde{u}_{nj}(\omega, t)\Big|_{t=0} = 0; & \omega \geq 0, \end{cases} \quad (5.15)$$

where

$$D\left(\sqrt{\lambda_{nj}^2 + \omega^2}\right) [\tilde{u}_{nj}(\omega, t)] \equiv \left[\frac{\partial^2}{\partial t^2} + \left(\lambda_{nj}^2 + \omega^2\right)\right] \tilde{u}_{nj}(\omega, t) \quad \text{and}$$

$$u_{nj}'(c, t) = \frac{\partial u_{nj}(z_j, t)}{\partial z_j} \Big|_{z_j=c}.$$

The derivation of (5.15) is based on the fact that the wave $U(g_j, t)$ ($g_j \in \Omega_j$) is an outgoing wave, and thus the amplitudes $u_{nj}(z_j, t)$ of all its partial components are zero at any time t for z_j large enough.

Continuing the functions $\tilde{u}_{nj}(\omega, t)$ and $u_{nj}'(0, t)$ by zero on the semiaxis $t < 0$, the generalized formulation of the Cauchy problem (5.15) [35] is obtained:

$$\begin{aligned} D\left(\sqrt{\lambda_{nj}^2 + \omega^2}\right) [\tilde{u}_{nj}(\omega, t)] &= -\sqrt{\frac{2}{\pi}}u_{nj}'(0, t) + \delta^{(1)}(t)\tilde{u}_{nj}(\omega, 0) \\ &\quad + \delta(t)\frac{\partial}{\partial t}\tilde{u}_{nj}(\omega, t)\Big|_{t=0} \\ &= -\sqrt{\frac{2}{\pi}}u_{nj}'(0, t); \quad \omega > 0, \quad -\infty < t < \infty, \end{aligned} \quad (5.16)$$

where $\delta(\dots)$ and $\delta^{(1)}(\dots)$ are the Dirac delta-function and its generalized derivative of the first order.

A convolution of the fundamental solution $G(\lambda, t) = \chi(t)\lambda^{-1} \sin \lambda t$ of the operator $D(\lambda)[\dots]$ with the right-hand side of the equation $D(\lambda)[u(t)] = f(t)$ gives its solution $u(t)$ [3, 35]. Here, $\chi(\dots)$ is the Heaviside step function. Therefore, the unknown functions $\tilde{u}_{nj}(\omega, t)$ from (5.16) can be represented as

$$\begin{aligned} \tilde{u}_{nj}(\omega, t) &= -\sqrt{\frac{2}{\pi}} \int_0^t \sin\left[(t-\tau)\sqrt{\lambda_{nj}^2 + \omega^2}\right] \frac{u_{nj}'(0, \tau)}{\sqrt{\lambda_{nj}^2 + \omega^2}} d\tau; \\ \omega &\geq 0, \quad t \geq 0. \end{aligned} \quad (5.17)$$

Applying the inverse transform (5.14) to (5.17), we get the originals $u_{nj}(z_j, t)$:

$$u_{nj}(z_j, t) = - \int_0^{t-z_j} J_0 \left[\lambda_{nj} \left((t-\tau)^2 - z_j^2 \right)^{1/2} \right] u_{nj}'(0, \tau) d\tau; \quad (5.18)$$

$$z_j \geq 0, \quad t \geq 0.$$

Multiplying (5.18) by $\mu_{nj}(\rho_j)$ and summing over all n , we obtain the *radiation condition* (RC) for the waves $U(g_j, t)$ outgoing towards $z_j = \infty$:

$$U(g_j, t) = - \sum_n \left\{ \int_0^{t-z_j} J_0 \left[\lambda_{nj} \left((t-\tau)^2 - z_j^2 \right)^{1/2} \right] \right. \\ \left. \times \left[\int_{\rho_{j(1)}}^{\rho_{j(2)}} \frac{\partial U(\rho_j, z_j, \tau)}{\partial z_j} \Big|_{z_j=0} \mu_{nj}(\rho_j) \rho_j d\rho_j \right] d\tau \right\} \mu_{nj}(\rho_j); \quad (5.19)$$

$$g_j = \{\rho_j, z_j\} \in \Omega_j, \quad t \geq z_j.$$

In (5.19), one should set $\rho_{j(1)} = 0$ and $\rho_{j(2)} = a_j$ for a circular waveguide Ω_j or $\rho_{j(1)} = b_j$ and $\rho_{j(2)} = a_j$ for a coaxial waveguide.

The equations (5.18) and (5.19) specify the operator $X_{0 \rightarrow z_j}(t)[u']$, which operates on the amplitudes $u_{nj}(z_j, t)$ according to the rule

$$u_{nj}(z_j, t) = X_{0 \rightarrow z_j}(t)[u_{nj}'(0, \tau)]; \quad (5.20)$$

$$z_j \geq 0, \quad t \geq z_j, \quad t - z_j \geq \tau \geq 0,$$

and the operator

$$U(g_j, t) = Z_{q_j \in \Gamma_j \rightarrow g_j \in \Omega_j}(t)[U'(q_j, \tau)]; \quad U'(q_j, \tau) = \frac{\partial U(g_j, \tau)}{\partial z_j} \Big|_{z_j=0}, \quad (5.21)$$

$$t \geq z_j, \quad t - z_j \geq \tau \geq 0.$$

The operators (5.20) and (5.21) allow to compute the values of $u_{nj}(z_j, t)$ and $U(g_j, t)$ in any point in the waveguide Ω_j knowing only their values on the virtual boundary Γ_j . The operators (5.20) and (5.21) are the so-called *transport operators* which relate near-zone and far-zone fields. They are discussed in more details in Sect. 5.3.3.

5.2.3 Nonlocal Exact Absorbing Conditions

Placing the observation point in (5.18) onto the virtual boundary Γ_j ($z_j = 0$), we obtain

$$u_{nj}(0, t) = - \int_0^t J_0[\lambda_{nj}(t - \tau)] u_{nj}'(0, \tau) d\tau; \quad t \geq 0. \tag{5.22}$$

Differentiating (5.22) with respect to t , we can write

$$\left[\frac{\partial}{\partial t} + \frac{\partial}{\partial z_j} \right] u_{nj}(z_j, t) \Big|_{z_j=0} = \lambda_{nj} \int_0^t J_1[\lambda_{nj}(t - \tau)] u_{nj}'(0, \tau) d\tau; \quad t \geq 0. \tag{5.23}$$

Here, the relationships $dJ_0(x)/dx = -J_1(x)$, $J_0(0) = 1$, and $\chi^{(1)}(t - \tau) = \delta(t - \tau)$ were used, $\chi^{(1)}(\dots)$ stands for the generalized derivative of $\chi(\dots)$.

Applying the Laplace transform

$$\tilde{f}(s) = \int_0^\infty f(t)e^{-st} dt \leftrightarrow f(t) = \frac{1}{2\pi i} \int_{\alpha-i\infty}^{\alpha+i\infty} \tilde{f}(s)e^{st} ds \tag{5.24}$$

to (5.23) and taking into account the relationships $\tilde{f}_1(s)\tilde{f}_2(s) \leftrightarrow \int_0^t f_1(t - \tau) f_2(\tau) d\tau$ (the convolution theorem), $\lambda^2 \left[\sqrt{s^2 + \lambda^2} (\sqrt{s^2 + \lambda^2} + s) \right]^{-1} \leftrightarrow \lambda J_1(\lambda t)$ [36], and $s\tilde{f}(s) - f(0) \leftrightarrow df(t)/dt$, we obtain the following expression in the space of images $\tilde{u}_{nj}(z, s)$:

$$\left[\frac{\partial}{\partial z_j} + s \right] \tilde{u}_{nj}(z_j, s) \Big|_{z_j=0} = \frac{\lambda_{nj}^2 \tilde{u}_{nj}'(0, s)}{\sqrt{s^2 + \lambda_{nj}^2} (\sqrt{s^2 + \lambda_{nj}^2} + s)}, \tag{5.25}$$

which is equivalent to

$$\tilde{u}_{nj}'(0, s) = - \left(s + \frac{\lambda_{nj}^2}{s + \sqrt{s^2 + \lambda_{nj}^2}} \right) \tilde{u}_{nj}(0, s). \tag{5.26}$$

Applying the inverse Laplace transform to (5.26), we return back to the originals:

$$\left[\frac{\partial}{\partial t} + \frac{\partial}{\partial z_j} \right] u_{nj}(z_j, t) \Big|_{z_j=0} = -\lambda_{nj} \int_0^t J_1[\lambda_{nj}(t-\tau)](t-\tau)^{-1} u_{nj}(0, \tau) d\tau; \tag{5.27}$$

$t \geq 0.$

Here, the formula $(s + \sqrt{s^2 + \lambda^2})^{-1} \leftrightarrow (\lambda t)^{-1} J_1(\lambda t)$ [37] was used.

To justify the use of the Laplace transform (5.24) when passing from (5.23) to (5.27), we refer to the estimates in [38]. From these estimates it follows that at the points g of any bounded subdomain of the domain Ω , the field $U(g, t)$ generated by a system of sources with compact supports cannot grow faster than $\exp(\alpha t)$ for $t \rightarrow \infty$, where $\alpha > 0$ is some constant. The estimates are valid for all electrodynamic structures whose spectrum of complex-valued eigenfrequencies $\{\bar{k}_n\}_n$ does not contain the points \bar{k}_m from the upper half-plane of the first (physical) sheet, which constitutes a natural domain of variation of the complex frequency parameter k [3]. All open structures considered in this section fall into this category [39].

Rewriting (5.22), (5.23), and (5.27) in terms of (5.6), we obtain:

$$U(\rho_j, 0, t) = - \sum_n \left\{ \int_0^t J_0[\lambda_{nj}(t-\tau)] \right. \\ \times \left. \left[\int_{\rho_{j(1)}}^{\rho_{j(2)}} \frac{\partial U(\rho_j, z_j, \tau)}{\partial z_j} \Big|_{z_j=0} \mu_{nj}(\rho_j) \rho_j d\rho_j \right] d\tau \right\} \tag{5.28}$$

$\times \mu_{nj}(\rho_j); \quad \rho_{j(1)} \leq \rho \leq \rho_{j(2)}, \quad t \geq 0,$

$$\left[\frac{\partial}{\partial t} + \frac{\partial}{\partial z_j} \right] U(\rho_j, z_j, t) \Big|_{z_j=0} = \sum_n \lambda_{nj} \left\{ \int_0^t J_1[\lambda_{nj}(t-\tau)] \right. \\ \times \left. \left[\int_{\rho_{j(1)}}^{\rho_{j(2)}} \frac{\partial U(\rho_j, z_j, \tau)}{\partial z_j} \Big|_{z_j=0} \mu_{nj}(\rho_j) \rho_j d\rho_j \right] d\tau \right\} \\ \times \mu_{nj}(\rho_j); \quad \rho_{j(1)} \leq \rho \leq \rho_{j(2)}, \quad t \geq 0, \tag{5.29}$$

and

$$\begin{aligned}
 \left[\frac{\partial}{\partial t} + \frac{\partial}{\partial z_j} \right] U(\rho_j, z_j, t) \Big|_{z_j=0} &= - \sum_n \lambda_{n,j} \left\{ \int_0^t J_1[\lambda_{n,j}(t-\tau)] \right. \\
 &\quad \times (t-\tau)^{-1} \left[\int_{\rho_{j(1)}}^{\rho_{j(2)}} U(\rho_j, 0, \tau) \mu_{n,j}(\rho_j) \rho_j d\rho_j \right] d\tau \left. \right\} \\
 &\quad \times \mu_{n,j}(\rho_j); \quad \rho_{j(1)} \leq \rho_j \leq \rho_{j(2)}, \quad t \geq 0.
 \end{aligned}
 \tag{5.30}$$

The relationships (5.28)–(5.30) are valid for all waves $U(g, t)$ outgoing into the waveguide Ω_j . The relationships (5.22), (5.23), and (5.27) deal with the space-time amplitudes $u_{n,j}(z_j, t)$ of all modes traveling towards $z_j = \infty$ on the boundary Γ_j , while the relationships (5.28)–(5.30) deal with the waves $U(g, t)$. The relationships (5.28)–(5.30) relate values of $U(g, t)$ with values of its derivatives on the virtual boundary Γ_j , and thus could be used as boundary conditions. The boundary conditions (5.28)–(5.30) are called *exact absorbing conditions* (EACs) because they are exact by derivation, and the wave $U(g, t)$ is not distorted crossing the boundary Γ_j ; there is no reflection back into the domain Ω_{int} , the wave $U(g, t)$ passes into the domain Ω_j completely, as if it is absorbed by that domain or by the virtual boundary Γ_j . The open problem (5.4) and the problem (5.4) with the bounded computation domain Ω_{int} together with any of EACs (5.28)–(5.30) on the virtual boundaries Γ_j , $j = 1, 2, \dots, J$ are equivalent (see Sect. 5.2.5). For the first time, the equations (5.22), (5.28) were used as EACs in [1].

EACs (5.28)–(5.30) are *nonlocal* in space (with respect to ρ_j) and in time: the function $U(\rho_j, z_j, t)$ and its derivatives at each point of the boundary Γ_j and at each moment of time are determined by the values of this function or its derivatives at all other points of the boundary and at all previous moments of time $\tau < t$. Numerical implementation of nonlocal EACs could be computationally expensive as discussed in Sect. 5.7. For practical applications, FFT-based acceleration of nonlocal EACs is used as detailed in Sect. 5.7.3 or nonlocal EACs are replaced with local ones as detailed next.

5.2.4 Local Exact Absorbing Conditions

Using the formula [34]

$$J_0(x) = \frac{2}{\pi} \int_0^{\pi/2} \cos(x \sin \varphi) d\varphi,$$

let us rewrite (5.22) as

$$u_{nj}(0, t) = -\frac{2}{\pi} \int_0^{\pi/2} \left\{ \int_0^t \cos [\lambda_{nj}(t - \tau) \sin \varphi] u_{nj}'(0, \tau) d\tau \right\} d\varphi; \quad t \geq 0. \quad (5.31)$$

Denote

$$w_{nj}(t, \varphi) = - \int_0^t \frac{\sin [\lambda_{nj}(t - \tau) \sin \varphi] u_{nj}'(0, \tau)}{\lambda_{nj} \sin \varphi} d\tau; \quad (5.32)$$

$$t \geq 0, \quad 0 \leq \varphi \leq \pi/2.$$

Then

$$\frac{\partial w_{nj}(t, \varphi)}{\partial t} = - \int_0^t \cos [\lambda_{nj}(t - \tau) \sin \varphi] u_{nj}'(0, \tau) d\tau,$$

and we have from (5.31) that

$$u_{nj}(0, t) = \frac{2}{\pi} \int_0^{\pi/2} \frac{\partial w_{nj}(t, \varphi)}{\partial t} d\varphi; \quad t \geq 0. \quad (5.33)$$

The integral form (5.32) is equivalent to the following differential form:

$$\begin{cases} \left[\frac{\partial^2}{\partial t^2} + \lambda_{nj}^2 \sin^2 \varphi \right] w_{nj}(t, \varphi) = -u_{nj}'(0, t); & t > 0 \\ w_{nj}(0, \varphi) = \frac{\partial w_{nj}(t, \varphi)}{\partial t} \Big|_{t=0} = 0. \end{cases} \quad (5.34)$$

Indeed, using the generalized formulation of the corresponding Cauchy problem, and the fundamental solution $G(\lambda, t) = \chi(t)\lambda^{-1} \sin \lambda t$ of the operator $D(\lambda) \equiv [d^2/dt^2 + \lambda^2]$ (see [3]), we can easily verify that the formulas (5.32) and (5.34) determine the same function $w_{nj}(t, \varphi)$.

Let us now multiply (5.33) and (5.34) by $\mu_{nj}(\rho_j)$ and sum over all n . As a result, taking into account that

$$\sum_n \lambda_{nj}^2 u_{nj}(z_j, t) \mu_{nj}(\rho_j) = -\frac{\partial}{\partial \rho_j} \frac{1}{\rho_j} \frac{\partial}{\partial \rho_j} \rho_j U(\rho_j, z_j, t)$$

and

$$\sum_n \lambda_{nj}^2 w_{nj}(t, \varphi) \mu_{nj}(\rho_j) = -\frac{\partial}{\partial \rho_j} \frac{1}{\rho_j} \frac{\partial}{\partial \rho_j} \rho_j W(\rho_j, t, \varphi)$$

for

$$W(\rho_j, t, \varphi) = \sum_n w_{nj}(t, \varphi) \mu_{nj}(\rho_j)$$

(see the problems (5.7), (5.8)), we obtain

$$U(\rho_j, 0, t) = \frac{2}{\pi} \int_0^{\pi/2} \frac{\partial W(\rho_j, t, \varphi)}{\partial t} d\varphi; \quad t \geq 0, \quad \rho_{j(1)} \leq \rho_j \leq \rho_{j(2)}, \quad (5.35a)$$

$$\begin{cases} \left[\frac{\partial^2}{\partial t^2} - \sin^2 \varphi \frac{\partial}{\partial \rho_j} \frac{1}{\rho_j} \frac{\partial}{\partial \rho_j} \rho_j \right] W(\rho_j, t, \varphi) = -\frac{\partial U(\rho_j, z_j, t)}{\partial z_j} \Big|_{z_j=0}; \\ \rho_{j(1)} < \rho_j < \rho_{j(2)}, \quad t > 0 \\ W(\rho_j, 0, \varphi) = \frac{\partial W(\rho_j, t, \varphi)}{\partial t} \Big|_{t=0} = 0, \quad \rho_{j(1)} \leq \rho_j \leq \rho_{j(2)}. \end{cases} \quad (5.35b)$$

Here, $W(\rho_j, t, \varphi)$ is an auxiliary function, which can be determined by solving the auxiliary initial boundary value problem (5.35b); $0 \leq \varphi \leq \pi/2$ is a numeric parameter.

The same manipulations with (5.23) and (5.27) result in the following local EACs different from (5.35a), (5.35b):

$$\begin{aligned} \left[\frac{\partial}{\partial t} + \frac{\partial}{\partial z_j} \right] U(\rho_j, z_j, t) \Big|_{z_j=0} &= \frac{2}{\pi} \int_0^{\pi/2} W(\rho_j, t, \varphi) \cos^2 \varphi d\varphi; \\ t \geq 0, \quad \rho_{j(1)} \leq \rho_j \leq \rho_{j(2)}, \end{aligned} \quad (5.36a)$$

$$\begin{cases} \left[\frac{\partial^2}{\partial t^2} - \cos^2 \varphi \frac{\partial}{\partial \rho_j} \frac{1}{\rho_j} \frac{\partial}{\partial \rho_j} \rho_j \right] W(\rho_j, t, \varphi) = -\frac{\partial}{\partial \rho_j} \frac{1}{\rho_j} \frac{\partial}{\partial \rho_j} \rho_j \\ \quad \times \left[\frac{\partial}{\partial z_j} U(\rho_j, z_j, t) \Big|_{z_j=0} \right]; \quad \rho_{j(1)} < \rho_j < \rho_{j(2)}, \quad t > 0 \\ W(\rho_j, 0, \varphi) = \frac{\partial W(\rho_j, t, \varphi)}{\partial t} \Big|_{t=0} = 0; \quad \rho_{j(1)} \leq \rho_j \leq \rho_{j(2)} \end{cases} \quad (5.36b)$$

and

$$\left[\frac{\partial}{\partial t} + \frac{\partial}{\partial z_j} \right] U(\rho_j, z_j, t) \Big|_{z_j=0} = \frac{2}{\pi} \int_0^{\pi/2} \frac{\partial W(\rho_j, t, \varphi)}{\partial t} \sin^2 \varphi d\varphi; \quad (5.37a)$$

$$t \geq 0, \quad \rho_{j(1)} \leq \rho_j \leq \rho_{j(2)},$$

$$\left\{ \begin{array}{l} \left[\frac{\partial^2}{\partial t^2} - \cos^2 \varphi \frac{\partial}{\partial \rho_j} \frac{1}{\rho_j} \frac{\partial}{\partial \rho_j} \rho_j \right] W(\rho_j, t, \varphi) = \frac{\partial}{\partial \rho_j} \frac{1}{\rho_j} \frac{\partial}{\partial \rho_j} \rho_j U(\rho_j, 0, t); \\ \rho_{j(1)} < \rho_j < \rho_{j(2)}, \quad t > 0 \\ W(\rho_j, 0, \varphi) = \frac{\partial W(\rho_j, t, \varphi)}{\partial t} \Big|_{t=0} = 0; \quad \rho_{j(1)} \leq \rho_j \leq \rho_{j(2)}. \end{array} \right. \quad (5.37b)$$

In derivation of (5.36a), (5.36b), the following formula was used [40]

$$J_1(x) = \frac{2}{\pi} \int_0^{\pi/2} \sin(x \cos \varphi) \cos \varphi d\varphi$$

along with the substitutions

$$w_{nj}(t, \varphi) = \lambda_{nj} \int_0^t \frac{\sin[\lambda_{nj}(t-\tau) \cos \varphi] u_{nj}'(0, \tau)}{\cos \varphi} d\tau; \quad t \geq 0, \quad 0 \leq \varphi \leq \pi/2,$$

while in the derivation of (5.37a), (5.37b), we applied the integral Poisson formula [34]

$$J_1(x) = \frac{2x}{\pi} \int_0^{\pi/2} \cos(x \cos \varphi) \sin^2 \varphi d\varphi$$

and

$$w_{nj}(t, \varphi) = -\lambda_{nj} \int_0^t \frac{\sin[\lambda_{nj}(t-\tau) \cos \varphi] u_{nj}(0, \tau)}{\cos \varphi} d\tau; \quad t \geq 0, \quad 0 \leq \varphi \leq \pi/2.$$

The auxiliary initial boundary value problems (5.35b), (5.36b), and (5.37b) should be supplemented by the following boundary conditions for all time moments $t \geq 0$

$$\left\{ \begin{array}{l} W(0, t, \varphi) = W(a_j, t, \varphi) = 0; \quad TE_0\text{-waves} \\ W(0, t, \varphi) = \frac{\partial(\rho_j W(\rho_j, t, \varphi))}{\partial \rho_j} \Big|_{\rho_j=a_j} = 0; \quad TM_0\text{-waves} \end{array} \right.$$

(for the domain Ω_j corresponding to a circular waveguide) and

$$\left\{ \begin{array}{l} W(b_j, t, \varphi) = W(a_j, t, \varphi) = 0; \quad TE_0\text{-waves} \\ \left. \frac{\partial(\rho_j W(\rho_j, t, \varphi))}{\partial \rho_j} \right|_{\rho_j=b_j} = \left. \frac{\partial(\rho_j W(\rho_j, t, \varphi))}{\partial \rho_j} \right|_{\rho_j=a_j} = 0; \quad TM_0\text{-waves} \end{array} \right.$$

(for the domain Ω_j corresponding to a coaxial waveguide).

The formulas (5.35a), (5.35b)–(5.37a), (5.37b), just like (5.28)–(5.30), exactly describe the behavior of the waves $U(g, t)$ on the boundary Γ_j , thus, they are EACs for the outgoing waves. In contrast with EACs (5.28)–(5.30), EACs (5.35a), (5.35b)–(5.37a), (5.37b) are *local* both in space and time: in (5.35a), (5.36a), and (5.37a) the function $U(g, t)$ and its derivatives at each point ρ_j of the boundary Γ_j and at each moment of time t are determined by the auxiliary function $W(\rho_j, t, \varphi)$ at the same point and the same moment of time.

5.2.5 Equivalence Theorem

EACs derived in Sects. 5.2.3, 5.2.4 allow us to replace the original open problem (5.4) with the closed (modified) problem

$$\left\{ \begin{array}{l} \left[-\varepsilon(g) \frac{\partial^2}{\partial t^2} - \sigma(g) \eta_0 \frac{\partial}{\partial t} + \frac{\partial^2}{\partial z^2} + \frac{\partial}{\partial \rho} \left(\frac{1}{\rho} \frac{\partial}{\partial \rho} \rho \right) \right] U(g, t) = F(g, t); \\ t > 0, \quad g \in \Omega_{\text{int}} \\ U(g, t)|_{t=0} = \varphi(g), \quad \left. \frac{\partial}{\partial t} U(g, t) \right|_{t=0} = \psi(g); \quad g = \{\rho, z\} \in \bar{\Omega}_{\text{int}} \\ \vec{E}_{\text{tg}}(p, t)|_{p=\{\rho, \phi, z\} \in \Sigma} = 0, \quad U(0, z, t) = 0 \quad \text{for } \{0, z\} \in \bar{\Omega}_{\text{int}}, \\ \text{and } D_{\text{add}}[U(g, t)]|_{g \in \Gamma_{\text{add}}} = 0; \quad t \geq 0 \end{array} \right. \quad (5.38)$$

and the total kit ($j = 1, 2, \dots, J$) of RCs (5.19) for the points $g \in \Omega_{\text{add}} = \bigcup_{j=1}^J \Omega_j$.

Below we prove that this replacement is equivalent, in other words, any solution to the problem (5.4) is at the same time a solution to the problem (5.38), (5.19) and vice versa. By $D_{\text{add}}[U(g, t)]|_{g \in \Gamma_{\text{add}}} = 0$, $\Gamma_{\text{add}} = \bigcup_{j=1}^J \Gamma_j$ we denote here the total kit ($j = 1, 2, \dots, J$) of EACs. It may be local or/and nonlocal EACs (5.28) to (5.30) and (5.35a), (5.35b) to (5.37a), (5.37b) in any combination.

The problem (5.4) is uniquely solvable in the space of generalized functions $W_2^1(\Omega^T)$. Its unique solution $U(g, t)$ is at the same time a solution to the problem

(5.38) from the Sobolev space $W_2^1(\Omega_{\text{int}}^T)$, where $\Omega_{\text{int}}^T = \Omega_{\text{int}} \times (0, T)$. This direct inclusion is trivial, it is proved by the derivations in Sects. 5.2.2 to 5.2.4. The inverse inclusion is true only if the generalized solution $U(g, t)$ to the problem (5.38) from the space $W_2^1(\Omega_{\text{int}}^T)$ is unique. Let us prove the uniqueness.

According to [33], the generalized solution to the problem (5.38) is an element $U(g, t)$ of the space $W_2^1(\Omega_{\text{int}}^T)$ which is equal to $\varphi(g)$ at $t = 0$ and satisfying the identity

$$\begin{aligned} & \int_{\Omega_{\text{int}}^T} \left[\varepsilon \frac{\partial U}{\partial t} \frac{\partial \gamma}{\partial t} - \left(\frac{1}{\rho^2} \frac{\partial}{\partial \rho} \rho U \right) \frac{\partial(\rho \gamma)}{\partial \rho} - \frac{\partial U}{\partial z} \frac{\partial \gamma}{\partial z} - \sigma \eta_0 \frac{\partial U}{\partial t} \gamma \right] dg dt \\ & + \int_{\Phi^T} \left[\left(\frac{1}{\rho} \frac{\partial}{\partial \rho} \rho U \right) \gamma \cos(\vec{n}, \vec{\rho}) + \frac{\partial U}{\partial z} \gamma \cos(\vec{n}, \vec{z}) \right] ds dt \\ & + \int_{\Omega_{\text{int}}} \varepsilon \psi \gamma(g, 0) dg = \int_{\Omega_{\text{int}}^T} F \gamma dg dt \end{aligned} \quad (5.39)$$

for any function $\gamma(g, t)$ from $W_2^1(\Omega_{\text{int}}^T)$ that is zero at $t = T$. Here, Φ^T is a lateral surface of the cylinder Ω_{int}^T ($\Phi^T = \Phi \times (0, T)$); Φ is the boundary of the domain Ω_{int} ; $\cos(\vec{n}, \vec{\rho})$ and $\cos(\vec{n}, \vec{z})$ are cosines of the angles between the outer normal \vec{n} to the surface Φ^T and the axes $\vec{\rho}$ and \vec{z} , respectively. An element of the end surfaces of the cylinder is $dg = \rho d\rho dz$. The identity (5.39) is obtained multiplying the equation from (5.38) by $\gamma(g, t)$ and integrating the result by parts in Ω_{int}^T [33, 41].

Assume that there exist two solutions to the problem (5.38) from the space $W_2^1(\Omega_{\text{int}}^T)$: $U_1(g, t)$ and $U_2(g, t)$. The difference between them $u(g, t) = U_1(g, t) - U_2(g, t)$ is a solution to the homogeneous problem similar to (5.38), so it satisfies the identity (see (5.39))

$$\begin{aligned} & \int_{\Omega_{\text{int}}^T} \left[\varepsilon \frac{\partial u}{\partial t} \frac{\partial \gamma}{\partial t} - \left(\frac{1}{\rho^2} \frac{\partial}{\partial \rho} \rho u \right) \frac{\partial(\rho \gamma)}{\partial \rho} - \frac{\partial u}{\partial z} \frac{\partial \gamma}{\partial z} - \sigma \eta_0 \frac{\partial u}{\partial t} \gamma \right] dg dt \\ & + \int_{\Phi^T} \left[\left(\frac{1}{\rho} \frac{\partial}{\partial \rho} \rho u \right) \gamma \cos(\vec{n}, \vec{\rho}) + \frac{\partial u}{\partial z} \gamma \cos(\vec{n}, \vec{z}) \right] ds dt = 0. \end{aligned} \quad (5.40)$$

Let us introduce an arbitrary $\tau \in (0, T)$ and consider the following function

$$\gamma(g, t) = \begin{cases} \int_t^\tau u(g, \zeta) d\zeta; & 0 < t < \tau \\ 0; & \tau < t < T \end{cases}.$$

It can be verified easily that $\gamma(g, t)$ has the generalized derivatives in Ω_{int}^T [41]

$$\frac{\partial \gamma(g, t)}{\partial t} = \begin{cases} -u(g, t); & 0 < t < \tau \\ 0; & \tau < t < T \end{cases}, \quad \frac{\partial \gamma(g, t)}{\partial \rho} = \begin{cases} \int_t^\tau \frac{\partial u(g, \zeta)}{\partial \rho} d\zeta; & 0 < t < \tau \\ 0; & \tau < t < T \end{cases},$$

$$\text{and } \frac{\partial \gamma(g, t)}{\partial z} = \begin{cases} \int_t^\tau \frac{\partial u(g, \zeta)}{\partial z} d\zeta; & 0 < t < \tau \\ 0; & \tau < t < T \end{cases}.$$

At the same time we have $\gamma(g, t)|_{t=T} = 0$. Substituting the function $\gamma(g, t)$ into the identity (5.40), we obtain:

$$\begin{aligned} & \int_{\Omega_{\text{int}}^\tau} \left[\varepsilon \frac{\partial u}{\partial t} u + \frac{1}{\rho^2} \left(\frac{\partial}{\partial \rho} \rho u \right) \left(\int_t^\tau \frac{\partial}{\partial \rho} \rho u(\zeta) d\zeta \right) \right. \\ & \left. + \frac{\partial u}{\partial z} \left(\int_t^\tau \frac{\partial}{\partial z} u(\zeta) d\zeta \right) + \sigma \eta_0 \frac{\partial u}{\partial t} \gamma \right] dg dt \\ & - \int_{\Phi^\tau} \left[\left(\frac{1}{\rho} \frac{\partial}{\partial \rho} \rho u \right) \gamma \cos(\vec{n}, \vec{\rho}) + \frac{\partial u}{\partial z} \gamma \cos(\vec{n}, \vec{z}) \right] ds dt = 0. \end{aligned} \tag{5.41}$$

Since [41]

$$\int_{\Omega_{\text{int}}^\tau} \left[k(g) f(g, t) \int_t^\tau f(g, \zeta) d\zeta \right] dg dt = \frac{1}{2} \int_{\Omega_{\text{int}}} k(g) \left(\int_0^\tau f(g, t) dt \right)^2 dg,$$

then

$$\int_{\Omega_{\text{int}}^\tau} \left[\frac{1}{\rho^2} \left(\frac{\partial}{\partial \rho} \rho u \right) \left(\int_t^\tau \frac{\partial}{\partial \rho} \rho u(\zeta) d\zeta \right) \right] dg dt = \frac{1}{2} \int_{\Omega_{\text{int}}} \frac{1}{\rho^2} \left(\int_0^\tau \frac{\partial}{\partial \rho} \rho u dt \right)^2 dg \geq 0 \tag{5.42}$$

and

$$\int_{\Omega_{\text{int}}^\tau} \left[\frac{\partial u}{\partial z} \left(\int_t^\tau \frac{\partial}{\partial z} u(\zeta) d\zeta \right) \right] dg dt = \frac{1}{2} \int_{\Omega_{\text{int}}} \left(\int_0^\tau \frac{\partial}{\partial z} u dt \right)^2 dg \geq 0. \tag{5.43}$$

Performing partial integration and taking into consideration that $\gamma(g, t)|_{t=\tau} = 0$ and $u(g, t)|_{t=0} = 0$, we also obtain

$$\int_{\Omega_{\text{int}}^{\varepsilon}} \left[\varepsilon \frac{\partial u}{\partial t} u \right] dg dt = \frac{1}{2} \int_{\Omega_{\text{int}}} \varepsilon [u(g, \tau)]^2 dg \geq 0 \quad (5.44)$$

and

$$\int_{\Omega_{\text{int}}^{\varepsilon}} \left[\sigma \frac{\partial u}{\partial t} \gamma \right] dg dt = - \int_{\Omega_{\text{int}}^{\varepsilon}} \left[\sigma u \frac{\partial \gamma}{\partial t} \right] dg dt = \int_{\Omega_{\text{int}}^{\varepsilon}} \sigma u^2 dg dt \geq 0. \quad (5.45)$$

Thus, all the volume integrals in the identity (5.41) are non-negative. Let us show that the integral

$$I_1(\tau) = - \int_{\Phi^{\varepsilon}} \left[\left(\frac{1}{\rho} \frac{\partial}{\partial \rho} \rho u \right) \gamma \cos(\vec{n}, \vec{\rho}) + \frac{\partial u}{\partial z} \gamma \cos(\vec{n}, \vec{z}) \right] ds dt \quad (5.46)$$

is non-negative as well. To this end, let us estimate the integral $I_1(\tau)$ for the case of TE_0 -waves, when (see [3, 8])

$$\begin{aligned} u(g, t) &= E_{\phi}, \quad E_{\rho} = E_z = H_{\phi} \equiv 0, \quad \text{and} \\ \frac{\partial H_{\rho}}{\partial t} &= \eta_0^{-1} \frac{\partial u}{\partial z}, \quad \frac{\partial H_z}{\partial t} = -\eta_0^{-1} \frac{1}{\rho} \frac{\partial(\rho u)}{\partial \rho} \end{aligned} \quad (5.47)$$

(the case of TM_0 -waves can be considered similarly). Thus

$$\begin{aligned} I_1(\tau) &= \eta_0 \int_{\Phi^{\varepsilon}} \left[\frac{\partial H_z}{\partial t} \gamma \cos(\vec{n}, \vec{\rho}) - \frac{\partial H_{\rho}}{\partial t} \gamma \cos(\vec{n}, \vec{z}) \right] ds dt \\ &= -\eta_0 \int_{\Phi^{\varepsilon}} \left[H_z \frac{\partial \gamma}{\partial t} \cos(\vec{n}, \vec{\rho}) - H_{\rho} \frac{\partial \gamma}{\partial t} \cos(\vec{n}, \vec{z}) \right] ds dt \\ &= \eta_0 \int_{\Phi^{\varepsilon}} [H_z u \cos(\vec{n}, \vec{\rho}) - H_{\rho} u \cos(\vec{n}, \vec{z})] ds dt \\ &= \eta_0 \int_{\Phi^{\varepsilon}} [H_z E_{\phi} \cos(\vec{n}, \vec{\rho}) - H_{\rho} E_{\phi} \cos(\vec{n}, \vec{z})] ds dt \\ &= \eta_0 \int_{\Gamma_{\text{add}} \times (0, \tau)} [H_z E_{\phi} \cos(\vec{n}, \vec{\rho}) - H_{\rho} E_{\phi} \cos(\vec{n}, \vec{z})] ds dt \\ &= \eta_0 \int_{\Gamma_{\text{add}} \times (0, \tau)} ([\vec{E} \times \vec{H}] \cdot \vec{n}) ds dt = \eta_0 I_2(\tau) \geq 0. \end{aligned} \quad (5.48)$$

The last step in the chain of transformations (5.48) requires explanation. The integral $I_2(\tau)$, which is accurate within a fixed factor, coincides with the

electromagnetic field energy radiated from the region $\Omega_{\text{int}} \times [0 \leq \phi \leq 2\pi]$ during the time $0 < t < \tau$ [42]. According to the condition $D_{\text{add}}[u(g, t)]|_{g \in \Gamma_{\text{add}}} = 0$ (the operator $D_{\text{add}}[\dots]$ here is given by (5.28)–(5.30) and (5.35a), (5.35b)–(5.37a), (5.37b)), the functions $\vec{E} = \{E_\rho, E_\phi, E_z\}$ and $\vec{H} = \{H_\rho, H_\phi, H_z\}$ correspond to the electromagnetic waves outgoing from the domain Ω_{int} , and the energy of the outgoing waves cannot be negative.

Then, from (5.41)–(5.45), (5.48) we have

$$\int_{\Omega_{\text{int}}} \varepsilon [u(g, \tau)]^2 dg = \eta_0 \int_{\Omega_{\text{int}}^T} \sigma u^2 dg dt = 0,$$

or, as τ could be arbitrary,

$$u(g, t) \equiv 0; \quad g \in \Omega_{\text{int}}, \quad 0 < t < T.$$

Thus, a solution to the modified problem (5.38) exists and it is unique. This result allows one to construct stable and convergent finite-difference or finite-element numerical schemes based on (5.38) for computing values of the field $U(g, t)$, $g \in \Omega$, $0 \leq t \leq T < \infty$ (see works [3, 28, 29, 33]) and proves the following statement.

Statement 5.2. *Let the problem (5.4) has a unique solution from the space $W_2^1(\Omega^T)$. Then, the problem (5.38) is uniquely solvable in the space $W_2^1(\Omega_{\text{int}}^T)$, and the closed problem (5.19), (5.38) is equivalent to the open problem (5.4).*

5.3 Compact Axially Symmetric Structures

5.3.1 Formulation of the Model Problem

Figure 5.3 shows the cross-section of an open compact axially symmetric ($\partial/\partial\phi \equiv 0$) resonant structure. Here, $\{\rho, \phi, z\}$ are cylindrical and $\{r, \vartheta, \phi\}$ are spherical coordinates. The 2-D initial boundary value problem describing evolutions of pulsed axially symmetric TE_0 - ($E_\rho = E_z = H_\phi \equiv 0$) and TM_0 -waves ($H_\rho = H_z = E_\phi \equiv 0$) in the open structures of this kind is given (see [3, 8]) by

$$\left\{ \begin{array}{l} \left[-\varepsilon(g) \frac{\partial^2}{\partial t^2} - \sigma(g) \eta_0 \frac{\partial}{\partial t} + \frac{\partial^2}{\partial z^2} + \frac{\partial}{\partial \rho} \left(\frac{1}{\rho} \frac{\partial}{\partial \rho} \rho \right) \right] U(g, t) = F(g, t); \\ t > 0, \quad g \in \Omega \\ U(g, t)|_{t=0} = \varphi(g), \quad \frac{\partial}{\partial t} U(g, t) \Big|_{t=0} = \psi(g); \quad g = \{\rho, z\} \in \bar{\Omega} \\ \vec{E}_{Tg}(p, t) \text{ and } \vec{H}_{Tg}(p, t) \text{ are continuous when crossing } \Sigma^{\varepsilon, \sigma} \\ \text{and } \vec{E}_{Tg}(p, t) \Big|_{p=\{\rho, \phi, z\} \in \Sigma} = 0, \quad U(0, z, t) = 0 \text{ for } |z| < \infty; \quad t \geq 0. \end{array} \right. \quad (5.49)$$

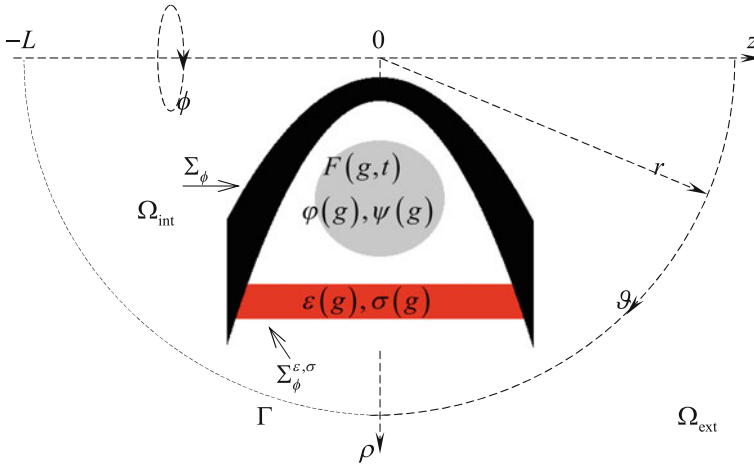


Fig. 5.3 Compact axially symmetric object

Here, $U(g, t) = E_\phi(g, t)$ for TE_0 -waves and $U(g, t) = H_\phi(g, t)$ for TM_0 -waves. The domain of analysis Ω is the part of the half-plane Ω_{total} bounded by the contours Σ_ϕ . The domains $\Omega_{\text{int}} = \{g = \{r, \vartheta\} \in \Omega : r < L\}$ and $\Omega_{\text{ext}} : \Omega = \Omega_{\text{int}} \cup \Omega_{\text{ext}} \cup \Gamma$ (free space) are separated by the virtual boundary $\Gamma = \{g = \{r, \vartheta\} \in \Omega : r = L\}$.

The functions $F(g, t)$, $\varphi(g)$, $\psi(g)$, $\sigma(g)$, and $\varepsilon(g) - 1$, which have compact supports in the closure of Ω , are supposed to satisfy the theorem on the unique solvability of the problem (5.49) in the Sobolev space $W_2^1(\Omega^T)$, $\Omega^T = \Omega \times (0, T)$, $T < \infty$ (see, for example, Statement 5.1 in Sect. 5.2). Current and instantaneous sources described by the functions $F(g, t)$ and $\varphi(g)$, $\psi(g)$ as well as all scatterers described by the piecewise constant functions $\varepsilon(g)$, $\sigma(g)$ and by the piecewise smooth contours Σ_ϕ and $\Sigma_\phi^{\varepsilon, \sigma}$ are located in the domain Ω_{int} . By $\Sigma = \Sigma_\phi \times [0, 2\pi]$ we denote perfectly conducting surfaces obtained by rotating the curves Σ_ϕ around the z -axis; $\Sigma^{\varepsilon, \sigma} = \Sigma_\phi^{\varepsilon, \sigma} \times [0, 2\pi]$ are similarly defined surfaces across which the relative permittivity $\varepsilon(g)$ and specific conductivity $\sigma(g)$ change step-wise.

5.3.2 Radiation Conditions for Outgoing Waves

In the domain Ω_{ext} , where the wave $U(g, t)$ propagates freely to infinity as $t \rightarrow \infty$, the 2-D initial boundary value problem (5.49) can be rewritten in the spherical coordinates in the following way [3, 7, 9]:

$$\left\{ \begin{array}{l} \left[-\frac{\partial^2}{\partial t^2} + \frac{1}{r} \frac{\partial^2}{\partial r^2} r + \frac{1}{r^2} \frac{\partial}{\partial \vartheta} \left(\frac{1}{\sin \vartheta} \frac{\partial}{\partial \vartheta} \sin \vartheta \right) \right] U(g, t) = 0; \\ \quad t > 0, \quad g \in \Omega_{\text{ext}} \\ U(g, t)|_{t=0} = 0, \quad \frac{\partial}{\partial t} U(g, t)|_{t=0} = 0; \quad g = \{r, \vartheta\} \in \Omega_{\text{ext}} \\ U(r, 0, t) = U(r, \pi, t) = 0; \quad r \geq L, \quad t \geq 0. \end{array} \right. \quad (5.50)$$

Let us represent the solution $U(r, \vartheta, t)$ of (5.50) as $U(r, \vartheta, t) = u(r, t)\mu(\vartheta)$. Separation of variables in (5.50) results into the homogeneous Sturm-Liouville problem with respect to the function $\tilde{\mu}(\cos \vartheta) = \mu(\vartheta)$

$$\left\{ \begin{array}{l} \left[\frac{d^2}{d\vartheta^2} + \text{ctg} \vartheta \frac{d}{d\vartheta} - \frac{1}{\sin^2 \vartheta} + \lambda^2 \right] \tilde{\mu}(\cos \vartheta) = 0; \quad 0 < \vartheta < \pi \\ \tilde{\mu}(\cos \vartheta)|_{\vartheta=0, \pi} = 0 \end{array} \right. \quad (5.51)$$

and the initial boundary value problem for $u(r, t)$

$$\left\{ \begin{array}{l} \left[-\frac{\partial^2}{\partial t^2} + \frac{\partial^2}{\partial r^2} - \frac{\lambda^2}{r^2} \right] r u(r, t) = 0; \quad r \geq L, \quad t > 0 \\ u(r, 0) = \frac{\partial}{\partial t} u(r, t)|_{t=0} = 0; \quad r \geq L. \end{array} \right. \quad (5.52)$$

Let us solve the problem (5.51) with respect to $\tilde{\mu}(\cos \vartheta)$ and λ . Change of variables $x = \cos \vartheta$, $\tilde{\mu}(x) = \tilde{\mu}(\cos \vartheta)$ yields the following boundary value problem for $\tilde{\mu}(x)$:

$$\left\{ \begin{array}{l} \left[(1-x^2) \frac{d^2}{dx^2} - 2x \frac{d}{dx} + \left(\lambda^2 - \frac{1}{1-x^2} \right) \right] \tilde{\mu}(x) = 0; \quad |x| < 1 \\ \tilde{\mu}(-1) = \tilde{\mu}(1) = 0. \end{array} \right. \quad (5.53)$$

With $\lambda^2 = \lambda_n^2 = n(n+1)$ for each $n = 1, 2, 3, \dots$ the equation (5.53) has two nontrivial linearly independent solutions in the form of the associated Legendre functions $P_n^1(x)$ and $Q_n^1(x)$. Taking into account the behavior of these functions in the vicinity of their singular points $x \rightarrow \pm 1$ [43], we obtain

$$\tilde{\mu}_n(\cos \vartheta) = \sqrt{(2n+1)/(2n(n+1))} P_n^1(\cos \vartheta). \quad (5.54)$$

The orthonormal (with the weight factor $\sin \vartheta$) system of functions $\tilde{\mu}_n(\cos \vartheta)$, $n = 1, 2, \dots$, which is complete in the space $L_2(0 < \vartheta < \pi)$, is nontrivial solution to the problem (5.51). Therefore, the solution to the initial boundary value problem (5.50) can be represented as

$$\begin{cases} U(r, \vartheta, t) = \sum_{n=1}^{\infty} u_n(r, t) \tilde{\mu}_n(\cos \vartheta); & r \geq L \\ u_n(r, t) = \int_0^{\pi} U(r, \vartheta, t) \tilde{\mu}_n(\cos \vartheta) \sin \vartheta d\vartheta, \end{cases} \quad (5.55)$$

where the space-time amplitudes $u_n(r, t)$ are the solution to the problem (5.52) for $\lambda^2 = \lambda_n^2$.

Our goal now is to derive RCs for the amplitudes $u_n(r, t)$ of the outgoing wave (5.55). Defining $w_n(r, t) = ru_n(r, t)$ and taking into account that $\lambda_n^2 = n(n + 1)$, we rewrite the equation in (5.52) as

$$\left[-\frac{\partial^2}{\partial t^2} + \frac{\partial^2}{\partial r^2} - \frac{n(n + 1)}{r^2} \right] w_n(r, t) = 0; \quad r \geq L, \quad t > 0. \quad (5.56)$$

Now subject it to the integral transform

$$\tilde{f}(\omega) = \int_L^{\infty} f(r) Z_{\gamma}(\omega, r) dr; \quad \omega \geq 0, \quad (5.57)$$

where the kernel $Z_{\gamma}(\omega, r) = r^a [\alpha(\omega)J_{\gamma}(\omega r) + \beta(\omega)N_{\gamma}(\omega r)]$ satisfies the equation [34]

$$\left[\frac{\partial^2}{\partial r^2} + \frac{1 - 2a}{r} \frac{\partial}{\partial r} + \omega^2 + \frac{a^2 - \gamma^2}{r^2} \right] Z_{\gamma}(\omega, r) = 0. \quad (5.58)$$

Here, $J_{\gamma}(\dots)$ and $N_{\gamma}(\dots)$ are the Bessel and Neumann cylindrical functions, $\alpha(\omega)$ and $\beta(\omega)$ are arbitrary functions independent of r , and a is a fixed real constant.

Applying the transform (5.57) to (5.56) with $a = 1/2$ and $\gamma = n + 1/2$, we obtain

$$\begin{aligned} & \int_L^{\infty} \left[-\frac{\partial^2}{\partial t^2} - \omega^2 \right] w_n(r, t) Z_{\gamma}(\omega, r) dr + Z_{\gamma}(\omega, r) \frac{\partial w_n(r, t)}{\partial r} \Big|_L^{\infty} \\ & - w_n(r, t) \frac{\partial Z_{\gamma}(\omega, r)}{\partial r} \Big|_L^{\infty} = 0. \end{aligned} \quad (5.59)$$

Since the ‘signal’ $w_n(r, t)$ propagates with a finite velocity, for any t we can always point a distance r which is not reached yet by this signal, in other words, such that for these t and r we have $w_n(r, t) \equiv 0$. Then we can rewrite the equation (5.59) in the form

$$\int_L^\infty \left[-\frac{\partial^2}{\partial t^2} - \omega^2 \right] w_n(r, t) Z_\gamma(\omega, r) dr - Z_\gamma(\omega, L) \frac{\partial w_n(r, t)}{\partial r} \Big|_{r=L} + w_n(L, t) \frac{\partial Z_\gamma(\omega, r)}{\partial r} \Big|_{r=L} = 0. \tag{5.60}$$

From (5.60) the simple differential equation for the images $\tilde{w}_n(\omega, t)$ of the functions $w_n(r, t)$ follows:

$$\left[\frac{\partial^2}{\partial t^2} + \omega^2 \right] \tilde{w}_n(\omega, t) = w_n(L, t) \frac{\partial Z_\gamma(\omega, r)}{\partial r} \Big|_{r=L} - Z_\gamma(\omega, L) \frac{\partial w_n(r, t)}{\partial r} \Big|_{r=L}; \quad \omega \geq 0, \quad t > 0. \tag{5.61}$$

In this equation, the values $\alpha(\omega)$ and $\beta(\omega)$ in $Z_\gamma(\omega, r)$ are not defined yet. With $\alpha(\omega) = -N_\gamma(\omega L)$ and $\beta(\omega) = J_\gamma(\omega L)$, the function $Z_\gamma(\omega, L) = \sqrt{L}[\alpha(\omega)J_\gamma(\omega L) + \beta(\omega)N_\gamma(\omega L)]$ in (5.61) vanishes, and the transform (5.57) turns into the Weber-Orr transform [43] with the known inverse

$$\begin{aligned} \tilde{f}(\omega) &= \int_L^\infty [J_\gamma(\omega L)N_\gamma(\omega r) - N_\gamma(\omega L)J_\gamma(\omega r)]f(r)\sqrt{r} dr \\ \leftrightarrow f(r) &= \sqrt{r} \int_0^\infty \frac{J_\gamma(\omega L)N_\gamma(\omega r) - N_\gamma(\omega L)J_\gamma(\omega r)}{J_\gamma^2(\omega L) + N_\gamma^2(\omega L)} \tilde{f}(\omega)\omega d\omega, \end{aligned} \tag{5.62}$$

while the coefficient of the first term in the right-hand side of (5.61) is

$$\begin{aligned} \frac{\partial Z_\gamma(\omega, r)}{\partial r} \Big|_{r=L} &= \frac{1}{2\sqrt{L}} [J_\gamma(\omega L)N_\gamma(\omega L) - N_\gamma(\omega L)J_\gamma(\omega L)] \\ &\quad + \omega \sqrt{L} [J_\gamma(\omega L)N'_\gamma(\omega L) - N_\gamma(\omega L)J'_\gamma(\omega L)] \\ &= \omega \sqrt{L} W\{J_\gamma(\omega L), N_\gamma(\omega L)\} = \frac{2}{\pi\sqrt{L}}. \end{aligned} \tag{5.63}$$

Here, $W\{J_\gamma(\omega L), N_\gamma(\omega L)\} = 2/(\pi\omega L)$ is the Wronskian [34]; $N'_\gamma(\omega L)$ and $J'_\gamma(\omega L)$ are the derivatives of the functions $N_\gamma(\omega L)$ and $J_\gamma(\omega L)$ with respect to their argument ωL .

Thus, applying the integral transform (5.62) to the problem (5.52) we obtain the following Cauchy problem for the images $\tilde{w}_n(\omega, t)$, $\omega \geq 0$, $n = 1, 2, 3, \dots$:

$$\begin{cases} \left[\frac{\partial^2}{\partial t^2} + \omega^2 \right] \tilde{w}_n(\omega, t) = g_n(\omega, t); & t > 0 \\ \left. \frac{\partial \tilde{w}_n(\omega, t)}{\partial t} \right|_{t=0} = \tilde{w}_n(\omega, 0) = 0. \end{cases} \tag{5.64}$$

Here, $g_n(\omega, t) = 2w_n(L, t)/(\pi\sqrt{L})$. In the generalized formulation (the functions $\tilde{w}_n(\omega, t)$ and $g_n(\omega, t)$ are extended with zero on the semiaxis $t \leq 0$), the problem (5.64) have the form [35]

$$\begin{aligned} \left[\frac{\partial^2}{\partial t^2} + \omega^2 \right] \tilde{w}_n(\omega, t) &= g_n(\omega, t) + \delta^{(1)}(t)\tilde{w}_n(\omega, 0) \\ + \delta(t)\frac{\partial}{\partial t} \tilde{w}_n(\omega, t) \Big|_{t=0} &= g_n(\omega, t); \quad -\infty < t < \infty, \end{aligned} \tag{5.65}$$

where $\delta(\dots)$ and $\delta^{(1)}(\dots)$ are the Dirac delta-function and its generalized derivative. The solutions $\tilde{w}_n(\omega, t)$ can be obtained as a result of the convolution $\tilde{w}_n(\omega, t) = [G * g_n]$ of the fundamental solution $G(\omega, t) = \chi(t)\omega^{-1} \sin \omega t = \omega^{-2}[\delta(t) \cos(\omega t) - d[\chi(t) \cos(\omega t)]/dt]$ of the operator $[\partial^2/\partial t^2 + \omega^2][G(\omega, t)]$ (see [3, 8, 35]) and the right-hand side of the equation (5.65):

$$\begin{aligned} \tilde{w}_n(\omega, t) &= \int_0^\infty G(\omega, t - \tau)g_n(\omega, \tau)d\tau \\ &= \frac{2}{\pi\omega^2\sqrt{L}} \left[w_n(L, t) - \int_0^t \cos[\omega(t - \tau)] \frac{\partial w_n(L, \tau)}{\partial \tau} d\tau \right]; \\ \omega \geq 0, \quad t \geq 0. \end{aligned} \tag{5.66}$$

Here, $\chi(\dots)$ is the Heaviside step-function and the following property of the convolution [35] was used in derivation of (5.66):

$$[\partial^\alpha f * g] = \partial^\alpha [f * g] = [f * \partial^\alpha g].$$

Let us subject the equation (5.66) to the inverse transform (5.62). Taking into consideration that [44]

$$\int_0^\infty \frac{J_\gamma(\omega L)N_\gamma(\omega r) - N_\gamma(\omega L)J_\gamma(\omega r)}{\omega [J_\gamma^2(\omega L) + N_\gamma^2(\omega L)]} d\omega = \frac{\pi}{2} \left(\frac{L}{r} \right)^\gamma; \quad L < r,$$

we obtain:

$$w_n(r, t) = \left(\frac{L}{r}\right)^{\gamma-1/2} w_n(L, t) - \frac{2}{\pi} \sqrt{\frac{r}{L}} \int_0^t F_\gamma(r, L, t - \tau) \frac{\partial w_n(L, \tau)}{\partial \tau} d\tau; \quad r > L, \quad (5.67)$$

$$F_\gamma(r, L, t - \tau) = \int_0^\infty \frac{\cos[\omega(t - \tau)] [J_\gamma(\omega L) N_\gamma(\omega r) - N_\gamma(\omega L) J_\gamma(\omega r)]}{\omega [J_\gamma^2(\omega L) + N_\gamma^2(\omega L)]} d\omega. \quad (5.68)$$

To compute the formula (5.67) efficiently, one should find an easy way to calculate the function $F_\gamma(r, L, t - \tau)$. To do this, first consider the following auxiliary integral

$$\tilde{F}_\gamma(r, L, t - \tau) = \int_{-\infty}^\infty \frac{H_\gamma^{(1)}(zr) \cos[z(t - \tau)]}{H_\gamma^{(1)}(zL) z} dz \quad (5.69)$$

along the real axis in the plane of the complex variable z . The critical point $z = 0$ is passed along the semi-circle C_δ of infinitely small radius δ in the upper half-plane; $H_\gamma^{(1)}(\dots)$ is the Hankel function of the first kind. The function $F_\gamma(r, L, t - \tau)$ is related to the integral in (5.69) by the easily verifiable equality

$$\frac{H_\gamma^{(1)}(zr)}{H_\gamma^{(1)}(zL)} - \frac{H_\gamma^{(1)}(e^{i\pi} zr)}{H_\gamma^{(1)}(e^{i\pi} zL)} = 2i \frac{J_\gamma(zL) N_\gamma(zr) - N_\gamma(zL) J_\gamma(zr)}{J_\gamma^2(zL) + N_\gamma^2(zL)},$$

in view of which

$$\begin{aligned} \tilde{F}_\gamma(r, L, t - \tau) &= \int_{-\infty}^{-\delta} \frac{H_\gamma^{(1)}(zr) \cos[z(t - \tau)]}{H_\gamma^{(1)}(zL) z} dz + \int_{\delta}^{\infty} \frac{H_\gamma^{(1)}(zr) \cos[z(t - \tau)]}{H_\gamma^{(1)}(zL) z} dz \\ &+ \int_{C_\delta} \frac{H_\gamma^{(1)}(zr) \cos[z(t - \tau)]}{H_\gamma^{(1)}(zL) z} dz = - \int_{\delta}^{\infty} \frac{H_\gamma^{(1)}(e^{i\pi} zr) \cos[z(t - \tau)]}{H_\gamma^{(1)}(e^{i\pi} zL) z} dz \\ &+ \int_{\delta}^{\infty} \frac{H_\gamma^{(1)}(zr) \cos[z(t - \tau)]}{H_\gamma^{(1)}(zL) z} dz - \pi i \left(\frac{L}{r}\right)^\gamma = 2i F_\gamma(r, L, t - \tau) - \pi i \left(\frac{L}{r}\right)^\gamma. \end{aligned} \quad (5.70)$$

Rewrite the function $\tilde{F}_\gamma(r, L, t - \tau)$ as

$$\tilde{F}_\gamma(r, L, t - \tau) = \frac{1}{2} \left\{ \int_{-\infty}^{\infty} \frac{H_\gamma^{(1)}(zr) \exp[iz(t - \tau)]}{H_\gamma^{(1)}(zL) z} dz + \int_{-\infty}^{\infty} \frac{H_\gamma^{(1)}(zr) \exp[-iz(t - \tau)]}{H_\gamma^{(1)}(zL) z} dz \right\}. \tag{5.71}$$

To calculate the integrals in the braces, we use the standard technique based on the Cauchy theorem and the Jordan lemma [45]. Since for $|zL| \geq \gamma$ with $z \rightarrow \infty$, the relationship $H_\gamma^{(1)}(zr)/H_\gamma^{(1)}(zL) \approx (L/r)^{1/2} \exp[iz(r - L)]$ is valid [34], then for $r - L > t - \tau$, the contours of integration in (5.71) can be closed by an arc of infinitely large radius in the upper half-plane of the complex variable z . For $r - L < t - \tau$, the contour of the first integral in (5.71) is closed in the upper half-plane, while the contour of the second integral is closed in the bottom half-plane. Taking into account that all singularities of the function $H_\gamma^{(1)}(zr)/H_\gamma^{(1)}(zL)$ are reduced to a finite number of simple poles at the points $z = z_s : \text{Im } z_s < 0$ ($s = 1, 2, \dots, n$) coinciding with zeros of the function $H_\gamma^{(1)}(zL)$ [36] and having regard to the asymptotic (for $z \rightarrow 0$) equality $H_\gamma^{(1)}(zr)/H_\gamma^{(1)}(zL) \approx (L/r)^\gamma$ and equality $dH_\gamma^{(1)}(zL)/dz = L [H_{\gamma-1}^{(1)}(zL) - \gamma H_\gamma^{(1)}(zL)/(zL)]$, we obtain

$$\tilde{F}_\gamma(r, L, t - \tau) = \begin{cases} -\pi i \left[\left(\frac{L}{r}\right)^\gamma + \sum_s \frac{H_\gamma^{(1)}(z_s r) \exp[-iz_s(t - \tau)]}{H_{\gamma-1}^{(1)}(z_s L) z_s L} \right]; & \tau < t - (r - L) \\ 0; & \tau > t - (r - L). \end{cases} \tag{5.72}$$

Substituting (5.72) into (5.70), we finally have:

$$F_\gamma(r, L, t - \tau) = \begin{cases} -\frac{\pi}{2} \sum_s \frac{H_\gamma^{(1)}(z_s r) \exp[-iz_s(t - \tau)]}{H_{\gamma-1}^{(1)}(z_s L) z_s L} \\ = -\frac{\pi}{2} S_\gamma(r, L, t - \tau); & \tau < t - (r - L) \\ \frac{\pi}{2} \left(\frac{L}{r}\right)^\gamma; & \tau > t - (r - L). \end{cases} \tag{5.73}$$

Summation in (5.73) can be performed over a half of the roots $z_s, s = 1, 2, \dots, n$ of the equation $H_\gamma^{(1)}(zL) = 0$, for example, taking into account only those lying in the fourth quadrant of the plane of complex variable z [36]. This inference stems

from the fact that the function $H_\gamma^{(1)}(zL)$, $\gamma = n + 1/2$ has n complex-valued zeros $z_s : \text{Im } z_s < 0$, which are located symmetrically with respect to the imaginary axis approximately on a finite arc connecting the points $zL = -n$ and $zL = n$ [36].

Calculation of the function $S_\gamma(r, L, t - \tau)$ and partial integration in (5.67) yield the following RC for the amplitudes $w_n(r, t) = r u_n(r, t)$, which determine the field $U(g, t)$ in the domain Ω_{ext} :

$$\begin{aligned}
 w_n(r, t) &= \left(\frac{L}{r}\right)^n w_n(L, t - (r - L)) + \sqrt{\frac{r}{L}} \int_0^{t-(r-L)} S_{n+1/2}(r, L, t - \tau) \frac{\partial w_n(L, \tau)}{\partial \tau} d\tau \\
 &= \left[\left(\frac{L}{r}\right)^n + \sqrt{\frac{r}{L}} S_{n+1/2}(r, L, r - L) \right] w_n(L, t - (r - L)) \\
 &\quad - \sqrt{\frac{r}{L}} \int_0^{t-(r-L)} w_n(L, \tau) \frac{\partial S_{n+1/2}(r, L, t - \tau)}{\partial \tau} d\tau; \\
 r &> L, \quad t \geq (r - L), \quad n = 1, 2, 3, \dots
 \end{aligned}
 \tag{5.74}$$

From the expansions in (5.55) and the condition for amplitudes in (5.74), we obtain RC for the wave $U(g, t)$ outgoing through the boundary Γ into the domain Ω_{ext} :

$$\begin{aligned}
 U(g, t) &= \sum_{n=1}^{\infty} \left\{ \left(\frac{L}{r}\right)^{n+1} \int_0^{\pi/2} U(L, \vartheta, t - (r - L)) \tilde{\mu}_n(\cos \vartheta) \sin \vartheta d\vartheta \right. \\
 &\quad + \sqrt{\frac{L}{r}} \int_0^{t-(r-L)} S_{n+1/2}(r, L, t - \tau) \\
 &\quad \left. \times \left[\int_0^{\pi/2} \frac{\partial U(L, \vartheta, \tau)}{\partial \tau} \tilde{\mu}_n(\cos \vartheta) \sin \vartheta d\vartheta \right] d\tau \right\} \tilde{\mu}_n(\cos \vartheta); \\
 g &= \{r, \vartheta\} \in \Omega_{\text{ext}}, \quad t \geq (r - L).
 \end{aligned}
 \tag{5.75}$$

With $r = L$, the equations (5.74) and (5.75) turn into identities. These RCs do not contain any directional derivative of the function $U(g, t)$ and, thus, can be implemented on a rectangular mesh of coordinates $g = \{\rho, z\}$ with minimal error. The peculiarities of utilization of these RCs as EACs are discussed in [8]. The modified (closed) problem obtained with (5.75) is following:

$$\left\{ \begin{array}{l} \left[-\varepsilon(g) \frac{\partial^2}{\partial t^2} - \sigma(g) \eta_0 \frac{\partial}{\partial t} + \frac{\partial^2}{\partial z^2} + \frac{\partial}{\partial \rho} \left(\frac{1}{\rho} \frac{\partial}{\partial \rho} \rho \right) \right] U(g, t) = F(g, t); \\ t > 0, \quad g \in \Omega_{\text{int}} \\ U(g, t)|_{t=0} = \varphi(g), \quad \frac{\partial}{\partial t} U(g, t)|_{t=0} = \psi(g); \quad g = \{\rho, z\} \in \bar{\Omega}_{\text{int}} \\ \vec{E}_{\text{tg}}(p, t) \text{ and } \vec{H}_{\text{tg}}(p, t) \text{ are continuous when crossing } \Sigma^{e, \sigma}, \\ \vec{E}_{\text{tg}}(p, t)|_{p=\{\rho, \phi, z\} \in \Sigma} = 0, \quad U(0, z, t) = 0 \quad \text{for } \{0, z\} \in \bar{\Omega}_{\text{int}} \\ \text{and } D[U(g, t)]|_{g \in \Gamma} = 0; \quad t \geq 0. \end{array} \right. \quad (5.76)$$

Statement 5.3. *Let the problem (5.49) has a unique solution from the space $W_2^1(\Omega^T)$. Then, the problem (5.76) is uniquely solvable in the space $W_2^1(\Omega_{\text{int}}^T)$ and the closed problem (5.75), (5.76) is equivalent to the open problem (5.49).*

5.3.3 Far-Field Zone Problem, Extended and Remote Sources

In contrast to approximate approaches to truncation of computation domains based on ABCs or PMLs, our approach is rigorous. This means that an original open problem and a modified closed (truncated) problem are equivalent. This allows to monitor a computational error and obtain reliable information about resonant wave scattering [3, 8]. It is noteworthy that using our approach we also solve without additional efforts the *far-field zone problem*. Namely, to find the field $U(g, t)$ at an arbitrary point in the external domain Ω_{ext} from values of $U(g, t)$ on any arc $r = M \leq L$, $0 \leq \vartheta \leq \pi$, lying entirely in the computation domain Ω_{int} and retaining all characteristics of the arc of the virtual boundary Γ . Thus in the case considered here, the equation (5.74) define the *transport operator* $X_{L \rightarrow r}(t)[u]$ which operates on the amplitudes $u_n(r, t)$ of the outgoing waves (5.55) according to the rule

$$u_n(r, t) = X_{L \rightarrow r}(t)[u_n(L, \tau)]; \quad r > L, \quad t \geq (r - L), \quad t - (r - L) \geq \tau \geq 0. \quad (5.77)$$

It allows one to calculate values of the amplitudes $u_n(r, t)$ anywhere in Ω_{ext} knowing their values only within Ω_{int} . The operator

$$U(g, t) = Z_{q \in \Gamma \rightarrow g \in \Omega_{\text{ext}}}(t)[U(q, \tau)]; \quad t \geq (r - L), \quad t - (r - L) \geq \tau \geq 0 \quad (5.78)$$

given by (5.75) allows to calculate values of the field $U(g, t)$ anywhere in Ω_{ext} knowing its values only within Ω_{int}

It is obvious that the efficiency of numerical algorithms based on (5.76) reduces if the support of the function $F(g, t)$ and/or the functions $\varphi(g)$ and $\psi(g)$ is extended

Let the relevant sources generate the field $U^i(g, t)$ in the half-plane $\Omega_{\text{total}} = \{g : \rho > 0, |z| < \infty\}$. In other words, let the function $U^i(g, t)$ be a solution to the following Cauchy problem:

$$\begin{cases} \left[-\frac{\partial^2}{\partial r^2} + \frac{\partial^2}{\partial z^2} + \frac{\partial}{\partial \rho} \left(\frac{1}{\rho} \frac{\partial}{\partial \rho} \rho \right) \right] U^i(g, t) = \tilde{F}(g, t); & t > 0, \quad g \in \Omega_{\text{total}} \\ U^i(g, t)|_{t=0} = \tilde{\varphi}(g), \quad \frac{\partial}{\partial t} U^i(g, t)|_{t=0} = \tilde{\psi}(g); & g = \{\rho, z\} \in \bar{\Omega}_{\text{total}} \\ U^i(0, z, t) = 0, \quad |z| < \infty; & t \geq 0. \end{cases} \tag{5.80}$$

It follows from (5.79), (5.80) that in the domain Ω_{ext} the function

$$U^s(g, t) = U(g, t) - U^i(g, t) \tag{5.81}$$

satisfies the equation

$$\begin{cases} \left[-\frac{\partial^2}{\partial t^2} + \frac{\partial^2}{\partial z^2} + \frac{\partial}{\partial \rho} \left(\frac{1}{\rho} \frac{\partial}{\partial \rho} \rho \right) \right] U^s(g, t) = 0; \\ t > 0, \quad g = \{\rho, z\} \in \Omega_{\text{ext}} \\ U^s(g, t)|_{t=0} = 0, \quad \frac{\partial}{\partial t} U^s(g, t)|_{t=0} = 0; \quad g \in \bar{\Omega}_{\text{ext}} \\ U^s(0, z, t) = 0; \quad |z| \geq L, \quad t \geq 0 \end{cases} \tag{5.82}$$

and determines the electromagnetic wave crossing the virtual boundary Γ in one direction only, namely, from Ω_{int} into Ω_{ext} .

The problems (5.82) and (5.50) are of the same kind. Therefore, repeating the transformations of Sect. 5.3.2, we obtain similarly to (5.75)

$$\begin{aligned} U^s(g, t) = & \sum_{n=1}^{\infty} \left\{ \left(\frac{L}{r} \right)^{n+1} \int_0^{\pi/2} U^s(L, \vartheta, t - (r - L)) \tilde{\mu}_n(\cos \vartheta) \sin \vartheta d\vartheta \right. \\ & + \sqrt{\frac{L}{r}} \int_0^{t-(r-L)} S_{n+1/2}(r, L, t - \tau) \\ & \left. \times \left[\int_0^{\pi/2} \frac{\partial U^s(L, \vartheta, \tau)}{\partial \tau} \tilde{\mu}_n(\cos \vartheta) \sin \vartheta d\vartheta \right] d\tau \right\} \tilde{\mu}_n(\cos \vartheta); \\ & g = \{r, \vartheta\} \in \Omega_{\text{ext}}, \quad t \geq (r - L). \end{aligned} \tag{5.83}$$

The open problem (5.79) can be replaced now with the equivalent closed problem

$$\left\{ \begin{array}{l} \left[-\varepsilon(g) \frac{\partial^2}{\partial t^2} - \sigma(g) \eta_0 \frac{\partial}{\partial t} + \frac{\partial^2}{\partial z^2} + \frac{\partial}{\partial \rho} \left(\frac{1}{\rho} \frac{\partial}{\partial \rho} \rho \right) \right] U(g, t) = F(g, t); \\ t > 0, \quad g \in \Omega_{\text{int}} \\ U(g, t)|_{t=0} = \varphi(g), \quad \frac{\partial}{\partial t} U(g, t) \Big|_{t=0} = \psi(g); \quad g = \{\rho, z\} \in \bar{\Omega}_{\text{int}} \\ \vec{E}_{\text{tg}}(p, t) \quad \text{and} \quad \vec{H}_{\text{tg}}(p, t) \quad \text{are continuous when crossing} \quad \Sigma^{\varepsilon, \sigma}, \\ \vec{E}_{\text{tg}}(p, t) \Big|_{p=\{\rho, \phi, z\} \in \Sigma} = 0, \quad U(0, z, t) = 0 \quad \text{for} \quad \{0, z\} \in \bar{\Omega}_{\text{int}} \\ \text{and} \quad D[U(g, t) - U^i(g, t)] \Big|_{g \in \Gamma} = 0; \quad t \geq 0. \end{array} \right. \quad (5.84)$$

The problem of extended and remote sources is solved. RC (5.83) allows one to shrink the computation domain of the problem (5.84) to the same domain Ω_{int} as in the case of compact sources $F(g, t)$, $\varphi(g)$, and $\psi(g)$ located in the immediate vicinity of scatterers.

To solve the problem (5.84) numerically, one has to solve the Cauchy problem (5.80) first, and determine the function $U^i(r, \vartheta, t)$ for points $g = \{r, \vartheta\}$ from the neighborhood of the boundary Γ (see the formulas (5.81)–(5.83)). Let us separate the transverse variable ρ in the problem (5.80) and represent its solution in the form [43]:

$$U^i(\rho, z, t) = \int_0^\infty v_\lambda(z, t) J_1(\lambda \rho) d\lambda, \quad (5.85)$$

$$\begin{aligned} v_\lambda(z, t) &= \int_0^\infty v_\mu(z, t) \delta(\mu - \lambda) d\mu = \lambda \int_0^\infty v_\mu(z, t) \left[\int_0^\infty J_1(\mu \rho) J_1(\lambda \rho) \rho d\rho \right] d\mu \\ &= \lambda \int_0^\infty \left[\int_0^\infty v_\mu(z, t) J_1(\mu \rho) d\mu \right] J_1(\lambda \rho) \rho d\rho = \lambda \int_0^\infty U^i(\rho, z, t) J_1(\lambda \rho) \rho d\rho. \end{aligned} \quad (5.86)$$

In order to find the functions $v_\lambda(z, t)$, one has to solve the following Cauchy problem for the 1-D Klein-Gordon equation:

$$\left\{ \begin{array}{l} \left[-\frac{\partial^2}{\partial t^2} + \frac{\partial^2}{\partial z^2} - \lambda^2 \right] v_\lambda(z, t) = F_\lambda(z, t); \quad t > 0, \quad |z| < \infty \\ v_\lambda(z, 0) = \varphi_\lambda(z), \quad \frac{\partial}{\partial t} v_\lambda(z, t) \Big|_{t=0} = \psi_\lambda(z); \quad |z| < \infty. \end{array} \right. \quad (5.87)$$

Here, $F_\lambda(z, t)$, $\varphi_\lambda(z)$, and $\psi_\lambda(z)$ are the amplitude coefficients in the integral presentation (5.85) for the functions $\tilde{F}(g, t)$, $\tilde{\varphi}(g)$, and $\tilde{\psi}(g)$, namely,

$$\begin{Bmatrix} F_\lambda(g, t) \\ \varphi_\lambda(g) \\ \psi_\lambda(g) \end{Bmatrix} = \lambda \int_0^\infty \begin{Bmatrix} \tilde{F}(g, t) \\ \tilde{\varphi}(g) \\ \tilde{\psi}(g) \end{Bmatrix} J_1(\lambda\rho) \rho d\rho.$$

Now, extending the functions $F_\lambda(z, t)$ and $v_\lambda(z, t)$ with zero on the interval $t \leq 0$, we pass on to the generalized version of the problem (5.87) [35]:

$$\begin{aligned} B(\lambda)[v_\lambda(z, t)] &\equiv \left[-\frac{\partial^2}{\partial t^2} + \frac{\partial^2}{\partial z^2} - \lambda^2 \right] v_\lambda(z, t) \\ &= F_\lambda(z, t) - \delta^{(1)}(t)\varphi_\lambda(z) - \delta(t)\psi_\lambda(z) \\ &= f_\lambda(z, t); \quad |t| < \infty, \quad |z| < \infty. \end{aligned} \tag{5.88}$$

Using the fundamental solution $G(z, t, \lambda) = (-1/2)\chi(t - |z|)J_0[\lambda(t^2 - z^2)^{1/2}]$ of the operator $B(\lambda)[v]$ and the well-known convolution property $[\partial^2 f * g] = \partial^2 [f * g] = [f * \partial^2 g]$ for generalized functions f and g [3, 35], the solution to the problem (5.88) is obtained in the following form:

$$\begin{aligned} v_\lambda(z, t) &= [G(z, t, \lambda) * f_\lambda(z, t)] = \int_0^\infty \int_{-\infty}^\infty G(z - z_1, t - \tau, \lambda) f_\lambda(z_1, \tau) dz_1 d\tau \\ &= -\frac{1}{2} \left\{ \int_0^t \int_{z_1: |z-z_1| < t-\tau} J_0 \left[\lambda \left((t-\tau)^2 - (z-z_1)^2 \right)^{1/2} \right] F_\lambda(z_1, \tau) dz_1 d\tau \right. \\ &\quad - \frac{\partial}{\partial t} \int_{z_1: |z-z_1| < t} J_0 \left[\lambda \left(t^2 - (z-z_1)^2 \right)^{1/2} \right] \varphi_\lambda(z_1) dz_1 \\ &\quad \left. - \int_{z_1: |z-z_1| < t} J_0 \left[\lambda \left(t^2 - (z-z_1)^2 \right)^{1/2} \right] \psi_\lambda(z_1) dz_1 \right\}; \quad t > 0, \quad |z| < \infty. \end{aligned} \tag{5.89}$$

The equations (5.89) and (5.85) completely determine the desired function $U^i(\rho, z, t)$. The equation (5.89) is similar to the Poisson formula [35], which describes a classic solution to the Cauchy problem for the wave equation in the spaces R^2 and R^3 . The formula (5.89) gives an explicit analytical representation for classic and generalized solutions to the Cauchy problem for 1-D Klein-Gordon equation.

Clearly the solution (5.81), (5.83), (5.84) to the problem (5.79) also remains valid in the case when instead of the sources $\tilde{F}(g, t)$, $\tilde{\varphi}(g)$, and $\tilde{\psi}(g)$ the field $U^i(g, t)$ generated by them is known in the domain Ω_{total} . Any nontrivial solution of the homogeneous wave equation

$$\left[-\frac{\partial^2}{\partial t^2} - + \frac{\partial^2}{\partial z^2} + \frac{\partial}{\partial \rho} \left(\frac{1}{\rho} \frac{\partial}{\partial \rho} \rho \right) \right] U^i(g, t) = 0; \quad t > 0, \quad g \in \Omega_{\text{total}} \quad (5.90)$$

could be chosen as the function $U^i(g, t)$.

5.3.4 Virtual Feed Lines in Compact Open Structures

A compact open electrodynamic structure with *input and output waveguides* is a difficult-to-simulate object. To deal with it, in some models [3, 8, 46, 47] an input waveguide is separated from the half-space where wave processes under study take place by a perfectly conducting infinite flange. However, in many cases, this approach is inapplicable because an infinite flange may introduce substantial distortions in the simulated processes.

Here we detail a different approach [3, 7, 8], which allows the presence of an arbitrary finite number of differently directed waveguides in a structure under study. It is expected that our approach introduces less distortions into the simulated processes. The ultimate conclusion on this matter can be made only comparing theoretical and experimental results. It is important that our approach allows one to solve initial boundary value problems for objects with input and output waveguides using methods developed for compact objects.

The essence of the approach is following (see Fig. 5.5). Each regular infinite waveguide is truncated to a finite length by a metal wall from the free-space side. Then the virtual boundary Γ_j is introduced inside the j th waveguide Ω_j at some distance away from the junction of the waveguide with a structure. The desired electromagnetic field on this boundary is subject to conditions identical to those in

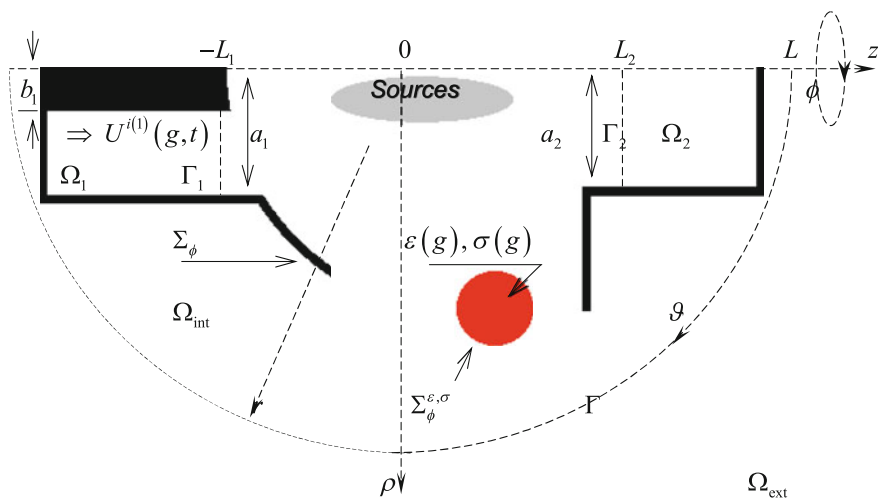


Fig. 5.5 Virtual feed lines in compact open structure

an infinite waveguide (see Sect. 5.2). In the input waveguide, the total field on the boundary Γ_j is a sum of the incident (from the domain Ω_j) wave and the outgoing waves. In the output waveguide, the total field on the boundary Γ_j is represented by the outgoing (into the domain Ω_j) waves. The domains Ω_j are excluded from the computation domain. In this way electrodynamic equivalency of the finite *virtual waveguide* (Ω_j) and the infinite *real waveguide* is achieved.

Let us discuss the details of this approach solving the following modified (closed) initial boundary value problem for a compact radiating structure with one input coaxial waveguide Ω_1 , and one output circular waveguide Ω_2 (Fig. 5.5):

$$\left\{ \begin{array}{l} \left[-\varepsilon(g) \frac{\partial^2}{\partial t^2} - \sigma(g) \eta_0 \frac{\partial}{\partial t} + \frac{\partial^2}{\partial z^2} + \frac{\partial}{\partial \rho} \left(\frac{1}{\rho} \frac{\partial}{\partial \rho} \rho \right) \right] U(g, t) = F(g, t); \\ t > 0, \quad g \in \Omega_{\text{int}} \\ U(g, t)|_{t=0} = \varphi(g), \quad \frac{\partial}{\partial t} U(g, t)|_{t=0} = \psi(g); \quad g = \{\rho, z\} \in \bar{\Omega}_{\text{int}} \\ \left\{ \begin{array}{l} \vec{E}_{Tg}(p, t), \quad \vec{H}_{Tg}(p, t) \text{ are continuous when crossing } \Sigma^{\varepsilon, \sigma} \\ \vec{E}_{Tg}(p, t)|_{p=\{\rho, \phi, z\} \in \Sigma} = 0, \quad U(0, z, t) = 0 \text{ for } \{0, z\} \in \bar{\Omega}_{\text{int}} \\ D_1[U(g, t) - U^{i(1)}(g, t)]|_{g \in \Gamma_1} = 0, \quad D_2[U(g, t)]|_{g \in \Gamma_2} = 0 \\ D[U(g, t)]|_{g \in \Gamma} = 0 \end{array} \right. ; \quad t \geq 0. \end{array} \right. \quad (5.91)$$

We adopted the same notation and assumptions to functions' properties as in the problems (5.49), (5.76). But the computation domain Ω_{int} now is the part of the half-plane Ω_{total} bounded by the contours Σ_ϕ together with the virtual boundaries Γ_j (input and output ports in the cross-sections $z_j = 0$ of the virtual waveguides Ω_j , $j = 1, 2$) and the spherical boundary $\Gamma = \{g = \{r, \vartheta\} : r = L\}$ separating the domains Ω_{int} and $\Omega_{\text{ext}} = \{g = \{r, \vartheta\} : r > L\}$ (free space).

The conditions $D_j[U]$ and $D[U]$ for the virtual boundaries Γ_j and Γ were described in Sects. 5.2.3, 5.2.4 and 5.3.2. The function

$$U^{i(1)}(g, t) = \sum_{n=0}^{\infty} v_{n1}(z, t) \mu_{n1}(\rho); \quad g = \{\rho, z\} \in \Omega_1 \quad (5.92)$$

$$n = \begin{cases} 1 & \text{for } TE_0\text{-waves} \\ 0 & \text{for } TM_0\text{-waves} \end{cases}$$

in the first of these conditions defines the wave incident on the boundary Γ_1 from the waveguide Ω_1 . This function and the source functions $F(g, t)$, $\varphi(g)$, and $\psi(g)$ are assumed to be given. It is assumed also that by the moment of time $t = 0$ the wave $U^{i(1)}(g, t)$ has not yet reached the boundary Γ_1 .

The equations

$$D_1[U(g, t) - U^{i(1)}(g, t)]|_{g \in \Gamma_1} = 0, \quad D_2[U(g, t)]|_{g \in \Gamma_2} = 0; \quad t \geq 0 \quad (5.93)$$

in (5.91) are EACs for the waves $U^{s(1)}(g, t) = U(g, t) - U^{i(1)}(g, t)$ and $U^{s(2)}(g, t) = U(g, t)$ traveling in the virtual waveguides Ω_1 and Ω_2 , respectively. Using EACs (5.93), we substantially simplify the model: the domains Ω_j are excluded from consideration, while EACs $D_j[U]$ describe wave transformation on the boundaries Γ_j which separate regular feeding waveguides from the main unit. These EACs allow waves arriving on Γ_j from the domain Ω_{int} to pass into the virtual domain Ω_j just like into a regular waveguide, without any deformations or reflections.

In Sect. 5.2 one can find six different versions of EAC $D_j[U]$ for virtual boundaries in cross-sections of circular or coaxial waveguides. We pick out two of them, nonlocal EAC (5.28) and local EAC (5.35a), (5.35b). Taking into consideration the location of the boundaries Γ_j (Γ_1 is in the plane $z = -L_1$ and Γ_2 is in the plane $z = L_2$), and the direction of propagation of the waves outgoing through these boundaries (towards $z = -\infty$ for Γ_1 and towards $z = \infty$ for Γ_2), we can rewrite (5.93) in the following form:

$$\begin{aligned}
 U(\rho, -L_1, t) - U^{i(1)}(\rho, -L_1, t) = & \sum_{n=1}^{\infty} \left\{ \int_0^t J_0[\lambda_{n1}(t - \tau)] \right. \\
 & \left. \begin{aligned}
 n= & \begin{cases} 1 \text{ for } TE_0\text{-waves} \\ 0 \text{ for } TM_0\text{-waves} \end{cases} \\
 & \times \left[\int_{b_1}^{a_1} \frac{\partial [U(\rho, z, \tau) - U^{i(1)}(\rho, z, \tau)]}{\partial z} \Big|_{z=-L_1} \mu_{n1}(\rho) \rho d\rho \right] d\tau \Big\} \\
 & \times \mu_{n1}(\rho); \quad b_1 \leq \rho \leq a_1, \quad t \geq 0,
 \end{aligned} \tag{5.94}
 \end{aligned}$$

$$\begin{aligned}
 U(\rho, L_2, t) = & - \sum_{n=1}^{\infty} \left\{ \int_0^t J_0[\lambda_{n2}(t - \tau)] \right. \\
 & \left. \times \left[\int_0^{a_2} \frac{\partial U(\rho, z, \tau)}{\partial z} \Big|_{z=L_2} \mu_{n2}(\rho) \rho d\rho \right] d\tau \right\} \\
 & \times \mu_{n2}(\rho); \quad 0 \leq \rho \leq a_2, \quad t \geq 0
 \end{aligned} \tag{5.95}$$

(nonlocal EACs) and

$$\begin{aligned}
 U(\rho, -L_1, t) - U^{i(1)}(\rho, -L_1, t) = & \frac{2}{\pi} \int_0^{\pi/2} \frac{\partial W(\rho, t, \varphi)}{\partial t} d\varphi; \quad t \geq 0, \\
 & b_1 \leq \rho \leq a_1,
 \end{aligned} \tag{5.96a}$$

$$\left\{ \begin{array}{l} \left[\frac{\partial^2}{\partial t^2} - \sin^2 \varphi \frac{\partial}{\partial \rho} \frac{1}{\rho} \frac{\partial}{\partial \rho} \rho \right] W(\rho, t, \varphi) \\ = \frac{\partial [U(\rho, z, t) - U^{i(1)}(\rho, z, t)]}{\partial z} \Bigg|_{z=-L_1}; \quad b_1 < \rho < a_1, \quad t > 0 \\ W(\rho, 0, \varphi) = \frac{\partial W(\rho, t, \varphi)}{\partial t} \Bigg|_{t=0} = 0, \quad b_1 \leq \rho \leq a_1, \end{array} \right. \quad (5.96b)$$

$$U(\rho, L_2, t) = \frac{2}{\pi} \int_0^{\pi/2} \frac{\partial W(\rho, t, \varphi)}{\partial t} d\varphi; \quad t \geq 0, \quad 0 \leq \rho \leq a_2, \quad (5.97a)$$

$$\left\{ \begin{array}{l} \left[\frac{\partial^2}{\partial t^2} - \sin^2 \varphi \frac{\partial}{\partial \rho} \frac{1}{\rho} \frac{\partial}{\partial \rho} \rho \right] W(\rho, t, \varphi) = -\frac{\partial U(\rho, z, t)}{\partial z} \Bigg|_{z=L_2}; \\ 0 < \rho < a_2, \quad t > 0 \\ W(\rho, 0, \varphi) = \frac{\partial W(\rho, t, \varphi)}{\partial t} \Bigg|_{t=0} = 0, \quad 0 \leq \rho \leq a_2 \end{array} \right. \quad (5.97b)$$

(local EACs).

The initial boundary value problems in (5.96a), (5.96b) and (5.97a), (5.97b) with respect to the auxiliary functions $W(\rho, t, \varphi)$ (φ is a numeric parameter) are supplemented with the following boundary conditions for all times $t \geq 0$:

$$\left\{ \begin{array}{l} W(b_1, t, \varphi) = W(a_1, t, \varphi) = 0; \quad TE_0\text{-waves} \\ \frac{\partial(\rho W(\rho, t, \varphi))}{\partial \rho} \Bigg|_{\rho=b_1} = \frac{\partial(\rho W(\rho, t, \varphi))}{\partial \rho} \Bigg|_{\rho=a_1} = 0; \quad TM_0\text{-waves} \end{array} \right. \quad (5.98)$$

(on the walls of coaxial waveguide Ω_1) and

$$\left\{ \begin{array}{l} W(0, t, \varphi) = W(a_2, t, \varphi) = 0; \quad TE_0\text{-waves} \\ W(0, t, \varphi) = \frac{\partial(\rho W(\rho, t, \varphi))}{\partial \rho} \Bigg|_{\rho=a_2} = 0; \quad TM_0\text{-waves} \end{array} \right. \quad (5.99)$$

(on the walls of circular waveguide Ω_2).

The incident wave $U^{i(1)}(g, t)$ and its derivative with respect to z on the boundary Γ_1 must be given by the sets of their space-time amplitudes $v(-L_1, t) = \{v_{n1}(-L_1, t)\}_n$ and $v'(-L_1, t) = \{\partial v_{n1}(z, t)/\partial z|_{z=-L_1}\}_n$ to implement EACs (5.94) and (5.96a). The functions $v_{n1}(-L_1, t)$, which should be non-zero on the finite interval $0 < T_1 \leq t \leq T_2 < T$ (T is the upper limit of the observation time), can be chosen practically arbitrarily. This choice is dictated by a specific problem and requirements of a numerical experiment. However, the set $v'(-L_1, t)$, which

determines the derivative of the wave $U^{i(1)}(g, t)$ on Γ_1 , cannot be chosen in an arbitrary way due to the *causality principle*. Each pair

$$V_{n1}(\rho, t) = \left\{ v_{n1}(-L_1, t)\mu_{n1}(\rho); \left[\frac{\partial v_{n1}(z, t)}{\partial z} \right]_{z=-L_1} \mu_{n1}(\rho) \right\}$$

is bound to be generated by a pulsed eigenmode $U_n^{i(1)}(g, t) = v_{n1}(z, t)\mu_{n1}(\rho)$ propagating in the waveguide Ω_1 in the direction of increasing z . This requirement is met if the functions comprising the pair $V_{n1}(\rho, t)$ satisfy the equation

$$v_{n1}(-L_1, t) = - \int_0^t J_0[\lambda_{n1}(t - \tau)] \frac{\partial v_{n1}(z, t)}{\partial z} \Big|_{z=-L_1} d\tau; \quad t \geq 0, \quad (5.100)$$

which is obtained from (5.22).

5.4 Characteristics of Steady-State and Transient Fields in Axially Symmetric Structures

5.4.1 Frequency-Domain Prototypes for Initial Boundary Value Problems

The solution $U(g, t)$ to the problem (5.75), (5.91) and the solution $\tilde{U}(g, k)$ to the problem

$$\left\{ \begin{array}{l} \left[\frac{\partial^2}{\partial z^2} + \frac{\partial}{\partial \rho} \left(\frac{1}{\rho} \frac{\partial}{\partial \rho} \rho \right) + \bar{\epsilon}(g)k^2 \right] \tilde{U}(g, k) = \bar{f}(g, k); \\ \qquad \qquad \qquad g = \{\rho, z\} \in \Omega_{\text{int}} \\ \tilde{E}_{tg}(p, k) \Big|_{p=\{\rho, \phi, z\} \in \Sigma} = 0, \quad \tilde{U}(0, z, k) = 0 \quad \text{for } \{0, z\} \in \bar{\Omega}_{\text{int}} \\ \tilde{E}_{tg}(p, k), \quad \tilde{H}_{tg}(p, k) \quad \text{are continuous when crossing } \Sigma^{\epsilon, \sigma} \\ \text{and boundaries } \Gamma \times [0, 2\pi], \quad \Gamma_j \times [0, 2\pi], \end{array} \right. \quad (5.101a)$$

$$\tilde{U}(g, k) = \sum_{n=1}^{\infty} \begin{cases} 1 & \text{for } TE_0\text{-waves} \\ 0 & \text{for } TM_0\text{-waves} \end{cases} \left[A_{n1}(k)e^{i\beta_{n1}(z+L_1)} + B_{n1}(k)e^{-i\beta_{n1}(z+L_1)} \right] \mu_{n1}(\rho);$$

$g \in \bar{\Omega}_1,$

(5.101b)

$$\tilde{U}(g, k) = \sum_{n=1}^{\infty} B_{n2}(k) e^{i\beta_{n2}(z-L_2)} \mu_{n2}(\rho); \quad g \in \bar{\Omega}_2, \quad (5.101c)$$

$$\tilde{U}(g, k) = \frac{1}{\sqrt{r}} \sum_{n=1}^{\infty} C_n(k) H_{n+1/2}^{(1)}(kr) \tilde{\mu}_n(\cos \vartheta); \quad g \in \bar{\Omega}_{\text{ext}} \quad (5.101d)$$

are related [3, 5] by the following integral transform

$$\tilde{f}(k) = \int_0^{\infty} f(t) e^{ikt} dt \leftrightarrow f(t) = \frac{1}{2\pi} \int_{i\alpha-\infty}^{i\alpha+\infty} \tilde{f}(k) e^{-ikt} dk; \quad 0 \leq \alpha \leq \text{Im } k. \quad (5.102)$$

This transform links time-domain characteristics $f(t)$ with frequency-domain characteristics $\tilde{f}(k)$. Here, $\tilde{U}(g, k) = \tilde{E}_\phi(g, k)$ for monochromatic TE_0 -waves and $\tilde{U}(g, k) = \tilde{H}_\phi(g, k)$ for monochromatic TM_0 -waves, k is the *complex wavenumber (frequency parameter or simply frequency)*, $\bar{\varepsilon}(g) = \varepsilon(g) + i\eta_0\sigma(g)/k$, $\tilde{f}(g, k) = \tilde{F}(g, k) + ik\bar{\varepsilon}(g)\varphi(g) - \varepsilon(g)\psi(g)$, $\tilde{F}(g, k) \leftrightarrow F(g, t)$, and

$$\beta_{nj} = \sqrt{k^2 - \lambda_{nj}^2}; \quad \text{Re } \beta_{nj} \text{ Re } k \geq 0, \quad \text{Im } \beta_{nj} \geq 0 \quad (5.103)$$

are the *longitudinal propagation numbers* of TE_{0n} - or TM_{0n} -modes which run along the waveguide Ω_j with the attenuation (when $\text{Im } \beta_{nj} > 0$) or without it (when $\text{Im } \beta_{nj} = 0$).

In the formulas (5.101b), (5.101c), the terms with complex-valued amplitudes A_{n1} correspond to the incident monochromatic wave $\tilde{U}^{i(1)}(g, k) \leftrightarrow U^{i(1)}(g, t)$ on the boundary Γ_1 , while the terms with amplitudes B_{n1} and B_{n2} correspond to the scattered (secondary) waves $\tilde{U}^{s(1)}(g, k) \leftrightarrow U^{s(1)}(g, t) = U(g, t) - U^{i(1)}(g, t)$ and $\tilde{U}^{s(2)}(g, k) \leftrightarrow U(g, t)$ in the waveguides Ω_1 and Ω_2 . If we correlate representations (5.6), (5.92) with (5.101b), (5.101c), it is evident that

$$\begin{aligned} A_{n1}(k) &\leftrightarrow v_{n1}(-L_1, t), & B_{n1}(k) &\leftrightarrow u_{n1}(-L_1, t), \\ B_{n2}(k) &\leftrightarrow u_{n2}(L_2, t), \end{aligned} \quad (5.104)$$

or, in other signs, $A_{n1}(k) = \tilde{v}_{n1}(-L_1, k)$, $B_{n1}(k) = \tilde{u}_{n1}(-L_1, k)$, $B_{n2}(k) = \tilde{u}_{n2}(L_2, k)$. Similar, from (5.55), (5.101d) we have too:

$$\frac{C_n(k) H_{n+1/2}^{(1)}(kr)}{\sqrt{r}} \leftrightarrow u_n(r, t) \quad \text{or} \quad \frac{C_n(k) H_{n+1/2}^{(1)}(kr)}{\sqrt{r}} = \tilde{u}_n(r, k). \quad (5.105)$$

In the boundary value problem (5.101a), (5.101b), (5.101c) (5.101d), the equations (5.101b) to (5.101d) represent the so-called *partial radiation conditions* [3, 5, 48], which reflect physically grounded requirement imposed on the total field outside the domain Ω_{int} , namely, that the field $\tilde{U}(g, k)$ in this region may not contain the waves incoming from infinity. The only exception is the incident wave, which in our case has the form:

$$\tilde{U}^{i(1)}(g, k) = \sum_n A_{n1}(k) e^{i\beta_{n1}(z+L_1)} \mu_{n1}(\rho); \quad g \in \bar{\Omega}_1. \quad (5.106)$$

5.4.2 Electrodynamic Characteristics of Open Axially Symmetric Structures

Consider now frequencies k such that $\text{Re } k > 0$ and $\text{Im } k = 0$ (physical values of k). Let also, an open axially symmetric structure (Fig. 5.5) is fed from the waveguide Ω_1 , and

$$\tilde{U}^{i(1)}(g, k) = \tilde{U}_p^{i(1)}(g, k) = A_{p1}(k) e^{i\beta_{p1}(z+L_1)} \mu_{p1}(\rho); \quad \text{Im } \beta_{p1} = 0 \quad (5.107)$$

(*undamped eigenwave*), and the domain Ω_{int} is free from sources ($\bar{f}(g, k) \equiv 0$). In the frequency-domain, a structure of this kind can be characterized by the *reflection coefficients* $R_{np}^{11}(k)$ (conversion coefficients of the p th incident mode into n th reflected mode) and the *transmission coefficients* $T_{np}^{21}(k)$ (conversion coefficients of the p th mode of the waveguide Ω_1 into n th mode of the waveguide Ω_2) given by the following formulas:

$$R_{np}^{11}(k) = \frac{B_{n1}}{A_{p1}} = \frac{\tilde{u}_{n1}(-L_1, k)}{\tilde{v}_{p1}(-L_1, k)}, \quad T_{np}^{21}(k) = \frac{B_{n2}}{A_{p1}} = \frac{\tilde{u}_{n2}(L_2, k)}{\tilde{v}_{p1}(-L_1, k)}. \quad (5.108)$$

It is evident that in real computation experiments, the first integral transform in (5.102) should be replaced with the following one:

$$\tilde{f}(k) = \int_0^T f(t) e^{ikt} dt. \quad (5.109)$$

Here, T is the upper limit of the observation time, and for all $t > T$ the function $f(t)$ in (5.102) is continued by zero.

The values

$$W_{\text{abs}}(k) = \frac{k^2}{\beta_{p1}\beta} \int_{\Omega_{\text{int}}} \text{Im } \bar{e}(g) \left| \tilde{E}(g, k) \right|^2 dg, \quad W_{np}^{11}(k) = \left| R_{np}^{11} \right|^2 \frac{\text{Re } \beta_{n1}}{\beta_{p1}}, \quad (5.110)$$

$$W_{np}^{21}(k) = \left| T_{np}^{21} \right|^2 \frac{\text{Re } \beta_{n2}}{\beta_{p1}}$$

($\beta = 1$ in the case of TE_0 -waves and $\beta = \eta_0^2$ in the case of TM_0 -waves, $dg = \rho d\rho dz$) specify the relative part of energy lost to absorption and diverted into each propagating mode in the waveguides Ω_1 and Ω_2 , where it is carried away from the open axially symmetric structure [3, 5, 8]. For any finite value of the frequency $k = 2\pi/\lambda$ (λ is the wavelength in free space) the number $N_j = \sum_n (\text{Re } \beta_{nj}/|\beta_{nj}|)$ of propagating modes for each waveguide Ω_j is finite. It follows from (5.110) that the relative portion of energy radiated into free space through the boundary Γ (the *radiating efficiency* or *antenna efficiency*) can be calculated by the formula

$$\eta(k) = 1 - W_{\text{abs}} - \sum_n \left(W_{np}^{11} + W_{np}^{21} \right). \quad (5.111)$$

The *normalized directional pattern* on the arc $r = M \geq L$

$$D(\vartheta, k, M) = \frac{\left| \tilde{E}_{tg}(M, \vartheta, k) \right|^2}{\max_{0 \leq \vartheta \leq \pi} \left| \tilde{E}_{tg}(M, \vartheta, k) \right|^2}; \quad 0 \leq \vartheta \leq 180^\circ, \quad K_1 \leq k \leq K_2 \quad (5.112)$$

determines the spatial orientation and the energy content of the propagating waves radiated into free space. Here, $\tilde{E}_{tg}(M, \vartheta, k)$ is the tangential (to the spherical surface $r = M$) component of the monochromatic electric field $\tilde{E}(g, k)$.

The *main lobe* of the pattern is directed at an angle $\bar{\vartheta}(k)$ such that $D(\bar{\vartheta}(k), k, M) = 1$. The value M defines a zone (near-field, intermediate, or far-field), for which the pattern $D(\vartheta, k, M)$ is calculated. We assume that the near-zone boundary is determined by $M = L$, while the far-zone boundary is determined by such M that its further growth does not lead to significant variations of $D(\vartheta, k, M)$ for all values of k under consideration.

Half-power beamwidth (HPBW) $\vartheta_{0.5}(k)$ is an angle between two directions of the main lobe, where the power reduces to the half of its maximum, i.e. $\vartheta_{0.5}(k) = |\vartheta^+ - \vartheta^-|$, where $D(\vartheta^+, k, M) = 0.5$ and $D(\vartheta^-, k, M) = 0.5$.

To obtain the pattern $D(\vartheta, k, M)$, one should solve the closed initial boundary value problem (5.91), then recalculate the values of $U(g, t)$ from the arc $r = L$ onto the arc $r = M$ using (5.75), determine $\vec{E}_{tg}(M, \vartheta, t)$ ($E_\phi(M, \vartheta, t)$ in the case of TE_0 -waves or $E_\vartheta(M, \vartheta, t)$ in the case of TM_0 -waves, see the formulas (5.19) in [3]), and finally invoke the transform (5.109).

Another sequence of operations is possible. Upon solving the initial boundary value problem (5.91), we determine (see the formulas (5.55)) a set of the amplitudes $u_n(L, t)$ and then determine the complex-valued amplitudes $C_n(k)$ using (5.105) and (5.109). The field $\tilde{E}_\phi(M, \vartheta, k)$ (in the case of TE_0 -waves) or the field $\tilde{H}_\phi(M, \vartheta, k)$ (in the case of TM_0 -waves) can be calculated then from (5.101d). For TM_0 -waves, we have $\tilde{E}_{Tg}(M, \vartheta, k)$ equals to $\tilde{E}_\vartheta(M, \vartheta, k)$, where

$$\tilde{E}_\vartheta(r, \vartheta, k) = \frac{\eta_0}{ik\bar{\epsilon}r} \frac{\partial [r\tilde{H}_\phi(r, \vartheta, k)]}{\partial r}. \tag{5.113}$$

The formula (5.113) is derived by applying the transform (5.102) to the equations (1.19) from [3].

Let now an open axially symmetric structure (see Fig. 5.5) is excited from the waveguide Ω_1 by the p th pulsed eigenwave (pulsed TE_{0p} - or TM_{0p} -wave)

$$U^{i(1)}(g, t) = U_p^{i(1)}(g, t) = v_{p1}(z, t)\mu_{p1}(\rho). \tag{5.114}$$

Let also the domain Ω_{int} is free from sources of pulsed waves, i.e. $F(g, t) \equiv 0$ and $\varphi(g) = \psi(g) \equiv 0$ in (5.91). The field $\{\vec{E}(g, t), \vec{H}(g, t)\}$, which is the solution to the problem (5.91), satisfies the following relation [5, 8]:

$$\underbrace{P^{s(1)} + P^{s(2)} + P^{i \times s(1)} + P}_A + \underbrace{\frac{1}{2} \frac{\partial}{\partial t} \int_{\Omega_{\text{int}}} \left(\eta_0 |\vec{H}|^2 + \frac{\epsilon}{\eta_0} |\vec{E}|^2 \right) dg}_B + \underbrace{\int_{\Omega_{\text{int}}} \sigma |\vec{E}|^2 dg}_C = \underbrace{-P^{i(1)}}_D. \tag{5.115}$$

This formula represents a relationship between instantaneous electromagnetic powers in the closure of the domain Ω_{int} [8, 42]: (A) is a sum of the instantaneous powers radiating through the boundaries Γ_j into the waveguides Ω_j ($P_j^s(t)$) and the instantaneous power radiating through the boundary Γ into free space ($P(t)$); (B) is the instantaneous power accumulated in the domain Ω_{int} ; (C) is the instantaneous absorbed power; and (D) is the instantaneous power incoming into the domain Ω_{int} through the boundary Γ_1 . Here,

$$P(t) = \int_{\Gamma} [(\vec{E} \times \vec{H}) \cdot \vec{n}] d\vartheta, \quad P^{s \text{ or } i(j)}(t) = \int_{\Gamma_j} [(\vec{E}^{s \text{ or } i(j)} \times \vec{H}^{s \text{ or } i(j)}) \cdot \vec{n}_j] \rho d\rho, \\ P^{i \times s(1)}(t) = \int_{\Gamma_1} [(\vec{E}^{s(1)} \times \vec{H}^{i(1)} + \vec{E}^{i(1)} \times \vec{H}^{s(1)}) \cdot \vec{n}_1] \rho d\rho, \tag{5.116}$$

\vec{n}_j and \vec{n} are the outer normals to the domain Ω_{int} on the boundaries Γ_j and Γ , $\vec{a} \times \vec{b}$ and $\vec{a} \cdot \vec{b}$ are the vector and scalar products of vectors \vec{a} and \vec{b} , \vec{E}^s or $i(j)$ and \vec{H}^s or $i(j)$ are electric and magnetic fields corresponding to the wave U^s or $i(j)(g, t)$ in the waveguide Ω_j (see comments after (5.93)).

The equation (5.115) is derived via simple manipulations with the Maxwell's equations

$$\text{rot}\vec{H} = \eta_0^{-1}\varepsilon\frac{\partial\vec{E}}{\partial t} + \sigma\vec{E}, \quad \text{rot}\vec{E} = -\eta_0\frac{\partial\vec{H}}{\partial t}. \quad (5.117)$$

Namely, the scalar product of the first equation in (5.117) by \vec{E} is subtracted from the scalar product of the second equation by \vec{H} . The resulting equation is integrated over the volume $\Omega_{\text{int}} \times [0, 2\pi]$. The term containing the volume integral of $\text{div}(\vec{E} \times \vec{H})$ is transformed then according to the Gauss divergence theorem [34]. The field $\{\vec{E}(g, t), \vec{H}(g, t)\}$, which is the solution to the problem (5.91), satisfies the Maxwell's equations (5.117) in all points of the domain $\bar{\Omega}_{\text{int}}$.

Bringing into correlation the notions of power and energy we can conclude that the integrals

$$\begin{aligned} W_{\text{feed}}^P(\Omega_1) &= -\int_0^T P^{i(1)}(t)dt, & W_{\text{rad}}^P(\Omega_{\text{ext}}) &= \int_0^T P(t)dt, \\ W_{\text{rad}}^P(\Omega_j) &= \int_0^T P^{s(j)}(t)dt, & W_{\text{abs}}^P(\Omega_{\text{int}}) &= \int_0^T \int_{\Omega_{\text{int}}} \sigma |\vec{E}|^2 dgdt, \\ W_{\text{cum}}^P(\Omega_{\text{int}}) &= \frac{1}{2} \int_{\Omega_{\text{int}}} \left(\eta_0 |\vec{H}|^2 + \frac{\varepsilon}{\eta_0} |\vec{E}|^2 \right) dg \Bigg|_{t=0}^{t=T} \end{aligned} \quad (5.118)$$

have the following physical meaning: $W_{\text{feed}}^P(\Omega_1)$ is the energy incoming into the axially symmetric system from the waveguide Ω_1 during the time interval $0 < t \leq T$; $W_{\text{rad}}^P(\Omega_{\text{ext}})$ and $W_{\text{rad}}^P(\Omega_j)$ represent the energy stored in pulses outgoing through the boundaries Γ and Γ_j into free space and into the waveguides Ω_j ; $W_{\text{cum}}^P(\Omega_{\text{int}})$ is the energy accumulated in the domain Ω_{int} ; and $W_{\text{abs}}^P(\Omega_{\text{int}})$ is the energy lost to absorption in the domain Ω_{int} . It is clear that

$$W_{\text{feed}}^P(\Omega_1) = W_{\text{rad}}^P(\Omega_{\text{ext}}) + W_{\text{rad}}^P(\Omega_1) + W_{\text{rad}}^P(\Omega_2) + W_{\text{cum}}^P(\Omega_{\text{int}}) + W_{\text{abs}}^P(\Omega_{\text{int}}). \quad (5.119)$$

Using (5.118) and (5.119), we can determine the *radiating efficiency of a pulsed antenna*

$$\eta_{\text{rad}} = \frac{W_{\text{rad}}^P(\Omega_{\text{ext}})}{W_{\text{feed}}^P(\Omega_1)} \quad (5.120)$$

and the *efficiency of energy accumulation* in an open axially symmetric resonator

$$\eta_{\text{cum}} = \frac{W_{\text{cum}}^P(\Omega_{\text{int}})}{W_{\text{feed}}^P(\Omega_1)}. \quad (5.121)$$

The ability of a pulsed antenna to concentrate the radiated energy in a certain direction is described by the *normalized pulsed pattern* on the arc $r = M$ [8, 19]:

$$D_{\text{puls}}(\vartheta, t, M) = \frac{U(M, \vartheta, t)}{\max_{\vartheta, t} |U(M, \vartheta, t)|}; \quad 0 \leq \vartheta \leq 180^\circ, \quad M \geq L, \quad (5.122)$$

$$T_1 \leq t \leq T_2 \leq T + M - L.$$

The results presented in [8, 19] show that $\tilde{D}_{\text{puls}}(\vartheta, k, M) \leftrightarrow D_{\text{puls}}(\vartheta, t, M)$ is also useful when investigating radiators of pulsed waves.

5.4.3 Spectral Characteristics of Open Resonators

It is known [3, 5, 48–50] that for k such that $\text{Im } k > 0$ and for any $\bar{f}(g, k) \in L_2(\Omega)$, $\tilde{U}^{i(1)}(g, k) = \tilde{U}_p^{i(1)}(g, k)$, the problem (5.101a), (5.101b), (5.101c), (5.101d) is uniquely solvable in the space $W_2^1(\Omega)$. And in this case, its *resolvent* (the operator $R^{-1}(k)[\dots]$ such that $\tilde{U}(g, k) = \tilde{U}(g, k, \bar{f}, A_{p1}(k)) = R^{-1}(k)[\bar{f}(g, k), A_{p1}(k)]$; $g \in \Omega$) is an analytical operator-function of the parameter k .

The natural boundaries of the analytical extension of resolving operators similar to $R^{-1}(k)[\dots]$ from the upper half-plane of the plane $\mathbb{C} = \{k : -\infty \leq \text{Re } k, \text{Im } k \leq +\infty\}$ are defined by some infinite-sheeted Riemann surfaces K [3, 5]. The kernels of resolvents (the Green functions $\tilde{G}(g, g_0, k)$ of associated boundary value problems) are in this case meromorphic functions of the complex-valued parameter k (in local variables on the surface K [45]). The sets of the poles $\{\bar{k}_n\}_n = \Theta_k$ of these functions are the *spectral sets* or simply the *spectra*. The elements \bar{k}_n of these sets (*eigenfrequencies*) correspond to the nontrivial solutions $\tilde{U}(g, \bar{k}_n) = \bar{u}(g, \bar{k}_n)$ of homogeneous boundary value problems. If the number of linearly independent solutions of this kind for $k = \bar{k}_n$ equals M ($\bar{u}(g, \bar{k}_n) = \bar{u}^{(m)}(g, \bar{k}_n)$; $m = 1, 2, \dots, M$), then the order of the pole \bar{k}_n of the resolvent $R^{-1}(k)[\dots]$ (and of the corresponding

Green function $\tilde{G}(g, g_0, k)$ is determined by the maximal value of $S(m)$, where $S(m) - 1$ is a number of associated with the *eigenfunction* $\bar{u}^{(m)}(g, \bar{k}_n)$ functions [3, 5, 51].

Solutions $\bar{u}(g, \bar{k}_n)$ define possible *free electromagnetic field oscillations* in open electrodynamic structures (open resonators). The spectrum points located in the vicinity of the real axis of the first (physical) sheet C_k of the surface K together with the corresponding free oscillations play a dominant role in the resonant response of a structure on any external excitation [3, 5, 8]. For the reliable physical analysis of resonant electromagnetic field transformations in space and time, it is necessary to use elements of the spectral theory: distribution of points $\bar{k}_n = \text{Re } \bar{k}_n + i \text{Im } \bar{k}_n$ in specified regions of the surface K , configuration of the fields $\bar{u}(g, \bar{k}_n)$, estimations of the *quality factor* $Q = \text{Re } \bar{k}_n / 2 |\text{Im } \bar{k}_n|$ for free oscillations, and so on.

We have shown previously how to calculate time- and frequency-domains characteristics using time-domain models. Now, we will discuss briefly how to obtain information about the spectrum Θ_k from these models. A few simple recipes from [20] will be quoted, which may be useful in consideration of various applied problems, as it was demonstrated in [5, 8, 24].

Let us consider the problem (5.75), (5.76) and

$$\left\{ \begin{array}{l} \left[\frac{\partial^2}{\partial z^2} + \frac{\partial}{\partial \rho} \left(\frac{1}{\rho} \frac{\partial}{\partial \rho} \rho \right) + \bar{\epsilon}(g)k^2 \right] \tilde{U}(g, k) = \bar{f}(g, k); \\ g = \{\rho, z\} \in \Omega_{\text{int}} \\ \tilde{E}_{tg}(p, k) \Big|_{p=\{\rho, \phi, z\} \in \Sigma} = 0, \quad \tilde{U}(0, z, k) = 0 \quad \text{for } \{0, z\} \in \bar{\Omega}_{\text{int}} \\ \tilde{E}_{tg}(p, k), \quad \tilde{H}_{tg}(p, k) \text{ are continuous when crossing } \Sigma^{\epsilon, \sigma} \\ \text{and boundary } \Gamma \times [0, 2\pi], \end{array} \right. \quad (5.123a)$$

$$\tilde{U}(g, k) = \frac{1}{\sqrt{r}} \sum_{n=1}^{\infty} C_n(k) H_{n+1/2}^{(1)}(kr) \tilde{\mu}_n(\cos \vartheta); \quad g \in \bar{\Omega}_{\text{ext}}, \quad (5.123b)$$

whose solutions are connected by the transform (5.102):

$$U(g, t) = \frac{1}{2\pi} \int_{ix-\infty}^{ix+\infty} \tilde{U}(g, k) e^{-ikt} dk; \quad \text{Re } k \geq \alpha \geq 0. \quad (5.124)$$

The surface K in this case coincides with the surface of the analytical extension of the function $\ln k$ [5, 48]: $k = 0$ is the logarithmic branch point; the sheets of the surface are cut along the semi-axis $\text{Re } k = 0, \text{Im } k < 0$. All poles of the resolvent

$R^{-1}(k)[\dots]$ of the problem (5.123a), (5.123b) on the first (physical) sheet C_k of the surface \mathbf{K} are located below the axis $\text{Im } k = 0$ [5, 48, 49]. Taking into consideration that by definition

$$\tilde{U}(g, k) = R^{-1}(k)[\bar{f}(g, k)] = \int_{\Omega} \tilde{G}(g, g_0, k) \bar{f}(g_0, k) dg_0, \tag{5.125}$$

and deforming the contour of integration in (5.124) downwards to the position $\text{Im } k = \beta < 0$ (the branch point is bypassed along the banks of the cut and an infinitesimal semi-circle), we obtain [20]:

$$\begin{aligned}
 U(g, t) = 2 \text{Im} \left\{ \sum_n \int_{\Omega} \underset{k=\bar{k}_n: \text{Re } \bar{k}_n > 0}{\text{Res}} [\tilde{G}(g, g_0, k) \bar{f}(g_0, k) e^{-ikt}] dg_0 \right. \\
 \left. + \sum_m \int_{\Omega} \underset{k=\underline{k}_m: \text{Re } \underline{k}_m > 0}{\text{Res}} [\tilde{G}(g, g_0, k) \bar{f}(g_0, k) e^{-ikt}] dg_0 \right\} + Q(g, t); \\
 g \in \Omega_{\text{int}}, \quad t > 0.
 \end{aligned} \tag{5.126}$$

The term $Q(g, t)$ in (5.126) sums up contributions of the singularities of $\tilde{U}(g, k)$, $k \in \mathbf{K}$ which are not swept when deforming the contour of integration in (5.124). Its estimation in the norm of the space $W_2^1(\Omega_{\text{int}})$ for large t is determined by the function $\bar{f}(g, k)$ when $k \rightarrow 0$ [38]. Thus, for example, if $\bar{f}(g, k) = O(k^p \ln^q k)$, where p and q are integers, then we have $\|Q(g, t)\| \leq \text{const}(\bar{f}) [t^{-p-1} \ln^{q-2} t]$. In (5.126), $\bar{k}_n \in \Theta_k$ are eigenfrequencies of an open resonator located on the first sheet of the surface \mathbf{K} between two straight lines $\text{Im } k = 0$ and $\text{Im } k = \beta < 0$, and numbered so that $\text{Im } \bar{k}_{n+1} \leq \text{Im } \bar{k}_n$. The number of such eigenfrequencies is finite [5, 20, 38, 48]. The values \underline{k}_m are poles of the function $\bar{f}(g, k)$ that do not coincide with elements of the spectral set Θ_k . All of them are assumed to be located in the plane C_k above the line $\text{Im } k = \beta < 0$.

Assume that all the poles $k = \bar{k}$ of the Green function $\tilde{G}(g, g_0, k)$ of the problem (5.123a), (5.123b) are simple. Without the loss of generality, it may be suggested that each eigenfrequency \bar{k} corresponds to a single free oscillation $\bar{u}(g, \bar{k})$.

Under these assumptions, the principal part $\Xi \tilde{G}$ of the Green function $\tilde{G}(g, g_0, k)$ in the vicinity of the pole $k = \bar{k}$ takes form [51]

$$\Xi \tilde{G}(g, g_0, k) = \frac{G_{-1}(g, g_0, \bar{k})}{k - \bar{k}} = \frac{\bar{u}(g, \bar{k}) \bar{w}^*(g_0, \bar{k}^*)}{k - \bar{k}}. \tag{5.127}$$

Here, $\bar{w}(g, \bar{k}^*)$ is the eigen element of the operator-function $\bar{R}(k) = [R(k^*)]^*$ corresponding to the eigenvalue \bar{k}^* [51]; the operator $R(k)[\dots]$ is inverse to the resolvent $R^{-1}(k)[\dots]$; $R(k)[\bar{U}(g, k)] = \bar{f}(g, k)$; and the asterisk ‘*’ stands for the complex conjugation. The symbols $G_l(g, g_0, \eta)$ and $f_l(g_0, \eta)$ (they will be introduced below) denote the coefficients at the terms $(k - \eta)^l$ in the Laurent expansion of the functions $\tilde{G}(g, g_0, k)$ and $\bar{f}(g_0, k)$ in the vicinity of the point $k = \eta$.

For the elements \bar{u} and \bar{w} we obtain from (5.127) and [20]

$$\tilde{G}(g, g_0, k) = \tilde{G}(g_0, g, k) = \tilde{G}^*(g, g_0, -k^*), \tag{5.128}$$

that

$$\bar{u}(g, \bar{k}) = \bar{w}^*(g, \bar{k}^*), \quad \bar{u}(g, \bar{k})\bar{w}^*(g_0, \bar{k}^*) = -\bar{u}^*(g, -\bar{k}^*)\bar{w}(g_0, -\bar{k}). \tag{5.129}$$

The results below are obtained from (5.126) to (5.129). These results may simplify significantly the analysis of the solutions $U(g, t)$ to the problem (5.75), (5.76).

- Let the function $\bar{f}(g, k)$ is free from singularities on the sheet C_k . From (5.126) it follows that

$$\begin{aligned} U(g, t) \approx & 2 \sum_{n: \text{Re } \bar{k}_n > 0} e^{t \text{Im } \bar{k}_n} |\bar{u}(g, \bar{k}_n)| |C(\bar{f}, \bar{k}_n)| \\ & \times \sin[\arg \bar{u}(g, \bar{k}_n) + \arg C(\bar{f}, \bar{k}_n) - t \text{Re } \bar{k}_n]; \end{aligned} \tag{5.130}$$

$g \in \Omega_{\text{int}}, \quad 0 < T_1 < t < T.$

Here,

$$C(f, \bar{k}_n) = \int_{\Omega} \bar{u}(g_0, \bar{k}_n) f(g_0, \bar{k}_n) dg_0 \tag{5.131}$$

and the value of T_1 is defined by such parameters as the duration of excitation, the presence of traps, absorbing elements, etc. From (5.130) it follows that the field $U(g, t)$ in the near-field zone of an open resonator is a superposition of the free oscillations $\bar{u}(g, \bar{k}_n)$ associated with the complex-valued eigenfrequencies \bar{k}_n . The lifetime of each oscillation in the domain Ω_{int} , as well as its rate of decay, are determined by the value $|\text{Im } \bar{k}_n|$ (or by the Q-factor $Q = \text{Re } \bar{k}_n / 2 |\text{Im } \bar{k}_n|$). The initial state (or the excitation level) is determined by the value $C(\bar{f}, \bar{k}_n)$ which reflects the degree of correlation of time- and frequency-domains characteristics of the field $\bar{u}(g, \bar{k}_n)$ with the source function $\bar{f}(g, k)$.

- Let the function $\bar{f}(g, k)$ has a single simple pole at the point $k = \underline{k}$ on the right-hand half-plane of the sheet C_k , and it does not coincide with any element \bar{k}_n of the set Θ_k . It follows from (5.126) that

$$\begin{aligned}
 U(g, t) \approx 2 \left\{ \sum_{n: \operatorname{Re} \bar{k}_n > 0} e^{t \operatorname{Im} \bar{k}_n} |\bar{u}(g, \bar{k}_n)| |C(\bar{f}, \bar{k}_n)| \right. \\
 \times \sin[\arg \bar{u}(g, \bar{k}_n) + \arg C(\bar{f}, \bar{k}_n) - t \operatorname{Re} \bar{k}_n] \\
 \left. + e^{t \operatorname{Im} \underline{k}} |\tilde{U}(g, \underline{k}, f_{-1})| \sin[\arg \tilde{U}(g, \underline{k}, f_{-1}) - t \operatorname{Re} \underline{k}] \right\}; \\
 g \in \Omega_{\text{int}}, \quad 0 < T_1 < t < T.
 \end{aligned} \tag{5.132}$$

In the formula (5.132), a new term arises, which is associated with a field of the frequency $\operatorname{Re} \underline{k}$. The spatial pattern of this field is determined by the solution $\tilde{U}(g, \underline{k}, f_{-1})$ of the elliptic problem $R(\underline{k})[\tilde{U}(g, \underline{k}, f_{-1})] = f_{-1}(g, \underline{k})$, and its amplitude decreases as $\exp(t \operatorname{Im} \underline{k})$. With $\operatorname{Im} \underline{k} = 0$ and sufficiently large values of t , this term will dominate in the field $U(g, t)$ due to the principle of limiting amplitude.

- Let the function $\bar{f}(g, k)$ has a single second-order pole at the point $k = \underline{k}$ on the right-hand half-plane of the sheet C_k , and it does not coincide with any element \bar{k}_n of the set Θ_k . In this case, we have:

$$\begin{aligned}
 U(g, t) \approx 2 \left\{ \sum_{n: \operatorname{Re} \bar{k}_n > 0} e^{t \operatorname{Im} \bar{k}_n} |\bar{u}(g, \bar{k}_n)| |C(\bar{f}, \bar{k}_n)| \right. \\
 \times \sin[\arg \bar{u}(g, \bar{k}_n) + \arg C(\bar{f}, \bar{k}_n) - t \operatorname{Re} \bar{k}_n] \\
 - te^{t \operatorname{Im} \underline{k}} |\tilde{U}(g, \underline{k}, f_{-2})| \cos[\arg \tilde{U}(g, \underline{k}, f_{-2}) - t \operatorname{Re} \underline{k}] \\
 + e^{t \operatorname{Im} \underline{k}} |\tilde{U}(g, \underline{k}, f_{-1}) + \tilde{U}_1(g, \underline{k}, f_{-2})| \\
 \left. \times \sin[\arg [\tilde{U}(g, \underline{k}, f_{-1}) + \tilde{U}_1(g, \underline{k}, f_{-2})] - t \operatorname{Re} \underline{k}] \right\}; \\
 g \in \Omega_{\text{int}}, \quad 0 < T_1 < t < T.
 \end{aligned} \tag{5.133}$$

Here,

$$\tilde{U}_1(g, \eta, f) = \int_{\Omega} G_l(g, g_0, \eta) f(g_0, \eta) dg_0. \tag{5.134}$$

With $\operatorname{Im} \underline{k} = 0$ and sufficiently large t , the contribution of free oscillations with complex-valued eigenfrequencies \bar{k}_n into the field $U(g, t)$ will be negligible. The field oscillating with frequency $k = \underline{k}$ will dominate. The spatial pattern of this field is determined by the solution $\tilde{U}(g, \underline{k}, f_{-2})$ of the elliptic problem $R(\underline{k})[\tilde{U}(g, \underline{k}, f_{-2})] = f_{-2}(g, \underline{k})$, and its amplitude increases proportionally with t . For small values of $|\operatorname{Im} \underline{k}| > 0$, the situation is basically the same, but the domination is not as striking as before.

- Let the simple poles $k = \underline{k}$ and $k = \bar{k}$ of the functions $\bar{f}(g, k)$ and $\tilde{G}(g, g_0, k)$ coincide ($\bar{k} = \underline{k}$). In this case,

$$\begin{aligned}
 U(g, t) \approx 2 \left\{ \sum_{n: \operatorname{Re} \bar{k}_n > 0; \bar{k}_n \neq \bar{k}} e^{t \operatorname{Im} \bar{k}_n} |\bar{u}(g, \bar{k}_n)| |C(\bar{f}, \bar{k}_n)| \right. \\
 \times \sin[\arg \bar{u}(g, \bar{k}_n) + \arg C(\bar{f}, \bar{k}_n) - t \operatorname{Re} \bar{k}_n] \\
 - t e^{t \operatorname{Im} \bar{k}} |\bar{u}(g, \bar{k})| |C(f_{-1}, \bar{k})| \cos[\arg \bar{u}(g, \bar{k}) + \arg C(f_{-1}, \bar{k}) - t \operatorname{Re} \bar{k}] \\
 + e^{t \operatorname{Im} \bar{k}} |\bar{u}(g, \bar{k})| |C(f_0, \bar{k})| \sin[\arg \bar{u}(g, \bar{k}) + \arg C(f_0, \bar{k}_n) - t \operatorname{Re} \bar{k}] \\
 \left. + e^{t \operatorname{Im} \bar{k}} |\tilde{U}_0(g, \bar{k}, f_{-1})| \sin[\arg \tilde{U}_0(g, \bar{k}, f_{-1}) - t \operatorname{Re} \bar{k}] \right\}; \\
 g \in \Omega_{\text{int}}, \quad 0 < T_1 < t < T.
 \end{aligned}$$

By superposing singularities of the Green function of the problem (5.123a), (5.123b) with singularities of the source function $\bar{f}(g, k)$, the field of the corresponding free oscillation can be forced to be dominating in the field $U(g, t)$. The values $|\operatorname{Im} \bar{k}|$ and $|C(f_{-1}, \bar{k})|$ determine how long the field

$$\begin{aligned}
 W(g, t) = -2t e^{t \operatorname{Im} \bar{k}} |\bar{u}(g, \bar{k})| |C(f_{-1}, \bar{k})| \\
 \times \cos[\arg \bar{u}(g, \bar{k}) + \arg C(f_{-1}, \bar{k}) - t \operatorname{Re} \bar{k}]
 \end{aligned}$$

will remain dominant.

Let us consider in more details one of the above-listed results, for example, the first one. Assume that an open resonator (note that we consider compact axially symmetric structures without feeding waveguides Ω_r) is excited by the current source $F(g, t)$ and $\varphi(g) = \psi(g) \equiv 0$. The frequency band occupied by this source is $K_1 \leq k \leq K_2$. Assume also that only the value of $k = \operatorname{Re} \bar{k}$ falls within this band; this k corresponds to the real part of the complex-valued eigenfrequency \bar{k} associated with a high-Q free oscillation $\bar{u}(g, \bar{k})$. The band occupied by the source is defined as the interval of real values of k such that the value $|\tilde{F}(g, k)| / \max_k |\tilde{F}(g, k)|$ of normalized spectral amplitudes of the function $F(g, t)$ exceeds 0.01. Assume also that the source is switched off at the moment of time $t = \bar{T}$. Then, according to (5.130), solving the problem (5.76) and monitoring the function $U(g, t)$, $g \in \Omega_{\text{int}}$, $t > \bar{T}$, we observe the field $\bar{u}(g, \bar{k})$ oscillating with the frequency $\operatorname{Re} \bar{k}$. Amplitudes of these oscillations are given by the function $|C(\bar{f}, \bar{k})|$; the formula (5.131) is the key to efficient excitation of an open resonator by the current source $F(g, t)$. For $\tau = t - \bar{T} > 0$ at any fixed point $g \in \Omega_{\text{int}}$ not coincident with the knot points of the field $\bar{u}(g, \bar{k})$, we obtain from (5.130) that

$$U(g, t) = U(\tau) \approx A \exp(\tau \operatorname{Im} \bar{k}) \sin(\tau \operatorname{Re} \bar{k} + a). \quad (5.135)$$

Comparing (5.135) with the function $U(g, t)$, which is obtained solving the problem (5.76) numerically, we estimate the values $\text{Re } \bar{k}$, $\text{Im } \bar{k}$, A , and a , which uniquely determine principal characteristics of the eigenoscillation $\bar{u}(g, \bar{k})$ (see, for example, Figs. 4.5 and 4.6 in [5]).

The analysis becomes more complicated if two eigenfrequencies \bar{k}_1 and \bar{k}_2 are so close that none of them can be separated even with a bandwidth reduction of the source $F(g, t)$ in the spectral domain (such reduction results in increased values of \bar{T} and T , and the duration of numerical experiment grows significantly). Assuming that the real parts of \bar{k}_1 and \bar{k}_2 fall within the band $K_1 \leq k \leq K_2$ occupied by the source $F(g, t)$, we obtain from (5.130) the following simplified formula:

$$U(g, t) = U(\tau) \approx U_1(\tau) + U_2(\tau) = A_1 \exp(\tau \text{Im } \bar{k}_1) \cos(\tau \text{Re } \bar{k}_1 + a_1) + A_2 \exp(\tau \text{Im } \bar{k}_2) \cos(\tau \text{Re } \bar{k}_2 + a_2); \quad \tau > 0. \quad (5.136)$$

Comparing (5.136) with the function $U(g, t)$, which is obtained solving the problem (5.76) numerically, and behavior of the curves which represent the global inner and the global outer envelopes of $U(\tau)$ (see Sect. 4.3.3 in [5]), we estimate all the values that specify the oscillations $\bar{u}(g, \bar{k}_j)$, namely $\text{Re } \bar{k}_j$, $\text{Im } \bar{k}_j$, A_j , and a_j ($j = 1, 2$).

5.5 Plane Models for Open Electrodynamic Structures

5.5.1 The Key Problem

In the closed initial boundary value problem

$$\left\{ \begin{array}{l} \left[-\varepsilon(g) \frac{\partial^2}{\partial t^2} - \sigma(g) \eta_0 \frac{\partial}{\partial t} + \frac{\partial}{\partial y^2} + \frac{\partial^2}{\partial z^2} \right] U(g, t) = F(g, t); \\ t > 0, \quad g = \{y, z\} \in \Omega_{\text{int}} \\ U(g, t)|_{t=0} = \varphi(g), \quad \frac{\partial}{\partial t} U(g, t)|_{t=0} = \psi(g); \quad g \in \bar{\Omega}_{\text{int}} \\ \left\{ \begin{array}{l} \vec{E}_{tg}(p, t), \quad \vec{H}_{tg}(p, t) \text{ are continuous when crossing } \Sigma^{\varepsilon, \sigma} \\ \vec{E}_{tg}(p, t)|_{p=\{x, y, z\} \in \Sigma} = 0, \quad D[U(g, t)]|_{g \in \Gamma} = 0 \\ D_1[U(g, t) - U^{i(1)}(g, t)]|_{g \in \Gamma_1} = 0, \quad D_2[U(g, t)]|_{g \in \Gamma_2} = 0 \end{array} \right. ; \quad t \geq 0 \end{array} \right. \quad (5.137)$$

we find all elements necessary for effective numerical analysis of the majority of 2-D (plane) models that can be found in practice (Fig. 5.6): (i) virtual parallel-plate waveguides Ω_j ($j = 1, 2$), which allow to study structures with infinite feeding and output lines just like bounded in space models; (ii) EACs $D_1[U(g, t) - U^{i(1)}(g, t)]|_{g \in \Gamma_1} = 0$ and $D_2[U(g, t)]|_{g \in \Gamma_2} = 0$, which allow errors-free replacement

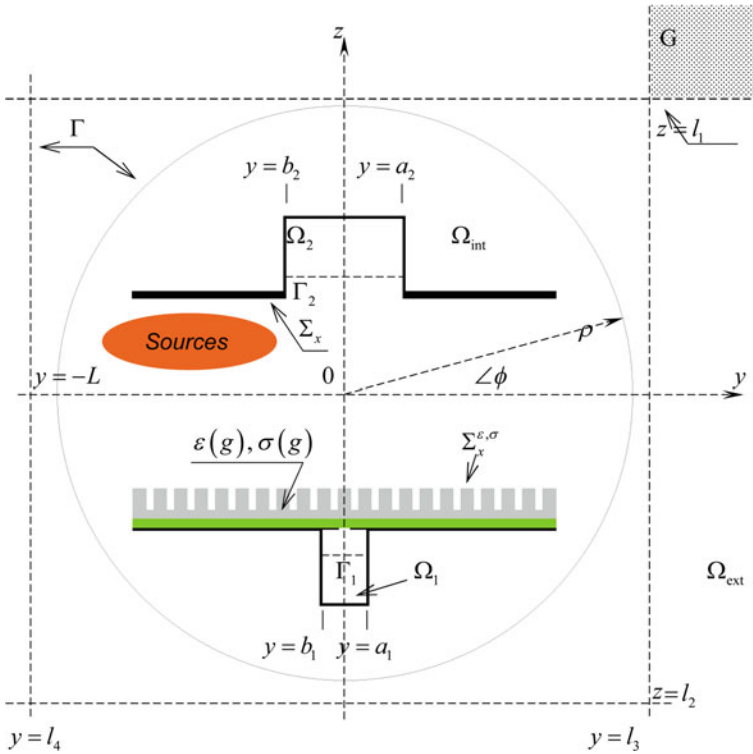


Fig. 5.6 Geometry of the key problem

of real infinite waveguides with finite virtual waveguides for simulations; (iii) EAC $D[U(g, t)]|_{g \in \Gamma} = 0$ on the cylindrical ($\Gamma = \{g = \{\rho, \phi\} \in \Omega_{total} : \rho = L\}$) or rectangular (see Fig. 5.6) virtual boundary Γ , which allows to truncate efficiently computation domains of open initial boundary value problems.

In (5.137), $\{x, y, z\}$ are the Cartesian coordinates and $\{\rho, \phi\}$ are the polar coordinates in the $y0z$ plane Ω_{total} ; $U(g, t) = E_x(g, t)$ for TE_0 - (E -polarized) waves ($\partial/\partial x = 0, E_y = E_z = H_x \equiv 0$) and $U(g, t) = H_x(g, t)$ for TM_0 - (H -polarized) waves ($\partial/\partial x = 0, H_y = H_z = E_x \equiv 0$). By $\Sigma = \Sigma_x \times [-\infty, \infty]$ we denote perfectly conducting surfaces obtained by moving the piecewise smooth contours Σ_x along the x -axis. $\Sigma^{e,\sigma} = \Sigma_x^{e,\sigma} \times [-\infty, \infty]$ are similarly defined surfaces across which the relative permittivity $\varepsilon(g)$ and specific conductivity $\sigma(g)$ change step-wise.

The functions $F(g, t), \varphi(g), \psi(g), \sigma(g)$, and $\varepsilon(g) - 1$, which have compact supports in the closure of Ω_{int} , are supposed to satisfy the theorem on unique solvability of the problem (5.137) in the Sobolev space $W_2^1(\Omega_{int}^T), \Omega_{int}^T = \Omega_{int} \times (0, T), T < \infty$. Current and instantaneous sources, which are given by the functions $F(g, t)$ and $\varphi(g), \psi(g)$, and all scatterers, which are given by the piecewise constant functions $\varepsilon(g), \sigma(g)$ and by the contours Σ_x and $\Sigma_x^{e,\sigma}$, are located in Ω_{int} .

The computation domain Ω_{int} is the part of the plane Ω_{total} bounded by the contours Σ_x together with the virtual boundaries Γ_1 and Γ_2 (input and output ports in the cross-sections $z = -L_1$ and $z = L_2$ of the virtual waveguides Ω_1 and Ω_2) and cylindrical or rectangular boundary Γ separating the domain Ω_{int} and the free space domain Ω_{ext} .

EACs $D_1[U - U^{i(1)}]$, $D_2[U]$ and $D[U]$ for the virtual boundaries are detailed below. They provide an ideal model for the outgoing waves

$$\begin{aligned}
 U^{s(1)}(g, t) &= U(g, t) - U^{i(1)}(g, t) \quad \text{in } \Omega_1, \\
 U^{s(2)}(g, t) &= U(g, t) \quad \text{in } \Omega_2, \\
 \text{and } U(g, t) &\quad \text{in } \Omega_{\text{ext}}.
 \end{aligned}
 \tag{5.138}$$

Namely, the outgoing waves cross the virtual boundaries without disturbance or reflection, as if they are absorbed by the virtual waveguides Ω_1, Ω_2 and by the part of free space Ω_{ext} . The function $U^{i(1)}(g, t)$ defines the wave incident on the virtual boundary Γ_1 from the waveguide Ω_1 . This function and the source functions $F(g, t)$, $\varphi(g)$, and $\psi(g)$ are assumed to be given. It is assumed also that by the moment of time $t = 0$ the wave $U^{i(1)}(g, t)$ has not yet reached the boundary Γ_1 .

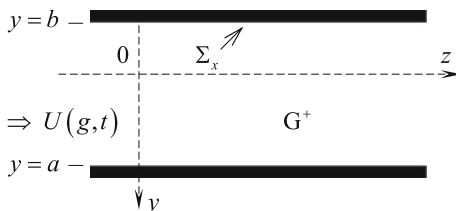
5.5.2 Exact Absorbing Conditions for Parallel-Plate Waveguides

Let us consider the following model problem (Fig. 5.7). A pulsed wave $U(g, t)$ propagating in a metal parallel-plate waveguide

$$G = \{g = \{y, z\} : b < y < a, \quad |z| < \infty\}$$

towards growing z is arriving on some imaginary boundary $z = 0$ at time moments $t > 0$. It is required to determine the field $U(g, t)$ in the closure of the domain $G^+ = \{g \in G : z > 0\}$ for $t > 0$. The corresponding equation has the following form:

Fig. 5.7 Virtual boundary $z = 0$ in the regular parallel-plate waveguide G



$$\begin{cases} \left[-\frac{\partial^2}{\partial t^2} + \frac{\partial}{\partial y^2} + \frac{\partial^2}{\partial z^2} \right] U(g, t) = 0; & t > 0, \quad g = \{y, z\} \in G^+ \\ U(g, t)|_{t=0} = 0, \quad \frac{\partial}{\partial t} U(g, t)|_{t=0} = 0; & g \in \bar{G}^+ \\ \vec{E}_{tg}(p, t)|_{p=\{x,y,z\} \in \Sigma} = 0; & t \geq 0. \end{cases} \tag{5.139}$$

The separation of variables in (5.139) yields the following representation for the solution $U(g, t)$:

$$U(g, t) = \sum_n u_n(z, t) \mu_n(y); \quad g \in \bar{G}^+ \quad t \geq 0. \tag{5.140}$$

The orthonormal system of transverse functions $\mu_n(y)$, which is complete in the space $L_2(b, a)$, is determined by a nontrivial solution to the homogeneous (spectral) problem

$$\begin{cases} \left[\frac{d^2}{dy^2} + \lambda_n^2 \right] \mu_n(y) = 0; & 0 < y < a \\ \mu_n(b) = \mu_n(a) = 0 \quad (E\text{-polarization}) \quad \text{or} \\ d\mu_n(y)/dy|_{y=b} = d\mu_n(y)/dy|_{y=a} = 0 \quad (H\text{-polarization}), \end{cases} \tag{5.141}$$

while the space-time amplitudes $u_n(z, t)$ of the wave $U(g, t)$ are determined by a solution to the initial boundary value problem

$$\begin{cases} \left[-\frac{\partial^2}{\partial t^2} + \frac{\partial^2}{\partial z^2} - \lambda_n^2 \right] u_n(z, t) = 0; & z > 0, \quad t > 0 \\ u_n(z, 0) = 0, \quad \frac{\partial}{\partial t} u_n(z, t)|_{t=0} = 0; & z \geq 0. \end{cases} \tag{5.142}$$

It is easy to show that in the case of E -polarized waves, $n = 1, 2, 3, \dots$, $\mu_n(y) = \sqrt{2/(a - b)} \sin[n\pi(y - b)/(a - b)]$, and $\lambda_n = n\pi/(a - b)$; and in the case of H -polarized waves, $n = 0, 1, 2, \dots$, $\mu_n(y) = \sqrt{(2 - \delta_0^n)/(a - b)} \times \cos[n\pi(y - b)/(a - b)]$ (δ_m^n is the Kronecker symbol), and $\lambda_n = n\pi/(a - b)$.

The problem (5.142) is studied in details in Sect. 5.2. It is evident that the relevant results may be easily adapted to the situation considered here. Therefore, omitting the intermediate constructions we immediately formulate the main conclusions.

- RCs for the amplitudes $u_n(z, t)$ and for the waves $U(g, t)$ have the form

$$u_n(z, t) = - \int_0^{t-z} J_0 \left[\lambda_n \left((t - \tau)^2 - z^2 \right)^{1/2} \right] u_n'(0, \tau) d\tau; \quad z \geq 0, \quad t \geq 0 \tag{5.143}$$

and

$$\begin{aligned}
 U(g, t) = & - \sum_n \left\{ \int_0^{t-z} J_0 \left[\lambda_n \left((t-\tau)^2 - z^2 \right)^{1/2} \right] \right. \\
 & \times \left. \left[\int_b^a \frac{\partial U(y, z, \tau)}{\partial z} \Big|_{z=0} \mu_n(y) dy \right] d\tau \right\} \mu_n(y); \tag{5.144} \\
 g = & \{y, z\} \in G^+, \quad t \geq z.
 \end{aligned}$$

Here and below, $n = 1, 2, 3, \dots$ in the case of E -polarized waves and $n = 0, 1, 2, \dots$ in the case of H -polarized waves.

- Nonlocal EACs for the amplitudes $u_n(z, t)$ and for the waves $U(g, t)$ may have one of the following forms:

$$u_n(0, t) = - \int_0^t J_0[\lambda_n(t-\tau)] u_n'(0, \tau) d\tau; \quad t \geq 0, \tag{5.145}$$

$$\left[\frac{\partial}{\partial t} + \frac{\partial}{\partial z} \right] u_n(z, t) \Big|_{z=0} = \lambda_n \int_0^t J_1[\lambda_n(t-\tau)] u_n'(0, \tau) d\tau; \quad t \geq 0, \tag{5.146}$$

$$\begin{aligned}
 \left[\frac{\partial}{\partial t} + \frac{\partial}{\partial z} \right] u_n(z, t) \Big|_{z=0} &= -\lambda_n \int_0^t J_1[\lambda_n(t-\tau)] (t-\tau)^{-1} u_n(0, \tau) d\tau; \tag{5.147} \\
 t &\geq 0
 \end{aligned}$$

and

$$\begin{aligned}
 U(y, 0, t) = & - \sum_n \left\{ \int_0^t J_0[\lambda_n(t-\tau)] \left[\int_b^a \frac{\partial U(y, z, \tau)}{\partial z} \Big|_{z=0} \mu_n(y) dy \right] d\tau \right\} \\
 & \times \mu_n(y); \quad b \leq y \leq a, \quad t \geq 0, \tag{5.148}
 \end{aligned}$$

$$\begin{aligned}
 \left[\frac{\partial}{\partial t} + \frac{\partial}{\partial z} \right] U(y, z, t) \Big|_{z=0} &= \sum_n \lambda_n \left\{ \int_0^t J_1[\lambda_n(t-\tau)] \right. \\
 & \times \left. \left[\int_b^a \frac{\partial U(y, z, \tau)}{\partial z} \Big|_{z=0} \mu_n(y) dy \right] d\tau \right\} \mu_n(y); \quad b \leq y \leq a, \quad t \geq 0, \tag{5.149}
 \end{aligned}$$

$$\left[\frac{\partial}{\partial t} + \frac{\partial}{\partial z} \right] U(y, z, t) \Big|_{z=0} = - \sum_n \lambda_n \left\{ \int_0^t J_1[\lambda_n(t - \tau)] \right. \\ \left. \times (t - \tau)^{-1} \left[\int_b^a U(y, 0, \tau) \mu_n(y) dy \right] d\tau \right\} \mu_n(y); \quad b \leq y \leq a, \quad t \geq 0. \quad (5.150)$$

- Local EACs for the waves $U(g, t)$ may have one of the following forms:

$$U(y, 0, t) = \frac{2}{\pi} \int_0^{\pi/2} \frac{\partial W(y, t, \varphi)}{\partial t} d\varphi; \quad t \geq 0, \quad b \leq y \leq a, \quad (5.151a)$$

$$\begin{cases} \left[\frac{\partial^2}{\partial t^2} - \sin^2 \varphi \frac{\partial^2}{\partial y^2} \right] W(y, t, \varphi) = - \frac{\partial U(y, z, t)}{\partial z} \Big|_{z=0}; \\ \quad b < y < a, \quad t > 0 \\ W(y, 0, \varphi) = \frac{\partial W(y, t, \varphi)}{\partial t} \Big|_{t=0} = 0, \quad b \leq y \leq a, \end{cases} \quad (5.151b)$$

$$\left[\frac{\partial}{\partial t} + \frac{\partial}{\partial z} \right] U(y, z, t) \Big|_{z=0} = \frac{2}{\pi} \int_0^{\pi/2} W(y, t, \varphi) \cos^2 \varphi d\varphi; \quad (5.152a) \\ t \geq 0, \quad b \leq y \leq a,$$

$$\begin{cases} \left[\frac{\partial^2}{\partial t^2} - \cos^2 \varphi \frac{\partial^2}{\partial y^2} \right] W(y, t, \varphi) = - \frac{\partial^2}{\partial y^2} \left[\frac{\partial}{\partial z} U(y, z, t) \Big|_{z=0} \right]; \\ \quad b < y < a, \quad t > 0 \\ W(y, 0, \varphi) = \frac{\partial W(y, t, \varphi)}{\partial t} \Big|_{t=0} = 0; \quad b \leq y \leq a \end{cases} \quad (5.152b)$$

or

$$\left[\frac{\partial}{\partial t} + \frac{\partial}{\partial z} \right] U(y, z, t) \Big|_{z=0} = \frac{2}{\pi} \int_0^{\pi/2} \frac{\partial W(y, t, \varphi)}{\partial t} \sin^2 \varphi d\varphi; \quad (5.153a) \\ t \geq 0, \quad b \leq y \leq a,$$

$$\left\{ \begin{array}{l} \left[\frac{\partial^2}{\partial t^2} - \cos^2 \varphi \frac{\partial^2}{\partial y^2} \right] W(y, t, \varphi) = \frac{\partial^2}{\partial y^2} U(y, 0, t); \\ \qquad \qquad \qquad b < y < a, \quad t > 0 \\ W(y, 0, \varphi) = \frac{\partial W(y, t, \varphi)}{\partial t} \Big|_{t=0} = 0; \quad b \leq y \leq a. \end{array} \right. \tag{5.153b}$$

The initial boundary value problems (5.151b), (5.152b), and (5.153b) are formulated with respect to the auxiliary functions $W(y, t, \varphi)$, and should be supplemented with the following boundary conditions for $t \geq 0$:

$$\left\{ \begin{array}{l} W(b, t, \varphi) = W(a, t, \varphi) = 0; \quad E\text{-polarization} \\ \frac{\partial W(y, t, \varphi)}{\partial y} \Big|_{y=b} = \frac{\partial W(y, t, \varphi)}{\partial y} \Big|_{y=a} = 0; \quad H\text{-polarization.} \end{array} \right.$$

Let us consider EACs (5.148) and (5.151a), (5.151b) in more details. Taking into consideration the location of the boundaries Γ_j in the problem (5.137) (in the plane $z = -L_1$ for the boundary Γ_1 and in the plane $z = L_2$ for Γ_2), and the direction of propagation for the waves outgoing through these boundaries (towards $z = -\infty$ for Γ_1 and towards $z = \infty$ for Γ_2), we can rewrite (5.148) and (5.151a), (5.151b) to explicitly show the operators $D_1[U - U^{i(1)}]$ and $D_2[U]$:

$$\begin{aligned} U(y, -L_1, t) - U^{i(1)}(y, -L_1, t) &= \sum_{n=1}^{\infty} \left\{ \int_0^t J_0[\lambda_{n1}(t - \tau)] \right. \\ &\quad \times \left. \left[\int_{b_1}^{a_1} \frac{\partial [U(y, z, \tau) - U^{i(1)}(y, z, \tau)]}{\partial z} \Big|_{z=-L_1} \mu_{n1}(y) dy \right] d\tau \right\} \\ &\times \mu_{n1}(y); \quad b_1 \leq y \leq a_1, \quad t \geq 0, \end{aligned} \tag{5.154}$$

$$\begin{aligned} U(y, L_2, t) &= - \sum_{n=1}^{\infty} \left\{ \int_0^t J_0[\lambda_{n2}(t - \tau)] \left[\int_{b_2}^{a_2} \frac{\partial U(y, z, \tau)}{\partial z} \Big|_{z=L_2} \mu_{n2}(y) dy \right] d\tau \right\} \\ &\times \mu_{n2}(y); \quad b_2 \leq y \leq a_2, \quad t \geq 0 \end{aligned} \tag{5.155}$$

(nonlocal EACs); and

$$U(y, -L_1, t) - U^{i(1)}(y, -L_1, t) = \frac{2}{\pi} \int_0^{\pi/2} \frac{\partial W(y, t, \varphi)}{\partial t} d\varphi; \quad t \geq 0, \tag{5.156a}$$

$$b_1 \leq y \leq a_1,$$

$$\begin{cases} \left[\frac{\partial^2}{\partial t^2} - \sin^2 \varphi \frac{\partial^2}{\partial y^2} \right] W(y, t, \varphi) = \frac{\partial [U(y, z, t) - U^{i(1)}(y, z, t)]}{\partial z} \Big|_{z=-L_1}; \\ b_1 < y < a_1, \quad t > 0 \\ W(y, 0, \varphi) = \frac{\partial W(y, t, \varphi)}{\partial t} \Big|_{t=0} = 0, \quad b_1 \leq y \leq a_1, \end{cases} \tag{5.156b}$$

$$U(y, L_2, t) = \frac{2}{\pi} \int_0^{\pi/2} \frac{\partial W(y, t, \varphi)}{\partial t} d\varphi; \quad t \geq 0, \quad b_2 \leq y \leq a_2, \tag{5.157a}$$

$$\begin{cases} \left[\frac{\partial^2}{\partial t^2} - \sin^2 \varphi \frac{\partial^2}{\partial y^2} \right] W(y, t, \varphi) = -\frac{\partial U(y, z, t)}{\partial z} \Big|_{z=L_2}; \\ b_2 < y < a_2, \quad t > 0 \\ W(y, 0, \varphi) = \frac{\partial W(y, t, \varphi)}{\partial t} \Big|_{t=0} = 0, \quad b_2 \leq y \leq a_2 \end{cases} \tag{5.157b}$$

(local EACs). Here, λ_{nj} and $\mu_{nj}(y)$ ($j = 1, 2$) are transverse eigenvalues and transverse eigenfunctions for the waveguide Ω_j . The wave $U^{i(1)}(g, t)$ incident on the boundary Γ_1 from the waveguide Ω_1 could be represented in the form

$$U^{i(1)}(g, t) = \sum_{n=1}^{\infty} v_{n1}(z, t) \mu_{n1}(y); \quad g = \{y, z\} \in \bar{\Omega}_1. \tag{5.158}$$

$$n = \begin{cases} 1 & \text{for } E\text{-case} \\ 0 & \text{for } H\text{-case} \end{cases}$$

The initial boundary value problems in (5.156a), (5.156b) and (5.157a), (5.157b) with respect to the auxiliary functions $W(y, t, \varphi)$ should be supplemented with the boundary conditions

$$\begin{cases} W(b_{1 \text{ or } 2}, t, \varphi) = W(a_{1 \text{ or } 2}, t, \varphi) = 0; \quad E\text{-polarization} \\ \frac{\partial W(y, t, \varphi)}{\partial y} \Big|_{y=b_{1 \text{ or } 2}} = \frac{\partial W(y, t, \varphi)}{\partial y} \Big|_{y=a_{1 \text{ or } 2}} = 0; \quad H\text{-polarization.} \end{cases}$$

5.5.3 Exact Absorbing Conditions for Cylindrical Virtual Boundary in Free Space

Let now all field sources and scatterers are located inside a circle of radius L with its center in the point $g = \{y, z\} = \{0, 0\}$ (see Fig. 5.6). Then within $\Omega_{\text{ext}} = \{g = \{\rho, \phi\} \in \Omega_{\text{total}} : \rho > L\}$ the E - or H -polarized wave $U(g, t)$ generated in Ω_{int} is the outgoing wave crossing the boundary $\Gamma = \{g = \{\rho, \phi\} \in \Omega_{\text{total}} : \rho = L\}$ only in one direction $\rho \rightarrow \infty$, and [3]

$$\begin{cases} \left[-\frac{\partial^2}{\partial t^2} + \frac{1}{\rho} \frac{\partial}{\partial \rho} \rho \frac{\partial}{\partial \rho} + \frac{1}{\rho^2} \frac{\partial^2}{\partial \phi^2} \right] U(g, t) = 0; \\ g = \{\rho, \phi\} \in \Omega_{\text{ext}}, \quad t > 0 \\ U(g, t)|_{t=0} = 0, \quad \frac{\partial}{\partial t} U(g, t)|_{t=0} = 0; \quad g \in \bar{\Omega}_{\text{ext}} \\ U(\rho, \phi, t) = U(\rho, \phi + 2\pi, t); \quad \rho \geq L, \quad t \geq 0. \end{cases} \quad (5.159)$$

The separation of variables with respect to ϕ in (5.159) yields

$$U(\rho, \phi, t) = \sum_n u_n(\rho, t) \mu_n(\phi); \quad g = \{\rho, \phi\} \in \bar{\Omega}_{\text{ext}}, \quad t \geq 0, \quad (5.160)$$

where $\mu_n(\phi) = (2\pi)^{-1/2} \exp(in\phi)$, $n = 0, \pm 1, \pm 2, \dots$ is the orthonormal system of transverse functions, which is complete in the space $L_2(0 < \phi < 2\pi)$. The space-time amplitudes $u_n(\rho, t)$ of the wave $U(\rho, \phi, t)$ are determined by a solution to the initial boundary value problem

$$\begin{cases} \left[-\frac{\partial^2}{\partial t^2} + \frac{1}{\rho} \frac{\partial}{\partial \rho} \rho \frac{\partial}{\partial \rho} - \frac{n^2}{\rho^2} \right] u_n(\rho, t) = 0; \quad \rho > L, \quad t > 0 \\ u_n(\rho, 0) = 0, \quad \frac{\partial}{\partial t} u_n(\rho, t) \Big|_{t=0} = 0; \quad \rho \geq L. \end{cases} \quad (5.161)$$

Let us multiply (5.161) by $\chi(\rho - L)$ and then apply the Hankel transform

$$\tilde{f}_n(\omega) = \int_0^\infty f_n(\rho) \rho J_{|n|}(\rho\omega) d\rho \leftrightarrow f_n(\rho) = \int_0^\infty \tilde{f}_n(\omega) \omega J_{|n|}(\rho\omega) d\omega. \quad (5.162)$$

Finally, for the images $\tilde{Z}_n(\omega, t)$ of the functions $Z_n(\rho, t) = u_n(\rho, t)\chi(\rho - L)$ we have

$$\begin{cases} D(\omega) [\tilde{Z}_n(\omega, t)] \equiv \left(\frac{\partial^2}{\partial t^2} + \omega^2 \right) \tilde{Z}_n(\omega, t) = \\ = L [u_n(L, t) J_{|n|}'(\omega L) - u_n'(L, t) J_{|n|}(\omega L)]; \quad \omega > 0, \quad t > 0 \\ \tilde{Z}_n(\omega, 0) = \frac{\partial}{\partial t} \tilde{Z}_n(\omega, t) \Big|_{t=0} = 0; \quad \omega \geq 0. \end{cases} \quad (5.163)$$

Here, $u_n'(L, t) = \partial u_n(\rho, t) / \partial \rho|_{\rho=L}$ and $J_{|n|}'(\omega L) = \partial J_{|n|}(\omega \rho) / \partial \rho|_{\rho=L}$. The derivation of (5.163) uses the formula [34] $-\omega^2 \tilde{f}_n(\omega) \leftrightarrow \left[\frac{d^2}{d\rho^2} + \frac{d}{\rho d\rho} - \frac{n^2}{\rho^2} \right] f_n(\rho)$, the chain of equalities

$$\begin{aligned} \chi(\rho - L) \left[\frac{1}{\rho} \frac{\partial}{\partial \rho} \rho \frac{\partial}{\partial \rho} \right] u_n(\rho, t) &= \chi(\rho - L) \left[\frac{1}{\rho} \frac{\partial}{\partial \rho} + \frac{\partial^2}{\partial \rho^2} \right] u_n(\rho, t) \\ &= \left[\frac{1}{\rho} \frac{\partial}{\partial \rho} + \frac{\partial^2}{\partial \rho^2} \right] Z_n(\rho, t) - \delta(\rho - L) \left[\frac{1}{\rho} + \frac{\partial}{\partial \rho} \right] u_n(\rho, t) \\ &\quad - \frac{\partial}{\partial \rho} [\delta(\rho - L) u_n(\rho, t)], \end{aligned}$$

and the equality $(\partial^{\alpha} f, \gamma) = (-1)^{|\alpha|} (f, \partial^{\alpha} \gamma)$ defining the generalized derivative $\partial^{\alpha} f$ ($\alpha = \{\alpha_i\}_{i=1}^n$ is the multiindex, $|\alpha| = \alpha_1 + \dots + \alpha_n$) of the generalized function $f(q)$, $q \in \mathbb{R}^n$ [35].

The problem (5.163) is similar to (5.15) studied in Sect. 5.2.2. Its solution

$$\tilde{Z}_n(\omega, t) = \frac{L}{\omega} \int_0^t \sin[\omega(t - \tau)] [u_n(L, \tau) J_{|n|}'(\omega L) - u_n'(L, \tau) J_{|n|}(\omega L)] d\tau$$

after the inverse Hankel transform (5.162) becomes

$$\begin{aligned} u_n(\rho, t) &= L \int_0^t [u_n(L, \tau) f_n'(L, \rho, t - \tau) - u_n'(L, \tau) f_n(L, \rho, t - \tau)] d\tau; \\ \rho &\geq L, \quad t \geq 0. \end{aligned} \tag{5.164}$$

The formula (5.164) describes the behavior of the amplitudes $u_n(\rho, t)$ of the outgoing cylindrical wave (5.160) propagating from the circle $\rho = L$ to any other circle with the radius $\rho > L$. Here,

$$f_n(r, \rho, t - \tau) = \int_0^{\infty} \sin[\omega(t - \tau)] J_{|n|}(\omega r) J_{|n|}(\omega \rho) d\omega \tag{5.165}$$

and $f_n'(L, \rho, t - \tau) = \partial f_n(r, \rho, t - \tau) / \partial r|_{r=L}$.

The integration in (5.165) is converted to the calculation of the first and the second kind Legendre functions $P_{|n|-1/2}(a)$ and $Q_{|n|-1/2}(-a)$ for the argument $a_{r,\rho} = [r^2 + \rho^2 - (t - \tau)^2] / (2\rho r)$ [44]:

$$\begin{aligned}
 f_n(r, \rho, t - \tau) &= \begin{cases} 0; & 0 < t - \tau < \rho - r \\ P_{|n|-1/2}(a_{r,\rho}) [2(r\rho)^{1/2}]; & \rho - r < t - \tau < \rho + r \\ -Q_{|n|-1/2}(-a_{r,\rho}) \cos(n\pi) / [\pi(r\rho)^{1/2}]; & \rho + r < t - \tau \end{cases} \\
 &= \chi[(t - \tau) - (\rho - r)] Q_{|n|-1/2}(-a_{r,\rho}) \cos(n\pi) / [\pi(r\rho)^{1/2}]; \quad 0 < t - \tau.
 \end{aligned}
 \tag{5.166}$$

At the last step in (5.166), we have used the well-known properties of the Legendre functions [40]: $\pi P_\nu(x) = \pi \cos(\nu\pi) P_\nu(-x) - 2 \sin(\nu\pi) Q_\nu(-x)$.

Considering [35, 40] that the value of $Q_{|n|-1/2}(-a_{r,\rho})$ at $t - \tau = \rho - r$ is

$$Q_{|n|-1/2}(-1) = \pi P_{|n|-1/2}(1) / 2 \cos(n\pi) = \pi / 2 \cos(n\pi),$$

while $\partial\chi[(t - \tau) - (\rho - r)] / \partial r = \delta[(t - \tau) - (\rho - r)]$, upon differentiation in (5.164) and summation of the results in accordance with (5.160), we obtain for $\rho \geq L$ and $t \geq 0$:

$$\begin{aligned}
 U(\rho, \phi, t) &= \frac{1}{2} \sqrt{\frac{L}{\rho}} U(L, \phi, t - \rho + L) + \frac{1}{\pi} \sqrt{\frac{L}{\rho}} \sum_n (-1)^n \mu_n(\phi) \\
 &\quad \times \int_0^{t-(\rho-L)} \left\{ \frac{u_n(L, \tau)}{2L} \left[Q_{|n|-1/2}'(-a_{L,\rho}) \left(\frac{\rho^2 - L^2 - (t - \tau)^2}{L\rho} \right) - Q_{|n|-1/2}(-a_{L,\rho}) \right] \right. \\
 &\quad \left. - u_n'(L, \tau) Q_{|n|-1/2}(-a_{L,\rho}) \right\} d\tau.
 \end{aligned}
 \tag{5.167}$$

Placing the observation point onto the virtual boundary $\rho = L$ in (5.167), we obtain EAC $D[U(g, t)]|_{g \in \Gamma} = 0$ for the problem (5.137):

$$\begin{aligned}
 U(L, \phi, t) &= \frac{2}{\pi} \sum_n (-1)^n \mu_n(\phi) \left[\int_0^t [u_n(L, \tau) \xi_n(t - \tau) - u_n'(L, \tau) \eta_n(t - \tau)] d\tau \right]; \\
 0 \leq \phi \leq 2\pi, \quad t \geq 0.
 \end{aligned}
 \tag{5.168}$$

In (5.167) and (5.168) the following notations were used: $\{Q_{|n|-1/2}'(-a) = \partial Q_{|n|-1/2}(x) / \partial x|_{x=-a}, \xi_n(t - \tau) = [2Q_{|n|-1/2}'(-a_{L,L})(a_{L,L} - 1) - Q_{|n|-1/2}(-a_{L,L})] (2L)^{-1}$, and $\eta_n(t - \tau) = Q_{|n|-1/2}(-a_{L,L})$.

5.5.4 Exact Absorbing Conditions for Rectangular Virtual Boundary in Free Space

Up to now we constructed EACs only for virtual boundaries which coincide with coordinate surfaces. In this section we demonstrate a different approach: we develop an EAC for a rectangular virtual boundary which detached components are orthogonal and have so-called corner points at intersections. In these points, EACs for different components of the virtual boundary must be matched neatly. This gives rise to a mathematically complicated [52, 53] auxiliary problem. Below we discuss one possible way to solve it rigorously, and obtain one more EAC for the problem (5.137).

Let now the virtual boundary Γ separating the domains Ω_{int} and Ω_{ext} in (5.137) is a rectangular boundary (Fig. 5.6). Then within $\Omega_{\text{ext}} = \Omega_{\text{total}} \setminus \{g = \{y, z\} \in \Omega_{\text{total}} : l_4 \leq y \leq l_3, l_2 \leq z \leq l_1\}$ the E - or H -polarized wave $U(g, t)$ generated in Ω_{int} is the outgoing wave crossing the boundary Γ only in one direction, and

$$\begin{cases} \left[-\frac{\partial^2}{\partial t^2} + \frac{\partial}{\partial y^2} + \frac{\partial^2}{\partial z^2} \right] U(g, t) = 0; & t > 0, \quad g = \{y, z\} \in \Omega_{\text{ext}} \\ U(g, t)|_{t=0} = 0, \quad \frac{\partial}{\partial t} U(g, t)|_{t=0} = 0; & g \in \bar{\Omega}_{\text{ext}}. \end{cases} \quad (5.169)$$

Subject the function $U(g, t)$ from (5.169) to the Fourier transforms

$$\begin{aligned} u_y(\lambda, z, t) &= \frac{1}{2\pi} \int_{-\infty}^{\infty} U(y, z, t) e^{i\lambda y} dy \leftrightarrow U(y, z, t) = \int_{-\infty}^{\infty} u_y(\lambda, z, t) e^{-i\lambda y} d\lambda, \\ u_z(y, \mu, t) &= \frac{1}{2\pi} \int_{-\infty}^{\infty} U(y, z, t) e^{i\mu z} dz \leftrightarrow U(y, z, t) = \int_{-\infty}^{\infty} u_z(y, \mu, t) e^{-i\mu z} d\mu \end{aligned} \quad (5.170)$$

and employ the technique from Sects. 5.2.2 and 5.2.3, which is applied there to the problem (5.9) for 1-D Klein-Gordon equations. Then

$$\left[\frac{\partial}{\partial t} \pm \frac{\partial}{\partial z} \right] u_y(\lambda, z, t) = -\lambda \int_0^t \frac{J_1(\lambda(t-\tau))}{t-\tau} u_y(\lambda, z, \tau) d\tau; \quad \begin{cases} z \geq l_1 \\ z \leq l_2 \end{cases}, \quad (5.171)$$

$$\left[\frac{\partial}{\partial t} \pm \frac{\partial}{\partial y} \right] u_z(y, \mu, t) = -\mu \int_0^t \frac{J_1(\mu(t-\tau))}{t-\tau} u_z(y, \mu, \tau) d\tau; \quad \begin{cases} y \geq l_3 \\ y \leq l_4 \end{cases}. \quad (5.172)$$

Nonlocal EACs (5.171) and (5.172), written in terms of the Fourier amplitudes of the field $U(g, t)$, truncate the computation domain of open plane problems to the

band $l_2 < z < l_1$ or $l_4 < y < l_3$. We will seek now conditions that are local in time and space. Following the scheme from Sect. 5.2.4, we obtain from (5.171), (5.172) and (5.170)

$$\left[\frac{\partial}{\partial t} \pm \frac{\partial}{\partial z} \right] U(g, t) = \frac{2}{\pi} \int_0^{\pi/2} \frac{\partial V_1(g, t, \varphi)}{\partial t} \sin^2 \varphi d\varphi; \quad (5.173a)$$

$$|y| \leq \infty, \quad \begin{cases} z \geq l_1, \\ z \leq l_2, \end{cases} \quad t \geq 0,$$

$$\left\{ \begin{array}{l} \left[\frac{\partial^2}{\partial t^2} - \cos^2 \varphi \frac{\partial^2}{\partial y^2} \right] V_1(g, t, \varphi) = \frac{\partial^2}{\partial y^2} U(g, t); \quad |y| < \infty, \quad t > 0 \\ \left. \frac{\partial V_1(g, t, \varphi)}{\partial t} \right|_{t=0} = V_1(g, t, \varphi)|_{t=0} = 0; \quad |y| \leq \infty \end{array} \right. \quad (5.173b)$$

and

$$\left[\frac{\partial}{\partial t} \pm \frac{\partial}{\partial y} \right] U(g, t) = \frac{2}{\pi} \int_0^{\pi/2} \frac{\partial V_2(g, t, \varphi)}{\partial t} \sin^2 \varphi d\varphi; \quad (5.174a)$$

$$\begin{cases} y \geq l_3, \\ y \leq l_4, \end{cases} \quad |z| \leq \infty, \quad t \geq 0,$$

$$\left\{ \begin{array}{l} \left[\frac{\partial^2}{\partial t^2} - \cos^2 \varphi \frac{\partial^2}{\partial z^2} \right] V_2(g, t, \varphi) = \frac{\partial^2}{\partial z^2} U(g, t); \quad |z| < \infty, \quad t > 0 \\ \left. \frac{\partial V_2(g, t, \varphi)}{\partial t} \right|_{t=0} = V_2(g, t, \varphi)|_{t=0} = 0; \quad |z| \leq \infty. \end{array} \right. \quad (5.174b)$$

Each of the four expressions (5.173a), (5.173b) and (5.174a), (5.174b) is *local EAC* which truncates the computation domain to the half-plane $z < l_1$, $z > l_2$, $y < l_3$ or $y > l_4$. The auxiliary differential (Cauchy) problems for the functions $V_1(g, t, \varphi)$ (z is some parameter) and $V_2(g, t, \varphi)$ (y is some parameter) are well posed.

When the domain truncated in this way is rectangular, all four equations of (5.173a), (5.173b) and (5.174a), (5.174b) must be taken into account. At the same time, the auxiliary differential problems must be completed with conditions at the ends where the boundaries $z = \text{const}$ and $y = \text{const}$ meet. There are several analytic ways to treat the problem of corner points. One of them, supposedly the clearest, is detailed below.

Initially, consider the first equations (with the plus signs) from (5.173a), (5.173b) and (5.174a), (5.174b). In Fig. 5.6, the domain Ω_{ext} quadrant, where these equations are valid simultaneously, is dotted. In this quadrant, consider the region $G = \{g = \{y, z\} : l_3 < y < l_3 + 2\pi; l_1 < z < l_1 + 2\pi\}$ and use here the following representation for the functions $f(g, t)$:

$$\begin{aligned}
 f(g, t) &= \frac{1}{2\pi i} \int_{\alpha-i\infty}^{\alpha+i\infty} \sum_{n,m=-\infty}^{\infty} \tilde{f}(n, m, s) e^{i(ny+mz)+st} ds; \quad \operatorname{Re} s \geq \beta \geq 0 \\
 &\leftrightarrow \tilde{f}(n, m, s) = \frac{1}{4\pi^2} \int_0^{\infty} \int_{l_1}^{l_1+2\pi} \int_{l_3}^{l_3+2\pi} f(g, t) e^{-i(ny+mz)-st} dy dz dt.
 \end{aligned} \tag{5.175}$$

For the amplitudes $\tilde{u} = \tilde{u}(n, m, s)$, $\tilde{v}_j(\varphi) = \tilde{v}_j(n, m, s, \varphi)$, and $\tilde{w}_j(\varphi) = \tilde{w}_j(n, m, s, \varphi)$, $j = 1, 2$, of the functions $U(g, t)$, $V_j(g, t, \varphi)$, and $W_j(g, t, \varphi) = V_j(g, t, \varphi) \cos^2 \varphi + U(g, t)$, we obtain:

$$(s + im)\tilde{u} = \frac{2s}{\pi} \int_0^{\pi/2} \sin^2 \varphi \tilde{v}_1 d\varphi, \quad (s + in)\tilde{u} = \frac{2s}{\pi} \int_0^{\pi/2} \sin^2 \varphi \tilde{v}_2 d\varphi, \tag{5.176}$$

$$\tilde{w}_1 = \frac{s^2}{s^2 + n^2 \cos^2 \varphi} \tilde{u}, \quad \tilde{w}_2 = \frac{s^2}{s^2 + m^2 \cos^2 \varphi} \tilde{u}, \tag{5.177}$$

$$\tilde{v}_1 = -\frac{n^2}{s^2 + n^2 \cos^2 \varphi} \tilde{u}, \quad \tilde{v}_2 = -\frac{m^2}{s^2 + m^2 \cos^2 \varphi} \tilde{u}, \tag{5.178}$$

$$s^2 + m^2 + n^2 = 0. \tag{5.179}$$

Now address the function

$$\begin{aligned}
 in\tilde{w}_1(\varphi) &= in\tilde{u} \frac{s^2}{s^2 + n^2 \cos^2 \varphi} \\
 &= \frac{s^2}{s^2 + n^2 \cos^2 \varphi} \left[-s\tilde{u} + \frac{2s}{\pi} \int_0^{\pi/2} \sin^2 \gamma \tilde{v}_2(\gamma) d\gamma \right] \\
 &= -s\tilde{u} \frac{s^2}{s^2 + n^2 \cos^2 \varphi} \left[1 + \frac{2 \sin^2 \varphi}{\pi} \int_0^{\pi/2} \frac{\sin^2 \gamma}{\cos^2 \varphi + \sin^2 \varphi \cos^2 \gamma} d\gamma \right] \\
 &\quad + \frac{2}{\pi} \int_0^{\pi/2} s\tilde{u} \frac{s^2}{s^2 + m^2 \cos^2 \gamma} \times \frac{\sin^2 \gamma}{\cos^2 \varphi + \sin^2 \varphi \cos^2 \gamma} d\gamma \\
 &= -\frac{s}{\cos \varphi} \tilde{w}_1(\varphi) + \frac{2}{\pi} \int_0^{\pi/2} s\tilde{w}_2(\gamma) \frac{\sin^2 \gamma}{\cos^2 \varphi + \sin^2 \varphi \cos^2 \gamma} d\gamma.
 \end{aligned} \tag{5.180}$$

Here, a successive usage of the equations (5.177), (5.176), (5.178) was made, the equality

$$\frac{s^2}{s^2 + an^2} \times \frac{s^2}{s^2 + bm^2} = \frac{a}{a + (1 - a)b} \times \frac{s^2}{s^2 + an^2} + \frac{b}{a + (1 - a)b} \times \frac{s^2}{s^2 + bm^2}$$

valid only if (5.179) and (5.177) holds.

The inverse transform of (5.180) yields

$$\left[\frac{\partial}{\partial t} + \cos \varphi \frac{\partial}{\partial y} \right] W_1(g, t, \varphi) = \frac{2c \cos \varphi}{\pi} \int_0^{\pi/2} \frac{\sin^2 \gamma}{\cos^2 \varphi + \sin^2 \varphi \cos^2 \gamma} \frac{\partial W_2(g, t, \gamma)}{\partial t} d\gamma;$$

$$z \geq l_1, \quad y \geq l_3.$$

The upper boundaries $z = l_1 + 2\pi$ and $y = l_3 + 2\pi$ of the region G, where the equation holds, are not mentioned, as the region G may be arbitrary in size.

Performing the operations described above for the function $im\tilde{w}_2(\varphi)$, which is the object of the present study, we obtain

$$\left[\frac{\partial}{\partial t} + \cos \varphi \frac{\partial}{\partial z} \right] W_2(g, t, \varphi) = \frac{2c \cos \varphi}{\pi} \int_0^{\pi/2} \frac{\sin^2 \gamma}{\cos^2 \varphi + \sin^2 \varphi \cos^2 \gamma} \frac{\partial W_1(g, t, \gamma)}{\partial t} d\gamma;$$

$$z \geq l_1, \quad y \geq l_3.$$

The expressions relating the auxiliary functions $W_1(g, t, \varphi)$ and $W_2(g, t, \varphi)$ in all four G-like regions resolve the problem of corner points. The auxiliary initial boundary value problems in (5.173a), (5.173b), (5.174a), (5.174b) equipped with the corresponding relation are well posed within the finite sections of the outer boundary Γ surrounding the rectangular domain Ω_{int} . The complete system of equations constituting EAC $D[U(g, t)]|_{g \in \Gamma} = 0$ for the problem (5.137) is

$$\left[\frac{\partial}{\partial t} \pm \frac{\partial}{\partial z} \right] U(g, t) = \frac{2}{\pi} \int_0^{\pi/2} \frac{\partial V_1(g, t, \varphi)}{\partial t} \sin^2 \varphi d\varphi;$$

$$l_4 \leq y \leq l_3, \quad \begin{cases} z = l_1, & t \geq 0, \\ z = l_2, & \end{cases} \tag{5.181a}$$

$$\left\{ \begin{aligned} \left[\frac{\partial^2 V_1(g, t, \varphi)}{\partial t^2} - \frac{\partial^2 W_1(g, t, \varphi)}{\partial y^2} \right] &= 0; & l_4 < y < l_3, \quad t > 0 \\ \left. \frac{\partial V_1(g, t, \varphi)}{\partial t} \right|_{t=0} &= V_1(g, t, \varphi)|_{t=0} = 0; & l_4 \leq y \leq l_3, \end{aligned} \right. \tag{5.181b}$$

$$\left[\frac{\partial}{\partial t} \pm \frac{\partial}{\partial y} \right] U(g, t) = \frac{2}{\pi} \int_0^{\pi/2} \frac{\partial V_2(g, t, \varphi)}{\partial t} \sin^2 \varphi d\varphi; \quad (5.182a)$$

$$\begin{cases} y = l_3, \\ y = l_4, \end{cases} \quad l_2 \leq z \leq l_1, \quad t \geq 0,$$

$$\begin{cases} \left[\frac{\partial^2 V_2(g, t, \varphi)}{\partial t^2} - \frac{\partial^2 W_2(g, t, \varphi)}{\partial z^2} \right] = 0; \quad l_2 < z < l_1, \quad t > 0 \\ \left. \frac{\partial V_2(g, t, \varphi)}{\partial t} \right|_{t=0} = V_2(g, t, \varphi)|_{t=0} = 0; \quad l_2 \leq z \leq l_1, \end{cases} \quad (5.182b)$$

$$\begin{cases} \left[\frac{\partial}{\partial t} \pm \cos \varphi \frac{\partial}{\partial y} \right] W_1(g, t, \varphi) = \frac{2 \cos \varphi}{\pi} \\ \times \int_0^{\pi/2} \frac{\sin^2 \gamma}{\cos^2 \varphi + \sin^2 \varphi \cos^2 \gamma} \frac{\partial W_2(g, t, \gamma)}{\partial t} d\gamma \\ \left[\frac{\partial}{\partial t} \pm \cos \varphi \frac{\partial}{\partial z} \right] W_2(g, t, \varphi) = \frac{2 \cos \varphi}{\pi} \\ \times \int_0^{\pi/2} \frac{\sin^2 \gamma}{\cos^2 \varphi + \sin^2 \varphi \cos^2 \gamma} \frac{\partial W_1(g, t, \gamma)}{\partial t} d\gamma \end{cases} ; \quad \begin{cases} + \\ + \end{cases} \rightarrow g = \{l_3, l_1\},$$

$$\begin{cases} + \\ - \end{cases} \rightarrow g = \{l_3, l_2\}, \quad \begin{cases} - \\ + \end{cases} \rightarrow g = \{l_4, l_1\}, \quad \begin{cases} - \\ - \end{cases} \rightarrow g = \{l_4, l_2\}. \quad (5.183)$$

Actually, the formulas (5.181a), (5.181b), (5.182a), (5.182b) and (5.183) should be considered together, as only together they can determine local EAC over the entire rectangular virtual boundary Γ . The equations (5.183) act here as boundary conditions in the auxiliary initial boundary value problems of (5.181a), (5.181b) and (5.182a), (5.182b). The symbols

$$\begin{cases} + \\ + \end{cases} \rightarrow g = \{l_3, l_1\}$$

choose the signs in the upper and lower equations for different corner points $g = \{y, z\}$.

5.5.5 Frequency-Domain Formalism and Main Characteristics of Open Plane Structures

The solution $U(g, t)$ to the problem (5.137), (5.167) (it is assumed that $\Gamma = \{g = \{\rho, \phi\} \in \Omega_{\text{total}} : \rho = L\}$) and the solution $\tilde{U}(g, k)$ to the problem

$$\left\{ \begin{array}{l} \left[\frac{\partial^2}{\partial y^2} + \frac{\partial^2}{\partial z^2} + \bar{\epsilon}(g)k^2 \right] \tilde{U}(g, k) = \bar{f}(g, k); \quad g = \{y, z\} \in \Omega_{\text{int}} \\ \tilde{E}_{tg}(p, k) \Big|_{p=\{x, y, z\} \in \Sigma} = 0 \quad \text{and} \quad \tilde{E}_{tg}(p, k), \quad \tilde{H}_{tg}(p, k) \\ \text{are continuous when crossing } \Sigma^{e, \sigma} \\ \text{and boundaries } \Gamma \times [|x| < \infty], \quad \Gamma_j \times [|x| < \infty], \end{array} \right. \quad (5.184a)$$

$$\tilde{U}(g, k) = \sum_{n=-\infty}^{\infty} \begin{cases} 1 & \text{for } E\text{-case} \\ 0 & \text{for } H\text{-case} \end{cases} \left[A_{n1}(k)e^{i\beta_{n1}(z+L_1)} + B_{n1}(k)e^{-i\beta_{n1}(z+L_1)} \right] \mu_{n1}(y); \quad g \in \bar{\Omega}_1, \quad (5.184b)$$

$$\tilde{U}(g, k) = \sum_{n=-\infty}^{\infty} B_{n2}(k)e^{i\beta_{n2}(z-L_2)} \mu_{n2}(y); \quad g \in \bar{\Omega}_2, \quad (5.184c)$$

$$n = \begin{cases} 1 & \text{for } E\text{-case} \\ 0 & \text{for } H\text{-case} \end{cases}$$

$$\tilde{U}(g, k) = \sum_{n=-\infty}^{\infty} C_n(k)H_n^{(1)}(k\rho)\mu_n(\phi); \quad g \in \bar{\Omega}_{\text{ext}} \quad (5.184d)$$

are related by the integral transform (5.102).

Here, $\tilde{U}(g, k) = \tilde{E}_x(g, k)$ for monochromatic E -polarized waves and $\tilde{U}(g, k) = \tilde{H}_x(g, k)$ for monochromatic H -polarized waves. The remaining designations like $\bar{f}(g, k)$, $\bar{\epsilon}(g)$, etc. and the electromagnetic characteristics $R_{np}^{11}(k)$, $T_{np}^{21}(k)$, etc. are the same as in Sects. 5.4.1 and 5.4.2. Below we highlight only differences in analysis as compared to that conducted above.

- From (5.160), (5.184d) we have in place of (5.105)

$$C_n(k)H_n^{(1)}(k\rho) \leftrightarrow u_n(\rho, t) \quad \text{or} \quad C_n(k)H_n^{(1)}(k\rho) = \tilde{u}_n(\rho, k). \quad (5.185)$$

- The element $dg = \rho d\rho dz$ in the integrals over the domain Ω_{int} in (5.110), (5.115), and (5.118) should be replaced by $dg = dydz$, while the element $\rho d\rho$ in (5.116) should be replaced by dy .

- The definition (5.112) of the *normalized directional pattern* changes to

$$D(\phi, k, M) = \frac{\left| \tilde{\vec{E}}_{tg}(M, \phi, k) \right|^2}{\max_{0 \leq \phi \leq 2\pi} \left| \tilde{\vec{E}}_{tg}(M, \phi, k) \right|^2}; \quad 0 \leq \phi \leq 360^\circ, \quad K_1 \leq k \leq K_2. \quad (5.186)$$

Here, $\tilde{\vec{E}}_{tg}(M, \phi, k)$ is the tangential (to the cylindrical surface $\{\rho = M \geq L, |x| \leq \infty\}$) component of the monochromatic electric field $\tilde{\vec{E}}(g, k)$.

- The definition (5.122) of the *normalized pulsed pattern* changes to

$$D_{\text{puls}}(\phi, t, M) = \frac{U(M, \phi, t)}{\max_{\phi, t} |U(M, \phi, t)|}; \quad 0 \leq \phi \leq 360^\circ, \quad M \geq L, \quad (5.187)$$

$$T_1 \leq t \leq T_2 \leq T + M - L.$$

5.6 3-D Vector Models

The 3-D vector problem

$$\left\{ \begin{array}{l} \left[\frac{\partial^2}{\partial x^2} + \frac{\partial^2}{\partial y^2} + \frac{\partial^2}{\partial z^2} - \text{grad div} - \varepsilon(g) \frac{\partial^2}{\partial t^2} - \sigma(g) \eta_0 \frac{\partial}{\partial t} \right] \vec{E}(g, t) \\ = \eta_0 \frac{\partial}{\partial t} \vec{j}(g, t) \equiv \vec{F}(g, t); \quad g = \{x, y, z\} \in \Omega_{\text{int}}, \quad t > 0 \\ \vec{E}(g, 0) = \vec{\varphi}(g), \quad \frac{\partial}{\partial t} \vec{E}(g, t) \Big|_{t=0} = \vec{\psi}(g); \quad g \in \bar{\Omega}_{\text{int}} \\ \left\{ \begin{array}{l} \vec{E}_{tg}(g, t), \quad \vec{H}_{tg}(g, t) \text{ are continuous when crossing } \Sigma^{\varepsilon, \sigma} \\ \vec{E}_{tg}(g, t) \Big|_{g \in \Sigma} = 0, \quad D[\vec{E}(g, t)] \Big|_{g \in \Gamma} = 0 \\ D_1[\vec{E}(g, t) - \vec{E}^{i(1)}(g, t)] \Big|_{g \in \Gamma_1} = 0, \quad D_2[\vec{E}(g, t)] \Big|_{g \in \Gamma_2} = 0 \end{array} \right. ; t \geq 0 \end{array} \right. \quad (5.188)$$

describes space-time transformations of the electromagnetic field $\vec{U}(g, t) = \{\vec{E}(g, t), \vec{H}(g, t)\}$ in compact open structures with input and output waveguides (Fig. 5.8). To solve it numerically, we must know how to construct EACs for virtual boundaries in cross-sections of different hollow waveguides ($D_1[\vec{E}(g, t) - \vec{E}^{i(1)}(g, t)] \Big|_{g \in \Gamma_1} = 0, D_2[\vec{E}(g, t)] \Big|_{g \in \Gamma_2} = 0$) and in free space ($D[\vec{E}(g, t)] \Big|_{g \in \Gamma} = 0$).

In (5.188), $\vec{E}(g, t) = \{E_x, E_y, E_z\}$ and $\vec{H}(g, t) = \{H_x, H_y, H_z\}$ are the vectors of electric and magnetic fields;

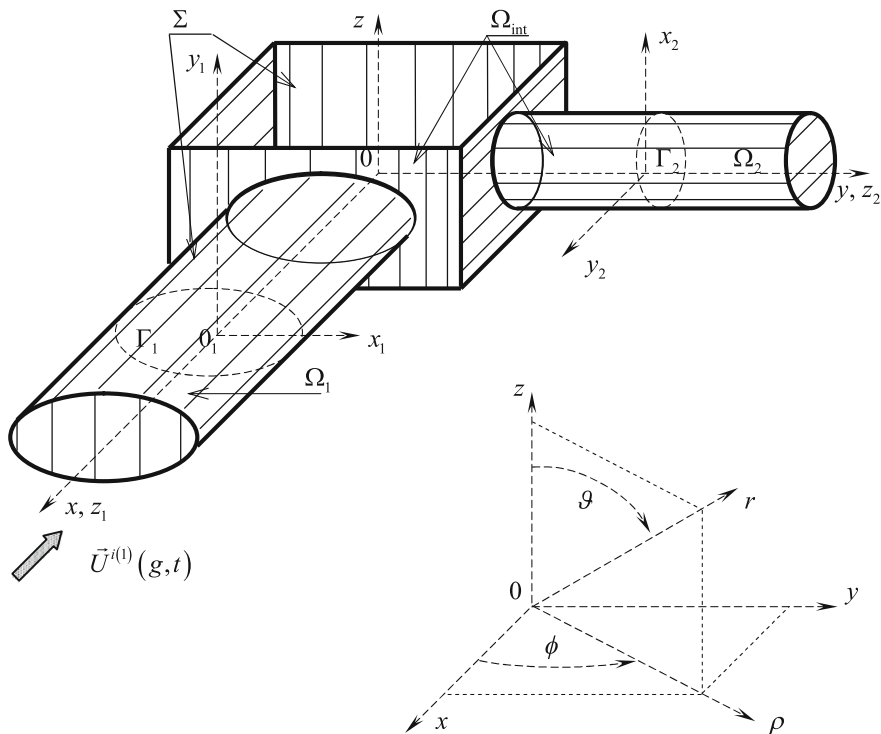


Fig. 5.8 Geometry of 3-D vector problem

$$-\eta_0 \frac{\partial}{\partial t} \vec{H}(g, t) = \text{rot} \vec{E}(g, t); \tag{5.189}$$

$\vec{j}(g, t)$ is the extraneous current density; $g = \{x, y, z\}$ is a point in the space \mathbb{R}^3 . The computation domain Ω_{int} is the part of the space \mathbb{R}^3 , bounded by the surfaces Σ together with the virtual boundaries Γ_1 and Γ_2 (input and output ports in the cross-sections of the virtual waveguides Ω_1 and Ω_2) and the spherical virtual boundary Γ separating the domains Ω_{int} and Ω_{ext} (free space). The surfaces Σ of perfectly conducting elements and the surfaces $\Sigma^{\varepsilon, \sigma}$ of discontinuities of material properties (of the piecewise smooth functions $\varepsilon(g)$ and $\sigma(g)$) are assumed to be sufficiently smooth. The function $\vec{E}^{i(1)}(g, t)$ in EAC in (5.188) represents a pulsed wave $\vec{U}^{i(1)}(g, t) = \{\vec{E}^{i(1)}(g, t), \vec{H}^{i(1)}(g, t)\}$, which is incident on the virtual boundary Γ_1 from the waveguide Ω_1 at $t > 0$.

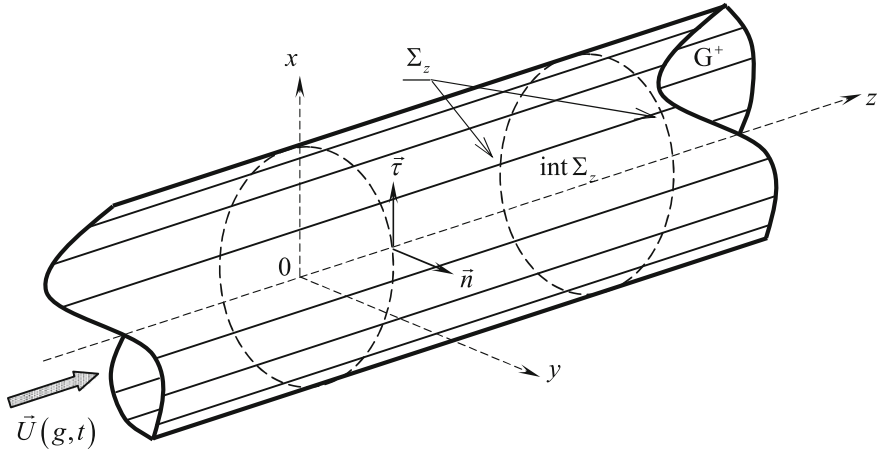


Fig. 5.9 The hollow regular waveguide G

5.6.1 Exact Absorbing Conditions for Regular Hollow Waveguides

Let us consider the following model problem (Fig. 5.9). A pulsed wave $\vec{U}(g, t)$, which propagates in a metal hollow waveguide $G = \{g = \{x, y, z\} : \{x, y\} \in \text{int}\Sigma_z, |z| < \infty\}$ towards increasing z , is incident on some virtual boundary $z = 0$ at the moments of time $t > 0$. It is required to find the field $\vec{U}(g, t)$ in the closure of the domain $G^+ = \{g \in G : z > 0\}$ for $t > 0$. The corresponding problem is

$$\begin{cases} \left[\Delta - \frac{\partial^2}{\partial t^2} \right] \vec{E}(g, t) = 0; & g \in G^+, \quad t > 0 \\ \vec{E}(g, 0) = \frac{\partial \vec{E}(g, t)}{\partial t} \Big|_{t=0} = 0; & g \in \bar{G}^+ \\ E_z(g, t)|_{g \in \Sigma} = (\vec{\tau} \cdot \vec{E}_\perp(g, t))|_{g \in \Sigma} = 0; & t \geq 0. \end{cases} \quad (5.190)$$

Here, $\vec{E} = E_z \vec{z} + \vec{E}_\perp$, $\vec{E}_\perp = E_x \vec{x} + E_y \vec{y}$; $\vec{a} \cdot \vec{b}$ is the scalar product of vectors \vec{a} and \vec{b} ; $\Delta = \partial^2 / \partial x^2 + \partial^2 / \partial y^2 + \partial^2 / \partial z^2$; $\Sigma = \Sigma_z \times (0 \leq z < \infty)$ are the walls of the regular waveguide G^+ ; Σ_z is the boundary contour of its cross-section by any coordinate plane $z = \text{const} \geq 0$; \vec{x} , \vec{y} , \vec{z} are the unit vectors of the coordinate axes; $\vec{\tau}$ and \vec{n} are the tangent and the normal to the contour Σ_z ; $\text{int}\Sigma_z$ is the domain in the plane $z = \text{const}$ bounded by Σ_z . The operator grad div in (5.188) is eliminated in (5.190) since the function grad div $\vec{E}(g, t)$ determines herein the volume density of induced charges $\rho(g, t)$, which is zero for all $t > 0$, if only $\rho(g, 0) = 0$ [8].

Applying the scalar *Borgnis functions* $U^E(g, t)$ and $U^H(g, t)$ (see [3, 32, 54]) such that

$$\begin{cases} \left(-\frac{\partial^2}{\partial t^2} + \Delta\right) \frac{\partial U^{E,H}(g, t)}{\partial t} = 0; & g \in G^+, \quad t > 0 \\ U^E(g, t)|_{g \in \Sigma} = \frac{\partial U^H(g, t)}{\partial \vec{n}} \Big|_{g \in \Sigma} = 0; & t \geq 0, \end{cases} \quad (5.191)$$

the general solution to the vector differential equation in (5.190) can be written as

$$E_x = \frac{\partial^2 U^E}{\partial x \partial z} - \frac{\partial^2 U^H}{\partial y \partial t}, \quad E_y = \frac{\partial^2 U^E}{\partial y \partial z} + \frac{\partial^2 U^H}{\partial x \partial t}, \quad E_z = \frac{\partial^2 U^E}{\partial z^2} - \frac{\partial^2 U^E}{\partial t^2}. \quad (5.192)$$

The field $\vec{E}(g, t)$ written in this form satisfies also the boundary conditions of the problem (5.190):

$$\begin{aligned} (\vec{\tau} \cdot \vec{E}_\perp)|_{\Sigma_z} &= \left(\frac{dx}{d\theta} \frac{\partial}{\partial x} + \frac{dy}{d\theta} \frac{\partial}{\partial y}\right) \frac{\partial}{\partial z} U^E - \left(\frac{dx}{d\theta} \frac{\partial}{\partial y} - \frac{dy}{d\theta} \frac{\partial}{\partial x}\right) \frac{\partial}{\partial t} U^H \\ &= \frac{d}{d\theta} \left(\frac{\partial}{\partial z} U^E\right) - \frac{\partial}{\partial \vec{n}} \left(\frac{\partial}{\partial t} U^H\right) = 0. \end{aligned}$$

Here, the contour Σ_z has been parametrized as $\Sigma_z = \Sigma_z(\theta) = \{x(\theta), y(\theta)\}_\theta$ and the following representations for the tangential and normal vectors to Σ_z is used [34]:

$$\vec{\tau} = \frac{dx}{d\theta} \vec{x} + \frac{dy}{d\theta} \vec{y}, \quad \vec{n} = -\frac{dy}{d\theta} \vec{x} + \frac{dx}{d\theta} \vec{y}.$$

Separating the transverse variables x and y in the problem (5.191), we obtain its solution in the form

$$U^{E,H}(x, y, z, t) = \sum_{n=1,0}^{\infty} u_n^{E,H}(z, t) \mu_n^{E,H}(x, y), \quad (5.193)$$

where $\{\mu_n^E(x, y)\}_{n=1}^{\infty}$ and $\{\mu_n^H(x, y)\}_{n=0}^{\infty}$ are the complete orthonormal systems of the solutions to the Sturm-Liouville problems for the equation $(\partial^2/\partial y^2 + \lambda^2)\mu = 0$ in the domain $\text{int}\Sigma_z$ and with the Dirichlet ($\mu^E(x, y)|_{\{x,y\} \in \Sigma_z} = 0$) or Neumann ($\partial \mu^H(x, y)/\partial \vec{n}|_{\{x,y\} \in \Sigma_z} = 0$) conditions on its boundary Σ_z . λ_n^E and λ_n^H are the eigenvalues associated with these solutions.

Substituting (5.193) into (5.192), the field $\vec{E}(g, t)$ can be written as

$$\begin{cases} E_z(g, t) = \sum_{n=1}^{\infty} u_{nz}(z, t) \zeta_{nz}(x, y) \\ \vec{E}_{\perp}(g, t) = \sum_{n=-\infty}^{\infty} u_{n\perp}(z, t) \vec{\zeta}_{n\perp}(x, y) \end{cases}; \quad t \geq 0, \quad z \geq 0. \quad (5.194)$$

The scalar functions $u_{nz}(z, t)$ and $u_{n\perp}(z, t)$ are solutions to the following initial boundary value problems:

$$\begin{cases} \left[-\frac{\partial^2}{\partial t^2} + \frac{\partial^2}{\partial z^2} - \alpha_{nz}^2 \right] u_{nz}(z, t) = 0; \quad t > 0, \quad z > 0 \\ u_{nz}(z, 0) = \frac{\partial}{\partial t} u_{nz}(z, t) \Big|_{t=0} = 0; \quad z \geq 0 \end{cases}, \quad n = 1, 2, 3, \dots, \quad (5.195)$$

$$\begin{cases} \left[-\frac{\partial^2}{\partial t^2} + \frac{\partial^2}{\partial z^2} - \alpha_{n\perp}^2 \right] u_{n\perp}(z, t) = 0; \quad t > 0, \quad z > 0 \\ u_{n\perp}(z, 0) = \frac{\partial}{\partial t} u_{n\perp}(z, t) \Big|_{t=0} = 0; \quad z \geq 0 \end{cases}, \quad n = 0, \pm 1, \pm 2, \dots \quad (5.196)$$

Here, $\alpha_{nz} = \lambda_n^E$; $\alpha_{n\perp} = \lambda_n^E$ for $n = 1, 2, 3, \dots$ and $\alpha_{n\perp} = \lambda_{-n}^H$ for $n = 0, -1, -2, \dots$; $\zeta_{nz} = \mu_n^E$; $\vec{\zeta}_{n\perp} = \alpha_{n\perp}^{-1} [(\partial \mu_n^E / \partial x) \vec{x} + (\partial \mu_n^E / \partial y) \vec{y}]$ for $n = 1, 2, 3, \dots$ and $\vec{\zeta}_{n\perp} = -\alpha_{n\perp}^{-1} [(\partial \mu_{-n}^H / \partial y) \vec{x} + (\partial \mu_{-n}^H / \partial x) \vec{y}]$ for $n = 0, -1, -2, \dots$

The inversion formulas for (5.194)

$$\begin{cases} u_{nz}(z, t) = \int_{\text{int}\Sigma_z} E_z(g, t) \zeta_{nz}(x, y) dx dy \\ u_{n\perp}(z, t) = \int_{\text{int}\Sigma_z} (\vec{E}_{\perp}(g, t) \cdot \vec{\zeta}_{n\perp}(x, y)) dx dy \end{cases} \quad (5.197)$$

can be obtained using the basic properties of the systems of functions $\mu_n^{E,H}(x, y)$. To see that the latter formula is true, consider the integrals

$$\begin{aligned} \int_{\text{int}\Sigma_z} \left[\left(\frac{\partial \mu_n^E}{\partial x} \vec{x} + \frac{\partial \mu_n^E}{\partial y} \vec{y} \right) \cdot \left(\frac{\partial \mu_m^E}{\partial x} \vec{x} + \frac{\partial \mu_m^E}{\partial y} \vec{y} \right) \right] dx dy &= \int_{\text{int}\Sigma_z} (\text{grad} \mu_n^E \cdot \text{grad} \mu_m^E) dx dy \\ &= - \int_{\text{int}\Sigma_z} \mu_m^E \Delta \mu_n^E dx dy + \int_{\Sigma_z} \mu_m^E \frac{\partial \mu_n^E}{\partial \vec{n}} ds = \begin{cases} 0; & m \neq n \\ (\lambda_n^E)^2; & m = n \end{cases} \end{aligned}$$

$$\begin{aligned}
& \int_{\text{int}\Sigma_z} \left[\left(-\frac{\partial\mu_n^H}{\partial y}\vec{x} + \frac{\partial\mu_n^H}{\partial x}\vec{y} \right) \cdot \left(-\frac{\partial\mu_m^H}{\partial y}\vec{x} + \frac{\partial\mu_m^H}{\partial x}\vec{y} \right) \right] dx dy \\
&= \int_{\text{int}\Sigma_z} [(\text{grad}\mu_n^H \times \vec{z}) \cdot (\text{grad}\mu_m^H \times \vec{z})] dx dy \\
&= \int_{\text{int}\Sigma_z} (\text{grad}\mu_n^H \cdot \text{grad}\mu_m^H) dx dy = \begin{cases} 0; & m \neq n \\ (\lambda_n^H)^2; & m = n \end{cases} \\
& \int_{\text{int}\Sigma_z} \left[\left(\frac{\partial\mu_n^E}{\partial x}\vec{x} + \frac{\partial\mu_n^E}{\partial y}\vec{y} \right) \cdot \left(-\frac{\partial\mu_m^H}{\partial y}\vec{x} + \frac{\partial\mu_m^H}{\partial x}\vec{y} \right) \right] dx dy = \int_P d\vec{P} \cdot \text{rot}\vec{\mu}_m^H \\
&= \int_{\Sigma_z} d\vec{\Sigma}_z \cdot \vec{\mu}_m^H = 0.
\end{aligned}$$

Here, $\vec{a} \times \vec{b}$ is the vector product of vectors \vec{a} and \vec{b} ; $\vec{\mu}_m^H = \mu_m^H \vec{z}$; P is the surface of the function $z = \mu_n^E(x, y)$ spanned on the contour Σ_z ; $d\vec{P} = [-(\partial\mu_n^E/\partial x)\vec{x} - (\partial\mu_n^E/\partial y)\vec{y} + \vec{z}]dx dy$ is the surface element of the surface P; $d\vec{\Sigma}_z = \vec{z}d\theta$ is the vector element of the contour Σ_z .

The problems (5.195) and (5.196) are identical with those considered in Sects. 5.2.2–5.2.4. Thus, omitting the tedious calculations, we address immediately to their solutions $u_n(z, t)$ ($u_n z(z, t)$ or $u_{n\perp}(z, t)$):

$$u_n(z, t) = - \int_0^t J_0 \left[\alpha_n \left((t - \tau)^2 - z^2 \right)^{1/2} \right] u_n'(0, \tau) d\tau; \quad z \geq 0, \quad t \geq 0. \quad (5.198)$$

Placing the observation point in (5.198) onto the virtual boundary $z = 0$, we obtain

$$u_n(0, t) = - \int_0^t J_0[\alpha_n(t - \tau)] u_n'(0, \tau) d\tau, \quad (5.199)$$

and then

$$\left. \left[\frac{\partial}{\partial z} + \frac{\partial}{\partial t} \right] u_n(z, t) \right|_{z=0} = -\alpha_n \int_0^t J_1[\alpha_n(t - \tau)] (t - \tau)^{-1} u_n(0, \tau) d\tau; \quad t \geq 0. \quad (5.200)$$

Setting $\alpha_n = \alpha_{nz}$, $n = 1, 2, 3, \dots$ in (5.198) to (5.200), we obtain RC and EAC for the amplitudes $u_{nz}(z, t)$ of the E_z -component of the outgoing wave $\vec{U}(g, t)$. With

$\alpha_n = \alpha_{n\perp}$, $n = 0, \pm 1, \pm 2, \dots$, we have precisely the same expressions for the amplitudes $u_{n\perp}(z, t)$ of the transverse electric field $\vec{E}_\perp(g, t)$ of the wave $\vec{U}(g, t)$.

Using (5.194) and (5.197), we rewrite the formulas (5.198)–(5.200):

$$\begin{aligned} \left\{ \begin{array}{l} E_z(x, y, z, t) \\ \vec{E}_\perp(x, y, z, t) \end{array} \right\} = & - \sum_{n=\left\{ \begin{array}{l} 1 \\ -\infty \end{array} \right\}}^{\infty} \left[\int_0^t J_0 \left\{ \begin{array}{l} \alpha_{nz} \\ \alpha_{n\perp} \end{array} \right\} \left((t-\tau)^2 - z^2 \right)^{1/2} \right] \\ & \times \int_{\text{int } \Sigma_z} \left\{ \begin{array}{l} (\partial E_z(x, y, z, \tau) / \partial z) |_{z=0} \cdot \xi_{nz}(x, y) \\ \left((\partial \vec{E}_\perp(x, y, z, \tau) / \partial z) |_{z=0} \cdot \vec{\xi}_{n\perp}(x, y) \right) \end{array} \right\} dx dy d\tau \left\{ \begin{array}{l} \xi_{nz}(x, y) \\ \vec{\xi}_{n\perp}(x, y) \end{array} \right\}; \\ & \{x, y\} \in \overline{\text{int } \Sigma_z}, \quad z \geq 0, \quad t \geq 0, \end{aligned} \quad (5.201)$$

$$\begin{aligned} \left\{ \begin{array}{l} E_z(x, y, 0, t) \\ \vec{E}_\perp(x, y, 0, t) \end{array} \right\} = & - \sum_{n=\left\{ \begin{array}{l} 1 \\ -\infty \end{array} \right\}}^{\infty} \left[\int_0^t J_0 \left\{ \begin{array}{l} \alpha_{nz} \\ \alpha_{n\perp} \end{array} \right\} (t-\tau) \right] \\ & \times \int_{\text{int } \Sigma_z} \left\{ \begin{array}{l} (\partial E_z(x, y, z, \tau) / \partial z) |_{z=0} \cdot \xi_{nz}(x, y) \\ \left((\partial \vec{E}_\perp(x, y, z, \tau) / \partial z) |_{z=0} \cdot \vec{\xi}_{n\perp}(x, y) \right) \end{array} \right\} dx dy d\tau \left\{ \begin{array}{l} \xi_{nz}(x, y) \\ \vec{\xi}_{n\perp}(x, y) \end{array} \right\}; \\ & \{x, y\} \in \overline{\text{int } \Sigma_z}, \quad t \geq 0, \end{aligned} \quad (5.202)$$

$$\begin{aligned} \left[\frac{\partial}{\partial z} + \frac{\partial}{\partial t} \right] \left\{ \begin{array}{l} E_z(x, y, z, t) \\ \vec{E}_\perp(x, y, z, t) \end{array} \right\} \Big|_{z=0} = & - \sum_{n=\left\{ \begin{array}{l} 1 \\ -\infty \end{array} \right\}}^{\infty} \left[\left\{ \begin{array}{l} \alpha_{nz} \\ \alpha_{n\perp} \end{array} \right\} \int_0^t J_1 \left\{ \begin{array}{l} \alpha_{nz} \\ \alpha_{n\perp} \end{array} \right\} (t-\tau) \right] (t-\tau)^{-1} \\ & \times \int_{\text{int } \Sigma_z} \left\{ \begin{array}{l} E_z(x, y, 0, \tau) \xi_{nz}(x, y) \\ \left(\vec{E}_\perp(x, y, 0, \tau) \cdot \vec{\xi}_{n\perp}(x, y) \right) \end{array} \right\} dx dy d\tau \left\{ \begin{array}{l} \xi_{nz}(x, y) \\ \vec{\xi}_{n\perp}(x, y) \end{array} \right\}; \\ & \{x, y\} \in \overline{\text{int } \Sigma_z}, \quad t \geq 0. \end{aligned} \quad (5.203)$$

From (5.200) it also follows that

$$\left[\frac{\partial}{\partial t} + \frac{\partial}{\partial z} \right] \left\{ \begin{array}{l} E_z(x, y, z, t) \\ \vec{E}_\perp(x, y, z, t) \end{array} \right\} \Big|_{z=0} = \frac{2}{\pi} \int_0^{\pi/2} \frac{\partial}{\partial t} \left\{ \begin{array}{l} W_z(x, y, t, \varphi) \\ \vec{W}_\perp(x, y, t, \varphi) \end{array} \right\} \sin^2 \varphi d\varphi; \quad (5.204a)$$

$$\{x, y\} \in \overline{\text{int } \Sigma_z}, \quad t \geq 0,$$

$$\left\{ \begin{aligned} & \left[\frac{\partial^2}{\partial t^2} - \cos^2 \varphi \left(\frac{\partial^2}{\partial x^2} + \frac{\partial^2}{\partial y^2} \right) \right] \left\{ \begin{aligned} & W_z(x, y, t, \varphi) \\ & \vec{W}_\perp(x, y, t, \varphi) \end{aligned} \right\} \\ & = \left(\frac{\partial^2}{\partial x^2} + \frac{\partial^2}{\partial y^2} \right) \left\{ \begin{aligned} & E_z(x, y, 0, t) \\ & \vec{E}_\perp(x, y, 0, t) \end{aligned} \right\}; \quad \{x, y\} \in \overline{\text{int } \Sigma_z}, \quad t > 0 \\ & \left\{ \begin{aligned} & W_z(x, y, 0, \varphi) \\ & \vec{W}_\perp(x, y, 0, \varphi) \end{aligned} \right\} = \partial \left\{ \begin{aligned} & W_z(x, y, t, \varphi) \\ & \vec{W}_\perp(x, y, t, \varphi) \end{aligned} \right\} / \partial t \Big|_{t=0} = 0; \quad \{x, y\} \in \overline{\text{int } \Sigma_z} \\ & \left\{ \begin{aligned} & W_z(x, y, t, \varphi) \\ & (\vec{\tau} \cdot \vec{W}_\perp(x, y, t, \varphi)) \end{aligned} \right\} \Big|_{\{x, y\} \in \Sigma_z} = 0; \quad t \geq 0. \end{aligned} \right. \tag{5.204b}$$

Each of EACs (5.202)–(5.204a), (5.204b) for the vector function $\vec{E}(g, t)$ determines its own operator $D_j[\dots]$ in EACs $D_1[\vec{E}(g, t) - \vec{E}^{i(1)}(g, t)]|_{g \in \Gamma_1} = 0$, $D_2[\vec{E}(g, t)]|_{g \in \Gamma_2} = 0$ in (5.188). The auxiliary scalar and vector functions $W_z(x, y, t, \varphi)$ and $\vec{W}_\perp(x, y, t, \varphi)$ are presented in the same bases of the transverse functions $\zeta_{nz}(x, y)$ and $\vec{\zeta}_{n\perp}(x, y)$ as the field $\vec{E}(g, t)$.

In contrast to (5.204a), (5.204b), EACs (5.202) and (5.203) are nonlocal both in time and space. It is important to note also the following essential distinction between EACs (5.202), (5.203) and EAC (5.204a), (5.204b). EACs (5.202), (5.203) require complete information on the eigenfunctions and eigenvalues of the Sturm-Liouville operator in the region $\text{int}\Sigma_z$ with the Dirichlet and Neumann conditions on its boundary Σ_z . Resolution of the corresponding problems may be too cumbersome and costly in terms of computer resources. EAC (5.204a), (5.204b) is free from this shortcoming and, hence, it should be preferred when analyzing structures for which the transverse functions for channels with outgoing waves cannot be found analytically.

The equations (5.198) and (5.201) specify the operator $X_{0 \rightarrow z}(t)[u']$, which operates on the amplitudes $u_n(z, t)$ of the outgoing wave (5.194) according to the rule

$$u_n(z, t) = X_{0 \rightarrow z}(t)[u_n'(0, \tau)]; \quad z \geq 0, \quad t \geq z, \quad t - z \geq \tau \geq 0 \tag{5.205}$$

and the operator

$$\begin{aligned} \vec{E}(g, t) &= Z_{q \rightarrow g}(t)[\vec{E}'(q, \tau)]; \quad \vec{E}'(q, \tau) = \frac{\partial \vec{E}(g, t)}{\partial z} \Big|_{z=0}, \\ g &= \{x, y, z\} \in G^+, \quad t \geq z, \quad t - z \geq \tau \geq 0, \end{aligned} \tag{5.206}$$

which operates on the field $\vec{E}(g, t)$. The operators (5.205) and (5.206) allow to compute the values of $u_n(z, t)$ and $\vec{E}(g, t)$ in any point in the waveguide G^+

knowing only their values on the virtual boundaries. The operators (5.205) and (5.206) are the so-called *transport operators* which relate near-zone and far-zone fields. They are discussed in more details in Sect. 5.3.3.

5.6.2 Radiation Conditions and Exact Absorbing Conditions for Spherical Virtual Boundary in Free Space

Turning back to the problem (5.188), we must formulate a condition on Γ for $\vec{E}(g, t)$ that does not distort the physical processes simulated. The virtual boundary $\Gamma = \{g = \{r, \vartheta, \phi\} : r = L\}$ is spherical, therefore, the problem

$$\begin{cases} \left[\Delta - \frac{\partial^2}{\partial t^2} \right] \vec{E}(g, t) = 0; & g \in \Omega_{\text{ext}}, \quad t > 0 \\ \vec{E}(g, 0) = 0, \quad \frac{\partial}{\partial t} \vec{E}(g, t)|_{t=0} = 0; & g \in \bar{\Omega}_{\text{ext}}, \end{cases} \quad (5.207)$$

whose solution represents the desired condition, should also be considered in the spherical coordinates $0 \leq r < \infty$, $0 \leq \vartheta \leq \pi$, $0 \leq \phi \leq 2\pi$. The expression for $\Delta \vec{E}(g, t)$ in spherical coordinates is too cumbersome (see, for example, [55]), which practically disables any analytical manipulations with the equation (5.207). Some intermediate derivations are needed to simplify the situation. Below we use the Borgnis functions for it. These are two scalar functions $U^E(g, t)$ and $U^H(g, t)$, which allow to determine all six components of the electromagnetic field vectors $\vec{E}(g, t)$ and $\vec{H}(g, t)$ (see [3, 32, 54]). Clearly we have worked in the region $\Omega_{\text{ext}} = \{g \in \mathbb{R}^3 : r > L\}$ where the relevant representations are valid and where all the analytical rearrangements are performed to obtain RC and EAC on the boundary Γ .

Following [32], we obtain such solutions $\vec{E}(g, t)$ for the wave equation from (5.207):

$$\begin{aligned} E_r &= \frac{\partial^2 U^E}{\partial r^2} - \frac{\partial^2 U^E}{\partial t^2}, & E_\vartheta &= \frac{1}{r} \left[\frac{\partial^2 U^E}{\partial r \partial \vartheta} - \frac{1}{\sin \vartheta} \frac{\partial^2 U^H}{\partial \phi \partial t} \right], \\ E_\phi &= \frac{1}{r} \left[\frac{1}{\sin \vartheta} \frac{\partial^2 U^E}{\partial r \partial \phi} + \frac{\partial^2 U^H}{\partial \vartheta \partial t} \right]. \end{aligned} \quad (5.208)$$

The functions $U^E(g, t)$ and $U^H(g, t)$, which specify *TM*- and *TE*-waves (with respect to the r -axis), satisfy the following equivalent (if $r \neq 0$) equations:

$$\begin{aligned} & \left[\frac{1}{r^2 \sin \vartheta} \frac{\partial}{\partial \vartheta} \left(\sin \vartheta \frac{\partial}{\partial \vartheta} \right) + \frac{1}{r^2 \sin^2 \vartheta} \frac{\partial^2}{\partial \phi^2} + \frac{1}{r^2} \frac{\partial}{\partial r} \left(r^2 \frac{\partial}{\partial r} \right) - \frac{\partial^2}{\partial t^2} \right] \frac{\partial U^{E,H}(g, t)}{r \partial t} \\ &= \left[-\frac{\partial^2}{\partial t^2} + \Delta \right] \frac{\partial U^{E,H}(g, t)}{r \partial t} \end{aligned} \quad (5.209)$$

and

$$\left[\frac{1}{r^2 \sin \vartheta} \frac{\partial}{\partial \vartheta} \left(\sin \vartheta \frac{\partial}{\partial \vartheta} \right) + \frac{1}{r^2 \sin^2 \vartheta} \frac{\partial^2}{\partial \phi^2} + \frac{\partial^2}{\partial r^2} - \frac{\partial^2}{\partial t^2} \right] \frac{\partial U^{E,H}(g,t)}{\partial t} = 0. \quad (5.210)$$

It is obvious that in the basis of the *tesseral spherical harmonics* [34]

$$\mu_{nm}(\vartheta, \phi) = \frac{1}{2} \sqrt{\frac{(2n+1)(n-|m|)!}{\pi(n+|m|)!}} P_n^{|m|}(\cos \vartheta) e^{im\phi};$$

$$n = 0, 1, 2, \dots, \quad m = 0, \pm 1, \pm 2, \dots, \pm n$$

($P_n^{|m|}(\dots)$ are the associated Legendre functions of the first kind of degree n and order $|m|$) they can be given by the expansions

$$U^{E,H}(g,t) = \sum_{n=0}^{\infty} u_n^{E,H}(r,t) \sum_{m=-n}^n \mu_{nm}(\vartheta, \phi). \quad (5.211)$$

The system of functions $\mu_{nm}(\vartheta, \phi)$ is complete on the sphere $0 \leq \vartheta \leq \pi$, $0 \leq \phi \leq 2\pi$, and for any two accessorial functions f_1 and f_2

$$[f_1 f_2^*]_{\perp} \equiv \int_0^{2\pi} d\phi \int_0^{\pi} f_1(\vartheta, \phi) f_2^*(\vartheta, \phi) \sin \vartheta d\vartheta = \begin{cases} 0; & f_1 \neq f_2 \\ 1; & f_1 = f_2 \end{cases} \quad (5.212)$$

(the superscript ‘*’ stands for the complex conjugation operation). The functions $\mu_{nm}(\vartheta, \phi)$ satisfy the equation [34]

$$\left[\frac{1}{\sin \vartheta} \frac{\partial}{\partial \vartheta} \left(\sin \vartheta \frac{\partial}{\partial \vartheta} \right) + \frac{1}{\sin^2 \vartheta} \frac{\partial^2}{\partial \phi^2} + n(n+1) \right] \mu_{nm}(\vartheta, \phi) = [\Delta_{\perp} + n(n+1)] \mu_{nm}(\vartheta, \phi) = 0. \quad (5.213)$$

From (5.209) to (5.211), and (5.213) we have the following equivalent equations to determine the space-time amplitudes $u_n^{E,H}(r,t)$ of the functions $U^{E,H}(g,t)$:

$$\left[-\frac{\partial^2}{\partial t^2} + \frac{\partial^2}{\partial r^2} - \frac{n(n+1)}{r^2} \right] \frac{\partial u_n^{E,H}(r,t)}{\partial t} = 0, \quad (5.214)$$

$$\left[-\frac{\partial^2}{\partial t^2} + \frac{1}{r^2} \frac{\partial}{\partial r} \left(r^2 \frac{\partial}{\partial r} \right) - \frac{n(n+1)}{r^2} \right] \frac{\partial u_n^{E,H}(r,t)}{r \partial t} = 0. \quad (5.215)$$

Let us rewrite now the vector $\vec{E}(g, t)$ in the form

$$\vec{E}(g, t) = -\frac{\partial^2 \vec{U}^E}{\partial t^2} + \text{grad} \frac{\partial U^E}{\partial r} - \text{rot} \frac{\partial \vec{U}^H}{\partial t}, \quad \vec{U}^{E,H}(g, t) = U^{E,H}(g, t) \vec{r}, \quad (5.216)$$

which is equivalent to (5.208). Substituting (5.211) into (5.216), we obtain

$$E_r(g, t) = \sum_{n,m} u_n^r(r, t) \mu_{nm}(\vartheta, \phi), \quad (5.217)$$

$$\begin{aligned} \vec{E}_\perp(g, t) &= E_\vartheta(g, t) \vec{\vartheta} + E_\phi(g, t) \vec{\phi} = \vec{E}_\perp^E(g, t) + \vec{E}_\perp^H(g, t) \\ &= \sum_{n,m} [u_n^{\perp,E}(r, t) \text{grad}_\perp \mu_{nm}(\vartheta, \phi) + u_n^{\perp,H}(r, t) \text{rot}_\perp \mu_{nm}(\vartheta, \phi)]. \end{aligned} \quad (5.218)$$

Here,

$$\text{grad}_\perp \equiv \vec{\vartheta} \frac{\partial}{\partial \vartheta} + \vec{\phi} \frac{1}{\sin \vartheta} \frac{\partial}{\partial \phi}, \quad \text{rot}_\perp \equiv \vec{\vartheta} \frac{1}{\sin \vartheta} \frac{\partial}{\partial \phi} - \vec{\phi} \frac{\partial}{\partial \vartheta},$$

while

$$u_n^r(r, t) = \left(-\frac{\partial^2}{\partial t^2} + \frac{\partial^2}{\partial r^2} \right) u_n^E(r, t) = \frac{n(n+1)}{r^2} u_n^E(r, t), \quad (5.219)$$

$$u_n^{\perp,E}(r, t) = \frac{1}{r} \frac{\partial u_n^E(r, t)}{\partial r}, \quad (5.220)$$

$$u_n^{\perp,H}(r, t) = -\frac{1}{r} \frac{\partial u_n^H(r, t)}{\partial t}. \quad (5.221)$$

On the other hand,

$$u_n^r(r, t) = [E_r(g, t) \mu_{nm}^*(\vartheta, \phi)]_\perp, \quad (5.222)$$

$$u_n^{\perp,E}(r, t) = [n(n+1)]^{-1} [(\vec{E}_\perp(g, t) \cdot \text{grad}_\perp \mu_{nm}^*(\vartheta, \phi))]_\perp, \quad (5.223)$$

$$u_n^{\perp,H}(r, t) = [n(n+1)]^{-1} [(\vec{E}_\perp(g, t) \cdot \text{rot}_\perp \mu_{nm}^*(\vartheta, \phi))]_\perp. \quad (5.224)$$

The equation (5.222) follows immediately from (5.212). To show that (5.223) and (5.224) are true, consider the equalities

$$\begin{aligned}
 & [\mathbf{grad}_\perp \mu_{ps}(\vartheta, \phi) \cdot \mathbf{grad}_\perp \mu_{nm}^*(\vartheta, \phi)]_\perp \\
 &= \int_0^{2\pi} \int_0^\pi \int_0^1 (\mathbf{grad}_{\mu_{ps}}(\vartheta, \phi) \cdot \mathbf{grad}_{\mu_{nm}^*}(\vartheta, \phi)) r^2 \sin \vartheta dr d\vartheta d\phi \\
 &= \int_{S(0,1)} (\mathbf{grad}_{\mu_{ps}}(\vartheta, \phi) \cdot \mathbf{grad}_{\mu_{nm}^*}(\vartheta, \phi)) dv \\
 &= - \int_{S(0,1)} \mu_{ps}(\vartheta, \phi) \Delta \mu_{nm}^*(\vartheta, \phi) dv + \int_{\partial S(0,1)} \mu_{ps}(\vartheta, \phi) \frac{\partial \mu_{nm}^*(\vartheta, \phi)}{\partial \vec{n}} ds \\
 &= - [\mu_{ps}(\vartheta, \phi) \Delta_\perp \mu_{nm}^*(\vartheta, \phi)]_\perp = \begin{cases} 0; & p \neq n \text{ or } s \neq m \\ n(n+1); & p = n \text{ and } s = m \end{cases},
 \end{aligned} \tag{5.225}$$

$$\begin{aligned}
 & [\mathbf{rot}_\perp \mu_{ps}(\vartheta, \phi) \cdot \mathbf{rot}_\perp \mu_{nm}^*(\vartheta, \phi)]_\perp \\
 &= [(\mathbf{grad}_\perp \mu_{ps}(\vartheta, \phi) \times \vec{r}) \cdot (\mathbf{grad}_\perp \mu_{nm}^*(\vartheta, \phi) \times \vec{r})]_\perp \\
 &= [\mathbf{grad}_\perp \mu_{ps}(\vartheta, \phi) \cdot \mathbf{grad}_\perp \mu_{nm}^*(\vartheta, \phi)]_\perp,
 \end{aligned}$$

$$\begin{aligned}
 & [\mathbf{grad}_\perp \mu_{ps}(\vartheta, \phi) \cdot \mathbf{rot}_\perp \mu_{nm}^*(\vartheta, \phi)]_\perp \\
 &= \int_0^{2\pi} \int_0^\pi \left[\frac{\partial \mu_{ps}(\vartheta, \phi)}{\partial \vartheta} \frac{\partial \mu_{nm}^*(\vartheta, \phi)}{\partial \phi} - \frac{\partial \mu_{ps}(\vartheta, \phi)}{\partial \phi} \frac{\partial \mu_{nm}^*(\vartheta, \phi)}{\partial \vartheta} \right] d\vartheta d\phi \\
 &\stackrel{\{\vartheta, \phi\}}{\downarrow} \\
 &\stackrel{\{x, y\}}{=} - \int_0^{2\pi} \int_0^\pi \mathbf{rot} [\mu_{nm}^*(x, y) \vec{z}] \cdot \left[- \frac{\partial \mu_{ps}(x, y)}{\partial x} \vec{x} - \frac{\partial \mu_{ps}(x, y)}{\partial y} \vec{y} + \vec{z} \right] dx dy \\
 &= - \int_M \mathbf{rot} [\mu_{nm}^*(x, y) \vec{z}] \cdot \vec{dm} = - \oint_K \vec{dr} \cdot \mu_{nm}^*(x, y) \vec{z} = 0.
 \end{aligned} \tag{5.226}$$

Here, $S(0, 1)$ is a solid sphere of the unit radius with the origin of coordinates as its center; $\partial S(0, 1)$ is its surface; \vec{n} is the outer normal to $\partial S(0, 1)$; $dv = r^2 \sin \vartheta dr d\vartheta d\phi$ is the volume element; M is the complex ‘surface’ of the function $z = \mu_{ps}(x, y)$, $\{x, y\} \in [0, \pi] \times [0, 2\pi]$, spanned on the complex ‘contour’ K ; \vec{dm} is the vector element of the area of this surface; and \vec{dr} is the vector element of the contour K . In the derivation of (5.225) were used the Green theorem and the equations (5.223), whereas in the derivation of (5.226) were used the Stokes theorem, the periodicity in ϕ of the spherical harmonics (the period is 2π), and the particular values $P_n^{|m|}(\pm 1) = 0$ for $n = 0, 1, 2, \dots$, $m = \pm 1, \pm 2, \dots, \pm n$ and $P_n(\pm 1) = (\pm 1)^n$, $\partial \mu_{n0}(\vartheta, \phi) / \partial \phi = 0$ for $n = 0, 1, 2, \dots$ [40, 43].

Rewrite now the equation (5.214) in the following form:

$$\left[-\frac{\partial^2}{\partial t^2} + \frac{\partial^2}{\partial r^2} - \frac{n(n+1)}{r^2} \right] u_n(r, t) = 0; \quad r \geq L, \quad t > 0. \quad (5.227)$$

Here, $u_n(r, t) = \partial u_n^{E,H}(r, t) / \partial t$ or $u_n(r, t) = u_n^{E,H}(r, t)$: since at the initial moment of time $t = 0$ the excitation is absent in Ω_{ext} , the functions $u_n^{E,H}(r, t)$ in this region satisfy the same equations as the functions $\partial u_n^{E,H}(r, t) / \partial t$ do.

As it was shown in Sect. 5.3.2 (see the equations (5.56)–(5.74)), we have the following solution for (5.227) with zero initial conditions:

$$\begin{aligned} u_n(r, t) &= \left(\frac{L}{r}\right)^n u_n(L, t - (r - L)) + \sqrt{\frac{r}{L}} \int_0^{t-(r-L)} S_{n+1/2}(r, L, t - \tau) \frac{\partial u_n(L, \tau)}{\partial \tau} d\tau \\ &= \left[\left(\frac{L}{r}\right)^n + \sqrt{\frac{r}{L}} S_{n+1/2}(r, L, r - L) \right] u_n(L, t - (r - L)) \\ &\quad - \sqrt{\frac{r}{L}} \int_0^{t-(r-L)} u_n(L, \tau) \frac{\partial S_{n+1/2}(r, L, t - \tau)}{\partial \tau} d\tau; \quad r > L, \quad t \geq (r - L), \quad n = 0, 1, 2, \dots \end{aligned} \quad (5.228)$$

To evaluate the amplitudes $u_n^{\perp,E}(r, t)$ of the transverse component $\vec{E}_{\perp}(g, t)$ of the electric field $\vec{E}(g, t)$ (see the formulas (5.218) and (5.220)), RCs for radial derivatives of the functions $u_n(r, t)$ should also be constructed. Through differentiation with respect to r in the first equality in (5.228) we obtain

$$\begin{aligned} \frac{\partial u_n(r, t)}{\partial r} &= -\frac{n}{r} \left(\frac{L}{r}\right)^n u_n(L, t - (r - L)) \\ &\quad - \left[\left(\frac{L}{r}\right)^n + \sqrt{\frac{r}{L}} S_{n+1/2}(r, L, r - L) \right] \frac{\partial u_n(L, \tau)}{\partial \tau} \Big|_{\tau=t-(r-L)} \\ &\quad + \sqrt{\frac{r}{L}} \int_0^{t-(r-L)} \left[\frac{S_{n+1/2}(r, L, t - \tau)}{2r} + \frac{\partial S_{n+1/2}(r, L, t - \tau)}{\partial r} \right] \frac{\partial u_n(L, \tau)}{\partial \tau} d\tau; \\ &\quad r > L, \quad t \geq (r - L), \quad n = 0, 1, 2, \dots \end{aligned} \quad (5.229)$$

The radial derivative of $S_{\gamma}(r, L, t - \tau)$ can be evaluated as easy as the function $S_{\gamma}(r, L, t - \tau)$ itself (see the formula (5.73)):

$$\frac{\partial S_{\gamma}(r, L, t - \tau)}{\partial r} = \frac{1}{L} \sum_{s=1}^n \frac{H_{\gamma}^{(1)\prime}(z_s r)}{H_{\gamma-1}^{(1)}(z_s L)} e^{-iz_s(t-\tau)}; \quad \tau < t - (r - L).$$

Now let us pass, using the expansions (5.212), (5.217) to (5.224), from RCs (5.228), (5.229) for the amplitudes of the Borgnis functions and their derivatives to RCs for the vector function $\vec{E}(g, t)$:

$$\begin{aligned}
E_r(g, t) = & \sum_{n,m} \left\{ \left(\frac{L}{r} \right)^{n+2} \left[E_r(L, \tilde{\vartheta}, \tilde{\phi}, t - (r-L)) \mu_{nm}^*(\tilde{\vartheta}, \tilde{\phi}) \right]_{\perp} \right. \\
& + \left. \left(\frac{L}{r} \right)^{3/2} \int_0^{t-(r-L)} S_{n+1/2}(r, L, t-\tau) \left[\frac{\partial E_r(L, \tilde{\vartheta}, \tilde{\phi}, \tau)}{\partial \tau} \mu_{nm}^*(\tilde{\vartheta}, \tilde{\phi}) \right]_{\perp} d\tau \right\} \\
& \times \mu_{nm}(\vartheta, \phi); \quad g = \{r, \vartheta, \phi\} \in \Omega_{\text{ext}}, \quad t \geq (r-L)
\end{aligned} \tag{5.230}$$

and

$$\begin{aligned}
\vec{E}_{\perp}(g, t) = & \sum_{n,m} \left\{ -\frac{1}{n+1} \left(\frac{L}{r} \right)^{n+2} \left[E_r(L, \tilde{\vartheta}, \tilde{\phi}, t - (r-L)) \mu_{nm}^*(\tilde{\vartheta}, \tilde{\phi}) \right]_{\perp} \right. \\
& + \frac{L}{n} \left[\left(\frac{L}{r} \right)^{n+1} + \sqrt{\frac{L}{r}} S_{n+1/2}(r, L, r-L) \right] \left[\frac{\partial E_r(L, \tilde{\vartheta}, \tilde{\phi}, \tau)}{\partial \tau} \Big|_{\tau=t-(r-L)} \mu_{nm}^*(\tilde{\vartheta}, \tilde{\phi}) \right]_{\perp} \\
& - \frac{L}{n} \sqrt{\frac{L}{r}} \int_0^{t-(r-L)} \left[\frac{S_{n+1/2}(r, L, t-\tau)}{2r} + \frac{\partial S_{n+1/2}(r, L, t-\tau)}{\partial r} \right] \\
& \times \left[\frac{\partial E_r(L, \tilde{\vartheta}, \tilde{\phi}, \tau)}{\partial \tau} \mu_{nm}^*(\tilde{\vartheta}, \tilde{\phi}) \right]_{\perp} d\tau \Big\} \text{grad}_{\perp} \mu_{nm}(\vartheta, \phi) \\
& + \frac{1}{n(n+1)} \left\{ \left(\frac{L}{r} \right)^{n+1} \left[\vec{E}_{\perp}(L, \tilde{\vartheta}, \tilde{\phi}, t - (r-L)) \cdot \text{rot}_{\perp} \mu_{nm}^*(\tilde{\vartheta}, \tilde{\phi}) \right]_{\perp} \right. \\
& + \left. \sqrt{\frac{L}{r}} \int_0^{t-(r-L)} S_{n+1/2}(r, L, t-\tau) \left[\frac{\partial \vec{E}_{\perp}(L, \tilde{\vartheta}, \tilde{\phi}, \tau)}{\partial \tau} \cdot \text{rot}_{\perp} \mu_{nm}^*(\tilde{\vartheta}, \tilde{\phi}) \right]_{\perp} d\tau \right\} \\
& \times \text{rot}_{\perp} \mu_{nm}(\vartheta, \phi); \quad g = \{r, \vartheta, \phi\} \in \Omega_{\text{ext}}, \quad t \geq (r-L).
\end{aligned} \tag{5.231}$$

There might be different approaches to the numerical implementation of RCs (5.230), (5.231) as EACs for the problem (5.180), but it is a subject of a separate study. It should be noted that the numerical implementation of EACs obtained from RCs (5.230), (5.231) does not require numerical differentiation with respect to the normal to the spherical virtual boundary Γ . This feature might appear unessential at the first glance, but it is very important in cases when these EACs, which are derived in spherical coordinates, are used to truncate computation domains on rectangular Cartesian grids.

Let us note also that RCs (5.230), (5.231) specify the *transport operator*

$$\vec{E}(g, t) = Z_{q \in \Gamma \rightarrow g \in \Omega_{\text{ext}}}(t) [\vec{E}(q, \tau)]; \quad t \geq L, \quad t - L \geq \tau \geq 0 \tag{5.232}$$

which allows to compute the values of $\vec{E}(g, t)$ in any point $g = \{r, \vartheta, \phi\}$ of the domain Ω_{ext} knowing only the values of $\vec{E}(g, t)$ on the virtual boundary Γ . Transport operators are discussed in more details in Sect. 5.3.3.

5.6.3 *TM-Excitation: Frequency-Domain Characteristics*

For situations described by the problem (5.188), the following important corollary [3, 8] exists: fields generated in the reflection (waveguide Ω_1) and transmission (waveguide Ω_2) zones of a waveguide (radiation into free space is absent) or a radiating unit (Fig. 5.8) are uniquely determined by their longitudinal (directed along the waveguide axes) components. Certainly it is not true for *TEM*-waves as their electromagnetic field is transverse with respect to the propagation direction. But now we eliminate this limitation. At this stage, simplifying the formalism as much as possible, we list characteristics whose analogs are widely used in physical and applied problems. Let us begin with simple definitions. First of all, we introduce the local coordinates $g_j = \{x_j, y_j, z_j\}$, $j = 1, 2$ for the waveguides Ω_1 and Ω_2 , as illustrated in Fig. 5.8. The wave $\vec{U}^{i(1)}(g_1, t) = \{\vec{E}^{i(1)}(g_1, t), \vec{H}^{i(1)}(g_1, t)\}$ in Ω_1 is the *TM*-wave when $H_z^{i(1)}(g_1, t) \equiv 0$, and is the *TE*-wave when $\vec{E}_z^{i(1)}(g_1, t) \equiv 0$.

Let the structure under consideration is excited by one of the *partial constituent* of the *TM*-wave, namely the *TM_p*-wave:

$$\begin{aligned} \vec{U}^{i(1)}(g_1, t) &= \vec{U}_{p(E)}^{i(1)}(g_1, t) : E_z^{i(1)}(g_1, t) = v_p^E(z_1, t) \mu_{p1}^E(x_1, y_1), \\ H_z^{i(1)}(g_1, t) &\equiv 0; \quad g_1 = \{x_1, y_1, z_1\} \in \bar{\Omega}_1, \quad t \geq 0. \end{aligned} \quad (5.233)$$

The waves $\vec{U}^s(g_1, t) = \vec{U}(g_1, t) - \vec{U}^{i(1)}(g_1, t)$ and $\vec{U}(g_2, t)$ generated in the domains Ω_1 and Ω_2 can be represented by their longitudinal components

$$\begin{aligned} \left\{ \begin{array}{l} E_z^s(g_1, t) \\ H_z^s(g_1, t) \end{array} \right\} &= \sum_{n=\begin{array}{l} \infty \\ 1 \\ 0 \end{array}} \left\{ \begin{array}{l} u_{nz,1}^{E \rightarrow E}(z_1, t) \\ u_{nz,1}^{E \rightarrow H}(z_1, t) \end{array} \right\} \left\{ \begin{array}{l} \mu_{n1}^E(x_1, y_1) \\ \mu_{n1}^H(x_1, y_1) \end{array} \right\}; \quad g_1 \in \bar{\Omega}_1, \quad t \geq 0 \end{aligned} \quad (5.234)$$

(reflected wave) and

$$\begin{aligned} \left\{ \begin{array}{l} E_z(g_2, t) \\ H_z(g_2, t) \end{array} \right\} &= \sum_{n=\begin{array}{l} \infty \\ 1 \\ 0 \end{array}} \left\{ \begin{array}{l} u_{nz,2}^{E \rightarrow E}(z_2, t) \\ u_{nz,2}^{E \rightarrow H}(z_2, t) \end{array} \right\} \left\{ \begin{array}{l} \mu_{n2}^E(x_2, y_2) \\ \mu_{n2}^H(x_2, y_2) \end{array} \right\}; \quad g_2 \in \bar{\Omega}_2, \quad t \geq 0 \end{aligned} \quad (5.235)$$

(transmitted wave in output waveguide). Here, we increase the number of indexes in the identifiers $v_{nz}(z, t)$, $u_{nz}(z, t)$, $\mu_n^E(x, y)$, and $\mu_n^H(x, y)$ in comparison with Sect. 5.6.1 to segregate notations for different domains (1 and 2) and different longitudinal components of the electromagnetic field ($\rightarrow E$ and $\rightarrow H$). The field generated by TM -waves is marked by $E \rightarrow$, and the field generated by TE -waves is marked by $H \rightarrow$. The expansions for H_z -component is written using the formulas

$$\eta_0 H_x = \frac{\partial^2 U^E}{\partial y \partial t} + \frac{\partial^2 U^H}{\partial x \partial z}, \quad \eta_0 H_y = -\frac{\partial^2 U^E}{\partial x \partial t} + \frac{\partial^2 U^H}{\partial y \partial z}, \quad \eta_0 H_z = \frac{\partial^2 U^H}{\partial z^2} - \frac{\partial^2 U^H}{\partial t^2}$$

[3, 32] complementing (5.192).

The frequency-domain counterparts of the time-domain representations (5.233) to (5.235) are:

$$\begin{aligned} \tilde{E}_z^{i(1)}(g_1, k) &= A_{pz,1}^E(k) \exp[-iz_1 \beta_{p1}^E(k)] \mu_{p1}^E(x_1, y_1), \\ \tilde{H}_z^{i(1)}(g_1, k) &= 0; \quad g_1 \in \bar{\Omega}_1, \end{aligned} \quad (5.236)$$

$$\left\{ \begin{array}{l} \tilde{E}_z^s(g_1, k) \\ \tilde{H}_z^s(g_1, k) \end{array} \right\} = \sum_{n=\begin{array}{l} \infty \\ 1 \\ 0 \end{array}} \left\{ \begin{array}{l} B_{nz,1}^{E \rightarrow E}(k) \exp[iz_1 \beta_{n1}^E(k)] \\ B_{nz,1}^{E \rightarrow H}(k) \exp[iz_1 \beta_{n1}^H(k)] \end{array} \right\} \left\{ \begin{array}{l} \mu_{n1}^E(x_1, y_1) \\ \mu_{n1}^H(x_1, y_1) \end{array} \right\}; \quad g_1 \in \bar{\Omega}_1 \quad (5.237)$$

(incident and reflected waves of the *steady-state field*) and

$$\left\{ \begin{array}{l} \tilde{E}_z(g_2, k) \\ \tilde{H}_z(g_2, k) \end{array} \right\} = \sum_{n=\begin{array}{l} \infty \\ 1 \\ 0 \end{array}} \left\{ \begin{array}{l} B_{nz,2}^{E \rightarrow E}(k) \exp[iz_2 \beta_{n2}^E(k)] \\ B_{nz,2}^{E \rightarrow H}(k) \exp[iz_2 \beta_{n2}^H(k)] \end{array} \right\} \left\{ \begin{array}{l} \mu_{n2}^E(x_2, y_2) \\ \mu_{n2}^H(x_2, y_2) \end{array} \right\}; \quad g_2 \in \bar{\Omega}_2 \quad (5.238)$$

(transmitted wave of the steady-state field in output waveguide). Here, $A_{pz,1}^E$, $B_{nz,1}^{E \rightarrow E}$, and so on are the complex-valued amplitudes of the monochromatic waves, which are the partial constituents of the longitudinal components of the steady-state field

$\tilde{U}(g, k) = \left\{ \tilde{E}(g, k), \tilde{H}(g, k) \right\}$; $\beta_{nj}^E(k) = \sqrt{k^2 - (\lambda_{nj}^E)^2}$ and $\beta_{nj}^H(k) = \sqrt{k^2 - (\lambda_{nj}^H)^2}$, $j = 1, 2$ are the longitudinal propagation numbers of these waves;

$\text{Re } \beta_{nj}^{E \text{ or } H}(k) \text{ Re } k \geq 0$ and $\text{Im } \beta_{nj}^{E \text{ or } H}(k) \geq 0$; $\tilde{f}(k) \leftrightarrow f(t)$ is the Laplace transform (5.102). The frequencies $k = (k_{nj}^E)^\pm = \pm |\lambda_{nj}^E|$ and $k = (k_{nj}^H)^\pm = \pm |\lambda_{nj}^H|$ are the *cutoff frequencies*. On these frequencies, the longitudinal propagation numbers

$\beta_{n_j}^E(k)$ and $\beta_{n_j}^H(k)$ (for TM_n - and TE_n -modes, respectively) vanish, as on larger frequencies monochromatic TM_n - and TE_n -modes propagate without decay. For majority of theoretical problems, k has real value and $k = 2\pi/\lambda$, where λ is the wavelength in free space. It is obvious that $A_{p z,1}^E(k) \leftrightarrow v_{p z,1}^E(0, t)$, $B_{n z,j}^{E \rightarrow E}(k) \leftrightarrow u_{n z,j}^{E \rightarrow E}(0, t)$, and $B_{n z,j}^{E \rightarrow H}(k) \leftrightarrow u_{n z,j}^{E \rightarrow H}(0, t)$. The amplitudes $B_{n z,j}^{E \rightarrow E}$ or $H(k)$ form the so-called scattering coefficients of a structure. They are the *reflection coefficients*

$$\begin{aligned} R_{n(E),p(E)}^{11} &= \frac{B_{n z,1}^{E \rightarrow E}(k)}{A_{p z,1}^E(k)}; \quad n = 1, 2, 3, \dots, \\ R_{n(H),p(E)}^{11} &= \frac{B_{n z,1}^{E \rightarrow H}(k)}{A_{p z,1}^E(k)}; \quad n = 0, 1, 2, \dots \end{aligned} \quad (5.239)$$

which characterize the efficiency of transformation of the p th mode of the monochromatic TM -wave $\tilde{U}^{i(1)}(g_1, k) \leftrightarrow \tilde{U}^{i(1)}(g_1, t)$ into the n th modes of the scattered field $\tilde{U}^s(g_1, k)$ in the waveguide Ω_1 ; and the *transmission coefficients*

$$\begin{aligned} T_{n(E),p(E)}^{21} &= \frac{B_{n z,2}^{E \rightarrow E}(k)}{A_{p z,1}^E(k)}; \quad n = 1, 2, 3, \dots, \\ T_{n(H),p(E)}^{21} &= \frac{B_{n z,2}^{E \rightarrow H}(k)}{A_{p z,1}^E(k)}; \quad n = 0, 1, 2, \dots \end{aligned} \quad (5.240)$$

which characterize the efficiency of excitation of the transmitted modes in the waveguide Ω_2 .

A portion of the energy feeding a waveguide or a radiating unit is redistributed between TE_n - and TM_n -modes propagating without decay in the waveguides Ω_1 and Ω_2 , i.e. between modes corresponding to the longitudinal propagation numbers $\beta_{n_j}^{E \text{ or } H}(k)$: $\text{Re } \beta_{n_j}^{E \text{ or } H}(k) > 0$. It is evident that the number of these modes is finite. Their ‘energy content’ (a portion of acquired energy) in case of $\text{Re } \beta_{p_1}^E(k) > 0$ and real k is defined by the following expressions [56]:

$$\begin{aligned} W_{n(E),p(E)}^{11} &= \left| R_{n(E),p(E)}^{11} \right|^2 \frac{\text{Re } \beta_{n_1}^E \left(\frac{\lambda_{p_1}^E}{\lambda_{n_1}^E} \right)^2}{(\lambda_{n_1}^E)^2 \beta_{p_1}^E}, \\ W_{n(E),p(E)}^{21} &= \left| T_{n(E),p(E)}^{21} \right|^2 \frac{\text{Re } \beta_{n_2}^E \left(\frac{\lambda_{p_1}^E}{\lambda_{n_2}^E} \right)^2}{(\lambda_{n_2}^E)^2 \beta_{p_1}^E}; \quad n = 1, 2, 3, \dots \end{aligned} \quad (5.241)$$

and

$$\begin{aligned}
 W_{n(H),p(E)}^{11} &= \eta_0^2 \left| R_{n(H),p(E)}^{11} \right|^2 \frac{\operatorname{Re} \beta_{n1}^H \left(\lambda_{p1}^E \right)^2}{\left(\lambda_{n1}^H \right)^2 \beta_{p1}^E}, \\
 W_{n(H),p(E)}^{21} &= \eta_0^2 \left| T_{n(H),p(E)}^{21} \right|^2 \frac{\operatorname{Re} \beta_{n2}^H \left(\lambda_{p1}^E \right)^2}{\left(\lambda_{n2}^H \right)^2 \beta_{p1}^E}; \quad n = 0, 1, 2, \dots
 \end{aligned} \tag{5.242}$$

If a radiating structure is made of a loss-free material, the value

$$\eta(k) = 1 - \left[\sum_{n=1}^{\infty} \left(W_{n(E),p(E)}^{11} + W_{n(E),p(E)}^{21} \right) + \sum_{n=0}^{\infty} \left(W_{n(H),p(E)}^{11} + W_{n(H),p(E)}^{21} \right) \right] \tag{5.243}$$

defines the *radiation efficiency*. The *normalized directional pattern* on the arc $r = M \geq L$

$$\begin{aligned}
 D(\vartheta, \phi, k, M) &= \frac{\left| \tilde{E}_{\perp}(M, \vartheta, \phi, k) \right|^2}{\max_{0 \leq \vartheta \leq \pi, 0 \leq \phi \leq 2\pi} \left| \tilde{E}_{\perp}(M, \vartheta, \phi, k) \right|^2}; \\
 0 \leq \vartheta \leq \pi, \quad 0 \leq \phi \leq 2\pi, \quad K_1 \leq k \leq K_2
 \end{aligned} \tag{5.244}$$

characterizes the distribution of the radiated field's power as a function of space directions and frequency. The pattern is computed in the near-, middle- or far-field region of a radiator and is defined thoroughly by the $\vec{E}_{\perp}(r, \vartheta, \phi, t)$ -component of the radiated into domain Ω_{ext} pulsed wave $\vec{U}(r, \vartheta, \phi, t)$. In this work, the normalized pattern definition, which depends on space and frequency, is preferred over the conventional one, which depends on space only and is evaluated at discrete frequencies [55], because it is obtained from time-domain simulations with no extra cost, and it allows easy and accurate detection of frequency dependent changes in the power distribution. $D(\vartheta, \phi, k, M)$ can be used to determine if all frequency components of a pulse propagate in the same direction or 'prefer' different ones causing spreading of a pulse in different directions.

The direction of the main beam is characterized by the angles $\bar{\vartheta}(k)$ and $\bar{\phi}(k)$. Along this direction the maximum radiation occurs, i.e. $D(\bar{\vartheta}(k), \bar{\phi}(k), k, M) = 1$.

5.6.4 *TE-Excitation: Frequency-Domain Characteristics*

Let the structure under consideration is excited now by one of the partial constituent of the *TE*-wave, namely the *TE_p*-wave or

$$\begin{aligned} \bar{U}^{i(1)}(g_1, t) = \bar{U}_{p(H)}^{i(1)}(g_1, t) : H_z^{i(1)}(g_1, t) = v_{p z, 1}^H(z_1, t) \mu_{p 1}^H(x_1, y_1), \\ E_z^{i(1)}(g_1, t) \equiv 0; \quad g_1 = \{x_1, y_1, z_1\} \in \bar{\Omega}_1, \quad t \geq 0 \end{aligned} \quad (5.245)$$

(in the case of time-dependent field) or

$$\begin{aligned} \tilde{U}^{i(1)}(g_1, k) = \tilde{U}_{p(H)}^{i(1)}(g_1, k) : \tilde{H}_z^{i(1)}(g_1, k) = A_{p z, 1}^H(k) \exp[-iz_1 \beta_{p 1}^H(k)] \\ \times \mu_{p 1}^H(x_1, y_1), \quad \tilde{E}_z^{i(1)}(g_1, k) = 0; \quad g_1 \in \bar{\Omega}_1, \quad t \geq 0 \end{aligned} \quad (5.246)$$

(in the case of steady-state field). For the longitudinal components of time-dependent and steady-state fields in the domains Ω_1 and Ω_2 we come to the equations which are almost identical to (5.234), (5.235) and (5.237), (5.238), only the symbol $E \rightarrow$ here, marking the field generated by *TM*-waves, must be substituted by the symbol $H \rightarrow$, marking the field generated by *TE*-waves. The *reflection and transmission coefficients*

$$\begin{aligned} R_{n(E), p(H)}^{11} = \frac{B_{n z, 1}^{H \rightarrow E}(k)}{A_{p z, 1}^H(k)}; \quad n = 1, 2, 3, \dots, \\ R_{n(H), p(H)}^{11} = \frac{B_{n z, 1}^{H \rightarrow H}(k)}{A_{p z, 1}^H(k)}; \quad n = 0, 1, 2, \dots, \end{aligned} \quad (5.247)$$

$$\begin{aligned} T_{n(E), p(H)}^{21} = \frac{B_{n z, 2}^{H \rightarrow E}(k)}{A_{p z, 1}^H(k)}; \quad n = 1, 2, 3, \dots, \\ T_{n(H), p(H)}^{21} = \frac{B_{n z, 2}^{H \rightarrow H}(k)}{A_{p z, 1}^H(k)}; \quad n = 0, 1, 2, \dots \end{aligned} \quad (5.248)$$

as well as the energy content of *TM_n*- and *TE_n*-waves propagating in the waveguides Ω_1 and Ω_2

$$\begin{aligned} W_{n(E), p(H)}^{11} = \eta_0^{-2} \left| R_{n(E), p(H)}^{11} \right|^2 \frac{\operatorname{Re} \beta_{n 1}^E \left(\lambda_{p 1}^H \right)^2}{\left(\lambda_{n 1}^E \right)^2 \beta_{p 1}^H}, \\ W_{n(E), p(H)}^{21} = \eta_0^{-2} \left| T_{n(E), p(H)}^{21} \right|^2 \frac{\operatorname{Re} \beta_{n 2}^E \left(\lambda_{p 1}^H \right)^2}{\left(\lambda_{n 2}^E \right)^2 \beta_{p 1}^H}; \quad n = 1, 2, 3, \dots, \end{aligned} \quad (5.249)$$

$$\begin{aligned}
 W_{n(H),p(H)}^{11} &= \left| R_{n(H),p(H)}^{11} \right|^2 \frac{\operatorname{Re} \beta_{n1}^H \left(\frac{\lambda_{p1}^H}{\lambda_{n1}^H} \right)^2}{\left(\lambda_{n1}^H \right)^2 \beta_{p1}^H}, \\
 W_{n(H),p(H)}^{21} &= \left| T_{n(H),p(H)}^{21} \right|^2 \frac{\operatorname{Re} \beta_{n2}^H \left(\frac{\lambda_{p1}^H}{\lambda_{n2}^H} \right)^2}{\left(\lambda_{n2}^H \right)^2 \beta_{p1}^H}; \quad n = 0, 1, 2, \dots,
 \end{aligned}
 \tag{5.250}$$

and the radiation efficiency

$$\eta(k) = 1 - \left[\sum_{n=1}^{\infty} \left(W_{n(E),p(H)}^{11} + W_{n(E),p(H)}^{21} \right) + \sum_{n=0}^{\infty} \left(W_{n(H),p(H)}^{11} + W_{n(H),p(H)}^{21} \right) \right]
 \tag{5.251}$$

change slightly too.

As for the normalized directional pattern $D(\vartheta, \phi, k, M)$, everything said in Sect. 5.6.3 remains valid for the case of TE -excitation.

5.7 Accurate and Efficient Calculations

5.7.1 General Questions

Standard discretization of closed 2-D or 3-D initial boundary value problems (see, for example, the problems (5.137) and (5.188)) by the finite-difference (FD) method [28] using a uniform rectangular mesh on the coordinates $g = \{y, z\}$ or $g = \{x, y, z\}$ leads to explicit computation schemes with the uniquely defined numerical solution $U(k, l, m) \approx U(y_k, z_l, t_m)$ or $\vec{E}(j, k, l, m) \approx \vec{E}(x_j, y_k, z_l, t_m)$. The approximation error is $O(\bar{h}^2)$, but could be improved, for example, using higher order schemes [57]; \bar{h} is the mesh step in space; \bar{l} is the mesh step in time t ; $x_j = j\bar{h}$, $y_k = k\bar{h}$, $z_l = l\bar{h}$, and $t_m = m\bar{l}$. In order to achieve desired second-order accuracy, all integrals are computed using the composite trapezoid rule and all one-sided first-order derivatives are approximated using the FD operators [58]

$$\left. \frac{df(x)}{dx} \right|_{x=x_j} \approx B_{\pm} [f(x_j)] = [\mp 3f(x_j) \pm 4f(x_{j\pm 1}) \mp f(x_{j\pm 2})] / 2\bar{h}.
 \tag{5.252}$$

The range of the $j = 0, \pm 1, \pm 2, \dots, J^{\pm}$, $k = 0, \pm 1, \pm 2, \dots, K^{\pm}$, $l = 0, \pm 1, \pm 2, \dots, L^{\pm}$, and $m = 0, 1, \dots, M$ integers depends on the size of the computation domain Ω_{int} and the length of the observation interval $[0, T]$: $g_{kl} = \{y_k, z_l\} \in \bar{\Omega}_{\text{int}}$ or $g_{jkl} = \{x_j, y_k, z_l\} \in \bar{\Omega}_{\text{int}}$ and $t_m \in [0, T]$. The condition

$$\frac{\eta\sqrt{n}\bar{l}}{\sqrt{\xi}\bar{h}} < 1 \quad \text{or/and} \quad \sqrt{2n\eta}\frac{\bar{l}}{\bar{h}} < 1; \quad \xi \leq \varepsilon^{-1}(g) \leq \eta, \quad (5.253)$$

$$g \in \Omega_{\text{int}} \in \mathbb{R}^n, \quad n = 2 \quad \text{or} \quad n = 3$$

ensures the uniform boundedness of the numerical solution $U(k, l, m)$ or $\vec{E}(j, k, l, m)$ with decreasing \bar{h} and \bar{l} (see the formulas (10.35) and (10.49) in [33]). FD schemes are stable, and the numerical solution $U(k, l, m)$ or $\vec{E}(j, k, l, m)$ tends to the solution $U(g_{kl}, t_m)$ or $\vec{E}(g_{kl}, t_m)$ of the original problem (5.137) or (5.188) [33].

5.7.2 Nonlocal or Local Conditions?

The computational complexity of FD-based solutions of modified (closed) problems depends on the type of EACs being discretized, nonlocal or local ones. In what follows, the computational complexity is derived not for the most general case: we consider the 2-D axially symmetric problem for an open radiating end of a coaxial waveguide with elongated central conductor over an infinite perfectly conducting plane (see Fig. 5.10 and paper [6]).

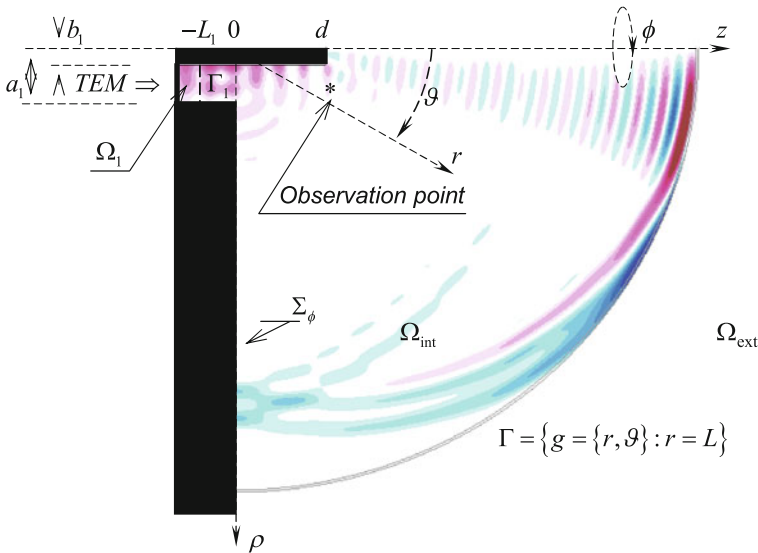


Fig. 5.10 Geometry of the test problem—open end of coaxial waveguide with elongated central conductor over infinite perfectly conducting plane

This example includes nonlocal or local EAC on the planar boundary Γ_1 and a nonlocal EAC similar to (5.75) on the semispherical ($0 \leq \vartheta \leq 90^\circ$) boundary Γ . They are (5.94), (5.96a), (5.96b) and

$$\begin{aligned}
 U(g, t) = & \sum_m \left\{ \left(\frac{L}{r} \right)^{m+1} \int_0^{\pi/2} U(L, \vartheta, t - (r - L)) \tilde{\mu}_m(\cos \vartheta) \sin \vartheta d\vartheta \right. \\
 & + \left. \sqrt{\frac{L}{r}} \int_0^{t-(r-L)} S_{m+1/2}(r, L, t - \tau) \left[\int_0^{\pi/2} \frac{\partial U(L, \vartheta, \tau)}{\partial \tau} \tilde{\mu}_m(\cos \vartheta) \sin \vartheta d\vartheta \right] d\tau \right\} \\
 & \times \tilde{\mu}_m(\cos \vartheta); \quad g = \{r, \vartheta\} \in \Omega_{\text{ext}}, \quad t \geq (r - L), \\
 & m = 2k \quad (\text{for } TE_0\text{-waves}) \quad \text{or} \\
 & m = 2k - 1 \quad (\text{for } TM_0\text{-waves}), \quad k = 1, 2, 3, \dots
 \end{aligned} \tag{5.254}$$

If the explicit three-layer $O(\hbar^2)$ -accurate FD scheme [6, 28] with nonlocal EACs (5.94) and (5.254) on Γ_1 and Γ is used, then its total computational cost is

$$S \approx \underbrace{O(PM)}_{C_{\text{FDTD}}} + \underbrace{O(N^{\text{mod}(i)} M^2)}_{C_{\Gamma_1}^{\text{precomp}}} + \underbrace{O(N_{\Omega_1}^{\text{mod}(s)} M^2)}_{C_{\Gamma_1}^{\text{nonloc}}} + \underbrace{O(N_{\Omega_{\text{ext}}}^{\text{mod}(s)} M^2)}_{C_{\Gamma}^{\text{nonloc}}}. \tag{5.255}$$

Here, the terms C_{FDTD} , $C_{\Gamma_1}^{\text{precomp}}$, $C_{\Gamma_1}^{\text{nonloc}}$, and $C_{\Gamma}^{\text{nonloc}}$ represent the computational costs of FD solution in Ω_{int} , precomputation of incident field's derivative, and numerical implementation of nonlocal EACs on Γ_1 and Γ , respectively. The integers P , M , $N^{\text{mod}(i)}$, $N_{\Omega_1}^{\text{mod}(s)}$ and $N_{\Omega_{\text{ext}}}^{\text{mod}(s)}$ are the total numbers of FD cells in the computation domain, the time steps, the modes in the incident wave $U^{i(1)}(g, t)$, and the modes of the secondary field taken into account in discretization of nonlocal EACs (5.94) and (5.254), respectively.

Replacement of nonlocal EAC (5.94) on the virtual boundary Γ_1 with local EAC (5.96a), (5.96b) yields a new estimate for the total computational cost:

$$S \approx \underbrace{O(PM)}_{C_{\text{FDTD}}} + \underbrace{O(N^{\text{mod}(i)} M^2)}_{C_{\Gamma_1}^{\text{precomp}}} + \underbrace{O(N^\varphi M)}_{C_{\Gamma_1}^{\text{loc}}} + \underbrace{O(N_{\Omega_{\text{ext}}}^{\text{mod}(s)} M^2)}_{C_{\Gamma}^{\text{nonloc}}}. \tag{5.256}$$

In (5.256), $C_{\Gamma_1}^{\text{loc}}$ represents the computational cost of numerical implementation of local EAC, the integer N^φ is the number of points needed to compute the integral over φ in local EAC. Comparing $C_{\Gamma_1}^{\text{loc}}$ in (5.256) with $C_{\Gamma_1}^{\text{nonloc}}$ in (5.255), it is clear that for large M utilization of local EAC might lead to a significant reduction in computational cost provided that $N_{\Omega_1}^{\text{mod}(s)} M \gg N^\varphi$. However, numerical experiments show that this condition may not always be satisfied: to obtain accurate results in resonant situations, N^φ must be high. This reduces the efficiency of local EACs. One can still use nonlocal EACs efficiently for the analysis of resonant situations, provided that the temporal convolutions in nonlocal EACs are computed fast. It could be achieved using the *blocked fast Fourier transform* based (FFT-based) acceleration scheme described below.

5.7.3 The Blocked FFT-Based Acceleration Scheme

The *FFT-based acceleration* scheme was presented in [59–61] and implemented for EACs in [6]. The FFT-based acceleration algorithm benefits from the temporal invariance of the convolutions present in all RCs and nonlocal EACs similar to (5.19), (5.28)–(5.30) and (5.75). The algorithm is applied to the discretized versions of these conditions, where the temporal convolutions are summations over discrete time samples. The operating principles of the algorithm are better explained using an example. Consider the discrete convolution

$$Y(m) = \sum_{q=0}^m J(m-q)X(q); \quad m = 0, 1, 2, \dots, M, \quad (5.257)$$

that results from (5.199) and (5.252). Here,

$$\begin{aligned} X(q) &\approx \bar{l} [3u_n(0, \tau_q) - 4u_n(-\bar{h}, \tau_q) + u_n(-2\bar{h}, \tau_q)] / 2\bar{h}, \\ Y(m) &\approx \bar{l} [3u_n(0, t_m) - 4u_n(-\bar{h}, t_m) + u_n(-2\bar{h}, t_m)] / 4\bar{h} - u_n(0, t_m), \\ J(m-q) &\approx J_0 [\alpha_n(t_m - \tau_q)] \end{aligned}$$

are the proper mesh functions and $Y(m)$, $m = 0, 1, 2, \dots, M$ represents the result of the convolution.

computed exactly using the discrete Fourier transform (DFT) [62], i.e. computing $\text{DFT}^{-1}[\text{DFT}[\bar{J}]\text{DFT}[\bar{X}]]$. In this expression, DFT is replaced with FFT without any numerical approximation for speed up. Since the large blocks are multiplied less often than the small ones and each block, which bigger than 1×1 , is multiplied using FFT, the computational complexity of the block-by-block multiplication (i.e., the discrete convolution in (5.257)) is reduced to $O(M \log^2 M)$ from $O(M^2)$.

Using the FFT-based acceleration technique described above for computing all temporal convolutions pertinent to nonlocal EAC in the problem under consideration (see Fig. 5.10), the computational complexity of the FD solution is reduced to

$$S \approx \underbrace{O(PM)}_{C_{\text{FDTD}}} + \underbrace{O\left(N^{\text{mod}(i)} M \log^2 M\right)}_{C_{\Gamma_1}^{\text{precomp, FFT}}} + \underbrace{O\left(N_{\Omega_1}^{\text{mod}(s)} M \log^2 M\right)}_{C_{\Gamma_1}^{\text{nonloc, FFT}}} + \underbrace{O\left(N_{\Omega_{\text{ext}}}^{\text{mod}(s)} M \log^2 M\right)}_{C_{\Gamma}^{\text{nonloc, FFT}}}. \quad (5.259)$$

Comparing (5.259) with (5.255) one concludes that $C_{\Gamma_1}^{\text{precomp, FFT}} \ll C_{\Gamma_1}^{\text{precomp}}$, $C_{\Gamma_1}^{\text{nonloc, FFT}} \ll C_{\Gamma_1}^{\text{nonloc}}$ and $C_{\Gamma}^{\text{nonloc, FFT}} \ll C_{\Gamma}^{\text{nonloc}}$ especially for large M . This results in significant savings in computational resources. Comparing (5.259) with (5.256), one can conclude that for $C_{\Gamma_1}^{\text{nonloc, FFT}} < C_{\Gamma_1}^{\text{loc}}$, $N_{\Omega_1}^{\text{mod}(s)} \log^2 M < N^\varphi$ should be satisfied. This is possible to achieve for resonant structures where N^φ is large [8]. It should be noted here that while comparing (5.259) and (5.256), $C_{\Gamma}^{\text{nonloc, FFT}} \ll C_{\Gamma}^{\text{nonloc}}$ is already satisfied.

Looking at the comparisons above, one can conclude the following: (i) the implementation of nonlocal EACs on spherical boundaries should always be accelerated using the blocked FFT-based algorithm as there are no equivalent local EACs; (ii) the implementation of nonlocal EACs on planar boundaries can be accelerated using the blocked FFT-based algorithm or equivalent local EACs may be used; one can compare $N_{\Omega_1}^{\text{mod}(s)} \log^2 M$ and N^φ , for example, to see which one will be more efficient; (iii) the FFT-based acceleration should be also used in preparation of the input data when expressions like (5.100) are used for computation of the spatial derivative of incoming signal.

It should be emphasized here again that no additional errors are introduced neither by the blocked FFT-based algorithm nor by the derivation of local EACs from nonlocal ones. Both of these approaches are exact.

5.7.4 Efficiency and Accuracy of the Blocked FFT-Based Acceleration Scheme. Numerical Results

Here we present numerical results that demonstrate the efficiency and accuracy of the blocked FFT-accelerated FD scheme with nonlocal/local EAC detailed above. Since the accuracy of EAC was the subject of several other publications (see [3, 8, 17] for example), the emphasis here is on the accuracy and efficiency of the blocked FFT-acceleration. Two different examples are considered. Both examples are run on a workstation with a 2.67 GHz Xeon CPU and 23.4 GB of RAM.

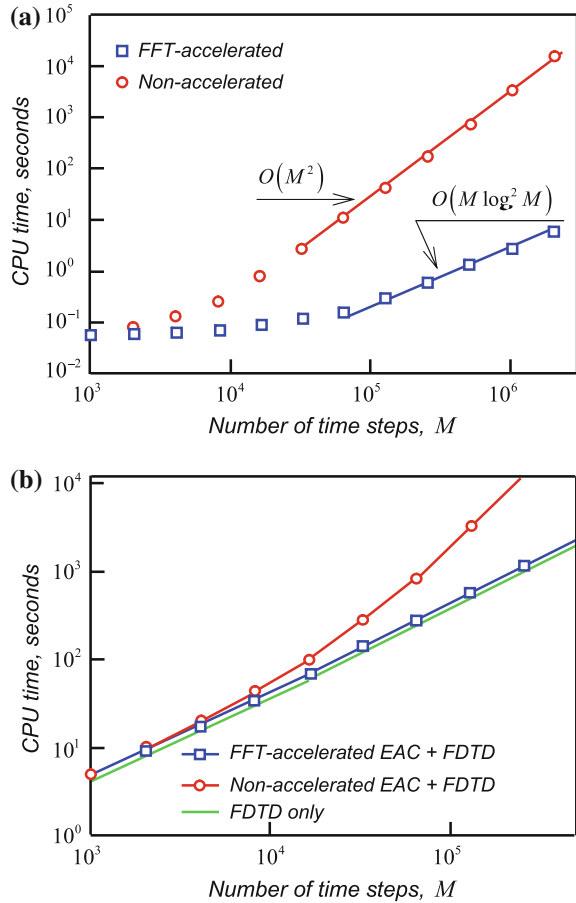
In the first example, the computational complexity estimates for $C_{\Gamma_1}^{\text{precomp, FFT}}$ and $C_{\Gamma_1}^{\text{precomp}}$ are verified and compared (without the FD calculation in Ω_{int}). To this end, a planar virtual boundary in the cross-section of a coaxial waveguide with the outer conductor radius $a_1 = 1.5$ and the inner conductor radius $b_1 = 0.9$ is considered (see Fig. 5.10) and the convolutions (5.100) are computed on this boundary (to be more precise, the discrete versions of (5.100) are computed). The space step is $\bar{h} = 0.01$, and the time step is $\bar{l} = 0.005$. The number of modes used for expanding the field $U^{i(1)}(g, t)$ is $N^{\text{mod}(i)} = 6$, the number of mesh cells used for discretizing the boundary equals to 61. Figure 5.11a presents the CPU times required by the blocked FFT-accelerated and non-accelerated computation while the number of time steps M is changed from 1000 to 2,000,000. As clearly shown here, theoretical estimates of the computational complexity are in good agreement with numerical experiment results. Also, Fig. 5.11a clearly shows that blocked FFT-accelerated computation becomes undoubtedly faster than non-accelerated computation when $M > 4000$.

The second example is designed to demonstrate the efficiency and accuracy of the blocked FFT-accelerated FD scheme. For this purpose, the same radiator, which was used as an example in the previous section to derive the computational complexity estimates is considered (see Fig. 5.10). The feeding structure is a coaxial waveguide with the outer conductor radius $a_1 = 1.0$ and the inner conductor radius $b_1 = 0.3$, the length of the elongated central conductor is $d = 1.57$. The space step is $\bar{h} = 0.02$, and the time step is $\bar{l} = 0.01$.

The structure is excited by a quasi-monochromatic *TEM*-signal (see (5.92) for *TM*₀-waves: $v_{n1}(z, t) \equiv 0, n = 1, 2, 3, \dots$), whose space-time amplitude $v_{01}(z, t)$ of the $H_\phi^{i(1)}$ -component is given on the boundary Γ_1 by the function $v_{01}(-L_1, t) = \cos(\tilde{k}t)$, where $\tilde{k} = 7.5$ is the central frequency. The virtual boundaries Γ_1 (planar) and Γ (spherical) are located at $z = -L_1 = -1.0$ and $r = L = 8.0$, respectively. Γ_1 is discretized using 36 cells, and the field $U^{s(1)}(\rho, z, t) = U(\rho, z, t) - U^{i(1)}(\rho, z, t)$ on Γ_1 is expanded using $N_{\Omega_1}^{\text{mod}(s)} = 5$ modes. Γ is discretized using 565 arc segments and the field $U(r, \vartheta, t)$ on it is expanded using $N_{\Omega_{\text{ext}}}^{\text{mod}(s)} = 30$ modes. The total number of mesh cells in the computation domain Ω_{int} is $P = 127,350$.

Figure 5.11b presents the CPU times required by the FD scheme with blocked FFT-accelerated EAC (see (5.259) for the computational complexity estimate), FD

Fig. 5.11 Radiator problem. CPU times versus number of time steps: **a** comparison of CPU times for FFT-accelerated and non-accelerated EAC; **b** comparison of total CPU times for FD schemes with FFT-accelerated and non-accelerated EAC and for the FD scheme itself. Reproduced courtesy of The Electromagnetics Academy



scheme with non-accelerated EAC (see (5.255) for the computational complexity estimate), and the FD scheme itself while the number of time steps M is changed from 1000 to 500,000. Figure 5.11b clearly demonstrates the efficiency of the blocked FFT-accelerated FD scheme.

To demonstrate that the blocked FFT-acceleration introduces only weak numerical noise in the solution, the H_ϕ -component for the field $U(\rho, z, t)$ computed at the point $\rho = 0.95$, $z = 1.7$ (see Fig. 5.10) by the FFT-accelerated and non-accelerated FD schemes are compared in Fig. 5.12. For this simulation, the same structure as in the previous one is utilized. $M = 8000$ and the radiator is excited by pulsed TEM -wave

$$\begin{aligned}
 U^{i(1)}(g, t) &= U_0^{i(1)}(g, t) : v_{01}(-L_1, t) \\
 &= 4 \cos[\tilde{k}(t - \tilde{T})] \sin[\Delta k(t - \tilde{T})] (t - \tilde{T})^{-1} \chi(\tilde{T} - t) = P_1(t),
 \end{aligned}$$

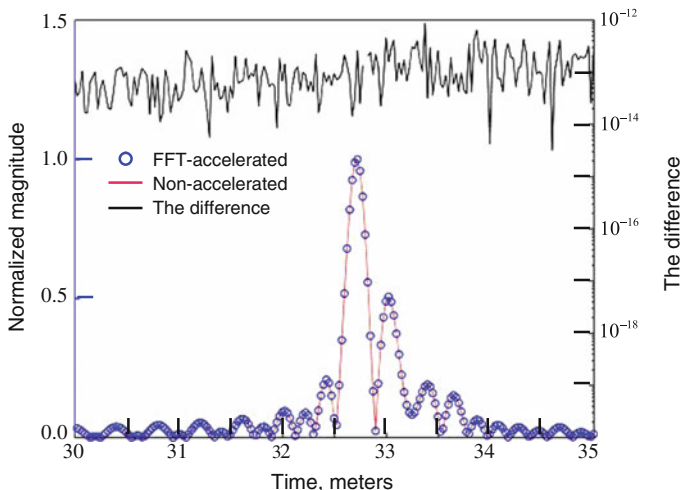
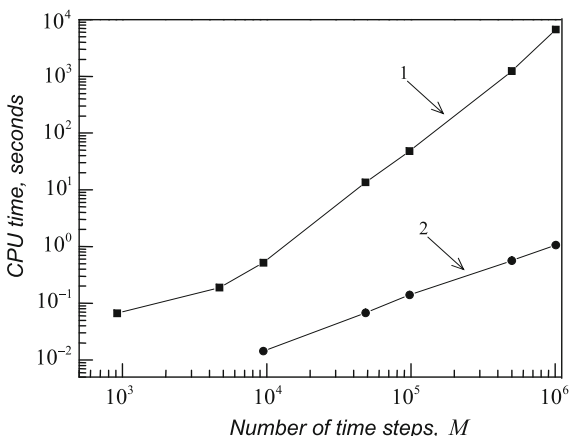


Fig. 5.12 The normalized magnitude of $|H_\phi(g, t)|$ recorded at the observation point and the difference between FFT-accelerated and nonaccelerated solutions ($\bar{h} = 0.01, \bar{l} = 0.005$). Reproduced courtesy of The Electromagnetics Academy

where $\tilde{k} = 7.5$ is the central frequency, $2\Delta k = 14.0$ is the bandwidth, $\tilde{T} = 30$ is the delay time, and $\bar{T} = 60$ is the signal duration. As expected the difference between two results is on the level of 10^{-13} , which is far below the error of the FD discretization scheme.

In closing it should be said that the optimized implementation of the blocked FFT-accelerated computation scheme described above was proposed in [63]. One result of this work we present in Fig. 5.13. Curve 1 shows the time of computing the convolution (5.200) of the signal

Fig. 5.13 Computation time for estimating the convolution integral (5.200). The calculations have been performed using the quadrature trapezoid formula (curve 1) and the optimized FFT-accelerated algorithm (curve 2)



$$\begin{aligned}
 u_n(0, t) &= S(t)P_1(t); \quad \tilde{k} = 6.25, \quad \Delta k = 2.75, \quad \tilde{T} = 25, \quad \bar{T} = 50, \\
 S(t) &= [x(t)]^2[3 - 2x(t)], \quad x(t) = t/25 \quad \text{for } 0 \leq t \leq 25 \\
 &\text{and } x(t) = (50 - t)/25 \quad \text{for } 25 \leq t \leq 50
 \end{aligned}$$

against the input array size. Curve 2 corresponds to the time of computing the same convolution using the optimized algorithm. For an array of one million elements, these times are equal to about 1.78 h and 1 s, respectively. The calculations were performed using a PC with a 3.0 GHz Intel Pentium 4 (Prescott) CPU and 4.0 GB of RAM.

5.7.5 Test Problems

Let an open axially symmetric resonator (a widening of a circular waveguide, see Fig. 5.14a) be excited from the domain Ω_1 by the pulsed TM_{01} -wave $U^{i(1)}(g, t) = U_1^{i(1)}(g, t)$ whose amplitude of the $E_\rho^{i(1)}$ -component equals $v_{11}^\rho(-L_1, t) = P_1(t)$; $\tilde{k} = 5.6, \Delta k = 2.1, \tilde{T} = 40, \bar{T} = 100$.

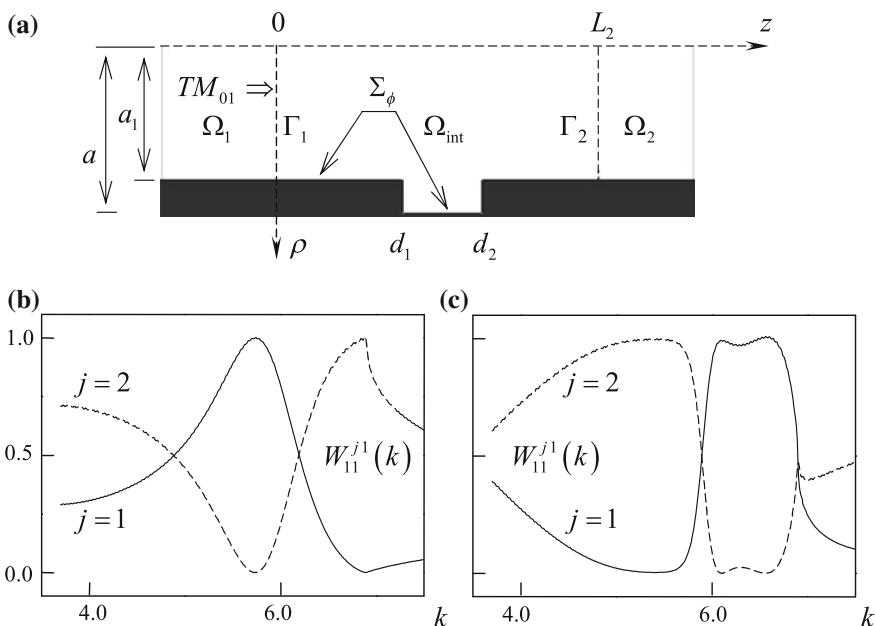


Fig. 5.14 a The widening of the circular waveguide ($a_1 = a_2 = 0.8, a = 1.0, L_1 = 0, d_1 = L_2 - d_2 = 0.5, k_{2j}^+ \approx 6.9$ is the cutoff frequency for TM_{02} -wave) and its energy characteristics: b $d_2 - d_1 = 0.3$ and c $d_2 - d_1 = 0.8$

The energy characteristics of the unit for two different lengths of its expanding part can be found in Fig. 5.14b, c ($\bar{h} = 0.005$, $\bar{l} = \bar{h}/2$, the number of modes of the secondary field taken into account in the discretization of nonlocal EAC similar to (5.94), (5.95) is equal to $N_{\Omega_1}^{\text{mod}(s)} = N_{\Omega_2}^{\text{mod}(s)} = 15$).

These characteristics replicate those obtained in [64] (see Fig. 93b in the book [64]) by one of the most reliable frequency-domain method, namely, the analytical regularization method [5, 39, 48, 65]. It is important that the results are practically identical as to determination of the points k of frequency band, at which a semi-transparent structure totally transmits ($W_{11}^{11}(k) = 0$, $W_{11}^{21}(k) = 1$) or totally reflects ($W_{11}^{11}(k) = 1$, $W_{11}^{21}(k) = 0$) the energy of the incident monochromatic TM_{01} -wave. The regimes of this kind are associated with excitation in the open waveguide resonator Ω_{int} of near-eigenmode oscillations [64, 66, 67]. Thus, the algorithms utilizing EACs adequately describe resonant situations.

Let now a cylindrical monopole extending the central conductor of coaxial feed line above the infinite perfectly conducting flange (see Fig. 5.15a: $a_1 = 0.00345$,

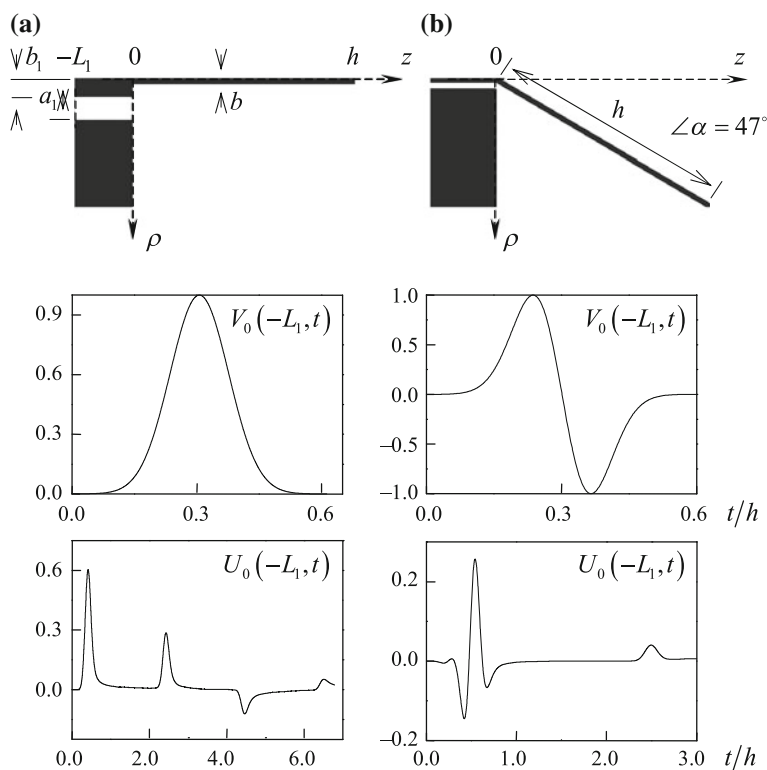


Fig. 5.15 The solutions to the test problems: **a** $\bar{h} = 0.00005$, $L = 0.13995$, $N_{\Omega_1}^{\text{mod}(s)} = 13$, $N_{\Omega_{\text{ext}}}^{\text{mod}(s)} = 40$; **b** $\bar{h} = 0.0001$, $L = 0.12$, $N_{\Omega_1}^{\text{mod}(s)} = 8$, $N_{\Omega_{\text{ext}}}^{\text{mod}(s)} = 35$

$b_1 = 0.0015$, $b = 0.00045$, $h = 0.1144$, $L_1 = 0.005$) be excited by the pulsed *TEM*-wave

$$U_0^{i(1)}(g, t) : v_{01}^\rho(-L_1, t) \sqrt{\ln(a_1/b_1)} = V_0(-L_1, t) \\ = \exp\left[-(t - \tilde{T})^2/4\tilde{\alpha}^2\right] \chi(2\tilde{T} - t) = P_2(t); \quad \tilde{T} = 0.035, \quad \tilde{\alpha} = 0.00569487$$

through the virtual boundary Γ_1 located in the cross-section $z = -L_1$ of the input waveguide.

The incident ($V_0(-L_1, t)$) and reflected ($U_0(-L_1, t)$) voltage pulses shown in Fig. 5.15a replicate in details (magnitude and sequence order of local extrema, distance between them, etc.) the same characteristics calculated for the same structure in the paper [68] (see Fig. 9b in [68]). Those pulses are determined by the $E_\rho(g, t)$ -components of the incident and reflected *TEM*-waves [69]:

$$\begin{Bmatrix} V_0(z, t) \\ U_0(z, t) \end{Bmatrix} = \begin{Bmatrix} v_{01}^\rho(z, t) \\ u_{01}^\rho(z, t) \end{Bmatrix} \int_{b_1}^{a_1} \mu_{01}^\rho(\rho) d\rho = \begin{Bmatrix} v_{01}^\rho(z, t) \\ u_{01}^\rho(z, t) \end{Bmatrix} \sqrt{\ln(a_1/b_1)}.$$

In [68], the experimental results for a prototype of a monopole antenna are also available. They agree well with the numerical results. The authors assert that nobody before could achieve better agreement between theory and experiment.

Our data are also in good agreement with the results obtained in [47] (see Fig. 2 in [47]) where a hollow conical monopole (Fig. 5.15b: $a_1 = 0.0023$, $b_1 = 0.001$, the slant height of cone is $h = 0.0997$, $L_1 = 0.01$) is illuminated by the pulsed *TEM*-wave

$$U_0^{i(1)}(g, t) : v_{01}^\rho(-L_1, t) \sqrt{\ln(a_1/b_1)} = V_0(-L_1, t) = AP_2(t)(\tilde{T} - t); \\ \tilde{T} = 0.03, \quad \tilde{\alpha} = 0.004533, \quad A = 257.186.$$

5.8 Conclusion

In this chapter, the problem of efficient truncation of computation domains of finite-difference or finite-element methods is discussed for 2-D and 3-D open (unbounded) electrodynamic structures. The original problem describing pulsed wave scattering on a compact waveguide discontinuity or on a compact free-space object is an initial boundary value problem formulated in an unbounded domain. EACs have been derived for virtual boundaries enveloping all sources and scatterers in order to truncate the computation domain and replace the original open

problem with an equivalent closed one formulated in now bounded computation domain.

It has been shown that for all situations under study, it is possible to prove that modified (closed) problems are uniquely solvable if original (open) problems are well-posed. The solutions to original and modified problems coincide; original and modified problems are equivalent. This result has been obtained by spreading the technique previously used in classical studies of initial boundary value problems with Dirichlet and Neumann boundary conditions (see, for example, [33, 41]) and for the first time applied for open problems with EACs in [9]. It can be now used for most problems involving EACs. Conceptually the proof of the equivalency completes the mathematical justification of the corresponding approach. The computation efficiency of the EACs-based approach was confirmed in a series of works [3, 8, 19, 21–27].

The EACs-based approach has been generalized to the case of extended and remote field sources. The analytical representation for transport operators converting near-zone fields into far-zone fields has been also derived.

Rigorous mathematical models of open compact structures are modified to fit applied problems involving structures of this kind. Models have been supplied with feeding waveguides to bridge the gap between models and real-world devices such as resonators and radiators of monochromatic and pulsed waves. Excitation of such structures as well as transformation of signals received by them is realized generally by means of various waveguides. The modifications allow to use almost with no changes the principal results associated with the efficient truncation of computation domains in problems for structures with feed lines. On this point, the idea of virtual waveguides with EACs in them is especially important.

Part of the chapter is devoted to practically important theoretical and methodological problems arising in the time-domain analysis of open resonators, namely, to relate spatial-temporal and spatial-frequency representations for electromagnetic field and to develop the algorithm for estimating principal electrodynamic characteristics of these structures.

The obtained analytic results together with a set of solvers and special programs developed by the authors and their colleague V. Pazynin were tested in numerical experiments devoted to testing and improving the EACs-based approach, and to calculation and physical analysis of electrodynamic characteristics of some open structures that are of interest to microwave theory and techniques [3, 8, 18, 19, 21–27].

In conclusion, it is worth noting once again that as opposed to the well-known approximate boundary conditions utilized by finite-difference and finite-element methods, namely ABCs and PMLs, EACs are exact by construction and do not introduce any additional error into algorithms and computations. This advantage is especially valuable in resonant situations, where numerical simulation requires large running time and calculating errors may grow unpredictably if an open problem is replaced by an insufficiently accurate closed problem.

References

1. Maikov, A.R., Sveshnikov, A.G., Yakunin, S.A.: A difference scheme for the non-stationary Maxwell equations in waveguide systems. *USSR Comput. Math. Math. Phys.* **26**(3), 130–138 (1986)
2. Sirenko, K.Y., Sirenko, Y.K.: Exact ‘absorbing’ conditions in the initial boundary value problems of the theory of open waveguide resonators. *Comput. Math. Math. Phys.* **45**(3), 490–506 (2005)
3. Sirenko, Y.K., Strom, S., Yashina, N.P.: *Modeling and Analysis of Transient Processes in Open Resonant Structures. New Methods and Techniques.* Springer, New York (2007)
4. Sirenko, K.Y., Sirenko, Y.K., Yashina, N.P.: Modeling and analysis of transients in periodic gratings. I. Fully absorbing boundaries for 2-D open problems. *J. Opt. Soc. Am. A* **27**(3), 532–543 (2010)
5. Sirenko, Y.K., Strom, S. (eds.): *Modern Theory of Gratings. Resonant Scattering: Analysis Techniques and Phenomena.* Springer, New York (2010)
6. Sirenko, K., Pazynin, V., Sirenko, Y., Bagci, H.: An FFT-accelerated FDTD scheme with exact absorbing conditions for characterizing axially symmetric resonant structures. *Prog. Electromagnet. Res.* **111**, 331–364 (2011)
7. Shafalyuk, O., Sirenko, Y., Smith, P.: Simulation and analysis of transient processes in open axially-symmetrical structures: method of exact absorbing boundary conditions. In: Zhurbenko, V. (ed.) *Electromagnetic Waves*, pp. 99–116. InTech, Rijeka (2011)
8. Kravchenko, V.F., Sirenko, Y.K., Sirenko, K.Y.: *Electromagnetic Wave Transformation and Radiation by the Open Resonant Structures. Modelling and Analysis of Transient and Steady-State Processes.* Fizmatlit, Moscow (2011) (in Russian)
9. Shafalyuk, O., Smith, P., Velychko, L.: Rigorous substantiation of the method of exact absorbing conditions in time-domain analysis of open electrodynamic structures. *Prog. Electromagnet. Res. B* **41**, 231–249 (2012)
10. Engquist, B., Majda, A.: Absorbing boundary conditions for the numerical simulation of waves. *Math. Comput.* **31**(139), 629–651 (1977)
11. Mur, G.: Absorbing boundary conditions for the finite-difference approximation of the time-domain electromagnetic-field equations. *IEEE Trans. Electromagnet. Capab.* **23**(4), 377–382 (1981)
12. Tirkas, P.A., Balanis, C.A., Renaut, R.A.: Higher order absorbing boundary conditions for FDTD-method. *IEEE Trans. Antennas Propag.* **40**(10), 1215–1222 (1992)
13. Mei, K.K., Fang, J.: Superabsorption—a method to improve absorbing boundary conditions. *IEEE Trans. Antennas Propag.* **40**(9), 1001–1010 (1992)
14. Berenger, J.-P.: A perfectly matched layer for the absorption of electromagnetic waves. *J. Comput. Phys.* **114**(1), 185–200 (1994)
15. Berenger, J.-P.: Three-dimensional perfectly matched layer for absorption of electromagnetic waves. *J. Comput. Phys.* **127**(2), 363–379 (1996)
16. Sacks, Z.S., Kingsland, D.M., Lee, R., Lee, J.F.: A perfectly matched anisotropic absorber for use as an absorbing boundary condition. *IEEE Trans. Antennas Propag.* **43**(12), 1460–1463 (1995)
17. Perov, A.O., Sirenko, Y.K., Yashina, N.P.: Explicit conditions for virtual boundaries in initial boundary value problems in the theory of wave scattering. *J. Electromagnet. Waves Appl.* **13**(10), 1343–1371 (1999)
18. Sirenko, Y.K., Velychko, L.G., Erden, F.: Time-domain and frequency-domain methods combined in the study of open resonance structures of complex geometry. *Prog. Electromagnet. Res.* **44**, 57–79 (2004)
19. Sirenko, K.Y., Pazynin, V.L.: Axially-symmetrical radiators of pulsed and monochromatic TE_{0n} - and TM_{0n} -waves. *Uspehi Sovremennoy Radioelektroniki* **4**, 52–69 (2006) (in Russian)
20. Velychko, L.G., Sirenko, Y.K., Velychko, O.S.: Time-domain analysis of open resonators. Analytical grounds. *Prog. Electromagnet. Res.* **61**, 1–26 (2006)

21. Sirenko, K.Y.: Slot resonances in axially symmetric radiators of pulse-modulated and monochromatic TM_{0n} -modes. *Telecommun. Radio Eng.* **66**(1), 9–21 (2007)
22. Sirenko, K.Y.: Splitting of super-broadband pulses by simple inhomogeneities of circular and coaxial waveguide. *Telecommun. Radio Eng.* **67**(16), 1415–1428 (2008)
23. Kuzmitchev, I.K., Melezhyk, P.M., Pazynin, V.L., Sirenko, K.Y., Sirenko, Y.K., Shafalyuk, O.S., Velychko, L.G.: Model synthesis of energy compressors. *Radiofizika I Elektronika* **13**(2), 166–172 (2008)
24. Velychko, L.G., Sirenko, Y.K.: Controlled changes in spectra of open quasi-optical resonators. *Prog. Electromagnet. Res. B* **16**, 85–105 (2009)
25. Sirenko, K.Y., Sirenko, Y.K., Yashina, N.P.: Modeling and analysis of transients in periodic gratings. II. Resonant wave scattering. *J. Opt. Soc. Am. A* **27**(3), 544–552 (2010)
26. Sirenko, K., Pazynin, V., Sirenko, Y., Bagci, H.: Compression and radiation of high-power short radio pulses. I. Energy accumulation in direct-flow waveguide compressors. *Progress In Electromagnetics Research* **116**, 239–270 (2011)
27. Sirenko, K., Pazynin, V., Sirenko, Y., Bagci, H.: Compression and radiation of high-power short radio pulses. II. A novel antenna array design with combined compressor/radiator elements. *Prog. Electromagnet. Res.* **116**, 271–296 (2011)
28. Taflov, A., Hagness, S.C.: *Computational Electrodynamics: The Finite-Difference Time-Domain Method*. Artech House, Boston (2000)
29. Rao, S.M. (ed.): *Time Domain Electromagnetics*. Academic Press, San Diego (1999)
30. Sirenko, K.Y.: Transport operators in the axially-symmetrical problems of the electrodynamics of pulsed waves. *Elektromagnitnye Volny I Elektronnye Sistemy* **11**(11), 15–26 (2006) (in Russian)
31. Kravchenko, V.F., Sirenko, K.Y., Sirenko, Y.K.: Transport operators and exact absorbing conditions in the plane problems of the electrodynamics of pulsed waves for compact open resonators with the waveguide feeder line. *Elektromagnitnye Volny I Elektronnye Sistemy* **14**(1), 4–19 (2009) (in Russian)
32. Borisov, V.V.: *Electromagnetic Fields of Transient Currents*. St. Petersburg University Press, St. Petersburg (1996) (in Russian)
33. Ladyzhenskaya, O.A.: *The Boundary Value Problems of Mathematical Physics*. Springer, New York (1985)
34. Korn, G.A., Korn, T.M.: *Mathematical Handbook for Scientists and Engineers*. McGraw-Hill, New York (1961)
35. Vladimirov, V.S.: *Equations of Mathematical Physics*. Dekker, New York (1971)
36. Abramowitz, M., Stegun, I.A. (eds.): *Handbook of Mathematical Functions*. Dover, New York (1972)
37. Bateman, H., Erdelyi, A.: *Tables of Integral Transforms*, vol. 1. McGraw-Hill, New York (1954)
38. Waynberg, B.R.: *Asymptotic Methods in the Equations of Mathematical Physics*. Moscow State University Press, Moscow (1982) (in Russian)
39. Sirenko, Y.K., Shestopalov, V.P., Yashina, N.P.: Free oscillations in coaxial-waveguide resonator. *Soviet J. Commun. Technol. Electron.* **32**(7), 60–67 (1987)
40. Gradshteyn, I.S., Ryzhik, I.M.: *Table of Integrals, Series, and Products*. Academic Press, San Diego, London (2000)
41. Mikhailov, V.P.: *Partial Differential Equations*. Mir Publishers, Moscow (1978)
42. Jackson, J.D.: *Classical Electrodynamics*. Wiley, New York (1975)
43. Bateman, H., Erdelyi, A.: *Higher Transcendental Functions*. McGraw-Hill, New York (1953)
44. Prudnikov, A.P., Brychkov, Y.A., Marichev, O.I.: *Integrals and Series*, vol. 2. Gordon & Breach, New York (1986)
45. von Hurwitz, A.: *Allgemeine Funktionentheorie und Elliptische Funktionen*. In: von Courant, R. (ed.) *Geometrische Funktionentheorie*. Springer, Berlin (1964) (in German)
46. Maloney, J.G., Smith, G.S., Scott, W.R.: Accurate computation of the radiation from simple antennas using the finite-difference time-domain method. *IEEE Trans. Antennas Propag.* **38**(7), 1059–1068 (1990)

47. Montoya, T.P., Smith, G.S.: A study of pulse radiation from several broad-band monopoles. *IEEE Trans. Antennas Propag.* **44**(8), 1172–1182 (1996)
48. Shestopalov, V.P., Tuchkin, Y.A., Poyedinchuk, A.Y., Sirenko, Y.K.: New solution methods for direct and inverse problems of the diffraction theory. In: *Analytical Regularization of the Boundary Value Problems in Electromagnetic Theory*. Osnova, Kharkov (1997) (in Russian)
49. Colton, D., Kress, R.: *Integral Equation Methods in Scattering Theory*. Wiley-Interscience, New York (1983)
50. Reed, M., Simon, B.: *Methods of Modern Mathematical Physics. Analysis of Operators*. Academic Press, New York, IV (1978)
51. Keldysh, M.V.: On the completeness of eigenfunctions of some classes of non-selfadjoint linear operators. *Russian Math. Surv.* **26**(4), 15–44 (1971)
52. Bamberger, A., Joly, P., Roberts, J.E.: Second order absorbing boundary conditions for the wave equation: a solution for the corner problem. *SIAM J. Numer. Anal.* **27**(2), 323–352 (1990)
53. Collino, F.: *Conditions Absorbantes D'ordre Eleve Pour des Modeles de Propagation D'onde Dans des Domaines Rectangulaires*. Rocquencourt, France: Report I.N.R.I.A. No.1790 (1993) (in French)
54. Levin, L.: *Theory of Waveguides: Techniques for Solution of Waveguide Problems*. Newnes-Butterworths, London (1975)
55. Balanis, C.A.: *Antenna Theory: Analysis and Design*. Wiley, New York (1982)
56. Velychko, L.G., Sirenko, Y.K., Vinogradova, E.D.: Analytical grounds for modern theory of two-dimensionally periodic gratings. In: Kishk, A. (ed.) *Solutions and Applications of Scattering, Propagation, Radiation and Emission of Electromagnetic Waves*, pp. 123–158. InTech, Rijeka (2012)
57. Kantartzis, N.V., Tsiboukis, T.D.: *High Order FDTD Schemes for Waveguide and Antenna Structures*. Morgan & Claypool, San Rafael, CA (2006)
58. Gerald, C.F., Wheatley, P.O.: *Applied Numerical Analysis*. Addison-Welsley, Boston (1999)
59. Bagci, H., Yilmaz, A.E., Lomakin, V., Michielssen, E.: Fast solution of mixed-potential time-domain integral equations for half-space environments. *IEEE Trans. Geosci. Remote Sens.* **43**(2), 269–279 (2005)
60. Bagci, H., Yilmaz, A.E., Jin, J.-M., Michielssen, E.: Fast and rigorous analysis of EMC/EMI phenomena on electrically large and complex structures loaded with coaxial cables. *IEEE Trans. Electromagnet. Capab.* **49**(2), 361–381 (2007)
61. Bagci, H., Yilmaz, A.E., Michielssen, E.: An FFT-accelerated time-domain multiconductor transmission line simulator. *IEEE Trans. Electromagnet. Capab.* **52**(1), 199–214 (2010)
62. Oppenheim, A.V., Schaffer, R.W., Buck, J.R.: *Discrete-Time Signal Processing*. Prentice-Hall, Englewood Cliffs, NJ (1999)
63. Pazynin, V.L.: Compression of frequency-modulated electromagnetic pulses in sections of regular waveguides. *Telecommun. Radio Eng.* **71**(20), 1833–1857 (2012)
64. Shestopalov, V.P., Kirilenko, A.A., Rud', L.A.: *Resonance Wave Scattering. Waveguide Discontinuities*, vol. 2. Naukova Dumka, Kiev (1986) (in Russian)
65. Shestopalov, V.P., Kirilenko, A.A., Masalov, S.A.: *Matrix Convolution-Type Equations in the Diffraction Theory*. Naukova Dumka, Kiev (1984) (in Russian)
66. Pochanina, I.E., Yashina, N.P.: Electromagnetic properties of open waveguide resonator. *Electromagnetics* **13**(3), 289–300 (1993)
67. Yashina, N.P.: Accurate analysis of coaxial slot bridge. *Microwave Opt. Technol. Lett.* **20**(5), 345–349 (1999)
68. Maloney, J.G., Smith, G.S.: A study of transient radiation from the Wu-King resistive monopole—FDTD analysis and experimental measurements. *IEEE Trans. Antennas Propag.* **41**(5), 668–676 (1993)
69. Shirman, Ya.D.: *Radio Ducts and Resonant Cavities*. Svyaz'izdat, Moscow (1959) (in Russian)

Chapter 6

High-Power Short Pulses Compression: Analysis and Modeling

Vadym Pazynin, Kostyantyn Sirenko and Yuriy Sirenko

Abstract The chapter discusses practically realizable algorithms of model synthesis of direct-flow compressors built on the basis of rectangular, circular or coaxial waveguides. Resonance and distributed switches have been designed to ensure effective energy accumulation and release into output waveguides or free space. The authors dwell on peculiarities of radiation of high-power short pulses by simple monopole antennas with coaxial feeding waveguides. They also design a novel phased antenna array, whose each radiating element is an active compressor. Particular attention is given to the study of such physical processes in compressors as energy accumulation, switching from the accumulation mode into the mode of energy release, and radiation of short high-power pulses into free space.

6.1 Introduction

This chapter presents our approach to studies of microwave energy compression, namely modeling, analysis, and design of compressors and radiators. *Energy compressor* is a device for converting long low-amplitude input pulses into short high-amplitude output pulses.

Design of a properly working energy compressor requires in-depth study of the energy accumulation process. As this process is non-monotonic in time, a real-time

V. Pazynin · Y. Sirenko
O.Ya. Usikov Institute for Radiophysics and Electronics,
National Academy of Sciences, Kharkiv, Ukraine
e-mail: pazynin@ire.kharkov.ua

Y. Sirenko
e-mail: yks@ire.kharkov.ua

K. Sirenko (✉)
King Abdullah University of Science and Technology, Thuwal, Saudi Arabia
e-mail: k.sirenko@gmail.com

Y. Sirenko
L.N. Gumilyov Eurasian National University, Astana, Republic of Kazakhstan

study is required to get an insight into all pertinent physical phenomena. In this chapter, we consider the processes inside a compressor, from the very beginning of excitation right to the accumulated energy release, in the time domain. We also discuss the influence of various parameters on the energy accumulation efficiency and, thus, the overall compressor performance.

The following topics are discussed in this chapter. First, the rigorous scheme to design and analyze energy compressors. Second, estimation of the influence on the compressor efficiency of various parameters. Third, studies of a monopole antenna mounted on a ground plane to demonstrate that compressed pulses can be efficiently radiated by simple antennas. Fourth, a novel array design, each of the array elements combines a compressor and a radiator. Fifth, the efficient scheme to determine the law of amplitude and frequency modulation of the input pulse for passive compressors based on hollow waveguides. Sixth, demonstration that the kinematical approximation is inapplicable for the rigorous description of broadband pulse propagation in dispersive systems.

One section in the book [1] is devoted to the model synthesis of *resonant quasi-optical devices*. An approach developed therein has been originally described in [2] as applied to microwave energy compressors. The approach includes the following steps: estimation of the functional capabilities of isolated components, matching these capabilities with the functionality of the unit as a whole, construction of the corresponding mathematical model, electrodynamic analysis and design of the unit and its components paying particular attention to optimization of the device.

Mathematically we deal here with *open boundary value problems* or *open initial boundary value problems*, i.e. problems whose domain of analysis is infinite in one or more directions. An efficient technique combining time-domain and frequency-domain methods have been proposed to solve this kind of problems. The basic idea was to use the so-called exact absorbing conditions (EACs) [1, 3–8], which are discussed in details in Chap. 5 of this book, in finite-difference or finite-element algorithms [9–11] and to invoke the time-domain analysis of open resonators [12–14]. EACs-enabled methods allow one to analyze initial boundary value problems in bounded domains and for long time intervals and to obtain reliable numerical data describing transient processes under resonant conditions [1, 2, 4, 7, 14–16]. EACs-enabled methods suit best for reliable and precise analysis of the energy accumulation process in *active compressors*, which are high-Q resonant systems excited by long pulses [17–19], and compressors' switches. We have also proposed to apply EACs-enabled methods to the study of the compression of frequency-modulated pulses propagating long distances in dispersive guiding structures like *passive compressors* [20]. The proposed algorithms are based on exact analytical representations for the so-called transport operators, which allow to compute far-zone fields knowing only near-zone fields (see Chap. 5 and [1, 7, 21–24]).

The developed methods and algorithms have been implemented in the special-purpose software packages for 2-D (and partially for 3-D) simulations and analysis of energy compressors and radiators of short high-power pulses. Devices under study are: (i) *cross-uniform regular waveguides* for passive compression,

(ii) *storage units* (waveguide and open resonators with metal, semitransparent, and frequency-selective mirrors), and (iii) *switches* (distributed grating-type switches for compressors on multimode waveguides and for resonant radiators, interference and resonant switches for compressors with single-mode output waveguides) for active compression.

In Sect. 6.2 we briefly consider models, which are employed in numerical experiments using EAC-enabled methods. A detailed discussion of these models and associated analytical results can be found in Chap. 5 of this book. In Sect. 6.3 we study in details the analysis and design of active microwave energy compressors. The methodology and results from Sect. 6.3 are used in Sect. 6.4 to study radiation of short pulses by a monopole antenna and to design a novel combined compressor/radiator antenna element for a phased array. Section 6.5 is devoted to the aforementioned algorithm for calculating the time profiles of pulses propagating in hollow waveguides.

We use SI, the International System of Units, for all physical parameters except the ‘time’ t that is the product of the natural time and the velocity of light in vacuum, thus t is measured in meters. In this chapter, dimensions are omitted as a rule. The obtained results are formulated in terms of relative values and can be generalized to all geometrically similar structures.

6.2 Exact Absorbing Conditions Method: 2-D Case

6.2.1 Planar Structures

Let $\vec{E}(g, t) = \{E_x, E_y, E_z\}$ and $\vec{H}(g, t) = \{H_x, H_y, H_z\}$ ($g = \{y, z\}$) be the electric and magnetic vectors of the E -polarized ($E_y = E_z = H_x \equiv 0$) or H -polarized ($H_y = H_z = E_x \equiv 0$) electromagnetic field. Let a planar structure (Fig. 6.1) be excited by a pulsed TE_{0n} - or TM_{0n} -wave $U_p^{i(1)}(g, t)$ incident onto the virtual boundary Γ_1 from the regular parallel-plate waveguide Ω_1 . Let also $\sigma(g, t) \geq 0$ be the specific conductivity of a locally inhomogeneous medium. Its time dependence allows us to simulate changes in compressor’s mode of operation. $\varepsilon(g) \geq 1$ and $\mu(g) \equiv 1$ are the relative permittivity and magnetic permeability of the medium; $\eta_0 = (\mu_0/\varepsilon_0)^{1/2}$ is the impedance of free space; ε_0 and μ_0 are the electric and magnetic constants of vacuum; $\{x, y, z\}$ are the Cartesian coordinates and $\{\rho, \phi\}$ are the polar coordinates in the yOz plane. By $\Sigma = \Sigma_x \times [|x| \leq \infty]$ we denote perfectly conducting surfaces obtained by moving the piecewise smooth curves Σ_x along the x -axis. $\Sigma^{\varepsilon, \sigma} = \Sigma_x^{\varepsilon, \sigma} \times [|x| \leq \infty]$ are the surfaces on which the functions $\varepsilon(g)$ and/or $\sigma(g, t)$ have discontinuities. Symbol ‘ \times ’ denotes the direct product of two sets.

The basis for all planar models considered in this chapter is the *closed* (i.e., formulated on a bounded computation domain) *initial boundary value problem*

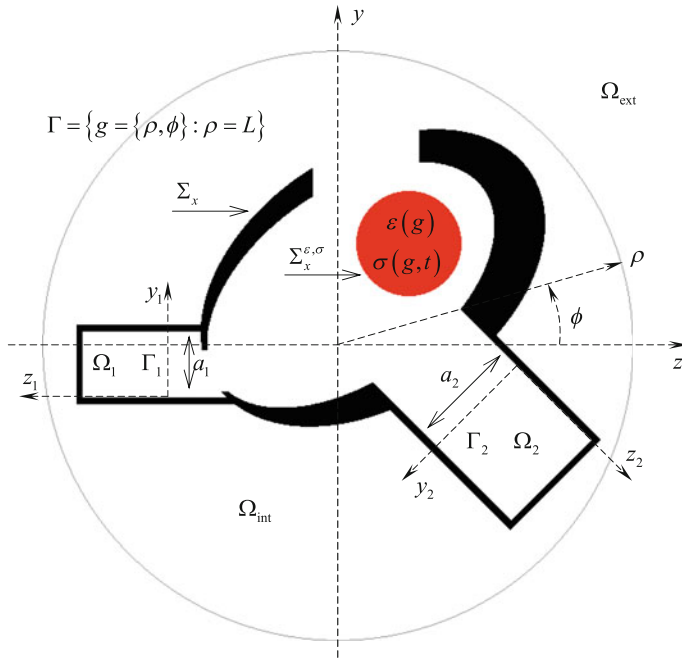


Fig. 6.1 Planar structure

$$\begin{cases}
 \left[-\varepsilon(g) \frac{\partial^2}{\partial t^2} - \eta_0 P + \frac{\partial^2}{\partial y^2} + \frac{\partial^2}{\partial z^2} \right] U(g, t) = 0; & t > 0, \quad g \in \Omega_{\text{int}} \\
 U(g, t)|_{t=0} = 0, \quad \frac{\partial}{\partial t} U(g, t)|_{t=0} = 0; & g = \{y, z\} \in \bar{\Omega}_{\text{int}} \\
 \vec{E}_{tg}(q, t) \text{ and } \vec{H}_{tg}(q, t) \text{ are continuous when crossing } \Sigma^{\varepsilon, \sigma}, \\
 \vec{E}_{tg}(q, t)|_{q=\{x, y, z\} \in \Sigma} = 0, \quad \text{and } D[U(g, t)]|_{g \in \Gamma} = 0, \\
 D_1[U(g, t) - U_p^{i(1)}(g, t)]|_{g \in \Gamma_1} = 0, \quad D_2[U(g, t)]|_{g \in \Gamma_2} = 0; & t \geq 0
 \end{cases} \quad (6.1a)$$

and the radiation conditions (RCs)

$$\begin{aligned}
 U(g_j, t) - \delta_j^1 U_p^{i(1)}(g_j, t) = & - \sum_{n=0}^{\infty} \begin{cases} \int_0^{t-z_j} J_0 \left[\lambda_{nj} \left((t-\tau)^2 - z_j^2 \right)^{1/2} \right] \\ 1 \text{ for } E \text{ - case} \\ 0 \text{ for } H \text{ - case} \end{cases} \\
 & \times \left[\int_{b_j^{(1)}}^{a_j^{(2)}} \frac{\left[\partial U(\tilde{y}_j, \tilde{z}_j, \tau) - \delta_j^1 U_p^{i(1)}(\tilde{y}_j, \tilde{z}_j, \tau) \right]}{\partial \tilde{z}_j} \Big|_{\tilde{z}_j=0} \mu_{nj}(\tilde{y}_j) d\tilde{y}_j \right] d\tau \Big\} \mu_{nj}(y_j); \\
 g_j = \{y_j, z_j\} \in \bar{\Omega}_j, \quad t \geq z_j, \quad j = 1, 2,
 \end{aligned} \quad (6.1b)$$

$$\begin{aligned}
U(\rho, \phi, t) &= \frac{1}{2} \sqrt{\frac{L}{\rho}} U(L, \phi, t - \rho + L) \\
&+ \frac{1}{\pi} \sqrt{\frac{L}{\rho}} \sum_{n=0, \pm 1, \pm 2, \dots} (-1)^n \mu_n(\phi) \int_0^{t-(\rho-L)} \left\{ \frac{u_n(L, \tau)}{2L} \right. \\
&\times \left[\mathcal{Q}'_{|n|-1/2}(-a_{L,\rho}) \left(\frac{\rho^2 - L^2 - (t - \tau)^2}{L\rho} \right) - \mathcal{Q}_{|n|-1/2}(-a_{L,\rho}) \right] \\
&\left. - u'_n(L, \tau) \mathcal{Q}_{|n|-1/2}(-a_{L,\rho}) \right\} d\tau; \quad \rho \geq L, \quad 0 \leq \phi \leq 2\pi, \quad t \geq 0
\end{aligned} \tag{6.1c}$$

for outgoing (into the domains Ω_j and $\Omega_{\text{ext}} = \{g = \{\rho, \phi\} : \rho > L, 0 \leq \phi \leq 2\pi\}$) pulsed waves. Here, $U(g, t) = E_x(g, t)$ and $P[U] \equiv \partial[\sigma(g, t)U(g, t)]/\partial t$ in the case of E -polarization, and $U(g, t) = H_x(g, t)$ and $P[U] \equiv \sigma(g, t) \times \partial U(g, t)/\partial t$ in the case of H -polarization.

The functions $\sigma(g, t)$ and $\varepsilon(g) - 1$, which have compact supports in the closure of Ω_{int} , are supposed to satisfy the theorem on the unique solvability of the problem (6.1a, 6.1b, 6.1c) in the Sobolev space $W_2^1(\Omega_{\text{int}} \times (0, T))$, $T < \infty$ [1, 8]. All scatterers described by the piecewise constant functions $\varepsilon(g)$, $\sigma(g, t)$ and by the piecewise smooth contours Σ_x and $\Sigma_x^{\varepsilon, \sigma}$ are located in Ω_{int} .

In (6.1b), $J_0(\dots)$ is the Bessel cylindrical function, δ_j^l is the Kronecker symbol, $g_j = \{y_j, z_j\}$ is the local coordinate system associated with the virtual waveguide Ω_j (see Fig. 6.1). In the parallel-plate waveguide Ω_j , the *transverse functions* $\mu_{nj}(y_j)$ form an orthonormal system, and λ_{nj} are the *transverse eigenvalues* associated with $\mu_{nj}(y_j)$. In the case of E -polarization, we have $\mu_{nj}(y_j) = \sqrt{2/a_j} \sin(n\pi y_j/a_j)$ and $\lambda_{nj} = n\pi/a_j$ ($n = 1, 2, 3, \dots$). In the case of H -polarization, we have $\mu_{nj}(y_j) = \sqrt{(2 - \delta_0^n)/a_j} \cos(n\pi y_j/a_j)$ and $\lambda_{nj} = n\pi/a_j$ ($n = 0, 1, 2, \dots$).

In (6.1c), $\mu_n(\phi) = (2\pi)^{-1/2} \exp(in\phi)$ ($n = 0, \pm 1, \pm 2, \dots$); $\mathcal{Q}_{|n|-1/2}(\dots)$ is the second-kind Legendre function; $\mathcal{Q}'_{|n|-1/2}(-a) = \partial \mathcal{Q}_{|n|-1/2}(x)/\partial x|_{x=-a}$; $a_{L,\rho} = [L^2 + \rho^2 - (t - \tau)^2] / (2\rho L)$; $u(\rho, t) = \{u_n(\rho, t)\}_n$ is the *evolutionary basis* for the outgoing (into free space) pulsed wave $U(\rho, \phi, t)$ which could be represented as

$$\begin{aligned}
U(\rho, \phi, t) &= \sum_n u_n(\rho, t) \mu_n(\phi); \quad g = \{\rho, \phi\} \in \bar{\Omega}_{\text{ext}}, \quad t \geq 0, \quad \text{and} \\
u_n(\rho, t) &= \int_0^{2\pi} U(\rho, \phi, t) \mu_n^*(\phi) d\phi
\end{aligned} \tag{6.2a}$$

(the asterisk ** stands for the complex conjugation); and $u_n'(L, \tau) = \partial u_n(\rho, t) / \partial \rho|_{\rho=L}$.

The computation domain Ω_{int} is the part of the yOz plane bounded by the contours Σ_x together with the virtual boundaries Γ_1 and Γ_2 (input and output ports in the cross-sections $z_1 = 0$ and $z_2 = 0$ of the virtual waveguides Ω_1 and Ω_2) and the cylindrical virtual boundary Γ separating the domains Ω_{int} and Ω_{ext} (free space).

The EAC operators $D_1[\dots]$, $D_2[\dots]$, and $D[\dots]$ are derived by placing the observation point in (6.1b) and (6.1c) onto the virtual boundaries Γ_1 , Γ_2 and Γ . The function $U_p^{i(1)}(g, t)$ in EAC $D_1[U(g, t) - U_p^{i(1)}(g, t)]|_{g \in \Gamma_1} = 0$ represents a pulsed wave incident on Γ_1 from Ω_1 . The following relations are true for this wave:

$$\begin{aligned} U_p^{i(1)}(g_1, t) &= v_{p1}(z_1, t)\mu_{p1}(y_1); \quad g_1 \in \Omega_1, \quad t \geq 0, \\ v_{p1}(z_1, t) &= \int_0^{a_1} U_p^{i(1)}(g_1, t)\mu_{p1}(y_1)dy_1. \end{aligned} \quad (6.2b)$$

Scattered waves traveling away from Ω_{int} in the waveguides Ω_1 and Ω_2 can be represented in the form

$$\begin{aligned} U^{s(1)}(g_1, t) &= U(g_1, t) - U_p^{i(1)}(g_1, t) = \sum_n u_{n1}(z_1, t)\mu_{n1}(y_1); \quad g_1 \in \Omega_1, \\ t \geq 0, \quad u_{n1}(z_1, t) &= \int_0^{a_1} U^{s(1)}(g_1, t)\mu_{n1}(y_1)dy_1 \end{aligned} \quad (6.2c)$$

and

$$\begin{aligned} U^{s(2)}(g_2, t) &= U(g_2, t) = \sum_n u_{n2}(z_2, t)\mu_{n2}(y_2); \quad g_2 \in \Omega_2, \quad t \geq 0, \\ u_{n2}(z_2, t) &= \int_0^{a_2} U^{s(2)}(g_2, t)\mu_{n2}(y_2)dy_2. \end{aligned} \quad (6.2d)$$

In the frequency domain, the formulas (6.2a, 6.2b, 6.2c, 6.2d) take the following form:

$$\tilde{U}(g, k) = \sum_{n=-\infty}^{\infty} C_n(k)H_n^{(1)}(k\rho)\mu_n(\phi); \quad g \in \bar{\Omega}_{\text{ext}}, \quad (6.3a)$$

$$\tilde{U}_p^{i(1)}(g_1, k) = A_{p1}(k) \exp(-i\beta_{p1}z_1)\mu_{p1}(y); \quad g \in \bar{\Omega}_1, \quad (6.3b)$$

$$\begin{aligned}\tilde{U}^{s(1)}(g_1, k) &= \tilde{U}(g_1, k) - \tilde{U}_p^{i(1)}(g_1, k) \\ &= \sum_{n=1}^{\infty} B_{n1}(k) \exp(i\beta_{n1}z_1) \mu_{n1}(y); \quad g \in \bar{\Omega}_1, \quad (6.3c) \\ n &= \begin{cases} 1 & \text{for } E\text{-case} \\ 0 & \text{for } H\text{-case} \end{cases}\end{aligned}$$

$$\begin{aligned}\tilde{U}^{s(2)}(g_2, k) &= \tilde{U}(g_2, k) = \sum_{n=1}^{\infty} B_{n2}(k) \exp(i\beta_{n2}z_2) \mu_{n2}(y); \quad g \in \bar{\Omega}_2. \\ n &= \begin{cases} 1 & \text{for } E\text{-case} \\ 0 & \text{for } H\text{-case} \end{cases}\end{aligned} \quad (6.3d)$$

Here, $A_{p1}(k) = \tilde{v}_{p1}(0, k) \leftrightarrow v_{p1}(0, t)$, $B_{nj}(k) = \tilde{u}_{nj}(0, k) \leftrightarrow u_{nj}(0, t)$, and $C_n(k)H_n^{(1)}(k\rho) = \tilde{u}_n(\rho, k) \leftrightarrow u_n(\rho, t)$ are the complex-valued amplitudes of monochromatic waves generating a steady-state field $\{\tilde{\vec{E}}(g, k), \tilde{\vec{H}}(g, k)\}$ in the domains Ω_j and Ω_{ext} ; $H_n^{(1)}(\dots)$ is the Hankel function of the first kind; $\beta_{nj}(k) = \sqrt{k^2 - \lambda_{nj}^2}$ are the *longitudinal propagation numbers* for the waveguide modes $U_n^{s(j)}(g_j, k) = B_{nj}(k) \exp(i\beta_{nj}z_j) \mu_{nj}(y)$ with $\text{Re } \beta_{nj}(k) \text{Re } k \geq 0$ and $\text{Im } \beta_{nj}(k) \geq 0$; k is the *complex wavenumber (frequency parameter or frequency)*; $\tilde{f}(k) \leftrightarrow f(t)$ stands for the Laplace transform

$$\tilde{f}(k) = \int_0^{\infty} f(t) e^{ikt} dt \leftrightarrow f(t) = \frac{1}{2\pi} \int_{i\alpha - \infty}^{i\alpha + \infty} \tilde{f}(k) e^{-ikt} dk; \quad 0 \leq \alpha \leq \text{Im } k. \quad (6.4)$$

The frequencies $k = k_{nj}^{\pm} = \pm |\lambda_{nj}|$ are the *cutoff frequencies*. On these frequencies, the longitudinal propagation numbers $\beta_{nj}(k)$ vanish, as on larger frequencies monochromatic modes $U_n^{s(j)}(g_j, k)$ propagate without decay.

Consider the values of k such that $\text{Re } k > 0$ and $\text{Im } k = 0$. In this case, the frequency parameter takes the physical value of $k = 2\pi/\lambda$, where λ is the wavelength in free space. Let also an open planar structure (Fig. 6.1) be fed from the waveguide Ω_1 by an undamped sinusoidal wave $\tilde{U}_p^{i(1)}(g_1, k)$ with $\text{Im } \beta_{p1} = 0$. Then the structure is completely described by the following characteristics.

- *Reflection and transmission coefficients*

$$R_{np}^{11}(k) = \left. \frac{\tilde{u}_{n1}(z_1, k)}{\tilde{v}_{p1}(z_1, k)} \right|_{z_1=0} = \frac{B_{n1}(k)}{A_{p1}(k)} \quad \text{and} \quad T_{np}^{21}(k) = \left. \frac{\tilde{u}_{n2}(z_2, k)}{\tilde{v}_{p1}(z_1, k)} \right|_{z_1=0} = \frac{B_{n2}(k)}{A_{p1}(k)},$$

which characterize the efficiency of transformation of the wave $\tilde{U}_p^{i(1)}(g_1, k)$ incoming from the waveguide Ω_1 into the waves $\tilde{U}_n^{s(1)}(g_1, k)$ and $\tilde{U}_n^{s(2)}(g_2, k)$ propagating in the waveguides Ω_1 and Ω_2 .

- *Energy distribution between waveguide modes*; the values

$$W_{np}^{11}(k) = \left| R_{np}^{11} \right|^2 \frac{\operatorname{Re} \beta_{n1}}{\beta_{p1}} \quad \text{and} \quad W_{np}^{21}(k) = \left| T_{np}^{21} \right|^2 \frac{\operatorname{Re} \beta_{n2}}{\beta_{p1}}$$

determine the relative parts of energy diverted into the waveguides Ω_1 and Ω_2 (the energy of the waves $\tilde{U}_n^{s(1)}(g_1, k)$ and $\tilde{U}_n^{s(2)}(g_2, k)$ propagating without decay).

- *Ohmic loss*; the value

$$W_{\text{abs}}(k) = \frac{k\beta}{\beta_{p1}} \int_{\Omega_{\text{int}}} \sigma(g) \left| \tilde{E}(g, k) \right|^2 dg \quad (6.5)$$

determine the relative part of energy lost to absorption. Here, $\beta = \eta_0$ in the case of E -polarized waves and $\beta = \eta_0^{-1}$ in the H -case; $dg = dydz$ is the surface element.

- *Radiation efficiency or antenna efficiency*, which is calculated by the formula

$$\eta(k) = 1 - W_{\text{abs}} - \sum_n \left(W_{np}^{11} + W_{np}^{21} \right).$$

- *Normalized directional pattern* on the arc $\rho = M \geq L$

$$D(\phi, k, M) = \frac{\left| \tilde{E}_{tg}(M, \phi, k) \right|^2}{\max_{0 \leq \bar{\phi} \leq 2\pi} \left| \tilde{E}_{tg}(M, \bar{\phi}, k) \right|^2}; \quad 0 \leq \phi \leq 360^\circ, \quad K_1 \leq k \leq K_2, \quad (6.6)$$

determines the spatial orientation and the energy content of the propagating waves radiated into free space. Here, $\tilde{E}_{tg}(M, \phi, k)$ is the tangential (to the cylindrical surface $\{q = \{\rho, \phi, x\}: \rho = M, 0 \leq \phi \leq 2\pi, |x| < \infty\}$) component of the monochromatic electric field $\tilde{E}(g, k)$.

- *Main lobe* of the pattern is directed at an angle $\bar{\phi}(k)$ such that $D(\bar{\phi}(k), k, M) = 1$.
- *Half-power beamwidth* $\phi_{0,5}(k)$ is an angle between two directions of the main lobe, where the power reduces to the half of its maximum, i.e. $\phi_{0,5}(k) = |\phi^+ - \phi^-|$, where $D(\phi^+, k, M) = 0.5$ and $D(\phi^-, k, M) = 0.5$.

- *Complex eigenfrequencies* $\bar{k}_m \in C_k$, where $\bar{k}_m = \text{Re } \bar{k}_m + i\text{Im}\bar{k}_m$, $\text{Im}\bar{k}_m < 0$. These frequencies ensure existence of nontrivial solutions $\tilde{U}(g, \bar{k}_m)$ to the boundary value (spectral) problem associated with the homogeneous problem in (6.1a, 6.1b, 6.1c), i.e. the problem with $U_p^{i(1)}(g, t) \equiv 0$. The function $\tilde{U}(g, \bar{k}_m)$ ($g \in \Omega_{\text{int}}$) represents a *free oscillation* with the eigenfrequency \bar{k}_m . The *quality factor* of the oscillation with the frequency \bar{k}_m is defined as $Q = \text{Re } \bar{k}_m / 2 |\text{Im}\bar{k}_m|$. Here, C_k is the first (physical) sheet of the Riemann surface, which determines natural boundaries for the analytical continuation in k of the boundary value problem associated with (6.1a, 6.1b, 6.1c) [1, 13].

The following time-domain characteristics are related with the energy accumulation:

- *Energy efficiency*

$$\gamma = \frac{W^{s(2)}(t_3; t_4)}{W^{i(1)}(t_1; t_2)} \quad \text{or} \quad \gamma = \frac{W^s(t_3; t_4)}{W^{i(1)}(t_1; t_2)}$$

is the output-to-input energy ratio. Here, $W^{i(1)}(t_1; t_2)$ and $W^{s(2)}(t_3; t_4)$ or $W^s(t_3; t_4)$ represent the total energy received by a compressor from the waveguide Ω_1 during the interval $t_1 < t < t_2$, and the energy transmitted into the domains Ω_2 or Ω_{ext} , respectively, during the interval $t_3 < t < t_4$. $W^{i \text{ or } s(j)}(t_3; t_4)$ and $W^s(t_3; t_4)$ are calculated using the following formulas:

$$W^{i \text{ or } s(j)}(t_{\text{start}}; t_{\text{finish}}) = (- \text{ or } +) \int_{t_{\text{start}}}^{t_{\text{finish}}} P^{i \text{ or } s(j)}(t) dt$$

$$\text{and } W^s(t_{\text{start}}; t_{\text{finish}}) = \int_{t_{\text{start}}}^{t_{\text{finish}}} P^s(t) dt,$$

where $-P^{i(1)}(t)$, $P^{s(2)}(t)$ and $P^s(t)$ represent the instantaneous power entering and leaving the domain Ω_{int} through the boundaries Γ_1 , Γ_2 , and Γ , respectively. The energy efficiency γ is a positive number less than or equal to one. Obviously, the closer γ to one, the more efficient compressor is.

- *Degree of compression* is the input-to-output pulse duration ratio:

$$\beta = \frac{T^{i(1)}}{T^{s(2)}} \quad \text{or} \quad \beta = \frac{T^{i(1)}}{T^s}.$$

Here, $T^{i(1)} = t_2 - t_1$ and $T^{s(2)}$ (or T^s) = $t_4 - t_3$ are the durations of the input and output pulses, respectively. The degree of compression β is a positive number greater than one.

- *Power gain* is a measure of compressor’s ability to increase the input power. Power gain $\theta = \beta \times \gamma$ is the product of degree of compression and energy

efficiency. It is clear that θ is the input-to-output average power ratio. The power gain θ is a positive number greater than one.

- *Instantaneous efficiency of energy accumulation* is the ratio of the energy accumulated in a storage unit to the total input energy by a given time. At the time t , it is

$$\gamma_{\text{accum}}(t) = \frac{W^{i(1)}(0;t) - W^{s(1)}(0;t) - W^{s(2)}(0;t) - W^s(0;t) - W^{\text{abs}}(0;t)}{W^{i(1)}(0;t)},$$

where $W^{s(1)}(t_1;t)$ is the energy reflected back into the feeding waveguide Ω_1 during the interval $t - t_1$, while $W^{\text{abs}}(t_1;t)$ is the energy lost to absorption. The meaning of the functions $W^{i(1)}(0;t)$ and $W^{s(2)}(0;t)$ is explained above. The characteristic $\gamma_{\text{accum}}(t)$ determines the optimal duration of excitation $T^{i(1)}$. As the reflected and transmitted instantaneous powers are non-monotonic functions of time, there exist intervals when the accumulated energy grows faster than the scattered energy. Also there exist intervals with the inverse dynamics and intervals without energy accumulation. For example, $T^{i(1)}$ can be chosen to obtain maximal energy efficiency γ . All one has to do is to stop the accumulation process at the instant of maximal $\gamma_{\text{accum}}(t)$.

The characteristics introduced above are based on the instantaneous Poynting theorem (the instantaneous power balance theorem), which has the following form for the structures under study [25]:

$$\underbrace{P^{s(1)}(t) + P^{s(2)}(t) + P^s(t) + P^{i \times s(1)}(t)}_1 + \underbrace{\frac{1}{2} \frac{\partial}{\partial t} \int_{\Omega_{\text{int}}} \left(\eta_0 |\vec{H}(g,t)|^2 + \frac{\varepsilon(g)}{\eta_0} |\vec{E}(g,t)|^2 \right) dg}_2 + \underbrace{\int_{\Omega_{\text{int}}} \sigma(g,t) |\vec{E}(g,t)|^2 dg}_{3} = -P^{i(1)}(t). \quad (6.7)$$

In (6.7) the following designations are used:

$$P^{i \text{ or } s(j)}(t) = \int_{\Gamma_j} \left([\vec{E}^{i \text{ or } s(j)}(g_j,t) \times \vec{H}^{i \text{ or } s(j)}(g_j,t)] \cdot \vec{n}_j \right) dy_j, \quad (6.8)$$

$$P^s(t) = \int_{\Gamma} ([\vec{E}^s(g,t) \times \vec{H}^s(g,t)] \cdot \vec{n}) d\phi,$$

$$P^{i \times s(1)}(t) = \int_{\Gamma_1} \left(\left[\vec{E}^{s(1)}(g_1, t) \times \vec{H}^{i(1)}(g_1, t) + \vec{E}^{i(1)}(g_1, t) \times \vec{H}^{s(1)}(g_1, t) \right] \cdot \vec{n}_1 \right) dy_1, \quad (6.9)$$

where \vec{n}_j and \vec{n} represent the outward (with respect to the domain Ω_{int}) unit normals to the boundaries Γ_j and Γ , respectively.

It follows from (6.7) that the sum of the instantaneous power reflected and transmitted from the domain Ω_{int} into the waveguides Ω_1 , Ω_2 and the domain Ω_{ext} through the boundaries Γ_1 , Γ_2 and Γ (the terms in brace ‘1’), the instantaneous power accumulated in Ω_{int} (brace ‘2’), and the instantaneous power dissipated in Ω_{int} (brace ‘3’) is equal to the instantaneous power incoming into Ω_{int} through Γ_1 (the right side of (6.7)). It is clear that the energies $W^{s(1)}(\dots)$, $W^{\text{abs}}(\dots)$, etc., which are required to calculate γ and $\gamma_{\text{accum}}(t)$, can be determined immediately from (6.7) by integrating the relevant terms over certain time intervals.

The *normalized pulsed pattern* describes the space (angular) and temporal distribution of the radiated pulse at a given distance [26]. It is defined as

$$D_{\text{puls}}(\phi, t, M) = \frac{U(M, \phi, t)}{\max_{\tilde{\phi}, \tau} |U(M, \tilde{\phi}, \tau)|}; \quad M \geq L, \quad 0 \leq \phi \leq 2\pi, \quad (6.10)$$

$$T_1 \leq t \leq T_2 \leq T + M - L.$$

This function allows one to estimate the distance where the radiated pulse retains its primary shape, and to study in detail its behavior (splitting, focusing, etc.) as the distance increases. The results presented in [7, 26] show that the values $\tilde{D}_{\text{puls}}(\phi, k, M) \leftrightarrow D_{\text{puls}}(\phi, t, M)$ are also highly informative in the study of radiators.

Disregarding ohmic loss (brace ‘3’ in (6.7)) and energy accumulation inside Ω_{int} (brace ‘2’ in (6.7)), the value

$$\xi(T) = \frac{W^{i(1)}(0; T) - W^{s(1)}(0; T) - W^{s(2)}(0; T)}{W^{i(1)}(0; T)}$$

defines the *time-domain radiation efficiency*. Here, T is the end of the observation time.

6.2.2 Axially Symmetric Structures

We will study the space-time and space-frequency transformations of symmetric ($\partial/\partial\phi \equiv 0$) electromagnetic waves in open axially symmetric structures (Fig. 6.2) by solving the following initial boundary value problem:

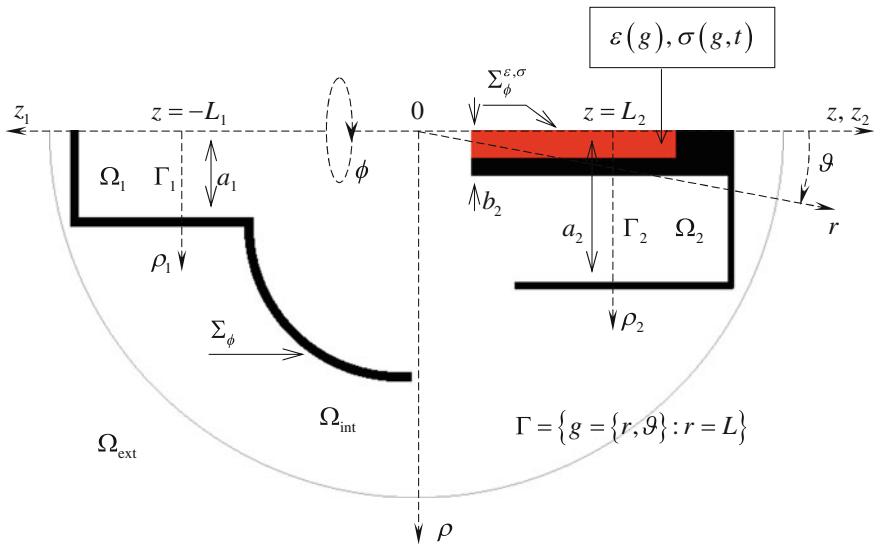


Fig. 6.2 Axially symmetric structure

$$\begin{cases}
 \left[-\varepsilon(g) \frac{\partial^2}{\partial r^2} - \eta_0 P + \frac{\partial^2}{\partial z^2} + \frac{\partial}{\partial \rho} \left(\frac{1}{\rho} \frac{\partial}{\partial \rho} \rho \right) \right] U(g, t) = 0; & t > 0, \quad g \in \Omega_{\text{int}} \\
 U(g, t)|_{t=0} = 0, \quad \frac{\partial}{\partial t} U(g, t)|_{t=0} = 0; & g = \{\rho, z\} \in \bar{\Omega}_{\text{int}} \\
 \vec{E}_{tg}(q, t), \quad \vec{H}_{tg}(q, t) \text{ are continuous when crossing } \Sigma^{\varepsilon, \sigma}, \\
 \vec{E}_{tg}(p, t)|_{q=\{\rho, \phi, z\} \in \Sigma} = 0, \quad U(0, z, t) = 0 \text{ for } \{0, z\} \in \bar{\Omega}_{\text{int}}, \\
 D_1 [U(g, t) - U_p^{i(1)}(g, t)]|_{g \in \Gamma_1} = 0, \quad D_2 [U(g, t)]|_{g \in \Gamma_2} = 0 \text{ and} \\
 D[U(g, t)]|_{g \in \Gamma} = 0; \quad t \geq 0,
 \end{cases} \tag{6.11a}$$

$$\begin{aligned}
 U(g_j, t) - \delta_j^1 U_p^{i(1)}(g_j, t) = & - \sum_n \left\{ \int_0^{t-z_j} J_0 \left[\lambda_{nj} \left((t-\tau)^2 - z_j^2 \right)^{1/2} \right] \right. \\
 & \times \left[\int_{b_j}^{a_j} \frac{\partial U(\tilde{\rho}_j, \tilde{z}_j, \tau) - \delta_j^1 U_p^{i(1)}(\tilde{\rho}_j, \tilde{z}_j, \tau)}{\partial \tilde{z}_j} \Big|_{\tilde{z}_j=0} \mu_{nj}(\tilde{\rho}_j) \tilde{\rho}_j d \tilde{\rho}_j \right] d\tau \Big\} \\
 & \times \mu_{nj}(\rho_j); \quad g_j = \{\rho_j, z_j\} \in \bar{\Omega}_j, \quad t \geq z_j,
 \end{aligned} \tag{6.11b}$$

$$\begin{aligned}
U(g, t) = & \sum_{n=1}^{\infty} \left\{ \left(\frac{L}{r} \right)^{n+1} \int_0^{\pi/2} U(L, \tilde{\vartheta}, t - (r - L)) \mu_n(\cos \tilde{\vartheta}) \sin \tilde{\vartheta} d\tilde{\vartheta} \right. \\
& + \sqrt{\frac{L}{r}} \int_0^{t-(r-L)} S_{n+1/2}(r, L, t - \tau) \\
& \times \left. \left[\int_0^{\pi/2} \frac{\partial U(L, \tilde{\vartheta}, \tau)}{\partial \tau} \mu_n(\cos \tilde{\vartheta}) \sin \tilde{\vartheta} d\tilde{\vartheta} \right] d\tau \right\} \mu_n(\cos \vartheta); \\
g = & \{r, \vartheta\} \in \Omega_{\text{ext}}, \quad t \geq (r - L).
\end{aligned} \tag{6.11c}$$

In the case of TE_0 -waves ($E_\rho = E_z = H_\phi \equiv 0$), we have $U(g, t) = E_\phi(g, t)$ and $P[U] \equiv \partial[\sigma(g, t)U(g, t)]/\partial t$. In the case of TM_0 -waves ($H_\rho = H_z = E_\phi \equiv 0$), we have $U(g, t) = H_\phi(g, t)$ and $P[U] \equiv \sigma(g, t)\partial U(g, t)/\partial t$. All other nonzero components (H_ρ, H_z in the case of TE_0 -waves and E_ρ, E_z in the case of TM_0 -waves) can be expressed via $U(g, t)$ [1]. $\sigma(g, t) \geq 0$ is the electric conductivity of a locally inhomogeneous medium, its time dependence allows us to simulate changes in compressor's mode of operation; $\varepsilon(g) \geq 1$ and $\mu(g) \equiv 1$ are the relative permittivity and magnetic permeability of the medium; $\eta_0 = (\mu_0/\varepsilon_0)^{1/2}$ is the impedance of free space; ε_0 and μ_0 are the electric and magnetic constants of vacuum; $\{\rho, \phi, z\}$ are the cylindrical coordinates and $\{r, \vartheta, \phi\}$ are the spherical coordinates. By $\Sigma = \Sigma_\phi \times [0, 2\pi]$ we denote perfectly conducting surfaces obtained by rotating the piecewise smooth curves Σ_ϕ around the z -axis. $\Sigma^{\varepsilon, \sigma} = \Sigma_\phi^{\varepsilon, \sigma} \times [0, 2\pi]$ are the surfaces on which the functions $\varepsilon(g)$ and/or $\sigma(g, t)$ have discontinuities.

The functions $\sigma(g, t)$ and $\varepsilon(g) - 1$, which have compact supports in the closure of Ω_{int} , are supposed to satisfy the theorem on the unique solvability of the problem (6.11a, 6.11b, 6.11c) in the Sobolev space $W_2^1(\Omega_{\text{int}} \times (0, T))$, $T < \infty$ [1, 8]. All scatterers defined by the piecewise constant functions $\varepsilon(g)$, $\sigma(g, t)$ and by the piecewise smooth contours Σ_ϕ and $\Sigma_\phi^{\varepsilon, \sigma}$ are located in the domain Ω_{int} .

In (6.11b), $g_j = \{\rho_j, z_j\}$ is the local coordinate system associated with the virtual waveguide Ω_j (see Fig. 6.2). In the circular or coaxial waveguide Ω_j , the *transverse functions* $\mu_{nj}(\rho_j)$ form an orthonormal system, and λ_{nj} are the *transverse eigenvalues* associated with $\mu_{nj}(\rho_j)$. Analytical representations for $\mu_{nj}(\rho_j)$ and λ_{nj} are well-known (see [1, 7] and Chap. 5) and for TE_0 -waves ($n = 1, 2, 3, \dots$) take the form:

$$\begin{cases} \mu_{nj}(\rho_j) = G_1(\lambda_{nj}, \rho_j) \sqrt{2} \left[a_j^2 G_0^2(\lambda_{nj}, a_j) - b_j^2 G_0^2(\lambda_{nj}, b_j) \right]^{-1/2}; \\ b_j < \rho_j < a_j \\ \lambda_{nj} > 0 \text{ are the roots of the equation } G_1(\lambda_j, a_j) = 0 \\ G_q(\lambda_j, \rho_j) = J_q(\lambda_j \rho_j) N_1(\lambda_j b_j) - N_q(\lambda_j \rho_j) J_1(\lambda_j b_j); \quad q = 0, 1 \end{cases}$$

(coaxial waveguide Ω_j), and

$$\begin{cases} \mu_{nj}(\rho_j) = J_1(\lambda_{nj}\rho_j)\sqrt{2}[a_j J_0(\lambda_{nj}a_j)]^{-1}; & 0 < \rho_j < a_j \\ \lambda_{nj} > 0 \text{ are the roots of the equation } & J_1(\lambda_j a_j) = 0 \end{cases}$$

(circular waveguide Ω_j). For TM_0 -waves we have:

$$\begin{cases} \mu_{nj}(\rho_j) = \tilde{G}_1(\lambda_{nj}, \rho_j)\sqrt{2}\left[a_j^2 \tilde{G}_1^2(\lambda_{nj}, a_j) - b_j^2 \tilde{G}_1^2(\lambda_{nj}, b_j)\right]^{-1/2} & \text{for} \\ n = 1, 2, \dots \text{ and } \mu_{nj}(\rho_j) = \left[\rho_j \sqrt{\ln(a_j/b_j)}\right]^{-1}; & b_j < \rho_j < a_j \\ \lambda_{nj} > 0 \text{ for } n = 1, 2, \dots \text{ are the roots of the equation} \\ \tilde{G}_0(\lambda_j, b_j) = 0 \text{ and } \lambda_{0j} = 0 \\ \tilde{G}_q(\lambda_j, \rho_j) = J_q(\lambda_j \rho_j)N_0(\lambda_j a_j) - N_q(\lambda_j \rho_j)J_0(\lambda_j a_j); & q = 0, 1 \end{cases}$$

(coaxial waveguide Ω_j , $n = 0, 1, 2, \dots$), and

$$\begin{cases} \mu_{nj}(\rho_j) = J_1(\lambda_{nj}\rho_j)\sqrt{2}[a_j J_1(\lambda_{nj}a_j)]^{-1}; & 0 < \rho_j < a_j \\ \lambda_{nj} > 0 \text{ are the roots of the equation } & J_0(\lambda_j a_j) = 0 \end{cases}$$

(circular waveguide Ω_j , $n = 1, 2, 3, \dots$). Here, $J_q(\dots)$ and $N_q(\dots)$ are the Bessel and Neumann cylindrical functions.

In (6.11c),

$$S_{n+1/2}(r, L, t - \tau) = \sum_s \frac{H_{n+1/2}^{(1)}(z_s r) \exp[-iz_s(t - \tau)]}{H_{n-1/2}^{(1)}(z_s L) z_s L},$$

where $z = z_s$: $\text{Im } z_s < 0$ ($s = 1, 2, \dots, n$) are zeros of the Hankel cylindrical function $H_{n+1/2}^{(1)}(zL)$; $\mu_n(\cos \vartheta) = \sqrt{(2n+1)/(2n(n+1))} P_n^1(\cos \vartheta)$, $n = 1, 2, \dots$ is a complete orthonormal (with the weight factor $\sin \vartheta$) system in the space $L_2(0 < \vartheta < \pi)$; $P_n^1(\dots)$ is the associated Legendre function of the first kind.

The computation domain Ω_{int} is the part of the half-plane $\Omega_{\text{total}} = \{g = \{\rho, z\} : \rho > 0, -\infty < z < \infty\}$ bounded by the contours Σ_ϕ together with the virtual boundaries Γ_1 and Γ_2 (input and output ports in the cross-sections $z = -L_1$ ($z_1 = 0$) and $z = L_2$ ($z_2 = 0$) of the virtual waveguides Ω_1 and Ω_2) and the spherical virtual boundary $\Gamma = \{g = \{\rho, \phi\} \in \Omega_{\text{total}} : r = L\}$ separating Ω_{int} and Ω_{ext} .

The EAC operators $D_1[\dots]$ and $D_2[\dots]$ are derived by placing the observation point in (6.11b) onto Γ_1 and Γ_2 , i.e. by putting $r = L$. This converts (6.11c) to the identity, which makes the discretization of $D[\dots]$ nontrivial [1, 7].

The function $U_p^{i(1)}(g, t)$ in EAC $D_1 \left[U(g, t) - U_p^{i(1)}(g, t) \right] \Big|_{g \in \Gamma_1} = 0$ represents a pulsed wave incident from the waveguide Ω_1 . The following relations are true for this wave:

$$\begin{aligned} U_p^{i(1)}(g_1, t) &= v_{p1}(z_1, t) \mu_{p1}(\rho_1); \quad g_1 \in \Omega_1, \quad t \geq 0, \\ v_{p1}(z_1, t) &= \int_{b_1}^{a_1} U_p^{i(1)}(g_1, t) \mu_{p1}(\rho_1) \rho_1 d\rho_1. \end{aligned} \quad (6.12a)$$

Reflected and transmitted pulsed waves outgoing into the waveguides Ω_1 and Ω_2 can be represented as

$$\begin{aligned} U^{s(1)}(g_1, t) &= U(g_1, t) - U_p^{i(1)}(g_1, t) = \sum_n u_{n1}(z_1, t) \mu_{n1}(\rho_1); \quad g_1 \in \Omega_1, \\ t \geq 0, \quad u_{n1}(z_1, t) &= \int_{b_1}^{a_1} U^{s(1)}(g_1, t) \mu_{n1}(\rho_1) \rho_1 d\rho_1 \end{aligned} \quad (6.12b)$$

and

$$\begin{aligned} U^{s(2)}(g_2, t) &= U(g_2, t) = \sum_n u_{n2}(z_2, t) \mu_{n2}(\rho_2); \quad g_2 \in \Omega_2, \quad t \geq 0, \\ u_{n2}(z_2, t) &= \int_{b_2}^{a_2} U^{s(2)}(g_2, t) \mu_{n2}(\rho_2) \rho_2 d\rho_2. \end{aligned} \quad (6.12c)$$

The following wave is radiated into free space:

$$\begin{aligned} U(r, \vartheta, t) &= \sum_n u_n(r, t) \mu_n(\vartheta); \quad g = \{r, \vartheta\} \in \bar{\Omega}_{\text{ext}}, \quad t \geq 0, \\ u_n(r, t) &= \int_0^\pi U(r, \vartheta, t) \sin \vartheta \mu_n(\cos \vartheta) d\vartheta. \end{aligned} \quad (6.12d)$$

Here, $v_{p1}(z_1, t)$, $u_{n1}(z_1, t)$, $u_{n2}(z_2, t)$, and $u_n(r, t)$ are the space-time amplitudes of the waves given by (6.12a, 6.12b, 6.12c, 6.12d).

In the frequency domain, the equations (6.12a, 6.12b, 6.12c, 6.12d) take the following form:

$$\tilde{U}_p^{i(1)}(g_1, k) = A_{p1}(k) \exp(-i\beta_{p1}z_1) \mu_{p1}(\rho_1); \quad g \in \bar{\Omega}_1, \quad (6.13a)$$

$$\begin{aligned} \tilde{U}^{s(1)}(g_1, k) &= \tilde{U}(g_1, k) - \tilde{U}_p^{i(1)}(g_1, k) \\ &= \sum_n B_{n1}(k) \exp(i\beta_{n1}z_1) \mu_{n1}(\rho_1); \quad g \in \bar{\Omega}_1, \end{aligned} \quad (6.13b)$$

$$\tilde{U}^{s(2)}(g_2, k) = \tilde{U}(g_2, k) = \sum_n B_{n2}(k) \exp(i\beta_{n2}z_2) \mu_{n2}(\rho_2); \quad g \in \bar{\Omega}_2, \quad (6.13c)$$

$$\tilde{U}(g, k) = \frac{1}{\sqrt{r}} \sum_{n=1}^{\infty} C_n(k) H_{n+1/2}^{(1)}(kr) \mu_n(\cos \vartheta); \quad g \in \bar{\Omega}_{\text{ext}}. \quad (6.13d)$$

Here, $A_{p1}(k) = \tilde{v}_{p1}(0, k) \leftrightarrow v_{p1}(0, t)$, $B_{nj}(k) = \tilde{u}_{nj}(0, k) \leftrightarrow u_{nj}(0, t)$, and $C_n(k) : C_n(k) H_{n+1/2}^{(1)}(kr) / \sqrt{r} = \tilde{u}_n(r, k) \leftrightarrow u_n(r, t)$ are the complex-valued amplitudes of monochromatic waves generating a steady-state field $\{\tilde{\vec{E}}(g, k), \tilde{\vec{H}}(g, k)\}$ in the domains Ω_j and Ω_{ext} ; $\beta_{nj}(k) = \sqrt{k^2 - \lambda_{nj}^2}$ are the *longitudinal propagation numbers* for the waveguide modes $U_n^{s(j)}(g_j, k) = B_{nj}(k) \exp(i\beta_{nj}z_1) \mu_{nj}(\rho_j)$, $\text{Re } \beta_{nj}(k) \text{Re } k \geq 0$ and $\text{Im } \beta_{nj}(k) \geq 0$; $\tilde{f}(k) \leftrightarrow f(t)$ is the Laplace transform (6.4).

The characteristics $R_{np}^{11}(k)$, $T_{np}^{21}(k)$, etc. are the same as in Sect. 6.2.1. Below we highlight only differences caused by switching from planar to axially symmetric structures.

- The element $dg = dydz$ in the integrals over the domain Ω_{int} in (6.5) and (6.7) should be replaced by $dg = \rho d\rho dz$, while the element dy in (6.8) and (6.9) should be replaced by $\rho d\rho$.
- The definition (6.6) of the *normalized directional pattern* changes to

$$D(\vartheta, k, M) = \frac{\left| \tilde{\vec{E}}_{tg}(M, \vartheta, k) \right|^2}{\max_{0 \leq \tilde{\vartheta} \leq \pi} \left| \tilde{\vec{E}}_{tg}(M, \tilde{\vartheta}, k) \right|^2}; \quad 0 \leq \vartheta \leq 180^\circ, \quad K_1 \leq k \leq K_2.$$

Here, $\tilde{\vec{E}}_{tg}(M, \vartheta, k)$ is the tangential (to the spherical surface $\{q = \{r, \vartheta, \phi\} : r = M, 0 \leq \vartheta \leq \pi, 0 \leq \phi \leq 2\pi\}$) component of the monochromatic electric field $\tilde{\vec{E}}(g, k)$.

- The definition (6.10) of the *normalized pulsed pattern* changes to

$$D_{\text{puls}}(\vartheta, t, M) = \frac{U(M, \vartheta, t)}{\max_{\tilde{\vartheta}, \tau} |U(M, \tilde{\vartheta}, \tau)|}; \quad 0 \leq \vartheta \leq 180^\circ, \quad M \geq L, \\ T_1 \leq t \leq T_2 \leq T + M - L.$$

6.3 Energy Accumulation in Direct-Flow Waveguide Compressors

Energy compressor is a device for converting long low-amplitude input pulses into short high-amplitude output pulses. Compressors accumulate the energy of an input pulse over a relatively long period of time and then release it in the form of a short high-power pulsed output. Efficient microwave pulse compression is required in several fields of science and engineering: compressors are used as components of particle accelerators [27, 28] and radars [29], in data transmission [30], energy transfer [31], plasma heating [32], and biological studies [33].

Design of a properly working energy compressor requires in-depth study of the energy accumulation process. This process, which involves formation of highly resonant high-power pulses in a storage unit, is non-monotonic in time. Hence, the real-time study is required to gain a better insight into all pertinent physical phenomena. In this section, we will consider the processes inside a compressor, from the very beginning of excitation right to the accumulated energy release, in the time domain. We will also discuss the influence of various parameters on the energy accumulation efficiency and, thus, the overall compressor performance. As an example, we will analyze in detail the energy accumulation in a rectangular direct-flow waveguide compressor working on TE_{0n} -waves. This chapter focuses on the development of the technique that allows rigorous and efficient solution of the problems associated with the design of compressors operating in VHF, UHF, SHF and EHF bands (from 300 MHz to 300 GHz). Here, we are dealing with compressors based on waveguide and open quasi-optical resonators, with resonant and distributed switches, the ones that release high-power short pulses into a feeder line and into free space.

The contributions of this section are twofold. In the first place, it presents the rigorous scheme to design and analyze energy compressors, which allows studying a compressor as a whole in contrast to the currently available design frameworks, which separately account for characteristics of isolated components. The second contribution is the estimation of the influence on the compressor efficiency of various parameters like geometry, duration of the excitation, accumulation and release processes' parameters, and others.

6.3.1 Slot Switches

Even simple structures can be used as switches in axially symmetric energy compressors. For example, narrow slots or narrow radial/coaxial grooves in inner or outer conductors of axially symmetric waveguide transformers (see Figs. 6.3, 6.4, 6.5, 6.6, 6.7).

The study of slots and grooves of this kind [7, 34–37] has shown that they may drastically affect the propagation and radiation of pulsed and sinusoidal *TEM*-

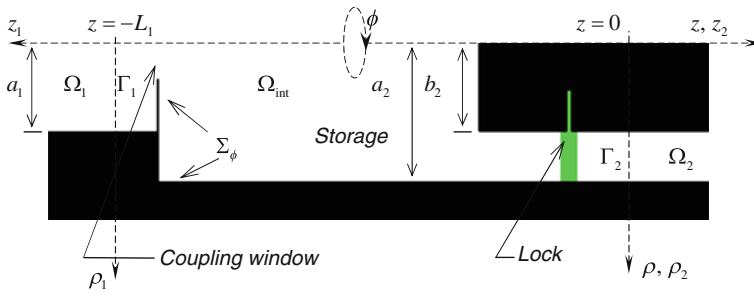
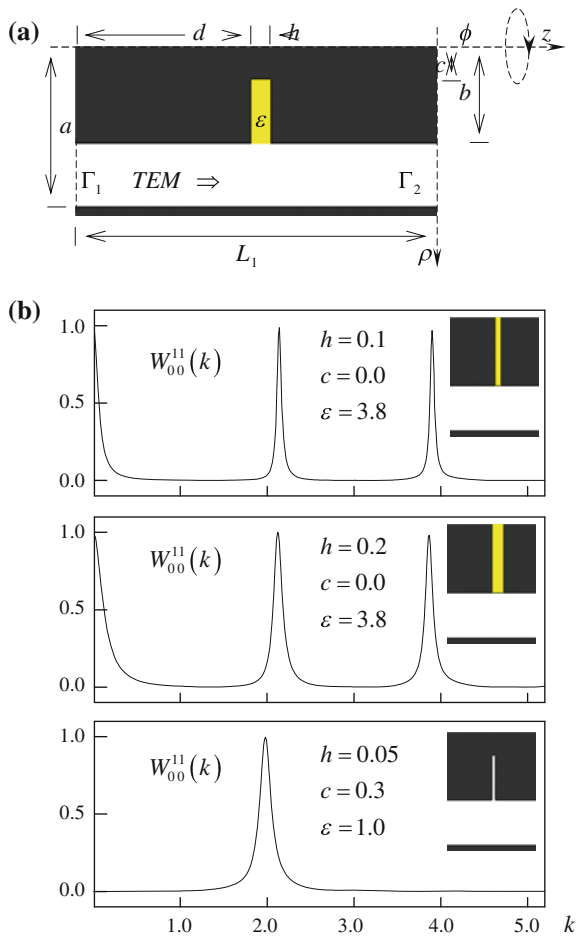


Fig. 6.3 Direct-flow compressor based on circular and coaxial waveguides

Fig. 6.4 **a** Slot resonator in coaxial waveguide ($a = 1.5$, $b = 0.9$, $d = 3.0$, $L_1 = 6.0$) and **b** its response on excitation by TEM -wave (single-mode operation $k_1^+ \approx 5.21$)



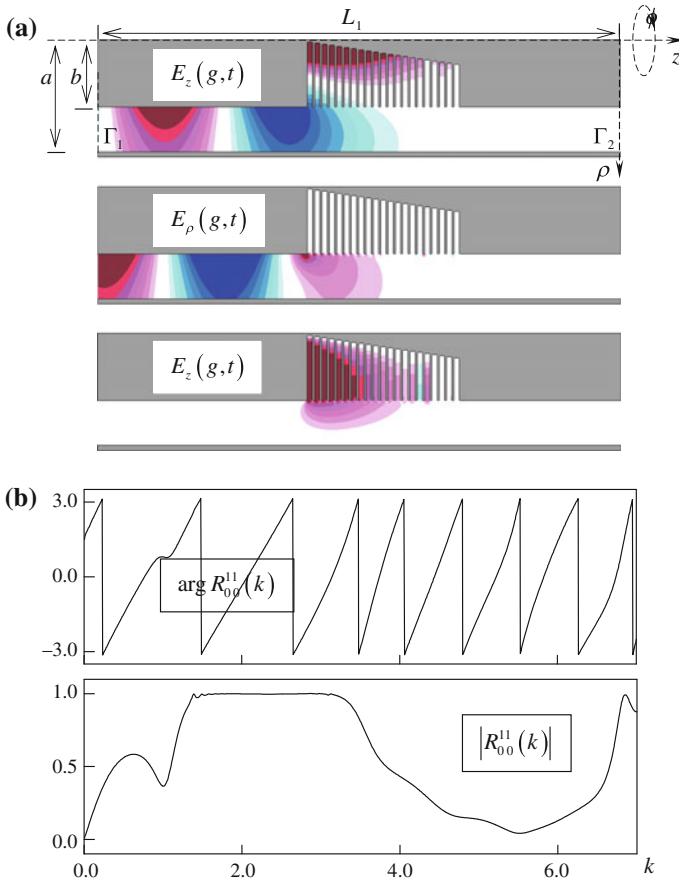
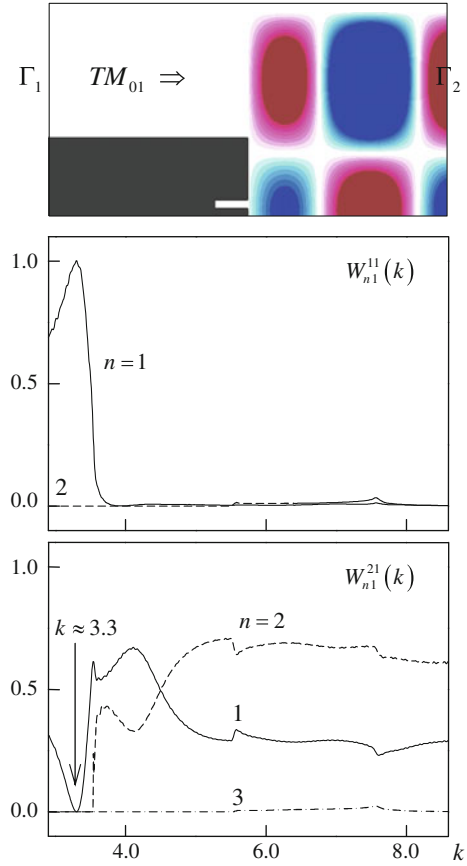


Fig. 6.5 A set of grooves in the inner conductor of a coaxial waveguide ($a = 1.0$, $b = 0.6$, $d = 2.0$, $L_1 = 5.0$, $\varepsilon = 1.0$): **a** the spatial distribution of the field intensity ($g \in \Omega_{\text{int}}$, $t = 45$); **b** the reflection coefficient $R_{00}^{11}(k)$ in the frequency band $0 \leq k \leq 7.0$ (single-mode operation, $k_1^+ \approx 7.83$)

waves. This is due to the so-called *slot resonances* (half-wave slot resonances and quarter-wave resonances in grooves) that can be excited in narrow radial or coaxial waveguides on *TEM*-waves.

Slot resonances can be used to lock energy release channels in direct-flow compressors based on circular and coaxial waveguides (see Fig. 6.3 and [2, 7]). Figure 6.4b shows that a *TEM*-wave is totally reflected by the short ($h = 0.1$) slot in the inner conductor on the frequencies $k = \text{Re } \bar{k}_1 \approx 2.14$ and $k = \text{Re } \bar{k}_2 \approx 3.9$, while the groove ($h = 0.05$, $c = 0.3$) in the inner conductor totally locks the coaxial waveguide on the frequency $k = \text{Re } \bar{k}_1 \approx 1.98$. Variation of the parameters h and c (Fig. 6.4a) results in a predictable change of complex eigenfrequencies $\bar{k} = \text{Re } \bar{k} + i \text{Im } \bar{k}$ that correspond to the slot resonances, and consequently, in a

Fig. 6.6 Total reflection of TM_{01} -wave by the step-junction of circular waveguide



predictable change of reflection parameters of a TEM -wave propagating in the single-mode coaxial waveguide.

We can also predict with confidence the action of a set of grooves [34, 37]. The groove with $h = 0.05$ and $c = 0.02$ resonates at $k = 1.4$, whereas the groove with $c = 0.22$ resonates at $k \approx 3.12$. The set of grooves in Fig. 6.5 completely locks the coaxial waveguide in the frequency band $k \in [k_{\text{lower}}, k_{\text{upper}}] = [1.6, 3.1]$. The bandwidth $BW = 2(k_{\text{upper}} - k_{\text{lower}}) / (k_{\text{upper}} + k_{\text{lower}}) \times 100\%$ equals 63.8% (Fig. 6.5b). Figure 6.5a demonstrates the process for the quasi-monochromatic signal

$$\begin{aligned}
 U_0^{i(1)}(g, t) &= v_{01}(z, t)\mu_{01}(\rho) : v_{01}^o(-L_1, t) = P(t) \cos[\tilde{k}(t - \tilde{T})] = F_1(t); \\
 \tilde{k} &= 2.7, \quad \tilde{T} = 0.5, \quad P(t) : 0.01 - 5 - 75 - 80, \quad g = \{\rho, z\} \in \Omega_1,
 \end{aligned}
 \tag{6.14}$$

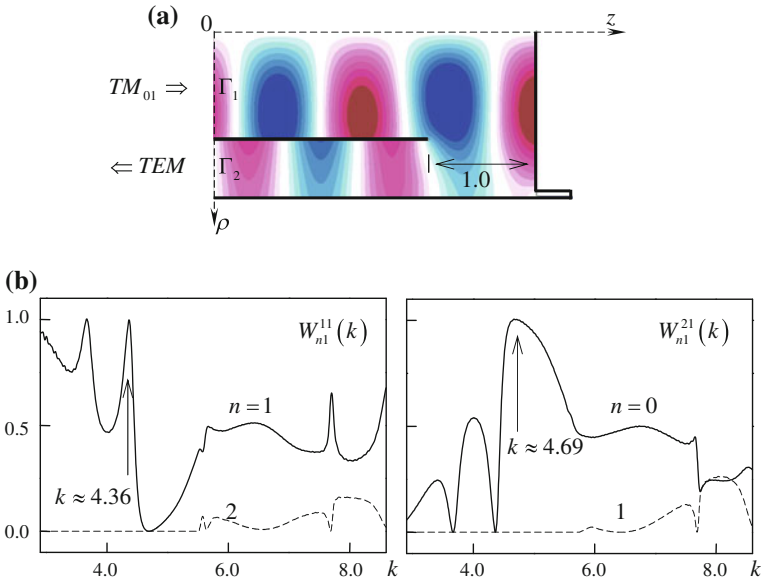


Fig. 6.7 Slot resonances. Total reflection of TM_{01} -wave of circular waveguide ($k \approx 4.36$) and total transformation of this wave into TEM -wave of coaxial waveguide ($k \approx 4.69$): **a** geometry of the wave converter (slot length and width are 0.33 and 0.02) and **b** energy response of the unit

where $v_{01}^{\rho}(z, t)$ is the space-time amplitude of the $E_{\rho}^{i(1)}(g, t)$ -component of the wave $U_0^{i(1)}(g, t)$ incoming from the waveguide Ω_1 (see the formula (6.12a); $\partial v_{01}^{\rho}(z, t)/\partial t = -\eta_0 \partial v_{01}(z, t)/\partial z$; \tilde{k} is the central frequency of the signal and $P(t) : t_1 - t_2 - t_3 - t_4$ is its trapezoidal envelope, which equals one for $t_2 < t < t_3$ and is zero for $t < t_1$ and $t > t_4$.

To extend the range of effects observed in structures of this kind, one can add narrow coaxial grooves (Figs. 6.6 and 6.7), which sustain low-Q free TEM -oscillations, to step junctions and U-turns of circular waveguides [7]. Properties exhibited by step junctions and U-turns with slot resonators are determined basically by the slot location (whether it is located along the line of nodes or along the line of antinodes of the H_{ϕ} -component of a wave propagating along the wide waveguide) and by the degree of matching of TM_{0n} -waves in the narrow and the wider waveguides.

In the waveguide step-junction with $a_1 = 1.0$, $a_2 = 1.56$, the TM_{02} -wave of the narrow waveguide is matched with the TM_{03} -wave of the wider waveguide: the cut-off points $k_{21}^+ \approx 5.52$ and k_{32}^+ are very nearly the same. A narrow coaxial groove cut along the line of antinodes of the H_{ϕ} -component of the second mode of the wider waveguide ($\rho = 1.5$, see Fig. 6.6) results in a new effect for step-junctions: the incident TM_{01} -wave is totally reflected back into the feeding waveguide. The width of the groove is 0.06 and the depth is 0.33. Only TM_{01} -waves propagate in both waveguides without decay.

An axially symmetric U-turn without slots and with the same parameters of the narrow and the wider waveguides totally reflects the incident TM_{01} -wave on the frequency $k \approx 3.68$ (the resonance on the modes locked in the section of the wider waveguide [38]). In the frequency band $4.0 < k < 5.0$, no less than 80% of the input energy is transformed into the energy of TEM -wave of the coaxial waveguide; the maximum is 86% at $k \approx 4.45$.

A narrow groove cut along the line of antinodes of the H_ϕ -component of the TM_{01} -wave in a section of the wider waveguide ($\rho = 1.23$) results in another point of total reflection ($k \approx 4.55$) and allows one to transport 95% of the input energy into the TEM -wave of the coaxial waveguide at $k \approx 4.8$.

In the U-turn, at the level of its outer wall (Fig. 6.7a), we observe at $k \approx 4.69$ the total transformation of the TM_{01} -wave of the circular waveguide into the TEM -wave of the coaxial waveguide (Fig. 6.7b). Within the frequency band $4.6 < k < 4.8$ ($BW \approx 4.0\%$), more than 98% of the input energy is transformed into the energy of TEM -wave. The frequencies on which the total reflection occurs (the locked-mode resonance at $k \approx 3.67$ and the slot resonance at $k \approx 4.36$) remain practically the same as before.

6.3.2 Active Compressors Based on Circular and Coaxial Waveguides

Active compressors (see, for example, [2, 7, 15–19]) contain, as a rule, two resonant units: a *storage unit* for accumulating an input energy, and a *switch*, which closes the output section during energy accumulation and opens it at the moment of release. The optimal matching of these units is an intricate problem. Its solution is based on the results and methods of spectral theory [1, 4, 7, 12–14, 39] and has to provide the following.

- Coincidence of the working frequencies $\text{Re } \bar{k}_{\text{stor}}$ and $\text{Re } \bar{k}_{\text{sw}}$ of the storage unit and the switch.
- Required dynamics of the field intensity growth in the storage unit and in the switch (it is determined by the Q-factors of the oscillations in the corresponding volumes, namely, by $\text{Im } \bar{k}_{\text{stor}}$ and $\text{Im } \bar{k}_{\text{sw}}$, by the deviation of the central frequency \tilde{k} of the input pulse from the compressor working frequency k_{work} , and by parameters of the *coupling window* between the feeder and the storage unit).
- Effective release (the eigenfrequencies \bar{k} of the unlocked storage in Fig. 6.8b may not be close to k_{work} in the complex plane C_k of the variable k).

Let us now outline, basing on [2], the algorithm for constructing the efficient electrodynamic model of a direct-flow compressor with a slot switch.

On the first stage, one should choose a prototype for a storage unit, namely, a waveguide resonator that is open only on the side of the feeding waveguide Ω_1 and is linked with it through a *beyond-cutoff diaphragm* (Fig. 6.8a). For the storage unit

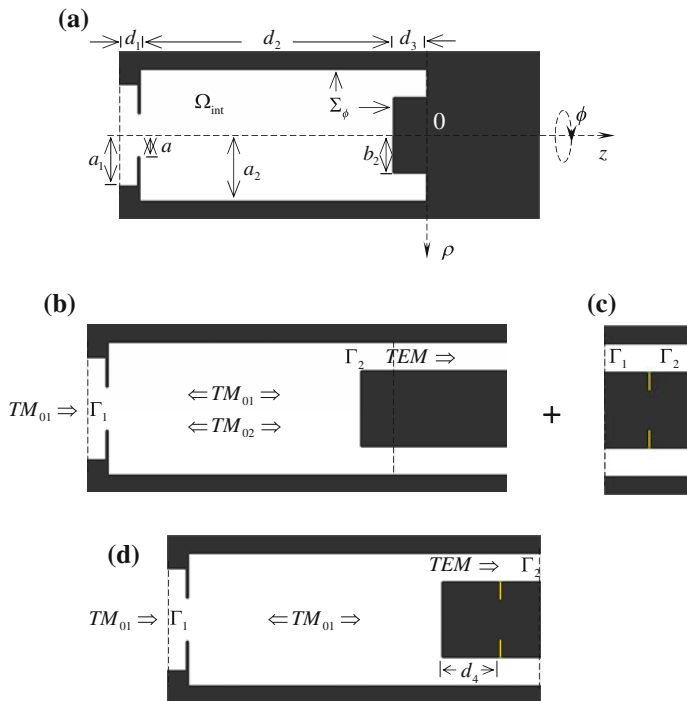


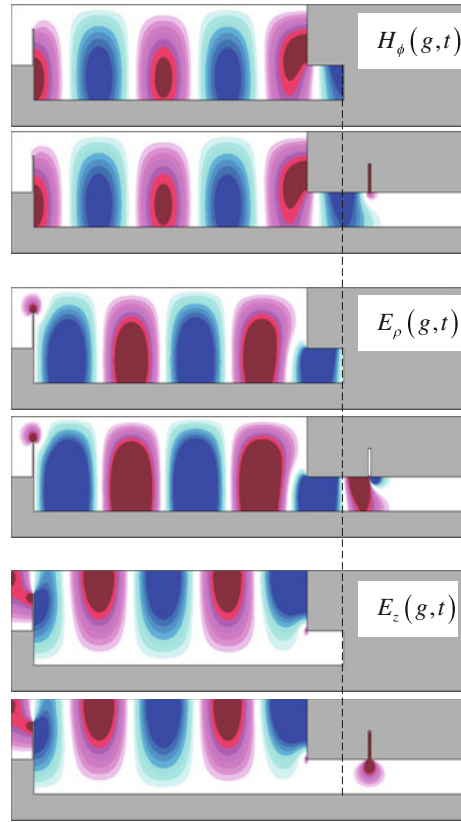
Fig. 6.8 Geometry of storage units with **a** open and **b** closed output ends: $a = 0.5$, $a_1 = 1.2$, $a_2 = 1.56$, $b_2 = 0.9$, $d_1 = 0.5$, $d_2 = 6.0$, $d_3 = 0.8$, $L_1 = d_1 + d_2 + d_3$; thickness c of diaphragm is 0.06. **c** Slot switch (slot depth and width are 0.44 and 0.06, permittivity of slot material is $\epsilon = 1.055$) and **d** compressor with slot switch ($d_4 = 1.34$)

shown in Fig. 6.8, the frequency band $K_1 < k < K_2$ where the waveguide Ω_1 and the closed coaxial output are single-mode is $2.3 < k < 4.5$. The dimensions a_2 and d_2 of the central part of the storage should be chosen such that the counter-propagating TM_{0m} -waves generating the TM_{0mm} -oscillation propagate without decay. Here m is the number of field variations along the z -axis. In the central circular waveguide shown in Fig. 6.8, the second propagating wave (TM_{02} -wave) appears at $k = k_2^+ \approx 3.54$ ($k_1^+ \approx 1.54$, $k_3^+ \approx 5.55$).

On the second step, one should calculate the complex-valued eigenfrequencies $\bar{k}_{\text{stor}, n} = \text{Re} \bar{k}_{\text{stor}, n} + i \text{Im} \bar{k}_{\text{stor}, n}$ of the storage resonator and to determine the quality factors and the field patterns for free oscillations associated with these frequencies. The working frequency k_{work} is assigned one of the values of $\text{Re} \bar{k}_{\text{stor}, n}$. It should be chosen in view of the following facts. A Q-factor and a type of the working oscillation determine the energy efficiency of the storage unit, while the difference between $\text{Re} \bar{k}_{\text{stor}, n}$ and the actual eigenfrequencies of the storage resonator with an open end (see Fig. 6.8b) determines, together with the parameter d_2 , the duration of the compressed pulse. Let us choose $k_{\text{work}} = 2.728$. A free oscillation with the

Fig. 6.9 Field patterns in resonator with closed end and in resonator with slot switch ($t = 910$). Excitation by TM_{01} -wave

$$U_1^{i(1)}(g, t): v_{11}^o(-L_1, t) = F_1(t); \bar{k} = 2.728, P(t): 0.1 - 5 - 1495 - 1499.9, \tilde{T} = 0.5$$

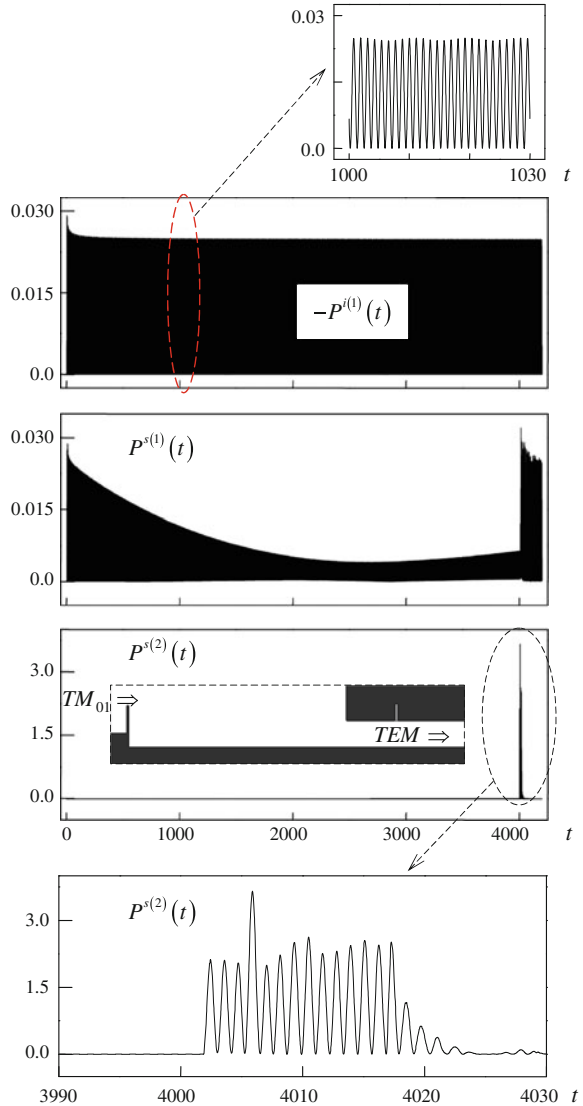


complex-valued eigenfrequency \bar{k}_{stor} : $\text{Re } \bar{k}_{\text{stor}} \approx 2.728$ is a high-Q oscillation whose field pattern is shown in Fig. 6.9.

On the third step, we design the slot switch that locks the coaxial output on the frequency $k_{\text{work}} = 2.728$ (see Fig. 6.8c) and then connect this switch with the open output of the storage such that the resonator with a closed output end (Fig. 6.8a) and the compressor as a whole (Fig. 6.8d) sustain the same high-Q oscillation at $k = k_{\text{work}}$. This can be easily done if $|R_{00}^{11}(k_{\text{work}})| \approx 1.0$, where $R_{00}^{11}(k)$ is the reflection coefficient for the slot discontinuity in the coaxial waveguide, by selecting a proper value of d_4 (see Figs. 6.8d and 6.9), which is uniquely determined by the value of $\arg R_{00}^{11}(k_{\text{work}})$ [2].

On the fourth step, one should refine the values of k_{work} ($\text{Re } \bar{k}_{\text{stor}}$) and Q for the resonant system as a whole, since these values vary slightly even with making the first three steps accurately, and then calculate the basic compressor characteristics for different in duration input quasi-monochromatic TM_{01} -pulses $U_1^{i(1)}(g, t)$ ($\bar{k} = k_{\text{work}}$).

Fig. 6.10 Input instantaneous power $(-P^{i(1)}(t))$, and instantaneous powers $P^{s(1)}(t)$ and $P^{s(2)}(t)$ radiated through Γ_1 (circular feeding) and Γ_2 (coaxial output)



Paper [2] presents the following results obtained at this stage (see also Fig. 6.10, where $U_1^{i(1)}(g, t) : v_{11}^o(-L_1, t) = F_1(t)$; $P(t) : 0.1 - 5 - 4195 - 4199.9$, $\tilde{k} = 2.723$, $\tilde{T} = 0.5$, and the observation time is $T = 4200$): $k_{\text{work}} = 2.723$ and $Q \approx 7160$; the degree of compression is $\beta = T^{i(1)}/T^{s(2)} \approx 190$; the energy efficiency is $\gamma = W^{s(2)}(4002; 4023)/W^{i(1)}(0; T^{i(1)}) \approx 0.51$; the power gain is $\theta = \beta \times \gamma \approx 97$. Here, $T^{i(1)} = 4000$ and $T^{s(2)} \approx 4023 - 4002 = 21$ are the input and the output pulse duration, respectively (almost all the accumulated energy is released through

the port Γ_2 in the time that is somewhat greater than the time required for the signal to pass twice the length of the storage unit); $W^{s(2)}(4002; 4023)$ and $W^{i(1)}(0; T^{i(1)})$ are the output and the input energy, respectively. During energy accumulation ($t \leq 4000$), the specific conductivity $\sigma(t)$ of the slot material equals zero, while in the release mode ($t > 4001$) it is equal to $5.8 \cdot 10^5$. Over a short period of time $4000 < t < 4001$, the function $\sigma(t)$ grows rapidly and linearly thus simulating a discharge in the slot with respect to the previously monotone increasing $E_z(g, t)$ -component (Fig. 6.9). This discharge converts the slot resonator into the section of a coaxial waveguide with a very weak inhomogeneity, and completely unlocks the compressor.

The results presented above show the validity of the basic steps in constructing the electromagnetic model of an energy compressor. We now turn our attention to the detailed study of special features in the energy accumulation process.

6.3.3 Distributed Switches and Active Compressors Based on Rectangular Waveguides

When dealing with planar models ($\partial/\partial x = 0$), we can analyze two types of waves: E -polarized waves (or TE_0 -waves) or H -polarized waves (or TM_0 -waves). In this section, we will consider TE_0 -waves, for which the following relations are valid:

$$U(g, t) = E_x(g, t), \quad E_y(g, t) = E_z(g, t) = H_x(g, t) \equiv 0, \\ \frac{\partial H_y}{\partial t} = -\eta_0^{-1} \frac{\partial E_x}{\partial z}, \quad \frac{\partial H_z}{\partial t} = \eta_0^{-1} \frac{\partial E_x}{\partial y}; \quad g = \{y, z\}$$

(see the equations (6.1a)–(6.1c) in Sect. 6.2.1 and [1, 7]).

Let the structure shown in Fig. 6.11 be excited by the pulsed TE_{01} -wave

$$U_1^{i(1)}(g, t) = v_{11}(z, t)\mu_{p1}(y) : v_{11}(-L_1, t) = 4 \frac{\sin[\Delta k(t - \tilde{T})] \cos[\tilde{k}(t - \tilde{T})]}{(t - \tilde{T})} \chi(\bar{T} - t) \\ = F_2(t); \quad \tilde{k} = 3.65, \quad \Delta k = 0.5, \quad \tilde{T} = 50, \quad \bar{T} = 100, \quad (6.15)$$

where \tilde{k} , Δk , \tilde{T} and \bar{T} stand for the central frequency of the signal, its band, delay time, and duration, respectively. A detailed description of the temporal and spectral characteristics of the pulse $F_2(t)$ could be found in the book [4], Fig. 4.3. In the frequency band $3.15 \leq k \leq 4.15$, the waveguides Ω_1 and Ω_2 sustain propagation of one and three undamped TE_{0n} -waves.

A compressor switch is a periodic system of quartz gas-discharge tubes ($\varepsilon = 3.8$) whose walls are 0.02 in thickness. Frequency characteristics of the accumulation mode and the release mode are presented in Fig. 6.12. Here $W_{n1}^{11}(k)$ ($W_{n1}^{21}(k)$) is the

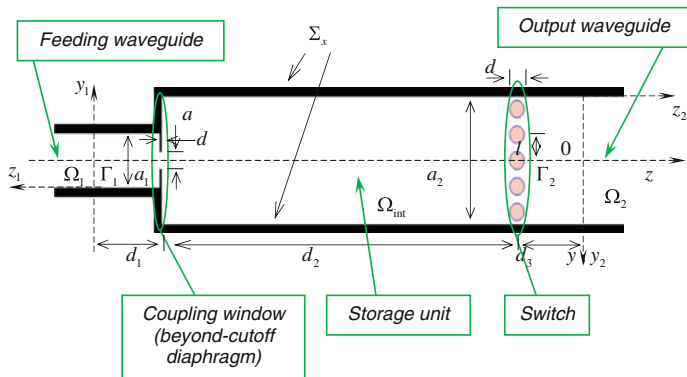
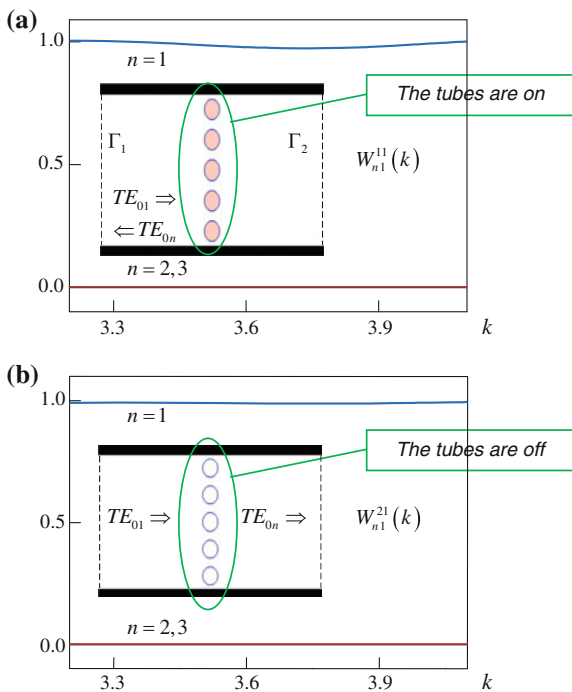


Fig. 6.11 Geometry of direct-flow compressor based on rectangular waveguide; $a = 0.4$, $a_1 = 1.28$, $a_2 = 3.0$, $L_1 = d_1 + d_2 + d_3 = 16.0$, $d_1 = 3.0$, $d_2 = 10.0$, $d_3 = 3.0$, $d = 0.06$, $l = 0.6$, $h = 0.4$; $z = -L_1$ ($z_1 = 0$) and $z = 0$ ($z_2 = 0$) are virtual boundaries. Reproduced courtesy of The Electromagnetics Academy

Fig. 6.12 Electrodynamics characteristics of the switch: **a** during energy accumulation (discharge tubes are on, switch is locked); and **b** during the release (discharge tubes are off, switch is unlocked). Reproduced courtesy of The Electromagnetics Academy



energy of the reflected (transmitted) TE_{0n} -wave if the TE_{01} -wave is incident on the virtual boundary Γ_1 . The material parameters of the gas in the switch are $\epsilon = 1.0$ and $\sigma = 5.7 \cdot 10^4$ for the accumulation mode and $\sigma = 0$ for the release mode.

By analyzing the resonant peaks of the spectral amplitudes $|\tilde{E}_x(g_1, k, \bar{T})|$ ($\tilde{E}_x(g, k, \bar{T}) \leftrightarrow E_x(g, t)\chi(t - \bar{T})$, see the formula (6.4) of the freely oscillating field $U(g, t)$, $g \in \Omega_{\text{int}}$, $t > \bar{T}$, determine seven values of $k \approx \text{Re } \bar{k}_{\text{stor}}$ (Fig. 6.13), choosing one of them as a working frequency for the compressor. Here, as before, $\text{Re } \bar{k}_{\text{stor}}$ is a real part of the complex-valued eigenfrequency \bar{k}_{stor} that corresponds to a high-Q free oscillation in the storage unit with a locked switch. The refined value of $\text{Re } \bar{k}_{\text{stor}}$, the oscillation pattern, and its quality factor can be found by exciting the compressor by a narrow-band Gaussian pulse

$$U_1^{i(1)}(g, t) : v_{1,1}(-L_1, t) = \exp\left[-(t - \tilde{T})^2 / 4\tilde{\alpha}^2\right] \cos[\tilde{k}(t - \tilde{T})]\chi(\tilde{T} - t) = F_3(t);$$

$$\tilde{k} \approx \text{Re } \bar{k}_{\text{stor}}, \quad \tilde{\alpha} = 20, \quad \tilde{T} = 100, \quad \bar{T} = 200, \quad g = \{y, z\} \in \Omega_1$$

(6.16)

and then studying the behavior of the functions $E_x(g_2, t)$, $t > \bar{T}$, where $g_2 \in \Omega_{\text{int}}$ is the point at the oscillation antinode (the relevant methodology is described in [12–14]). In Fig. 6.13, the peak marked ‘6’ corresponds to the $TE_{0,1,12}$ -oscillation (see Fig. 6.14b). Its Q-factor $Q \approx 6600$ ($\text{Re } \bar{k}_{\text{stor}} \approx 3.953$, $\text{Im } \bar{k}_{\text{stor}} \approx -0.0003$) is sufficient to construct the compressor.

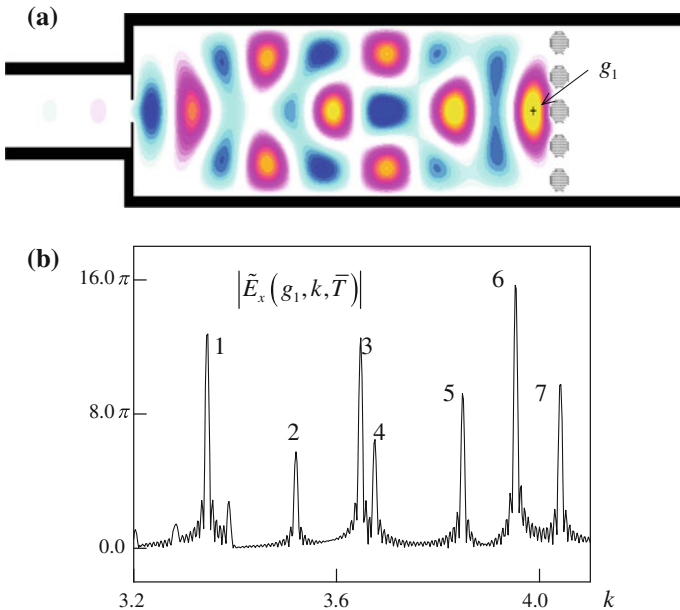


Fig. 6.13 Excitation of compressor by broadband pulse: **a** field pattern of $E_x(g, t)$ at $t = 902$; **b** spectral amplitudes $|\tilde{E}_x(g_1, k, \bar{T})|$ of free-oscillating field in antinodal point g_1

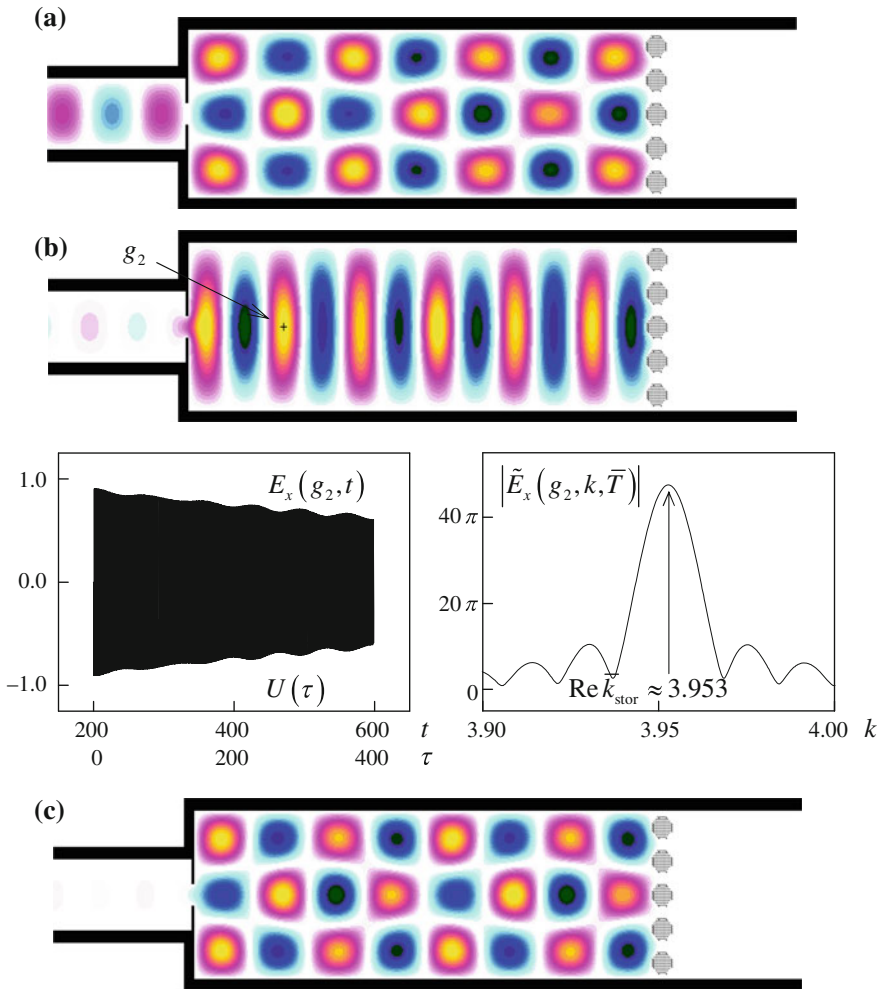


Fig. 6.14 Excitation of compressor by narrowband Gaussian pulse (6.16) with varying central frequency $\tilde{k} = \text{Re } \bar{k}_{\text{stor}}$: **a** $\tilde{k} = 3.85$ (fifth point in Fig. 6.13b); **b** $\tilde{k} = 3.95$ (sixth point), $\tilde{E}_x(g_2, k, \bar{T}) \leftrightarrow E_x(g_2, t)\chi(t - \bar{T})$; **c** $\tilde{k} = 4.04$ (seventh point). All field patterns are at $t = 210.5$ (free oscillation, $E_x(g, t)$ -component). Reproduced courtesy of The Electromagnetics Academy

To get complete information on the accumulation modes that can be realized in the compressor (see Fig. 6.15), calculate the eigenfrequencies $\bar{k}_{\text{stor}} = \text{Re } \bar{k}_{\text{stor}} + i \text{Im } \bar{k}_{\text{stor}}$ for $H_{0,1,12}$ -oscillations in the storage units with various dimensions of the coupling window between the feeder and the resonator and then excite each structure by a long quasi-monochromatic TE_{01} -pulse $U_1^{i(1)}(g, t) : \tilde{k} = \text{Re } \bar{k}_{\text{stor}}$. It is clear that the functions $u_{11}(-L_1, t)$ and $u_{12}(0, t)$ (the space-time amplitudes of the pulsed TE_{01} -waves outgoing into the waveguides Ω_1 and Ω_2) determine the

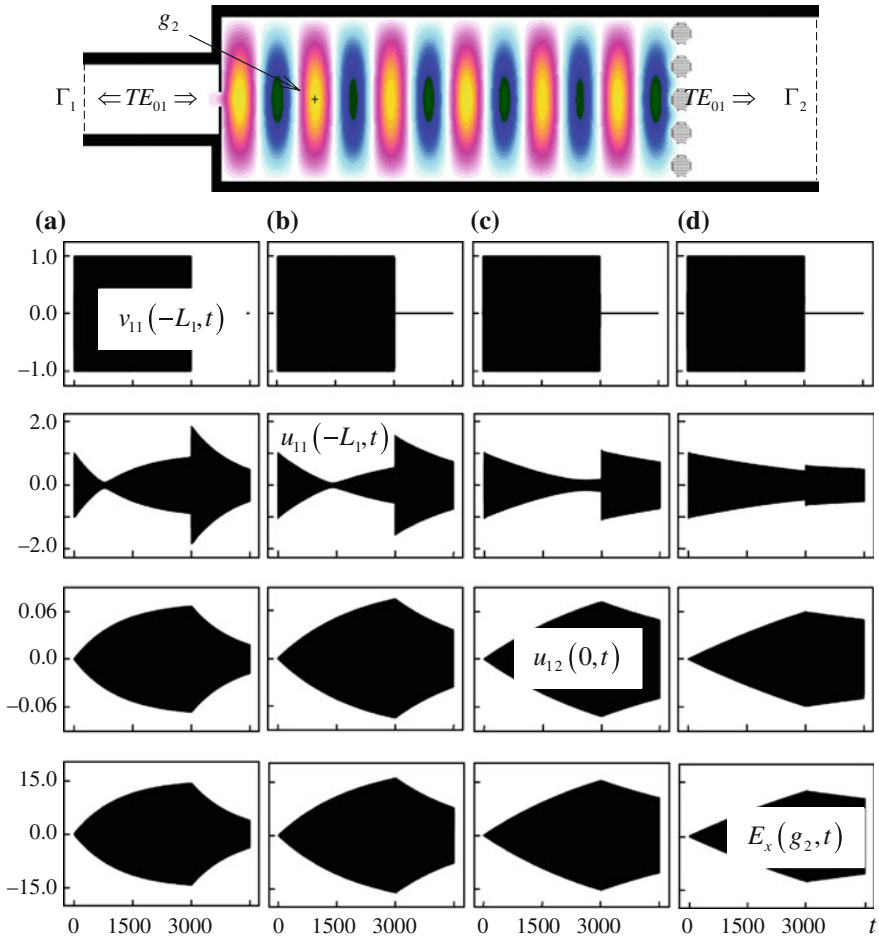


Fig. 6.15 Excitation of compressor with varying size of coupling window by long quasi-monochromatic pulse $U_1^{(1)}(g, t): v_{11}(-L_1, t) = F_1(t)$, $\tilde{T} = 1.0$, $P(t) : 0.1 - 5 - 3000 - 3004.9$, $T = 4500$ with varying central frequency \tilde{k} : **a** $a = 0.4$, $\tilde{k} = 3.953$; **b** $a = 0.36$, $\tilde{k} \approx 3.9546$; **c** $a = 0.32$, $\tilde{k} \approx 3.95625$; **d** $a = 0.28$, $\tilde{k} \approx 3.9575$. Reproduced courtesy of The Electromagnetics Academy

efficiency of energy accumulation $\gamma_{\text{accum}}(t)$ at each moment of time from the interval $0 < t < 3000$, while the function $E_x(g_2, t)$ specifies the amplitude of the signal obtained as a result of compression, the rate of its rise, and its limiting values. From the behavior of these functions, one can easily estimate the limiting duration $T^{i(1)}$ of the input pulse. Exceeding this value will result in substantial reduction in the compressor efficiency, and the amplitude of the compressed pulse will not gain even a slight increase.

When the size of the coupling window is fixed (i.e., fixed quality factor of the storage resonator), the accumulation efficiency depends only on the duration of the accumulation mode. The behavior of this non-monotonic dependence is almost the same for high-Q and low-Q resonators. The growing quality factor will cause the signal amplitude and the time, required to obtain the same value of γ_{accum} , to increase. As we can see, when constructing an electromagnetic model of a compressor, one should take into consideration and critically estimate a great body of options.

Let us consider in greater detail the compressor whose size of the coupling window is $a = 0.32$ (see Fig. 6.15c; $\text{Re}\bar{k}_{\text{stor}} \approx 3.95625$). Even with a slight deviation of the central frequency \tilde{k} of the input pulse from the value $\tilde{k} = \text{Re}\bar{k}_{\text{stor}}$, the compressor may lose its ability to accumulate energy, Fig. 6.16. Even 0.01% error in \tilde{k} may turn the storage unit to an ordinary reflecting inhomogeneity.

We have chosen the $TE_{0,1,12}$ -oscillation as a working oscillation; the working frequency of the compressor is $k_{\text{work}} = 3.95625 \approx \text{Re}\bar{k}_{\text{stor}}$, its Q-factor is $Q \approx 7912.5$ ($\text{Im}\bar{k}_{\text{stor}} \approx -0.00025$) Let us excite the structure by a long quasi-monochromatic TE_{01} -pulse $U_1^{i(1)}(g, t) : v_{1,1}(-L_1, t) = F_1(t); \tilde{k} = k_{\text{work}}, P(t) : 0.1 - 5 - 10100 - 10104.9, \tilde{T} = 1.0$. Let us also set the following operating

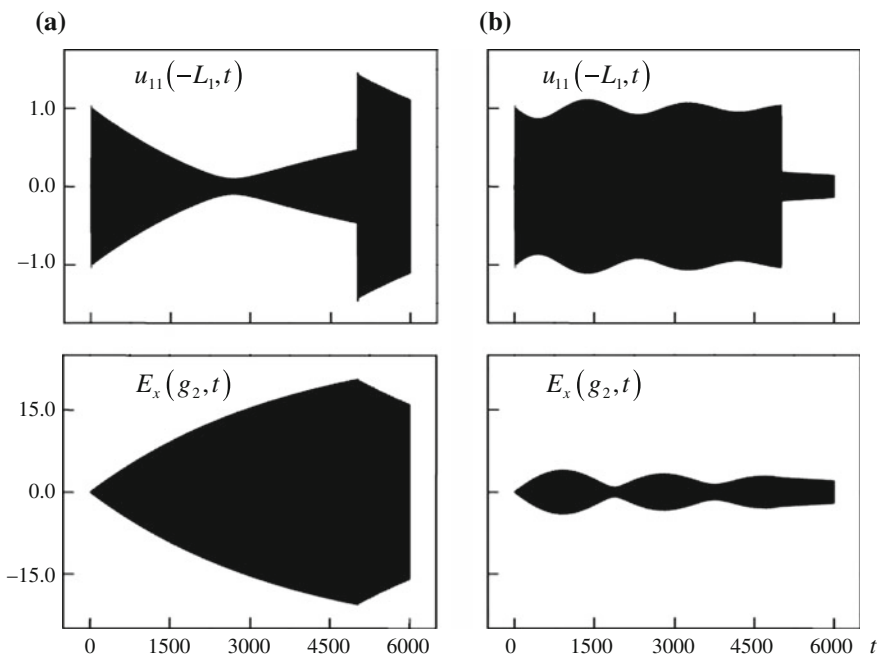


Fig. 6.16 Influence of central frequency \tilde{k} of incident TE_{01} -pulse ($U_1^{i(1)}(g, t) : v_{11}(0, t) = F_1(t), \tilde{T} = 1.0, P(t) : 0.1 - 5 - 5000 - 5004.9, T = 6000$) on compressor's ability to accumulate energy: **a** central frequency coincides with working frequency: $\tilde{k} = k_{\text{work}} = 3.95625$; **b** central frequency is slightly different: $\tilde{k} = 3.953$. Reproduced courtesy of The Electromagnetics Academy

Table 6.1 Energy accumulation efficiency at different observation times t

	$t = 2500$	5000	7500	10000
$\gamma_{\text{accum}}(t) \approx$	0.691	0.8	0.736	0.637
$\alpha(t) \approx$	0.509	0.774	0.906	0.981

regime for the switch (Fig. 6.12): during the time period until $t = 10000$ the switch is locked, for the moments of time $t > 10001$ it is open, and in the time interval $10000 \leq t \leq 10001$ the specific conductivity of the gas in the discharge tubes varies from $\sigma(t) = 5.7 \cdot 10^4$ to $\sigma(t) = 0$.

In Table 6.1 are given the energy accumulation efficiency $\gamma_{\text{accum}}(t)$ and the relative field-intensity level $\alpha(t) = \max_{0 < \tau \leq t} |E_x(g_2, \tau)| / \max_{\tau > 0} |E_x(g_2, \tau)|$ at the working oscillation antinode for different times (see also Fig. 6.17a–c).

The energy accumulation is completed and the accumulated energy is released at $t = T^{i(1)} = 10000$; a high-power short pulse crosses the boundary Γ_2 in a time $T^{s(2)} \approx 10025.5 - 10004 = 21.5$ (Fig. 6.17d). The degree of compression is $\beta = T^{i(1)} / T^{s(2)} \approx 465$; the efficiency is $\gamma = W^{s(2)}(10004; 10025.5) / W^{i(1)}(0; T^{i(1)}) \approx 0.6238$; the power gain is $\theta = \beta \times \gamma \approx 290$. The output pulse duration $T^{s(2)}$ is somewhat greater than the double length of the storage unit (see Fig. 6.11), what is predictable since the unlocked storage unit is not a resonant structure.

Notice that on the interval $10004 < t < 10025.5$ the amplitudes of the function $P^{s(2)}(t)$ are 325 and 16250 times greater than the maximal amplitudes of the functions $P^{i(1)}(t)$ and $P^{s(2)}(t)$ on the interval $0 < t < 10000$. The compressor efficiency is slightly below the accumulation efficiency $\gamma_{\text{accum}}(T^{i(1)})$ since a part of the accumulated energy is distributed among a short intense spike in the reflected signal (see Fig. 6.17) and the tail of the main pulse.

From the value of $k_{\text{work}} = 3.95625$ rad/m we determine the working wavelength $\lambda_{\text{work}} \approx 1.588$ m of the compressor whose storage unit is of length $d_2 = 10.0$ m (Fig. 6.11). The accumulation time required to obtain those characteristics is 33.3564 μs ; the pulse duration is 71.7163 ns. It should be noted that the results can be easily extended to any other geometrically similar structures. Thus, for example, the working wavelength $\lambda_{\text{work}} \approx 8$ mm requires the storage unit 50.38 mm in length and 168.042 ns of the accumulation time. The duration of the pulse formed by such a compressor will be 361.291 ps.

6.4 Radiation of High-Power Short Pulses

Almost any paper on microwave energy compression focuses on the design of a compressor as a whole [2, 19] or its (isolated) components [40, 41], on the generation of compressed pulses [42, 43], or, rarely, on the details of the energy accumulation [2, 15]). However, the design of a compressor and the generation of high-power short pulses are just one aspect of the problem. In most of applications,

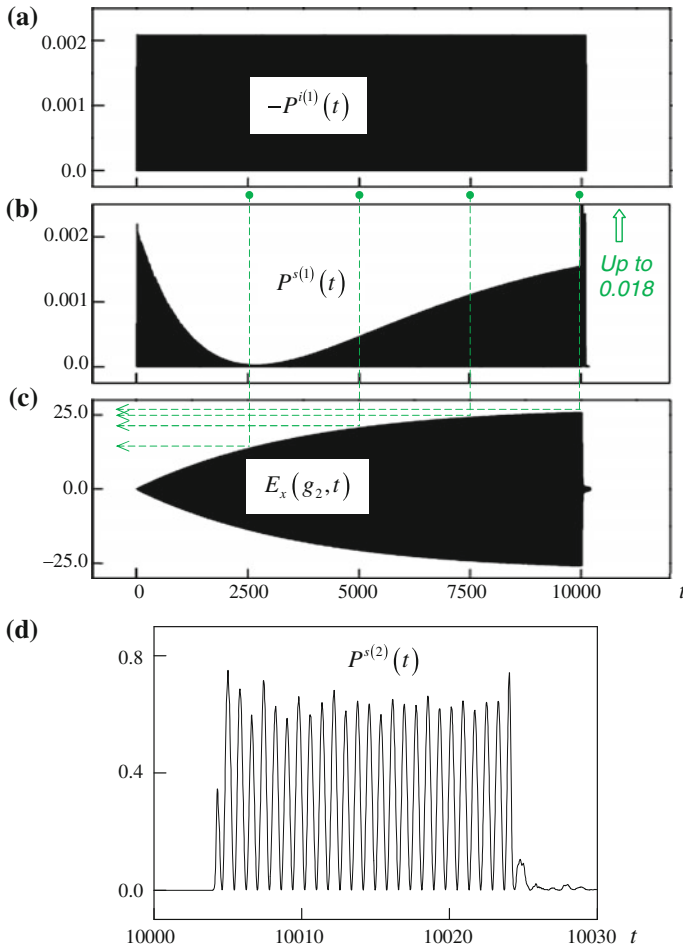


Fig. 6.17 Accumulation and release of energy ($a = 0.32$): **a** instantaneous power of excitation; **b** instantaneous power of wave reflected back into Ω_1 ; **c** $E_x(g, t)$ in antinodal point g_2 ; **d** instantaneous power of compressed pulse. Reproduced courtesy of The Electromagnetics Academy

an output pulse has to be transmitted to a load without significant distortion [27, 44] or to an antenna to be radiated [45, 46]. Propagation of a compressed pulse through waveguides is quite easy for study and understanding. However, the topic of radiation of compressed pulses is practically untouched. This section is intended to fill this gap.

The output of a microwave compressor is a high-power short pulse. The bandwidth of the compressed pulse is determined mostly by the spectral content of the input pulse and by the dynamics of energy accumulation and release processes. Since the compressor is a resonant device, the bandwidth of the compressed pulse is

not wide. No specially designed antenna is required to efficiently radiate a compressed pulse; in other words, one can use even simple antennas [7, 16, 26, 36, 47] to radiate a compressed pulse with low distortion. The corresponding antenna arrays can be used in specific applications.

The contributions of this section are twofold. First of all, it studies radiation of a short pulse from a monopole antenna mounted on a ground plane. The purpose of this study is to demonstrate that compressed pulses can be efficiently radiated by simple antennas. Besides, a novel array design is presented; each of the array elements combines a compressor and a radiator. The proposed design allows one to eliminate the feeder line between the compressor and the radiator and thus reduces the overall size and weight of the array. It also reduces the pulse distortion and absorption loss since the distance covered by the pulse in lossy and dispersive waveguides is reduced. Additionally, the proposed design has the advantage of compressing the pulse right before it is radiated. Therefore, one can use array components that do not necessarily designed for working with high power.

6.4.1 Radiation of Compressed Pulses by Simple Antennas

In this section, characteristics of a simple monopole antenna, which is mounted on an infinite ground plane and excited by a compressed pulse, which is an output of axially symmetric compressor (see Sect. 6.3.2), are studied. These studies are carried out in two steps. First, the characteristics of the monopole, namely the frequency-domain radiation efficiency and the power and pulse patterns, are obtained under a broadband excitation to observe all possible modes of operation. The interesting features of the obtained characteristics are pointed out. Then, the geometry of the monopole antenna is modified so that the antenna can be joined to the output waveguide of the axially symmetric compressor from Sect. 6.3.2, and the characteristics of the modified monopole under the compressed pulse excitation are studied.

The geometry of a monopole mounted on an infinite ground plane is shown in Fig. 6.18a. The antenna represents an elongated inner conductor of a coaxial waveguide over an infinite flange. Its geometrical dimensions are set as $a_1 = 1.0$, $b_1 = 0.3$, and $d = 1.57$. The electromagnetic wave transformations in this structure are described by the 2-D initial boundary value problem (6.11a, 6.11b, 6.11c), where in this case $0 \leq \vartheta \leq 90^\circ$. To calculate the electrodynamic characteristics of the monopole in a wide frequency band, the monopole is illuminated by a broadband pulse. Since the output of the axially symmetric compressor is a *TEM*-mode pulse, the monopole is excited by a wideband pulse of the same type. The excitation is implemented by setting $U_0^{i(1)}(g, t) : v_{01}^\rho(-L_1, t) = F_2(t)$, $\bar{T} = 100$, $L_1 = 0.5$, $T = 150$ and $\tilde{k} = 8$, $\Delta k = 7.5$, $\tilde{T} = 30$ (for the results presented in Fig. 6.18) or $\tilde{k} = 15$, $\Delta k = 10$, $\tilde{T} = 25$ (for the results presented in Figs. 6.19 and 6.20). These

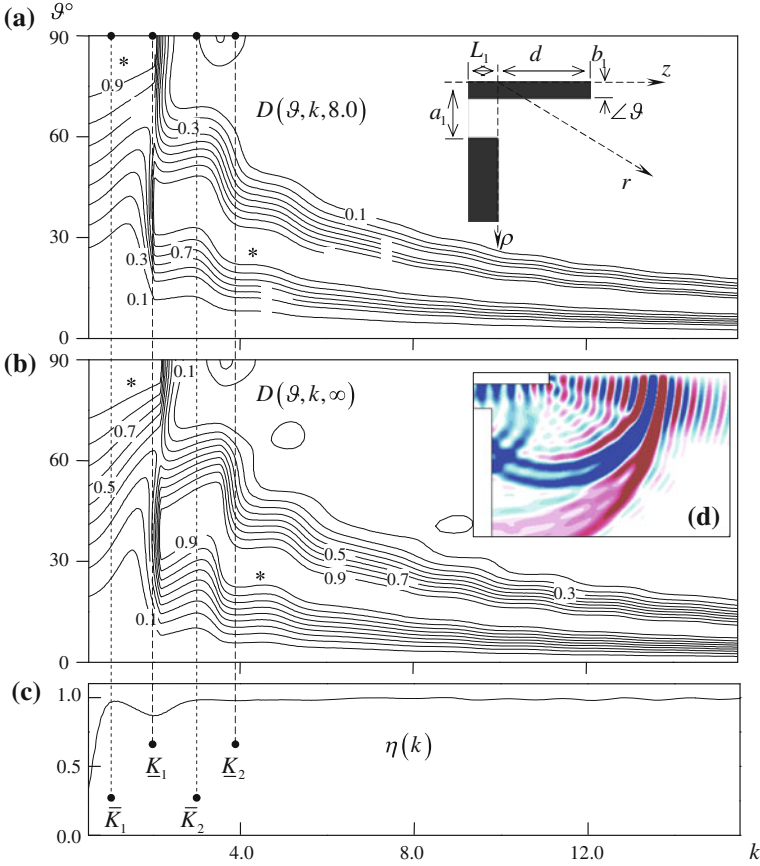


Fig. 6.18 TM_0 -waves. Characteristics of monopole: normalized power patterns $D(\vartheta, k, M)$ for **a** $M = L = 8.0$ and **b** $M = \infty$; **c** frequency-domain radiation efficiency $\eta(k)$; **d** spatial distribution of $H_\phi(g, t)(g \in \Omega_{\text{int}})$ at $t = 35$. Asterisks denote domains where $D(k, \vartheta, M) > 0.9$

signals occupy the frequency bands $0.5 \leq k \leq 15.5$ and $5.0 \leq k \leq 25.0$, within which the monopole exhibits the following behavior [7, 26].

The frequency-domain radiation efficiency, $\eta(k)$, grows monotonically from zero to $\bar{\eta}_1 \approx 1$ within the frequency band $0 < k < \bar{K}_1$ (see Fig. 6.18c). The first local maximum $\bar{\eta}_1$ of the function $\eta(k)$ occurs at $k = \bar{K}_1$, which approximately corresponds to $\lambda = 4d$; the second local maximum $\bar{\eta}_2$ occurs at $k = \bar{K}_2$, which approximately corresponds to $3\lambda = 4d$. It is obvious that the peaks are associated with the quarter-wave resonances. The first local minimum $\underline{\eta}_1$ of the function $\eta(k)$ occurs at $k = \underline{K}_1$, which approximately corresponds to $\lambda = 2d$, the second local minimum $\underline{\eta}_2$ occurs at $k = \underline{K}_2$, which approximately corresponds to $\lambda = d$. Clearly the minima are associated with the half-wave resonances.

For the frequencies $k > k_{21}^+ \approx 8.93$ (k_{n1}^+ are the cut-off frequencies of TM_{0n} -waves in the waveguide Ω_1), the frequency-domain radiation efficiency $\eta(k)$ is close to one. The normalized power pattern, $D(\vartheta, k, M)$, changes smoothly with increasing k , and its main lobe is gradually getting narrow and finally reaches the stable direction of $\bar{\vartheta}(k) < 10^\circ$ (see Figs. 6.18 and 6.19a).

In the frequency band $k < k_{11}^+$ (single-wave range) and at the beginning of the double-wave range, the function $D(\vartheta, k, M)$ changes abruptly in the vicinities of the points $k = \underline{K}_n$: the main lobe gets much closer to the z -axis and becomes narrower, and then smoothly turns back in the direction of large ϑ (Fig. 6.18a, b). This means that a pulse could be strongly distorted if its central frequency coincides with any of the frequency points \underline{K}_n .

For $0 < k < \underline{K}_1$ (relatively low frequencies), the radiated waves propagate transversely to the axis of symmetry (z -axis, see Fig. 6.18a, b). Hence, this mode of operation allows using a monopole as a feeding element for planar structures and paracylinder pulsed antennas.

The power patterns $D(\vartheta, k, M)$ on the boundary of the near-field zone (Fig. 6.18a: $M = L = 8.0$), in the intermediate-field region (Fig. 6.19a: $M = 30$), and in the far-field zone (Fig. 6.18b: $M = \infty$) differ moderately.

The pulse $U_0^{i(1)}(g, t)$, whose spectral amplitudes are non-zero only for $k > k_{11}^+$, is radiated without forerunner pulse, and its low-amplitude tail cannot compete with the main pulse (see the pulsed pattern $D_{\text{puls}}(\vartheta, t, 30)$ in Fig. 6.19b). The time-domain radiation efficiency $\xi(T)$ is higher than 0.97. The radiated signal is well-focused and propagates in the direction of $\bar{\vartheta}$, which is determined by the central frequency \tilde{k} of the pulse $U_0^{i(1)}(g, t)$: the larger \tilde{k} corresponds to the smaller $\bar{\vartheta}$ (see Fig. 6.19b, c, where $\tilde{k} = 15$ and $\bar{\vartheta} \approx 7^\circ$).

The spectral amplitudes of the signal $U_0^{i(1)}(g, t)$ in the band $k_{11}^+ < k < k_{21}^+$ are comparable with those in the band $k > k_{21}^+$, but the shape of the radiated pulse only partially replicates the shape of the primary signal (Fig. 6.20). Most of the low-frequency spectral components are scattered in the sector $\bar{\vartheta} + 5^\circ < \vartheta < 50^\circ$ (Fig. 6.19). For the primary signal $U_0^{i(1)}(g, t)$, which is free from those components, a monopole turns into a near-perfect antenna, whose efficiency is $\xi(T) \approx 0.98$. The radiated pulse is well-focused and retains the shape and the spectral composition of the primary signal.

Part of the information and reasoning presented above might be considered as predictable or well-known, but when collected together, they provide a deep insight into the physics of wave radiation from monopole antennas.

Let now a monopole antenna mounted on an infinite ground plane is fed by the output signal of the axially symmetric microwave compressor that was designed in Sect. 6.3.2. Recall that the output pulse here is the short high-power TEM -pulse $U(g, t) = U^{s(2)}(g, t) = u_{02}(z, t)\mu_{02}(\rho)$ ($g = \{\rho, z\} \in \Omega_2$), which was released into the coaxial output waveguide Ω_2 (see Fig. 6.10). The central frequency of this pulse is $\tilde{k} = 2.723$, its bandwidth is in the band $2.5 \leq k \leq 2.9$, and its duration is $T^{s(2)} \approx 21$.

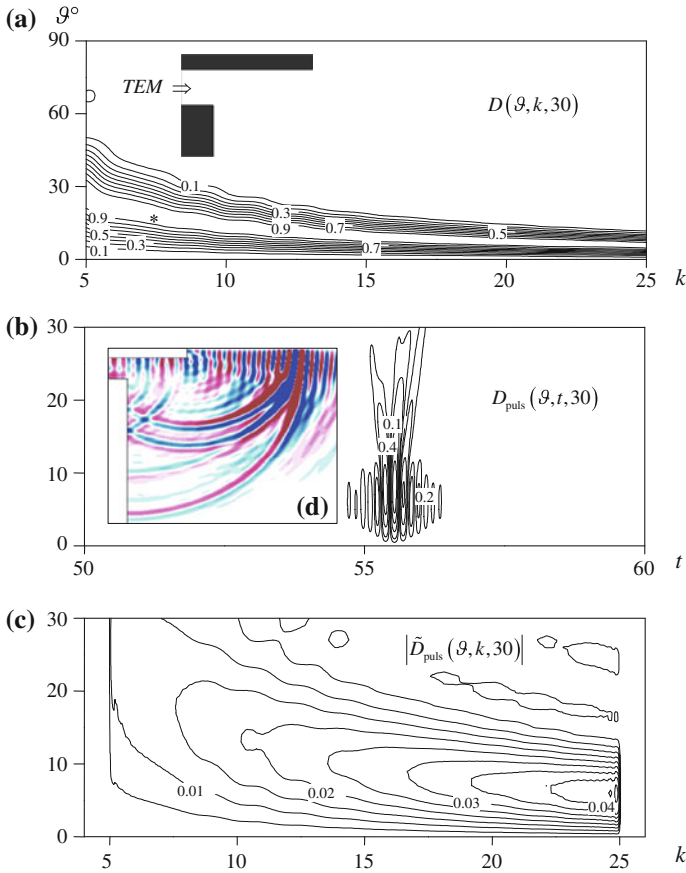


Fig. 6.19 Excitation of monopole by pulsed TEM-wave: **a** directional pattern ($M = 30$, intermediate-field region); **b** pulsed pattern; **c** spectral amplitudes of pulsed pattern and **d** field pattern for $H_\phi(g, t)(g \in \Omega_{\text{int}})$ at $t = 30$

The radii of the inner and the outer conductors of the waveguide Ω_2 are 0.9 and 1.56, respectively.

The modified monopole antenna (see Fig. 6.21a) is designed from the simple monopole studied above. The feeding waveguide Ω_1 of this antenna is interfaced with the coaxial waveguide Ω_2 of the compressor ($a_1 = 1.56$, $b_1 = 0.9$). The radiator replicates (a one-third scale model) the geometry of the monopole, whose characteristics are presented in Figs. 6.18, 6.19, 6.20 ($c + b_1 = 3.0$, $d = 4.71$). The modified monopole antenna is excited by the compressed pulse $U_0^{i(1)}(g, t)$: $v_{01}^\rho(-L_1, t) = u_{02}^\rho(0, t + 3980)$, $t > 0$, $\bar{T} = 100$, $T = 150$. Its time signature is shown in Fig. 6.21b.

Taking into account the frequency band $k = \tilde{k} \pm 0.2 = 2.723 \pm 0.2$ of the compressed pulse and studying the data associated with the band $k = 3\tilde{k} \approx 8.17 \pm 0.7$ in

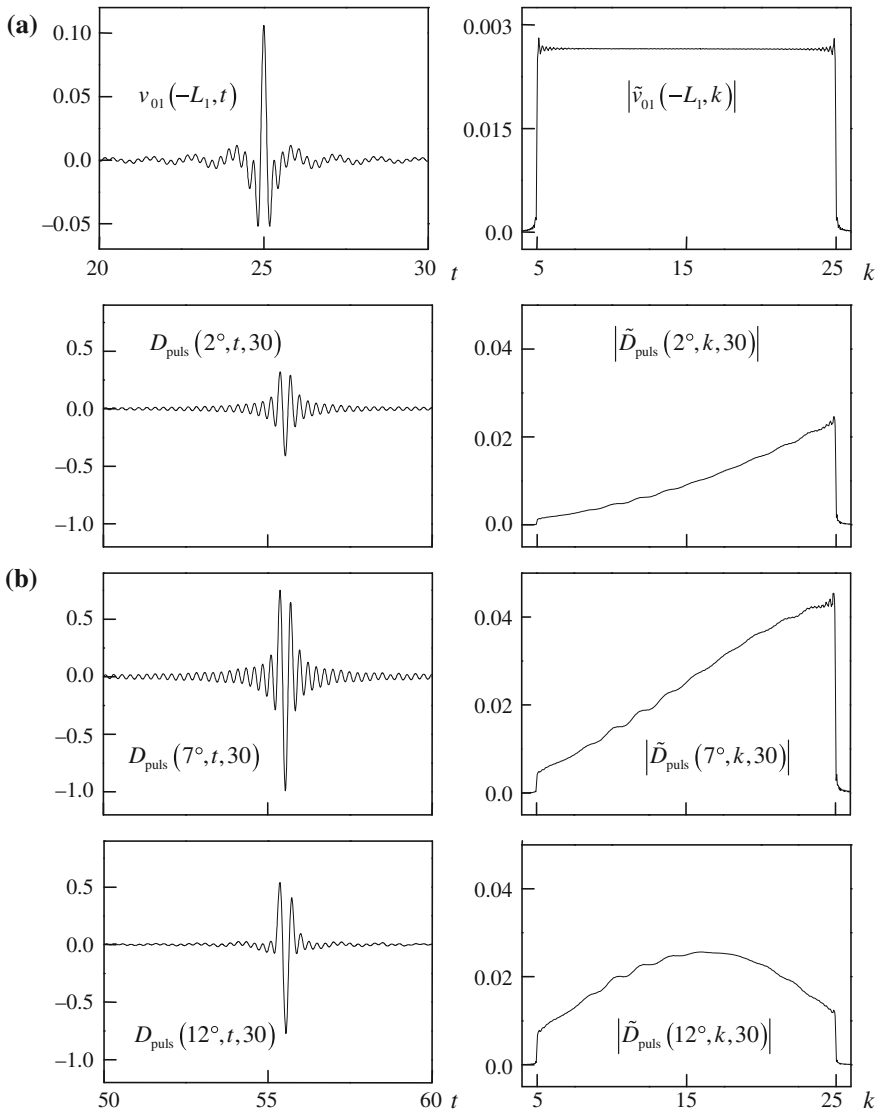


Fig. 6.20 Temporal and spatial amplitudes of **a** H_ϕ -component of primary TEM -pulse $U_0^{i(1)}(g, t)$ and **b** pulsed patterns $D_{\text{puls}}(\vartheta, t, 30)$ for various ϑ

Figs. 6.18, 6.19, 6.20 (the threefold increase in frequency is caused by the changes in the monopole geometry), one can state with confidence that the efficiency and the directivity of radiation from the modified monopole will be rather high. The simulation data fully confirm this statement (see Figs. 6.21c and 6.22): the time-domain radiation efficiency is $\xi(T) \approx 0.981$, the frequency-domain radiation efficiency

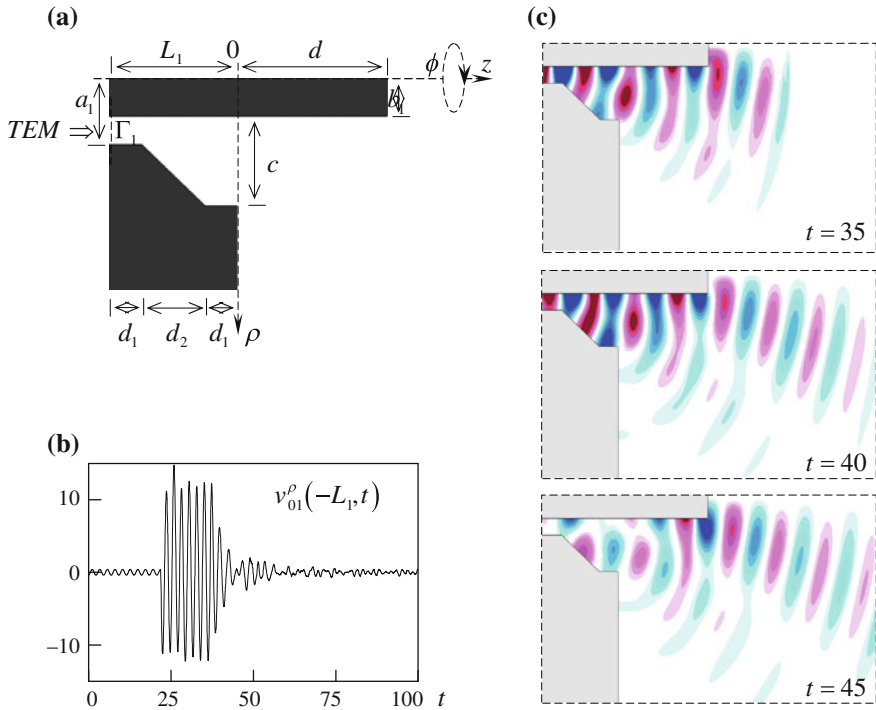


Fig. 6.21 **a** Geometry of modified monopole ($d_1 = 1.0, d_2 = 2.0, L_1 = 2d_1 + d_2$); **b** time signature of input (compressed) pulse: amplitude of E_p -component of TEM -wave $U_0^{i(1)}(g, t)$ on Γ_1 ; **c** field patterns of $H_{\phi}(g, t), g \in \Omega_{int}$. Reproduced courtesy of The Electromagnetics Academy

varies from $\eta = 0.965$ (at $k \approx 2.87$) до $\eta = 0.999$ (at $k \approx 2.6$), the direction of the main lobe of the pulsed pattern is $\vartheta_{puls} \approx 15^\circ$ and the half-amplitude beamwidth of this lobe is $\vartheta_{puls, 0.5} \approx 13^\circ$ (see Fig. 6.22). The weak side lobe ($\vartheta \approx 45^\circ$) is caused by the radiation of the undamped TM_{01} -mode, which is excited in the wider coaxial waveguide when $k > 1.47$.

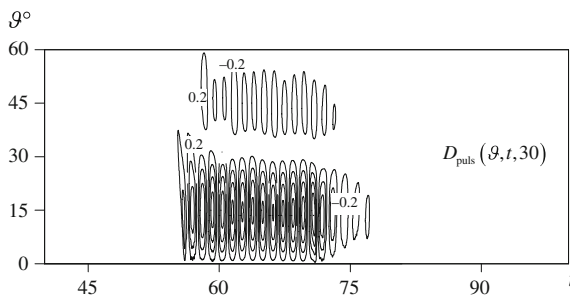


Fig. 6.22 Normalized pulsed pattern $D_{puls}(\vartheta, t, M), M = 30$

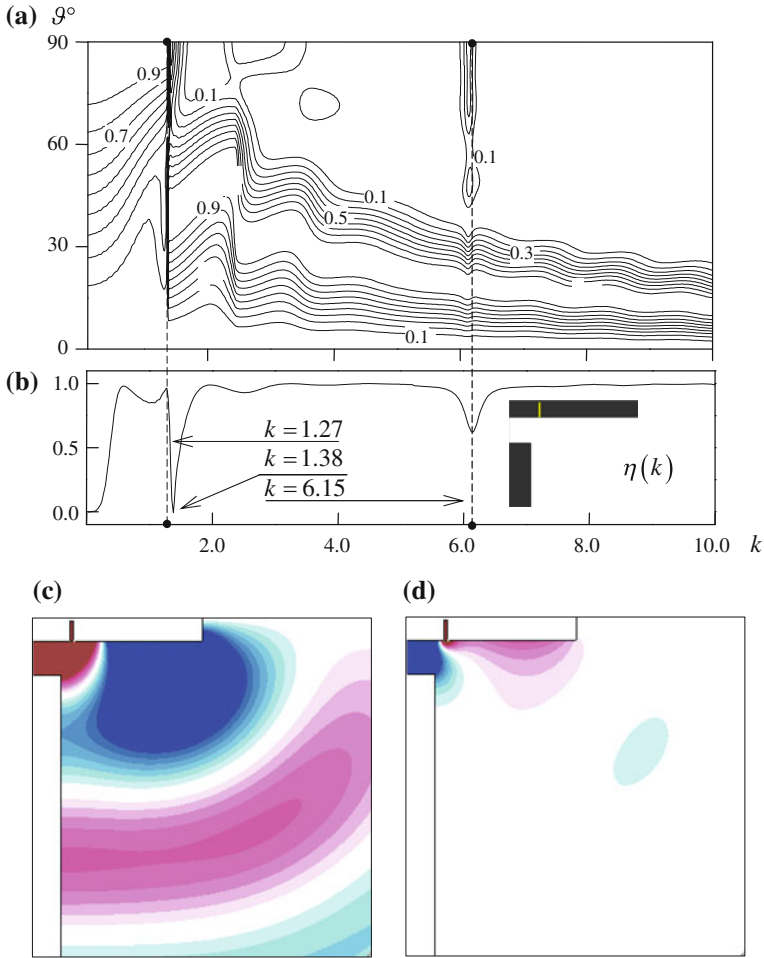


Fig. 6.23 Narrow transverse groove ($\varepsilon = 4.0$) in monopole. **a** Directional pattern and **b** radiation efficiency. Field pattern for $H_\phi(g, t)$; excitation by quasi-monochromatic *TEM*-waves with central frequencies $\tilde{k} = 1.27$ (**c**—maximal radiation efficiency) and $\tilde{k} = 1.38$ (**d**—antenna ‘blindness’)

In conclusion of the discussion, we point to the result [36], which makes important additions to the traditional understanding of the characteristics that can be achieved by using simple monopole antennas. Transverse quarter-wave groove in the extension of the central conductor of the feeding line (see Fig. 6.23, where the groove width is 0.06, the groove depth is 0.36; the plane $z = 0.2$ bisects the groove) significantly changes the behaviour of the function $\eta(k)$ in the vicinity of the point $k \approx 1.3$, which corresponds to the first half-wave resonance along the monopole length d . Here, in accord with the notation of Fig. 6.18a, $a_1 = 1.0$, $b_1 = 0.4$, $d = 2.5$, and $L_1 = 0.5$).

The patterns $D(\vartheta, k, \infty)$ for the radiators with a groove and without it (Figs. 6.18b and 6.23a) are almost the same. The only distinction is the presence of side lobes in the radiation field of the modified antenna in the vicinity of the second quarter-wave groove resonance ($k \approx 6.15$). The values of $D(\vartheta, k, \infty)$ for these lobes are less than 0.3 (for the lobe with the lower value of $\bar{\vartheta}$) and 0.4.

The groove position with respect to the plane $z = 0$ is an important parameter in the control of the basic radiator characteristics. For example, if the groove is shifted along the z -axis for a distance of 1.2, then the radiation efficiency would fall to 35% at $k \approx 1.28$ and would grow to 100% at $k \approx 1.42$. The distinctions in the radiation characteristics are caused basically by the phase difference between the oscillation in the groove and the wave guided by the monopole. It is easily observable from the spatial distributions of the function $H_\phi(g, t)$ in Fig. 6.23c (maximal radiation efficiency; zero phase difference) and in Fig. 6.23d (minimal radiation efficiency; opposite phases).

Even though the results presented in this section show that a monopole antenna can be used efficiently for radiating short pulses, more complex antennas or antenna arrays might be needed for solving some specific problems. More directive radiation patterns can be obtained using advanced antennas such as horn-type or reflector antennas, or arrays of the elements of this kind [4, 7, 26]. In the next section, the radiation of compressed pulses from phased antenna arrays is discussed and a new design, where each of the array elements is constructed by combining a radiator and a microwave compressor, is proposed.

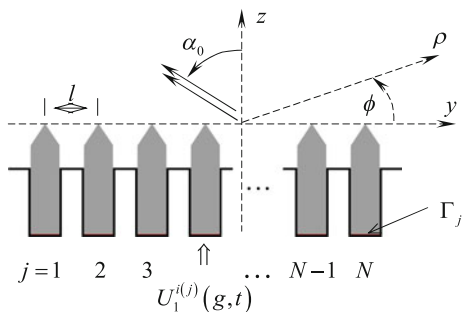
6.4.2 Novel Antenna Array Design with Combined Compressor/Radiator Elements

Analysis and design of phased antenna arrays [48] are based basically on the methods and results of grating theory. To calculate actual constructions, rather universal and reliable 3-D models are required. However, many vital issues, in particular, questions associated with the physics of wave transformation in phased antenna arrays, can be successfully resolved using 2-D models. Below a series of such problems are considered basing on the approaches and results of the previous sections and book [4].

In [4], a 2-D phased array (see Fig. 6.24: a planar model contains 13 radiating elements being excited by TE_{01} -waves of rectangular feeding waveguides) was designed, whose radiation efficiency $\eta_{\text{array}}(k)$ in the frequency band $168 \leq k \leq 251$ ($f = 8 \div 12\text{GHz}$, $k = 2\pi/\lambda = 2\pi\sqrt{\epsilon_0\mu_0}f$) and for the scanning sector $45^\circ \leq \phi \leq 135^\circ$ does not fall below 0.9.

The function $\eta_{\text{array}}(k)$ obviously extends $\eta(k)$ to the case of compact grating structures with more than one feeding waveguides. The width $\phi_{0.5}(k)$ of the main (and actually the sole) lobe of the pattern for this phased array varies from 7.0° ($k = 251$, $\bar{\phi} = 90^\circ$) to 13.9° ($k = 168$, $\bar{\phi} = 90^\circ \pm 45^\circ$), while its directivity $\bar{\phi}(k)$

Fig. 6.24 Geometry of 2-D phased array



fully complies with the expected one: $\bar{\phi}(k) = 75^\circ$ for $\Delta t = \sin(15^\circ)l \approx 0.36$, $\bar{\phi}(k) = 60^\circ$ for $\Delta t = \sin(30^\circ)l \approx 0.7$, and $\bar{\phi}(k) = 45^\circ$ for $\Delta t = \sin(45^\circ)l \approx 0.99$. When operating in the pulse mode and for $\Delta t = \sin(-\alpha_0)l$, the beam associated with the zeroth spatial harmonic of the infinite grating goes away from the grating at an angle of α_0 [4]. The angle $\alpha_0 = \phi - 90^\circ$ is measured from the z -axis anticlockwise; l is the grating period. The value Δt is the delay in the excitation of the radiating elements such that if the first grating element is excited by the wave $U_1^{i(1)}(y, z, t)$, then the second one is excited by the wave $U_1^{i(2)}(y, z, t) = U_1^{i(1)}(y - l, z, t + \Delta t)$, and so on.

Let us modify the grating investigated in [4] in such a way that having the period of $l = 1.4$, it can form and directionally radiate high-power short pulses in the frequency band $1.68 \leq k \leq 2.51$. Taking into account a hundred-fold reduction in the frequency (as compared with the prototype from [4]) and the necessity of building the resonance storage unit in the antenna-feeder path, choose the radiating element whose geometry is shown in Fig. 6.25a.

Following the technique presented in the previous section, let us excite the radiator by the TE_{01} -pulse that occupies the frequency band of interest. From the behavior of the spectral amplitudes $\tilde{u}_{11}(-L_1, k, 250) \leftrightarrow u_{11}(-L_1, t)\chi(t - 250)$ of the signal $U^{s(1)}(g, t)$, $t \geq 250$ outgoing into the rectangular virtual waveguide Ω_1 (see Fig. 6.25b and [12–14]) determine the frequency corresponding to a high-Q free oscillation in the storage unit: $k \approx \text{Re} \bar{k}_{\text{stor}} \approx 2.329$. Exciting the storage resonator with a quasi-monochromatic signal $U_1^{i(1)}(g, t)$: $v_{11}(-L_1, t) = F_3(t)$, $\bar{k} = 2.329$, $\tilde{\alpha} = 22$, $\tilde{T} = 100$, $\bar{T} = 200$ (a narrow-band Gaussian pulse) and then analyzing the behavior of the function $U(g, t)$, $t > 200$ at the antinode (Fig. 6.26), we determine the mode of oscillation ($TE_{0,1,3}$), the imaginary part of its complex-valued eigenfrequency ($\text{Im} \bar{k}_{\text{stor}} \approx -0.00095$) and the Q-factor ($Q \approx 1225.8$).

Some data for the radiating element operating in the accumulation mode are presented in Fig. 6.27 and in Table 6.2.

Here as before $\gamma_{\text{accum}}(t)$ is the energy accumulation efficiency over the interval $(0, t)$, while $\alpha(t)$ defines the relative level of the field strength at the antinode of the working oscillation. For $t \geq 4500$, the function $\alpha(t)$ reaches one: $\alpha(t) \approx 1$. There is

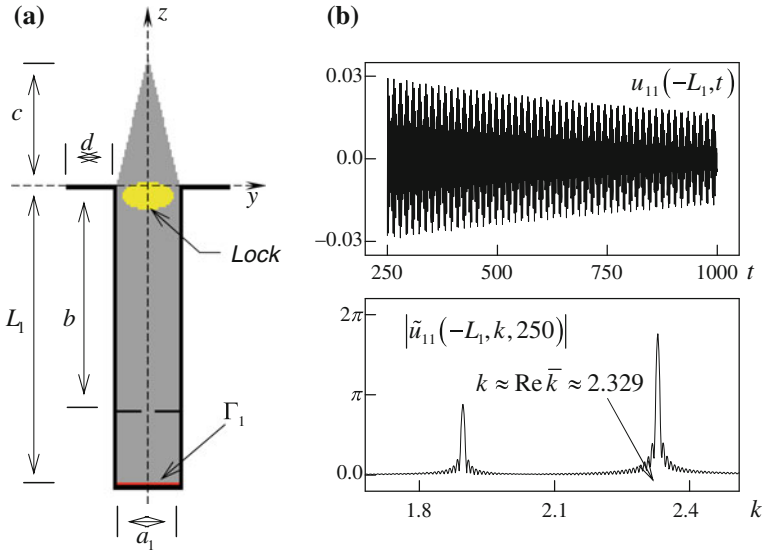


Fig. 6.25 **a** Geometry of radiating element: $a_1 = 1.32$; $b = 3.6$; $c = 2.0$; $d = 1.0$; $L_1 = 4.8$; thickness of metal walls is 0.08; the diaphragm thickness is 0.04; size of the diaphragm window is 0.28; permittivity of dielectric parts is $\epsilon = 2.5$ everywhere including the lock, for which $\sigma(t) = 5.7 \cdot 10^4$ in accumulation mode and $\sigma(t) = 0$ in release mode. **b** Excitation by TE_{01} -wave $U_1^{i(1)}(g, t) = v_{11}(z, t)\mu_{11}(y) : v_{11}(-L_1, t) = F_2(t)$, $\tilde{k} = 2.1$, $\tilde{T} = 100$, $\bar{T} = 200$, $T = 1000$. Reproduced courtesy of The Electromagnetics Academy

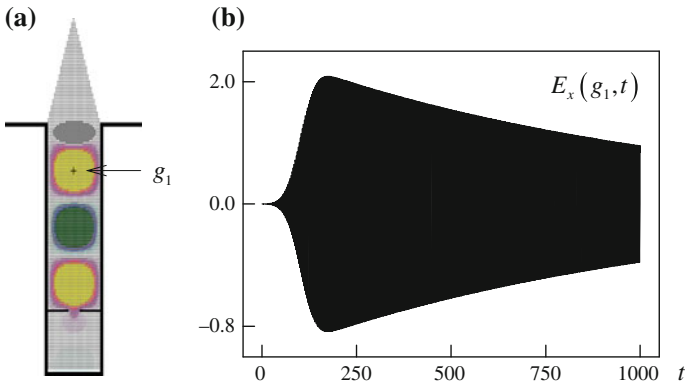


Fig. 6.26 Excitation by quasi-monochromatic TE_{01} -wave: **a** field pattern of $E_x(g, t)$ at $t = 250$ (free oscillation mode); **b** E_x in g_1 . Reproduced courtesy of The Electromagnetics Academy

no point in further accumulation of energy. For $T^{i(1)} > 4500$, the device efficiency drastically decreases, while the amplitude of the compressed pulse is no longer growing. Notice that the data in Tables 6.1 and 6.2 correlate well. With different

Fig. 6.27 Excitation in accumulation mode by long quasi-monochromatic pulse $U_1^{i(1)}(g, t): v_{11}(-L_1, t) = F_1(t)$, $\tilde{k} = 2.329$, $P(t): 0.1 - 5 - 4000 - 4004.9$, $\tilde{T} = 1.0$, $T = 4000$. The instantaneous **a** input and **b** output power on the boundary Γ_1 **c** the electric field strength at the point $g = g_1$. Reproduced courtesy of The Electromagnetics Academy

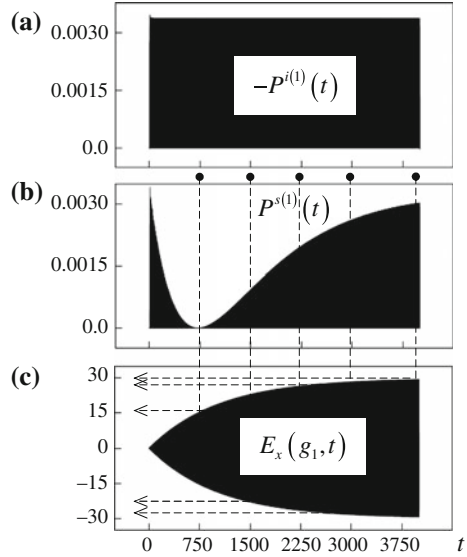


Table 6.2 Energy accumulation efficiency at different observation times t

	$t = 750$	1500	2250	3000	4000
$\gamma_{\text{accum}}(t) \approx$	0.74	0.81	0.72	0.61	0.49
$\alpha(t) \approx$	0.52	0.78	0.90	0.96	0.99

resonators, working oscillation modes, working frequencies, and quality factors, the parameters of the accumulation processes calculated for those portions of the t -axis, where the functions $P^{s(1)}(t)$ ($u_{11}(-L_1, t)$) behave qualitatively the same, are close. This observation provides the means of controlling the compressor operational parameters.

Let us consider the accumulation mode with $T^{i(1)} \approx 3000$ and excite the radiator with the storage unit and the plain radiator (Fig. 6.28) by a long quasi-monochromatic pulse

$$U_1^{i(1)}(g, t) : v_{11}(-L_1, t) = F_1(t); \quad (6.17)$$

$$\tilde{k} = k_{\text{work}} = 2.329, \quad P(t) : 0.1 - 5 - 3095 - 3099.9, \quad \tilde{T} = 1.0.$$

The conductivity of the switch, the piecewise linear function $\sigma(t)$, equals $5.7 \cdot 10^4$ for $t \leq 2994$ and is zero for $t \geq 2995$. At the instant of time $t = T^{i(1)} = 2995$, a high-power short pulse is released and passes the point $g = g_2$ in a time $T^{s(2)} \approx 3015 - 3000 = 15$ (see Fig. 6.28a). The degree of compression is equal to $\beta = T^{i(1)} / T^{s(2)} \approx 199.7$; the efficiency is $\gamma \approx 0.608$; the power gain is $\theta = \beta \times \gamma \approx 121.4$. In the interval $3000 < t < 3015$, the amplitude of the compressed pulse passing the point $g = g_2$ is 13 times greater than the amplitude of the uncompressed

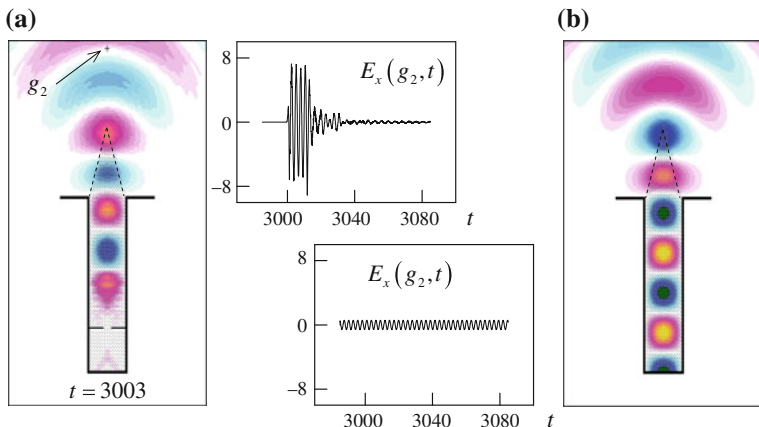


Fig. 6.28 Radiation of **a** compressed and **b** uncompressed pulses under excitation by long quasi-monochromatic pulse (6.17). Reproduced courtesy of The Electromagnetics Academy

pulse. The compressor efficiency is somewhat below the accumulation efficiency $\gamma_{\text{accum}}(T^{i(1)})$, since a part of the accumulated energy falls on the pulse tail (see the function $E_x(g_2, t)$ for $t \geq 3015$ in Fig. 6.28a).

To simulate the shaping and directional radiation of short high-power pulses, compose a grating of 13 identical radiators. The grating period is $l = 1.4$. Let the first radiator is fed by the wave $U_1^{i(1)}(y, z, t)$ (see the formula (6.17)), the second one — by $U_1^{i(2)}(y, z, t) = U_1^{i(1)}(y - l, z, t + \Delta t)$; $\Delta t = \sin(-\alpha_0)l$, $|\alpha_0| < 45^\circ$, and so on. The first radiator is released at $t = t_1 = 2995$, the second one — at $t = t_2 = t_1 + \Delta t$, and so on. The energy accumulation in each of the elementary radiators lasts for equal time intervals. The numerical results for $\Delta t = \sin(30^\circ)l \approx 0.7$ are presented in Fig. 6.29. The amplitudes of the pulse with a near-flat front are somewhat greater than the amplitudes of the pulses formed by isolated elements. These pulses are of the same duration. The radiation directivity is very high, the width of the main lobe of the pattern ($\bar{\phi}(k) \approx 60^\circ$) does not exceed the value $\phi_{0.5} = 8.3^\circ$ in the frequency band occupied by the pulse. As the value $\Delta t = \sin(-\alpha_0)l$ changes within the range $0 \leq |\Delta t| \leq 0.99$, the scanning sector of the high-power short pulse in the half-space $z > 0$ is $|\alpha_0| \leq 45^\circ$.

6.5 Compression of Frequency-Modulated Electromagnetic Pulses in Hollow Waveguides

The idea of *passive compression* of radio-frequency pulses has been formulated long ago (see, for example, [49–54]). If a section of a dispersive waveguide is fed by a pulse modulated in frequency and amplitude according to a certain law, then it

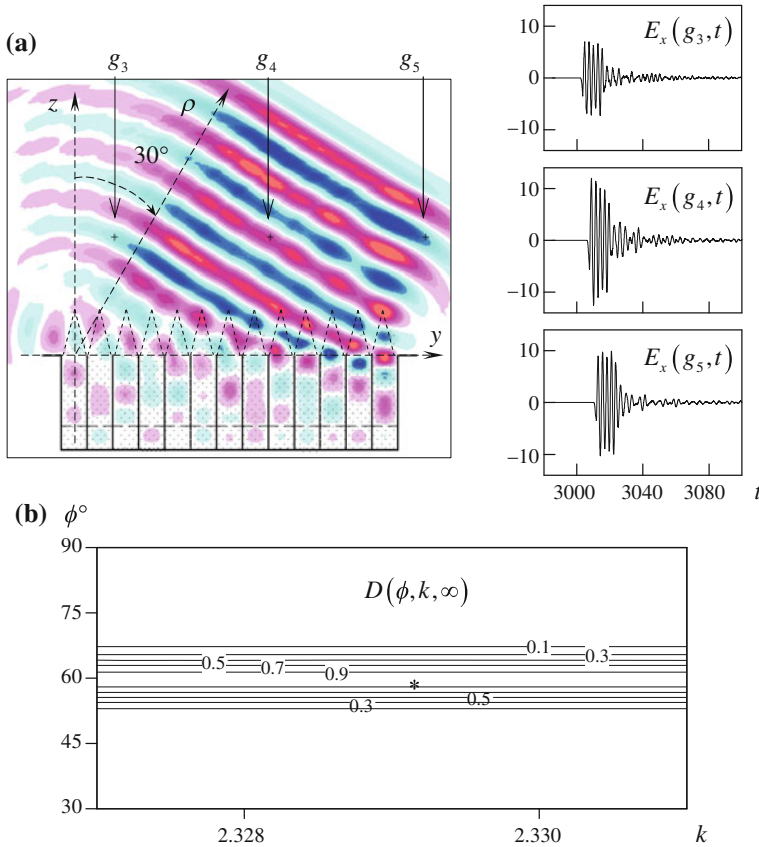


Fig. 6.29 Compression and radiation by the grating of 13 elements. **a** Field pattern of $E_x(g, t)$ ($g \in \Omega_{\text{int}}, t = 3014$) and $E_x(g, t)$ in near-field zone. **b** Directional pattern in frequency band of primary pulse $U_1^{i(1)}(g, t)$

is possible to make all the frequency components of the pulse to arrive in-phase and simultaneously at a certain point. It would be accompanied by an increase in the pulse amplitude and a decrease in its length. The main theoretical problem which should be solved in this situation is to determine the law of amplitude and frequency modulation of the input pulse.

Despite the apparent simplicity of this problem and a great number of theoretical and experimental studies on the subject [49–58], the results to date seem to be rather modest. For example, the attained compression factor (degree of compression), i.e., the input-to-output pulse length ratio, is several tens at best. The progress observed in the field over the last fifty years concerns basically the transition to shorter wavelengths rather than increasing the degree of compression. This situation may be explained by the inadequate efficiency of mathematical models, which

precede full-scale physical experiments. In our opinion the main shortcoming of the works we are familiar with is explicit or implicit use of the so-called *kinematic approximation* (see, for example, [58]), in the context of which the input pulse is represented (often purely conceptually) as a continuous chain of particles (wave packets) each entering the dispersive element of a compressor with its own time delay. Assuming (without any foundation) that the frequency dependencies of the particle speed and of the electromagnetic wave group velocity in a waveguiding section of a compressor coincide, the kinematic equations of motion are used to determine both the time delays, i.e., the law of frequency modulation of the input pulse, and the optimum length of the dispersive element, i.e., the distance that particles pass to meet at one point. Undoubtedly, the kinematic representation describes qualitatively physical processes in a compressor. However, as shown below, it proves to be a very crude approximation and is unsuitable for rigorous modeling and design.

In this section the possibility of pulse compression in regular homogeneous waveguides of arbitrary cross-section is discussed. The main advantages of the approach we have developed are the use of rigorous methods for calculating electrodynamic characteristics and accurate numerical experiments, whose results can be replicated in actual devices. The main idea for determining the required modulation law is in solving first an inverse problem. If we know the pulse shape to be obtained, then applying this pulse to the output of the dispersive system and changing the time variable t by $-t$, we obtain the required input pulse. Once the time profile of the input signal is found, there is no problem to determine its modulation law. Such numerical experiments were first suggested in paper [59]. The approach is universal and can be easily applied to any dispersive medium (at least linear one) or waveguiding systems.

6.5.1 Transport Operators for Regular Waveguides

The well-known dependence of the relative group velocity $v_n(k) = \sqrt{1 - (k_n^+/k)^2}$ on the frequency k [60] suggests that the compression of frequency-modulated pulses can be observed even in simple dispersive systems like regular waveguides. Here k_n^+ is the cutoff frequency of the n th mode. For numerical simulation of this effect the robust and efficient algorithm is required, which is capable to calculate transformations of the time profile of a pulsed n th mode during its travel through a waveguide. Works [1, 3, 6, 7, 21–23] introduce the transport operators in two arbitrary cross-sections of a hollow regular semi-infinite waveguide with perfectly conducting walls. One of the operators for the space-time amplitudes $u_n(z, t)$ of any longitudinal or transverse component of the n th waveguide mode is the formula (5.198) in Chap. 5:

$$u_n(z, t) = \mp \int_0^t J_0 \left[\alpha_n \left((t - \tau)^2 - z^2 \right)^{1/2} \right] u'_n(0, \tau) d\tau; \quad t \geq 0. \tag{6.18}$$

From (6.18) it follows [1, 3, 7] that

$$u_n(0, t) = \mp \int_0^t J_0 [\alpha_n(t - \tau)] u'_n(0, \tau) d\tau; \quad t \geq 0 \tag{6.19}$$

and

$$\left[\pm \frac{\partial}{\partial z} + \frac{\partial}{\partial t} \right] u_n(z, t) \Big|_{z=0} = -\alpha_n \int_0^t J_1 [\alpha_n(t - \tau)] (t - \tau)^{-1} u_n(0, \tau) d\tau; \quad t \geq 0. \tag{6.20}$$

Here, $u'_n(a, t) = \partial u_n(z, t) / \partial z|_{z=a}$; $J_m(\dots)$ are the Bessel functions; z is supposed to be the longitudinal axis of a waveguide and the upper and the lower signs correspond to the waves propagating toward increasing and decreasing z , respectively. Magnitudes of the transverse eigenvalues α_n depend on a waveguide type and the wave polarization and can be calculated analytically for waveguides with simple cross-section geometry. The values of α_n (that are equal to λ_{nj}) for parallel-plate, circular and coaxial waveguides are given in Sects. 6.2.1 and 6.2.2. The transverse eigenvalues α_n for waveguides with more complex geometry can be determined numerically.

The transport operators are exact in the sense that they strictly follow from the Maxwell’s equations. For this reason, they can be used with no restrictions when investigating the transformation of a pulse with arbitrary waveform during its travel through a waveguide. In particular, the signal spectrum can be different from zero at frequencies above and below the cutoff point [24]. This property is of the highest importance in numerical experiments. Any inaccuracy in calculating the time dependence of the input signal, which gives rise to spectral components below the cutoff point, is not disastrous for algorithms implementing EACs like (6.18)–(6.20). All such components are damped rapidly as the pulse propagates along a waveguide.

Now let us formulate the main steps of the algorithm of recalculation of the time-dependent profile $u_n(0, t)$ from the reference cross-section $z = 0$ onto the arbitrary waveguide cross-section z . Let the initial signal $u_n(0, t)$ be specified within the interval $0 \leq t \leq T(0)$, and the output signal is to be determined for the interval $0 \leq t \leq T(z)$, $T(z) \geq T(0)$. Since the function $u_n(0, t)$ is determined on a uniform time grid with the step size \bar{l} , which is independent of the parameter α_n , it might occur that the period T_j of the Bessel function oscillations in the convolutions of (6.18)–(6.20) would be comparable with or even smaller than \bar{l} . For such values of

α_n and \bar{l} it becomes impossible to calculate the relevant integrals exactly. To prevent such situations, let us introduce a parameter κ to control the accuracy of mesh approximation of the Bessel function. If the inequality $T_J/\bar{l} \geq \kappa$ holds, then the convolutions are calculated using the function $u_n(0, t)$ with the preset step size \bar{l} . Otherwise, the function $u_n(0, t)$ is redefined on a grid with the mesh size small enough. It has been found experimentally that to provide the acceptable accuracy, it is sufficient to select κ between 10^3 and 10^4 . The value of T_J can be estimated using the asymptotic formula [61]

$$J_m(\alpha_n t) \approx \sqrt{\frac{2}{\pi \alpha_n t}} \cos\left(\alpha_n t - \frac{m\pi}{2} - \frac{\pi}{4}\right),$$

from which follows immediately $T_J = 2\pi/\alpha_n$.

The algorithm for recalculating the pulse waveform $u_n(0, t) \rightarrow u_n(z, t)$ includes the following steps.

- Test the time step size \bar{l} to satisfy the condition $T_J/\bar{l} \geq \kappa$.
- Calculate $\partial u_n(0, t)/\partial t$ over the interval $0 \leq t \leq T(0)$. To do this, we use the five-point approximation formulas for the first-order differentiation [62].
- Calculate $\partial u_n(z, t)/\partial z|_{z=0}$ by the formula (6.20) for $0 \leq t \leq T(z)$. It is assumed that $u_n(0, t) \equiv \partial u_n(0, t)/\partial t \equiv 0$ for $T(0) < t \leq T(z)$.
- Calculate $u_n(z, t)$ by the formula (6.18) for the interval $0 \leq t \leq T(z)$.

One may often encounter difficulties calculating the convolution integrals during implementation of the described algorithm. The direct use of the trapezoid rule, the Simpson rule, etc. requires about $O(M^2)$ (M is the dimension of the array to be convolved) floating-point operations, which would make the formulas (6.18)–(6.20) impractical for rather long pulses. To solve this problem, an algorithm has been suggested in [5] for calculating such convolutions using the fast Fourier transform (FFT) which requires only about $O(M \log M)$ operations. In [24] a modification of this algorithm is presented which is faster and more efficient.

6.5.2 Pulse Compression in Regular Waveguides

Now consider the compression of frequency-modulated pulses in regular waveguides by using the algorithm described in the previous section. A general scheme of the relevant numerical experiment is as follows.

1. Select the pulse time profile to be obtained at the compressor output.
2. Solve the inverse problem. It is necessary to find the time profile at the given distance z knowing the time profile of the pulse from step 1 at the cross-section $z = 0$ of the waveguide compressor.
3. Find the amplitude and frequency modulation laws for the pulse from step 2.

4. Construct the pulse using the modulation laws from step 3 and changing the time variable from t to $-t$.
5. Solve the direct problem. The pulse from step 4 is used to excite the structure, and its time dependence at the distance z is to be determined.

The pulse waveform to be obtained is determined by the device application. There are many options available for the initial pulse. We will use the pulse

$$\begin{aligned}
 u_n(0, t) &= 4S(t) \cos[6.25(t - 25)] \sin[2.75(t - 25)](t - 25)^{-1}; \quad 0 \leq t \leq 50, \\
 S(t) &= [x(t)]^2 [3 - 2x(t)], \quad x(t) = \begin{cases} t/25; & 0 \leq t \leq 25 \\ (50 - t)/25; & 25 \leq t \leq 50 \end{cases}
 \end{aligned}
 \tag{6.21}$$

which propagates in a regular homogeneous waveguide of arbitrary cross-section. Here, $u_n(z, t)$ is the amplitude of the n th waveguide mode. The function $S(t)$, which is composed of two splines, is introduced for convenience of calculations. It is intended for smoothing the source edges and allows more accurate calculation of the time derivatives at the moments when the source switches on, $t = 0$, and switches off, $t = 50$. The selection of such waveform is easily explainable. When the switch-on and switch-off times go to minus and plus infinity, respectively, the amplitude spectrum of the signal $u_n(0, t)$ tends to a constant level within the frequency band $k \in [6.25 - 2.75, 6.25 + 2.75]$, while outside of this band it vanishes. Thus, the formula (6.21) can be considered as an approximate representation of the Dirac delta-function, whose spectrum is uniform within the band $-\infty < k < \infty$. The unique properties of the delta-function make it a key tool in theoretical electrodynamics and signal processing theory, in particular when investigating the pulse responses of dynamic systems. Thus, it seems quite attractive to use its approximate analog when simulating the operation of actual physical devices. The time step size of a discrete representation of the function $u_n(0, t)$ is $\bar{l} = 0.002$. The time dependence of the function (6.21) and its amplitude spectrum are shown in Fig. 6.30.

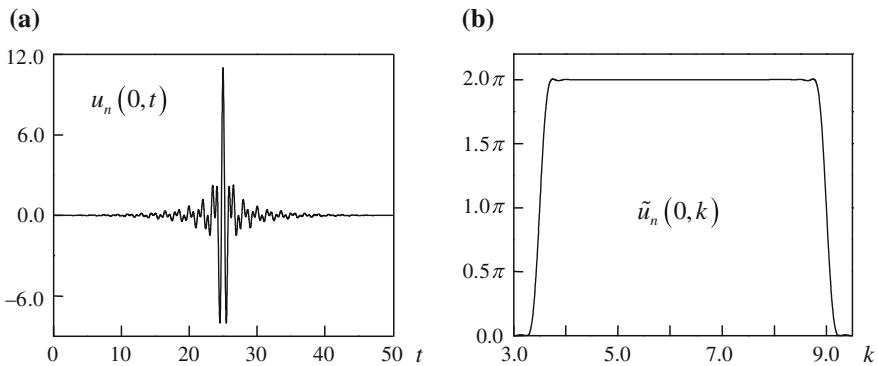


Fig. 6.30 **a** The pulse (6.21) and **b** its amplitude spectrum

In order to solve the inverse problem, it is necessary to specify the waveguide type and the operating mode. Since the waveguide type in the formulas (6.18)–(6.20) is determined exclusively by the parameter α_n , it does not matter what waveguide would be chosen for a dispersive system. The final result will be the same for different waveguides with identical α_n . Thus, let us consider the transformation of the TE_{01} -mode ($n = 1$) in a hollow parallel-plate waveguide of height $a = 1.0$. The obtained results can be easily extended (by scaling) to waveguides with other transverse dimensions when needed. The cutoff frequencies of the selected waveguide are $k_n^+ = n\pi$; and the pulse's spectrum (Fig. 6.30b) occupies the single-mode and two-mode propagation range.

Figure 6.31a shows transformations of the pulse (6.21) during its propagation along the waveguide at the distances $z = 100$, $z = 1000$ and $z = 10000$ from the reference cross-section $z = 0$. With the selected scaling factor, the function $u_1(z, t + z)$ oscillates so fast that the area occupied by the pulse seems to be completely filled. More detailed information on these characteristics can be obtained from the modulation laws below. As can be seen, the pulse length increases almost proportionally to the distance traveled. Therefore, it is possible, theoretically, to construct a compressor with an arbitrary large degree of compression, by increasing the waveguide length unlimitedly. From the practical point of view, it is pointless, as all characteristics of such compressor will be confined due to loss in the walls.

Now let us find the laws of amplitude and frequency modulations (the functions $A(t)$ and $k(t)$) of the pulses $u_1(z, t + z)$. The window Laplace transform (see also (6.4)).

$$\tilde{f}(k, t) = \int_0^{\infty} f(\tau) W\left(\tau - t + \frac{w}{2}\right) e^{ik\tau} d\tau \quad (6.22)$$

makes it possible to visually represent signal changes in the time-frequency coordinates and to check the carrier frequency for uniqueness. Figure 6.32a, b show results of applying the transform (6.22) to the initial function $u_1(0, t)$ and to the function $u_1(1000, t + 1000)$ using the Hamming window [63] $W(t) = 0.54 - 0.46 \cos(2\pi t/w)$ of the width $w = 8.0$. Each spectrum in Fig. 6.32b has been calculated for the respective position of the time window and normalized to one:

$$\tilde{f}^{\text{norm}}(t, k) = \tilde{f}(t, k) / \max_k \tilde{f}(t, k).$$

The bold curve corresponds to $\tilde{u}_1^{\text{norm}} = 1.0$ and actually demonstrates the frequency modulation law. However, it is not practical to apply the window transform (6.22) for determining the exact time dependence of $k(t)$ since it requires very small

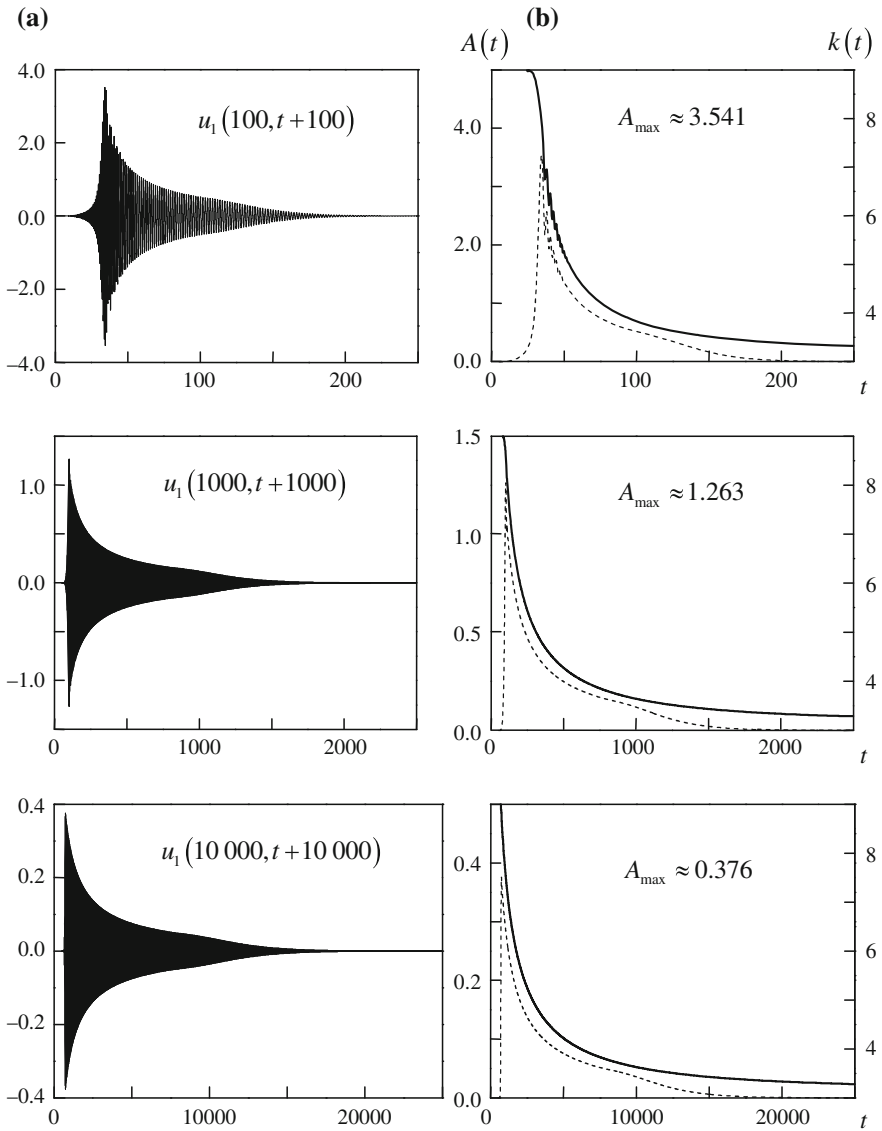


Fig. 6.31 **a** The pulse at distance 100, 1000 and 10000 m (waveguide heights) from reference cross-section and **b** functions of its amplitude (*dashed line*) and frequency (*solid line*) modulation

frequency step, two-coordinate interpolation formulas, etc. As a result, the complexity of computer programs and the computation time increase.

In the present work, a simpler and more effective procedure was adopted instead of finding simultaneously the frequency and amplitude modulation laws. First, the sequences of zeros $t_{01}, t_{02}, t_{03}, \dots, t_{0N}$ and extremes $t_1, t_2, t_3, \dots, t_{N-1}$ of the wanted

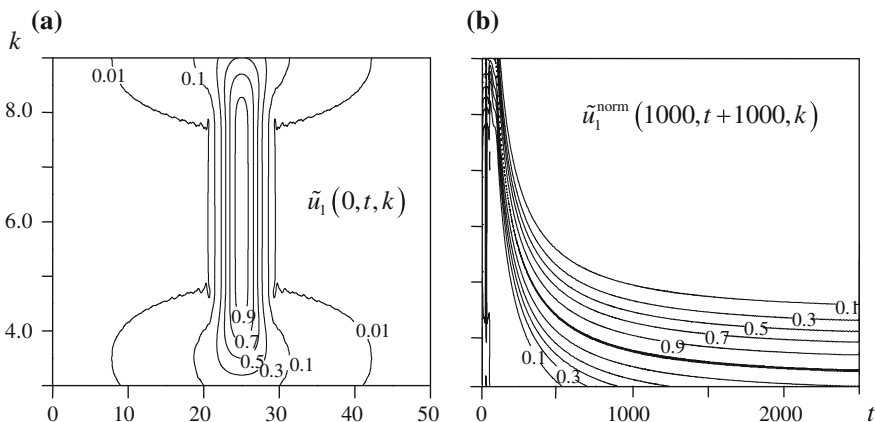


Fig. 6.32 Window Laplace transforms of functions **a** $u_1(0, t)$ and **b** $u_1(1000, t + 1000)$

function $f(t)$ were determined within the given time interval $[T_0, T_1]$. The zeros and extremes were arranged according to the inequalities

$$T_0 \leq t_{0,1} < t_1 < t_{0,2} < \dots < t_{0,i} < t_i < t_{0,i+1} < \dots < t_{0,N-1} < t_{N-1} < t_{0,N} \leq T_1.$$

Then for every time point t_j , the amplitude and frequency were calculated following the rule:

$$A(t_j) = |f(t_j)| \quad \text{and} \quad k(t_j) = \pi / (t_{0,j+1} - t_{0,j}).$$

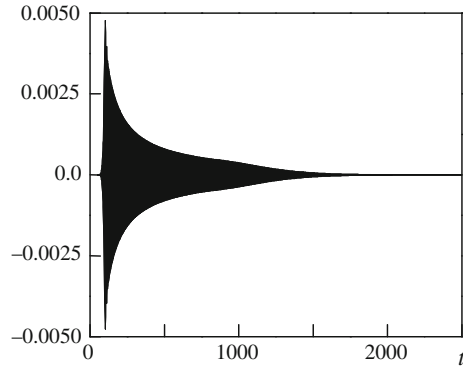
If for further calculations the amplitude and frequency for the times other than t_j should be known, then the quadratic interpolation formulas are used. The numerical experiments have proved that this way to estimate $A(t)$ and $k(t)$ is more efficient than using the window Laplace transform as it provides more accurate results and requires shorter computation time.

Finally, in order to recover the initial function $f(t)$ uniquely from the found modulation laws [64]

$$f^{\text{recon}}(t) = A(t) \sin \left[\varphi_0 + \int_{t_{0,1}}^t k(\tau) d\tau \right]; \quad t_{0,1} \leq t \leq t_{0,N}, \quad (6.23)$$

it is also necessary to know the signal phase φ_0 at the initial time. Since the reconstruction was performed for the interval $[t_{0,1}, t_{0,N}]$, we have $f^{\text{recon}}(t_{0,1}) = 0$, and $\varphi_0 = 0$ if $f(t_1) > 0$, and $\varphi_0 = \pi$ if $f(t_1) < 0$.

Fig. 6.33 Reconstruction error for $u_1(1000, t + 1000)$ recovered from the found amplitude and frequency modulation laws



The described algorithm of determining the modulation laws and recovering the initial signal was applied to the pulses $u_1(z, t + z)$ with $z = 100$, $z = 1000$, and $z = 10\,000$ (see Fig. 6.31a) and provided acceptable accuracy. Figure 6.31b shows time dependences of the amplitudes (left scale) and frequencies (right scale) calculated for these pulses. Figure 6.33 presents the time dependence of the absolute error $u_1(1000, t + 1000) - u_1^{\text{recon}}(1000, t + 1000)$ of reconstruction of the signal $u_1(1000, t + 1000)$. As can be seen, the error is three orders of magnitude smaller than the value of the function itself (the integral in (6.23) was calculated numerically using the trapezoidal formula).

The presence of noticeable oscillations in the signal amplitude and frequency at the distance $z = 100$ from the reference cross-section (Fig. 6.31b) makes this pulse unsuitable for practical use. At greater z the frequency modulation law is monotonous. Such pulses are of greatest interest to study.

On the next step, the signal $u_1^{\text{recon}}(z, t + z)$ ($t_{0,1} \leq t \leq t_{0,N}$) is used to reconstruct the reversed in time signal

$$u_1^{\text{recon}(-)}(0, t) = u_1^{\text{recon}}(z, t_{0,N} - t + z)$$

($0 \leq t \leq t_{0,N} - t_{0,1}$), which is to be incident on the reference cross-section of the waveguide $z = 0$. The time profile of this pulse in the cross-section z is described by the function, which will be referred as $u_1^{\text{recon}(-)}(z, t + z)$. Both of the signals, $u_1^{\text{recon}(-)}(0, t)$ and $u_1^{\text{recon}(-)}(1000, t + 1000)$ ($t_{0,1} \approx 50.19$, $t_{0,N} \approx 2499.03$), are shown in Fig. 6.34. As can be seen from Fig. 6.30a, the initial pulse $u_1(0, t)$ has been reconstructed with a high accuracy. The minor difference is due to the truncated long-lasting ringing tail of $u_1^{\text{recon}(-)}(1000, t + 1000)$ for $t > 2500$. By increasing the length of this pulse, it is possible, at least in theory, to reproduce the profile of the desired signal with any degree of accuracy.

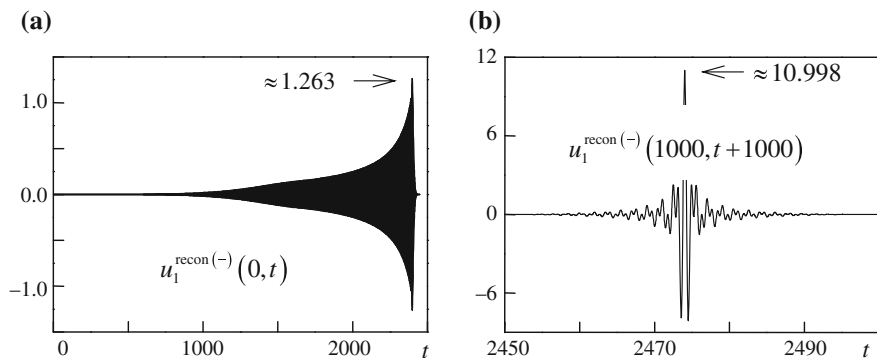


Fig. 6.34 **a** Pulse $u_1^{\text{recon}(-)}(z, t)$ within reference cross-section $z = 0$ and **b** its profile within cross-section $z = 1000$

The compressor based on the section of a regular waveguide, which transforms the pulse $u_1^{\text{recon}(-)}(0, t)$ into $u_1^{\text{recon}(-)}(1000, t + 1000)$, has the following characteristics: (i) the *amplitude gain* (output-to-input signal maximum magnitude ratio) is $\alpha \approx 10.998/1.263 \approx 8.708$; (ii) the degree of compression (input-to-output pulse length ratio) is $\beta \approx 2448.84/50 \approx 48.98$; (iii) the energy efficiency (output-to-input pulse energy ratio) is $\gamma \approx 1$; (iv) the *power gain* (product of the compression factor by the efficiency) is $\theta = \beta \times \gamma \approx 48.98$. These characteristics were calculated assuming no loss in the waveguide walls.

A more detailed description of these results can be found in [24], which also demonstrates the non-applicability of the kinematic approximation in the study of compression processes even in simplest dispersive systems. The frequency modulation laws for the pulses $u_1(z, t + z)$ and $u_1^{\text{recon}(-)}(0, t)$ calculated in the context of our rigorous approach and in the context of the kinematic theory [58] differ rather substantially. Even greater differences are found when determining the optimal length of a compressor.

Thus, the kinematic conception that a pulse moves as a superposition of particles is too rough for adequate modeling of physical processes even in a simple case where a dispersive element is a section of a regular waveguide. Using this approximation, it is difficult to answer the question: ‘What should be the frequency and amplitude modulation law of the input pulse?’ This question is of the highest importance in numerical and full-scale experiments since the knowledge of the dispersion law of a specific device does not mean the knowledge of the frequency modulation law of an input pulse.

6.6 Conclusion

The chapter presents our approach to studies of microwave energy compression and radiation, namely modeling, analysis, and design of compressors and radiators. Our approach is based on highly-accurate EACs-enabled time-domain numerical methods, which are detailed in Chap. 5.

As follows from the name, the pillars of EACs-enabled methods are exact absorbing conditions (EACs). Being imposed on virtual boundaries, EACs allow truncation of unbounded physical domains of interest to bounded computation domains without introduction of any additional errors or distortion of wave processes. EACs-enabled methods are especially appropriate for the analysis and synthesis of microwave energy compressors and radiators of high-power short pulses, since design of such devices requires simulation tools for accurate and efficient analysis of long-duration wave interactions with resonant structures.

In Sect. 6.3 we studied several problems concerning analysis and synthesis of active microwave energy compressors. In order to successfully design such devices, the in-depth understanding of nonmonotonic behavior of high-power pulses inside storage units becomes a necessity. This can be achieved using a design scheme that heavily depends on time-domain analysis. In this work, the physical processes inside microwave energy compressors have been extensively studied in the time domain, from the very beginning of the excitation right until the end of the energy release. The methodology and the results presented in Sect. 6.3 were used in Sect. 6.4 to design a novel combined compressor/radiator antenna element for a phased array.

The radiation of a short pulse from a monopole antenna mounted on a ground plane has also been studied. It has been demonstrated that compressed pulses can be efficiently radiated by simple antennas. A novel array design, where each of the array elements is constructed by combining a compressor and a radiator, has been presented. The new design allows one to reduce the overall size and weight of the array, pulse distortion and absorption loss. Besides, the proposed design has the advantage of compressing a pulse right before it is radiated, allowing the use of components that cannot handle high power in the rest of array. This design idea was applied to a phased antenna array, which is intended for generation and directional radiation of high-power short pulses and shares the basic advantage of common phased arrays, namely, rapid electronic beam steering without moving an array itself.

The substantial part of this chapter is devoted to the rigorous algorithm for calculating the time profiles of electromagnetic pulses propagating in hollow waveguides of arbitrary cross-sections with perfectly conducting walls. An efficient computation scheme has been suggested for calculating the frequency and amplitude modulation laws for pulses to be compressed. It has been shown that the kinematic approximation is inapplicable for the rigorous description of broadband pulse propagation in dispersive systems.

References

1. Sirenko, Y.K., Strom, S., Yashina, N.P.: Modeling and Analysis of Transient Processes in Open Resonant Structures. *New Methods and Techniques*. Springer, New York (2007)
2. Kuzmitchev, I.K., Melezykh, P.M., Pazynin, V.L., Sirenko, K.Y., Sirenko, Y.K., Shafalyuk, O.S., Velychko, L.G.: Model synthesis of energy compressors. *Radiofizika I Elektronika* **13**(2), 166–172 (2008)
3. Sirenko, K.Y., Sirenko, Y.K.: Exact ‘absorbing’ conditions in the initial boundary value problems of the theory of open waveguide resonators. *Comput. Math. Math. Phys.* **45**(3), 490–506 (2005)
4. Sirenko, Y.K., Strom, S. (eds): *Modern Theory of Gratings. Resonant Scattering: Analysis Techniques and Phenomena*. Springer, New York (2010)
5. Sirenko, K., Pazynin, V., Sirenko, Y., Bagci, H.: An FFT-accelerated FDTD scheme with exact absorbing conditions for characterizing axially symmetric resonant structures. *Prog. Electromagn. Res.* **111**, 331–364 (2011)
6. Shafalyuk, O., Sirenko, Y., Smith, P.: Simulation and analysis of transient processes in open axially-symmetrical structures: Method of exact absorbing boundary conditions. In: Zhurbenko V. (ed.): *Electromagnetic Waves*, pp. 99–116. InTech, Rijeka (2011)
7. Kravchenko, V.F., Sirenko, Y.K., Sirenko, K.Y.: *Electromagnetic Wave Transformation and Radiation by the Open Resonant Structures. Modelling and Analysis of Transient and Steady-State Processes*. Fizmathlit, Moscow (2011). (in Russian)
8. Shafalyuk, O., Smith, P., Velychko, L.: Rigorous substantiation of the method of exact absorbing conditions in time-domain analysis of open electrodynamic structures. *Prog. Electromagn. Res. B* **41**, 231–249 (2012)
9. Taflove, A., Hagness, S.C.: *Computational Electrodynamics: the Finite-Difference Time-Domain Method*. Artech House, Boston (2000)
10. Jin, J.: *The Finite Element Method in Electromagnetics*. Wiley, New York (2002)
11. Liu, M., Sirenko, K., Bagci, H.: An efficient discontinuous Galerkin finite-element method for highly accurate solution of Maxwell equations. *IEEE Trans. Antennas Propag.* **60**(8), 3992–3998 (2012)
12. Sirenko, Y.K., Velychko, L.G., Erden, F.: Time-domain and frequency-domain methods combined in the study of open resonance structures of complex geometry. *Prog. Electromagn. Res.* **44**, 57–79 (2004)
13. Velychko, L.G., Sirenko, Y.K., Velychko, O.S.: Time-domain analysis of open resonators. Analytical grounds. *Prog. Electromagn. Res.* **61**, 1–26 (2006)
14. Velychko, L.G., Sirenko, Y.K.: Controlled changes in spectra of open quasi-optical resonators. *Prog. Electromagn. Res. B* **16**, 85–105 (2009)
15. Sirenko, K., Pazynin, V., Sirenko, Y., Bagci, H.: Compression and radiation of high-power short radio pulses. I. Energy accumulation in direct-flow waveguide compressors. *Prog. Electromagn. Res.* **116**, 239–270 (2011)
16. Sirenko, K., Pazynin, V., Sirenko, Y., Bagci, H.: Compression and radiation of high-power short radio pulses. II. A novel antenna array design with combined compressor/radiator elements. *Prog. Electromagn. Res.* **116**, 271–296 (2011)
17. Tantawi, S.G., Ruth, R.D., Vlieks, A.E., Zolotarev, M.: Active high-power RF pulse compression using optically switched resonant delay lines. *IEEE Trans. Microw. Theory Tech.* **45**(8), 1486–1492 (1997)
18. Artemenko, S.N., Avgustinovich, V.A., Kaminsky, V.L., Chumerin, P.Y., Yushkov, Y.G.: Experimental investigation of a 25-mw microwave (3-cm range) compressor prototype. *Tech. Phys.* **45**(12), 1608–1611 (2000)
19. Vikharev, A.L., Gorbachev, A.M., Ivanov, O.A., Isaev, V.A., Kuzikov, S.V., Kolysko, A.L., Movshevich, B.Z., Hirshfield, J., Gold, S.H.: Active Bregg compressor of 3-cm wavelength microwave pulses. *Radiophys. Quantum Electron.* **51**(7), 539–555 (2008)

20. Samsonov, S.V., Phelps, A.D.R., Bratman, V.L., Denisov, G.G., Cross, A.W., Ronald, K., He, W., Yin, H.: Compression of frequency-modulated pulses using helically corrugated waveguides and its potential for generating multigigawatt RF radiation. *Phys. Rev. Lett.* **92** (11), 118301-1–118301-4 (2004)
21. Sirenko, Y.K., Yashina, N.P. Time domain theory of open waveguide resonators: canonical problems and a generalized matrix technique. *Radio Sci.* **38**(2), VIC 26-1–VIC 26-12 (2003)
22. Sirenko, K.Y.: Transport operators in the axially-symmetrical problems of the electrodynamics of pulsed waves. *Elektromagnitnye Volny I Elektronnye Sistemy*, **11**(11), 15–26 (2006). (in Russian)
23. Kravchenko, V.F., Sirenko, K.Y., Sirenko, Y.K.: Transport operators and exact absorbing conditions in the plane problems of the electrodynamics of pulsed waves for compact open resonators with the waveguide feeder line. *Elektromagnitnye Volny I Elektronnye Sistemy*, **14** (1), 4–19 (2009). (in Russian)
24. Pazyinin, V.L.: Compression of frequency-modulated electromagnetic pulses in sections of regular waveguides. *Telecommun. Radio Eng.* **71**(20), 1833–1857 (2012)
25. Karmel, P.R., Colef, G.D., Camisa, R.L.: *Introduction to Electromagnetic and Microwave Engineering*. Wiley, New York (1998)
26. Sirenko, K.Y., Pazyinin, V.L.: Axially-symmetrical radiators of pulsed and monochromatic TM_{0n} - and TM_{0n} -waves. *Uspehi Sovremennoy Radioelektroniki* **4**, 52–69 (2006). (in Russian)
27. Bossart, R., Brown, P., Mourier, J., Syratchev, I.V., Tanner, L.: High-power microwave pulse compression of klystrons by phase-modulation of high-Q storage cavities. CERN CLIC-Notes, no.592, (2004)
28. Vikharev, A.L., Ivanov, O.A., Gorbachev, A.M., Kuzikov, S.V., Isaev, V.A., Koldanov, V.A., Lobaev, M.A., Hirshfield, J.L., LaPointe, M.A., Nezhevenko, O.A., Gold, S.H., Kinkead, A. K.: Active compression of RF pulses. In: Hirshfield J.L., Petelin M.I. (eds) *Quasi-Optical Control of Intense Microwave Transmission*, pp. 199–218. Springer, Netherlands (2005)
29. Yushkov, Y.G., Badulin, N.N., Batsula, A.P., Mel'nikov, A.I., Novikov, S.A., Razin, S.V., Shoshin, E.L.: A nanosecond pulse-compression microwave radar. *Telecommun. Radio Eng.* **54**(2), 92–98 (2000)
30. Schamiloglu, E.: High power microwave sources and applications. In: 2004 IEEE MTT-S Digest, pp. 1001–1004 (2004)
31. Benford, J.: Space applications of high-power microwaves. *IEEE Trans. Plasma Sci.* **36**(3), 569–581 (2008)
32. Gaponov-Grekhov, A.V., Granatstein, V.L.: *Applications of High-Power Microwaves*. Artech House, Boston (1994)
33. Bluhm, H.: *Pulsed Power Systems. Principles and Applications*. Springer, Berlin (2006)
34. Pazyinin, V.L., Sirenko, K.Y.: Transformation of TM_{0n} - and TM_{0n} -waves by axially-symmetrical waveguide units. Slot resonances. *Elektromagnitnye Volny I Elektronnye Sistemy*, **10**(10), 21–26 (2005). (in Russian)
35. DeLoach, B.C.: Radial-line coaxial filters in the microwave region. *IEEE Trans. Microw. Theory Tech.* **11**(1), 50–55 (1963)
36. Sirenko, K.Y.: Slot resonances in axially symmetric radiators of pulse-modulated and monochromatic TM_{0n} -modes. *Telecommun. Radio Eng.* **66**(1), 9–21 (2007)
37. Chernobrovkin, R.E., Ivanchenko, I.V., Korolev, A.M., Popenko, N.A., Sirenko, K.Y.: The novel microwave stop-band filter. *Active and Passiv. Electron. Compon.* **2008**(745368) (2008)
38. Shestopalov, V.P., Kirilenko, A.A., Rud', L.A.: *Resonance Wave Scattering. Vol.2. Waveguide Discontinuities*. Naukova Dumka, Kiev (1986). (in Russian)
39. Velychko, L.G., Sirenko, Y.K., Vinogradova, E.D.: Analytical grounds for modern theory of two-dimensionally periodic gratings. In: Kishk A. (ed) *Solutions and Applications of Scattering, Propagation, Radiation and Emission of Electromagnetic Waves*, pp. 123–158. InTech, Rijeka (2012)
40. Andreev, A.D., Farr, E.G., Schamiloglu, E.: A simplified theory of microwave pulse compression. *Circuit and Electromagnetic System Design Notes*, no. 57, (2008)

41. Avgustinovich, V.A., Artemenko, S.N., D'yachenko, V.F., Kaminskii, V.L., Novikov, S.A., Yushkov, Yu.G.: A study of the switching of the microwave compressor switch in a circular waveguide. *Instrum. Exp. Tech.* **52**(4), 547–550 (2009)
42. Faillon, G., Durand, A.-J.: Microwave pulse generator incorporating a pulse compressor. U.S. Patent 6768266 (2004)
43. Artemenko, S.N.: Formation of nanosecond RF pulses in an autogenerator by resonance compression of microwave energy. *Radiophys. Quantum Electron.* **41**(7), 616–624 (1998)
44. Farr, E.G., Bowen, L.H., Prather, W.D., Baum, C.E.: Microwave pulse compression experiments at low and high power. *Circuit and Electromagnetic System Design Notes*, no.63 (2010)
45. Benford, J.: Space applications of high-power microwaves. *IEEE Trans. Plasma Sci.* **36**(3), 569–581 (2008)
46. Giri, D.V., Tesche, F.M., Baum, C.E.: An overview of high-power electromagnetics (HPEM) radiating and conducting systems. *Circuit and Electromagnetic System Design Notes*, no.50 (2006)
47. Balanis, C.A.: *Antenna Theory: Analysis and Design*. Wiley, New York (1982)
48. Amitay, N., Galindo, V., Wu, C.P.: *Theory and Analysis of Phased Array Antennas*. Wiley, New York (1972)
49. Ramp, H.O., Wingrove E.R.: Principles of pulse compression. *IRE Trans. Mil. Electron.*, **MIL-5**(2), 109–116 (1961)
50. Thor R.C.: A large time-bandwidth product pulse-compression technique. *IRE Trans. Mil. Electron.* **MIL-6**(2), 169–173 (1962)
51. Bongiani, W.L., Harrington, J.B.: Ultrawide bandwidth pulse compression in YIG. *Proc. IEEE* **54**(8), 1074–1075 (1966)
52. Bromley, R.A., Callan, B.E.: Use of a waveguide dispersive line in an f.m. pulse-compression system. *Proc. IEEE* **114**(9), 1213–1218 (1967)
53. Gökgör, H.S., Minakovic, B.: Circular TE_{01} periodic waveguide as delay line for pulse compression. *Electron. Lett.* **7**(20), 607–608 (1971)
54. Shirman, Y.D.: *Signal Resolution and Compression*. Sovetskoe Radio, Moscow (1974). (in Russian)
55. Thirios, E.C., Kaklamani, D.I., Uzunoglu, N.K.: Pulse compression using a periodically dielectric loaded dispersive waveguide. *Prog. Electromag. Res.* **48**, 301–333 (2004)
56. McStravick, M., Samsonov, S.V., Ronald, K., Mishakin, S.V., He, W., Denisov, G.G., Whyte, C.G., Bratman, V.L., Cross, A.W., Yong, A.R., MacInnes, P., Robertson, C.W., Phelps, A.D.R.: Experimental results on microwave pulse compression using helically corrugated waveguide. *J. Appl. Phys.* **108**(5), 054908-1–054908-4 (2010)
57. Burt, G., Samsonov, S.V., Bratman, V.L., Denisov, G.G., Phelps, A.D.R., Ronald, K., He, W., Young, A.R., Cross, A.W., Konoplev, I.V.: Microwave pulse compression using a helically corrugated waveguide. *IEEE Trans. Plasma Sci.* **33**(2), 661–667 (2005)
58. Bratman, V.L., Denisov, G.G., Samsonov, S.V., Cross, A.W., Ronald, K., Phelps, A.D.R.: A technique of obtaining multigigawatt peak power through compression of microwave pulses radiated by a relativistic BWT in a helically corrugated waveguide. *Izvestiya Vuzov. Radiofizika*, **50**(1), 40–53 (2007). (in Russian)
59. Pazyinin, V.L.: On rigorous simulation of FM pulses compression in the hollow regular waveguides. *Radiofizika I Elektronika*, **17**(3), 30–34 (2012). (in Russian)
60. Levin, L.: *Theory of Waveguides: Techniques for Solution of Waveguide Problems*. Newnes-Butterworths, London (1975)
61. Gradshteyn, I.S., Ryzhik, I.M.: *Table of Integrals, Series, and Products*. Academic Press, San Diego, London (2000)
62. Abramowitz, M., Stegun, I.A. (eds.): *Handbook of Mathematical Functions*. Dover, New York (1972)
63. Marple, S.L.: *Digital Spectral Analysis with Applications*. Prentice-Hall, New Jersey (1987)
64. Southworth, G.C.: *Principles and Application of Waveguide Transmission*. D. Van Nostrand Co., New York (1950)

Chapter 7

Diffraction Radiation Phenomena: Physical Analysis and Applications

Seil Sautbekov, Kostyantyn Sirenko, Yuriy Sirenko, Alexey Vertiy
and Anatoliy Yevdokymov

Abstract The chapter is devoted to the problems of analysis and applied usage of the diffraction radiation phenomena, which are exploited in antennas and generators for millimeter and submillimeter waves. The diffraction radiation occurs when surface waves of open waveguides or eigenfields of charged-particle beams are transformed by periodic gratings into radiated fields. Main properties of the diffraction radiation phenomena have been studied using the given-current approximation and rigorous methods taking into account actual size of devices exploiting the phenomena. The algorithm of experimental synthesis of planar diffraction antennas with record-breaking low side lobes level has been developed and applied to design a real-world device.

7.1 Introduction

Advances in the electrodynamic theory of gratings (see, for example, [1–13]) have always played an important role in the development of related areas of science and technology. Nowadays optics, spectroscopy, physics and engineering of millimeter

S. Sautbekov · Y. Sirenko · A. Vertiy
L.N. Gumilyov Eurasian National University, Astana, Republic of Kazakhstan
e-mail: sautbek@mail.ru

Y. Sirenko
e-mail: yks@ire.kharkov.ua

A. Vertiy
e-mail: alexey.vertiy@gmail.com

K. Sirenko (✉)
King Abdullah University of Science and Technology,
Thuwal, Saudi Arabia
e-mail: k.sirenko@gmail.com

Y. Sirenko · A. Yevdokymov
O.Ya. Usikov Institute for Radiophysics and Electronics,
National Academy of Sciences, Kharkiv, Ukraine
e-mail: yevdok@ire.kharkov.ua

and submillimeter waves, high-power electronics, quantum radio physics, solid state physics, acoustics, and resonance quasi-optics benefit from new methods and models of the gratings theory, its results and novel effects. Gratings ability to change their transparency over maximal limits and controllability of energy transfer between waves propagating in different directions allows to use gratings as polarization and frequency filters, anti-reflection and scattering coatings, screens of various types and purposes, selective mirrors for dispersive open resonators, pattern-forming structures. One major field of diffraction gratings application is antenna equipment, in particular, antennas exploiting the *effect of diffraction radiation* [14–18] or *diffraction antennas*. When this effect occurs, exponentially decreasing surface eigenwaves of any open guiding structure (or eigenfields of charged-particle beams in diffraction electronics) are transformed by nearby periodic structures into radiation fields [19–23], whose characteristics (directivity, energy efficiency, frequency band, scanning sector, etc.) are optimized to suit practical requirements.

In this chapter, extending our results from [16, 18], we consider in more details the diffraction radiation effect (Sect. 7.3) and methodological grounds for model and experimental synthesis of diffraction antenna components and units (Sect. 7.4). In Sect. 7.5, we present the unique *low-side-lobe planar antenna* [16] for millimeter-wave radars. The presented theoretical results have been obtained for 2-D planar and axially symmetric objects. Electrodynamical analysis of these objects (finite and infinite gratings, planar and circular dielectric waveguides, etc.) is based on the numerical resolution of *open initial boundary value problems*, whose computation domains are truncated using *exact absorbing conditions* (EACs). All relevant analytical results are given in Sect. 7.2 and Chap. 5.

We use SI, the International System of Units, for all physical parameters except the ‘time’ t that is the product of the natural time and the velocity of light in vacuum, thus t is measured in meters. In this chapter, dimensions are omitted as a rule. According to SI, all geometrical parameters (a, b, c , etc.) are given in meters. However, this is obviously not a serious obstacle to extend the results to any other geometrically similar structure. For example, if some parameter a of a model problem corresponds to the parameter a_r of a real problem and $a_r/a = \alpha$, then to construct the solution to the real problem, all quantities of the model problem involving dimension [m] (meters) should be multiplied by the factor α , while quantities involving dimension [m⁻¹] should be divided by α .

7.2 Periodic Structures and Dielectric Waveguides: Analysis Techniques

7.2.1 Plane Models for Infinite Gratings: Time-Domain Representations

Space-time transformations of E - ($E_y = E_z = H_x \equiv 0$) and H -polarized ($H_y = H_z = E_x \equiv 0$) waves in the near-field zone of a *one-dimensionally periodic grating* (see Fig. 7.1: structures are uniform along the x -axis ($\partial/\partial x = 0$) and periodic with the period l along the y -axis) are described by the following scalar problem:

$$\left\{ \begin{array}{l} \left[-\varepsilon(g) \frac{\partial^2}{\partial z^2} - \sigma(g) \eta_0 \frac{\partial}{\partial t} + \frac{\partial^2}{\partial y^2} + \frac{\partial^2}{\partial z^2} \right] U(g, t) = F(g, t); \\ g = \{y, z\} \in \Omega, \quad t > 0 \\ U(g, 0) = \varphi(g), \quad \frac{\partial}{\partial t} U(g, t)|_{t=0} = \psi(g); \quad g \in \bar{\Omega} \\ \vec{E}_{tg}(q, t) \text{ and } \vec{H}_{tg}(q, t), \text{ where } q = \{x, y, z\}, \text{ are continuous} \\ \text{when crossing } \Sigma^{\varepsilon, \sigma} \text{ and } \vec{E}_{tg}(q, t)|_{q \in \Sigma} = 0; \quad t \geq 0. \end{array} \right. \quad (7.1)$$

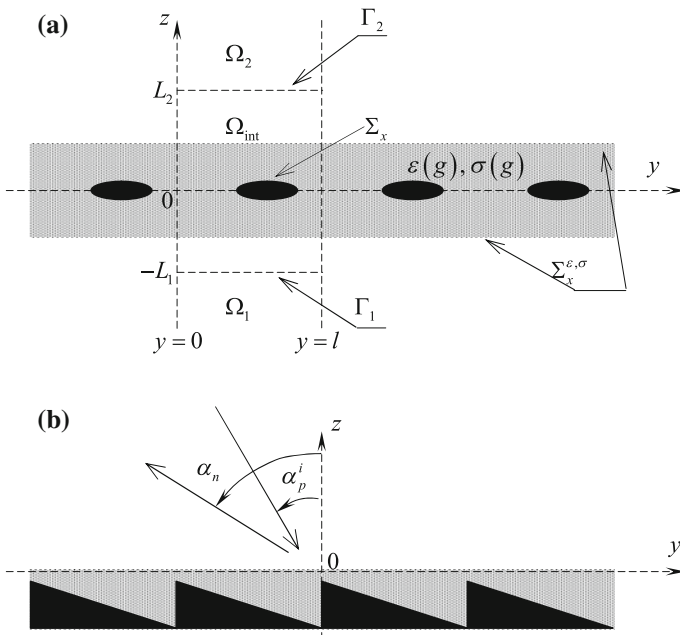


Fig. 7.1 1-D periodic structures: **a** semitransparent grating and **b** reflective grating

Here, $U(g, t) = E_x(g, t)$ in the case of E -polarization and $U(g, t) = H_x(g, t)$ in the case of H -polarization; $\vec{E}(g, t) = \{E_x, E_y, E_z\}$ and $\vec{H}(g, t) = \{H_x, H_y, H_z\}$ are the electric and magnetic field vectors; $\{x, y, z\}$ are the Cartesian coordinates; the piecewise-constant functions $\sigma(g) \geq 0$ and $\varepsilon(g) \geq 1$ are the specific conductivity and the relative permittivity of dielectric elements; $\eta_0 = (\mu_0/\varepsilon_0)^{1/2}$ is the impedance of free space; ε_0 and μ_0 are the electric and magnetic vacuum constants. The surfaces $\Sigma = \Sigma_x \times [|x| \leq \infty]$ of perfectly conducting elements of a grating and the surfaces $\Sigma^{\varepsilon, \sigma}$ of discontinuities of its material parameters are assumed to be sufficiently smooth.

It is known [9, 12, 24] that the *initial boundary value problem* (7.1) can be formulated such that it is uniquely solvable in the Sobolev space $W_2^1(\Omega \times (0, T))$, where $(0, T) = \{t : 0 < t < T < \infty\}$ is the observation interval. Let us suppose that all necessary conditions for the single-valued solvability of the problem (7.1) are fulfilled (the *source functions* $\varphi(g)$, $\psi(g)$, and $F(g, t)$ have compact supports in the closure $\bar{\Omega}$ of the domain Ω , and so on) and discuss the following important question.

The analysis domain Ω is the part of the yOz plane bounded by Σ_x . Ω is unbounded, and should be truncated to solve the problem (7.1) numerically.

For this purpose, let us introduce the complex-valued functions $f_p^{\text{new}}(g, t, \Phi)$, $|\Phi| < \infty$ or $f_p^{\text{new}}(g, t, \Phi)$, $|\Phi| \leq 0.5$, which are the Fourier images of the real-valued functions $f(g, t)$ ($\varphi(g)$, $\psi(g)$ and $F(g, t)$) describing the true sources:

$$\begin{aligned}
 f(y, z, t) &= \int_{-\infty}^{\infty} \tilde{f}(z, t, \Phi) e^{2\pi i \Phi y / l} d\Phi = \int_{-\infty}^{\infty} f^{\text{new}}(y, z, t, \Phi) d\Phi \\
 \leftrightarrow f^{\text{new}}(y, z, t, \Phi) &= \frac{\exp(2\pi i \Phi y / l)}{l} \int_{-\infty}^{\infty} f(y_1, z, t) e^{-2\pi i \Phi y_1 / l} dy_1,
 \end{aligned}
 \tag{7.2}$$

$$\begin{aligned}
 f(y, z, t) &= \int_{-\infty}^{\infty} \tilde{f}(z, t, \Phi) e^{2\pi i \Phi y / l} d\Phi = \sum_{p=-\infty}^{\infty} \int_{-0.5}^{0.5} \tilde{f}(z, t, \Phi + p) e^{2\pi i (\Phi + p)y / l} d\Phi \\
 &= \sum_{p=-\infty}^{\infty} \int_{-0.5}^{0.5} \tilde{f}_p(z, t, \Phi) e^{i\Phi_p y} d\Phi = \sum_{p=-\infty}^{\infty} \int_{-0.5}^{0.5} f_p^{\text{new}}(y, z, t, \Phi) d\Phi \\
 \leftrightarrow f_p^{\text{new}}(y, z, t, \Phi) &= \frac{\exp(i\Phi_p y)}{l} \int_{-\infty}^{\infty} f(y_1, z, t) e^{-i\Phi_p y_1} dy_1,
 \end{aligned}
 \tag{7.3}$$

$$\Phi_p = 2\pi(\Phi + p) / l.$$

From (7.2) and (7.3) it follows that

$$f^{\text{new}} \left\{ \frac{\partial f^{\text{new}}}{\partial y} \right\} (y+l, z, t, \Phi) = e^{2\pi i \Phi} f^{\text{new}} \left\{ \frac{\partial f^{\text{new}}}{\partial y} \right\} (y, z, t, \Phi) \quad (7.4)$$

and

$$f_p^{\text{new}} \left\{ \frac{\partial f_p^{\text{new}}}{\partial y} \right\} (y+l, z, t, \Phi) = e^{2\pi i \Phi} f_p^{\text{new}} \left\{ \frac{\partial f_p^{\text{new}}}{\partial y} \right\} (y, z, t, \Phi). \quad (7.5)$$

The use of the quasiperiodic sources $f^{\text{new}}(g, t, \Phi)$ or $f_p^{\text{new}}(g, t, \Phi)$ together with the superposition principle allows one to restrict the domain of analysis to $\Omega^{\text{new}} = \{g = \{y, z\} \in \Omega : 0 < y < l\}$ (to the part of the *Floquet channel* $R = \{g : 0 < y < l\}$). The problem (7.1) is represented in one of the following equivalent forms:

$$U(g, t) = \int_{-\infty}^{\infty} U^{\text{new}}(g, t, \Phi) d\Phi, \quad (7.6a)$$

$$\left\{ \begin{array}{l} \left[-\varepsilon(g) \frac{\partial^2}{\partial t^2} - \sigma(g) \eta_0 \frac{\partial}{\partial t} + \frac{\partial^2}{\partial y^2} + \frac{\partial^2}{\partial z^2} \right] U^{\text{new}}(g, t) = F^{\text{new}}(g, t); \\ g = \{y, z\} \in \Omega^{\text{new}}, \quad t > 0 \\ U^{\text{new}}(g, 0) = \varphi^{\text{new}}(g), \quad \frac{\partial}{\partial t} U^{\text{new}}(g, t) \Big|_{t=0} = \psi^{\text{new}}(g); \quad g \in \overline{\Omega}^{\text{new}} \\ \vec{E}_{t_g}^{\text{new}}(q, t) \quad \text{and} \quad \vec{H}_{t_g}^{\text{new}}(q, t) \quad \text{are continuous when} \\ \text{crossing } \Sigma^{\varepsilon, \sigma}, \quad \vec{E}_{t_g}^{\text{new}}(q, t) \Big|_{q=\{x, y, z\} \in \Sigma} = 0, \quad \text{and} \\ U^{\text{new}} \left\{ \frac{\partial U^{\text{new}}}{\partial y} \right\} (l, z, t) = e^{2\pi i \Phi} U^{\text{new}} \left\{ \frac{\partial U^{\text{new}}}{\partial y} \right\} (0, z, t); \quad t \geq 0, \end{array} \right. \quad (7.6b)$$

or

$$U(g, t) = \sum_{p=-\infty}^{\infty} \int_{-0.5}^{0.5} U_p^{\text{new}}(g, t, \Phi) d\Phi \quad (7.7a)$$

$$\left\{ \begin{array}{l} \left[-\varepsilon(g) \frac{\partial^2}{\partial t^2} - \sigma(g) \eta_0 \frac{\partial}{\partial t} + \frac{\partial^2}{\partial y^2} + \frac{\partial^2}{\partial z^2} \right] U_p^{\text{new}}(g, t) = F_p^{\text{new}}(g, t); \\ g = \{y, z\} \in \Omega^{\text{new}}, \quad t > 0 \\ U_p^{\text{new}}(g, 0) = \varphi_p^{\text{new}}(g), \quad \frac{\partial}{\partial t} U_p^{\text{new}}(g, t) \Big|_{t=0} = \psi_p^{\text{new}}(g); \quad g \in \overline{\Omega}^{\text{new}} \\ \left(\vec{E}_p^{\text{new}} \right)_{t_g}(q, t) \quad \text{and} \quad \left(\vec{H}_p^{\text{new}} \right)_{t_g}(q, t) \quad \text{are continuous when} \\ \text{crossing } \Sigma^{\varepsilon, \sigma}, \quad \left(\vec{E}_p^{\text{new}} \right)_{t_g}(q, t) \Big|_{q=\{x, y, z\} \in \Sigma} = 0; \quad \text{and} \\ U_p^{\text{new}} \left\{ \frac{\partial U_p^{\text{new}}}{\partial y} \right\} (l, z, t) = e^{2\pi i \Phi} U_p^{\text{new}} \left\{ \frac{\partial U_p^{\text{new}}}{\partial y} \right\} (0, z, t); \quad t \geq 0. \end{array} \right. \quad (7.7b)$$

The problems (7.6b) and (7.7b) are open since the domain Ω^{new} extends to infinity along the z -axis. It is a serious handicap to the use of finite-difference or finite-element methods [25, 26] for numerical solution. On the virtual boundaries Γ_1 and Γ_2 of the domain $\Omega_{\text{int}} = \{g \in \Omega^{\text{new}} : -L_1 < z < L_2\}$ containing all sources and grating’s elements (Fig. 7.1), the fields $U^{\text{new}}(g, t)$ and $U_p^{\text{new}}(g, t)$ are formed by *outgoing pulsed waves*. This lets us replace (7.6b) and (7.7b) with the following closed problem (see [10, 12] and Chap. 5 in this book)

$$\left\{ \begin{array}{l} \left[-\varepsilon(g) \frac{\partial^2}{\partial t^2} - \sigma(g) \eta_0 \frac{\partial}{\partial t} + \frac{\partial^2}{\partial y^2} + \frac{\partial^2}{\partial z^2} \right] U(g, t) = F(g, t); \\ g = \{y, z\} \in \Omega_{\text{int}}, \quad t > 0 \\ U(g, 0) = \varphi(g), \quad \frac{\partial}{\partial t} U(g, t) \Big|_{t=0} = \psi(g); \quad g \in \overline{\Omega}_{\text{int}} \\ \vec{E}_{\text{tg}}(q, t) \quad \text{and} \quad \vec{H}_{\text{tg}}(q, t) \quad \text{are continuous when} \\ \text{crossing } \Sigma^{\varepsilon, \sigma}, \quad \vec{E}_{\text{tg}}(q, t) \Big|_{q=\{x, y, z\} \in \Sigma} = 0, \\ U \left\{ \frac{\partial U}{\partial y} \right\} (l, z, t) = e^{2\pi i \Phi} U \left\{ \frac{\partial U}{\partial y} \right\} (0, z, t) \quad \text{for } -L_1 < z < L_2, \\ \text{and } D_1[U(g, t)] \Big|_{g \in \Gamma_1} = 0, \quad D_2[U(g, t)] \Big|_{g \in \Gamma_2} = 0; \quad t \geq 0 \end{array} \right. \quad (7.8a)$$

(the superscript ‘new’ is omitted) and the formulas

$$U(y, z, t) = \sum_{n=-\infty}^{\infty} \left\{ \int_0^{t+(L_1+z)} J_0 \left[\Phi_n \left((t-\tau)^2 - (L_1+z)^2 \right) \right] \times \left[\int_0^l \frac{\partial U(\tilde{y}, \tilde{z}, \tau)}{\partial \tilde{z}} \Big|_{\tilde{z}=-L_1} \mu_n^*(\tilde{y}) d\tilde{y} \right] d\tau \right\} \mu_n(y); \quad (7.8b)$$

$$0 \leq y \leq l, \quad z \leq -L_1, \quad t \geq 0,$$

$$U(y, z, t) = - \sum_{n=-\infty}^{\infty} \left\{ \int_0^{t-(z-L_2)} J_0 \left[\Phi_n \left((t-\tau)^2 - (z-L_2)^2 \right) \right] \times \left[\int_0^l \frac{\partial U(\tilde{y}, \tilde{z}, \tau)}{\partial \tilde{z}} \Big|_{\tilde{z}=L_2} \mu_n^*(\tilde{y}) d\tilde{y} \right] d\tau \right\} \mu_n(y); \quad (7.8c)$$

$$0 \leq y \leq l, \quad z \geq L_2, \quad t \geq 0,$$

which calculate the field $U(g, t)$ in the domains $\Omega_1 = \{g = \{y, z\} \in R : z < -L_1\}$ and $\Omega_2 = \{g = \{y, z\} \in R : z > L_2\}$ from its values on the virtual boundaries Γ_j , $j = 1, 2$. Here, $J_m(\dots)$ are the Bessel cylindrical functions and the asterisk ‘*’ stands for the complex conjugation. The transverse functions $\mu_n(y) = l^{-1/2} \exp(i\Phi_n y)$, $n = 0, \pm 1, \pm 2, \dots$, $\Phi_n = (n + \Phi)2\pi/l$ form a complete orthonormal system in the Floquet channel R . Thus, for $g = \{y, z\} \in \overline{\Omega}_j$ and $t > 0$ the following representations for the sought-for field are correct:

$$U(g, t) = \sum_{n=-\infty}^{\infty} u_{nj}(z, t) \mu_n(y) \quad \text{and} \quad u_{nj}(z, t) = \int_0^l U(g, t) \mu_n^*(y) dy. \quad (7.9)$$

The EACs operators $D_1[U(g, t)]|_{g \in \Gamma_1} = 0$ and $D_2[U(g, t)]|_{g \in \Gamma_2} = 0$ are obtained by substituting the values $z = -L_1$ and $z = L_2$ into (7.8b) and (7.8c).

Suppose all sources are relocated from the domain Ω_{int} into the domain Ω_2 , where they generate the pulsed wave

$$U^{i(2)}(g, t) = \sum_{n=-\infty}^{\infty} v_n z(z, t) \mu_n(y); \quad g = \{y, z\} \in \Omega_2, \quad t \geq 0, \quad (7.10)$$

which is incident onto the boundary Γ_2 at $t > 0$. Then the problem (7.8a, 7.8b, 7.8c) should be rewritten in the form:

$$\left\{ \begin{array}{l} \left[-\varepsilon(g) \frac{\partial^2}{\partial t^2} - \sigma(g) \eta_0 \frac{\partial}{\partial t} + \frac{\partial^2}{\partial y^2} + \frac{\partial^2}{\partial z^2} \right] U(g, t) = 0; \quad g \in \Omega_{\text{int}}, \quad t > 0 \\ U(g, 0) = 0, \quad \frac{\partial}{\partial t} U(g, t)|_{t=0} = 0; \quad g \in \bar{\Omega}_{\text{int}} \\ \vec{E}_{\text{tg}}(q, t) \quad \text{and} \quad \vec{H}_{\text{tg}}(q, t) \quad \text{are continuous when crossing} \quad \Sigma^{\varepsilon, \sigma}, \\ \vec{E}_{\text{tg}}(q, t)|_{q=\{x, y, z\} \in \Sigma} = 0, \quad U \left\{ \frac{\partial U}{\partial y} \right\} (l, z, t) = e^{2\pi i \Phi} U \left\{ \frac{\partial U}{\partial y} \right\} (0, z, t) \\ \text{for} \quad -L_1 < z < L_2, \quad \text{and} \quad D_1[U(g, t)]|_{g \in \Gamma_1} = 0, \\ D_2[U(g, t) - U^{i(2)}(g, t)]|_{g \in \Gamma_2} = 0; \quad t \geq 0, \end{array} \right. \quad (7.11a)$$

$$U(y, z, t) = \sum_{n=-\infty}^{\infty} \left\{ \int_0^{t+(L_1+z)} J_0 \left[\Phi_n \left((t-\tau)^2 - (L_1+z)^2 \right) \right] \right. \\ \left. \times \left[\int_0^l \frac{\partial U(\tilde{y}, \tilde{z}, \tau)}{\partial \tilde{z}} \Big|_{\tilde{z}=-L_1} \mu_n^*(\tilde{y}) d\tilde{y} \right] d\tau \right\} \mu_n(y); \quad (7.11b)$$

$$0 \leq y \leq l, \quad z \leq -L_1, \quad t \geq 0,$$

$$U(y, z, t) - U^{i(2)}(y, z, t) = - \sum_{n=-\infty}^{\infty} \left\{ \int_0^{t-(z-L_2)} J_0 \left[\Phi_n \left((t-\tau)^2 - (z-L_2)^2 \right) \right] \right. \\ \left. \times \left[\int_0^l \frac{\partial [U(\tilde{y}, \tilde{z}, \tau) - U^{i(2)}(\tilde{y}, \tilde{z}, \tau)]}{\partial \tilde{z}} \Big|_{\tilde{z}=L_2} \mu_n^*(\tilde{y}) d\tilde{y} \right] d\tau \right\} \mu_n(y); \quad (7.11c)$$

$$0 \leq y \leq l, \quad z \geq L_2, \quad t \geq 0.$$

7.2.2 Plane Models for Infinite Gratings: Frequency-Domain Representations

The solution $\tilde{U}(g, k)$ to the problem

$$\left\{ \begin{array}{l} \left[\frac{\partial}{\partial t} + \frac{\partial^2}{\partial y^2} + \frac{\partial^2}{\partial z^2} + \bar{\varepsilon}(g)k^2 \right] \tilde{U}(g, k) = 0; \quad g \in \Omega_{\text{int}} \\ \tilde{E}_{\text{tg}}(q, k), \quad \tilde{H}_{\text{tg}}(q, k) \quad \text{are continuous when crossing } \Sigma^{\varepsilon, \sigma} \\ \text{and boundaries } \Gamma_j \times [|x| \leq \infty], \quad \tilde{E}_{\text{tg}}(q, k) \Big|_{q=\{x,y,z\} \in \Sigma} = 0, \quad \text{and} \\ \tilde{U} \left\{ \frac{\partial \tilde{U}}{\partial y} \right\} (l, z, k) = e^{2\pi i \Phi} \tilde{U} \left\{ \frac{\partial \tilde{U}}{\partial y} \right\} (0, z, k) \quad \text{for } -L_1 \leq z \leq L_2, \end{array} \right. \quad (7.12a)$$

$$\tilde{U}(g, k) = \sum_{n=-\infty}^{\infty} B_{n1}(k) e^{-i\gamma_n(z+L_1)} \mu_n(y); \quad g \in \bar{\Omega}_1, \quad (7.12b)$$

$$\tilde{U}(g, k) = \sum_{n=-\infty}^{\infty} \left[A_{n2}(k) e^{-i\gamma_n(z-L_2)} + B_{n2}(k) e^{i\gamma_n(z-L_2)} \right] \mu_n(y); \quad g \in \bar{\Omega}_2 \quad (7.12c)$$

and the solution $U(g, t)$ to the problem (7.11a, 7.11b, 7.11c) can be related [12] by the following integral transform

$$\tilde{f}(k) = \int_0^{\infty} f(t) e^{ikt} dt \quad \leftrightarrow \quad f(t) = \frac{1}{2\pi} \int_{i\alpha-\infty}^{i\alpha+\infty} \tilde{f}(k) e^{-ikt} dk; \quad 0 \leq \alpha \leq \text{Im } k. \quad (7.13)$$

Here, $\tilde{U}(g, k) = \tilde{E}_x(g, k)$ for monochromatic E -polarized waves and $\tilde{U}(g, k) = \tilde{H}_x(g, k)$ for H -polarized waves, k is the complex wavenumber (frequency parameter or frequency), $\bar{\varepsilon}(g) = \varepsilon(g) + i\eta_0\sigma(g)/k$,

$$\gamma_n = \sqrt{k^2 - \Phi_n^2}; \quad \text{Re } \gamma_n \text{Re } k \geq 0, \quad \text{Im } \gamma_n \geq 0, \quad \text{and } \Phi_n = (n + \Phi)2\pi/l \quad (7.14)$$

are the vertical and horizontal wavenumbers for spatial harmonics (plane waves) propagating in the domains Ω_j with attenuation (when $\text{Im } \gamma_n > 0$) or without it (when $\text{Im } \gamma_n = 0$). According to (7.13), the time-dependence for monochromatic components of any signal is $\exp(-ikt)$.

In the formulas (7.12b), (7.12c), the terms with complex-valued amplitudes A_{n2} correspond to the monochromatic wave $\tilde{U}^{i(2)}(g, k) \leftrightarrow U^{i(2)}(g, t)$ incident on the boundary Γ_2 , while the terms with amplitudes B_{n1} and B_{n2} correspond to the scattered (secondary) waves $\tilde{U}^{s(1)}(g, k) \leftrightarrow U^{s(1)}(g, t) = U(g, t)$ and $\tilde{U}^{s(2)}(g, k) \leftrightarrow U^{s(2)}(g, t) = U(g, t) - U^{i(2)}(g, t)$ in Ω_1 and Ω_2 . If we correlate (7.9) and (7.10) with (7.12b) and (7.12c), it becomes evident that

$$A_{n2}(k) \leftrightarrow v_{n2}(L_2, t), \quad B_{n1}(k) \leftrightarrow u_{n1}(-L_1, t), \quad B_{n2}(k) \leftrightarrow u_{n2}(L_2, t). \quad (7.15)$$

Consider now frequencies k such that $\text{Re } k > 0$ and $\text{Im } k = 0$ (*physical values of the frequency parameter* $k = 2\pi/\lambda$, λ is the wavelength). Let also, as previously, a grating (Fig. 7.1) be excited from the domain Ω_2 , but

$$\tilde{U}^{i(2)}(g, k) = \tilde{U}_p^{i(2)}(g, k) = A_{p2}(k)e^{-i\gamma_p(z-L_2)}\mu_p(y). \quad (7.16)$$

In the frequency domain, a periodic structure is characterized by the *reflection coefficient* $R_{np}^{22}(k)$ (coefficient of conversion of the p th incident harmonic into the n th reflected harmonic) and the *transmission coefficient* $T_{np}^{12}(k)$ (coefficient of conversion of the p th incident harmonic into the n th transmitted harmonic) given by the following formulas:

$$R_{np}^{22}(k) = \frac{B_{n2}}{A_{p2}} = \frac{\tilde{u}_{n2}(L_2, k)}{\tilde{v}_{p2}(L_2, k)}, \quad T_{np}^{12}(k) = \frac{B_{n1}}{A_{p2}} = \frac{\tilde{u}_{n1}(-L_1, k)}{\tilde{v}_{p2}(L_2, k)}. \quad (7.17)$$

The elements $R_{np}^{22}(k)$ and $T_{np}^{12}(k)$ of the *generalized scattering matrices* $\left\{R_{np}^{22}(k)\right\}_{n,p=-\infty}^{\infty}$ and $\left\{T_{np}^{12}(k)\right\}_{n,p=-\infty}^{\infty}$ are related by the *energy balance equations*

$$\sum_{n=-\infty}^{\infty} \left[\left| R_{np}^{22} \right|^2 + \left| T_{np}^{12} \right|^2 \right] \begin{Bmatrix} \text{Re } \gamma_n \\ \text{Im } \gamma_n \end{Bmatrix} = \begin{Bmatrix} \text{Re } \gamma_p + 2\text{Im } R_{pp}^{22} \text{Im } \gamma_p \\ \text{Im } \gamma_p - 2\text{Im } R_{pp}^{22} \text{Re } \gamma_p \end{Bmatrix} - \frac{k^2}{\beta_0} \begin{Bmatrix} W_1 \\ W_2 \end{Bmatrix};$$

$$p = 0, \pm 1, \pm 2, \dots \quad (7.18)$$

and by the *reciprocity relations*

$$\frac{R_{np}^{22}(\Phi)}{\gamma_p(\Phi)} = \frac{R_{-p,-n}^{22}(-\Phi)}{\gamma_{-n}(-\Phi)}, \quad \frac{T_{np}^{12}(\Phi)}{\gamma_p(\Phi)} = \frac{T_{-p,-n}^{21}(-\Phi)}{\gamma_{-n}(-\Phi)};$$

$$n, p = 0, \pm 1, \pm 2, \dots, \quad (7.19)$$

which are the corollaries from the Pointing theorem on complex power and the Lorentz lemma [2, 12, 27]. It should be obvious that for excitation from the domain Ω_1 , the matrices $\left\{R_{np}^{11}(k)\right\}_{n,p=-\infty}^{\infty}$ and $\left\{T_{np}^{21}(k)\right\}_{n,p=-\infty}^{\infty}$ are determined in the same way. In (7.18), we have used the following designations:

$$\beta_0 = \left\{ \begin{array}{l} \varepsilon_0 \\ \mu_0 \end{array} \right\}, \quad W_1 = \frac{\eta_0 \varepsilon_0}{k} \int_{\Omega_{\text{int}}} \sigma(g) \left| \tilde{E}(g, k) \right|^2 dg, \quad \text{and}$$

$$W_2 = \left\{ \begin{array}{l} + \\ - \end{array} \right\} \int_{\Omega_{\text{int}}} \left[\mu_0 \left| \tilde{H}(g, k) \right|^2 - \varepsilon(g) \varepsilon_0 \left| \tilde{E}(g, k) \right|^2 \right] dg; \quad \left\{ \begin{array}{l} E - \text{case} \\ H - \text{case} \end{array} \right\}.$$

Every harmonic of the field $\tilde{U}^{s(j)}(g, k)$, for which $\text{Im } \gamma_n = 0$ and $\text{Re } \gamma_n > 0$, is a homogeneous plane wave propagating away from a grating at the angle $\alpha_n = -\arcsin(\Phi_n/k)$ into the *reflection zone* ($z > L_2$), and at the angle $\alpha_n = \pi + \arcsin(\Phi_n/k)$ into the *transmission zone* ($z < -L_1$). All angles are measured anticlockwise from the z -axis in the plane $y0z$ (Fig. 7.1).

For $\text{Re } \gamma_p > 0$, the angle $\alpha_p^i = \arcsin(\Phi_p/k)$ is the angle of incidence of the wave $\tilde{U}_p^{i(2)}(g, k)$ onto a grating. It is obvious that the travelling direction of each homogeneous harmonic of the secondary field depends on its number n , as well as on the values of k and α_p^i . The angle between the propagation directions of the primary and the $(-m)$ th reflected plane wave $2\alpha = \alpha_p^i - \alpha_{-m}$ is determined from the equation $kl \sin(\alpha_p^i - \alpha) \cos \alpha = \pi(p + m)$. At $\alpha = 0$ the corresponding harmonic propagates countercurrent to the incident wave. Initiation of the nonspecular reflected mode of this kind is called the *autocollimation* phenomenon. According to (7.18), the values

$$W_{\text{abs}}(k) = \frac{k^2}{\beta_0 |\gamma_p^i|} W_1, \quad W_{np}^{22}(k) = \left| R_{np}^{22} \right|^2 \frac{\text{Re } \gamma_n}{|\gamma_p|}, \quad W_{np}^{12}(k) = \left| T_{np}^{12} \right|^2 \frac{\text{Re } \gamma_n}{|\gamma_p|} \quad (7.20)$$

determine the relative part of energy lost to absorption and directed by a grating into the relevant spatial harmonic.

If a grating is excited by an inhomogeneous plane wave ($\text{Im } \gamma_p > 0$), the *near-field to far-field conversion efficiency* is determined by the value of $\text{Im } R_{pp}^{22}$ (see (7.18)), which in this case is nonnegative and

$$\text{Im } R_{pp}^{22} = \frac{1}{2} \left[\sum_n \left(W_{np}^{22} + W_{np}^{12} \right) + W_{\text{abs}} \right] \quad (7.21)$$

as follows from (7.19) and the equalities $\Phi_n(\Phi) = -\Phi_{-n}(-\Phi)$ and $\gamma_n(\Phi) = \gamma_{-n}(-\Phi)$, one can study the excitation of a grating by an inhomogeneous plane wave in the context of conventional for the gratings theory diffraction problems: a structure is excited by homogeneous plane waves $\tilde{U}_{-n}^{i(2)}(g, k, -\Phi)$ and $\tilde{U}_{-n}^{i(1)}(g, k, -\Phi)$, and the coefficients of conversion into damped $(-p)$ th spatial harmonics $R_{-p, -n}^{22}(-\Phi)$ and $T_{-p, -n}^{21}(-\Phi)$ are calculated.

7.2.3 Infinite Gratings as Open Resonators or Open Waveguides

Main peculiarities of the near-field to far-field conversion are associated with the so-called *normal modes*. When modes of this kind are excited in a grating, it operates as an open resonator or an open waveguide. One can simulate such operating modes by extending analytically *homogeneous (spectral) frequency-domain problems* (see, for example, the problem (7.12a, 7.12b, 7.12c) for $\tilde{U}^{i(2)}(g, k) \equiv 0$) into a range of complex values of one of spectral parameters: the frequency k or the *longitudinal propagation number* Φ [12]. The domain of analytical extension coincides with the infinite-sheeted Riemann surfaces K (real-valued Φ is fixed, $k \in K$ is a complex-valued spectral parameter) or F ($k > 0$ is fixed, $\Phi \in F$ is a spectral parameter) with the *real algebraic branch points* $k_n^\pm : \gamma_n(k_n^\pm) = 0$ and $\Phi_n^\pm : \gamma_n(\Phi_n^\pm) = 0$, $n = 0, \pm 1, \pm 2, \dots$. On the real axis of the first (physical) sheet of the Riemann surface K the following conditions hold true: $\text{Re } \gamma_n \text{Re } k \geq 0$ and $\text{Im } \gamma_n \geq 0$ (see (7.14)). They are consistent with the physically understandable requirement that the fields $\tilde{U}^{s(1)}(g, k)$ and $\tilde{U}^{s(2)}(g, k)$ do not contain waves incoming from infinity. Similarly, on the real axis of the first sheet of F we have: $\text{Re } \gamma_n \geq 0$ and $\text{Im } \gamma_n \geq 0$.

The set Θ_k of eigenfrequencies \bar{k}_n is the *frequency spectral set* or the *frequency spectra* if for complex-valued frequencies $k = \bar{k}_n \in K$, the spectral problem has nontrivial solutions $\tilde{U}(g, \bar{k}_n) = \bar{u}(g, \bar{k}_n)$. Every solution of this kind corresponds to a *free oscillation* at the *eigenfrequency* \bar{k}_n in a grating. Likewise one can define the set Θ_Φ of propagation constants $\bar{\Phi}_n$ of surface, leaky, and piston-like *eigenwaves* $\tilde{U}(g, \bar{\Phi}_n) = \bar{u}(g, \bar{\Phi}_n)$ [8]. For gratings under consideration, the sets Θ_k and Θ_Φ are countable sets without finite accumulation points. A detailed discussion of spectral sets, localization and dynamics of their elements on the surfaces K and F as well as the relation between anomalous or resonant scattering of monochromatic and pulsed waves by periodic structures and generation in these structures of high-quality free oscillations and weak decaying eigenwaves can be found in [12].

7.2.4 Some Further Comments

- The field of a density-modulated electron flow, whose instantaneous charge density can be written as $\rho \delta(z - a) \exp[i((k/\beta)y - kt)]$, is H -polarized field with

$$\tilde{H}_x(y, z, k) = 2\pi\rho\beta e^{i[\sqrt{k^2 - (k/\beta)^2}|z-a| + (k/\beta)y]} [|z - a|/(z - a)]; \quad z \neq a \quad (7.22)$$

[19]. Here, $\delta(\dots)$ is the Dirac delta-function, ρ and k are the modulation amplitude and the modulation frequency of the flow, and $\beta < 1$ is its relative velocity.

From (7.16) and (7.22) it follows that the flow-generated field is a solution to the problem (7.12a, 7.12b, 7.12c) (*H*-case), where the incident wave is

$$\tilde{U}^{i(2)}(g, k) = \tilde{U}_p^{i(2)}(g, k) = A_p \mu_p(k) e^{-i\gamma_p(z-L_2)} \mu_p(y); \quad L_2 \leq z < a \quad (7.23)$$

with $A_p \mu_p(k) = -2\pi\rho\beta\sqrt{l} \exp\left[-k(a-L_2)\sqrt{(1/\beta)^2-1}\right]$ and $\Phi_p = k/\beta$.

- In the subsequent considerations of electrodynamic models (Sect. 7.3), we deal with the following structures: infinite one-dimensionally periodic gratings and plane density-modulated electron flows, whose description is given in this section; finite planar and axially symmetric gratings and open waveguides (information on these structures can be found in Chap. 5); infinite planar dielectric waveguides.
- Represent the *x*-component of *E*- or *H*-polarized eigenwave of a planar waveguide (Fig. 7.2; $\partial/\partial x = 0$) as

$$\tilde{U}(g, \bar{\chi}) = \bar{u}(g, \bar{\chi}) = \begin{cases} B_2 \exp[i\gamma(\bar{\chi})(z-b) + i\bar{\chi}y]; & z \geq b \\ [C \exp[-i\gamma_\varepsilon(\bar{\chi})(z-b)] + D \exp[i\gamma_\varepsilon(\bar{\chi})(z-a)]] \\ \quad \times \exp[i\bar{\chi}y]; & a \leq z \leq b \\ B_1 \exp[-i\gamma(\bar{\chi})(z-a) + i\bar{\chi}y]; & z \leq a. \end{cases} \quad (7.24)$$

Here, $\bar{\chi}$ is the complex-valued *longitudinal propagation number* for the eigenwave $\bar{u}(g, \bar{\chi})$; $\gamma(\chi) = \sqrt{k^2 - \chi^2}$ (a branch of the square root is determined by the point $\bar{\chi}$ location on the two-sheeted Riemann surface *X* with the algebraic branch points $\chi^\pm = \pm k$ (Fig. 7.3)); $\gamma_\varepsilon(\chi) = \sqrt{k^2\varepsilon - \chi^2}$ (one can choose any branch of the root).

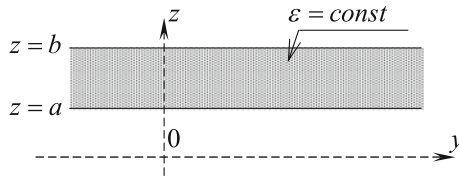


Fig. 7.2 Planar dielectric waveguide

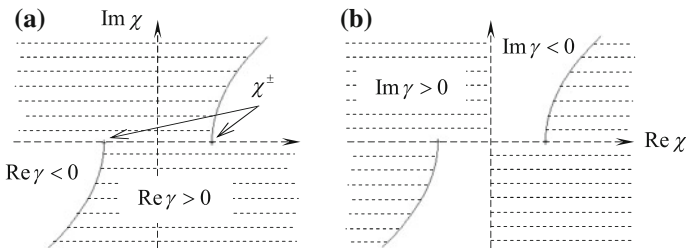


Fig. 7.3 $\gamma(\chi)$ distribution on the first sheet of *X*: **a** $\text{Re } \gamma(\chi)$ and **b** $\text{Im } \gamma(\chi)$

The continuity condition of the wave tangential components on the boundaries $z = b$ and $z = a$ of the partial domains in (7.24) leads to the homogeneous system of linear algebraic equations

$$\begin{cases} (B_2 \pm B_1) - (C \pm D)(1 \pm e_\varepsilon) = 0 \\ (B_2 \pm B_1)\gamma + (C \pm D)(1 \mp e_\varepsilon)\alpha\gamma_\varepsilon = 0, \end{cases} \quad (7.25)$$

which is resolvable nontrivially for the values of $\chi = \bar{\chi} \in X$ satisfying the following *dispersion equation*:

$$(1 \mp e_\varepsilon)\alpha\gamma_\varepsilon(\chi) + (1 \pm e_\varepsilon)\gamma(\chi) = 0. \quad (7.26)$$

Here, $e_\varepsilon = \exp[i\gamma_\varepsilon(\chi)(b - a)]$; $\alpha = 1$ for E -polarized wave and $\alpha = \varepsilon^{-1}$ for H -polarized wave; the upper signs in (7.25), (7.26) correspond to symmetric with respect to the plane $z = (a + b)/2$ waves ($B_2 = B_1$, $C = D$), while the bottom signs correspond to antisymmetric waves ($B_2 = -B_1$, $C = -D$).

On the axis $\text{Re } \chi$ of the first (physical) sheet of X we have: $\text{Re } \gamma(\chi) \geq 0$ and $\text{Im } \gamma(\chi) \geq 0$. It follows from the physically evident requirement that the field $\bar{u}(g, \bar{\chi})$ does not contain waves incoming from infinity. The values of $\gamma(\chi)$ determine the quarters of the χ -plane where the branch cuts should lie. They are given by the curves $k^2 - (\text{Re } \chi)^2 + (\text{Im } \chi)^2 = 0$, $\text{Re } \chi \text{Im } \chi \geq 0$. The functions $\text{Re } \gamma(\chi)$ and $\text{Im } \gamma(\chi)$ are shown in Fig. 7.3 for the points χ of the first sheet of the surface X . For χ from the second sheet, the values of $\text{Re } \gamma(\chi)$ and $\text{Im } \gamma(\chi)$ have opposite signs.

An eigenwave, whose field strength is exponentially decreasing with the distance from the dielectric layer ($\text{Im } \gamma(\bar{\chi}) > 0$), is a *surface wave*, otherwise ($\text{Im } \gamma(\bar{\chi}) \leq 0$) it is a *leaky wave*. A wave $\bar{u}(g, \bar{\chi})$ is called a *real wave* if $\text{Im } \chi = 0$, and a *complex wave* if $\text{Im } \chi \neq 0$. A real surface wave is a *true wave*. Its relative phase velocity $\beta = k/\bar{\chi} < 1$ and thus it is a *slow wave*.

- The points χ , $-\chi$, and χ^* lie on the same sheet of the surface X , and the following relations are true for them: $\gamma(\chi) = \gamma(-\chi)$, $\gamma^*(\chi) = \gamma(\chi^*)$. Then the points $\chi = \bar{\chi}$, $\chi = -\bar{\chi}$, $\chi = \bar{\chi}^*$, and $\chi = -\bar{\chi}^*$ are the solutions to the dispersion equation (7.26). The points $\bar{\chi}$ and $-\bar{\chi}$ lie on the same sheet of X , and the points $\bar{\chi}^*$, $-\bar{\chi}^*$ on the other sheet. These facts provide some insight into the behavior of the eigenvalues $\bar{\chi}$ under changing $b - a$, ε , and k . The longitudinal propagation numbers move on the surface X in sets of four $\{\bar{\chi}, -\bar{\chi}, \bar{\chi}^*, -\bar{\chi}^*\}$. For example, if $\text{Im } \bar{\chi} = 0$, then in order to transform a real wave into a complex wave with wiggling the corresponding parameters around, it is necessary to collide a real wave with another real wave. In other words, two waves simultaneously emerge in the domain of complex-valued $\bar{\chi}$ from the point on the real axis of χ , where projections of their longitudinal propagation numbers on the first sheet of X coincide. The collided real waves are transformed into complex waves; the eigenvalues $\bar{\chi}$ acquire equal in magnitude and opposite in sign imaginary increments.

7.3 Diffraction Radiation Phenomena

7.3.1 Reflecting Gratings in the Field of a Density-Modulated Electron Flow

Suppose $A_{p,2}(k) = A_{1,2}(k) = 1$ ($p = 1$) and $L_2 = 0$ in (7.23). Consider behavior of the functions $W_{01}^{22}(\beta, \alpha_0, \dots)$ (see (7.20) and (7.21)), which determine the transformation efficiency of the eigenfield of density-modulated electron flow into fundamental ($n = 0$) spatial harmonic of the secondary field outgoing into the reflection zone of a periodic structure at an angle of α_0 . We study numerical data obtained for perfectly-conducting lamellar and echelette gratings for $\beta > 0.9$. This range is interesting for developers of relativistic devices of diffraction electronics. Radiation characteristics of reflecting gratings in the field of slow electron beams ($0 < \beta < 0.5$) have been studied extensively in [20, 28].

From $\Phi_p = k/\beta$ and $\alpha_n = -\arcsin(\Phi_n/k)$ (see Sects. 7.2.2 and 7.2.4) we have (for $p = 1$ and $n = 0$) $\beta = \kappa/(1 - \kappa \sin \alpha_0)$. This formula relates the electron velocity β , the angle α_0 , and the nondimensional frequency parameter $\kappa = l/\lambda = kl/2\pi$, where λ is the flow modulation wavelength.

The radiation energy $W_{01}^{22}(\beta, \alpha_0, \delta, \theta)$ of the zeroth spatial harmonic is presented in Fig. 7.4 as a function of the relative height $\delta = h/l$ of a lamellar grating for different values of α_0 , β , and $\theta = d/l$. The functions $W_{01}^{22}(\delta)$ are almost periodic. The period decreases as β increases; an increase in α_0 causes the oscillation period to increase too. The maximum value of $W_{01}^{22}(\delta)$ grows as β increases and θ decreases. For large β (for high velocity of electron beam) gratings with lesser groove height are required to implement the regime with the maximal intensity of

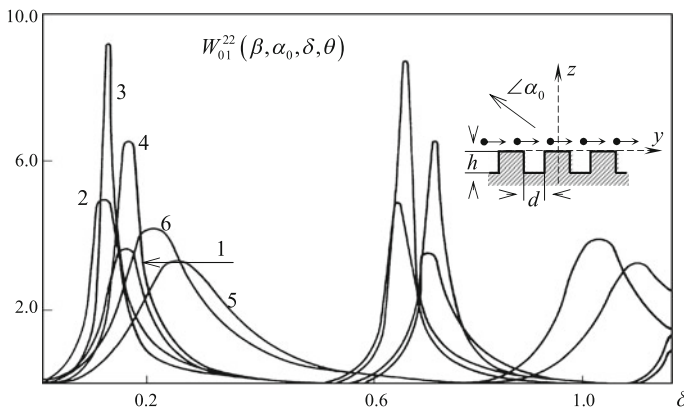


Fig. 7.4 Radiation intensity as function of relative height of lamellar grating grooves: 1 – $W_{01}^{22}(0.9, 1.0^\circ, \delta, 0.4)$; 2 – $W_{01}^{22}(0.95, 1.0^\circ, \delta, 0.4)$; 3 – $W_{01}^{22}(0.95, 1.0^\circ, \delta, 0.2)$; 4 – $W_{01}^{22}(0.9, 1.0^\circ, \delta, 0.2)$; 5 – $W_{01}^{22}(0.9, 35^\circ, \delta, 0.4)$; 6 – $W_{01}^{22}(0.95, 35^\circ, \delta, 0.4)$

the radiation into the zeroth spatial harmonic. The corresponding height for a vertical radiation is less than for $\alpha_0 > 0$.

We emphasize a favorable, in technical respect, tendency for a decrease of the required groove depth to gain the optimum diffraction radiation characteristics with increasing β . Thus, the values of h/l for the near-vertical radiation ($\alpha_0 = 1^\circ$) are approximately equal to 0.15 and 0.121 for $\beta = 0.9$ and $\beta = 0.95$, respectively. This tendency gets more evident as β gets closer to 1.0. It is shown by the behavior of the level curves of W_{01}^{22} in the plane with coordinates β and δ (Fig. 7.5). It follows that the requirements imposed on the stability of the electron flow velocity have to grow as β increases because a small variation in stability for $\beta > 0.99$ and fixed δ and α_0 can cause an abrupt decrease of the diffraction radiation intensity. For $\beta < 0.99$ the requirements imposed on the stability of the beam velocity can be far more lenient (the level curves of $W_{01}^{22}(\beta, \delta)$ are almost parallel to the β -axis).

Observation of the level curves for W_{01}^{22} in the plane with coordinates β and θ allows one to investigate in detail the radiation characteristics of lamellar gratings of various groove width. Thus, for example, for $\beta < 0.93$ (Fig. 7.6) a decrease of groove width is followed initially by a progressive and monotonic increase of the radiation intensity. Then it decreases in its passage through the maximum $W_{01}^{22}(\theta) \approx 4.0 \div 7.0$, which is reached in the band $0.2 < \theta < 0.4$. The greater is β , the sharper is a decrease. In the range $0.93 < \beta < 0.98$, the functions $W_{01}^{22}(\beta, \alpha_0, \delta, \theta) = W_{01}^{22}(\beta, 1.0^\circ, 0.135, \theta)$ have several local extrema. For wide

Fig. 7.5 Level curves $W_{01}^{22}(\beta, 31^\circ, \delta, 0.4) = \text{const}$ of energy radiated into free space on the fundamental spatial harmonic

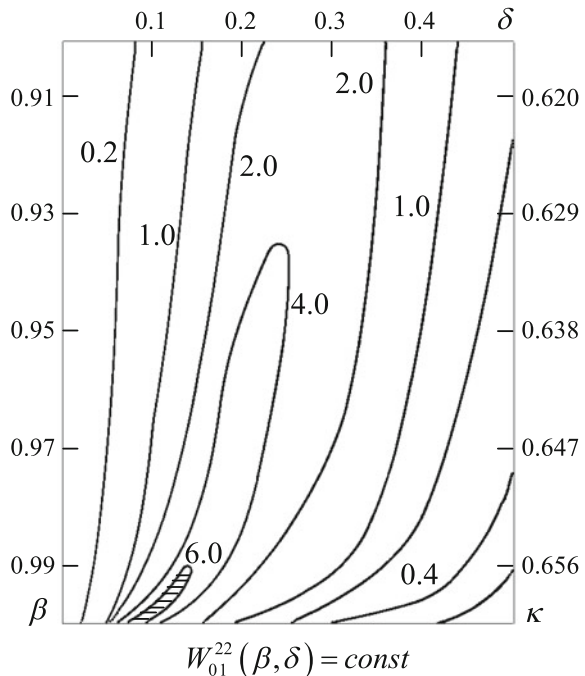
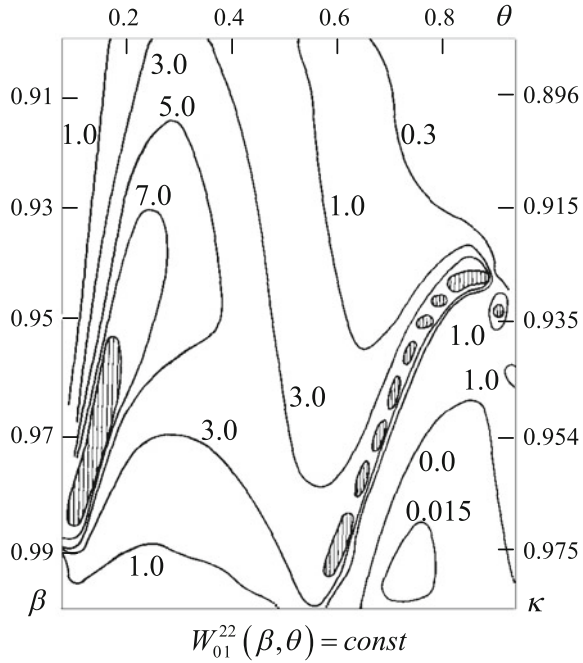


Fig. 7.6 Level curves $W_{01}^{22}(\beta, 1.0^\circ, 0.135, \theta) = \text{const}$ of energy radiated into free space in near-vertical direction. Shaded area corresponds to $W_{01}^{22}(\beta, \theta) \geq 10.0$



grooves ($\theta > 0.6$), the best performance is possible only if electron beams are highly velocity-stabilized. Such ranges of β and θ form separate islands with the values $W_{01}^{22}(\beta, \theta) \geq 10.0$ in the relevant plane. The islands lie along a line; crossing this line towards large β and θ causes the diffraction radiation intensity to decrease sharply (to $W_{01}^{22} < 0.1$). The tendency for a growth of maximum values of $W_{01}^{22}(\theta)$ as β increases for small θ changes into the opposite one for $\beta > 0.98$. For the near-vertical radiation, it is worthwhile to use gratings with filling factor close to 0.5 in order to gain high levels of W_{01}^{22} . Initiation of the islands with high radiation intensity in the region $\beta > 0.94$ and $\theta > 0.5$ is associated with the excitation of near-free oscillations. A necessary condition to enter this resonant region (where high-Q free oscillations can exist) remains the same as in the case of excitation by a homogeneous plane wave [12].

As noted above, the groove depth that is necessary to gain the optimal values of W_{01}^{22} decreases substantially as β increases. This mechanism being most conspicuous for $\beta > 0.99$ is typical only for beams with velocities close to the velocity of light. Recall [20, 28] that for $\beta < 0.5$ it has not been found noticeable deviations of h/λ from the value $h/\lambda \approx 0.22$ with the maximum of W_{01}^{22} .

When passing to relativistic beams one can observe a peculiarity affecting essentially the radiation pattern. The number of sliding points (points at which new propagating harmonics arise and the Wood's anomalies are displayed) on the interval

$|\alpha_0| < \pi/2$ increases with increasing β . The degree of the radiation pattern roughness increases accordingly. Figure 7.7 presents the level curves of $W_{01}^{22}(\alpha_0, \delta)$. The dashed lines denote the lower boundaries of the radiation zones for the minus first, minus second, and minus third harmonics. In the region $-2^\circ < \alpha_0 < 90^\circ$, where only the fundamental harmonic radiates, the near-vertical directions correspond to the maximal intensity. The curves in Fig. 7.7 confirm the mechanism described above, namely, the closer is the radiation direction to a vertical one, the lesser has to be the groove depth to achieve the best performance. The peak of the radiation diagram is shifting towards larger α_0 as δ increases. A crevasse is found near the boundary where the radiation on the minus first harmonic ($\alpha_0 = -2.14^\circ$) comes into existence. The closer is δ to optimal values, the steeper becomes this crevasse. The initiation of the radiation on the minus second ($\alpha_0 = -22.5^\circ$) and minus third ($\alpha_0 = -33.8^\circ$) harmonics is marked by the similar crevasses. The function $W_{n1}^{22}(\alpha_0, \delta)$ for the harmonics with near-sliding propagation directions increases sharply.

As a result of scattering by an echelette grating of a plane inhomogeneous H -polarized wave generated by a modulated electron flow (Fig. 7.8), an intensive radiation may occur in near-vertical direction for large β . For $\beta < 0.4$ reasonable

Fig. 7.7 Level curves $W_{01}^{22}(0.93, \alpha_0, \delta, 0.4) = \text{const}$

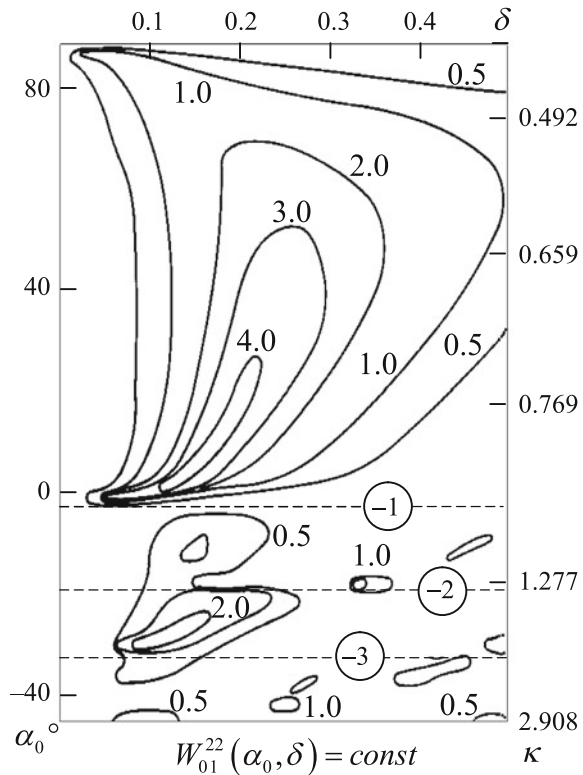
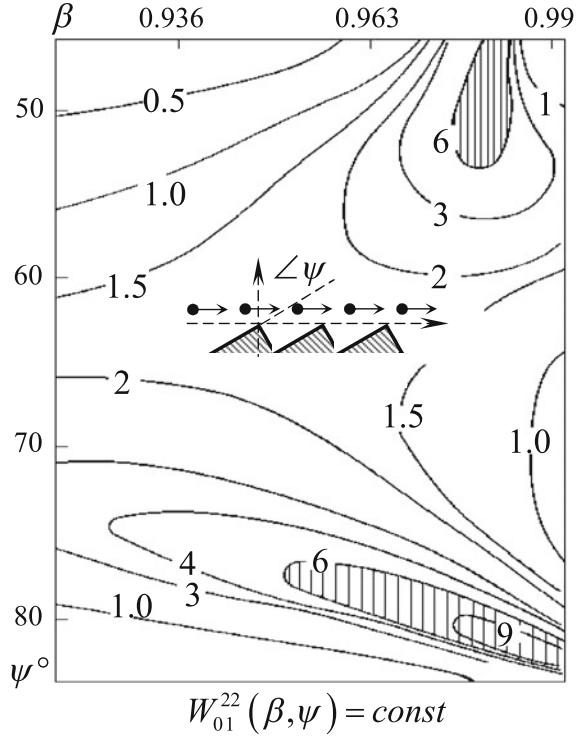


Fig. 7.8 High radiation intensity zones with $W_{01}^{22}(\beta, 1^\circ, \psi) \geq 6.0$ for echelette gratings



values of $W_{01}^{22}(\beta, \alpha_0, \psi)$ could be obtained only in the angular range $\alpha_0 > 80^\circ$ [28]. Figure 7.8, where the level curves of $W_{01}^{22}(\beta, 1.0^\circ, \psi)$ are presented, allows one to distinguish two principal zones for which the level of radiation can be greater than $W_{01}^{22} = 6.0$, i.e. the radiation characteristics as good as for a lamellar grating can be attained for an echelette grating. This is an important result because the production of lamellar gratings with optimized profile becomes problematic with shortening of excitation wavelengths, however, the present-day manufacturing technique for echelette gratings is well-developed both in optical and in microwave ranges.

In Fig. 7.8, one of high radiation intensity zones corresponds to deep grooves with $\psi \approx 45^\circ \div 55^\circ$, another one corresponds to shallow grooves with $\psi \approx 75^\circ \div 82^\circ$ (rippled surface). Echelette gratings with the intermediate value $\psi \approx 65^\circ$ are characterized by the stability of diffraction radiation under variations of β . For $\beta < 0.95$ the maximal radiation intensity in near-vertical direction is reached for echelette gratings with $\psi \approx 74^\circ$.

In relativistic diffraction electronics, echelette gratings are best suited for strong vertical radiation resulting from the interaction of an electron flow with a weakly profiled periodic structure. In particular, this is evident from the curves presented in Fig. 7.9 for $\beta = 0.93$; a neighborhood of the point $\alpha_0 = 0, \psi = 78^\circ$ corresponds to the radiation zone with $W_{01}^{22}(\alpha_0, \psi) \geq 4.0$.

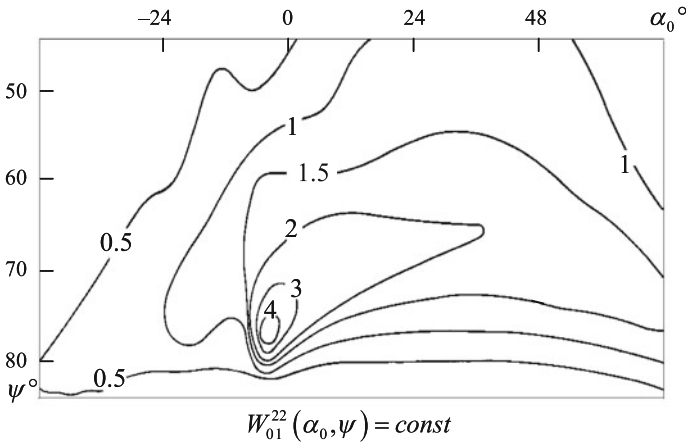


Fig. 7.9 Intensive near-vertical radiation ($W_{01}^{22}(0.93, \alpha_0, \psi) \geq 4.0$) under interaction of electron flow with slightly grooved echelette grating

The obtained results allow one to choose optimal parameters for lamellar and echelette gratings, which are the most-used periodic structures in various devices of relativistic diffraction electronics. The above-described mechanisms simplify substantially the design of structures from their output characteristics and can serve as a basis for creating new intense radiation sources and units in millimeter and sub-millimeter ranges. It is evident that we can read these results in the context of a structure ‘planar dielectric waveguide—grating’: from (7.16) and (7.24) it follows that we can study a waveguide-generated field by solving the problem (7.12a, 7.12b, 7.12c) for the incident wave (7.23) with $A_{p2}(k) = B_1(k)\sqrt{l} \exp[i\gamma_p(a - L_2)]$ and $\Phi_p = \bar{\chi}$.

It should be noted that the approach to study the transformation of eigenwaves of a planar waveguide into propagating spatial harmonics of a periodic structure (*near-field to far-field conversion*) fails to account for the interaction of those harmonics with a waveguide and a decrease of the amplitude $B_1(k)$ of the wave $\bar{u}(g, \bar{\chi})$ as it propagates along the y -axis, which is natural for real situations. This is the so-called *given-field approximation* and its range of accuracy can be evaluated within the framework of more accurate models (see, for example, Sects. 7.3.2–7.3.4).

Some results obtained in the framework of this approximation related to the near-field to far-field conversion on an infinite grating are discussed below. In the covered frequency band $0.36 \leq \kappa = l/\lambda = lk/2\pi \leq 0.64$, the H -polarized wave (7.23) with $A_{p2}(k) = 1, p = 1, \Phi = -0.35$ generated by a modulated electron flow ($\Phi_1 = k/\beta k$) or by a planar waveguide ($\Phi_1 = \bar{\chi}$) produces in its reflection zone only one undamped wave (harmonic with $n = 0$), which moves away from a grating at the angle $\alpha_0 = -\arcsin(\Phi_0/k) = -\arcsin(\Phi/\kappa)$ (Fig. 7.10a).

The functions $W_{01}^{22}(\kappa)$ depicted in Fig. 7.10b reflect the transformation efficiency. A curve with the number j ($j = 1, 2, \dots, 5$) corresponds to a reflecting grating with the same number. The following gratings are considered (Fig. 7.10a):

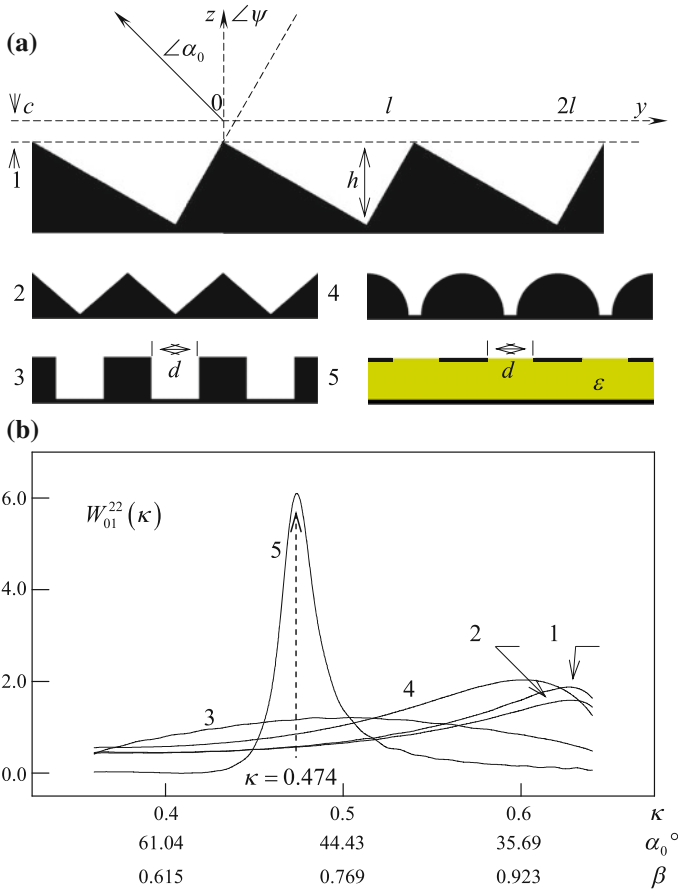


Fig. 7.10 **a** Geometry of gratings ($\delta = h/l = 0.43, c/l = 0.013, L_2 = 0, \psi = 30^\circ, \theta = d/l = 0.5, \varepsilon = 2.5$) and **b** their ability to near-field to far-field conversion

the echelette grating with rectangular grooves, the symmetric echelette, the lamellar grating, the semi-cylindrical grating and the strip grating on a dielectric layer. All the gratings are equal in depth h with the equal period l ; the strip thickness equals $0.0064l$. But just one of them (the grating number 5) is capable of reradiating energy efficiently into the far-field region. This ability shows up in a narrow frequency band in the vicinity of the point $\kappa = 0.474$, for which $\alpha_0 \approx 47.6^\circ$. The less intensive *reversed radiation* (the angle between travelling directions of the incident wave and the outgoing plane wave is greater than 90°) and in far wider band of κ (see curve 3 in Fig. 7.10a) is provided by the metal lamellar grating.

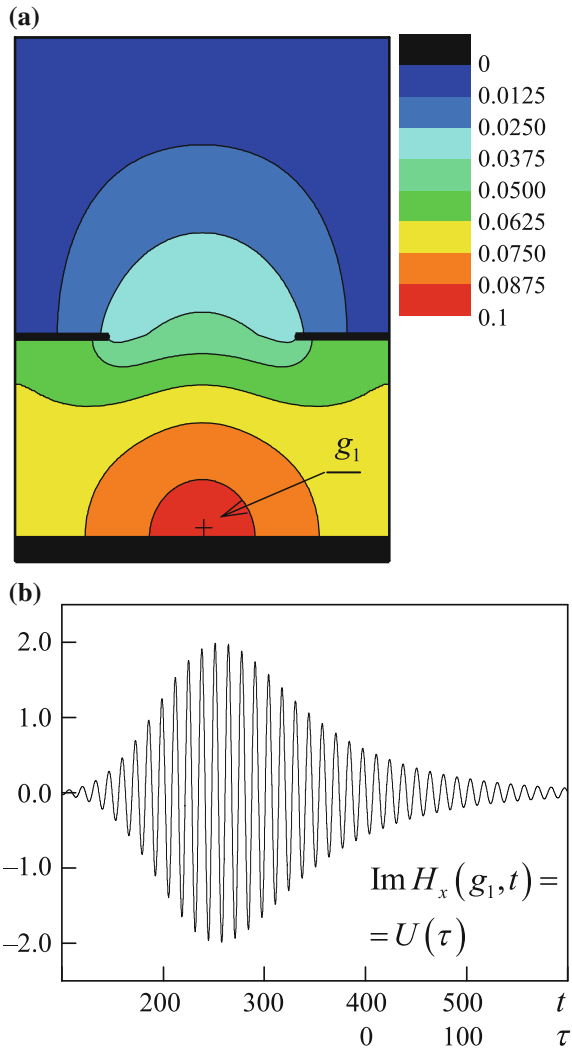
Let now the grating number 5 ($l = 2\pi$; for such l we have $|k| = |\kappa|; L_2 = 4.0$) be excited by the pulsed plane wave $U^{i(2)}(g, t) = U_0^{i(2)}(g, t) = v_{02}(z, t) \times \mu_0(y); \Phi = -0.35, g \in \Omega_2, t \geq 0$ such that

$$v_{02}(L_2, t) = \exp\left[-(t - \tilde{T})^2 / 4\tilde{\alpha}^2\right] \times \cos[\tilde{k}(t - \tilde{T})] \chi(\bar{T} - t) = F_1(t) \quad (7.27)$$

with $\tilde{k} = 0.474$, $\tilde{\alpha} = 35$, $\tilde{T} = 200$, $\bar{T} = 400$. Here \tilde{k} , \tilde{T} , and \bar{T} are the central frequency, the delay time, and the signal duration, respectively. The parameter $\tilde{\alpha}$ determines the frequency band $[\tilde{k} - b(\gamma)/\tilde{\alpha}, \tilde{k} + b(\gamma)/\tilde{\alpha}]$, where the normalized spectral amplitudes $\tilde{F}_1(k)$ of the function $F_1(t)$ do not fall below some given level $\gamma > 0$ (see details in book [12], Sect. 4.3.2).

In Fig. 7.11, the free-oscillating field $H_x(g, t)$, $g \in \Omega_{\text{int}}$, $t > \bar{T}$ (once the source has been switched off) is depicted.

Fig. 7.11 **a** Space distribution of $|H_x(g, t)|$ at $t = 560$ and **b** function $\text{Im} H_x(g_1, t) = U(\tau)$, $\tau = t - \bar{T}$



The anomalous peak of intensity of $W_{01}^{22}(k)$ at the point $k = 0.474$ results from the generation in the structure of low- Q eigenoscillations ($Q = \text{Re } \bar{k}/2|\text{Im } \bar{k}| \approx 24$) associated with the complex eigenfrequency $\bar{k} \approx 0.474 - i0.0098$. Configuration of these oscillations is shown in Fig. 7.11a, while their quality factors are determined by the envelope of the function $U(\tau)$, $\tau \geq 0$ (Fig. 7.11b). The technique used here for estimating spectral characteristics of open periodic resonators from their response on a pulse excitation was proposed in [29] and discussed in detail in [12].

7.3.2 Finite Gratings: Plane and Axially Symmetric Models

The closed initial boundary value problems

$$\left\{ \begin{array}{l} \left[-\varepsilon(g) \frac{\partial^2}{\partial t^2} - \sigma(g) \eta_0 \frac{\partial}{\partial t} + \frac{\partial^2}{\partial y^2} + \frac{\partial^2}{\partial z^2} \right] U(g, t) = 0; \quad t > 0, \quad g \in \Omega_{\text{int}} \\ U(g, t)|_{t=0} = 0, \quad \frac{\partial}{\partial t} U(g, t)|_{t=0} = 0; \quad g = \{y, z\} \in \bar{\Omega}_{\text{int}} \\ \vec{E}_{\text{tg}}(q, t) \quad \text{and} \quad \vec{H}_{\text{tg}}(q, t) \quad \text{are continuous when crossing} \quad \Sigma^{\varepsilon, \sigma}, \\ \vec{E}_{\text{tg}}(q, t)|_{q=\{x, y, z\} \in \Sigma} = 0, \quad \text{and} \quad D[U(g, t)]|_{g \in \Gamma} = 0, \\ D_1[U(g, t) - U^{i(1)}(g, t)]|_{g \in \Gamma_1} = 0, \quad D_2[U(g, t)]|_{g \in \Gamma_2} = 0; \quad t \geq 0, \end{array} \right. \quad (7.28a)$$

$$\left\{ \begin{array}{l} \left[-\varepsilon(g) \frac{\partial^2}{\partial t^2} - \sigma(g) \eta_0 \frac{\partial}{\partial t} + \frac{\partial^2}{\partial z^2} + \frac{\partial}{\partial \rho} \left(\frac{1}{\rho} \frac{\partial}{\partial \rho} \rho \right) \right] U(g, t) = 0; \\ t > 0, \quad g = \{\rho, z\} \in \Omega_{\text{int}} \\ U(g, t)|_{t=0} = 0, \quad \frac{\partial}{\partial t} U(g, t)|_{t=0} = 0; \quad g = \{\rho, z\} \in \bar{\Omega}_{\text{int}} \\ \vec{E}_{\text{tg}}(q, t) \quad \text{and} \quad \vec{H}_{\text{tg}}(q, t) \quad \text{are continuous when crossing} \quad \Sigma^{\varepsilon, \sigma}, \\ \vec{E}_{\text{tg}}(q, t)|_{q=\{\rho, \phi, z\} \in \Sigma} = 0, \quad U(0, z, t) = 0 \quad \text{for} \quad \{0, z\} \in \bar{\Omega}_{\text{int}}, \\ \text{and} \quad D[U(g, t)]|_{g \in \Gamma} = 0, \quad D_1[U(g, t) - U^{i(1)}(g, t)]|_{g \in \Gamma_1} = 0, \\ D_2[U(g, t)]|_{g \in \Gamma_2} = 0; \quad t \geq 0 \end{array} \right. \quad (7.28b)$$

describe space-time transformations of the electromagnetic field $\{\vec{E}(g, t), \vec{H}(g, t)\}$ in planar ($\partial/\partial x = 0$, Fig. 7.12a) and axially symmetric ($\partial/\partial \phi = 0$, Fig. 7.12b) structures, on which a pulsed wave $\{\vec{E}^{i(1)}(g, t), \vec{H}^{i(1)}(g, t)\}$ is incident through the virtual boundary Γ_1 in a cross-section of the virtual waveguide Ω_1 (for details see Sects. 5.2, 5.3 and 5.5 and [9, 12, 13]). In the context of this formulation, the diffraction radiation phenomena are described accurately, without distortions which inevitably accompany the given-field or given-current approximations. Besides, in the context of this model one can calculate energy and phase characteristics of the processes that have to be studied prior to designing devices exploiting the near-field to far-field conversion.

In (7.28a, 7.28b) $U(g, t) = E_x(g, t)$ or $U(g, t) = E_\phi(g, t)$ in the case of TE_0 -waves ($E_y = E_z = H_x \equiv 0$ or $E_\rho = E_z = H_\phi \equiv 0$) and $U(g, t) = H_x(g, t)$ or $U(g, t) = H_\phi(g, t)$ in the case of TM_0 -waves ($H_y = H_z = E_x \equiv 0$ or

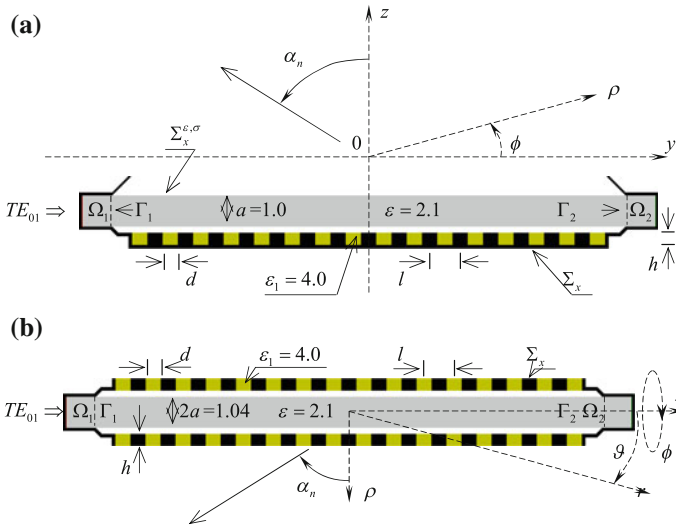


Fig. 7.12 **a** Planar and **b** axially symmetric models of diffraction radiation antenna: $l = 1.0$, $d = 0.5$, $h = 0.4$; impact parameter $c = 0.2$. Drawings are in proportion

$H_\rho = H_z = E_\phi \equiv 0$); $\varepsilon(g) \geq 1$ and $\sigma(g) \geq 0$ are the relative permittivity and the specific conductivity of nondispersive and nonmagnetic materials; $\eta_0 = (\mu_0/\varepsilon_0)^{1/2}$ is the impedance of free space; ε_0 and μ_0 are the electric and magnetic constants of vacuum; $g = \{y, z\}$ or $g = \{\rho, z\}$ is a point in 2-D space \mathbb{R}^2 ; $q = \{x, y, z\}$ or $q = \{\rho, \phi, z\}$ is a point in 3-D space \mathbb{R}^3 . By $\Sigma = \Sigma_x \times [-\infty, \infty]$ and $\Sigma = \Sigma_\phi \times [0, 2\pi]$ we denote perfectly conducting surfaces, while $\Sigma^{e,\sigma} = \Sigma_x^{e,\sigma} \times [-\infty, \infty]$ and $\Sigma^{e,\sigma} = \Sigma_\phi^{e,\sigma} \times [0, 2\pi]$ stand for surfaces on which the medium material parameters (the functions $\varepsilon(g)$ and $\sigma(g)$) have discontinuities. In the problem (7.28a) for planar structures, the domain of analysis Ω_{int} is the part of the plane $y0z$ bounded by the contours Σ_x and the virtual boundaries Γ_j ($j = 1, 2$) and $\Gamma = \{g = \{\rho, \phi\} : \rho = L, 0 \leq \phi \leq 2\pi\}$ (by $\{\rho, \phi\}$ we denote the polar coordinates in the plane $y0z$). In the problem (7.28b) for axially symmetric structures, the domain of analysis Ω_{int} is the part of the half-plane $\rho > 0$ bounded by Σ_ϕ , the axis of symmetry $\rho = 0$ and the virtual boundaries Γ_j ($j = 1, 2$) and $\Gamma = \{g = \{r, \vartheta\} : r = L, 0 \leq \vartheta \leq \pi\}$ ($\{r, \vartheta, \phi\}$ are the spherical coordinates). All scatterers, which are given by the piecewise constant functions $\varepsilon(g)$, $\sigma(g)$ and piecewise smooth contours Σ_x , Σ_ϕ and $\Sigma_x^{e,\sigma}$, $\Sigma_\phi^{e,\sigma}$ are located in Ω_{int} . If the functions $\varepsilon(g) - 1$ and $\sigma(g)$ have compact supports in the closure $\bar{\Omega}_{\text{int}}$ of the domain Ω_{int} then the problems (7.28a, 7.28b) are uniquely solvable in the Sobolev space $W_2^1(\Omega_{\text{int}} \times [0, T])$, $T < \infty$ [12, 24].

The EACs operators $D_1[U - U^{i(1)}]$, $D_2[U]$, and $D[U]$ were constructed in Chap. 5 (see also [12]). When they are used for the computation domain truncation, they do not introduce any additional errors into simulations of the behavior of the

pulsed waves $U^{s(1)}(g, t) = U(g, t) - U^{i(1)}(g, t)$, $U^{s(2)}(g, t) = U(g, t)$, and $U(g, t)$ outgoing through the virtual boundaries Γ_1 , Γ_2 , and Γ into the virtual waveguides Ω_1 , Ω_2 and the free-space domain Ω_{ext} [9, 12, 29]. The function

$$U^{i(1)}(g, t) = \sum_n^{\infty} v_{n1}(y, t) \mu_{n1}(z); \quad g = \{y, z\} \in \overline{\Omega}_1 \quad \text{or}$$

$$U^{i(1)}(g, t) = \sum_n^{\infty} v_{n1}(z, t) \mu_{n1}(\rho); \quad g = \{\rho, z\} \in \overline{\Omega}_1,$$

which determines the wave $\{\vec{E}^{i(1)}(g, t), \vec{H}^{i(1)}(g, t)\}$ coming on the boundary Γ_1 from the waveguide Ω_1 is assumed to be given along with the functions $\varepsilon(g)$, $\sigma(g)$ and the contours Σ_x , $\Sigma_x^{e, \sigma}$, etc. Suppose also that by the moment of time $t = 0$ the incident wave has not yet reached the boundary Γ_1 . The transverse eigenfunctions $\mu_{nj}(z)$, $\mu_{nj}(\rho)$ ($j = 1, 2$) of the waveguides Ω_j form orthonormal bases, they can be found in [9]; $v_{n1}(y, t)$ and $v_{n1}(z, t)$ are the space-time amplitudes of the pulsed eigenwaves of the waveguide Ω_1 , which form the incident wave $U^{i(1)}(g, t)$.

The solution $U(g, t)$ to the problems (7.28a, 7.28b) can be obtained by standard finite-difference or finite-element methods [25, 26] for the points $g \in \Omega_{\text{int}}$ and $t \in [0, T]$ ($T < \infty$), and then extended from the boundary Γ into the domain Ω_{ext} using the so-called transport operators. These operators allow to compute far-zone fields knowing only near-zone fields, see Chap. 5 and [9, 12].

Applying the integral transform $\tilde{f}(k) = \int_0^T f(t) e^{ikt} dt$, the time-domain solution $U(g, t)$ is converted into the frequency-domain solution $\tilde{U}(g, k)$ [12], whereby we can calculate amplitude-frequency characteristics, which are necessary for the physical analysis. Some of them are:

- *field patterns* for $\vec{E}(g, k)$ and $\vec{H}(g, k)$ in the domains Ω_{int} and Ω_{ext} ;
- *radiation efficiency*

$$\eta(k) = 1 - W_{\text{abs}} - \sum_{n,p} \left(W_{np}^{11} + W_{np}^{21} \right);$$

- *directional pattern* on the arc $\rho = M \geq L$ or $r = M \geq L$

$$D(\phi, k, M) = \frac{\left| \tilde{E}_{tg}(M, \phi, k) \right|^2}{\max_{0 \leq \phi \leq 2\pi} \left| \tilde{E}_{tg}(M, \phi, k) \right|^2}; \quad 0 \leq \phi \leq 360^\circ \quad \text{or}$$

$$D(\vartheta, k, M) = \frac{\left| \tilde{E}_{tg}(M, \vartheta, k) \right|^2}{\max_{0 \leq \vartheta \leq \pi} \left| \tilde{E}_{tg}(M, \vartheta, k) \right|^2}; \quad 0 \leq \vartheta \leq 180^\circ; \quad K_1 \leq k \leq K_2;$$

- *orientation of the main lobe*, which is determined by the angle $\bar{\phi}(k)$ or $\bar{\vartheta}(k)$ such that $D(\bar{\phi}(k) \text{ or } \bar{\vartheta}(k), k, M) = 1.0$;
- $\phi_{0.5}(k)$ or $\vartheta_{0.5}(k)$, which are the *width of the main lobe* at a level of $D(\phi \text{ or } \vartheta, k, M) = 0.5$, and others [9, 12].

Here $k = 2\pi/\lambda > 0$, the observation interval is $0 \leq t \leq T$ and $f(t)$ is taken zero for $t > T$, $\vec{E}_{tg}(M, \phi, k)$ or $\vec{E}_{tg}(M, \vartheta, k)$ is the tangential component of the harmonic electric field $\vec{E}(q, k)$ on the cylindrical surface $\rho = M \geq L$ or the spherical surface $r = M \geq L$, W_{abs} is the ratio of the energy lost in the imperfect materials and the energy of the incident p th waveguide mode, $W_{np}^{j1}(k)$ is the ratio of the energy of the n th eigenwave outgoing through the waveguide Ω_j and the energy of the p th waveguide mode incident from the waveguide Ω_1 . The functions $D(\phi, k, M)$ and $D(\vartheta, k, M)$ determine the spatial orientation and the energy content of waves radiated into free space via the virtual boundary Γ . The value M defines a zone (near-field, intermediate, or far-field), for which the pattern is calculated.

7.3.3 Near-Field to Far-Field Conversion by Finite Periodic Structures. Plane Models

Consider a radiating structure whose section by the plane $x = \text{const}$ is depicted in Fig. 7.12a. It is a planar dielectric waveguide ($\varepsilon = 2.1$) of the width a with parallel-plate virtual waveguides Ω_j ($j = 1, 2$) on its ends. The flanges of the virtual waveguides are inclined at an angle of 45° . At a distance of c below the waveguide, a diffraction grating of length $15l$ is placed, where l is the grating period. The pulsed TE_{01} -wave

$$U^{i(1)}(g, t) = U_1^{i(1)}(g, t) = v_{11}(y, t)\mu_{11}(z); \quad g = \{y, z\} \in \bar{\Omega}_1 \quad (7.29)$$

is incident on the structure through the virtual boundary Γ_1 . The cutoff points of the first three sinusoidal TE_{0n} -waves in the waveguides Ω_1 and Ω_2 are $k_1^+ \approx 2.17$, $k_2^+ \approx 4.33$ and $k_3^+ \approx 6.5$.

First assume that

$$v_{11}(y : g \in \Gamma_1, t) = 4 \frac{\sin[\Delta k(t - \tilde{T})]}{(t - \tilde{T})} \cos[\tilde{k}(t - \tilde{T})]\chi(\bar{T} - t) = F_2(t) \quad (7.30)$$

and $\tilde{k} = 4.4$, $\Delta k = 2.0$, $\tilde{T} = 40$, $\bar{T} = 80$, $T = 300$. Here, $\chi(\dots)$ is the Heaviside step function, \tilde{k} is the central frequency of the pulse, \tilde{T} and \bar{T} are its delay time and duration. The pulse $F_2(t)$ occupies the frequency band $\tilde{k} - \Delta k \leq k \leq \tilde{k} + \Delta k$ [12], in our case it is $2.4 \leq k \leq 6.4$. Only two sinusoidal waves, TE_{01} -wave and TE_{02} -wave, are undamped in the waveguides Ω_j .

Figure 7.13 presents the characteristics of a finite grating illuminated by the surface wave $A(z, k) \exp[i\bar{\chi}(k)y]$ guided by a dielectric layer. In order to make sense of these results, one should invoke the information on the propagation constant $\bar{\chi}(k)$ in the band $2.4 \leq k \leq 6.4$. It is also important to understand what kind of the field is generated if a plane inhomogeneous monochromatic wave with the longitudinal propagation constant $\Phi_1(k) = \bar{\chi}(k)$ ($k < |\Phi_1(k)|$) is incident on an infinite grating of period l .

We start with some well-known facts [2, 3, 12] (see also Sects. 7.2.1, 7.2.2). The spatial harmonics $B_n(k) \exp[i\gamma_n(k)z] \exp[i\Phi_n(k)y]$, $n = 0, \pm 1, \pm 2, \dots$ are generated in the reflection zone $z > 0$ of an infinite grating by an inhomogeneous plane monochromatic wave. These harmonics are homogeneous ($n : k > |\Phi_n|$) and inhomogeneous ($n : k < |\Phi_n|$) plane waves propagating towards growing z with zero or exponential decay. The number of harmonics with $k > |\Phi_n|$ is finite for any finite k . Each of these homogeneous plane waves outgoes from a grating at an angle of

$$\alpha_n(k) = -\arcsin[\Phi_n(k)/k] \tag{7.31}$$

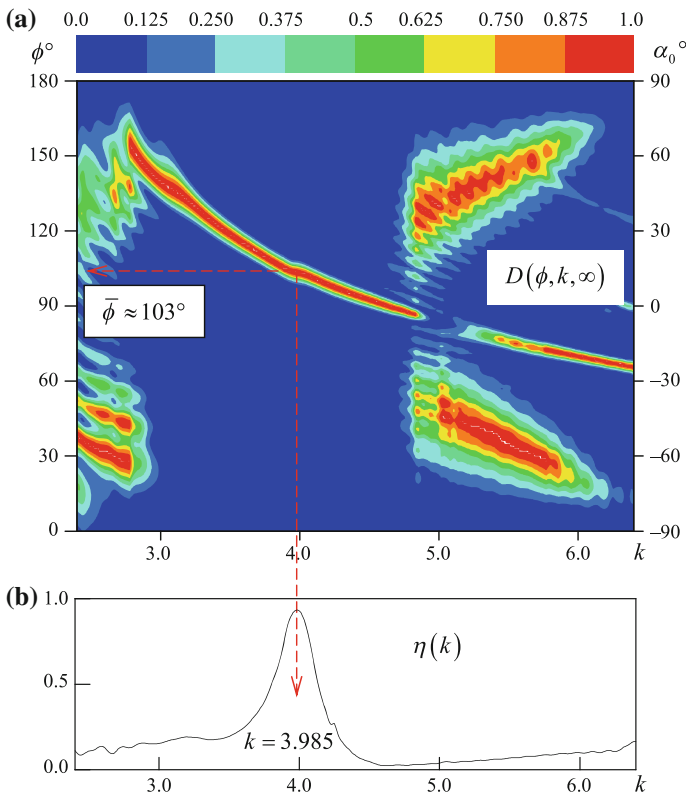


Fig. 7.13 **a** Directional pattern $D(\phi, k, \infty)$ and **b** radiation efficiency $\eta(k)$ of planar antenna

(Fig. 7.12a) and carries away the energy released as a result of scattering of the inhomogeneous wave. Here, $\gamma_n(k) = \sqrt{k^2 - \Phi_n^2(k)}$ ($\text{Re } \gamma_n(k) \geq 0, \text{Im } \gamma_n(k) \geq 0$), $\Phi_n = (n + \Phi)2\pi/l = \Phi_1 + 2\pi(n - 1)/l$; Φ is the real number and $|\Phi| \leq 0.5$.

The values of $\bar{\chi}(k)$ (Fig. 7.14) we obtain by calculating the phase incursion $\zeta(k) = \arg \bar{E}_x(g_2, k) - \arg \bar{E}_x(g_1, k) = \bar{\chi}(k)$ of the field $\bar{E}_x(g, k)$ caused by the displacement of the observation point along the dielectric waveguide axis from the point $g = \{z, y_1\}$ into the point $g = \{z, y_2\}$ ($y_2 - y_1 = 1.0$).

As we can see from Fig. 7.14, the zeroth harmonic is detached from a grating and propagating if $2.7 < k < 2.8$. At the instant the harmonic leaves a grating we have $k = |\Phi_0(k)|$ and $\phi = 90^\circ + \alpha_0 = 180^\circ$, that is the incipient homogeneous plane wave is sliding along the grating's surface. The analog of this propagating harmonic forms the main lobe of the pattern of the radiator under study in the bands $2.8 < k < 4.8$ and $5.8 < k < 6.4$. The minus first propagating harmonic emerges in the reflection zone of an infinite grating when $5.2 < k < 5.3$, but analog of this harmonic in the situation under study has little effect on the directional pattern $D(\phi, k, \infty)$.

It is clear now why the pattern does not have a sharp main lobe for $k < 2.8$, but as before the reasons of the phenomenon observed in the band $4.8 < k < 5.8$ are not evident. For the directional pattern function, two large ranges of variation of ϕ and k with the high level of $D(\phi, k, \infty)$ are clearly defined. These domains are almost symmetric about the direction $\phi = 90^\circ$. It turns out that the associated pattern lobes are shaped by the leaky waves of the planar dielectric waveguide (fast waves or waves with $\bar{\chi}(k) < k$), which are generated efficiently near the open ends of the virtual waveguides Ω_1 and Ω_2 , but decay rapidly when moving towards each other (Fig. 7.15a). This inference is also confirmed by the results presented in Fig. 7.15b: in the frequency band where the lobes (which occurrence cannot be predicted by the classic theory of gratings) are observed, the excitation level of the TE_{02} -wave in the input waveguide Ω_1 rises sharply. This means that the higher eigenwave of the dielectric waveguide appears at the output of Ω_1 . And its field pattern is identical to the one of the TE_{02} -wave of a closed waveguide.

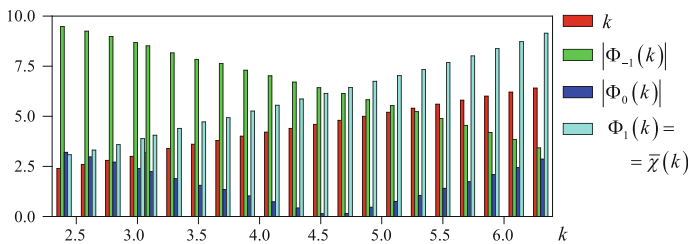


Fig. 7.14 Propagation constant $\bar{\chi}(k) = \Phi_1(k)$ of surface wave of planar waveguide and associated values of longitudinal propagation constants $|\Phi_m(k)|$ for the zeroth and minus first spatial harmonics of infinite grating of period $l = 1.0$

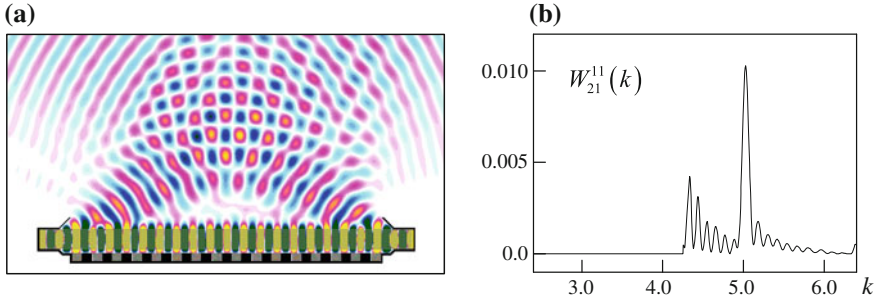


Fig. 7.15 **a** Excitation of planar radiating structure by the pulse (7.32), $\tilde{k} = 5.4$. Space distribution of $E_x(g, t)$ at $t = 60$. **b** Level of reflected wave in Ω_1

The antenna radiation efficiency is not high over the whole frequency band under consideration. The sole exception is the neighborhood of the point $k = 3.985$ (see Fig. 7.13b). As we can see from simple calculations, it is caused by a half-wave resonance: the wavelength of the TE_{01} -wave propagating along the grating grooves is $\lambda_w = 2\pi / \sqrt{k^2 \varepsilon_1 - (\pi/d)^2} \approx 0.83$ ($\lambda = 2\pi/k\sqrt{\varepsilon_1} \approx 0.79$), while the groove depth is 0.4. At the frequency $k = 3.985$, we have $\bar{\chi}(k) = \Phi_1 \approx 5.35$, and an infinite grating according to the formula (7.31) directs the zeroth spatial harmonic at an angle of $\alpha_0(k) = 13.53^\circ$ ($\phi = 103.53^\circ$). The accurately calculated beam direction $\bar{\phi}(k)$ for $k = 3.985$ is 103° .

Let now a quasi-monochromatic (narrowband) TE_{01} -pulse $U_1^{j(1)}(g, t)$ be incident on the structure. Assume also that the amplitude of its $E_x(g, t)$ -component is

$$v_{11}(y : g = \{y, z\} \in \Gamma_1, t) = P(t) \cos[\tilde{k}(t - \tilde{T})] = F_3(t), \quad (7.32)$$

with $\tilde{k} = 3.985$, $\tilde{T} = 5$, $P(t) : 0.01 - 5 - 75 - 80$ and $T = 200$. As before, \tilde{k} is the central frequency of the signal; $P(t) : t_1 - t_2 - t_3 - t_4$ is its trapezoidal envelope, which equals zero for $t < t_1$, $t > t_4$ and 1 for $t_2 < t < t_3$. Figure 7.16 presents the results of this numerical experiment. The finite grating radiates a wave with almost plane front (Fig. 7.16a). This radiation is narrow-beamed as the width of the main lobe at the level $D(\phi, k, \infty) = 0.5$ is $\phi_{0.5}(k) = 5.6^\circ$ (Fig. 7.16b). $\bar{\phi}(k) \approx 103^\circ$, which means that a simple metal grating provides the so-called *backscattered radiation* [30] without any negative-refractive-index materials. On the frequency corresponding to the maximal radiation efficiency ($\eta(k) \approx 0.94$) one can observe a low-Q resonance [12, 29], the field intensity in the grating grooves decreases rapidly once the source is switched off (Fig. 7.16c).

Figure 7.16d presents some characteristics, which are of exceptional importance in design of antennas exploiting the diffraction radiation phenomenon [14–17]. It

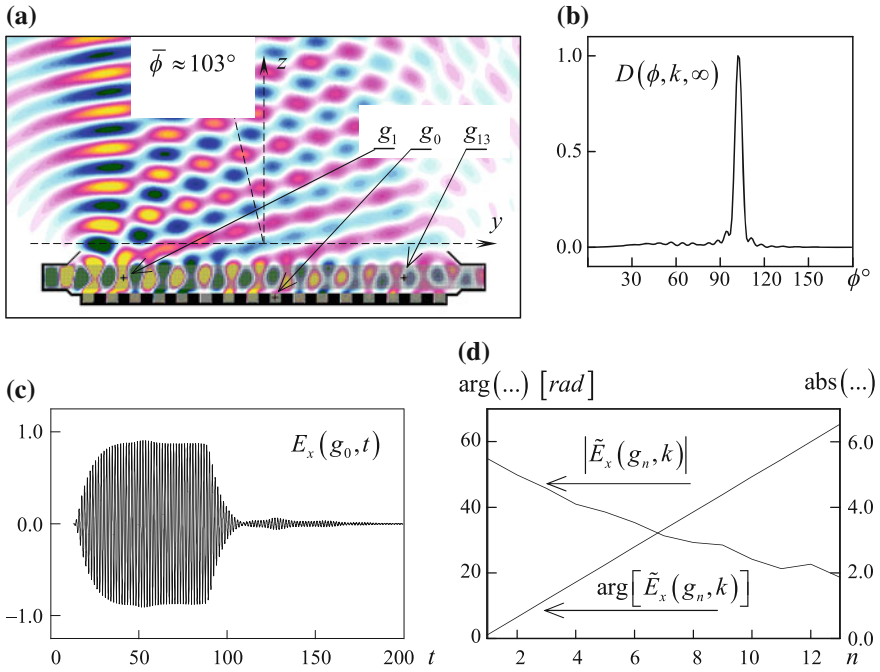


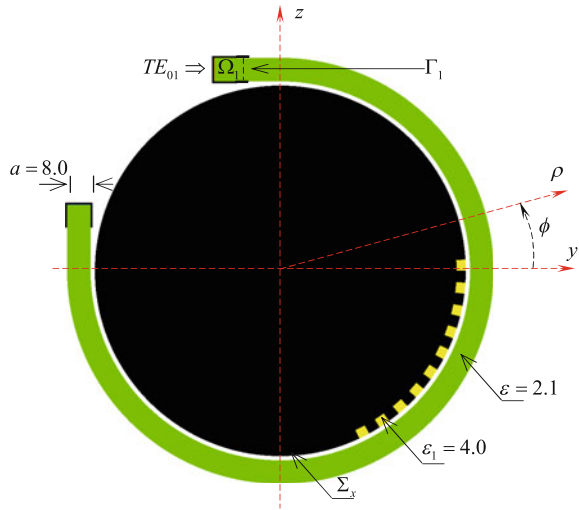
Fig. 7.16 Excitation of planar structure by the pulse (7.32), $\tilde{k} = 3.985$: **a** Space distribution of $E_x(g, t)$ at $t = 60$; **b** directional pattern $D(\phi, k, \infty)$ for $k = 3.985$; **c** $E_x(g, t)$ -component at $g = g_0$; **d** distribution of $\tilde{E}_x(g_n, k)$ for $k = 3.985$ over radiator's aperture

turns out that the phase distortions can be minimized even for rather long apertures. At the same time, the averaged distribution of the field over short gratings ($6 \div 8$ periods in length) is such that the field can be easily controlled by changing the *impact parameter* (distance between grating and dielectric waveguide) and the groove depth. Short gratings of this kind can be assembled together to comprise structures with large apertures and required amplitude-phase field distributions on them or, in other words, structures with specified directional patterns. Thus, the above-described algorithm for model synthesis of diffraction radiation antennas can be efficiently used to design new products.

Let us take a brief look at diffraction radiation effects in structures with finite gratings lying on a surface of a metal circular cylinder (Figs. 7.17 and 7.18).

When simulating the incidence of a pulsed TE_{01} -wave, which is given by (7.29), (7.30) and occupying the band $0.29 \leq k \leq 0.79$, onto the boundary Γ_1 from the virtual waveguide Ω_1 , we obtained the characteristics $D(\phi, k, \infty)$ and $\eta(k)$ very similar to the ones shown in Fig. 7.13. The basic distinction in the patterns is that

Fig. 7.17 Geometry of cylindrical antenna: grating period is 10.0; grooves width and depth are 5.0 and 4.0; the impact parameter is $c = 0.8$; cylinder radius is $\rho = 80$; dielectric waveguide width is a ; permittivity of dielectric in the grooves is $\varepsilon_1 = 4.0$



the lobes corresponding to the zeroth spatial harmonic of the planar antenna are now split. Their irregularity and width grow as the number of periods of the grating increases. This effect makes cylindrical antennas with gratings comprising $6 \div 10$ periods unsuitable for the generation of narrow-beam radiation. The only exception is a radiator with the grating five periods in length. It exhibits the directivity acceptable for potential users on the peak of $\eta(k) \approx 0.6$ at $k = 0.42$, which corresponds to a half-wave resonance of the TE_{01} -wave in the grating groove. However, the radiation efficiency of this structure is lower as compared to the gratings of six ($\eta(k) \approx 0.67$), eight ($\eta(k) \approx 0.78$) and ten ($\eta(k) \approx 0.84$) periods in length.

The radiation characteristics of the structure with the grating five periods in length do not vary substantially when the cylinder rotates. Rotation of the cylinder results in the same rotation of the main lobe of the pattern $D(\phi, k, \infty)$ (see Fig. 7.18). This effect may be exploited in scanning antennas including antennas for Squint-Mode SAR Systems [31]. However, in order to implement these possibilities, cylindrical radiators of good performance are required and a series of full-scale experiments verifying theoretical results should be conducted.

7.3.4 Near-Field to Far-Field Conversion by Finite Periodic Structures. Axially Symmetric Models

Axially symmetric antennas (Fig. 7.12b) differ from planar antennas discussed in the previous section in that their radiation field is formed by the waves transmitted through a periodic structure. These waves will be called spatial harmonics, as well

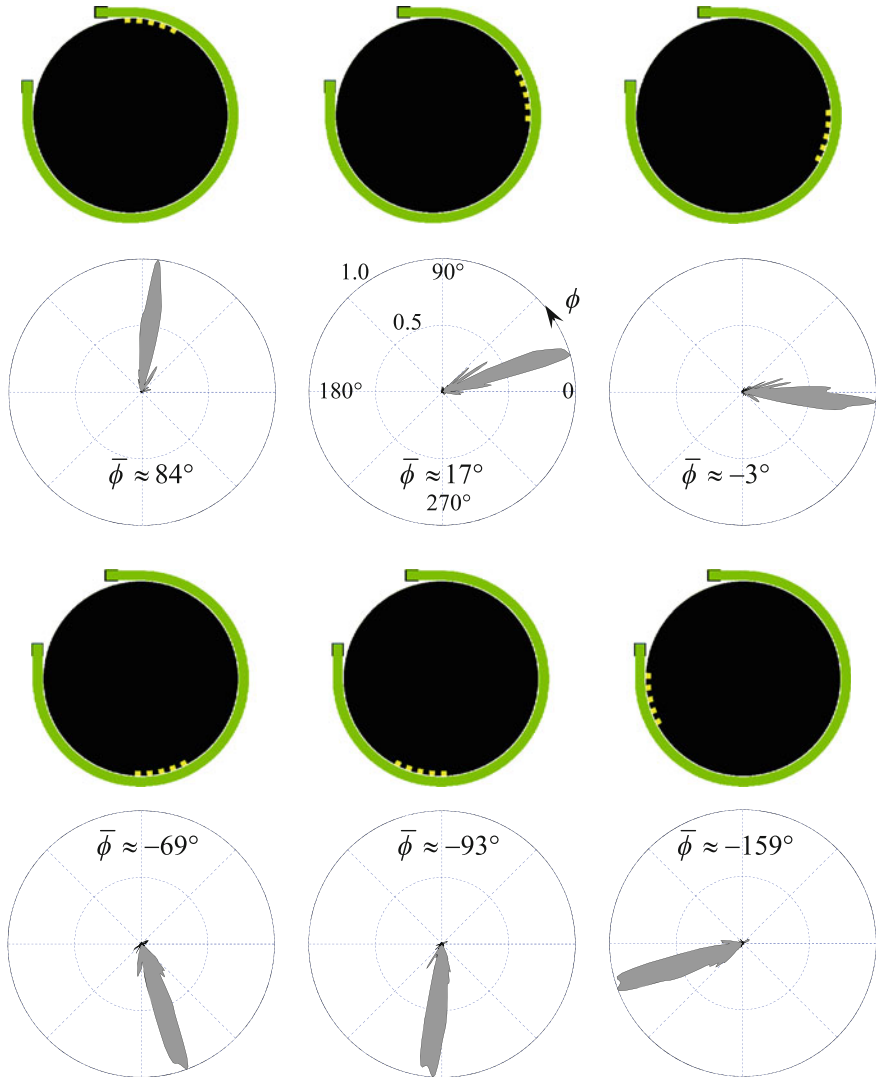


Fig. 7.18 Beam scanning by rotating cylindrical diffraction antenna, $k = 0.42$

as the waves $B_n(k)H_1^{(1)}[\gamma_n(k)\rho] \exp[i\Phi_n(k)z]$ ($n = 0, \pm 1, \pm 2, \dots, \rho > a + c + h$) comprising the secondary field of an infinite axially symmetric grating being excited by the surface wave $A(\rho, k) \exp[i\bar{\chi}(k)z]$ of an infinite circular dielectric waveguide. They are given the common name because of qualitatively identical contribution of these waves into the radiation field. For the same reason, we can invoke a series of well-known concepts of the classical theory of gratings when interpreting numerical results obtained for finite periodic structures.

Let a pulsed TE_{01} -wave $U^{i(1)}(g, t) = U_1^{i(1)}(g, t)$ ($g = \{\rho, z\} \in \Omega_1$) be incident on the antenna shown in Fig. 7.12b. The amplitude of its $E_\phi(g, t)$ -component is $v_{11}(z : g \in \Gamma_1, t) = F_2(t)$ with $\tilde{k} = 7.0$, $\Delta k = 1.5$, $\tilde{T} = 40$, $\bar{T} = 80$, $T = 300$. The pulse $F_2(t)$ occupies the frequency band $5.5 \leq k \leq 8.5$. TE_{01} -wave is the only undamped sinusoidal wave propagating in the circular waveguides Ω_j ($k_1^+ \approx 5.08$, $k_2^+ \approx 9.31$). Basic characteristics of the axially symmetric antenna within this band are presented in Fig. 7.19.

If a surface wave of an infinite circular dielectric waveguide whose propagation constant is $\bar{\gamma}(k) = \Phi_1(k)$ be incident onto an infinite axially symmetric grating, the zeroth spatial harmonic will propagate in its transmission zone without decay (or more precisely, without exponential decay) for $5.5 \leq k \leq 8.5$ (see Fig. 7.20: $k > |\Phi_0(k)|$ for all k). The minus first harmonic propagates if $5.8 \leq k \leq 5.9$. In this band, the inequality $k < |\Phi_{-1}(k)|$ is replaced by $k > |\Phi_{-1}(k)|$. The minus second harmonic propagates if $8.3 \leq k \leq 8.4$. The phase front of the n th propagating harmonic is perpendicular to the direction $\vartheta_n(k) = \alpha_n(k) + 90^\circ$ (see the formula (7.31)

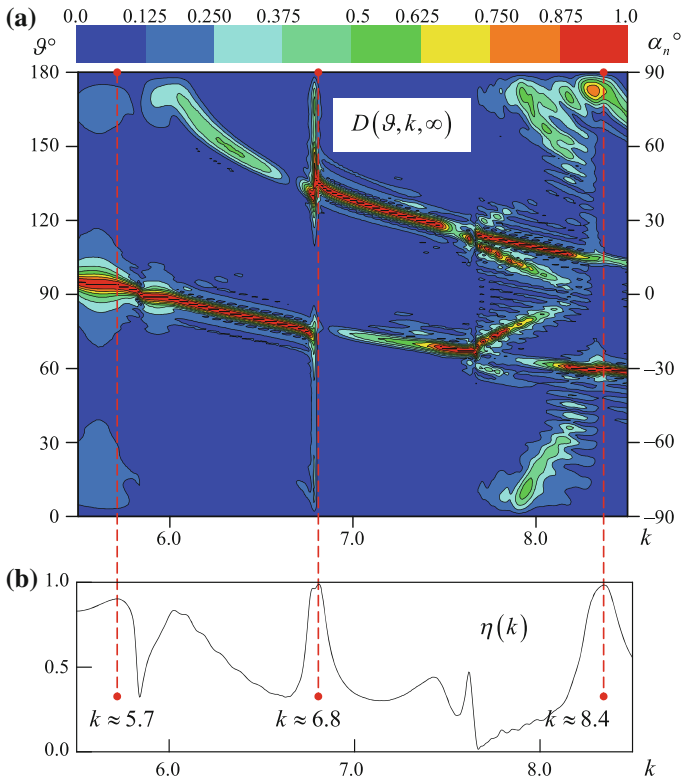


Fig. 7.19 **a** Directional pattern $D(\vartheta, k, \infty)$ and **b** radiation efficiency $\eta(k)$ of axially symmetric antenna

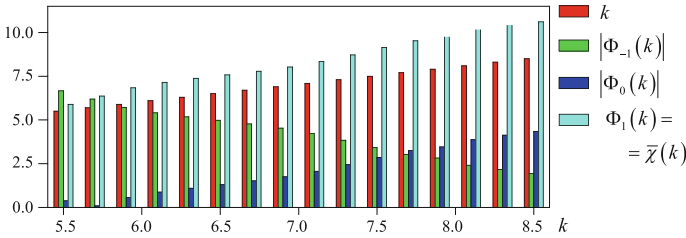


Fig. 7.20 Same as in Fig. 7.14 but for circular dielectric waveguide and axially symmetric infinite grating with period $l = 1.0$

and Fig. 7.12b) for all $0 \leq \phi \leq 2\pi$. This allows us to unambiguously determine the contribution of each harmonic into the radiation in the far-field zone from the function $D(\vartheta, k, \infty)$ given in Fig. 7.19a.

The radiation efficiency at some points from the band under study is high enough: $\eta(k) \approx 0.9$ at $k_1 = 5.7$ and $\eta(k) \approx 0.99$ at $k_2 = 6.8$ and $k_3 = 8.4$ (Fig. 7.19b). Exciting the axially symmetric antenna by a quasi-monochromatic signal whose central frequency coincides with the frequencies k_1, k_2, k_3 (Fig. 7.21), we can determine (i) which resonances in the grating's slots cause the sharp increase of $\eta(k)$ and how fronts of the outgoing waves are oriented (see the curves for $E_\phi(g, t)$ at $t = 195$), and (ii) how the orientation of the fronts correlate with the direction of the basic lobes of $D(\vartheta, k, \infty)$. It worth to point the half-wave resonance of the TE_{02} -wave on the frequency $k = 6.8$. It results in an abnormally abrupt change of the orientation of the main lobe from the direction $\vartheta_0(k)$ to $\vartheta_{-1}(k)$ (Fig. 7.19a).

Let us take a close look at the results presented in Fig. 7.21 for $k = 8.4$. Three main lobes of the pattern $D(\vartheta, k, \infty)$ are oriented at $\vartheta_0 \approx 61^\circ$, $\vartheta_{-1} \approx 106^\circ$ and $\vartheta_{-2} \approx 173^\circ$. From Fig. 7.20 we have for $k = 8.4$: $\bar{\chi}(k) = \Phi_1(k) \approx 10.5$, $\Phi_0(k) \approx 4.22$, $\Phi_{-1}(k) \approx -2.06$ and $\Phi_{-2}(k) \approx -8.34$. With these values of the longitudinal propagation constants, the spatial harmonics numbered 0, -1 and -2 propagate in the directions $\alpha_0 \approx -30.1^\circ$ ($\vartheta_0 \approx 59.9^\circ$), $\alpha_{-1} \approx 14.2^\circ$ ($\vartheta_{-1} \approx 104.2^\circ$) and $\alpha_{-2} \approx 83.1^\circ$ ($\vartheta_{-2} \approx 173.1^\circ$), respectively. The accurate calculation of these angles yields the results close to those obtained from the calculation based on the knowledge of exact value of the propagation constant $\bar{\chi}(k)$ and assumptions common for the given-field approximation (see Sect. 3.1).

A decrease of the grating period results in predictable changes of the patterns $D(\vartheta, k, \infty)$ (Fig. 7.22). The number of the lobes associated with propagating harmonics is reduced. At the same time, the remaining lobes are coming closer (for the common values of k) to the direction $\vartheta = 180^\circ$, which determines the sliding operation mode of a spatial harmonic. For example, the antenna with the grating whose period is reduced to $l = 0.8$ radiates at its best on two different spatial

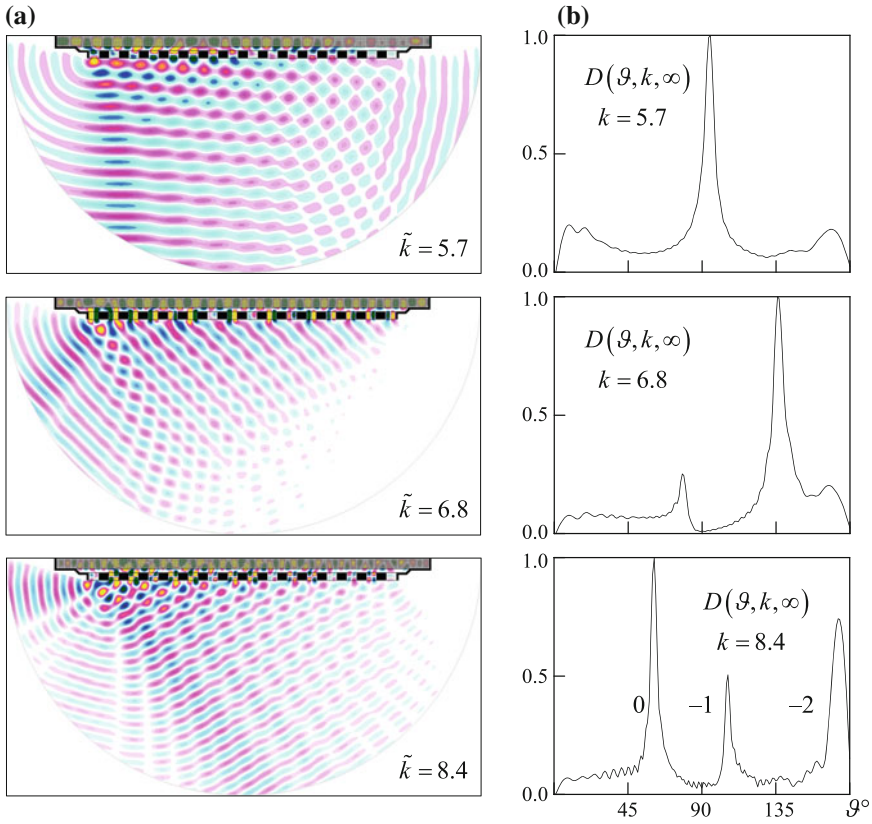


Fig. 7.21 Excitation of axially symmetric antenna from Ω_1 by the pulse (7.32): $P(t)$: 0.01–5–195–200, $T = 300$ and $\tilde{k} = 5.7, \tilde{k} = 6.8, \tilde{k} = 8.4$. **a** Space distribution of $E_\phi(g, t)$ at $t = 195$ and **b** directional patterns for different k

harmonics with $k = 5.8$ ($\eta(k) = 0.998$) and $k = 8.4$ ($\eta(k) = 0.963$); the radiation directions fall within the range $\vartheta > 90^\circ$ (reversed radiation).

If the slot size remains practically unchanged with reduction of the grating period, we can predict with confidence that most of the resonances associated with extreme points of the function $\eta(k)$ retains. The supporting results are presented in Figs. 7.19 and 7.22.

Let us consider the radiator displayed in Fig. 7.23a. It is a section of the Goubau line placed inside a semi-transparent grating of thick dielectric rings. Let also a pulsed TEM -wave $U_0^{i(1)}(g, t) : v_{01}(z : g \in \Gamma_1, t) = F_2(t)$ ($\tilde{k} = 6.0, \Delta k = 2.5, \tilde{T} = 30, \bar{T} = 60, T = 350$) be incident on the radiator. The incident wave occupies the frequency band $3.5 < k < 8.5$. Within this band, the only wave propagating

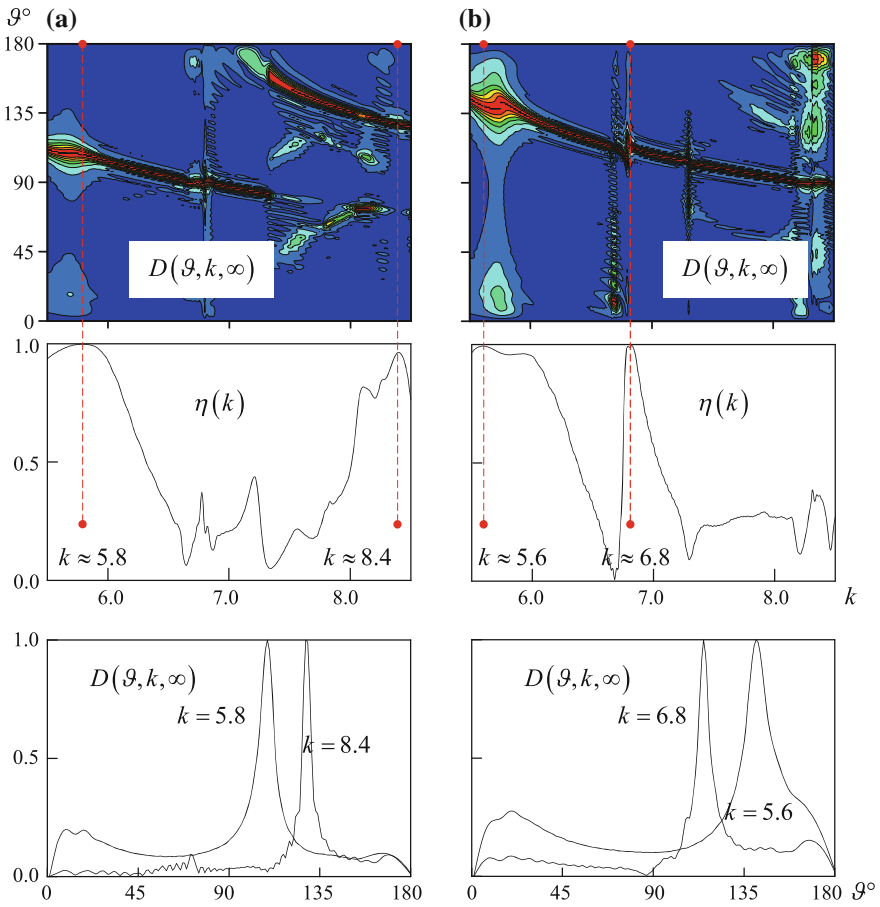


Fig. 7.22 Directional patterns $D(\vartheta, k, \infty)$ and radiation efficiency $\eta(k)$ of axially symmetric structures with semitransparent ($d = 0.5$) gratings of periods **a** 0.8 and **b** 0.6

without decay in the waveguides Ω_j is a sinusoidal *TEM*-wave. The functions $D(\vartheta, k, \infty)$ and $\eta(k)$ are plotted in Fig. 7.23b, c. As we can see, qualitatively they differ little from those obtained before (Figs. 7.13, 7.19 and 7.22). As to the quantitative difference, it can be significant in the following situations: (i) considerable difference between the propagation constants $\bar{\gamma}(k)$ of surface waves traveling in the sections of the open waveguides and (ii) considerable difference in the geometry of the gratings used for surface-to-spatial wave conversion and, as a consequence [2, 11], in the redistribution of radiated energy between propagating spatial harmonics.

It worth to note the existence of sufficiently wide frequency bands, where the radiation efficiency $\eta(k)$ is above 0.98. These are the bands $3.59 \leq k \leq 4.25$, $5.6 \leq k \leq 6.05$ and $8.06 \leq k \leq 8.22$, whose widths are 17%, 8%, and 2%,

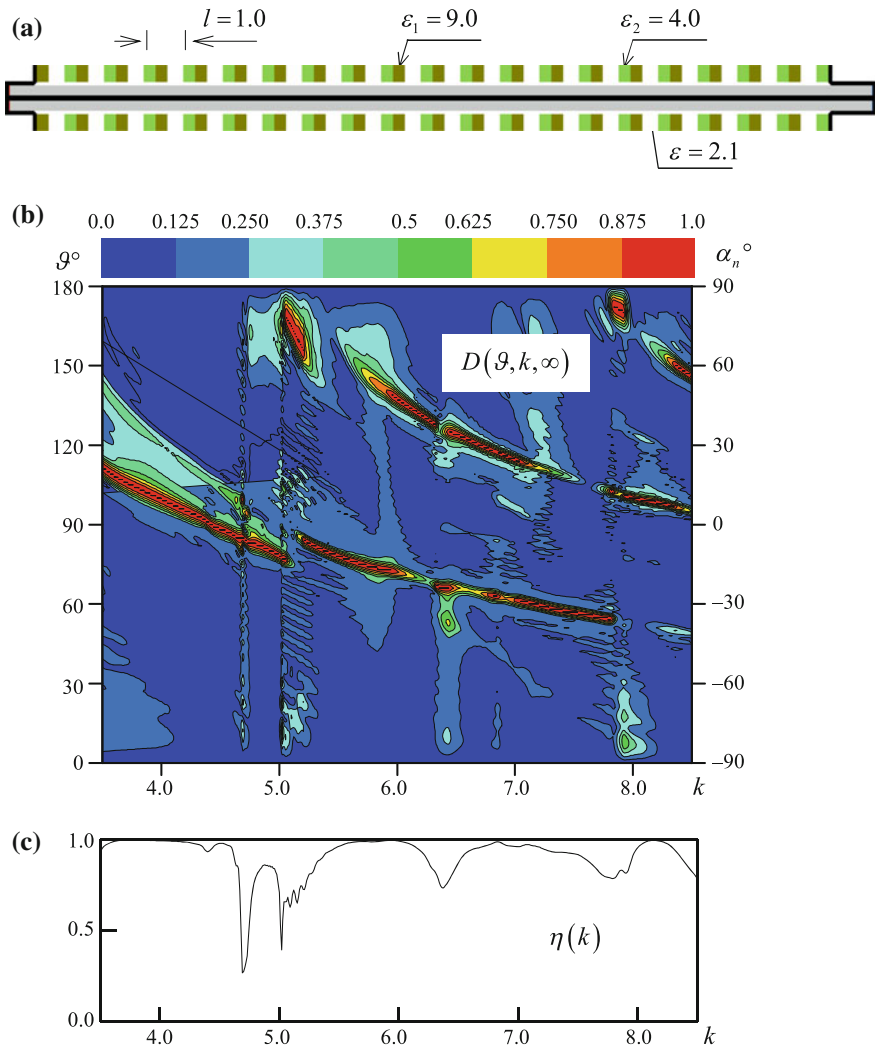


Fig. 7.23 a Axially symmetric antenna—Goubau line and dielectric rings grating: inner conductor radius is 0.06, outer radius of dielectric cover is 0.3, thickness and width of dielectric rings are 0.4 and 0.3, $c = 0.08$. Drawing is in proportion. b Directional pattern $D(\vartheta, k, \infty)$ and c radiation efficiency $\eta(k)$ of the antenna

respectively. The behavior of the directional pattern is quite predictable. In the vicinity of frequencies corresponding to small $\eta(k)$, the number of lobes increases abruptly, while the main lobes change their orientation twice from the direction associated with one spatial harmonic to the direction corresponding to the other one, if only such opportunity exists.

7.4 Synthesis of Diffraction Antenna Components and Units

Most of optimization problems considered in this section can be resolved theoretically, in particular by the methods discussed above. However, we give preference to the experimental approach. There are some reasons for our choice. First of all, we believe it would be appropriate to demonstrate potential of experimental methods as was done previously for theoretical approaches, since they inevitably must be invoked passing from theoretical research to new devices. At the same time, the emphasis in this section is on the methodology, which is equally applicable to both theoretical and experimental technique used for solving a specific problem. And finally, in the next section we present the unique diffraction antenna, which is a product of the experimental technique outlined below.

7.4.1 Synthesis of Radiators with Predetermined Amplitude-Phase Field Distribution on the Aperture

Consider a radiator formed by a *ridge dielectric waveguide* (RDW) and a lamellar grating (Fig. 7.24). The radiator of this kind was used in the airfield surveillance radar discussed in [32]. In the dielectric waveguide made from fluoroplastic ($\epsilon = 2.05$), the surface wave with the *moderating coefficient* $\gamma(k) = \beta^{-1}(k) = \bar{\chi}(k)/k = 1.243$ for $\lambda = 2\pi/k = \lambda_{\text{work}} = 8.3$ mm propagates, where λ_{work} is the working wavelength. The components E_y and E_z dominate in the electric field. Being scattered by the grating, the surface wave gives rise to the horizontally-polarized spatial outgoing wave. The vector \vec{H} of this wave is directed normally to the $y0z$ plane, which is called ‘horizontal’ due to typical antenna orientation in radar installations.

RDW is fitted with a horn-type source of slow surface waves. Its total loss is 0.2 dB, of which the radiation loss is 0.1 dB. The *standing wave ratio* (SWR) does not exceed 1.15 in the frequency band $34 \text{ GHz} \leq f \leq 38 \text{ GHz}$ ($7.89 \text{ mm} \leq \lambda \leq 8.82 \text{ mm}$).

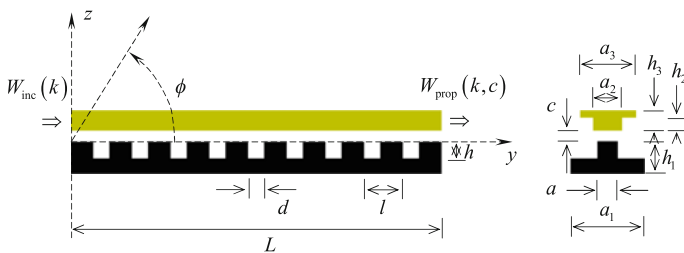


Fig. 7.24 ‘RDW—grating’ radiator: $a_1 = 77$ mm, $a_2 = 7.0$ mm, $a_3 = 40$ mm, $h_1 = 5.5$ mm, $h_2 = 3.1$ mm, $h_3 = 5.5$ mm

An efficient antenna can be constructed around the radiator under consideration providing three following problems are resolved [17]. The first problem is to determine the grating period l and the grating geometry (parameters d and h) with the following requirements in mind: (i) a slow surface wave with the propagation constant $\bar{\chi}(k) = \Phi_1(k)$ produces in the reflection zone only one propagating spatial harmonic (zeroth harmonic), which is directed within the angle range $90^\circ < \phi \leq 150^\circ$ and (ii) sufficiently high efficiency of the surface-to-spatial wave conversion (for planar infinite gratings this parameter is defined by the function $W_{01}^{22}(k)$) and minimal phase distortions (minimal variations in $\bar{\chi}(k)$ due to a waveguide-grating field coupling). The second problem is to gain the required field-amplitude distribution on the radiator aperture by selecting the waveguide-grating separation $c(y)$ throughout the length of the interaction region $0 \leq y \leq L$. The resolution of this problem allows to construct an antenna with the given radiation efficiency and *side-lobe level* (SLL) of its directional pattern in the plane $y0z$ [33]. The third problem is to determine and minimize aperture phase distortions, which are characterized by the deviation $\Delta\psi(y)$ of the field phase $\psi(y)$ from the straight line connecting the points $\psi(0)$ and $\psi(L)$.

In [32] the first problem was resolved experimentally for $l = 6.2$ mm (with this period we have $\phi_0(k) = 95.49^\circ$), $d = 2.0$ mm, $h = 1.5$ mm and $a = 4.0$ mm (see also Fig. 7.24). The authors used a radiator with a grating of length $L_{\text{prot}} = 250$ mm and measured such characteristics of the structure ‘surface wave line—grating’ like the input-to-output power ratio $W_{\text{inc}}(k)/W_{\text{prop}}(k, c)$ and $\gamma(k, c)$ for various values of the impact parameter c . The results of measurements of several suitable gratings (electrodynamical characteristics of periodic structures of this kind were analyzed in detail in [2, 11, 20]) let them to select the one that best meets the requirements in (ii) above.

At the next stage, we chose the grating length $L = 2000$ mm such that the directional pattern in the plane $y0z$ has sufficiently narrow main lobe. From the required field-amplitude distribution on the aperture, which is determined by the function $W_{\text{rad}}^{\text{norm}}(k, y) = W_{\text{rad}}(k, y) / \max_{0 \leq y \leq L} [W_{\text{rad}}(k, y)]$ (normalized radiated energy), and the linear loss in the surface wave line, we calculated the power taken by each period of the grating. Then, using the function $W_{\text{inc}}(k)/W_{\text{prop}}(k, c)$ measured earlier for the grating 250 mm long (Fig. 7.25), we determined the magnitude of c for each period and consequently $c(y)$ along the whole length of the interaction region $0 \leq y \leq 2000$ mm. Provided high precision of measurements, this approach exhibits good agreement between the resulting data with those expected.

As the distance $r > 0$ from the planar dielectric waveguide increases, the field intensity decreases as $\exp[-\alpha(k)r]$, where $\alpha(k) = \text{Im} \sqrt{k^2 - \bar{\chi}^2(k)}$ (see Sect. 7.2.4). RDW differs from the planar waveguide with the same moderating coefficient in that the field decreases more steeply with the distance away from its surface facing the grating. The approximate formula for the field decrease is $\exp[-\alpha(k)r] \sqrt{r_0/(r_0 + r)}$, where r_0 is the distance between the plane $z = c$ and the point at which the power flux density is maximal within the RDW cross-section

Fig. 7.25 Energy response of ‘RDW—grating’ structure 250 mm in length

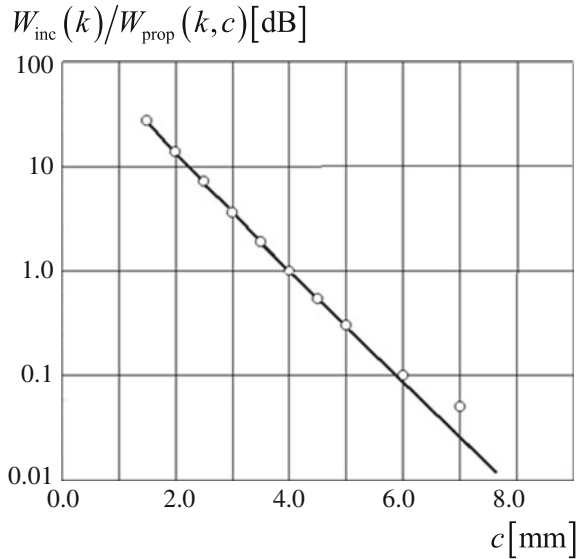


(Fig. 7.24). The corresponding power takeoff is plotted in Fig. 7.25 (solid line) for the following parameters: $\gamma(k) = 1.243$, $\lambda_{work} = 8.3$ mm and $r_0 = 3.0$ mm. This curve corresponds to the experimentally obtained value of $W_{inc}(k)/W_{prop}(k, c)$ for $c = 1.5$ mm and agrees well with the measurement data (circles) obtained for greater (up to $c = 5.0$ mm) grating-RDW distances. The data calculated by this algorithm is required for accurate determination of the function $c(y)$ along the entire interaction region, where at some points a drop to 10^{-4} dB is registered for $c \approx 12.0$ mm ($c \approx 1.45\lambda_{work}$). The point is that the range where the drop can be measured rather precisely is $1.0 \div 30.0$ dB. Therefore the discrepancy between the measured and calculated data in Fig. 7.25 for $W_{inc}(k)/W_{prop}(k, c) < 0.1$ dB is caused by the increased measurement error for small values of the power takeoff.

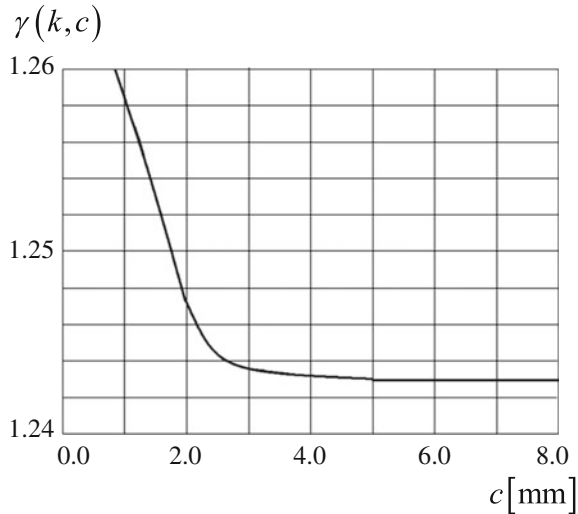
When solving the second problem, consideration must be given to some general restrictions on the shape of the field-amplitude distribution along the antenna aperture $0 \leq y \leq L$:

$$f(y) = \eta + (1 - \eta)g\left(\frac{2y - L}{L}\right); \quad 0 \leq \eta \leq 1$$

and for $|p| \leq 1 \quad g(p) \geq 0, \quad \max g(p) = 1.$

This function must be sufficiently smooth and may not become zero, including its values at the ends of the interaction region. Therefore, such widely used distributions as cosine distribution $g(p) = \cos(p\pi/2)$ (see Table 4.1 in [33]) or cosine-squared distribution $g(p) = \cos^2(p\pi/2)$ can be used only with a pedestal η of height not less than 0.01. It should be mentioned that with a cosine-squared

Fig. 7.26 Moderating coefficient for ‘RDW—grating’ structure 250 mm in length



distribution, a pedestal $\eta = 0.1$ produces the first side lobes at the level of -42.64 dB.

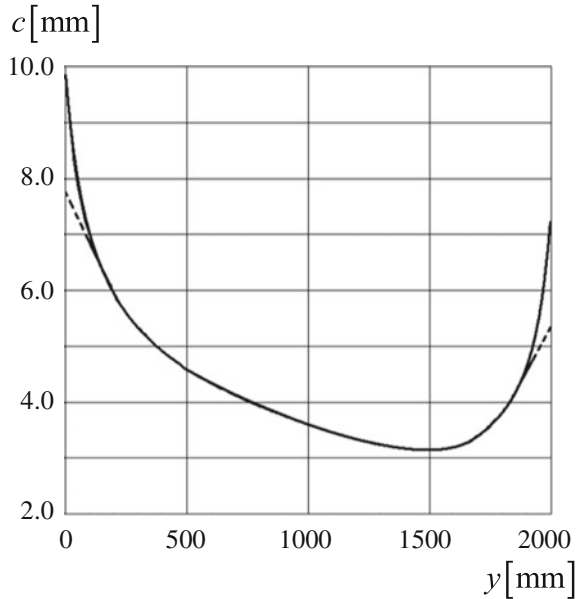
At the third stage, using the previously calculated and measured functions $c(y)$ for $0 \leq y \leq L$ and $\gamma(k, c)$, we estimated phase distortions on the aperture, which are caused by a relationship between the moderating coefficient $\gamma(k)$ and the waveguide-grating gap c (Fig. 7.26).

To measure the moderating coefficient $\gamma(k, c)$, we used the radiator with the grating 250 mm in length and the 8-mm phase meter with Doppler frequency shifter [32]. The values of $\gamma(k)$ for different c were determined from the phase incursion over a finite distance along the interaction region (see Sect. 7.3.3). The radiator input and output were very well matched with the phase meter that provided precision of measurements at a level of about 0.2° .

As seen from Fig. 7.26, the moderating coefficient $\gamma(k, c)$ rises sharply for $c < 2.5$ mm, that is why this value of c was chosen as ultimately permissible. The phase $\psi(y)$ at some point y corresponding to a certain grating period is a sum of the phase incursions over all preceding periods. These incursions can be easily calculated from the impact parameter c corresponding to each grating period and the local value of the function $\gamma(k, c)$. Since it is not easy to visualize the incursion $\Delta\gamma(k, c) = \gamma(k, c) - \gamma(k, \infty)$ for $c > 3.0$ mm due to the plotting scale in Fig. 7.26, we give some numerical data: $\Delta\gamma(k, c) = 6.5 \cdot 10^{-4}$ for $c = 3.0$ mm, $\Delta\gamma(k, c) = 2.3 \cdot 10^{-4}$ for $c = 4.0$ mm, and $\Delta\gamma(k, c) = 4.6 \cdot 10^{-5}$ for $c = 5.0$ mm. If the antenna aperture size is greater than 100 wavelengths, then even such small phase deviations must be taken into account when calculating the directional pattern.

The above-described methodology may be followed to construct an antenna whose SLL does not exceed -20 dB and the main lobe width approximates 0.3° for the pattern in the plane $y0z$. This performance can be reached if the amplitude

Fig. 7.27 Impact parameter $c(y)$



distribution on the aperture is cosine with the pedestal $\eta = 0.03$ (the field drop is -30 dB at the aperture ends). The function $c(y)$ calculated for this distribution with allowance made for linear loss in the dielectric waveguide at a level of 0.85 dB/m is depicted in Fig. 7.27 by the solid line. The values of c vary from 3.15 mm to 9.7 mm over the interaction interval $0 \leq y \leq L$. The dashed line corresponds to the profile $c(y)$ of the constructed antenna. The discrepancy between the calculated and realized functions $c(y)$ stems from the fact that only eight points of fixation in 250 mm intervals starting with the point $y = 125$ mm provide the required bending of RDW. For the same reason the field drop at the aperture edges in the constructed antenna reduced from the expected -30 dB to -20 dB (Fig. 7.28).

Fig. 7.28 Calculated (solid line) and measured (circles) amplitude field distribution over aperture

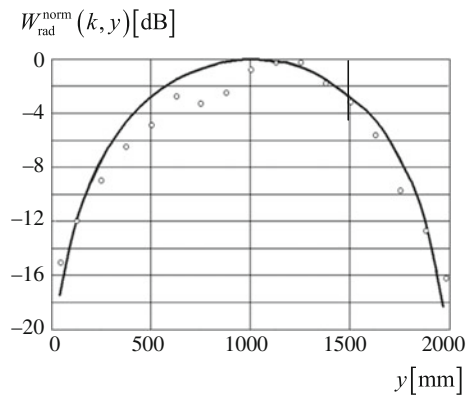
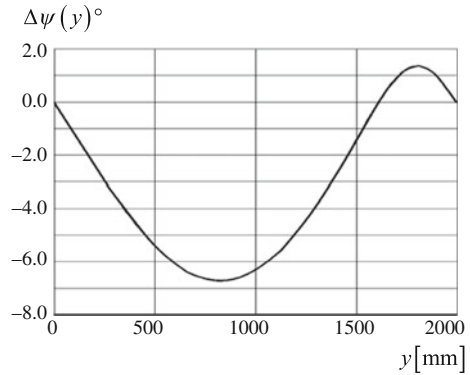


Fig. 7.29 Phase distortions on aperture



The measured and computed values for the function $W_{\text{rad}}^{\text{norm}}(k, y)$, which is representative of the field-amplitude distribution over the antenna aperture, agree closely. The total loss of the ‘RDW—grating’ system is 1.25 dB, which includes the material loss in the guiding line and the load loss at the end of this line.

The function $\Delta\psi(y)$ defining phase distortions on the aperture, which was calculated from $\gamma(k, c)$ for the actual profile $c(y)$, is presented in Fig. 7.29. In Fig. 7.30, the calculated directional patterns for the cosine-on-pedestal amplitude distribution without phase distortions and the actual amplitude-phase distribution (see Figs. 7.28 and 7.29) are depicted by the solid and dashed lines, respectively. The total effect of the amplitude and phase distortions is moderate—the maximum of the directional pattern is deflected gently towards the aperture normal, the side lobes are slightly asymmetric, while their level falls. From the results obtained it may be concluded that eight points of fixation of RDW would be ample to get satisfactory amplitude-phase field distribution on the aperture 2000 mm in length.

The directional pattern of the actual antenna in the plane yOz is shown in Fig. 7.31. Its width is $\phi_{0.5} = 0.27^\circ$ (or $\phi_{-3.0\text{dB}} = 0.27^\circ$), SLL is -21.7 dB. When the calculated SLL (Fig. 7.30) is compared with the SLL obtained experimentally, it is apparent that some additional disregarded sources of amplitude-phase distortions

Fig. 7.30 Calculated horizontal directional patterns as illustration of impact of aperture phase distortions

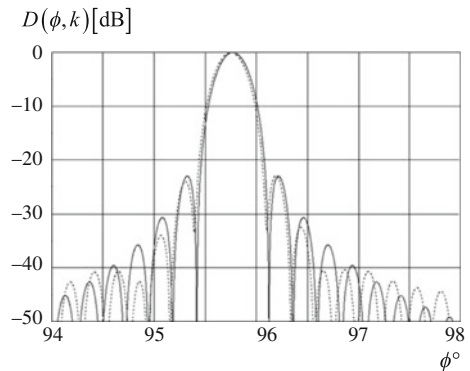
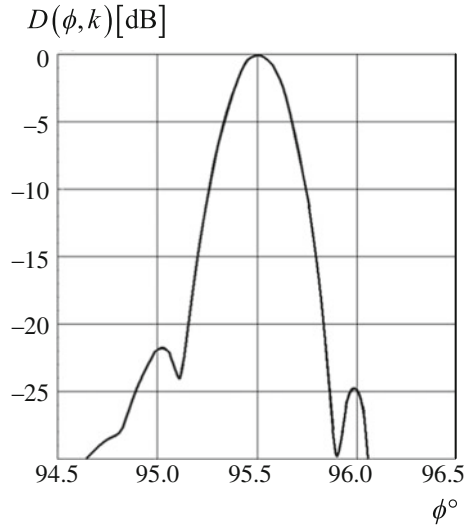


Fig. 7.31 Measured horizontal directional pattern



occur. However, the actual SLL exceeds the calculated values insignificantly (1.2 dB), which is quite satisfactory. On the whole, all these rather good results have been obtained owing to optimal dimensions of the dielectric waveguide and the grating geometry as well as to minimal manufacturing errors.

It should be noted that all experimental and numerical data discussed above were obtained for the working wavelength $\lambda = \lambda_{\text{work}} = 8.3 \text{ mm}$.

7.4.2 Maintenance of Antenna Operability on Coupling Level

Table 7.1 presents values of the function $c(y)$ which result in the cosine-squared field distribution on the aperture to decay down to -14 dB at its edges (see Table 7.2, first row) for $\lambda = \lambda_{\text{work}} = 8.8 \text{ mm}$ ($\gamma(k_{\text{work}}) = 1.254$) and the following radiator parameters: $l = 6.5 \text{ mm}$, $d = 2.0 \text{ mm}$, $h = 1.6 \text{ mm}$, $L = 1830 \text{ mm}$, $a = 12.0 \text{ mm}$ (and, see Fig. 7.24, $a_1 = 28 \text{ mm}$, $a_2 = 8.0 \text{ mm}$, $a_3 = 40 \text{ mm}$, $h_1 = 8.0 \text{ mm}$, $h_2 = 3.5 \text{ mm}$, $h_3 = 6.2 \text{ mm}$). When calculating $c(y)$, we used the energy responses from the antenna segment 201.5 mm in length.

The data in Table 7.2 allows to estimate the influence of uniform deviations on the calculated function $c(y)$ (first row). The first column lists new impact parameter functions. In the second and third columns, field-amplitude distributions and directional patterns associated with these profiles are given. The main lobe width $\phi_{0.5}(k)$ is 0.325° in all cases. The calculated directional patterns take no account of phase distortions. The taken into account linear loss is 1.0 dB/m .

Table 7.1 Calculated values of impact parameter

y [mm]	$c(y)$ [mm]
10	6.49
110	6.25
310	5.22
510	4.29
710	3.63
910	3.17
1110	2.88
1315	2.80
1510	3.11
1710	3.79
1810	3.95

To increase the antenna efficiency, small impact parameters must be used, which results in a growth of phase distortions. That is why the field drop at the output of the interaction region at a level of -14 dB ($AE = 75\%$) is a compromise from the standpoint of phase distortions and possible thermal expansions or compressions of the antenna parts. Such a choice results in a reasonable precision of measurements as it is well known that it is difficult to determine the field drop at a level of -20 dB and below.

The data presented in Table 7.2 testify that even considerable growth or reduction of the impact parameter (e.g., due to variations of ambient temperature) does not cause operating irregularity of the diffraction antenna. In fabrication of antennas of this kind, reasonably large deviations of the function $c(y)$ from the calculated values may be tolerated.

Let us consider the influence of deviations of $c(y)$ from its initial values over small variation intervals of y on the antenna performance. Such deviations may occur if we use separate points of fixation when making the profile $c(y)$ (see Table 7.1). The results presented in the first and second rows of Table 7.3 are calculated for the cases where the value of $c(y)$ is increased by 0.2 mm and 0.4 mm, respectively, at the point $y = 1100$ mm on the aperture, while the data in the third and fourth rows correspond to $c(y)$ being decreased in the same way. The antenna efficiency reduces predictably in the first two cases and increases in the two others, where field coupling between the waveguide and the grating increases slightly on a small portion of the interaction area. In all cases, one can observe considerable distortions of the field-amplitude distribution over the aperture together with the marked increase of SLL. The presented data allow to conclude that the acceptable deviation of $c(y)$ may not exceed 0.1 mm at separate points. However, as was shown previously, a smooth and uniform variation of the impact parameter well over this value results in only insignificant change in the antenna performance.

In closing, it may be noted that the width of the directional pattern measured in the plane yOz with the initial parameters given in Table 7.1 agrees with the calculated one while SLL does not exceed -27 dB.

Table 7.2 Impact of uniform deviations of $c(y)$

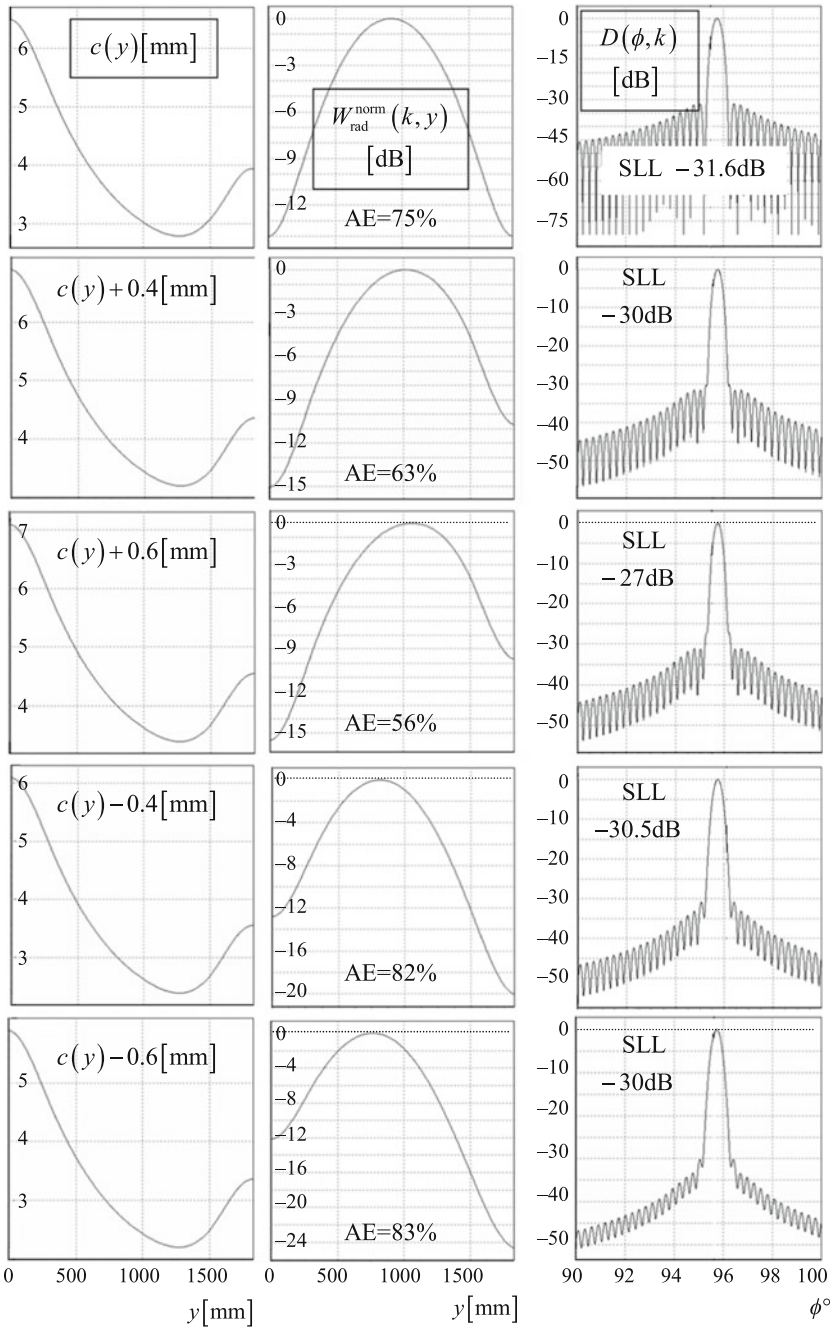
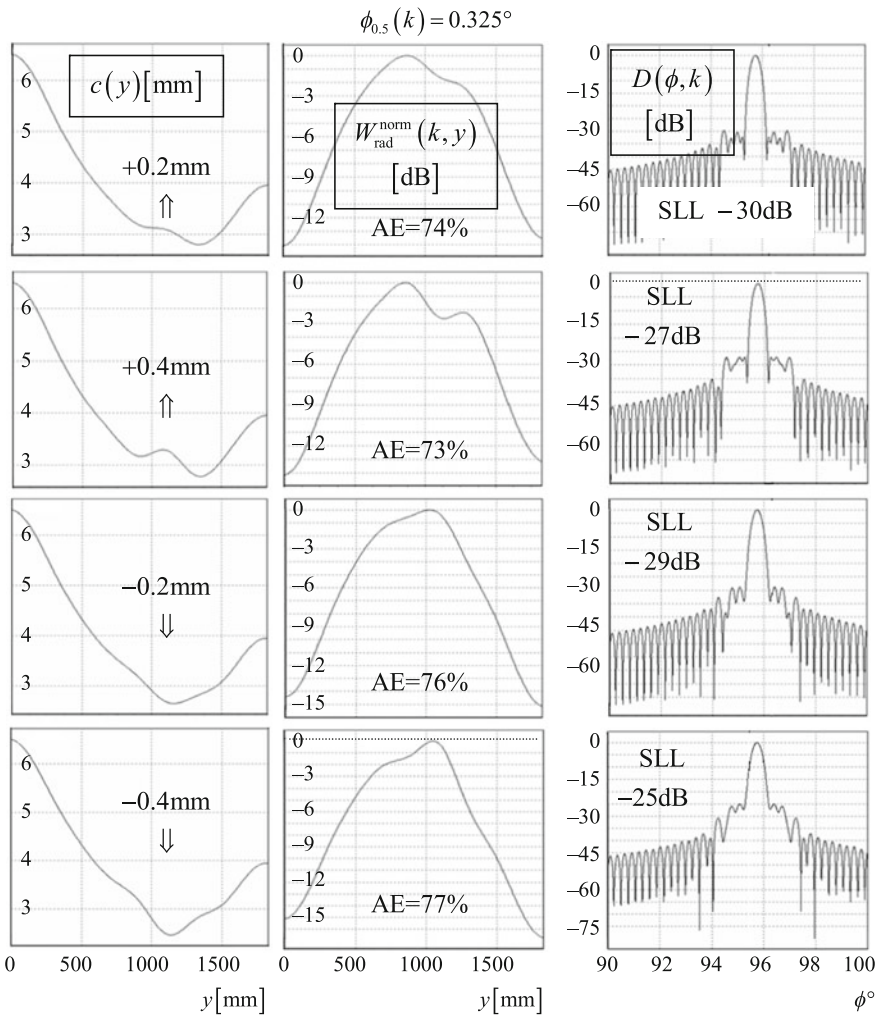


Table 7.3 Impact of local deviations of $c(y)$



7.5 The Low-Side-Lobe Planar Antenna

7.5.1 Radiator's Characteristics

Consider a radiator incorporating a planar dielectric waveguide (PDW) and a lamellar grating (Fig. 7.32a). The dielectric waveguide made from fluoroplastic ($\epsilon = 2.05$) sustains propagation of the surface TM_{11} -wave with the moderating

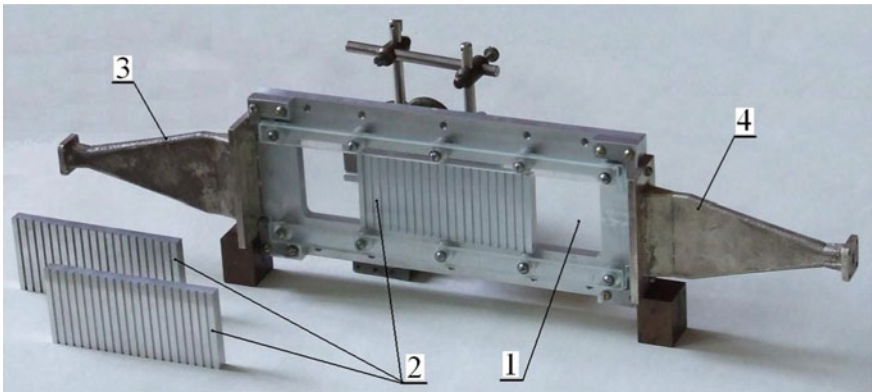
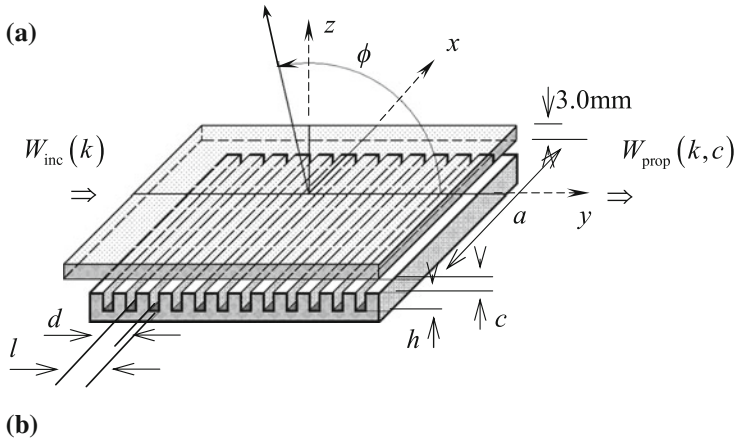


Fig. 7.32 **a** Geometry of ‘PDW—grating’ radiator. **b** Prototype with reduced aperture ($60 \times 125 \text{ mm}^2$): 1—PDW; 2—three changeable diffraction gratings; 3 and 4—input and output horns

coefficient $\gamma(k) = 1.23$ for $\lambda = \lambda_{\text{work}} = 8.824 \text{ mm}$ ($f_{\text{work}} = 34 \text{ GHz}$). Scattering on the grating, this wave gives rise to a horizontally polarized spatial outgoing wave (the vector \vec{H} is almost perpendicular to the $y0z$ plane) with a cylindrical phase front in the plane $x0z$. The radiator of this kind is a principal unit of the low-side-lobe planar antenna, whose design and characteristics were first described in [16].

In the course of experiments with the radiator of the length $L_{\text{prot}} = 125 \text{ mm}$ (Fig. 7.32b), among three gratings having groove depths $h = 2.2 \text{ mm}$, $h = 1.75 \text{ mm}$, $h = 1.4 \text{ mm}$ and the common parameters $l = 6.2 \text{ mm}$, $d = 2.0 \text{ mm}$, $a = 52.0 \text{ mm}$, we selected the one with $h = 1.75 \text{ mm}$ which demonstrated high efficiency in the surface-to-spatial wave transformation (Fig. 7.33) and the smallest phase distortions for $c > 3.0 \text{ mm}$ (Fig. 7.34). It is precisely these values that were thereafter considered as acceptable values of the impact parameter.

Fig. 7.33 Energy response of ‘RDW—grating’ structure 125 mm in length recalculated to length of 100 mm

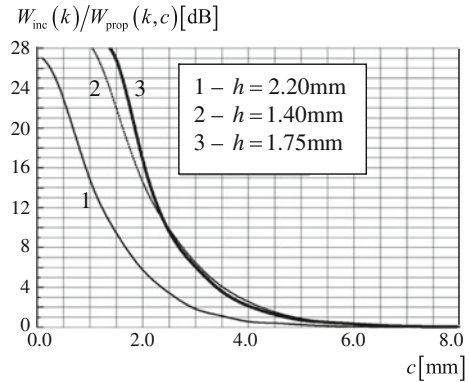
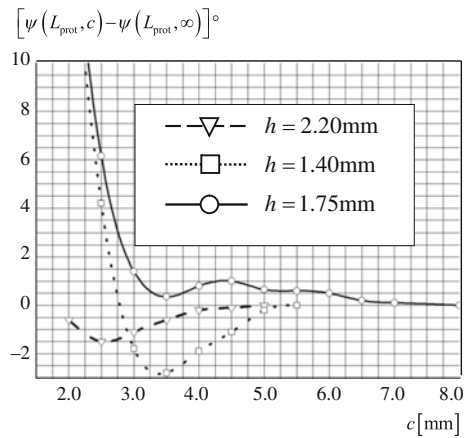


Fig. 7.34 Measured phase incursions at output of prototype 125 mm in length caused by PDW—grating field coupling for various c



In the reflection zone of an infinite grating, a surface wave with the given moderation gives rise to only one (nonzero) propagating spatial harmonic outgoing into free space at an angle of $\phi_0(k) = 101.11^\circ$ for $k_{work} \approx 0.712$ rad/mm. This means that the main lobe of the directional pattern is directed at 10° to the aperture normal. This deflection ensures low SWR and no impact of the energy remaining in PDW after the surface wave passage over the grating and reflection from its end on the level of the first side lobes.

When calculating a sample of a planar antenna with the interaction region of length $L = 1000$ mm and SLL below -30 dB, we utilized the data on the field distribution functions and the associated directional patterns given in [33]. To obtain the given SLL, the cosine-squared with a pedestal field distribution is required on the aperture. Different values of η result in field distributions with different drops at the ends of the interval $0 \leq y \leq L$ and different SLL of the directional patterns. For example, the pedestal $\eta = 1.0$ corresponds to uniform field distribution on the aperture (the field drop is 0.0 dB at the ends); the expected SLL

is -13.25 dB. With $\eta = 0.1$, the field drop at the ends is -22.0 dB, and SLL is -42.64 dB. With $\eta = 0.0$, the field drop is -60.0 dB, and SLL is -31.17 dB.

The problem set above can be solved by utilizing the cosine-squared distribution with the pedestal $\eta = 0.2$. With this distribution, the field drop at the aperture edges is -14 dB and the expected SLL is -31.41 dB. The impact factor $c(y)$ and the phase distortions $\Delta\psi(y)$ calculated for this distribution are depicted in Fig. 7.35. They are required to set up the experimental sample of the antenna. The calculated directional pattern shown in Fig. 7.36 indicates that the required side-lobe level may be achieved.

In the above-mentioned calculations, we used experimentally obtained data of the function $\gamma(k, c)$ (Table 7.4) and took into account 1.0 dB/m linear loss in PDW.

7.5.2 Antenna Design

An antenna embodiment plays an important role in ensuring the stability of its parameters in a wide range of temperatures, under static and dynamic loads, and

Fig. 7.35 Calculated impact parameter $c(y)$ and phase distortions $\Delta\psi(y)$ for aperture 1000 mm in length

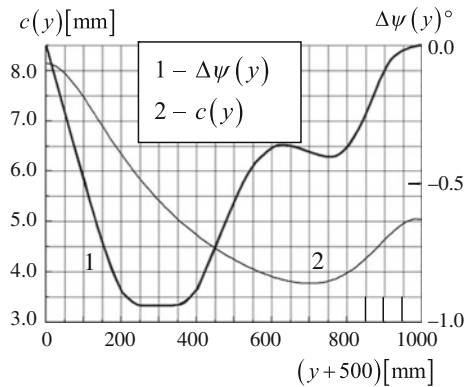


Fig. 7.36 Calculated horizontal directional pattern with field drop of -14 dB

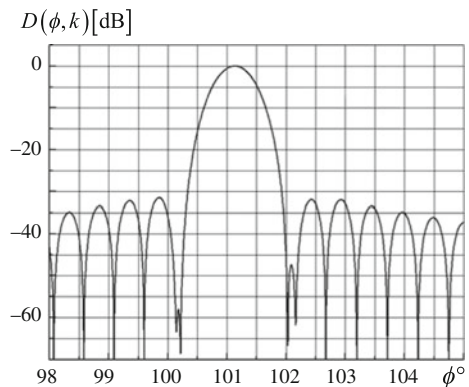


Table 7.4 Moderating coefficient as function of impact parameter

$c(y)[\text{mm}]$	$\gamma(k, c)$
1.0	1.249947
1.5	1.236864
2.0	1.233314
2.5	1.231206
3.0	1.230275
3.5	1.230069
4.0	1.230157
4.5	1.230196
5.0	1.230128
5.5	1.230118
6.0	1.230098
6.5	1.230039
7.0	1.230002
7.5	1.230001
8.0	1.230000
12.0	1.230000

vibrations. Additionally, a complete hermeticity may be needed to protect against moisture and precipitation. An antenna should be sufficiently rigid in construction with high precision of fabrication and assembly of its parts. Usually, when sealing hermetically, an entire antenna is placed into a protective housing with a radio-transparent window. In our design, it has been modified and resulted in a significant reduction of weight and dimensions of the device.

The dimensions of the antenna aperture are $200 \times 1000 \text{ mm}^2$, and the thicknesses of the grating, the dielectric waveguide, and the excitation device are within a few millimeters. Such dimensions of the antenna constituent parts do not provide the required flexural rigidity in the horizontal plane and torsional rigidity, so we added the base (marked '1' in Fig. 7.37a) and the bracing frame (marked '2') on the reverse side of the aperture.

The base is intended for mounting on it such antenna parts as five diffraction gratings ('3', Fig. 7.37a) the dielectric waveguide ('4'), the horn-lens excitation unit with an output waveguide and a return bend. Each diffraction grating 9.0 mm thick provides local rigidity over the area $200 \times 200 \text{ mm}^2$ in size. In the assembly of the antenna, the rigidity increases and reaches the required value when installing it on the bracing frame. Total sealing encloses only the antenna itself without the bracing frame. They are separated by a sealing sheet. The antenna enclosed in a protective housing represents a self-contained construction that can be mounted on any flat surface with the deviation from flatness of no more than $\pm 0.1 \text{ mm}$ and fixed with twelve screws. The points of fixation match gratings' junctions or edges, so the surface of the assembled diffraction grating meets the flatness requirements both over the $200 \times 200 \text{ mm}^2$ area and over the total area $200 \times 1000 \text{ mm}^2$.

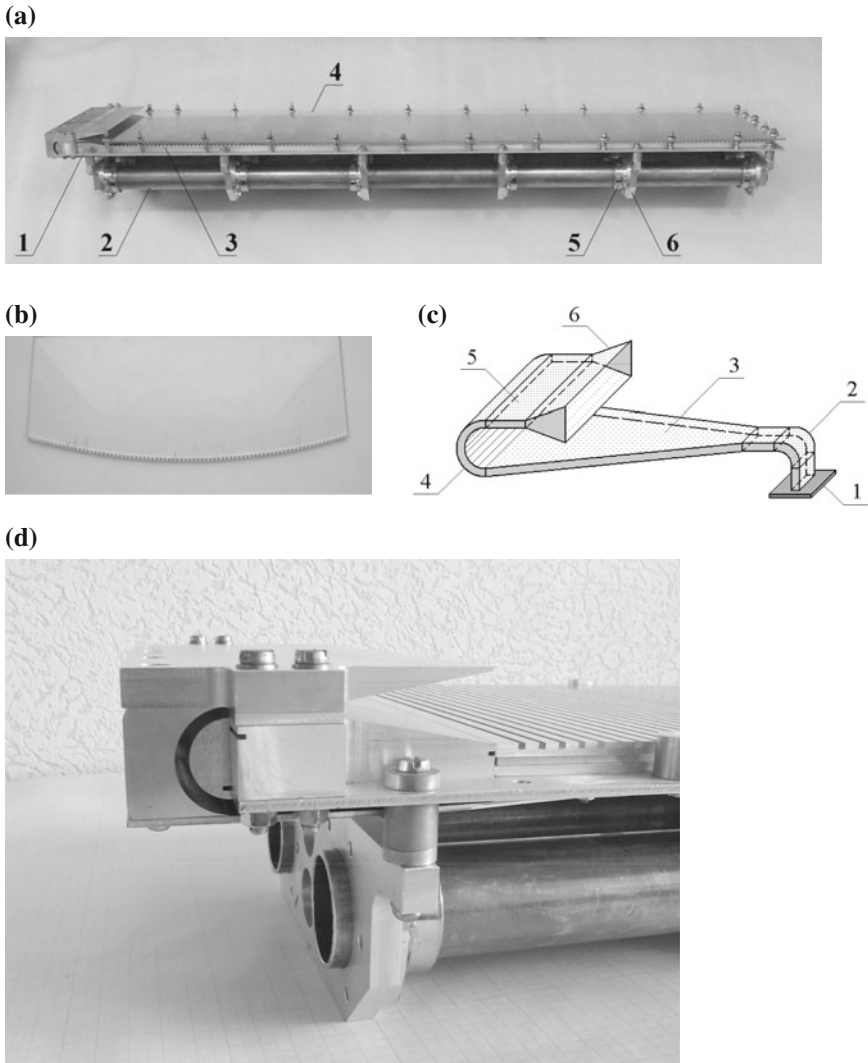


Fig. 7.37 **a** Experimental prototype of planar antenna [16], **b** PDW with antireflection lens, **c** exciter of PDW, and **d** return bend

The bracing frame consists of two pipes (aluminum alloy) 40 mm in diameter and 1050 mm long. Using the flanges ‘5’, the ribs ‘6’ are secured to the pipes. During the fabrication, six ribs are processed simultaneously, including their holes 40 mm in diameter, and hence, straightness of the pipes ensures sufficient flatness of the frame. The center-to-center distances of the ribs equal 210, 210, 210, 200, and 200 mm measured from the excitation unit. Strength of the ribs and pipes is sufficient to be securely fastened to a rotary device or any other bearing part.

The diffraction gratings are the most important and accurately fabricated parts. The period is maintained with the tolerance of ± 0.02 mm. Upon assembling (up to the length of $L = 1000$ mm), the distance between two arbitrary grooves is nearly multiple of the period $l = 6.2$ mm. Once the base is mounted on the bracing frame, the tolerance on flatness of the grating surface is 0.25 mm. The gratings interface together at the grooves bottom without clearance and are attached to the base by six screws each.

The dielectric waveguide (marked '4' in Fig. 7.37a) is made from polystyrene sheet 3.0 mm in nominal thickness. The average thickness of a sheet varies between 2.8 mm and 3.0 mm, however, extreme deviation from the mean value may not exceed ± 0.02 mm. PDW is attached to the base by twenty seven studs with adjustable height and spring blank holders to provide sliding fit and to compensate for thermal expansion of the polystyrene sheet. A planar lens with a focal distance of 582.7 mm and 14.31 mm thick is installed at the waveguide input. The lens refractor is hyperbolic in shape. At the antenna end, under the dielectric waveguide, a matching absorber is pasted in. Rubber with metal powder filling proved itself to be the best absorbing material.

The lens refractor may be equipped with an antireflection layer in the form of a grating (Fig. 7.37b), which results in the lower reflection coefficient and thus in the lower SWR of the antenna as a whole. To do this, a lens with a smooth surface is first fabricated and then grooves 1.75 mm in depth, 1.5 mm in width and with a period of 2.5 mm are milled.

PDW is excited through the horn (marked '3' in Fig. 7.37c) loaded on the biplanar metal waveguide with return bend '4'. For the horn upper wall, the base is used and a cover 1.0 mm long is used as the bottom wall. Aluminum alloy sheets used for these details should be free from scratches, corrosion marks, and other defects. The horn side walls 4.0 mm thick are positioned at an angle of 9.5° to the antenna axis. The return bend (Fig. 7.37d) provides also a smooth transition from the four-millimeter section to the three-millimeter section, which corresponds to the thickness of the dielectric waveguide. In the horn throat, the feeding waveguide of inner dimensions 7.2×3.4 mm² is installed. This waveguide is equipped with the flange '1' 24×24 mm² in size and the *E*-plane bend '2'. A correcting lens is placed in the planar waveguide '5'. The configuration of this kind reduces the number of reflecting surfaces on the way to the planar waveguide, and, as a result, decreases the total SWR of the waveguide transmission line. The horn marked '6' matches the parallel-plate waveguide with PDW.

7.5.3 *Experimental Data*

Below are given the results obtained for the frequency $f_{\text{work}} = 34$ GHz ($\lambda_{\text{work}} = 8.824$ mm), which coincides with the center of the antenna working frequency band. On typical spatial orientation of the antenna (yOz is the horizontal

plane, xOz is the vertical plane), its polarization is horizontal and the magnitude of the cross-component is below -40 dB. The antenna losses measured by means of registering SWR comprise 1.7 dB. They are a sum of the loss in the exciter of PDW 0.72 m in length (1.0 dB) and the loss in the planar waveguide up to its center (0.7 dB). Thus, the antenna intrinsic loss is 0.7 dB.

The measured SWR is 1.12 . Notice that prior the blooming of the lens, SWR was 1.25 , while the loss in the PDW excitation unit was 0.2 dB higher.

Figure 7.38a presents the measured antenna directional pattern in the vertical plane. From a number of measurements, we obtain the mean width of the pattern of 2.95° at a level of -3.0 dB. Due to the dielectric lens installed at the driven end of PDW, the field drops at the aperture edges $x = \pm a/2$ faster, which results in the reduction of the lateral radiation level down to -25 dB in the vertical plane. It would have been -23 dB for the cosine-shape distribution. The effect of this kind is common to horn-lens antennas with a convex first refractor. In short-focus systems, it is more pronounced. Application of a short-focus lens will allow to reduce SLL in the vertical plane by another $2 \div 6$ dB.

The measured antenna directional pattern in the horizontal plane is shown in Fig. 7.38b. Its shape agrees with the calculated one (Fig. 7.36). A set of measurements gave the mean width of the pattern of 0.64° at a level of -3.0 dB. The operational integrity of the antenna is retained in the frequency band 34 ± 0.5 GHz with possible variations of the main lobe orientation as low as 1.0° per 1% of frequency variation. SLL in the horizontal plane is coincident with the calculated data and equals -31.4 dB. The shape of the side lobes suggests unsuspected phase distortions associated with possible inaccurate fabrication of individual parts and assembly errors. It is also possible that there exist other neglected energy leakage paths. As a whole, the problem may be considered as resolved since we have

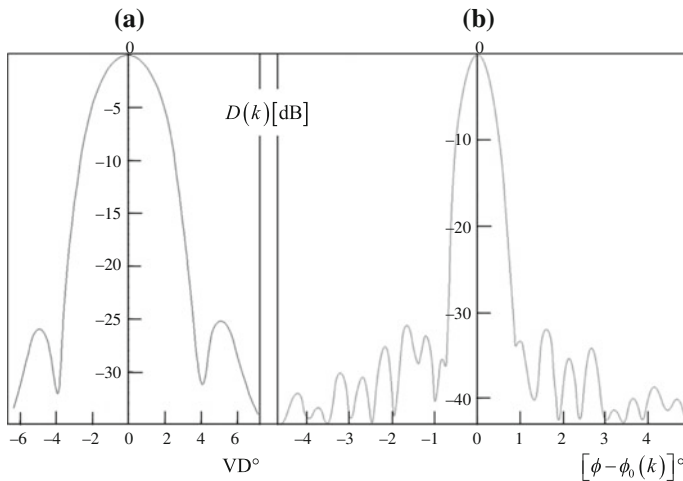


Fig. 7.38 Experimental **a** vertical and **b** horizontal directional patterns. VD is vertical deviation

proved experimentally the possibility to form directional patterns with SLL below -30 dB for diffraction radiation antennas. Further reduction of SLL is possible provided other amplitude distribution is realized on the aperture and the assembling accuracy control is more rigid.

The *antenna directive gain* (ADG) obtained from the measured widths of the directional patterns in the vertical and horizontal planes is 42.7 dB. The measurement of the *antenna power gain* (APG) by the substitution technique with an aid of a reference horn-lens antenna (APG = 33.8 dB) yields the elevation of +7.6 dB. From the difference between ADG and APG, we determine the total loss in the designed planar antenna, it is 1.3 dB. Previously, we estimated the total loss by registering SWR, it was 1.7 dB. The difference of 0.4 dB is due to oversized losses caused by phase distortions in planar guided-wave structures when estimating the loss by registering SWR. That oversized estimation has nothing to do with the structural ohmic loss. Thus, we may consider that the antenna loss is about 1.3 dB.

The planar antenna with hermetic housing weights 16 kg. The antenna finds its use in stationary and movable, ground-based and sea-based millimeter-waves scanning radars as well as in side-looking radars. Long-standing testing of actual antennas of this kind demonstrates their reliability, stability, and tolerance for adverse environmental conditions [17].

7.6 Conclusion

Diffraction gratings illuminated by surface waves of open waveguides or by density-modulated charged-particle beams are capable of forming a narrow-beam radiation. This effect is used in antenna and electronic devices, specifically in diffraction radiation generators and antennas. In this chapter, we first decided to look into this area in detail. We presented the models making possible more detailed observations of the processes associated with the near-field to far-field conversion by infinite and finite periodic structures. The efficient experimental approach to design parts and units for diffraction antennas was elaborated. We obtained a number of new physical results, which are of theoretical and applied interest. In particular, the low-side-lobe planar antenna prototype was designed and tested, which experimentally proved the possibility of diffraction radiation antennas to form a directional pattern with SLL below -30 dB.

References

1. Amitay, N., Galindo, V., Wu, C.P.: Theory and Analysis of Phased Array Antennas. Wiley, New York (1972)
2. Shestopalov, V.P., Lytvynenko, L.M., Masalov, S.A., Sologub, V.G.: Wave Diffraction by Gratings. Kharkov State University Press, Kharkov (1973). (in Russian)

3. Petit, R. (ed.): *Electromagnetic Theory of Gratings*. Springer, New York (1980)
4. Chandezon, J., Maystre, D., Raoult, G.: A new theoretical method for diffraction gratings and its numerical application. *J. Opt. (Paris)* **11**(4), 235–241 (1980)
5. Li, L., Granet, G., Plumey, J.P., Chandezon, J.: Some topics in extending the C-method to multilayer-coated gratings of different profiles. *Pure Appl. Opt.* **5**(2), 141–156 (1996)
6. Sirenko, Y.K., Velychko, L.G.: Diffraction grating profile reconstruction: simple approaches to solving applied problems. *Electromagnetics* **19**(2), 211–221 (1999)
7. Sirenko, Y.K., Velychko, L.G., Karacuha, E.: Synthesis of perfectly conducting gratings with an arbitrary profile of slits. *Inverse Prob.* **15**(2), 541–550 (1999)
8. Neviere, M., Popov, E.: *Light Propagation in Periodic Media: Differential Theory and Design*. Marcel Dekker, New York (2003)
9. Sirenko, Y.K., Strom, S., Yashina, N.P.: *Modeling and Analysis of Transient Processes in Open Resonant Structures: New Methods and Techniques*. Springer, New York (2007)
10. Sirenko, K.Y., Sirenko, Y.K., Yashina, N.P.: Modeling and analysis of transients in periodic gratings. I. Fully absorbing boundaries for 2-D open problems. *J. Opt. Soc. Am. A* **27**(3), 532–543 (2010)
11. Sirenko, K.Y., Sirenko, Y.K., Yashina, N.P.: Modeling and analysis of transients in periodic gratings. II. Resonant wave scattering. *J. Opt. Soc. Am. A* **27**(3), 544–552 (2010)
12. Sirenko, Y.K., Strom, S. (eds.): *Modern Theory of Gratings. Resonant Scattering: Analysis Techniques and Phenomena*. Springer, New York (2010)
13. Granet, G., Melezhhik, P., Sirenko, K., Yashina, N.: Time-and-frequency domains approach to data processing in multiwavelength optical scatterometry of dielectric gratings. *J. Opt. Soc. Am. A* **30**(3), 427–436 (2013)
14. Lee, J.W., Eom, H.J., Park, K.H., Chun, W.J.: TM-wave radiation from grooves in a dielectric-covered ground plane. *IEEE Trans. Antennas Propag.* **49**(1), 104–105 (2001)
15. Melezhhik, P.N., Sidorenko, Y.B., Provalov, S.A., Andrenko, S.D., Shilo, S.A.: Planar antenna with diffraction radiation for radar complex of millimeter band. *Radioelectron. Commun. Syst.* **53**(5), 233–240 (2010)
16. Yevdokymov, A.P., Kryzhanovskiy, V.V., Sirenko, Y.K.: A planar extremely high frequency diffraction radiation antenna. *Elektromagnitnye Volny I Elektronnye Sistemy* **16**(6), 53–61 (2011). (in Russian)
17. Yevdokymov, A.P.: Diffraction radiation antennas. *Fizicheskie Osnovy Priborostroeniya* **2**(1), 108–125 (2013). (in Russian)
18. Sautbekov, S., Sirenko, K., Sirenko, Y., Yevdokimov, A.: Diffraction radiation phenomena: physical analysis and applications. *IEEE Antennas Propag. Mag.* **57**(5), 73–93 (2015)
19. Tretyakov, O.A., Tretyakova, S.S., Shestopalov, V.P.: Electromagnetic wave radiation by electron beam mowing over diffraction grating. *Radiotekhnika I Elektronika* **10**(7), 1233–1243 (1965). (in Russian)
20. Shestopalov, V.P.: *Physical Foundation of the Millimeter and Sub Millimeter Waves Technique. Vol. I. Open structures*. VSP Books Inc., Utrecht, Netherland & Tokyo, Japan (1997)
21. Sirenko, Y.K., Velychko, L.G.: The features of resonant scattering of plane inhomogeneous waves by gratings: model problem for relativistic diffraction electronics. *Telecommun. Radio Eng.* **55**(3), 33–39 (2001)
22. Kesar, A.S., Hess, M., Korbly, S.E., Temkin, R.J.: Time- and frequency-domain models for Smith-Purcell radiation from a two-dimensional charge moving above a finite length grating. *Phys. Rev. E* **71**, 016501-1–016501-9 (2005)
23. Zhang, P., Zhang, Ya., Hu, M., Liu, W., Zhou, J., Liu, S.: Diffraction radiation of a sub-wavelength hole array with dielectric medium loading. *J. Phys. D: Appl. Phys.* **45**, 145303-1–145303-8 (2012)
24. Ladyzhenskaya, O.A.: *The Boundary Value Problems of Mathematical Physics*. Springer, New York (1985)
25. Taflov, A., Hagness, S.C.: *Computational Electrodynamics: The Finite-Difference Time-Domain Method*. Artech House, Boston (2000)

26. Rao, S.M. (ed.): Time Domain Electromagnetics. Academic Press, San Diego (1999)
27. Rothwell, E.J., Cloud, M.J.: Electromagnetics. CRC Press, New York (2001)
28. Masalov, S.A.: On a possibility of using an echelette in the diffraction radiation generators. *Ukrainskiy Fizicheskiy Zhurnal* **25**(4), 570–574 (1980). (in Russian)
29. Velychko, L.G., Sirenko, Y.K., Velychko, O.S.: Time-domain analysis of open resonators. Analytical grounds. *Prog. Electromagnet. Res.* **61**, 1–26 (2006)
30. Chen, H., Chen, M.: Flipping photons backward: reversed Cherenkov radiation. *Mater. Today* **14**(1-2), 34–41 (2011)
31. Park, S.-H., Park, J.-I., Kim, K.-T.: Motion compensation for squint mode spotlight SAR imaging using efficient 2D interpolation. *Prog. Electromagnet. Res.* **128**, 503–518 (2012)
32. Yevdokymov, A.P., Kryzhanovskiy, V.V.: Antenna for 8 mm range airfield control radar set. *Elektromagnitnye Volny I Elektronnye Sistemy* **13**(6), 46–52 (2008). (in Russian)
33. Kuhn, R.: *Mikrowellen Antennen*. Veb Verlag Technik, Berlin (1964). (in German)

Index

A

Abrupt waveguide discontinuities, 108
Accretive-accumulative operator, 161
Accretive contraction, 137
Active compressors, 328, 348
Actual real-valued sources, 193
Adiabatic approximation, 7, 18
Adjoint matrix, 94
Adjoint orthoprojectors, 138
Algebraic branch points, 219
Amplitude and phase of trapezoids, 22
Amplitude gain, 381
Analytical solution, 63
Anisotropic medium, 91
Antenna directive gain (ADG), 440
Antenna efficiency, 266, 334
Antenna power gain (APG), 440
Artificial boundaries, 195
Asymmetric Epstein layer, 54
Attenuation, 394
Autocollimation, 396

B

Backscattered radiation, 414
Banach algebra, 119
Banach spaces, 113
Bandwidth, 346
Barnes representation, 56
Beyond-cutoff diaphragm, 348
Bianisotropic medium, 92
Biisotropic, 63
Biisotropic medium, 63
Biisotropic plane stratified medium, 2
Bilinear tensor-scalar product of
vector-functions, 115
Blocked fast Fourier transform, 314
Borgnis functions, 200, 295

C

Cagniard-de Hoop method (CHM), 2, 41
Cagniard method, 40
Canonical symmetry, 143
Carleman's two-element boundary value
problem, 5
Cauchy-Poincaré theorem, 7, 15
Causality principle, 263
Cayley transformation, 121
Characteristic equation, 223
Closed initial boundary value problem, 329
Closed problem, 188
Coastal refraction problem, The, 3
Compact finite-meromorphic
operator-function, 222
Compact operator, 127
Complete and orthonormal set, 112
Complex eigenfrequencies, 335
Complex power theorem, 209
Complex-valued (nonphysical) values of real
parameters, 217
Complex-valued sources and waves, 193
Complex wave, 399
Complex wavenumber, 264, 333, 394
Condition number, 128
Condition on the sharp edge, 138
Continuously varying parameters, 63
Coupling window, 348
Cramer rule, 107
Cramped unitary operators, 116
Creeping waves, 31
Criterion of the boundary 'sharpness', 2
Criterion of the interface 'sharpness', 54
Cross-section method, 21
Cross-uniform regular waveguides, 328
Current sources, 229
Cutoff frequencies, 307, 333
Cycle slipping (CS) phenomenon, 2, 22, 84

D

Damped harmonics, 215
 Degree of compression, 335
 Diffraction antennas, 388
 Diffuse boundary, 62
 Directional pattern, 410
 Dirichlet conditions, 107
 Dispersion equation, 399
 Distorting coating, 83, 85
 Distortion, 3
 Double-negative media, 2
 Double-positive media, 2
 Dyadic Green's function (DGF), 91

E

Earth-ionosphere waveguide, 2
 Edge condition, 110
 Effect of diffraction radiation, 388
 Efficiency of energy accumulation, 269
 Eigenfrequency, 220, 269, 397
 Eigenfunction, 270
 Eigenvector of reflection matrix, 131
 Eigenwaves, 397
 Elementary excitation, 205
 Energy balance equations, 209, 395
 Energy compressor, 327, 343
 Energy conservation law, 2
 Energy content, 214
 Energy distribution between waveguide modes, 334
 Energy efficiency, 335
 Epstein transition layer, 2
 Equation of the second kind, 222
 Evolutionary bases, 203
 Evolutionary basis, 331
 Exact absorbing conditions (EACs), 188, 225, 237, 297
 Exact absorbing conditions, 388
 Exact nonlocal and local absorbing conditions, 195
 Explicit computational schemes, 188

F

Factorization function, 6
 Factorization method, 27
 Faraday effect, 63
 Far-field zone problem, 254, 255
 FFT-based acceleration, 314
 Field patterns, 410
 First (physical) sheet, 219
 Floquet channel, 391
 Free electromagnetic field oscillations, 270
 Free oscillation, 220, 335, 397
 Frequency, 264, 333, 394

Frequency dispersive media, 189
 Frequency parameter, 264, 333, 394
 Frequency spectra, 397
 Frequency spectral set, 397
 Fresnel formulas, 72, 103
 Fully discrete method, 129
 Fundamental solution, 199

G

Galerkin procedure, 107, 121
 Generalized operator Fresnel formulas, 105
 Generalized scattering matrices, 395
 Given-field approximation, 405
 Green function, 7

H

Half-power beamwidth (HPBW), 266
 Half-power beamwidth, 334
 Helmholtz equation, 7
 Hermitian conjugation, 116
 Hilbert space, 104
 Homogeneous (spectral) frequency-domain problems, 397
 Hypersingular integral operator, 139

I

Idempotent operators, 122
 Illusion optics, 83
 Impact parameter, 415
 Initial boundary value problem, 390
 Input and output waveguides, 259
 Instantaneous efficiency of energy accumulation, 336
 Instantaneous sources, 229
 Integral convolution equations, 1
 Integral Green formula, 4
 Integral operator of Hilbert-Schmidt type, 139
 Isotropic dispersive media, 189

K

Kinematic approximation, 373
 Krein space, 178
 Kummer's formula, 66

L

Leaky wave, 399
 Left-handed media, 71
 Local, 241
 Local EACs, 280, 287
 Locally inhomogeneous dispersive media, 189
 Longitudinal propagation number, 397, 398
 Longitudinal propagation numbers, 264, 333, 342
 Loran series, 220

Lorentz lemma, 210
 Low-side-lobe planar antenna, 388

M

Main lobe, 266, 334
 Masking coating, 83, 85
 Matrix of the problem, 131
 Matrix product, 176
 Medium impedance, 104
 Meromorphic Fredholm theorem, 220, 222
 Metamaterial coating, 3
 Method of simple iteration, 180
 Method of successive approximations, 180
 Method of transformation operators, 188
 Mittra rule, 107
 Mode interconversion, 24
 Moderating coefficient, 423
 Modified Cagniard contour, 41
 Modified problem, 227
 Moving longitudinal magnetic dipole, 2

N

Near-field to far-field conversion, 405
 Near-field to far-field conversion efficiency, 396
 Negative refraction (NR) phenomenon, 2, 71
 Newton-Raphson method, 35
 Nonlocal, 237
 Nonlocal EACs, 279, 286
 Normalized directional pattern, 266, 292, 309, 334, 342
 Normalized pulsed pattern, 269, 292, 337, 342
 Normal modes, 397

O

Observation interval, 194
 Ohmic loss, 334
 Olver's uniform asymptotic representation, 35
 One-dimensionally periodic grating, 389
 Open (unbounded) initial boundary value problems, 226
 Open boundary value problems, 328
 Open initial boundary value problem, 188
 Open initial boundary value problems, 328, 388
 Open periodic resonator, 217
 Operator Fresnel formulas, 105
 Orientation of the main lobe, 411
 Original initial boundary value problem, 227
 Orthoprojectors, 116, 122
 Outgoing pulsed waves, 392

P

Parallelogram rule, 163

Parseval equality, 6
 Partial constituent, 306
 Partial radiation conditions, 265
 Passive compression, 371
 Passive compressors, 328
 Physical values of the frequency parameter, 395
 Point spectrum, 220
 Pontryagin space, 106, 128
 Portal operator, 116
 Portal operator matrix, 151
 Power gain, 335, 381
 Poynting theorem, 209
 Poynting vector, 76, 104
 Practical convergence, 113
 Problem of corner points, 287
 Problem of extended and remote sources, 255
 Projection method, 130
 Propagating harmonics, 215

Q

Qualitative explanation, 23
 Quality factor, 270, 335
 Quasi-Hermitian, 127

R

Radar image, 3
 Radiating efficiency, 266
 Radiating efficiency of a pulsed antenna, 269
 Radiation condition (RC), 226, 234, 278, 297, 330
 Radiation efficiency, 309, 311, 334, 410
 Radiation-forming region, The, 61
 Real algebraic branch points, 397
 Real wave, 399
 Real waveguide, 260
 Reciprocity relations, 211, 395
 Reflection and transmission coefficients, 310, 333
 Reflection and transmission matrix operators, 104
 Reflection coefficient, 208, 265, 308, 395
 Reflection zone, 396
 Regularization, 222
 Relative convergence, 107
 Replacement of the image, 83
 Resolvent, 222, 269
 Resonant quasi-optical devices, 328
 Reversed radiation, 406
 Riccati-Bessel functions, 81
 Ridge dielectric waveguide (RDW), 423
 Riemann problem, 5
 Riemann surface, 75

S

Saddle-point technique, 6
 Second Lorentz lemma, 123
 Sesquilinear Hermitian Q - form, 178
 Side-lobe level (SLL), 424
 Similarity operator', 115
 Single-mode regime, 214
 Slot resonances, 345
 Slow wave, 399
 Smooth transition equations, 4
 Sobolev space, 110
 Source functions, 390
 Space-time amplitudes, 231, 278, 283
 Spatial harmonics, 394
 Spectra, 269
 Spectral amplitude of the pulse, 201
 Spectral sets, 269
 Spectral theory, 188
 Spectrum of reflection matrix, 132
 Standing wave ratio, 423
 Stationary dispersive media, 189
 Steady-state field, 307
 Step-by-step progression through time layers, 207
 Storage units, 329, 348
 Strong projection convergence, 134
 Superposition principle, 193
 Surface of analytic continuation of the canonical Green function, 218
 Surface wave, 399
 Switches, 329, 348

T

Tensor product, 94

Tesseral spherical harmonics, 301
 Three-element Carleman's problem, 3
 Threshold frequencies or sliding points, 213
 Threshold value, 37
 Time-domain radiation efficiency, 337
 Transformation operators, 205
 Transformation optics, 79
 Transition radiation, 54
 Transmission coefficient, 209, 265, 308, 395
 Transmission zone, 396
 Transporting operators, 205
 Transport operators, 227, 234, 254, 300, 305
 Transverse eigenvalues, 230, 331, 339
 Transverse functions, 230, 278, 283, 331, 339
 True wave, 399

U

Undamped eigenwave, 265

V

Vavilov-Cherenkov radiation, 54
 Vertical and horizontal wavenumbers, 394
 Virtual boundary, 226
 Virtual waveguide, 260

W

Watson method, 24
 Watson transformation, 31
 Wave flow, 78
 Width of the main lobe, 411
 Wiener-Hopf method, 1